frontiers | Research Topics

Pulmonary hypertension in the modern era: Science and clinical practice, volume II

Edited by
Harm Jan Bogaard, Vinicio De Jesus Perez and Elena Goncharova

Published in
Frontiers in Medicine

ISSN 1664-8714
ISBN 978-2-83251-710-9
DOI 10.3389/978-2-83251-710-9

About Frontiers

Frontiers is more than just an open access publisher of scholarly articles: it is a pioneering approach to the world of academia, radically improving the way scholarly research is managed. The grand vision of Frontiers is a world where all people have an equal opportunity to seek, share and generate knowledge. Frontiers provides immediate and permanent online open access to all its publications, but this alone is not enough to realize our grand goals.

Frontiers journal series

The Frontiers journal series is a multi-tier and interdisciplinary set of open-access, online journals, promising a paradigm shift from the current review, selection and dissemination processes in academic publishing. All Frontiers journals are driven by researchers for researchers; therefore, they constitute a service to the scholarly community. At the same time, the *Frontiers journal series* operates on a revolutionary invention, the tiered publishing system, initially addressing specific communities of scholars, and gradually climbing up to broader public understanding, thus serving the interests of the lay society, too.

Dedication to quality

Each Frontiers article is a landmark of the highest quality, thanks to genuinely collaborative interactions between authors and review editors, who include some of the world's best academicians. Research must be certified by peers before entering a stream of knowledge that may eventually reach the public - and shape society; therefore, Frontiers only applies the most rigorous and unbiased reviews. Frontiers revolutionizes research publishing by freely delivering the most outstanding research, evaluated with no bias from both the academic and social point of view. By applying the most advanced information technologies, Frontiers is catapulting scholarly publishing into a new generation.

What are Frontiers Research Topics?

Frontiers Research Topics are very popular trademarks of the *Frontiers journals series*: they are collections of at least ten articles, all centered on a particular subject. With their unique mix of varied contributions from Original Research to Review Articles, Frontiers Research Topics unify the most influential researchers, the latest key findings and historical advances in a hot research area.

Find out more on how to host your own Frontiers Research Topic or contribute to one as an author by contacting the Frontiers editorial office: frontiersin.org/about/contact

Pulmonary hypertension in the modern era: Science and clinical practice, volume II

Topic editors

Harm Jan Bogaard — Amsterdam University Medical Center, Netherlands
Vinicio De Jesus Perez — Stanford University, United States
Elena Goncharova — University of California, Davis, United States

Citation

Bogaard, H. J., De Jesus Perez, V., Goncharova, E., eds. (2023). *Pulmonary hypertension in the modern era: Science and clinical practice, volume II*. Lausanne: Frontiers Media SA. doi: 10.3389/978-2-83251-710-9

Table of contents

frontiers | Frontiers in Medicine

TYPE Editorial
PUBLISHED 06 February 2023
DOI 10.3389/fmed.2023.1136157

OPEN ACCESS

EDITED AND REVIEWED BY
Chunxue Bai,
Fudan University, China

*CORRESPONDENCE
Harm J. Bogaard
✉ hj.bogaard@amsterdamumc.nl

SPECIALTY SECTION
This article was submitted to Pulmonary Medicine, a section of the journal Frontiers in Medicine

RECEIVED 02 January 2023
ACCEPTED 25 January 2023
PUBLISHED 06 February 2023

CITATION
Bogaard HJ, Goncharova EA and de Jesus Perez VA (2023) Editorial: Pulmonary hypertension in the modern era: Science and clinical practice, Volume II.
Front. Med. 10:1136157.
doi: 10.3389/fmed.2023.1136157

Editorial: Pulmonary hypertension in the modern era: Science and clinical practice, Volume II

Harm J. Bogaard[1]*, Elena A. Goncharova[2] and Vinicio A. de Jesus Perez[3]

[1]Department of Pulmonary Medicine, Amsterdam University Medical Center, Amsterdam, Netherlands, [2]Division of Pulmonary, Critical Care and Sleep Medicine, Lung Center, Department of Internal Medicine, Davis School of Medicine, University of California, Davis, Davis, CA, United States, [3]Division of Pulmonary, Allergy and Critical Care Medicine, Stanford University Medical Center, Stanford, CA, United States

KEYWORDS

pulmonary hypertension, right ventricle, microbiome, COVID-19, senescence, metabolism, inflammation

Editorial on the Research Topic
Pulmonary hypertension in the modern era: Science and clinical practice, Volume II

In 2021, this journal launched a Research Topic dedicated to translational science and clinical practice in pulmonary hypertension. Volume I of this topic was highly successful, with many valuable contributions from scientists across the globe. Because not all submitted papers could be accommodated in this first Volume, Frontiers in Medicine released Volume II of this topic on Pulmonary Hypertension.

Pulmonary hypertension is a devastating condition of high pulmonary pressures and right heart failure that, if untreated, leads to premature death. Research into disease mechanisms and optimal treatment remain of highest importance. In this volume, researchers from China, the United States and Europe provide important new insights into the diagnosis and management of pulmonary hypertension. First, in a study from Kunming, China, the microbiome in broncho-alveolar lavage fluid is compared between normal controls and pediatric patients with pulmonary arterial hypertension (PAH) associated with congenital left to right shunts (Ma et al.). The authors show an altered spectrum of microbes in pediatric PAH patients that is strongly correlated to a disturbed metabolomic profile. They speculate that metabolomic biomarkers may inform on clinical diagnosis, treatment, and prognosis of pediatric PAH patients. This volume also contains two valuable contributions on the diagnosis of chronic thromboembolic hypertension (CTEPH). Clinical scientists from Stanford University, Palo Alto, USA, conducted a survey to assess agreement amongst clinicians for initial therapy choice in patients with pulmonary hypertension in the context of chronic lung disease, or group 3 pulmonary hypertension (Thomas et al.). Although management guidelines discourage the routine use of PAH-targeted therapies in these patients, over 90% of respondents agreed that they would treat cases with severe group 3 pulmonary hypertension with some form of PAH-targeted therapy. For mild pulmonary hypertension and mild lung disease cases, <50% of respondents chose to start PAH-specific therapy. There was overall poor agreement between respondents in the choice to use mono-, double, or triple combination therapy with PAH-specific agents. This study shows wide practice variation and a strong need for further studies in this field. Le Pennec et al. from France address the current lack of consensus on the use of specific criteria for the interpretation of Ventilation/Perfusion (V/Q) lung scintigraphy to screen for CTEPH. In a group of 226 patients with newly diagnosed pulmonary hypertension,

of whom one quarter were ultimately diagnosed with CTEPH, the optimal diagnostic cut-off for interpretation was 2.5 segmental mismatched perfusion defects. An interpretation based on perfusion defects only provided similar sensitivity but lower specificity. As scintigraphy retained its central position in the diagnosis of CTEPH in the new ERS/ESC pulmonary hypertension guidelines, this study provides valuable additive guidance for a proper diagnosis of CTEPH. Shahin et al. from Sheffield, UK, described the use of cardiac magnetic resonance the assess prognosis and predict the response to pulmonary endarterectomy (PEA) in CTEPH. While right ventricular ejection fraction predicted outcome in patients not undergoing PEA, measures of left atrial volume index were associated with outcome after PEA surgery. This study highlights the prognostic value of imaging cardiac structure and function in CTEPH and the importance of considering left heart disease in patients considered for PEA.

The COVID-19 pandemic has brought forth a new disease entity whose long-term impact on public health continue to evolve as many survivors are now suffering from Post-Acute Sequelae of SARS-CoV-2 (PASC), a condition in which individuals experience a wide range of physical and mental symptoms after their initial infection. The manuscript by Oliveira et al. focuses on the cardiopulmonary sequelae of COVID-19 infection which include right ventricular dysfunction, pulmonary hypertension, thrombosis, and lung fibrosis. Acknowledging the many knowledge gaps pertaining to these topics, the authors provide a list of research priorities to direct attention to the most urgent questions to be addressed in an effort to anticipate the health care needs that these patients will require as the pandemic continues to evolve over the next few years.

Moving from clinical to the basic sciences, the study by Kyi et al. included in the collection tackles the contribution of cellular senescence in triggering vascular cell accumulation in the distal pulmonary arterioles of PAH patients. In a series of elegant experiments, the investigators demonstrate that accumulation of the senescence marker $p16^{INK4a}$ in pulmonary endothelial cells drives the production of endothelial-derived growth factors (e.g., PDGF) that promote the expansion of smooth muscle cells in the medial layer, a phenomenon that can be attenuated in *p16* $^{fl/fl}$*-Cdh5(PAC)-Cre* ^{ERT2} (*p16* $^{i\Delta EC}$) mice after tamoxifen induction. These studies provide compelling evidence that targeting senescence could be a viable therapeutic strategy in the management of PAH. Further, the study by Lin et al. takes a bioinformatics-based strategy to interrogate four publicly available datasets in an effort to identify prospective biomarkers and therapeutic targets in PAH. Among the genes identified in their robust analysis, TXNRD1 was selected for validation given its predictive performance and correlation with several hemodynamic parameters of PAH. Beyond the identification of TXNRD1, the most important aspect of the work is the demonstration that application of bioinformatics can accelerate the discovery of new mechanisms and targets using accumulating datasets being generated from Omics studies.

Continuing to uncover molecular mechanisms driving hyper-proliferation of pulmonary vascular cells in PAH, recent study by Jiang et al. investigated the role of lipogenesis in increased proliferation and apoptosis resistance of PAH PA smooth muscle cells. The authors found that, in contrast to healthy subjects, distal PA smooth muscle cells from PAH patients' lungs have enhanced lipogenesis, which is supported by up-regulation of key fatty acid synthesis enzymes ATP-citrate lyase, acetyl-CoA carboxylase, and fatty acid synthase. Importantly, the authors demonstrate that active lipogenesis is required for increased proliferation and survival of PA smooth muscle cells in PAH and provide strong evidence that there is a mechanistic link between glycolysis, lipogenesis, and the proliferation of human PAH PA smooth muscle cells, which is regulated by SIRT7/JNK-Akt axis. This study offers strong molecular basis for further investigations to determine the potential attractiveness of targeting abnormal lipogenesis to reduce pulmonary vascular remodeling and PAH.

Inflammation plays important role in PAH pathogenesis and supports multiple molecular and metabolic abnormalities involved in the initiation and progression of this deadly disease. The review article from Foley et al. discusses the role of inflammasome activation in the pathogenesis of PAH. Inflammasomes are multi-protein complexes that initiate and amplify immune responses induced by infectious or sterile inflammatory stimuli. Aberrant activation of inflammasomes has been implicated in various pulmonary and cardiovascular diseases. This timely and important review provides detailed overview of our current knowledge about inflammasome activation in immune and resident pulmonary vascular cells as it relates to the pathogenesis of PAH. The authors also provide in depth discussion of potential drug development to inhibit inflammasomes and their downstream effectors to treat PAH. Further emphasizing important role of inflammation and translational significance of transforming growth factor-β (TGF-β) superfamily signaling in dysregulated vascular cell proliferation in PAH, Andre et al. provide comprehensive review of the TGF-β superfamily mechanisms in PAH pathogenesis and expertly summarize the interaction of TGF-β superfamily signaling with the inflammation and mechanobiological forces. The authors also discuss emerging therapeutic strategies to restore SMAD signaling and reverse pulmonary vascular remodeling and overall PAH.

The right ventricle (RV) dysfunction is one of the most important determinants of survival in patients with pulmonary hypertension, but the age-related RV changes either in health or disease are not well-understood. To note, aging is associated with alterations in pulmonary vasculature and RV hemodynamics, and there is higher prevalence of pulmonary hypertension in the elderly. Using male Sprague-Dawley rats as a model, Sharifi Kia et al. report their pilot findings demonstrating effects of healthy aging on the structure, function, and biomechanical properties of RV. Specifically, the authors provide strong evidence suggesting that healthy aging could promote RV remodeling *via* increased peak pressures, cardiomyocyte loss, fibrosis, fiber reorientation, and altered mechanical properties. These findings improve our understanding of age-related changes in the RV fitness, which may play important role in response to disease, and call for further investigations to determine how age contributes to the disease progression in patients with pulmonary hypertension.

Author contributions

All authors listed have made a substantial, direct, and intellectual contribution to the work and approved it for publication.

Conflict of interest

The authors declare that the research was conducted in the absence of any commercial or financial relationships that could be construed as a potential conflict of interest.

Publisher's note

frontiers in Medicine

ORIGINAL RESEARCH
published: 03 December 2021
doi: 10.3389/fmed.2021.764815

Prescription Patterns for Pulmonary Vasodilators in the Treatment of Pulmonary Hypertension Associated With Chronic Lung Diseases: Insights From a Clinician Survey

Christopher A. Thomas[1], Justin Lee[2], Roberto J. Bernardo[3], Ryan J. Anderson[1], Vladimir Glinskii[1], Yon K. Sung[1], Kristina Kudelko[1], Haley Hedlin[2], Andrew Sweatt[1], Steven M. Kawut[4], Rishi Raj[1†], Roham T. Zamanian[1*†] and Vinicio de Jesus Perez[1*†]*

[1] Department of Pulmonary, Allergy and Critical Care Medicine, Stanford University, Stanford, CA, United States, [2] Quantitative Sciences Unit, Department of Medicine, Stanford University, Stanford, CA, United States, [3] Division of Pulmonary, Critical Care and Sleep Medicine, The University of Oklahoma Health Sciences Center, Tulsa, OK, United States, [4] Pulmonary, Allergy and Critical Care Medicine Division, Perelman School of Medicine at the University of Pennsylvania, Philadelphia, PA, United States

Background: Pulmonary hypertension is a complication of chronic lung diseases (PH-CLD) associated with significant morbidity and mortality. Management guidelines for PH-CLD emphasize the treatment of the underlying lung disease, but the role of PH-targeted therapy remains controversial. We hypothesized that treatment approaches for PH-CLD would be variable across physicians depending on the type of CLD and the severity of PH.

Methods and Results: Between May and July 2020, we conducted an online survey of PH experts asking for their preferred treatment approach in seven hypothetical cases of PH-CLD of varying severity. We assessed agreement amongst clinicians for initial therapy choice using Fleiss' kappa calculations. Over 90% of respondents agreed that they would treat cases of severe PH in the context of mild lung disease with some form of PH-targeted therapy. For cases of severe PH in the context of severe lung disease, over 70% of respondents agreed to use PH-targeted therapy. For mild PH and mild lung disease cases, <50% of respondents chose to start PH-specific therapy. There was overall poor agreement between respondents in the choice to use mono-, double or triple combination therapy with PH-specific agents in all cases.

Conclusion: Although management guidelines discourage the routine use of PH-targeted therapies to treat PH-CLD patients, most physicians choose to treat patients with some form of PH-targeted therapy. The choice of therapy and treatment approach are variable and appear to be influenced by the severity of the PH and the underlying lung disease.

Keywords: pulmonary hypertension, chronic lung disease, vasodilators, survey, group 3 PH

OPEN ACCESS

Edited by:
Silvia Ulrich,
University Hospital Zürich, Switzerland

Reviewed by:
Joan Albert Barberà,
Hospital Clínic de Barcelona, Spain
Cheng Jun Hu,
University of Colorado, United States

***Correspondence:**
Vinicio de Jesus Perez
vdejesus@stanford.edu
Rishi Raj
rishi.raj@stanford.edu
Roham T. Zamanian
zamanian@stanford.edu

†These authors have contributed equally to this work

Specialty section:
This article was submitted to Pulmonary Medicine, a section of the journal Frontiers in Medicine

Received: *26 August 2021*
Accepted: *25 October 2021*
Published: *03 December 2021*

Citation:
Thomas CA, Lee J, Bernardo RJ, Anderson RJ, Glinskii V, Sung YK, Kudelko K, Hedlin H, Sweatt A, Kawut SM, Raj R, Zamanian RT and de Jesus Perez V (2021) Prescription Patterns for Pulmonary Vasodilators in the Treatment of Pulmonary Hypertension Associated With Chronic Lung Diseases: Insights From a Clinician Survey. Front. Med. 8:764815. doi: 10.3389/fmed.2021.764815

INTRODUCTION

Pulmonary hypertension (PH) associated with chronic lung disease (PH-CLD) is a subgroup of group 3 PH associated with significant morbidity and mortality (1, 2). Although PH-CLD is relatively common, the pathophysiology is quite diverse and complex, and even mild PH in the setting of CLD has been associated with reduced functional status and worse outcomes (3). Diagnosis of PH-CLD remains challenging even for the most experienced medical professionals. When patients have a diagnosis of CLD and PH, the clinician must use data from lung imaging, pulmonary function tests, and right heart catheterization (RHC) to confirm the diagnosis and phenotype of patients according to disease severity. As such, PH-CLD presents many diagnostic and therapeutic challenges to even the most experienced clinicians.

Current consensus guidelines recommend treating the primary lung disease and advise against routine use of PH-targeted drugs in PH-CLD (1). However, clinicians may favor treating PH-CLD empirically with pulmonary vasodilators, although the clinical benefit of monotherapy or combination therapy in this setting remains controversial. In April 2021, following the results of the INCREASE study, inhaled treprostinil became the first and only drug approved by the Food and Drug Administration (FDA) for the treatment of PH associated with interstitial lung disease (ILD) (4). For other PH-targeted therapies, the data remains controversial and may even indicate that certain drugs increase the risk of complications in PH-CLD. For example, the use of ambrisentan and riociguat is contraindicated in patients with PH associated with idiopathic pulmonary fibrosis (IPF) and idiopathic interstitial pneumonia based on clinical studies demonstrating an increased incidence of morbidity related to these drugs (5, 6). As such, it is advisable to avoid empirical use of endothelin receptor antagonists and riociguat in PH-CLD.

At present, there is limited data on the practice patterns of physicians who treat PH-CLD in terms of their approach to using PH-targeted agents. A 2015 survey of treatment practices for non-Group 1 PH patients at national PH referral centers reported that 80% of Group 3 PH received PH-targeted therapy (7). Since then, there has been no reassessment to determine whether the attitudes toward PH-CLD have changed following the publication of the 2018 6th World Symposium on PH (6th WSPH) proceedings (8). Moreover, despite the safety concerns with use of endothelin receptor antagonists or riociguat (5, 6), it is unclear whether physicians rely on these drugs when choosing to empirically treat patients with CLD or whether they favor the use of mono- or combination therapy in a manner similar to the current standard of care for Group 1 PH patients.

Given the lack of consensus regarding the use of PH-targeted therapies in CLD, we hypothesized that agreement to treat with PH-targeted drugs would be higher in cases of severe PH-CLD and that use of monotherapy would be preferred over combination therapy. Our goal was to understand the current attitudes among PH professionals regarding the treatment of PH-CLD and how disease severity dictates the decision to choose a specific approach to treatment.

It must be noted that this study reflects the attitude of physicians toward the use of PH medications to treat PH-CLD prior to the publication of the INCREASE trial and approval of inhaled treprostinil for PH-ILD in April 2021.

METHODS

We created an online survey to gather information on the treatment preferences of clinicians who manage PH-CLD. The survey was created using the Qualtrics survey tool provided by Stanford University. The survey was reviewed by the Stanford University Institutional Review Board and granted exempt status. The survey included eight demographic questions on clinician training backgrounds, experience with PH-CLD, and institution location and type (see **Appendix I** for survey details). We submitted the survey for dissemination to the following organizations' email listservs: the Pulmonary Hypertension Clinicians and Researchers (PHCR) network, the American College of Chest Physicians (ACCP), and the American Thoracic Society (ATS) pulmonary circulation assembly. We chose these listservs because they are well-known organizations with broad distribution to the PH clinician community. The survey was conducted between May and July 2020, and respondents were asked to complete the survey only once. Responses were anonymous, and all data was stored in the secure online Qualtrics database.

The survey included seven hypothetical cases designed by PH and ILD experts at Stanford University. We chose to focus the clinical cases on IPF and chronic obstructive pulmonary disease (COPD) as these two disease entities are commonly representative of PH-CLD. Each case included the patient's age, biological sex, CLD diagnosis, WHO functional class, pulmonary function test (PFT) values, echocardiography results, RHC hemodynamics, and 6-min walk distance (6MWD) (see **Figure 1** for an example case, and the **Appendix** for the survey including all cases). Cases were based on the current definitions of PH-CLD from the 6th World Symposium on Pulmonary Hypertension (1): (1) *CLD without PH*: mPAP < 21 mmHg, or mPAP 21–24 with PVR < 3 WU, (2) *CLD with mild PH*: mPAP 21–24 mmHg

Abbreviations: ACCP, American College of Chest Physicians; ATS, American Thoracic Society; CI, Cardiac index; CLD, Chronic lung disease; COPD, Chronic obstructive pulmonary disease; CTEPH, Chronic thromboembolic pulmonary hypertension; CTD, Connective tissue disease; DLCO, Diffusing capacity of the lungs for carbon monoxide; ERA, Endothelin receptor antagonist; FDA, Food and drug administration; FVC, Forced vital capacity; FEV1, Forced expiratory volume in 1 second; IPF, Idiopathic pulmonary fibrosis; HIV, Human Immunodeficiency Virus; ILD, Interstitial lung disease; IV, intravenous; VO2 max, maximal rate of oxygen consumption; mPAP, mean pulmonary artery pressure; NYHA, New York Heart Association; PDE5 inhibitor, Phosphodiesterase-5 inhibitor; PAH, Pulmonary arterial hypertension; PCWP, Pulmonary capillary wedge pressure; PFT, Pulmonary function test; PH, Pulmonary hypertension; PH-CLD, Pulmonary hypertension associated with chronic lung disease; PHCR, Pulmonary Hypertension Clinicians and Researchers; PVR, Pulmonary vascular resistance; RHC, Right heart catheterization; RV, Right ventricle; 6MWD, Six minute walk distance; SC, subcutaneous; TR, tricuspid regurgitation; V/Q scan, ventilation/perfusion scan; WU, Wood units; WHO, World Health Organization; 6th WSPH, 6th World Symposium on PH.

Demographics	
Age	65
Sex	Male
Disease	Mild IPF with limited parenchymal involvement
WHO Functional Class	II
PFTs	
FEV1/FVC ratio	0.75
FVC (% predicted)	80%
DLCO (% predicted)	60%
Echo	normal biventricular size and function, normal valves

Right Heart Catheterization	
mPAP	28 mmHg
PVR	3.8 WU
PCWP	11 mmHg
CI	2.8 L/min/m^2
Other Testing	
6MWD	500 meters
VO2 Max	18 ml/min/kg
V/Q Scan	Low probability for PE
Autoimmune serologies	Negative
Kidney and liver function	Normal
HIV	Negative

What would be your initial therapeutic approach to treating the pulmonary hypertension in this patient?

FIGURE 1 | Example PH-CLD case from the survey (case 1—Mild IPF/Mild PH).

IPF	COPD
Mild IPF / Mild PH (Case 1)	Mild COPD / Mild PH (Case 5)
Advanced IPF / Mild PH (Case 2)	-
Mild IPF / Severe PH (Case 3)	Mild COPD / Severe PH (Case 6)
Advanced IPF / Severe PH (Case 4)	Severe COPD / Severe PH (Case 7)

FIGURE 2 | PH-CLD phenotypes for each of the seven hypothetical cases. Severe PH was defined as a mPAP > 35 mmHg, severe IPF was defined as FVC < 70%, and severe COPD was defined as FEV1 < 60%. These values were based on the 6th WSPH Group 3 task force recommendations (1).

with PVR > 3 WU, or mPAP 25–34, (3) *CLD with severe PH*: mPAP > 35 mmHg, or mPAP > 25 mmHg and low cardiac index (CI< 2.0 l/min/m^2). The cases were created using different combinations of mild to severe CLD and PH and designed to be straightforward regarding the severity of both the lung disease and the PH. Four cases were created with "severe" PH, defined as an mPAP > 35 mmHg. Of these cases, two were paired with a "mild" CLD diagnosis (i.e., Group 1 PH-like phenotype), and another two were "severe" PH paired with advanced CLD. The case designs are summarized in **Figure 2**.

We included other variables to make the overall clinical picture clear and to eliminate the possibility of other etiologies of PH [i.e., connective tissue diseases (CTD) or chronic thromboembolic pulmonary hypertension (CTEPH)]. To keep the survey as short as possible, we chose not to include the combination of severe COPD and mild PH because the treatment choice variability was likely to be relatively low (i.e., most would choose no PH-targeted treatment).

After reading the cases, clinicians were first asked, "What would be your initial therapeutic approach to treating pulmonary hypertension in this patient?" The answer choices for this question were "no medical therapy," "single-agent therapy," "double agent therapy," or "triple agent therapy." If they chose no medical therapy, the survey proceeded to the next case. If they decided on single, double or triple agent therapy, respondents were asked to pick a specific combination therapy regimen [e.g., phosphodiesterase-5 inhibitor (PDE5 inhibitor), endothelin receptor antagonist (ERA), or prostacyclin analog]. See the **Appendix** for complete answer choices.

The primary analysis was agreement amongst clinicians for initial therapy choice (i.e., 0 vs. 1 vs. 2 vs. 3 drug therapy) for each of the 7 cases. This analysis was done using Fleiss' kappa calculations (9) amongst all survey respondents who answered all seven cases. As a sensitivity analysis, Fleiss' kappa was also calculated amongst US practicing clinicians. Additionally, Fleiss' kappa was calculated for the subset of IPF and COPD cases. Finally, Fleiss' kappa was calculated separately for both pulmonologists and cardiologists. Fleiss' kappa values can range from −1 to 1, with negative values indicating more disagreement than expected by chance, positive values below

TABLE 1 | Demographic characteristics of the survey respondents.

Demographics of those who answered at least one case (*N* = 87)	
Title (%)	
Attending physician/consultant	84 (96.6%)
Physician-in-training	1 (1.1%)
Nurse practitioner	2 (2.3%)
Training background (%)	
Pulmonary medicine training	60 (69%)
Cardiology medicine training	26 (29.9%)
Other clinicians	1 (1.1%)
Years in practice [median (IQR)]	12 [6–20]
Practicing in the United States (%)	80 (92%)
Institution type (%)	
Pulmonary hypertension center of comprehensive care	39 (48.8%)
Pulmonary hypertension regional clinical program	4 (5.0%)
Academic center without PHA designation	28 (35.0%)
Community practice without PHA designation	7 (8.8%)
Other	2 (2.5%)
Percentage of time spent practicing clinical medicine [%, median (IQR)]	75.0 [60.0–81.0]
Percentage of time spent treating pulmonary hypertension patients [%, median (IQR)]	50.0 [30.0–76.0]
Unique group 3 pulmonary hypertension patients in the past year of practice [#, median (IQR)]	30.0 [20.0–50.0]

IQR, interquartile range.

0.40 suggesting poor agreement beyond what is expected by chance, and values >0.75 suggesting excellent agreement (10). All analyses were conducted with R version 3.5.1, and the "likert" R package (11) version 1.3.5 was used to plot responses by case.

RESULTS

Demographic characteristics for respondents who responded to at least one of the cases are shown in **Table 1**. Hundred clinicians responded to at least one survey question, 87 clinicians responded to at least 1 case, and 76 clinicians completed the entire survey. Though we disseminated the survey to three international organizations, most respondents (92%) reported practicing in the United States. Responses provided for each of the seven cases were analyzed globally (**Figure 3**) and specialty (**Figure 4**).

In cases with severe PH (regardless of the severity of the lung disease), clinicians were more likely to choose some form of PH therapy (71–94%) rather than no therapy. Over half (58–66%) of the clinicians chose no PH therapy in the three cases with mild PH. In the "Group 1-like" cases [Case 3 (mild IPF and severe PH) and Case 6 (mild COPD and severe PH)], more than 90% of clinicians chose some form of PH treatment. In Case 3, 39% of clinicians chose single-agent therapy, 48% chose double agent therapy, and 7% chose triple agent therapy, for a total of 94% of clinicians selecting some form of PH therapy. In Case 6, 33% of clinicians chose single-agent treatment, 50% chose double agent therapy, and 8% chose triple agent therapy, for a total of 91% of clinicians selecting some form of PH therapy.

In the other cases [Case 4 (advanced IPF and severe PH) and Case 7 (severe COPD and severe PH)], more than 70% of clinicians chose some form of therapy. In Case 4, 37% of clinicians chose single-agent treatment, 23% chose double agent therapy, and 12% chose triple treatment, for a total of 73% of clinicians chose some form of PH therapy. In Case 7, 37% of clinicians chose single-agent treatment, 24% chose double agent therapy, and 11% chose triple treatment, for a total of 71% of clinicians selecting some sort of PH therapy.

In the cases of mild PH [Case 1 (mild IPF and mild PH), Case 2 (advanced IPF and mild PH), and Case 5 (mild COPD and mild PH)], over half (58–66%) of the clinicians chose not to start PH therapy.

Fleiss' Kappa Analyses

Fleiss' kappa calculation for the overall analysis yielded a value of 0.12 (**Table 2**). This value is consistent with poor overall agreement among the 76 clinicians who completed all 7 cases regarding choosing between the number of therapies (i.e., 0, 1, 2, or 3 PH therapies). Agreement for IPF specific case questions (Cases 1, 3, and 4) and COPD-specific case questions (Cases 5, 6, and 7) was also poor with kappa values of 0.13 and 0.10, respectively (**Table 2**). We excluded Case 2 (advanced IPF and mild PH) from this analysis because its corresponding case (severe COPD and mild PH) was not included in the survey. The Fleiss' kappa for survey respondents who reported practicing in the US and who completed the entire survey ($n = 70$) was similarly low (0.11) for all cases, which is consistent with poor agreement among US clinicians (**Table 3**). We also calculated Fleiss' kappa for pulmonologists ($n = 53$) and cardiologists ($n = 23$) who completed the entire survey (**Tables 4**, **5**). The Fleiss' kappa for pulmonologists (0.13) was slightly higher than that of all survey respondents, and the Fleiss' kappa for the cardiologists (0.07) was slightly lower than that for all survey respondents.

Individual Medication Choices for Severe PH Cases

We describe Cases 3 and 6 (mild lung disease with severe PH) as a "Group 1-like" phenotype. In Case 3 (mild IPF and severe PH), 39, 48, and 7% of clinicians chose single, double, and triple agent therapy, respectively. Of those clinicians who chose single-agent therapy ($n = 32$), 52% chose a PDE5 inhibitor, 45% chose an inhaled prostacyclin analog, 3.2% chose an endothelin receptor antagonist (ERA), and a single respondent did not choose a specific therapy. Of those clinicians who chose double agent therapy ($n = 39$), 55% chose the combination of a PDE5 inhibitor and an ERA, 32% chose the combination of a PDE5 inhibitor and an inhaled prostacyclin analog, and the remainder of clinicians chose various other combinations. There was no predominant combination for those who decided on triple agent therapy ($n = 6$), with clinicians selecting multiple combinations of PDE5 inhibitors, ERAs, oral/inhaled/IV/SQ prostacyclins,

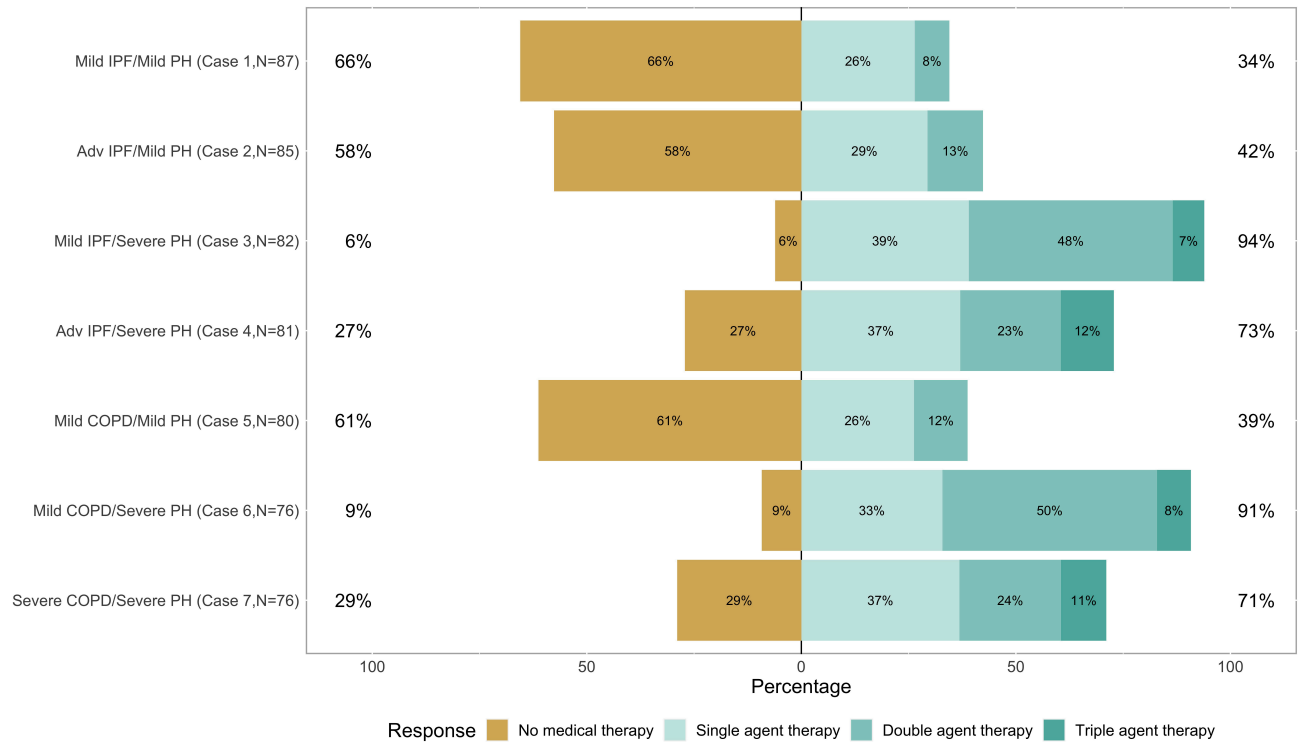

FIGURE 3 | Plot of the responses to each of the seven cases.

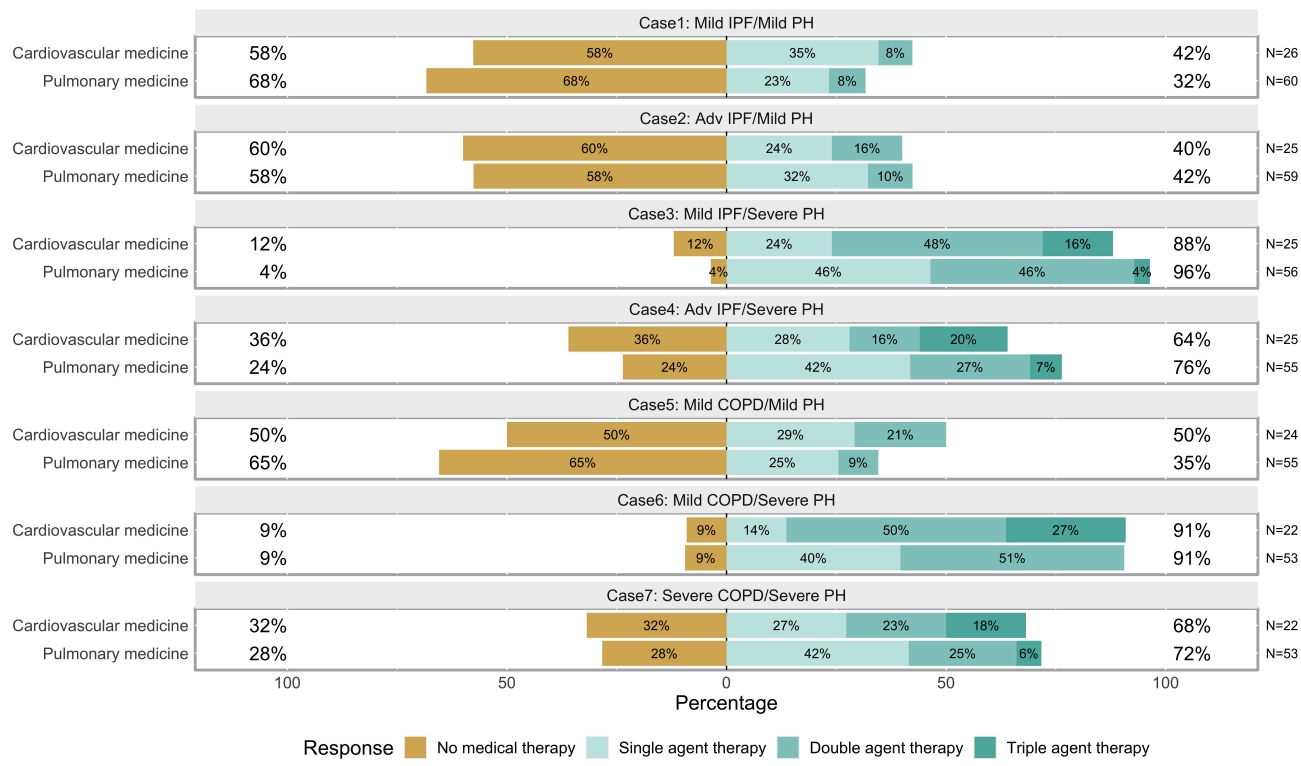

FIGURE 4 | Plot of the responses to each of the seven cases by specialty.

TABLE 2 | Fleiss' Kappa calculations for all respondents who completed the entire survey ($n = 76$).

Measuring agreement on:	Number of raters	Kappa: all cases	Kappa: IPF cases only	Kappa: COPD cases only
Number of therapies (0, 1, 2, 3)	76	0.12	0.13	0.10
None vs. any therapy	76	0.23	0.27	0.21

TABLE 3 | Fleiss' Kappa calculations for US respondents who completed the entire survey ($n = 70$).

Measuring agreement on:	Number of raters	Kappa: all cases	Kappa: IPF cases only	Kappa: COPD cases only
Number of therapies (0, 1, 2, 3)	70	0.11	0.12	0.10
None vs. any therapy	70	0.24	0.28	0.23

TABLE 4 | Fleiss' Kappa calculations for respondents who identified as pulmonologists and completed the entire survey ($n = 53$).

Measuring agreement on:	Number of raters	Kappa: all cases	Kappa: IPF cases only	Kappa: COPD cases only
Number of therapies (0, 1, 2, 3)	53	0.13	0.14	0.12
None vs. any therapy	53	0.25	0.31	0.23

TABLE 5 | Fleiss' kappa for survey respondents who identified as cardiologists and completed the entire survey ($n = 22$).

Measuring agreement on:	Number of raters	Kappa: all cases	Kappa: IPF cases only	Kappa: COPD cases only
Number of therapies (0, 1, 2, 3)	22	0.07	0.07	0.05
None vs. any therapy	22	0.14	0.14	0.12

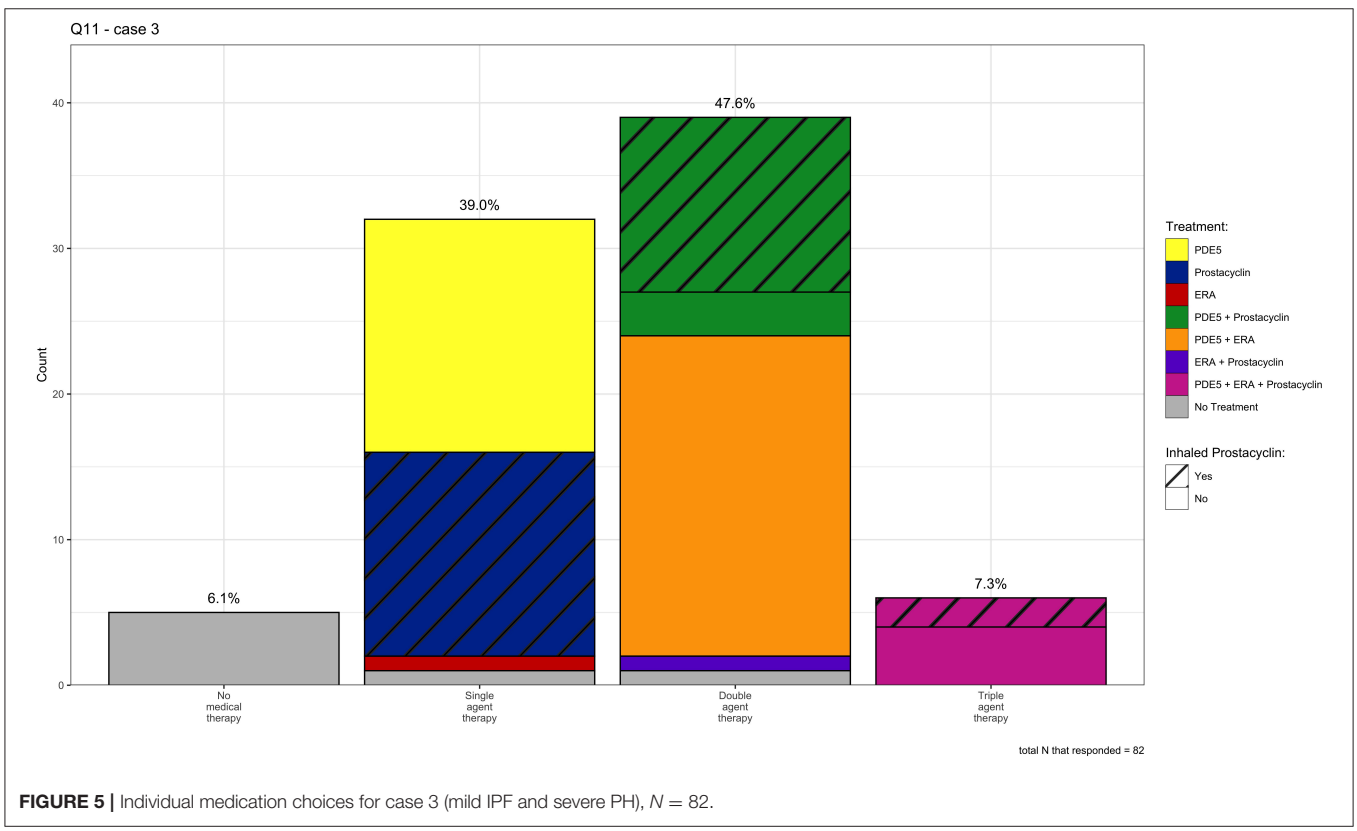

FIGURE 5 | Individual medication choices for case 3 (mild IPF and severe PH), $N = 82$.

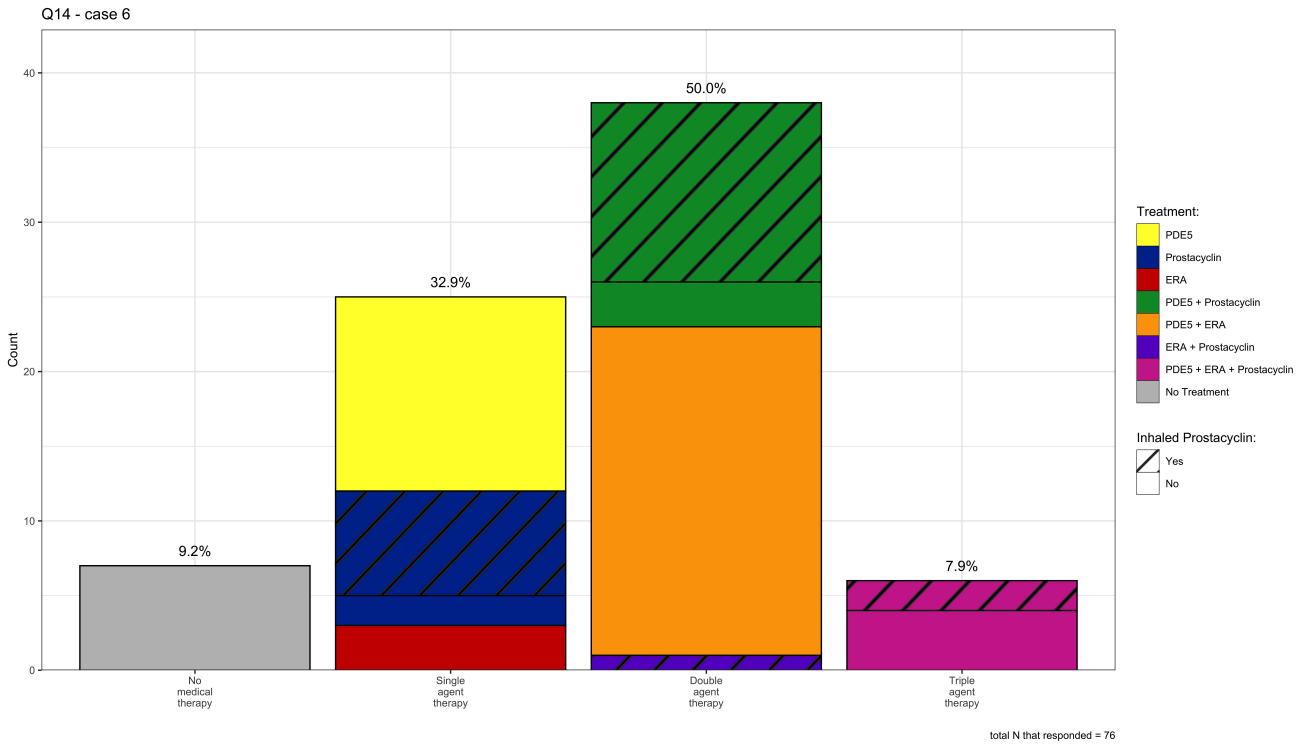

FIGURE 6 | Individual medication choices for case 6 (mild COPD and severe PH), $N = 76$.

and riociguat. See **Figure 5** for a visual representation of the individual answer choices for Case 3.

In Case 6 (mild COPD and severe PH), 33, 50, and 8% of clinicians chose single, double, and triple agent therapy, respectively. Of those clinicians who chose single-agent therapy ($n = 25$), 52% chose a PDE5 inhibitor, 28% chose an inhaled prostacyclin analog, and 12% chose an ERA. The remainder chose either an oral or IV/SQ prostacyclin. Of those clinicians who chose double agent therapy ($n = 38$), 58% chose the combination of PDE5 inhibitor and an ERA, 29% chose the combination of a PDE5 inhibitor and an inhaled prostacyclin analog, and the remainder of clinicians ($n = 5$) chose various other combinations. For those who decided on triple agent therapy, there was again not a predominant medication combination. See **Figure 6** for a visual representation of the individual answer choices for Case 6.

In Case 4 (advanced IPF and severe PH), 37, 24, and 12% of clinicians chose single, double, and triple agent therapy, respectively. Of those clinicians who chose single-agent therapy ($n = 30$), 53% chose an inhaled prostacyclin analog, and 40% chose a PDE5 inhibitor. Of those clinicians who chose double agent therapy ($n = 19$), 74% chose the combination of a PDE5 inhibitor and an inhaled prostacyclin analog. Of those who decided on triple agent therapy ($n = 10$), there was no predominant combination.

In Case 7 (severe COPD and severe PH), 37, 24, and 11% of clinicians chose single, double and triple agent therapy, respectively. Of those clinicians who chose single-agent therapy ($n = 28$), 50% chose a PDE5 inhibitor, and 43% chose an inhaled prostacyclin analog. Of those clinicians who chose double agent therapy ($n = 18$), 39% chose the combination of PDE5 inhibitor and an inhaled prostacyclin analog, and 33% chose the combination of a PDE5 inhibitor and an IV/SQ prostacyclin analog. Of those clinicians who chose triple agent therapy, the predominant therapy choice was the combination of a PDE5 inhibitor, an ERA, and an IV/SQ prostacyclin analog. See the **Appendix** for all answer choices to every case.

DISCUSSION

In this study, we sought to characterize treatment preferences for PH-CLD. We hypothesized that there would be a wide variation in treatment practices among clinicians who treat this patient population. In cases with mild PH (mPAP < 35 mmHg), clinicians predominantly chose no medical therapy, whereas in cases with severe PH (mPAP > 35 mmHg), clinicians were more likely to select PH therapy regardless of the severity of CLD. More than 90% of clinicians chose to treat patients with severe PH and mild CLD, while >70% chose to treat patients with severe PH and advanced CLD with PH-targeted therapies. There were clear patterns in selecting some form of medical treatment for the severe PH cases and no medical treatment for the mild PH cases. However, the Fleiss' kappa analysis of treatment strategy (i.e., 0 vs. 1 vs. 2 vs. 3 drug therapies) revealed poor overall agreement

among clinicians regarding the initial treatment strategy. Our data shows that many clinicians would be inclined to treat PH-CLD with PH-targeted therapies even though these drugs, with the notable exception of inhaled treprostinil, are not approved for this indication.

Some observations in the choice of PH-targeted therapy are worth highlighting in light of reports questioning the safety of certain drugs and the approval of inhaled treprostinil almost a year after the survey was conducted. In the two cases with a "Group 1-like PH" phenotype, PDE5 inhibitors were the predominant choice, regardless of whether the clinician chose single, double or triple agent therapy. Several studies have been conducted to determine whether the treatment of COPD or ILD patients with PH with sildenafil offers some clinical benefit, but the data remains inconclusive (12–17). Interestingly, in case 3 (mild IPF and severe PH), many clinicians chose dual therapy with a PDE5 inhibitor and an ERA, despite evidence that the use of ERAs could worsen hypoxia without an increase in efficacy (18, 19). The ARTEMIS-IPF study was terminated prematurely because an interim analysis indicated that ambrisentan-treated patients with IPF were more likely to have disease progression and require hospitalizations due to respiratory decompensation (5). Of note, a parallel study to study ambrisentan in PH-CLD (ARTEMIS-PH) was also terminated by the results were never published. Regarding prostacyclins, there was a preference toward using inhaled prostacyclins as either monotherapy or in combination with other drugs (most often PDE5 inhibitors). This preference may have been motivated by multiple studies predating the recently completed INCREASE study suggesting that inhaled treprostinil can improve hemodynamics and functional capacity in PH-CLD (20–22). Of note, there was similarly poor agreement for the IPF vs. COPD cases and among both pulmonologists and cardiologists. The lack of agreement between disease subgroups or subspecialists likely reflects the wide variation in treatment practices, regardless of chronic lung disease type or training background.

Our study differs from the 2015 Trammel et al. (7) in several important ways. Besides capturing the present attitudes of clinicians familiar with the new 6th WSPH clinical definition of group 1 and group 3 PH (8), our survey is based on the use of hypothetical yet "real world" cases to assess the level of agreement amongst individual experts in their decision to treat or not to treat PH-IPF and PH-COPD. In contrast, the 2015 survey was designed to collect information from respondents on their diagnostic approach, their definition of "out of proportion" PH-CLD, and the percentage of non-group 1 patients treated with either single or combination PH-targeted therapy at their centers. This approach predated the current clinical classification of group 3 severity proposed by Nathan and colleagues at the 6th WSPH, which was used to design our cases (1). Also, it is worth noting that the 2015 Trammel study also included group 2 PH patients, another group for which no treatment guidelines currently exist. Despite their differences, our study complements the data captured in the 2015 survey by Trammel and should serve as a benchmark for future surveys on attitudes to PH-CLD treatment following the approval of inhaled treprostinil for PH-ILD.

There are several limitations to our study. We recognize that these are simplified cases and treatment plans that don't necessarily reflect complex real-world clinical scenarios and include common comorbidities and other treatment options such as pulmonary rehabilitation, palliative care, and lung transplant. We also acknowledge that the lack of details regarding the clinical context of individual cases may have led clinicians to select specific approaches that may not reflect their approach to management. Also, as this was a convenience sample, we were unable to calculate the response rate or characterize the non-respondents and likely selection bias. The respondents were overwhelmingly from the United States, and thus our survey results cannot be generalized to any other countries.

Despite these limitations, this survey data provides important information regarding current clinician treatment practices for the use of PH-targeted therapy in PH-CLD. We found that most clinicians chose to treat severe PH in patients with severe lung disease, despite a lack of treatment guidelines or approved medical therapies at the time of this survey. We strongly recommend that all clinicians closely adhere to published guidelines for patients with PH-CLD, which emphasize early referral to PH centers of comprehensive care and individualized treatment planning by experienced clinicians.

While our survey was administered before the results of the INCREASE trial had been published or the FDA had approved inhaled treprostinil, our data show that inhaled therapy is already part of many clinicians' treatment practices in PH-CLD. Use of inhaled prostanoids in PH in COPD patients also appears to be favored and reflects the interest in this treatment modality currently being tested in the ongoing PERFECT study evaluating the safety and efficacy of inhaled treprostinil in COPD patients (NCT03496623).

CONCLUSION

Most clinicians who care for PH-CLD patients associated with IPF and COPD favor empirical therapy with PH targeted therapy despite the lack of consensus guidelines. The decision to offer treatment may be guided by the severity of the PH independent of the status of the CLD. Whereas, respondents favored the use of inhaled prostanoids, overall agreement regarding the use of one or multiple drug classes was low. Given the number of respondents that chose to use ERAs, it is vital to educate the medical community regarding the risks associated with PH-targeted therapies in PH-CLD. Thus, our results raise concern regarding the lack of proper guidance for the use of PH therapies in PH-CLD and stress the need for updated and perhaps better-informed guidelines.

DATA AVAILABILITY STATEMENT

The original contributions presented in the study are included in the article/**Supplementary Material**, further inquiries can be directed to the corresponding author/s.

GUARANTOR STATEMENT

VJP is the guarantor of the content of the manuscript.

AUTHOR CONTRIBUTIONS

VJP and RZ had full access to all the data in the study and take responsibility for its integrity and the data analysis and revised the manuscript for important intellectual content. All authors contributed to study design, data analysis, manuscript writing, and reviewed and revised the manuscript.

FUNDING

This work was supported by an NIH R01 HL134776 and R01 HL139664 to VJP.

SUPPLEMENTARY MATERIAL

The Supplementary Material for this article can be found online at: https://www.frontiersin.org/articles/10.3389/fmed.2021.764815/full#supplementary-material

REFERENCES

1. Nathan SD, Barbera JA, Gaine SP, Harari S, Martinez FJ, Olschewski H, et al. Pulmonary hypertension in chronic lung disease and hypoxia. *Eur Respir J*. (2019) 53:1801914. doi: 10.1183/13993003.01914-2018
2. Seeger W, Adir Y, Barbera JA, Champion H, Coghlan JG, Cottin V, et al. Pulmonary hypertension in chronic lung diseases. *J Am Coll Cardiol*. (2013) 62:D109–16. doi: 10.1016/j.jacc.2013.10.036
3. Behr J, Nathan SD. Pulmonary hypertension in interstitial lung disease: screening, diagnosis and treatment. *Curr Opin Pulm Med*. (2021) 27:396–404. doi: 10.1097/MCP.0000000000000790
4. Waxman A, Restrepo-Jaramillo R, Thenappan T, Ravichandran A, Engel P, Bajwa A, et al. Inhaled treprostinil in pulmonary hypertension due to interstitial lung disease. *N Engl J Med*. (2021) 384:325–34. doi: 10.1056/NEJMoa2008470
5. Raghu G, Behr J, Brown KK, Egan JJ, Kawut SM, Flaherty KR, et al. Treatment of idiopathic pulmonary fibrosis with ambrisentan: a parallel, randomized trial. *Ann Intern Med*. (2013) 158:641–9. doi: 10.7326/0003-4819-158-9-201305070-00003
6. Nathan SD, Behr J, Collard HR, Cottin V, Hoeper MM, Martinez FJ, et al. Riociguat for idiopathic interstitial pneumonia-associated pulmonary hypertension (RISE-IIP): a randomised, placebo-controlled phase 2b study. *Lancet Respir Med*. (2019) 7:780–90. doi: 10.1016/S2213-2600(19)30250-4
7. Trammell AW, Pugh ME, Newman JH, Hemnes AR, Robbins IM. Use of pulmonary arterial hypertension-approved therapy in the treatment of non-group 1 pulmonary hypertension at US referral centers. *Pulm Circ*. (2015) 5:356–63. doi: 10.1086/681264
8. Thomas CA, Anderson RJ, Condon DF, de Jesus Perez VA. Diagnosis and management of pulmonary hypertension in the modern era: insights from the 6th World Symposium. *Pulm Ther*. (2020) 6:9–22. doi: 10.1007/s41030-019-00105-5
9. Zapf A, Castell S, Morawietz L, Karch A. Measuring inter-rater reliability for nominal data - which coefficients and confidence intervals are appropriate? *BMC Med Res Methodol*. (2016) 16:93. doi: 10.1186/s12874-016-0200-9
10. Hallgren KA. computing inter-rater reliability for observational data: an overview and tutorial. *Tutor Quant Methods Psychol*. (2012) 8:23–34. doi: 10.20982/tqmp.08.1.p023
11. Sullivan GM, Artino AR Jr. Analyzing and interpreting data from likert-type scales. *J Grad Med Educ*. (2013) 5:541–2. doi: 10.4300/JGME-5-4-18
12. Rao RS, Singh S, Sharma BB, Agarwal VV, Singh V. Sildenafil improves six-minute walk distance in chronic obstructive pulmonary disease: a randomised, double-blind, placebo-controlled trial. Indian *J Chest Dis Allied Sci*. (2011) 53:81–5.
13. Blanco I, Santos S, Gea J, Guell R, Torres F, Gimeno-Santos E, et al. Sildenafil to improve respiratory rehabilitation outcomes in COPD: a controlled trial. *Eur Respir J*. (2013) 42:982–92. doi: 10.1183/09031936.00176312
14. Goudie AR, Lipworth BJ, Hopkinson PJ, Wei L, Struthers AD. Tadalafil in patients with chronic obstructive pulmonary disease: a randomised, double-blind, parallel-group, placebo-controlled trial. *Lancet Respir Med*. (2014) 2:293–300. doi: 10.1016/S2213-2600(14)70013-X
15. Vitulo P, Stanziola A, Confalonieri M, Libertucci D, Oggionni T, Rottoli P, et al. Sildenafil in severe pulmonary hypertension associated with chronic obstructive pulmonary disease: a randomized controlled multicenter clinical trial. *J Heart Lung Transplant*. (2017) 36:166–74. doi: 10.1016/j.healun.2016.04.010
16. Han MK, Bach DS, Hagan PG, Yow E, Flaherty KR, Toews GB, et al. Sildenafil preserves exercise capacity in patients with idiopathic pulmonary fibrosis and right-sided ventricular dysfunction. *Chest*. (2013) 143:1699–708. doi: 10.1378/chest.12-1594
17. Keir GJ, Walsh SL, Gatzoulis MA, Marino PS, Dimopoulos K, Alonso R, et al. Treatment of sarcoidosis-associated pulmonary hypertension: a single centre retrospective experience using targeted therapies. *Sarcoidosis Vasc Diffuse Lung Dis*. (2014) 31:82–90.
18. Stolz D, Rasch H, Linka A, Di Valentino M, Meyer A, Brutsche M, et al. A randomised, controlled trial of bosentan in severe COPD. *Eur Respir J*. (2008) 32:619–28. doi: 10.1183/09031936.00011308
19. Judson MA, Highland KB, Kwon S, Donohue JF, Aris R, Craft N, et al. Ambrisentan for sarcoidosis associated pulmonary hypertension. *Sarcoidosis Vasc Diffuse Lung Dis*. (2011) 28:139–45.
20. Baughman RP, Judson MA, Lower EE, Highland K, Kwon S, Craft N, et al. Inhaled iloprost for sarcoidosis associated pulmonary hypertension. *Sarcoidosis Vasc Diffuse Lung Dis*. (2009) 26:110–20.
21. Faria-Urbina M, Oliveira RKF, Agarwal M, Waxman AB. Inhaled treprostinil in pulmonary hypertension associated with lung disease. *Lung*. (2018) 196:139–46. doi: 10.1007/s00408-017-0081-7
22. Bajwa AA, Shujaat A, Patel M, Thomas C, Rahaghi F, Burger CD. The safety and tolerability of inhaled treprostinil in patients with pulmonary hypertension and chronic obstructive pulmonary disease. *Pulm Circ*. (2017) 7:82–8. doi: 10.1086/689291

Conflict of Interest: The authors declare that the research was conducted in the absence of any commercial or financial relationships that could be construed as a potential conflict of interest.

Publisher's Note: All claims expressed in this article are solely those of the authors and do not necessarily represent those of their affiliated organizations, or those of the publisher, the editors and the reviewers. Any product that may be evaluated in this article, or claim that may be made by its manufacturer, is not guaranteed or endorsed by the publisher.

frontiers in Medicine

BRIEF RESEARCH REPORT
published: 10 January 2022
doi: 10.3389/fmed.2021.751338

The Effects of Healthy Aging on Right Ventricular Structure and Biomechanical Properties: A Pilot Study

Danial Sharifi Kia[1], *Yuanjun Shen*[2,3], *Timothy N. Bachman*[1,2], *Elena A. Goncharova*[1,2,3,4], *Kang Kim*[1,2,5,6,7,8,9] *and Marc A. Simon*[10]*

[1] Department of Bioengineering, University of Pittsburgh, Pittsburgh, PA, United States, [2] Pittsburgh Heart, Lung, Blood and Vascular Medicine Institute, University of Pittsburgh and University of Pittsburgh Medical Center, Pittsburgh, PA, United States, [3] Davis School of Medicine Lung Center, University of California, Davis, Davis, CA, United States, [4] Division of Pulmonary, Allergy and Critical Care Medicine, School of Medicine, University of Pittsburgh, Pittsburgh, PA, United States, [5] Heart and Vascular Institute, University of Pittsburgh Medical Center, Pittsburgh, PA, United States, [6] Division of Cardiology, School of Medicine, University of Pittsburgh, Pittsburgh, PA, United States, [7] McGowan Institute for Regenerative Medicine, University of Pittsburgh, Pittsburgh, PA, United States, [8] Department of Mechanical Engineering and Materials Science, University of Pittsburgh, Pittsburgh, PA, United States, [9] Center for Ultrasound Molecular Imaging and Therapeutics, University of Pittsburgh, Pittsburgh, PA, United States, [10] Division of Cardiology, Department of Medicine, University of California, San Francisco, San Francisco, CA, United States

OPEN ACCESS

Edited by:
Sandeep Sahay, Weill Cornell Medical College of Cornell University, United States

Reviewed by:
Roberto J. Bernardo, University of Oklahoma Health Sciences Center, United States
Soban Umar, University of California, Los Angeles, United States
Werner Seeger, University of Giessen, Germany

***Correspondence:**
Marc A. Simon
marc.simon@ucsf.edu

Specialty section:
This article was submitted to Pulmonary Medicine, a section of the journal Frontiers in Medicine

Received: *31 July 2021*
Accepted: *01 December 2021*
Published: *10 January 2022*

Citation:
Sharifi Kia D, Shen Y, Bachman TN, Goncharova EA, Kim K and Simon MA (2022) The Effects of Healthy Aging on Right Ventricular Structure and Biomechanical Properties: A Pilot Study. Front. Med. 8:751338. doi: 10.3389/fmed.2021.751338

Healthy aging has been associated with alterations in pulmonary vascular and right ventricular (RV) hemodynamics, potentially leading to RV remodeling. Despite the current evidence suggesting an association between aging and alterations in RV function and higher prevalence of pulmonary hypertension in the elderly, limited data exist on age-related differences in RV structure and biomechanics. In this work, we report our preliminary findings on the effects of healthy aging on RV structure, function, and biomechanical properties. Hemodynamic measurements, biaxial mechanical testing, constitutive modeling, and quantitative transmural histological analysis were employed to study two groups of male Sprague-Dawley rats: control (11 weeks) and aging (80 weeks). Aging was associated with increases in RV peak pressures (+17%, $p = 0.017$), RV contractility (+52%, $p = 0.004$), and RV wall thickness (+38%, $p = 0.001$). Longitudinal realignment of RV collagen (16.4°, $p = 0.013$) and myofibers (14.6°, $p = 0.017$) were observed with aging, accompanied by transmural cardiomyocyte loss and fibrosis. Aging led to increased RV myofiber stiffness (+141%, $p = 0.003$), in addition to a bimodal alteration in the biaxial biomechanical properties of the RV free wall, resulting in increased tissue-level stiffness in the low-strain region, while progressing into decreased stiffness at higher strains. Our results demonstrate that healthy aging may modulate RV remodeling via increased peak pressures, cardiomyocyte loss, fibrosis, fiber reorientation, and altered mechanical properties in male Sprague-Dawley rats. Similarities were observed between aging-induced remodeling patterns and those of RV remodeling in pressure overload. These findings may help our understanding of age-related changes in the cardiovascular fitness and response to disease.

Keywords: right ventricular remodeling, aging, right ventricular biomechanics, ventricular structure, hemodynamics

INTRODUCTION

Healthy aging is associated with alterations in right ventricular (RV) structure and function in subjects with no underlying cardiopulmonary disease (1–5). Aging has been shown to result in pulmonary artery (PA) remodeling (6, 7) and increased pulmonary vascular resistance (5, 8). Echocardiographic studies on RV function have found a strong positive correlation between aging and PA systolic pressures (9, 10). This, in turn, may lead to increased RV afterload and RV remodeling (11, 12), altered contraction dynamics (13), and decreased global and segmental RV systolic strains (14). Previous work has demonstrated that healthy aging results in diminished RV hypertrophy in response to pressure overload (11, 15). Age-related differences exist in the survival rates of pulmonary hypertension (PH) patients in which older patients show more severe characteristics with poor response to therapeutic interventions (16, 17).

In recent years, biomechanical analysis techniques have been employed to better understand the underlying mechanisms of RV remodeling (18–21) and have closely linked RV biomechanics to physiological function (22). Despite the evidence suggesting an association between aging and alterations in RV structure/function, the literature has focused on younger animal models and limited data exist on age-associated differences in RV biomechanics. Similar to RV adaption to pressure overload in PH, alterations in PA resistance and systolic pressures with healthy aging have the potential to trigger RV remodeling, leading to altered organ, tissue, and fiber-level biomechanics.

In this work, we present our pilot findings on the effects of healthy aging on RV biomechanical properties. Our study provides preliminary insights into how healthy aging may modulate RV remodeling and lays the groundwork for future studies to further evaluate the age-related differences in RV response to pressure overload.

METHODS

The data acquired during this study are available from the corresponding author on reasonable request. A total of 15 male Sprague-Dawley rats corresponding to young (controls, ∼11 weeks, weighing 327 ± 9 g, $n_{Control} = 9$) and old (∼80 weeks, weighing 789 ± 3 g, $n_{Aging} = 6$) age groups were studied using a multi-scale biomechanical analysis framework. Historical data from a recent study in our laboratory (18) was used for the control animals in this work. An ∼70-week age difference was considered sufficient to study the effects of healthy aging on RV structure/function in the absence of pathological events arising with senescence in older animals, previously reported to begin at ∼85 weeks in rats (23). The young and old rats in this work correspond to ∼15 and 55 years in human age, respectively (23). 11-week old rats were chosen for our control group to facilitate comparison of our findings on the effects of aging with previous work on RV biomechanics in murine models, which typically utilize rats of this age (19, 24, 25). **Figure 1** summarizes the experimental procedures and analysis techniques used in this study. As further demonstrated in **Supplementary Figure 1**, $n = 6$ animals were dedicated to each group to study the effects of aging on RV hemodynamics, morphology, and biomechanical properties. Histological analysis for the aging cohort, was performed on a sub-set ($n = 3$) of the 6 animals used for hemodynamics and biomechanical analysis, mainly due to the limited availability of aging animals. In the control group, however, we were able to have 3 separate animals dedicated to histological analysis. Hemodynamic and morphological measurements were performed on these 3 additional control animals, in order to confirm normal RV function. All animal procedures were approved by University of Pittsburgh's IACUC (protocol# 18113872 and 19126652).

Hemodynamic and Morphological Measurements

Using standard techniques (19), *in-vivo* terminal invasive pressure catheterization was performed on both groups ($n_{Control} = 8$; $n_{Aging} = 5$). Open-chest hemodynamic measurements were performed under anesthesia induced via inhalation of isoflurane, while the animals were placed on a heated table (37°C) and monitored using a rectal probe. Pressure waveforms were then acquired using a conductance catheter and analyzed for common hemodynamic metrics of RV function. Due to lack of cuvette calibration of catheters for conversion of volume measurements from relative-volume-units to absolute measurements, only pressure-based hemodynamic data are reported and compared in the current work. RV heart rate was calculated by evaluating the periodicity of the waveforms (peak-to-peak time). Peak pressures were characterized as the maximum pressure experienced by the RV during a cardiac cycle (P_{max}), while end-diastolic pressures were identified as pressures at the point of the maximum second derivative of the waveforms, $\left(\frac{d^2p}{dt^2}\right)$ max. Load-dependent measures of RV contractility and relaxation were, respectively, calculated by evaluating the maximum and minimum of the time derivatives of pressure waveforms ($\frac{dp}{dt}$max and $\frac{dp}{dt}$min). Contractility index was then obtained using the ratio of $\frac{dp}{dt}$max over the maximum pressure experienced by the RV over a cardiac cycle (RV peak pressure; P_{max}). Additionally, the time-constant of RV relaxation (tau) was calculated as (26):

$$\ln(P) = -\frac{1}{\tau} \cdot t + B \quad (1)$$

Where P represents the RV pressure waveform beginning at $\frac{dp}{dt}$min until the minimum RV pressure experienced during a cardiac cycle (P_{min}), B is an intercept, t represents the time during a cardiac cycle, and τ (tau) is the time-constant of RV relaxation, measured via linear regression of equation 1 to the acquired pressure waveforms in MATLAB (Mathworks, Natick, MA). Hemodynamic parameters for each animal were evaluated using average measurements from at least three consecutive cycles, except for tau, which was obtained from a single beat (due to limitations of our custom hemodynamic analysis subroutines for estimation of tau).

Following hemodynamic measurements, the heart was harvested and arrested by placement in cardioplegic solution

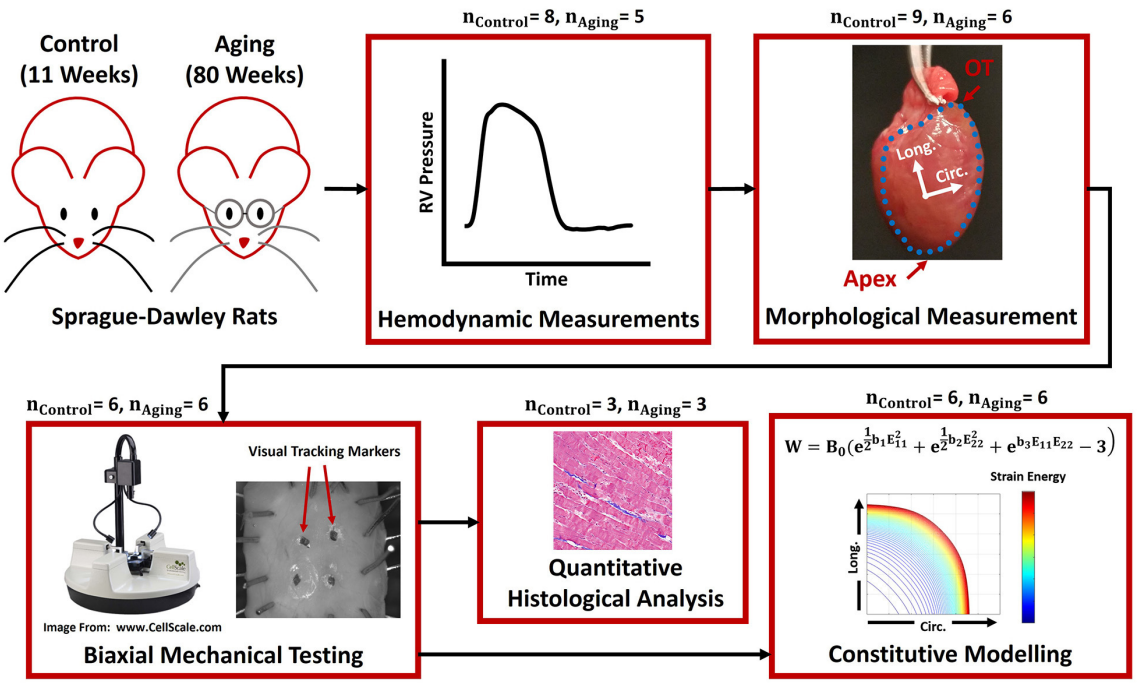

FIGURE 1 | The framework used to study RV remodeling with healthy aging. *In vivo* terminal invasive hemodynamic measurements were performed on young controls and aging Sprague-Dawley rats, followed by harvesting the heart and morphological measurements, biaxial mechanical testing, constitutive modeling, and quantitative transmural histological analysis. The blue dots in the "Morphological Measurement" panel demonstrate the boundaries of the RV free wall, while the Circ-Long coordinate system indicates the orientation of square specimens harvested for mechanical testing. RV, Right ventricle; OT, Outflow tract; Circ, Circumferential; Long, Longitudinal.

(27). Subsequently, the RV free wall (RVFW) was dissected and measurements were acquired for the Fulton index [ratio of RV weight to weight of the left ventricle (LV) + intraventricular septum] and RVFW thickness ($n_{Control} = 9$, $n_{Aging} = 6$). All measurements were performed in air, at room temperature (23°C), using a scale (0.1 mg readability; Mettler-Toledo International Inc., Columbus, OH) and a thickness gauge (0.025 mm precision; L. S. Starrett Company, Athol, MA).

Biomechanical Characterization

Following morphological measurements, square specimens with a circumferential-longitudinal orientation (**Figure 1**) were harvested from the RVFW to undergo biaxial mechanical testing ($n_{Control} = 6$, $n_{Aging} = 6$). Specimens were mounted on a BioTester testing device (CellScale, Waterloo, ON, Canada), using a suture and pulley mechanism for minimal shear loading (28). Samples were then submerged in modified Krebs solution with 2,3-Butanedione monoxime and oxygen to ensure tissue viability (27). Our previous work (19) has shown that this media bath can effectively maintain tissue viability up to 90 min, via passive diffusion. All measurements in this study were concluded within 45–80 min of harvesting the heart.

RVFW mechanical properties were characterized using multi-protocol displacement-controlled biaxial loading scenarios (1:1, 1:2, 2:1, 1:4, 4:1, 1:6, and 6:1 displacement ratios). Previous work has demonstrated that this loading protocol can effectively capture the biaxial RVFW properties under a wide range of possible strains (18, 27, 29), generating adequate data for parameter characterization of constitutive models. Each specimen underwent 15 cycles of 1:1 displacement-controlled preconditioning, before the start of data acquisition. Four visual tracking markers were placed on the epicardial surface of the RVFW specimens and marker displacements (recorded using a CCD camera) were post-processed via standard techniques (27, 29, 30) to obtain the deformation gradient tensor (F), using a four-node finite-element approximation (31). Components of the Green–Lagrange strain tensor (E) were then calculated as $E = \frac{1}{2}(F^TF - I)$, where I is the identity tensor. Biaxial force measurements and initial specimen dimensions were used to obtain the 1st Piola-Kirchhoff stress tensor (P) by calculating the ratio of forces in the deformed configuration over the cross-sectional area in the reference configuration. The 2nd Piola-Kirchhoff stress tensor (S) was then evaluated as $S = F^{-1}P$. Stress-strain data was post-processed under a plane-stress approximation, using a finite deformation analysis framework in Mathcad (PTC, Needham, MA).

Using previously established techniques (19, 32), equibiaxial strain-controlled responses of RVFW specimens were interpolated from the acquired multi-protocol displacement-controlled experimental data via biharmonic spline interpolations in MATLAB (**Supplementary Figure 2**). As previously discussed, equibiaxial strain-controlled responses

are accompanied by unique tissue kinematics with no fiber rotations (33) and, therefore, could be used to estimate fiber-level mechanical properties from tissue-level measurements, independent of fiber orientation and splay (19, 21, 32). Effective fiber-ensemble (EFE) stresses, representing the fiber-level response of combined collagen and myofiber bundles, were then estimated from tissue-level measurements as (19, 32):

$$S_{EFE} = (S_{11})_{Equibiaxial} + (S_{22})_{Equibiaxial} \quad (2)$$

Here, S_{EFE} represents the EFE stress of the combined collagen-myofiber bundles, and $(S_{11})_{Equibiaxial}$ and $(S_{22})_{Equibiaxial}$ are the interpolated biaxial tissue-level 2nd Piola-Kirchhoff stresses under equibiaxial strains, respectively, in the circumferential and longitudinal directions. We assumed the initial nearly-linear, low-strain portion of the EFE stress-strain responses to be mostly dominated by myofibers, while collagen fibers dominated the high-strain response following recruitment (18, 34) (**Supplementary Figure 3**). To categorize the data before and after collagen recruitment, equation 2 was differentiated with respect to EFE strain (E_{EFE}), to evaluate the changes in EFE stiffness ($TM_{EFE} = \frac{\partial S_{EFE}}{\partial E_{EFE}}$; where TM_{EFE} is the EFE stiffness). For specimens in both groups, we observed a relatively constant-stiffness region (relatively linear stress-strain behavior, dominated by myofibers), followed by beginning of collagen recruitment and an abrupt increase in EFE stiffness (**Supplementary Figure 4**). The strain at which collagen fibers begin recruitment was defined as the point where there is a significant elevation in EFE stiffness compared to the stiffness trends prior to that point. This was quantified as the point where TM_{EFE} (EFE stiffness) was significantly elevated outside of the $Z = 4.417$ confidence interval of the distribution of TM_{EFE} measurements before that point. A Z-value of 4.417 (99.999% confidence interval) was chosen as a threshold for maximal confidence in the detected increase in stiffness, avoiding false detection of collagen recruitment strain due to potential fluctuations in the low-strain data, resulting from data acquisition noise. The EFE strain at the $n+1$th point of the EFE stiffness-strain plot (**Supplementary Figure 4**) was defined as the collagen recruitment strain, if:

$$(TM_{EFE})_{n+1} > \frac{1}{n}\sum_{1}^{n}(TM_{EFE})_n + 4.417 * \frac{\sqrt{\frac{\sum_1^n\left[(TM_{EFE})_n - \frac{1}{n}\sum_1^n (TM_{EFE})_n\right]^2}{n-1}}}{\sqrt{n}} \quad (3)$$

Here, $(TM_{EFE})_{n+1}$ is the EFE stiffness at the $n+1$th point of the EFE stiffness-strain data (**Supplementary Figure 4**). The right-hand side of the inequality represents the upper bound of the TM_{EFE} confidence interval based on the TM_{EFE} data up to the n^{th} point. The beginning of collagen recruitment was defined as the first point where the inequality in equation 3 is satisfied. The EFE stress-strain data before collagen recruitment was then used for myofiber stiffness estimations, using a rule-of-mixtures approach (18, 19, 35):

$$(TM_{EFE})_{Before\ Collagen\ Recruitment} = \phi_{Myofiber}TM_{Myofiber} + \phi_{Collagen}TM_{Collagen} \quad (4)$$

Where $(TM_{EFE})_{Before\ Collagen\ Recruitment}$ is the slope of the line fitted to the initial low-strain portion of the EFE stress-strain curve (**Supplementary Figure 5**), $\phi_{Myofiber}$ and $\phi_{Collagen}$ represent the myofiber and collagen area fractions in RVFW specimens (measures of tissue content; acquired from histological measurements), and $TM_{Myofiber}$ and $TM_{Collagen}$ are the effective myofiber and collagen stiffnesses, respectively. Assuming the initial portion of the stress-strain data to be dominated by myofibers (minimal collagen recruitment, $TM_{Collagen} = 0$), effective myofiber stiffness for each specimen was estimated as:

$$TM_{Myofiber} = \frac{(TM_{EFE})_{Before\ Collagen\ Recruitment}}{\phi_{Myofiber}} \quad (5)$$

Additionally, a non-linear anisotropic constitutive model (36) was used to model the response of the RVFW specimens in each cohort:

$$W = B_0(e^{\frac{1}{2}b_1E_{11}^2} + e^{\frac{1}{2}b_2E_{22}^2} + e^{b_3E_{11}E_{22}} - 3) \quad (6)$$

Here, W is the strain energy density, E_{11} and E_{22}, respectively, represent the circumferential and longitudinal (apex-to-base) Green-Lagrange strains, B_0 is a scaling factor and b_1, b_2 and b_3 are metrics for the circumferential, longitudinal and in-plane coupling stiffness of the RVFW, respectively (19). 2nd Piola–Kirchhoff stress components were obtained by differentiating equation 6 with respect to Green-Lagrange strain:

$$(S_{11})_{Model-Predicted} = \frac{\partial W}{\partial E_{11}} = B_0(b_1E_{11}e^{\frac{1}{2}b_1E_{11}^2} + b_3E_{22}e^{b_3E_{11}E_{22}})$$
$$(S_{22})_{Model-Predicted} = \frac{\partial W}{\partial E_{22}} = B_0(b_2E_{22}e^{\frac{1}{2}b_2E_{22}^2} + b_3E_{11}e^{b_3E_{11}E_{22}}) \quad (7)$$

Where $(S_{11})_{Model-Predicted}$ and $(S_{22})_{Model-Predicted}$ are the model-predicted stress components in the circumferential and longitudinal directions, respectively. Using equation 7 and the acquired multi-protocol experimental stress-strain data, model parameters were estimated for each specimen using a trust-region-reflective non-linear least-squares optimization algorithm in MATLAB, to minimize the difference between model-predicted and experimentally acquired data. A R^2 measure was used to evaluate the goodness of fit. Cohort-specific strain energy maps in the low-strain and high-strain regions were then generated by taking the average of all strain energy distributions in the circumferential-longitudinal strain space for specimens in each cohort, facilitating holistic model-based evaluation of RVFW biomechanical properties over a wide range of loading scenarios.

Quantitative Histological Analysis

Transmural histological staining was performed on a sub-group of specimens ($n_{Control} = 3$, $n_{Aging} = 3$) to quantify the

effects of aging on RV fiber architecture. Sample sizes were chosen based on our previous work showing minimal between-sample variabilities in RV content and fiber architecture (18, 19). Specimen fixation was carried out using 10% neutral buffered formalin followed by staining of RVFW specimens using Masson's trichrome, resulting in collagen fibers stained in blue and myofibers in red/pink. A total of 11–17 sections were obtained for each specimen, from epi to endocardium, at 50–75 μm increments. Transmural area fractions of collagen and myofibers were then quantified via manual RGB-based thresholding of the histological images (collagen: blue, myofibers: red/pink) to analyze the effects of aging on RVFW composition. Area fractions were calculated as the ratio of the area occupied by respective blue/red pixels, divided by the total area within the region of interest. In addition, cardiomyocyte width was measured from the histological data to investigate the role of aging in RV hypertrophy (40 measurements performed on each specimen at different sites along the myofibers). Furthermore, similar to previous work (18), the orientation of RVFW collagen and myofibers and the coherency of collagen fiber distributions were quantified transmurally, using gradient-based image analysis techniques (37). Following segmentation of histological sections based on the appropriate RGB threshold, local image gradients at each section were used to construct the structure tensor of the gradient map in order to analyze the transmural orientation of RVFW collagen and myofibers (18, 19, 37):

$$\mathrm{T} = \begin{bmatrix} \iint \mathrm{R}(x,y)\mathrm{I_x}(x,y)\mathrm{I_x}(x,y)\mathrm{d}x\mathrm{d}y & \iint \mathrm{R}(x,y)\mathrm{I_x}(x,y)\mathrm{I_y}(x,y)\mathrm{d}x\mathrm{d}y \\ \iint \mathrm{R}(x,y)\mathrm{I_x}(x,y)\mathrm{I_y}(x,y)\mathrm{d}x\mathrm{d}y & \iint \mathrm{R}(x,y)\mathrm{I_y}(x,y)\mathrm{I_y}(x,y)\mathrm{d}x\mathrm{d}y \end{bmatrix} \tag{8}$$

Here, T is the symmetric positive-definite structure tensor, R(x,y) is a gaussian weighting function which specifies the integration region of interest (37), and I_x and I_y are the partial spatial derivatives of the histological image (I), respectively, in x and y directions. The 1st eigen vector of T indicates the dominant fiber orientation at each histological section (19, 37). For all data presented in this work, 0° corresponds to the circumferential direction, while +90° points toward the apex-to-base (longitudinal) direction. Moreover, using the eigen values of the structure tensor in equation 8, collagen fiber coherency was evaluated as:

$$\mathrm{C} = \frac{\lambda_1 - \lambda_2}{\lambda_1 + \lambda_2} \times 100 \tag{9}$$

where λ_1 and λ_2 correspond to the 1st and 2nd eigen values of the structure tensor T (37). 0% collagen fiber coherency corresponds to a sparse (non-coherent), randomly distributed fiber architecture, while 100% coherency indicates a highly-aligned, tightly packed, continuous (coherent) collagen fiber distribution (38).

A total of 66 histological sections were analyzed for the control and aging groups. We performed linear interpolations to report the histological data on an equally-spaced grid, against normalized tissue thickness (0–100% thickness). In case of data categorization (Epi, Mid and Endo groups), the data between 0 and 20% thickness were used for the epicardium, while the data between 80 and 100% thickness correspond to the endocardium. Orientation analysis and image segmentation were performed using the OrientationJ toolbox (37, 39) in ImageJ (imagej.nih.gov).

Statistical Analysis

Data are presented with mean ± standard error of the mean. Sample normality and homogeneity of variances were assessed using the Shapiro–Wilk test and Bartlett's test of homoscedasticity. Circular statistics was employed for fiber orientation analysis, using the Watson–Williams test in the CircStat toolbox (40) in MATLAB. For all other data, in case of normality and homoscedasticity, a two-sided unpaired student's *t*-test was used for statistical comparisons, while non-normal distributions were compared using Mann–Whitney *U*-tests. For all purposes, $p < 0.05$ was considered statistically significant. Statistical analyses were performed in the R software package (R Foundation for Statistical Computing, Vienna, Austria).

RESULTS

RV Hemodynamics and Morphology

Healthy aging did not show an effect on the heart rate (**Figure 2A**; 271.5 ± 11.7 vs. 292.3 ± 14.1 BPM for Aging-vs.-Control; $p = 0.326$). Aging resulted in increased RV peak pressures (**Figure 2B**; 26.8 ± 0.9 vs. 23.0 ± 0.9 mmHg for Aging-vs.-Control; $p = 0.017$), while showing a modest non-significant effect on end-diastolic pressures (**Figure 2C**; 1.9 ± 0.4 vs. 1.3 ± 0.1 mmHg for Aging-vs.-Control; $p = 0.085$). Effects of aging on the load-dependent measures of RV contractility and relaxation are shown in **Figure 2D**. Aging significantly increased $\frac{dp}{dt}$max (1,611.7 ± 90.5 vs. 1,063.8 ± 101.7 mmHg/s for Aging-vs.-Control; $p = 0.004$) but did not demonstrate any effects on $\frac{dp}{dt}$min (−823.9 ± 60.4 vs. −814.7 ± 85.5 mmHg/s for Aging-vs.-Control; $p = 0.940$). Increased contractility index was observed for the aging group (**Figure 2E**; 60.1 ± 2.2 vs. 45.8 ± 3.5 1/s for Aging-vs.-Control; $p = 0.012$), while the time-constant of RV relaxation (tau) remained unchanged (**Figure 2F**; 10.7 ± 1.6 vs. 9.9 ± 0.8 ms for Aging-vs.-Control; $p = 0.595$).

Healthy aging led to increased RVFW thickness (0.90 ± 0.05 vs. 0.65 ± 0.05 mm for Aging-vs.-Control; $p = 0.001$), while not affecting the Fulton index (0.26 ± 0.03 vs. 0.27 ± 0.01 mg/mg for Aging-vs.-Control; $p = 0.140$). Moreover, aging was associated with decreased RV and LV weight normalized to body weight ($\frac{\text{RV Weight}}{\text{Body Weight}}$: 0.05 ± 0.007% vs. 0.06 ± 0.003% for Aging-vs.-Control, $p = 0.026$; $\frac{\text{LV Weight}}{\text{Body Weight}}$: 0.18 ± 0.007% vs. 0.23 ± 0.009% for Aging-vs.-Control, $p = 0.0005$). Specimen-specific RVFW thickness and Fulton index measurements are reported in **Supplementary Table 1**.

RVFW Biomechanical Properties

Aging demonstrated a bimodal effect on the RVFW biaxial properties by resulting in increased circumferential and longitudinal stiffness under lower strains, while progressing to

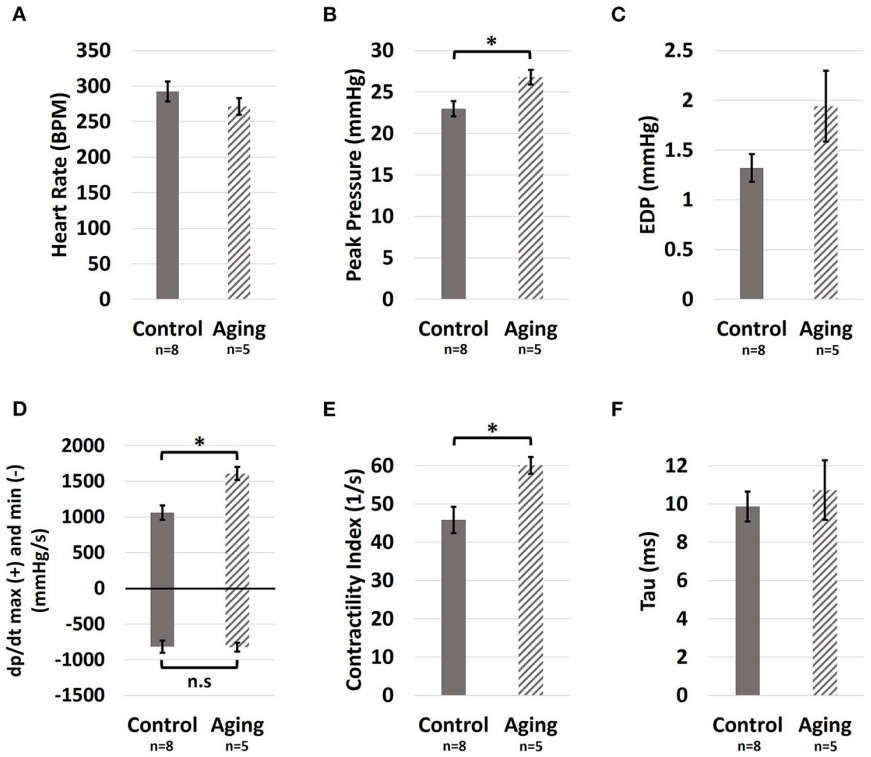

FIGURE 2 | Hemodynamic measures of the effects of healthy aging on RV **(A)** Heart rate, **(B)** Peak pressure, **(C)** End-diastolic pressure, **(D)** $\frac{dp}{dt}$ max (positive side) and $\frac{dp}{dt}$ min (negative side), **(E)** Contractility index, and **(F)** The preload-independent measure of relaxation (tau). Healthy aging significantly increased RV peak pressures and the load-dependent measures of RV contractility ($\frac{dp}{dt}$ max and contractility index), while not affecting the heart rate, end-diastolic pressures (EDP), and relaxation function ($\frac{dp}{dt}$ min and tau). Error bars represent standard error of the mean (SEM). *Indicates $p < 0.05$. RV, Right ventricle; BPM, Beats per minute; EDP, End-diastolic pressure; $\frac{dp}{dt}$ max and min, Load-dependent measures of RV contractility and relaxation; n.s, Non-significant.

decreased biaxial stiffness at higher strains (**Figure 3A**). A similar effect was observed on the EFE (effective fiber-ensemble) stress-strain properties of combined RVFW collagen-myofiber bundles (**Figure 3B**). Using a rule-of-mixtures approach, this translated into increased effective myofiber stiffness (**Figure 3C**; 159.5 ± 23.6 vs. 66.2 ± 5.2 kPa for Aging-vs.-Control; $p = 0.003$), while no significant effects were observed on collagen recruitment strain (**Figure 3D**; 11.9 ± 0.7% vs. 10.4 ± 0.9% for Aging-vs.-Control; $p = 0.197$). Specimen-specific constitutive model parameters for each group are shown in **Supplementary Table 2**. Overall, the employed model showed an acceptable fit quality (R^2) to our experimental data ($R^2 = 0.95 \pm 0.01$ and 0.96 ± 0.01 for Aging and Control, respectively). Age-specific strain energy maps, representing the combined effects of all model parameters, are demonstrated in **Figures 3E,F** for each cohort at the low-strain and high-strain regions.

Quantitative Transmural Histology

Representative histological sections for each group are demonstrated in **Figure 4A**. Aging resulted in increased cardiomyocyte width (**Figure 4B**; 25.42 ± 0.34 vs. 14.94 ± 0.64 μm for Aging-vs.-Control; $p = 0.0001$). Quantifying the transmural orientation of RVFW fibers revealed myofiber (**Figure 4C**) and collagen (**Figure 4D**) reorientation toward the longitudinal direction at sub-endocardial levels. Overall, myofibers showed similar orientations to collagen fibers. Aging significantly shifted the overall orientation of myofibers (circular mean of transmural fiber angles, dotted lines in **Figure 4C**) by 14.6° toward the longitudinal direction (**Figure 4E**; $p = 0.017$). Similarly, the overall orientation of collagen fibers was shifted by 16.4° ($p = 0.013$). Aging also resulted in cardiomyocyte loss and decreased myofiber area fractions at both epicardium (**Figure 4F**; 90.8 ± 0.3% vs. 95.3 ± 0.7% for Aging-vs.-Control; $p = 0.004$) and endocardium (**Figure 4F**; 82.4 ± 1.5% vs. 95.3 ± 1.9% for Aging-vs.-Control; $p = 0.007$). Furthermore, aging led to RVFW fibrosis and increased collagen area fractions at epicardium (**Figure 4G**; 5.3 ± 0.4% vs. 3.4 ± 0.3% for Aging-vs.-Control; $p = 0.015$) and the mid-ventricular region (**Figure 4G**; 5.0 ± 0.4% vs. 3.4 ± 0.3% for Aging-vs.-Control; $p = 0.037$). Analyzing the coherency of collagen architectures revealed decreased coherency at the endocardium (**Figure 4H**; 10.4 ± 1.1% vs. 19.7 ± 1.1% for Aging-vs.-Control; $p = 0.003$), while showing no effects on the other regions.

DISCUSSION

In this pilot study of the effects of healthy aging on RV remodeling, we found aging associated with (1) increased RV peak pressures and contractility; (2) increased RVFW thickness

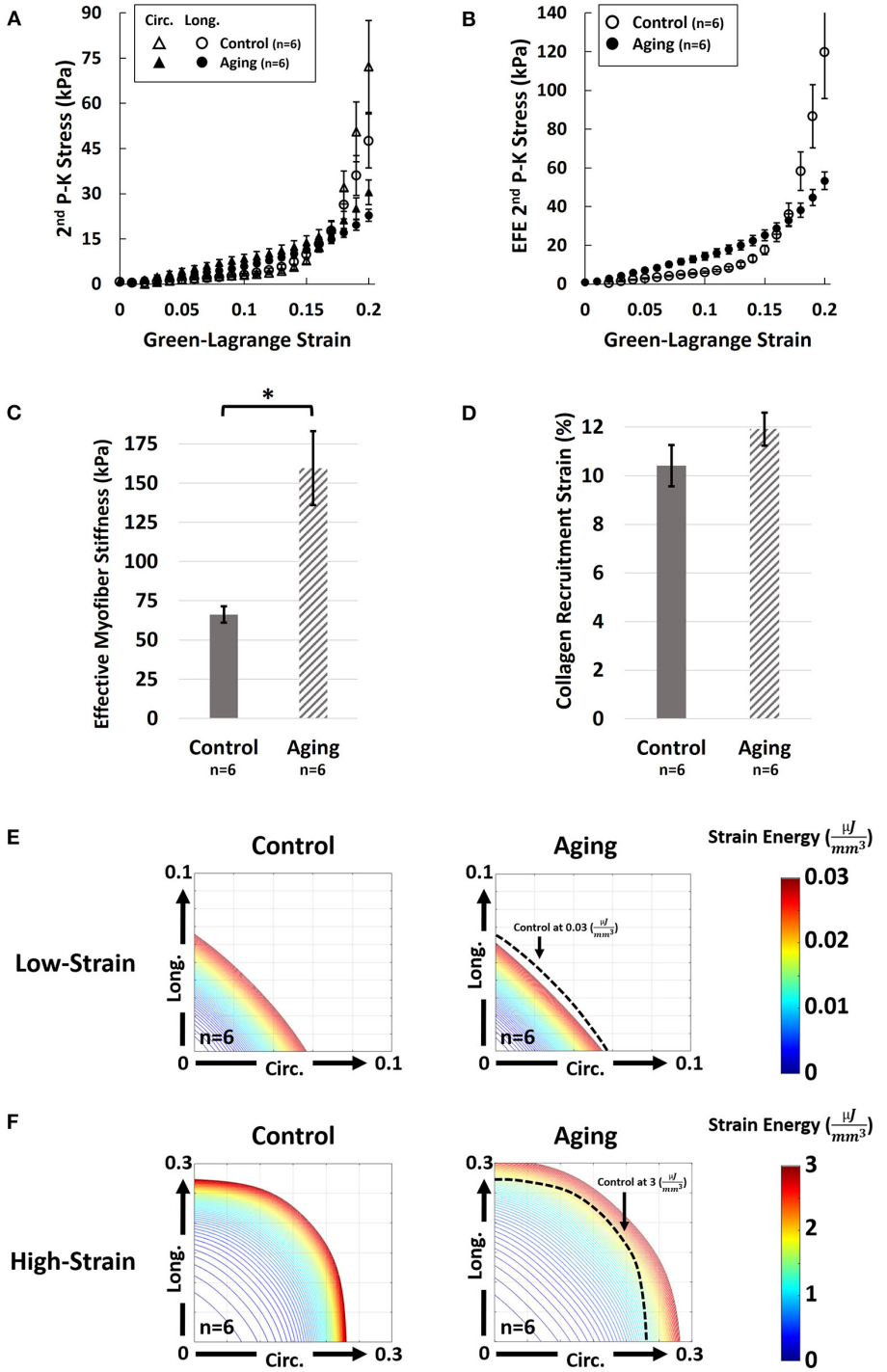

FIGURE 3 | Effects of healthy aging on **(A)** Biaxial mechanical properties of RV myocardium, **(B)** Effective fiber-ensemble (EFE) mechanical properties of combined collagen-myofiber bundles, **(C)** Effective myofiber stiffness, **(D)** Collagen recruitment strain, **(E)** Strain energy maps of the RVFW in the low-strain region (circumferential-longitudinal strain space), and **(F)** Strain energy maps of the RVFW in the high-strain region. Healthy aging modulates the biomechanical properties of the RVFW in a bimodal manner by resulting in increased circumferential and longitudinal stiffness under lower strains, while progressing to decreased biaxial stiffness at higher strains. Significant myofiber stiffening was observed with healthy aging. Specimens in the aging cohort demonstrate higher levels of strain energy at equivalent levels of deformation compared to controls in the low strain region (indicating RVFW stiffening), while showing lower strain energy in the high-strain region (indicating a more compliant RVFW). Error bars represent standard error of the mean (SEM).*Indicates $p < 0.05$. RV, Right ventricle; RVFW, Right ventricular free wall; 2nd P-K Stress, 2nd Piola-Kirchhoff stress; Circ, Circumferential; Long, Longitudinal; EFE 2nd P-K Stress, Effective fiber-ensemble 2nd Piola-Kirchhoff stress.

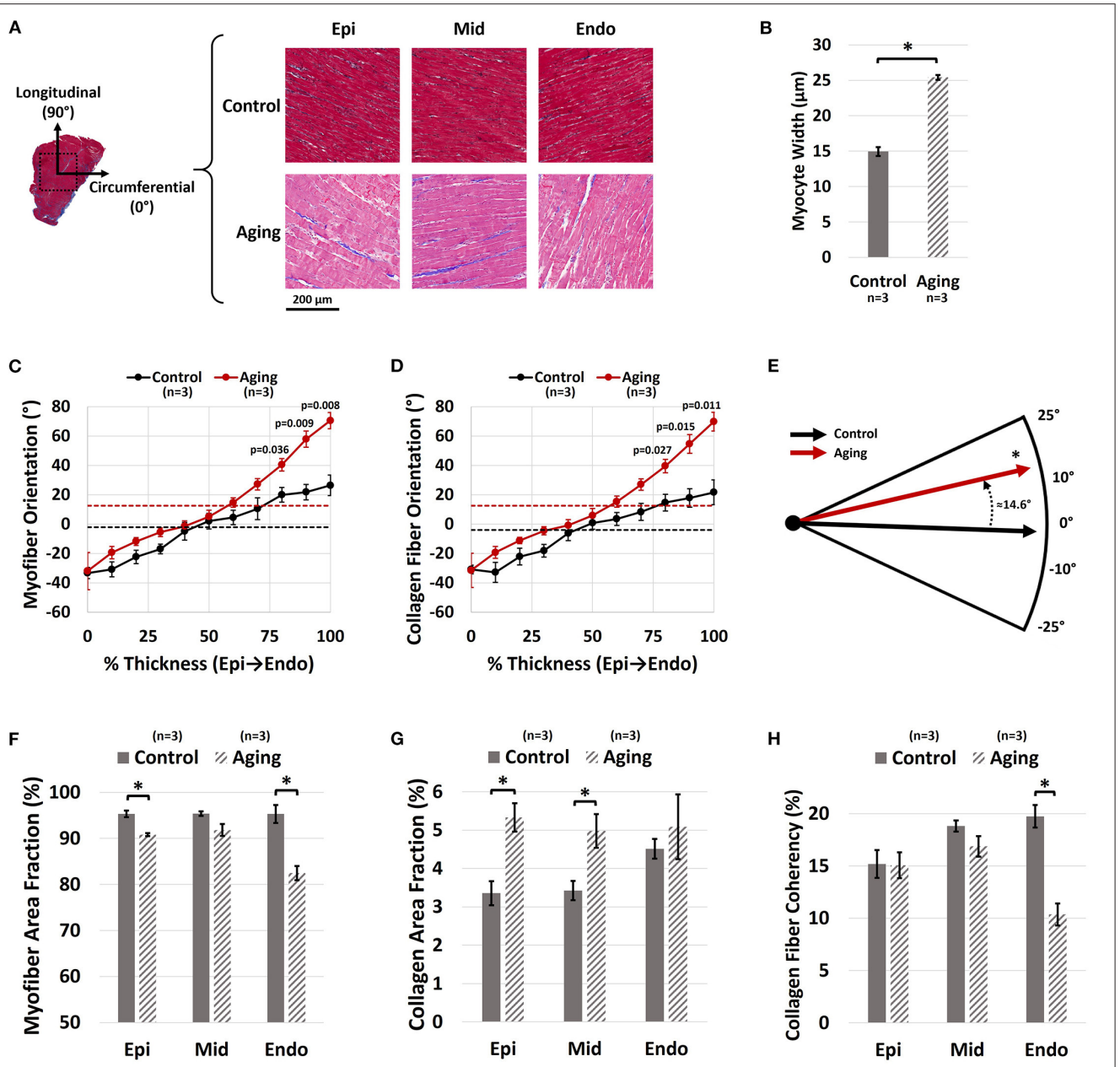

FIGURE 4 | Histological analysis of the effects of healthy aging on RV structure. **(A)** Representative transmural histological sections of the RVFW (Red/Pink: Myofiber, Blue: Collagen) and effects of aging on **(B)** Cardiomyocyte hypertrophy (myocyte width), **(C)** Transmural myofiber orientations, **(D)** Transmural collagen fiber orientations, **(E)** Dominant myofiber orientations, **(F)** Transmural myofiber content (area fraction), **(G)** Transmural collagen content (area fraction), and **(H)** Transmural collagen fiber coherency. Healthy aging results in cardiomyocyte hypertrophy, in addition to reorientation of sub-endocardial collagen and myofibers toward the longitudinal direction. This is accompanied by cardiomyocyte loss, RVFW fibrosis, and decreased collagen fiber coherency. Error bars represent standard error of the mean (SEM). *Indicates $p < 0.05$. RV, Right ventricle; RVFW, Right ventricular free wall; Epi, Epicardium; Mid, Mid-ventricular region; Endo, Endocardium.

in proportion to increased LV size; (3) longitudinal reorientation of collagen/myofibers, with transmural cardiomyocyte loss and RVFW fibrosis; and (4) increased effective myofiber stiffness. The increase in RV peak pressures (**Figure 2B**) is consistent with previous reports of increased PA pressures with healthy aging (9, 10). Increased PA pressures impose an increased afterload on the RV, leading to elevated RV pressures. Furthermore, cardiomyocyte width (**Figure 4B**) and RVFW thickness (**Supplementary Table 1**) increased with aging, leading to increased organ-level contractility (**Figures 2D,E**). Interestingly, these changes are similar to those seen in a PH model in young animals (18). Increased RVFW thickness was accompanied by reduced ratios of RV and LV weight normalized to body weight of the animals. This indicate RV

growth with aging that is not proportional to the increase in body weight (reduced $\frac{RV\ Weight}{Body\ Weight}$ ratio), similar to previous reports of LV growth (41). Moreover, consistent with prior work (12, 42), reduced cardiomyocyte area fraction (**Figure 4F**) and RVFW fibrosis (**Figure 4G**) were noted with aging. Reduced cardiomyocyte area fraction in the RVFW increases the hemodynamic load on the remaining myocytes (43), possibly explaining the observed hypertrophy and stiffening patterns (**Figures 4B**, **3C**).

Histological analyses revealed reorientation of endocardial collagen and myofibers, resulting in a longitudinal shift in dominant transmural fiber orientations (**Figure 4E**). Similar patterns of longitudinal fiber reorientation have been reported with PH (18, 34). Unlike PH, where elevated RV pressures may stimulate transmural fiber reorientation (20, 44), fiber realignment in aging may have different underlying mechanisms. A potential candidate, pending further investigation, is RV fiber reorientation due to volumetric growth of the RVFW with healthy aging (kinematic shift). Further analysis using growth-and-remodeling frameworks may facilitate decoupling the effects of growth-induced reorientation from fiber remodeling due to other mechanisms.

Fiber reorientation (**Figures 4C,D**) and increased transmural change in fiber angles with aging led to a less anisotropic biaxial mechanical response (**Figure 3A**) with bimodal alterations in RVFW biaxial properties (**Figure 3**). Specimens in the aging cohort demonstrated higher levels of strain energy at equivalent levels of deformation compared to controls in the low-strain region (indicating RVFW myofiber stiffening), while showing lower strain energy in the high-strain region (indicating more compliant collagen in the RVFW) (**Figures 3E,F**). Moreover, aging led to increased effective myofiber stiffness (**Figure 3C**). Potential underlying mechanisms of myofiber stiffening include myocyte remodeling due to cell loss, as well as reduced titin phosphorylation (45). Increased myofiber stiffness and reduced tissue-level ventricular stiffness at high strains have been previously documented in separate studies on age-related LV remodeling (46, 47). Despite alterations in tissue-level properties, the time-constant of RV relaxation (tau) did not show any changes with aging. It should be noted that, in addition to passive tissue properties, RV relaxation velocities can also affect tau and alterations in relaxation velocities have the potential to offset the changes in mechanical properties at the organ level. However, no direct measurement of relaxation velocities was performed in this work. Interestingly, we have previously observed myofiber stiffening to be accompanied by an increase in tau in response to PH in male Sprague-Dawley rats (19). A potential explanation for the observed differences with healthy aging compared to PH could be the severity of elevations in RV pressures and higher levels of hypertrophy in PH compared to aging-induced remodeling, that may manifest in concurrent changes in myofiber-level RV relaxation velocities and myocyte stiffening, affecting the time constant of RV relaxation at the organ-level. The underlying mechanisms of the observed effect warrant further cell and fiber-level investigation of aging-induced alterations in RV myocyte mechanics in future work.

No effects on the collagen recruitment strain (measure of collagen crimp) were observed with healthy aging (**Figure 3D**). However, aging led to RVFW fibrosis and increased collagen area fractions (**Figure 4G**). Despite an increased collagen content with similar levels of crimp to young controls, tissue-level stiffness of the specimens in the aging group was reduced in the high-strain region, when collagen fibers are recruited. This indicates a potential reduction in the intrinsic fiber-level stiffness of collagen fibers with aging. Additionally, reduced collagen fiber coherency was detected at the endocardial levels (**Figure 4H**), indicating a more sparse and isotropic distribution of collagen fibers (38). This has the potential to affect the load transfer mechanism of endocardial collagen, contributing to reduced stiffness at the tissue level. Ongoing research focuses on evaluation of lysyl oxidase-mediated alterations in collagen cross-linking with healthy aging, as a potential mechanism of reduced collagen network stiffness.

There are limitations to the experimental and modeling techniques used in this study. We only analyzed the effects of healthy aging in male animals. Previous work has shown sex-related differences in RV mechanics in PH (48–50), mainly due to the protective effects of the female sex hormone 17β-estradiol (estrogen). Recent studies on sex difference in RV-PA coupling in the setting of PH and heart failure with preserved ejection fraction have demonstrated superior adaptive remodeling in female patients leading to preserved RV-PA coupling at rest and under exercise, while male patients demonstrated impaired contractile function in response to increased afterload and lower RV-PA coupling (51, 52). While, the exact underlying mechanisms of the observed effects remain unknown (52) and, to the best of our knowledge, to date no data exist on sex-related differences in RV biomechanics with healthy aging, estrogen-mediated effects have the potential to affect the observed patterns in our work via altered adaptation in the myocyte contractile apparatus, potentially leading to different levels of structural and biomechanical remodeling. Sex-related difference in RV remodeling with healthy aging is an important topic necessitating further investigation in future studies. Moreover, as a first step toward better understanding of the effects of healthy aging on RV remodeling, the current work evaluated the changes in RV mechanics in the absence of analyzing LV structure/function and pulmonary hemodynamics. Due to the interdependence of RV and LV function (53), the observed effects may not be independent of potential age-related changes in LV hemodynamics or biomechanical properties. Biventricular analysis of the effects of healthy aging on RV and LV structure, function, and biomechanics, as well as pulmonary mechanics, is an important topic to be investigated in future research. Despite low variability and strong statistics, the small sample size of our pilot study limited our ability to investigate detailed interactions between aging, gender, and disease, which will require future studies with larger sample sizes. Furthermore, lack of molecular studies to evaluate the underlying mechanisms of the observed effects at the tissue and fiber level remains another limitation of the current work, requiring further investigation in future studies. We employed a phenomenological constitutive model

for analyzing our biomechanical data; future work will focus on structurally-informed constitutive models of RV myocardium (21) to couple the histologically measured tissue architecture to biaxial properties. Different batches of staining solution used for each group resulted in different shades of cardiomyocyte staining for control vs. aging (red vs. pink). However, this had minimal effects on our findings as segmentation thresholds for myofibers and collagen were individually selected for each histological section. While, to the best of our knowledge, there has been no reports of biaxial testing-induced permanent alterations in soft tissue fiber architectures, lack of a dedicated group for histological analysis of the aging cohort remains a limitation of this work.

In summary, our results demonstrate that healthy aging may modulate RV remodeling via increased peak pressures, cardiomyocyte loss, fibrosis, fiber reorientation, and altered mechanical properties. While this can help our understanding of age-related changes in the cardiovascular fitness and response to disease, these findings need to be considered in light of potential sex-differences in RV remodeling and the limitations of the current work.

DATA AVAILABILITY STATEMENT

The raw data supporting the conclusions of this article will be made available by the authors, without undue reservation.

ETHICS STATEMENT

The animal study was reviewed and approved by University of Pittsburgh Institutional Animal Care and Use Committee (IACUC).

AUTHOR CONTRIBUTIONS

DS: conception of the study, data acquisition, analysis and interpretation, and drafting the manuscript. YS: conception of the study, data acquisition, interpretation, and drafting the manuscript. TB: data analysis and interpretation and drafting the manuscript. EG, KK, and MS: conception of the study, data interpretation, and drafting the manuscript. All authors contributed to the article and approved the submitted version.

FUNDING

This study was supported by the American Heart Association (AHA-20PRE35210429, DS; AHA Postdoctoral Fellowship 826806, YS) and the National Institutes of Health (NIH Grants 1R01AG058659, 2P01HL103455, and UL1 TR001857, MS; 2R01HL130261, 2R01HL113178, and R01HL150638, EG). The funding sources had no involvement in design of the study, data acquisition or interpretation.

ACKNOWLEDGMENTS

A pre-print based on this work is available online in an open-access repository (54). The data discussed in this work has been included as a chapter in the PhD dissertation of the first author (DS).

SUPPLEMENTARY MATERIAL

The Supplementary Material for this article can be found online at: https://www.frontiersin.org/articles/10.3389/fmed.2021.751338/full#supplementary-material

REFERENCES

1. Innelli P, Esposito R, Olibet M, Nistri S, Galderisi M. The impact of ageing on right ventricular longitudinal function in healthy subjects: a pulsed tissue doppler study. *Eur J Echocardiogr.* (2009) 10:491–8. doi: 10.1093/ejechocard/jen313
2. D'Andrea A, Vriz O, Carbone A, Ferrara F, Di Maio M, Cocchia R, et al. The impact of age and gender on right ventricular diastolic function among healthy adults. *J Cardiol.* (2017) 70:387–95. doi: 10.1016/j.jjcc.2016.12.005
3. Fiechter M, Fuchs TA, Gebhard C, Stehli J, Klaeser B, Stähli BE, et al. Age-related normal structural and functional ventricular values in cardiac function assessed by magnetic resonance. *BMC Med Imag.* (2013) 13:1–6. doi: 10.1186/1471-2342-13-6
4. Nakou ES, Parthenakis FI, Kallergis EM, Marketou ME, Nakos KS, Vardas PE. Healthy aging and myocardium: a complicated process with various effects in cardiac structure and physiology. *Int J Cardiol.* (2016) 209:167–75. doi: 10.1016/j.ijcard.2016.02.039
5. Granath A, Jonsson B, Strandell T. Circulation in healthy old men, studied by right heart catheterization at rest and during exercise in supine and sitting position. *Acta Med Scand.* (1964) 176:425–46. doi: 10.1111/j.0954-6820.1964.tb00949.x
6. Sicard D, Haak AJ, Choi KM, Craig AR, Fredenburgh LE, Tschumperlin DJ. Aging and anatomical variations in lung tissue stiffness. *Am J Physiol Lung Cell Mol Physiol.* (2018) 314:L946–55. doi: 10.1152/ajplung.00415.2017
7. Hosoda Y, Kawano K, Yamasawa F, Ishii T, Shibata T, Inayama S. Age-dependent changes of collagen and elastin content in human aorta and pulmonary artery. *Angiology.* (1984) 35:615–21. doi: 10.1177/000331978403501001
8. Ehrsam RE, Perruchoud A, Oberholzer M, Burkart F, Herzog H. Influence of age on pulmonary haemodynamics at rest and during supine exercise. *Clin Sci.* (1983) 65:653–60. doi: 10.1042/cs0650653
9. Lam CSP, Borlaug BA, Kane GC, Enders FT, Rodeheffer RJ, Redfield MM. Age-associated increases in pulmonary artery systolic pressure in the general population. *Circulation.* (2009) 119:2663–70. doi: 10.1161/CIRCULATIONAHA.108.838698
10. Kane GC, Sachdev A, Villarraga HR, Ammash NM, Oh JK, McGoon MD, et al. Impact of age on pulmonary artery systolic pressures at rest and with exercise. *Echo Res Pract.* (2016) 3:53–61. doi: 10.1530/ERP-16-0006
11. Chouabe C, Ricci E, Amsellem J, Blaineau S, Dalmaz Y, Favier R, et al. Effects of aging on the cardiac remodeling induced by chronic high-altitude hypoxia in rat. *Am J Physiol Hear Circ Physiol.* (2004) 287:H1246–53. doi: 10.1152/ajpheart.00199.2004
12. Anversa P, Palackal T, Sonnenblick EH, Olivetti G, Meggs LG, Capasso JM. Myocyte cell loss and myocyte cellular hyperplasia in the hypertrophied aging rat heart. *Circ Res.* (1990) 67:871–85. doi: 10.1161/01.RES.67.4.871
13. Effron MB, Bhatnagar GM, Spurgeon HA, Ruaño-Arroyo G, Lakatta EG. Changes in myosin isoenzymes, ATPase activity, and contraction duration in rat cardiac muscle with aging can be modulated by thyroxine. *Circ Res.* (1987) 60:238–45. doi: 10.1161/01.RES.60.2.238
14. Chia EM, Hsieh CHC, Boyd A, Pham P, Vidaic J, Leung D, et al. Effects of age and gender on right ventricular systolic and diastolic function using

two-dimensional speckle-tracking strain. *J Am Soc Echocardiogr.* (2014) 27:1079–86.e1. doi: 10.1016/j.echo.2014.06.007
15. Kuroha M, Isoyama S, Ito N, Takishima T. Effects of age on right ventricular hypertrophic response to pressure-Overload in rats. *J Mol Cell Cardiol.* (1991) 23:1177–90. doi: 10.1016/0022-2828(91)90206-2
16. Hoeper MM, Huscher D, Ghofrani HA, Delcroix M, Distler O, Schweiger C, et al. Elderly patients diagnosed with idiopathic pulmonary arterial hypertension: results from the COMPERA registry. *Int J Cardiol.* (2013) 168:871–80. doi: 10.1016/j.ijcard.2012.10.026
17. Ling Y, Johnson MK, Kiely DG, Condliffe R, Elliot CA, Gibbs JSR, et al. Changing demographics, epidemiology, and survival of incident pulmonary arterial hypertension: results from the pulmonary hypertension registry of the United Kingdom and Ireland. *Am J Respir Crit Care Med.* (2012) 186:790–6. doi: 10.1164/rccm.201203-0383OC
18. Sharifi Kia D, Benza E, Bachman TN, Tushak C, Kim K, Simon MA. Angiotensin receptor-neprilysin inhibition attenuates right ventricular remodeling in pulmonary hypertension. *J Am Heart Assoc.* (2020) 9:e015708. doi: 10.1161/JAHA.119.015708
19. Hill MR, Simon MA, Valdez-Jasso D, Zhang W, Champion HC, Sacks MS. Structural and mechanical adaptations of right ventricle free wall myocardium to pressure overload. *Ann Biomed Eng.* (2014) 42:2451–65. doi: 10.1007/s10439-014-1096-3
20. Avazmohammadi R, Mendiola EA, Li DS, Vanderslice P, Dixon RAF, Sacks MS. Interactions between structural remodeling and hypertrophy in the right ventricle in response to pulmonary arterial hypertension. *J Biomech Eng.* (2019) 141:0910161–13. doi: 10.1115/1.4044174
21. Avazmohammadi R, Hill MR, Simon MA, Zhang W, Sacks MS. A novel constitutive model for passive right ventricular myocardium: evidence for myofiber–collagen fiber mechanical coupling. *Biomech Model Mechanobiol.* (2017) 16:561–81. doi: 10.1007/s10237-016-0837-7
22. Jang S, Vanderpool RR, Avazmohammadi R, Lapshin E, Bachman TN, Sacks M, et al. Biomechanical and hemodynamic measures of right ventricular diastolic function: translating tissue biomechanics to clinical relevance. *J Am Heart Assoc.* (2017) 6:1–10. doi: 10.1161/JAHA.117.006084
23. Quinn R. Comparing rat's to human's age: how old is my rat in people years? *Nutrition.* (2005) 21:775–7. doi: 10.1016/j.nut.2005.04.002
24. Akazawa Y, Okumura K, Ishii R, Slorach C, Hui W, Ide H, et al. Pulmonary artery banding is a relevant model to study the right ventricular remodeling and dysfunction that occurs in pulmonary arterial hypertension. *J Appl Physiol.* (2020) 129:238–46. doi: 10.1152/japplphysiol.00148.2020
25. Avazmohammadi R, Mendiola EA, Soares JS, Li DS, Chen Z, Merchant S, et al. A computational cardiac model for the adaptation to pulmonary arterial hypertension in the rat. *Ann Biomed Eng.* (2019) 47:138–53. doi: 10.1007/s10439-018-02130-y
26. Weiss JL, Frederiksen JW, Weisfeldt ML. Hemodynamic determinants of the time course of fall in canine left ventricular pressure. *J Clin Invest.* (1976) 58:751–60. doi: 10.1172/JCI108522
27. Valdez-Jasso D, Simon MA, Champion HC, Sacks MS. A murine experimental model for the mechanical behaviour of viable right-ventricular myocardium. *J Physiol.* (2012) 590:4571–84. doi: 10.1113/jphysiol.2012.233015
28. Sacks MS. A method for planar biaxial mechanical testing that includes in-plane shear. *J Biomech Eng.* (1999) 121:551–5. doi: 10.1115/1.2835086
29. Sacks MS, Chuong CJ. Orthotropic mechanical properties of chemically treated bovine pericardium. *Ann Biomed Eng.* (1998) 26:892–902. doi: 10.1114/1.135
30. Zhang W, Feng Y, Lee C-H, Billiar KL, Sacks MS. A generalized method for the analysis of planar biaxial mechanical data using tethered testing configurations. *J Biomech Eng.* (2015) 137:064501–13. doi: 10.1115/1.4029266
31. Humphrey JD, Vawter DL, Vito RP. Quantification of strains in biaxially tested soft tissues. *J Biomech.* (1987) 20:59–65. doi: 10.1016/0021-9290(87)90267-3
32. Fata B, Zhang W, Amini R, Sacks MS. Insights into regional adaptations in the growing pulmonary artery using a meso-scale structural model: effects of ascending aorta impingement. *J Biomech Eng.* (2014) 136:0210091–13. doi: 10.1115/1.4026457
33. Sacks MS. Incorporation of experimentally-derived fiber orientation into a structural constitutive model for planar collagenous tissues. *J Biomech Eng.* (2003) 125:280–7. doi: 10.1115/1.1544508
34. Avazmohammadi R, Hill M, Simon M, Sacks M. Transmural remodeling of right ventricular myocardium in response to pulmonary arterial hypertension. *APL Bioeng.* (2017) 1:016105. doi: 10.1063/1.5011639
35. Humphrey JD, Rajagopal KR. A constrained mixture model for growth and remodeling of soft tissues. *Math Model Methods Appl Sci.* (2002) 12:407–30. doi: 10.1142/S0218202502001714
36. Choi HS, Vito RP. Two-dimensional stress-strain relationship for canine pericardium. *J Biomech Eng.* (1990) 112:153–9. doi: 10.1115/1.2891166
37. Rezakhaniha R, Agianniotis A, Schrauwen JTC, Griffa A, Sage D, Bouten CVC, et al. Experimental investigation of collagen waviness and orientation in the arterial adventitia using confocal laser scanning microscopy. *Biomech Model Mechanobiol.* (2012) 11:461–73. doi: 10.1007/s10237-011-0325-z
38. Clemons TD, Bradshaw M, Toshniwal P, Chaudhari N, Stevenson AW, Lynch J, et al. Coherency image analysis to quantify collagen architecture: implications in scar assessment. *RSC Adv.* (2018) 8:9661–9. doi: 10.1039/C7RA12693J
39. Püspöki Z, Storath M, Sage D, Unser M. Transforms and operators for directional bioimage analysis: A survey. *Adv Anat Embryol Cell Biol.* (2016) 219:69–93. doi: 10.1007/978-3-319-28549-8_3
40. Berens P. CircStat: a MATLAB toolbox for circular statistics. *J Stat Softw.* (2009) 31:1–21. doi: 10.18637/jss.v031.i10
41. Joseph DR. The ratio between the heart-weight and body-weight in various animals. *J Exp Med.* (1908) 10:521–8. doi: 10.1084/jem.10.4.521
42. Walker EM, Nillas MS, Mangiarua EI, Cansino S, Morrison RG, Perdue RR, et al. Age-associated changes in hearts of male fischer 344/Brown Norway F1 rats. *Ann Clin Lab Sci.* (2006) 36:427–38. Available online at: http://www.annclinlabsci.org/content/36/4/427.long
43. Fajemiroye JO, Cunha LC Da, Saavedra-Rodríguez R, Rodrigues KL, Naves LM, Mourão AA, et al. Aging-induced biological changes and cardiovascular diseases. *Biomed Res Int.* (2018) 2018:1–14. doi: 10.1155/2018/7156435
44. Gomez AD, Zou H, Bowen ME, Liu X, Hsu EW, McKellar SH. Right ventricular fiber structure as a compensatory mechanism in pressure overload: a computational study. *J Biomech Eng.* (2017) 139:0810041–10. doi: 10.1115/1.4036485
45. Rain S, Handoko ML, Trip P, Gan CTJ, Westerhof N, Stienen GJ, et al. Right ventricular diastolic impairment in patients with pulmonary arterial hypertension. *Circulation.* (2013) 128:2016–25. doi: 10.1161/CIRCULATIONAHA.113.001873
46. Cappelli V, Forni R, Poggesi C, Reggiani C, Ricciardi L. Age-dependent variations of diastolic stiffness and collagen content in rat ventricular myocardium. *Arch Physiol Biochem.* (1984) 92:93–106. doi: 10.3109/13813458409071133
47. Lieber SC, Aubry N, Pain J, Diaz G, Kim SJ, Vatner SF. Aging increases stiffness of cardiac myocytes measured by atomic force microscopy nanoindentation. *Am J Physiol Hear Circ Physiol.* (2004) 287:H645–51. doi: 10.1152/ajpheart.00564.2003
48. Lahm T, Frump AL, Albrecht ME, Fisher AJ, Cook TG, Jones TJ, Yakubov B, Whitson J, Fuchs RK, Liu A, et al. 17β-Estradiol mediates superior adaptation of right ventricular function to acute strenuous exercise in female rats with severe pulmonary hypertension. *Am J Physiol Lung Cell Mol Physiol.* (2016) 311:L375–88. doi: 10.1152/ajplung.00132.2016
49. Liu A, Philip J, Vinnakota KC, Van den Bergh F, Tabima DM, Hacker T, et al. Estrogen maintains mitochondrial content and function in the right ventricle of rats with pulmonary hypertension. *Physiol Rep.* (2017) 5:e13157. doi: 10.14814/phy2.13157
50. Liu A, Schreier D, Tian L, Eickhoff JC, Wang Z, Hacker TA, et al. Direct and indirect protection of right ventricular function by estrogen in an experimental model of pulmonary arterial hypertension. *Am J Physiol Hear Circ Physiol.* (2014) 307:H273–83. doi: 10.1152/ajpheart.00758.2013
51. Singh I, Oliveira RKF, Heerdt PM, Pari R, Systrom DM, Waxman AB. Sex-related differences in dynamic right ventricular-pulmonary vascular coupling in heart failure with preserved ejection fraction. *Chest.* (2021) 159:2402–16. doi: 10.1016/j.chest.2020.12.028
52. Tello K, Richter MJ, Yogeswaran A, Ghofrani HA, Naeije R, Vanderpool R, et al. Sex differences in right ventricular-pulmonary arterial coupling in pulmonary arterial hypertension. *Am J Respir Crit Care Med.* (2020) 202:1042–6. doi: 10.1164/rccm.202003-0807LE

53. Santamore WP, Dell'Italia LJ. Ventricular interdependence: significant left ventricular contributions to right ventricular systolic function. *Prog Cardiovasc Dis.* (1998) 40:289–308. doi: 10.1016/S0033-0620(98)80049-2
54. Sharifi Kia D, Shen Y, Bachman TN, Goncharova EA, Kim K, Simon MA. Effects of healthy aging on right ventricular structure and biomechanical properties. *bioRxiv*. (2020) 1–19. doi: 10.1101/2020.09.08.288332

Conflict of Interest: MS: Research support from Aadi. Steering committee for Janssen. Consultancy fees from Acceleron and Bial. DS is employed by Align Technology, Inc.

The remaining authors declare that the research was conducted in the absence of any commercial or financial relationships that could be construed as a potential conflict of interest.

Publisher's Note: All claims expressed in this article are solely those of the authors and do not necessarily represent those of their affiliated organizations, or those of the publisher, the editors and the reviewers. Any product that may be evaluated in this article, or claim that may be made by its manufacturer, is not guaranteed or endorsed by the publisher.

frontiers in Medicine

REVIEW
published: 13 January 2022
doi: 10.3389/fmed.2021.826557

Inflammasome Activation in Pulmonary Arterial Hypertension

Anna Foley[1], *Benjamin E. Steinberg*[1,2] *and Neil M. Goldenberg*[1,2*]

[1] Department of Physiology, University of Toronto, Toronto, ON, Canada, [2] Department of Anesthesia and Pain Medicine, The Hospital for Sick Children, The University of Toronto, Toronto, ON, Canada

Inflammasomes are multi-protein complexes that sense both infectious and sterile inflammatory stimuli, launching a cascade of responses to propagate danger signaling throughout an affected tissue. Recent studies have implicated inflammasome activation in a variety of pulmonary diseases, including pulmonary arterial hypertension (PAH). Indeed, the end-products of inflammasome activation, including interleukin (IL)-1β, IL-18, and lytic cell death ("pyroptosis") are all key biomarkers of PAH, and are potentially therapeutic targets for human disease. This review summarizes current knowledge of inflammasome activation in immune and vascular cells of the lung, with a focus on the role of these pathways in the pathogenesis of PAH. Special emphasis is placed on areas of potential drug development focused on inhibition of inflammasomes and their downstream effectors.

Keywords: pulmonary hypertension, inflammasome, macrophage, endothelial, vascular remodeling

OPEN ACCESS

Edited by:
Elena Goncharova, University of California, Davis, United States

Reviewed by:
Laszlo Farkas, The Ohio State University, United States
Rahul Kumar, University of California, San Francisco, United States

***Correspondence:**
Neil M. Goldenberg
neil.goldenberg@sickkids.ca

Specialty section:
This article was submitted to Pulmonary Medicine, a section of the journal Frontiers in Medicine

Received: *01 December 2021*
Accepted: *20 December 2021*
Published: *13 January 2022*

Citation:
Foley A, Steinberg BE and Goldenberg NM (2022) Inflammasome Activation in Pulmonary Arterial Hypertension. Front. Med. 8:826557. doi: 10.3389/fmed.2021.826557

THE INFLAMMASOME

Inflammasomes are multi-protein complexes involved in sensing both endogenous and exogenous cellular stress (**Figure 1**) (1). Inflammasomes can respond to a variety of pathogen-associated molecular patters (PAMP's) and damage-associated molecular patters (DAMP's) based on the identity of the pattern recognition receptor (PRR) within the complex (2). In general, inflammasome pathways consist of a receptor, adaptor, and effectors. Five receptor proteins have been confirmed to form the "canonical" inflammasomes to date: nucleotide-binding oligomerization domain (NOD), leucine-rich repeat (LRR)-containing proteins (NLR) family members NLRP1, NLRP3, and NLRC4 as well as the proteins absent in melanoma 2 (AIM2) and pyrin (3). In addition to the canonical pathways, there is also the non-canonical pathway in which caspase-4/5 in humans and caspase-11 in mice are activated directly by intracellular triggers (4). Recognition of inflammatory stimuli results in the activation and oligomerization of the complex that often includes the adaptor protein, apoptosis associated speck-like protein (ASC). The oligomerization with ASC, which contains a caspase recruitment domain (CARD), establishes the activation platform for the pro-inflammatory caspase that facilitates the formation of the functional inflammasome complex (5). The NLRP3 inflammasome is the best characterized and will be the pathway of focus in this review.

The formation of the NLRP3 inflammasome complex allows the proximity-induced autocatalytic activation of pro-caspase-1 to cleaved caspase-1. The role of caspase-1 downstream is the cleavage of cytokines such as pro-IL-1β and pro-IL-18 to their biologically active forms. Caspase-1 additionally cleaves gasdermin D (GSDMD), a protein in which the N terminal subunits assemble into a multi-unit complex to form a plasma membrane pore. The inner diameter of this pore is 21.5 nm and is the main route of egress for mature cytosolic cytokines into the extracellular space (6).

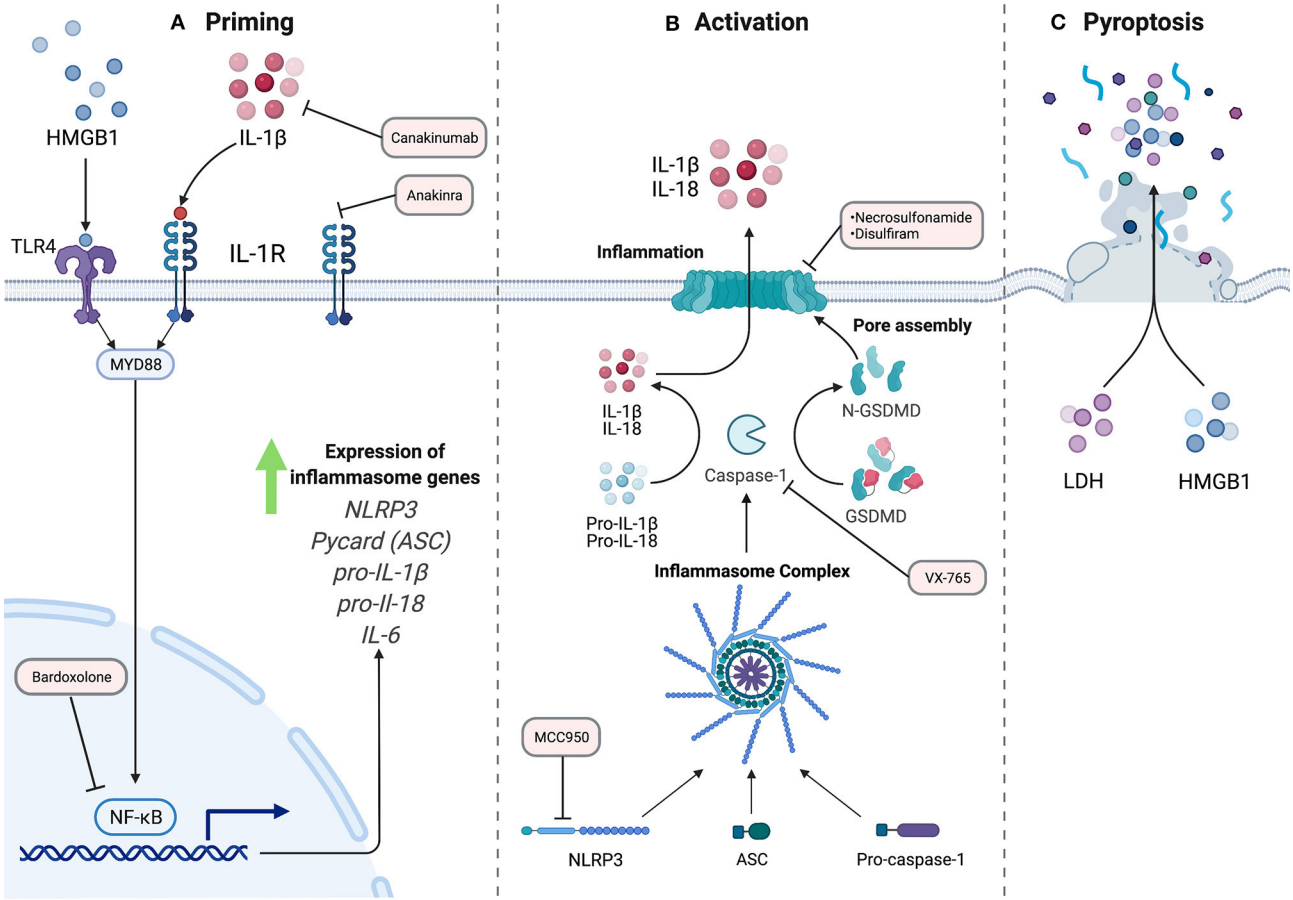

FIGURE 1 | The NLRP3 Inflammasome Pathway. A two-signal model for NLRP3 inflammasome activation. **(A)** Priming, signal 1, is accomplished by extracellular ligands through receptors such as Toll-like receptors. This results in activation of transcription factor NF-κB and subsequent upregulation of inflammasome machinery and pro-inflammatory components. **(B)** Activation, signal 2, which can be achieved by a variety of stimuli resulting in the assembly of the inflammasome complex. Activated caspase-1 cleaves inflammatory cytokines, including pro-IL-1B and pro-IL-18 into their active forms. Additionally, GSDMD is cleaved to allow for N-terminal oligomerization and pore formation at the plasma membrane for release of mature cytokines. **(C)** In some conditions, the cell can undergo pro-inflammatory cell death termed pyroptosis, with frank rupture of the cell, and subsequent release of large macromolecules into the extracellular space, including danger-associated molecular patterns like HMGB1, and pro-inflammatory molecules like ATP, histones, and nucleic acids. The red rectangles indicate steps in the inflammasome pathway that can be targeted pharmacologically, and current agents that work at these steps.

Largely non-selective, the GSDMD pore allows free passage of appropriately sized molecules between the cytosol and the extracellular space. In some conditions, these pores lead to lytic cell death, termed pyroptosis (7). This pro-inflammatory cell death pathway requires the protein ninjurin-1 (NINJ1) through a mechanism that has yet to be defined in detail (8). Following cell membrane rupture, larger proteins such as the potent signaling molecule high-mobility group box 1 (HMGB1) are released into the extracellular environment, propagating inflammatory signals to neighboring cells (9). While this process is best described in immune cells, evidence exists for inflammasome activation in non-immune cells as well, including vascular endothelial cells (10–12).

Triggers and Effectors

The most commonly described stimulus for inflammasome activation *in vitro* involves two steps: a priming step followed by an activation trigger (13). The priming signal is accomplished by extracellular ligands for Toll-like receptors (TLRs), such as bacterial lipopolysaccharide, and results in the activation of the transcription factor NF-κB. This signal upregulates NLRP3, pro-IL-1β, and other inflammasome components, as those proteins are not expressed at a sufficient level in a resting cell for activation (13).

The NLRP3 inflammasome is activated by a wide variety of stimuli that are different in both their physical structure and their chemical nature. As a result of these differences, it is suspected that these diverse stimuli all converge in a common cellular event that activates the inflammasome (5). Potassium efflux through the plasma membrane is critical to multiple NLRP3 inflammasome activators such as bacterial pore-forming toxins and extracellular ATP. Effectively serving as a type of DAMP, extracellular ATP activates the purinergic P2X receptor 7 (P2X7), which is an ion channel selective for Na^+, K^+, and

Ca^{2+} ions. The ATP-gated receptor initiates the depletion of the K^+ concentration in the cell (14). Furthermore, the decrease of K^+ concentration in the cell alone is sufficient for inflammasome activation (15). The potassium sensor for the NLRP3 pathway is still an area of investigation. However, there is some work that demonstrates NEK7, of the NIMA-related kinase family, as an essential protein that acts downstream of potassium efflux leading to the association of NEK7 with NLRP3 for the assembly of the inflammasome and subsequent activation (16, 17).

Mitochondrial dysfunction, resulting in production of mitochondrial reactive oxygen species (mtROS) and release of mitochondrial DNA, is considered another activator of the NLRP3 pathway. Gross et al. demonstrated that mtROS led to NLRP3 activation in a K^+ independent mechanism (18). Mitochondrial DNA, which can be oxidized by mtROS showed similar findings of inflammasome activation in mouse bone marrow derived macrophages (BMDM's) (19). The link between mitochondria and inflammasomes is of special interest given the known role of mitochondrial dysfunction in PAH. Indeed, mitochondrial DNA can directly activate both the NLRP3 and AIM2 inflammasomes (20). The proliferative phenotype of PAH can be at least partially attributed to mitochondrial metabolism. The Warburg phenomenon—glycolysis and lactate metabolism even in the presence of oxygen—allows cells to maintain a highly proliferative state [reviewed in (21)]. Furthermore, mitochondrial fission stimulates fibroblast proliferation in the vasculature and right ventricle, driving adverse remodeling (22). Interestingly, these phenomena link to both activation and regulation of inflammasomes. The oligomerization of GSDMD is controlled by the Ragulator-Rag complex upstream of the master metabolic regulator, mTOR (23). Linking through the mitochondria, GSDMD pore formation was enhanced by mitochondrial dysfunction, as seen through loss of mitochondrial membrane potential and mROS production (23). Together, these data suggest that conditions favoring mitochondrial dysfunction, as seen in PAH, favor inflammasome activation. Additionally, treatments targeting metabolic dysfunction, such as metformin, are under intensive investigation clinically (24).

PULMONARY ARTERIAL HYPERTENSION

Pulmonary Hypertension (PH) is highly fatal disease defined by a mean pulmonary arterial pressure >20 mmHg at rest (25). Pulmonary Arterial Hypertension (PAH) is classified by the World Health organization as Group 1 PH, and is characterized by elevated pulmonary vascular resistance and lung vascular remodeling (26). This remodeling consists of alterations in the structure and growth of all three layers of the vessel—the intima, media and adventitia—resulting in the high pulmonary vascular resistance, right ventricular failure and ultimately death (27). In recent years, the importance of inflammation in the pathogenesis of pulmonary hypertension has received greater attention. The immune cell infiltrates observed in diseased vessels in both human and animal models of PH include cells such as T cells, B cells, neutrophils, macrophages, and others (27). In addition to the presence of autoantibodies, both PH animal models and PAH patients have shown high levels of cytokines that are relevant to the effectors of inflammasome activation (28). The presence of inflammasome products in PAH patients, as well as the efficacy of cytokine blockade in treating PAH in patients and animal models have provided the rationale for targeting inflammasomes in PAH therapy. In the remaining sections, we will review pre-clinical and clinical evidence for blocking inflammasomes in PAH, and will suggest future targets for such a strategy (**Figure 2**).

Pre-clinical Evidence

The NLRP3 inflammasome and its downstream components have been investigated in the context of many pulmonary diseases such as COPD, asthma, cystic fibrosis and pulmonary fibrosis (29–32). There are multiple lines of *in vitro* and animal model evidence implicating inflammasomes in the pathogenesis of PAH (**Table 1**). Following chronic hypoxia, mice lacking the inflammasome adaptor, ASC, were protected from elevated right ventricular systolic pressure (RVSP) and right ventricular hypertrophy (33). Furthermore, $ASC^{-/-}$ mice demonstrated no pulmonary increase in caspase-1, IL-18, or IL-1β abundance, in contrast to wildtype controls. Surprisingly, NLRP3 knockout mice developed disease to a similar extent as wildtype, with no significant difference in right ventricular systolic pressure (RVSP) or cytokine levels (33). These data are consistent with possible compensation for loss of an individual inflammasome type by others, since loss of NLRP3 has no effect, but loss of ASC which is required for most inflammasomes, is protective.

Downstream of inflammasome activation, IL-1β and its receptor, IL-1R, are involved in the pathogenesis of PH in animal models. Within hours of exposure to hypoxia, IL-1β, IL-1R, and the IL-1R adaptor, MyD88, are upregulated in the lungs of mice (34). Knockout mice lacking either MyD88 or IL-1R are protected from hypoxic PH, as are those treated with the IL-1R receptor blocker, anakinra (34). Either genetic or pharmacological blockade of IL-1R reduced macrophage infiltration into hypoxic mouse lungs. In cultured pulmonary artery smooth muscle cells, IL-1β stimulated proliferation in an IL-1R and MyD88 dependent fashion (34). Together, these results indicate a key role for signaling through IL-1R in PH. Interestingly, blockade of IL-1β also has the beneficial effect of inhibiting upstream inflammasomes. There are several possibilities for how this effect evolves. There is potential for upstream negative feedback, but more intriguingly, the role of MyD88 and NF-κB sets up the possibility of breaking a cycle of self-amplification of inflammasome signaling. While IL-1β is a product of inflammasome activation, its receptor engages MyD88 and NF-κB, in a similar manner to TLR. Therefore, IL-1β can then induce its own upregulation in both an autocrine and paracrine manner. Blockade of the IL-1R, hence, can break this cycle, leading to profound dampening of this system. Indeed, the involvement of TLR signaling in inflammasome pathways opens a variety of potential routes to targeting important mechanisms of PAH development pharmacologically. TLR4, downstream of HMGB1, is known to drive PAH development in multiple models (35, 36). Additionally, NF-κB, downstream of TLR4 and MyD88, induces the expression of IL-6, itself sufficient for driving PH development in mice (37). Lastly, an important "gut-lung axis"

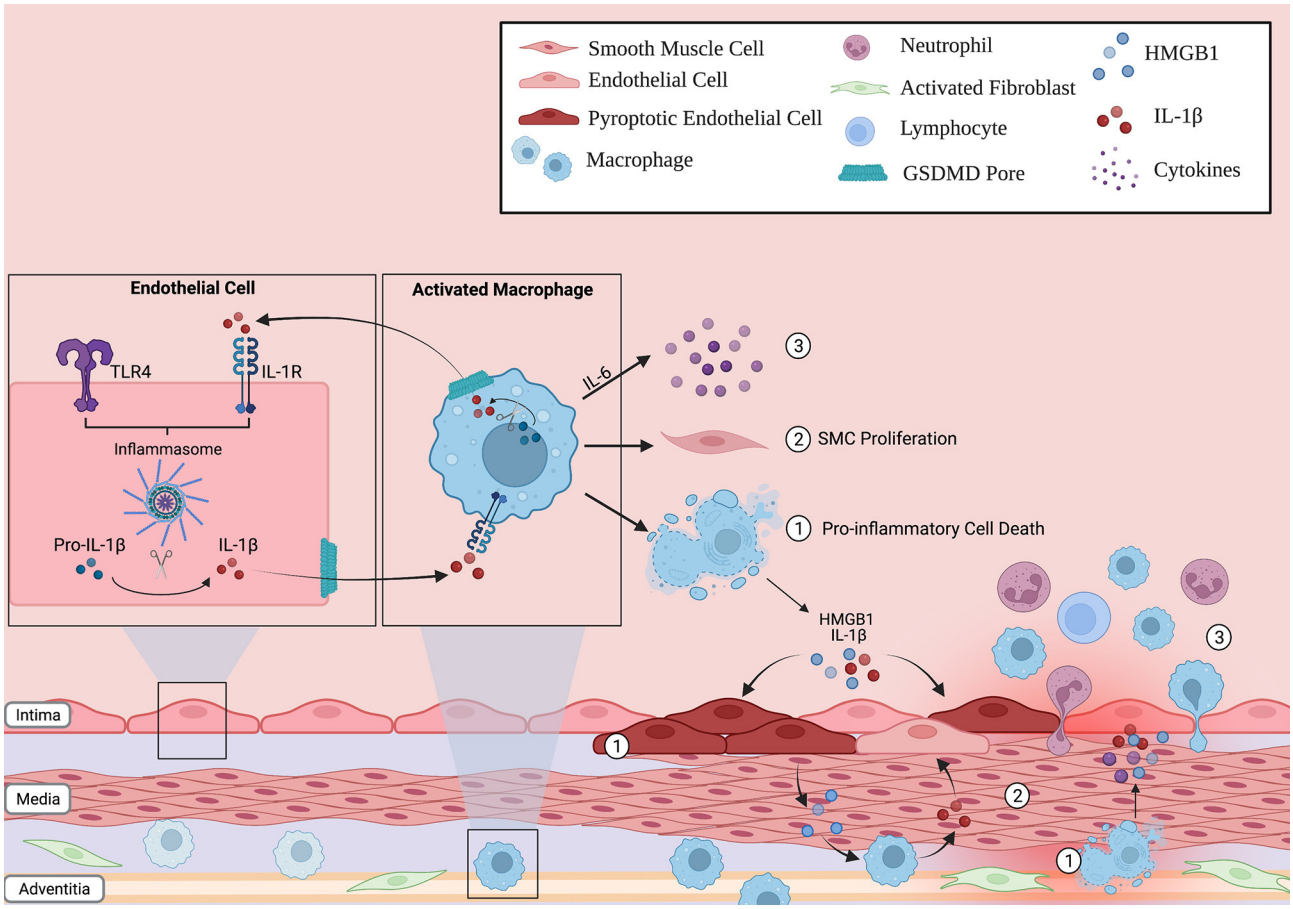

FIGURE 2 | Inflammasome action in the lung vascular environment. Immune cells (such as macrophages) and non-immune cells (endothelial cells) can respond to stress, activate the inflammasome pathway and undergo pyroptosis. The release of pro-inflammatory cytokines through the GSDMD pore, such as IL-1B, can propagate inflammation in neighboring cells by inducing their own transcription in a paracrine fashion. As such, the innate immune response can be amplified through the lung vasculature. In addition, these activated cells can (1) release other potent signaling molecules, such as HMGB1, into the environment following lytic cell death, (2) increase smooth muscle cell (SMC) proliferation in the medial layer of the vessel, and (3) release cytokines such as IL-6 that recruit other inflammatory cells to the vessel wall. Overall, this creates a vicious inflammatory cycle that, over time, contributes to the characteristic pulmonary vascular remodeling seen in PAH patients.

has been identified, whereby bacterial lipopolysaccharide from the gut stimulate adverse remodeling and inflammation in the lung in PAH and heart failure (38). Together, these systems all converge upon the same signaling players, setting up a tempting possibility whereby breaking this chain via inflammasome inhibition may target multiple important pathogenic pathways in PAH.

Downstream of canonical inflammasome activation, the adaptor protein ASC, and the serine protease, caspase-1, are activated and begin cleaving further downstream substrates. In addition to the data presented above, both of these proteins are involved in PH development in model systems. The double stranded RNA kinase (PKR) is upregulated by Type 1 interferons, and is typically activated during viral infection (39). PKR has been shown to directly bind NLRP3, and loss of PKR inhibits release of IL-1β, IL-18, and HMGB1 (40). Recently, PKR was found to be activated in the pulmonary vessels of both monocrotaline-treated and Sugen-hypoxia treated rats (41). PKR inhibition prevented PH development in these models, and was found to block ASC activation and subsequent release of IL-1β and HMGB1 (41). Mechanistically, PKR was found to promote HMGB1 and cytokine release from endothelial cells, leading to proliferation of cocultured smooth muscle cells (41). These data add a significant regulatory protein to the inflammasome pathway, which can potentially be targeted clinically.

Caspase-1 inhibition has also been explored in PH models. As expected, caspase-1 knockout mice are relatively protected from hypoxic PH, and caspase-1 induced smooth muscle cell proliferation (42). Of note, re-introduction of exogenous IL-1β and IL-18 in caspase-1 knockouts restored the PH phenotype, suggesting that downstream cytokine release is the key role of caspase-1 in this model. Clearly, blockade of canonical inflammasomes can inhibit a variety of important proteins in PH models, and are the subject of substantial clinical and translational inquiry.

TABLE 1 | Pre-clinical and clinical evidence for inflammasomes in PAH.

Molecule	Pre-clinical	Clinical	Drug target	References
NLRP3	*NLRP3*$^{-/-}$ mice were not protected from hypoxic PH	NS	MCC950	(33, 53–55)
ASC	*ASC*$^{-/-}$ mice protected from hypoxic PH and RV hypertrophy, with decreased IL-1β and IL-6	NS	None	(33)
Caspase-1	• Increased lung expression of active caspase-1 in chronic hypoxic mice • Caspase-1 induces smooth muscle cell proliferation	NS	VX-765	(33, 42, 56)
Gasdermin D	NS	NS	Necrosulfonamide Disulfiram	(57, 58)
IL-1β/IL-1R	• IL-1β stimulates smooth muscle cell proliferation • *IL-1R*$^{-/-}$ mice protected from chronic hypoxic PH	Increased serum IL-1 correlates with worse outcomes in PAH	Anakinra Canakinumab	(34, 49–51)
NF-κB	Induces expression of IL-6 and drives PH in mice	NF-κB inhibitor in Phase 3 clinical trial	Bardoxolone	(37, 52)
HMGB1	• Anti-HMGB1 antibody rescues PH in Sugen-hypoxia and monocrotaline rats • Stimulates pulmonary endothelial cell proliferation	Increased HMGB1 in idiopathic and CHD-associated PAH	None	(35, 36, 48)

This table summarizes current pre-clinical and clinical evidence for the involvement of inflammasomes in PAH. NS, not studied. See text for details.

While the majority of work in the field focuses on inflammasome activation in macrophage, several other cell types have been shown to also express and activate this pathway, including neutrophils (43), epithelial cells (44), and interestingly for PAH, endothelial cells (45). In acute lung injury models, pulmonary artery endothelial cells were shown to activate inflammasomes and undergo pyroptosis (46). These results establish an intriguing possibility whereby inflammasome activation has an immune effect, as well as a direct effect on the pulmonary vasculature, stimulating cell death, cytokine release, elevated intracellular calcium concentration, and other critical events of known importance in the pathogenesis of PAH. Targeting such a mechanism may, therefore, have pleiotropic effects in a complex disease like PAH.

CLINICAL EVIDENCE

Broadly speaking, the importance of inflammation in vascular remodeling in PAH is well-accepted (25, 27, 47). Evidence for the importance of inflammasome activation in PAH patients comes from both biomarkers and interventional studies (**Table 1**). Indeed, inflammasome activation is broadly applicable to a wide variety of pulmonary diseases (1). In PAH, levels of HMGB1—itself released from pyroptotic cells—are elevated in patients with idiopathic or congenital heart disease-associated PAH (36, 48). Serum IL-1β is elevated in PAH patients and has been shown to correlate with worse outcomes (49). Proof of principle for IL-1β blockade, taken from the preclinical studies detailed above, allowed for the CANTOS trial to examine this approach in patients with atherosclerosis (50). In this large randomized controlled trial, IL-1β blockade with canakinumab decreased both recurrent cardiac events and indices of inflammation. This approach has now been tested in PAH patients, albeit on a smaller scale. Six patients with PAH and right ventricular failure were given anakinra, an IL-1R antagonist. While hemodynamic measures were unchanged over the 3-month study, there was a significant improvement in heart failure symptoms, and a decrease in C-reactive protein levels (51).

Attempts at clinical translation of inflammasome-based therapies will likely grow rapidly in the coming years. Indeed, a variety of drugs are poised for trial, or have themselves entered trials already. The priming step of inflammasome activation largely depends on toll-like receptor-mediated activation of NF-κB (52). To this end, the NF-κB inhibitor bardoxolone, has been in Phase 3 trial in PAH patients, although this trial was recently stopped due to safety concerns surrounding COVID-19 (NCT 02657356). NLRP3 itself can be inhibited by drugs such as MCC-950, which has also shown efficacy in models of cardiac ischemia, aortic disease, and other inflammatory conditions (53, 54). Effective in a variety of models and species, MCC-950 may prove to be an important clinical therapeutic in the future (55). The catalytic action of caspase-1 itself can be targeted by the pro-drug VX-765 [reviewed in (56)]. Further downstream, the effector pore of inflammasome activation, gasdermin D, can be targeted by necrosulfonamide, or the repurposed drug, disulfiram (57, 58). Downstream effectors released from the gasdermin D pore can also be targeted, including the use of anakinra or canakinumab to block IL-1β, or tocilizumab to block IL-6. All of these drugs are undergoing extensive clinical investigation. Together, a wide variety of drugs are under investigation that target inflammasome activity at nearly all steps in the pathway. However, their tolerability, specificity, and overall immunosuppressive side effects will need to be carefully considered and monitored.

SUMMARY

Inflammasome activation interfaces with PAH across several important elements. Pro-inflammatory cytokines, lytic cell death, leukocyte infiltration, and even endothelial dysfunction can all be stimulated via the activation of inflammasomes in the lung vasculature. Fittingly, this area is an intensive research focus across the continuum of basic translational science and clinical trials. Given the multiple potential points of pharmacological intervention available, inflammasome targeting may prove to be a viable treatment option for PAH patients in the future. Fine-tuning this system, as with all potentially immunosuppressive therapies, will be a key consideration going forward.

Importantly, PAH represents a syndrome arising from a huge range of inciting etiologies. One of the key challenges going forward will be in determining the precise populations that are most likely to benefit from inflammasome-targeted therapy. Important work remains in characterizing biomarkers of inflammasome activation in patients with PAH arising from diverse causes. Several such efforts are underway currently, and have reported novel potential groupings of PAH patients based on sequencing efforts (59, 60). Once a systematic assessment has been made, clinical trials can begin in targeted populations most likely to derive benefit from these translational therapies.

AUTHOR CONTRIBUTIONS

AF and NG conceived the concept, wrote the manuscript, and prepared figures. BS conceived the concept, edited the manuscript, and prepared figures. All authors contributed to the article and approved the submitted version.

FUNDING

NG was supported by an Early Career Scientist Award from the Canadian Lung Association, AstraZeneca Canada and the CIHR.

REFERENCES

1. McVey MJ, Steinberg BE, Goldenberg NM. Inflammasome activation in acute lung injury. *Am J Physiol-Lung Cell Mol Physiol.* (2021) 320:L165–78. doi: 10.1152/ajplung.00303.2020
2. Schroder K, Tschopp J. The inflammasomes. *Cell.* (2010) 140:821–32. doi: 10.1016/j.cell.2010.01.040
3. Broz P, Dixit VM. Inflammasomes: mechanism of assembly, regulation and signalling. *Nat Rev Immunol.* (2016) 16:407–20. doi: 10.1038/nri.2016.58
4. Brubaker SW, Brewer SM, Massis LM, Napier BA, Monack DM. A rapid caspase-11 response induced by IFNγ priming is independent of guanylate binding proteins. *iScience.* (2020) 23:101612. doi: 10.1016/j.isci.2020.101612
5. Kelley N, Jeltema D, Duan Y, He Y. The NLRP3 inflammasome: an overview of mechanisms of activation and regulation. *Int J Mol Sci.* (2019) 20:3328. doi: 10.3390/ijms20133328
6. Xia S, Zhang Z, Magupalli VG, Pablo JL, Dong Y, Vora SM, et al. Gasdermin D pore structure reveals preferential release of mature interleukin-1. *Nature.* (2021) 593:607–11. doi: 10.1038/s41586-021-03478-3
7. Kist M, Vucic D. Cell death pathways: intricate connections and disease implications. *EMBO J.* (2021) 40:e106700. doi: 10.15252/embj.2020106700
8. Kayagaki N, Kornfeld OS, Lee BL, Stowe IB, O'Rourke K, Li Q, et al. NINJ1 mediates plasma membrane rupture during lytic cell death. *Nature.* (2021) 591:131–6. doi: 10.1038/s41586-021-03218-7
9. Volchuk A, Ye A, Chi L, Steinberg BE, Goldenberg NM. Indirect regulation of HMGB1 release by gasdermin D. *Nat Commun.* (2020) 11:4561. doi: 10.1038/s41467-020-18443-3
10. Pandey A, Shen C, Feng S, Man SM. Cell biology of inflammasome activation. *Trends Cell Biol.* (2021) 31:924–39. doi: 10.1016/j.tcb.2021.06.010
11. Peeters PM, Perkins TN, Wouters EF, Mossman BT, Reynaert NL. Silica induces NLRP3 inflammasome activation in human lung epithelial cells. *Part Fibre Toxicol.* (2013) 10:3. doi: 10.1186/1743-8977-10-3
12. Sand J, Haertel E, Biedermann T, Contassot E, Reichmann E, French LE, et al. Expression of inflammasome proteins and inflammasome activation occurs in human, but not in murine keratinocytes. *Cell Death Dis.* (2018) 9:24. doi: 10.1038/s41419-017-0009-4
13. Bauernfeind FG, Horvath G, Stutz A, Alnemri ES, MacDonald K, Speert D, et al. Cutting edge: NF-κB activating pattern recognition and cytokine receptors license NLRP3 inflammasome activation by regulating NLRP3 expression. *J Immunol.* (2009) 183:787–91. doi: 10.4049/jimmunol.0901363
14. Pelegrin P. P2X7 receptor and the NLRP3 inflammasome: partners in crime. *Biochem Pharmacol.* (2021) 187:114385. doi: 10.1016/j.bcp.2020.114385
15. Muñoz-Planillo R, Kuffa P, Martínez-Colón G, Smith BL, Rajendiran TM, Núñez G. K+ Efflux is the common trigger of NLRP3 inflammasome activation by bacterial toxins and particulate matter. *Immunity.* (2013) 38:1142–53. doi: 10.1016/j.immuni.2013.05.016
16. He Y, Zeng MY, Yang D, Motro B, Núñez G. NEK7 is an essential mediator of NLRP3 activation downstream of potassium efflux. *Nature.* (2016) 530:354–7. doi: 10.1038/nature16959
17. Liu H, Gu C, Liu M, Liu G, Wang Y. NEK7 mediated assembly and activation of NLRP3 inflammasome downstream of potassium efflux in ventilator-induced lung injury. *Biochem Pharmacol.* (2020) 177:113998. doi: 10.1016/j.bcp.2020.113998
18. Groß CJ, Mishra R, Schneider KS, Médard G, Wettmarshausen J, Dittlein DC, et al. K + efflux-independent NLRP3 inflammasome activation by small molecules targeting mitochondria. *Immunity.* (2016) 45:761–73. doi: 10.1016/j.immuni.2016.08.010
19. Shimada K, Crother TR, Karlin J, Dagvadorj J, Chiba N, Chen S, et al. Oxidized mitochondrial DNA activates the NLRP3 inflammasome during apoptosis. *Immunity.* (2012) 36:401–14. doi: 10.1016/j.immuni.2012.01.009
20. Trachalaki A, Tsitoura E, Mastrodimou S, Invernizzi R, Vasarmidi E, Bibaki E, et al. Enhanced IL-1β release following NLRP3 and AIM2 inflammasome stimulation is linked to mtROS in airway macrophages in pulmonary fibrosis. *Front Immunol.* (2021) 12:661811. doi: 10.3389/fimmu.2021.661811
21. Dasgupta A, Wu D, Tian L, Xiong PY, Kimberly J, Chen K, et al. Mitochondria in the pulmonary vasculature in health and disease: oxygen-sensing, metabolism, and dynamics. *Comprehens Physiol.* (2011) 10:713–65. doi: 10.1002/cphy.c190027
22. Tian L, Potus F, Wu D, Dasgupta A, Chen KH, Mewburn J, et al. Increased Drp1-mediated mitochondrial fission promotes proliferation and collagen production by right ventricular fibroblasts in experimental pulmonary arterial hypertension. *Front Physiol.* (2018) 9:828. doi: 10.3389/fphys.2018.00828
23. Evavold CL, Hafner-Bratkovič I, Devant P, D'Andrea JM, Ngwa EM, Boršić E, et al. Control of gasdermin D oligomerization and pyroptosis by the Ragulator-Rag-mTORC1 pathway. *Cell.* (2021) 184:4495–511.e19. doi: 10.1016/j.cell.2021.06.028
24. Brittain EL, Niswender K, Agrawal V, Chen X, Fan R, Pugh ME, et al. Mechanistic phase II clinical trial of metformin in pulmonary arterial hypertension. *J Am Heart Assoc.* (2020) 9:e018349. doi: 10.1161/JAHA.120.018349

25. Goldenberg NM, Rabinovitch M, Steinberg BE. Inflammatory basis of pulmonary arterial hypertension. *Anesthesiology.* (2019) 131:898–907. doi: 10.1097/ALN.0000000000002740
26. Sysol JR, Machado RF. Classification and pathophysiology of pulmonary hypertension. *Contin Cardiol Educ.* (2018) 4:2–12. doi: 10.1002/cce2.71
27. Rabinovitch M, Guignabert C, Humbert M, Nicolls MR. Inflammation and immunity in the pathogenesis of pulmonary arterial hypertension. *Circ Res.* (2014) 115:165–75. doi: 10.1161/CIRCRESAHA.113.301141
28. Hu Y, Chi L, Kuebler WM, Goldenberg NM. Perivascular inflammation in pulmonary arterial hypertension. *Cells.* (2020) 9:2338. doi: 10.3390/cells9112338
29. Yang W, Ni H, Wang H, Gu H. NLRP3 inflammasome is essential for the development of chronic obstructive pulmonary disease. *Int J Clin Exp Pathol.* (2015) 8:13209–16.
30. Dostert C, Pétrilli V, Van Bruggen R, Steele C, Mossman BT, Tschopp J. Innate immune activation through Nalp3 inflammasome sensing of asbestos and silica. *Science.* (2008) 320:674–7. doi: 10.1126/science.1156995
31. Iannitti RG, Napolioni V, Oikonomou V, De Luca A, Galosi C, Pariano M, et al. IL-1 receptor antagonist ameliorates inflammasome-dependent inflammation in murine and human cystic fibrosis. *Nat Commun.* (2016) 7:10791. doi: 10.1038/ncomms10791
32. Kim RY, Pinkerton JW, Essilfie AT, Robertson AAB, Baines KJ, Brown AC, et al. Role for NLRP3 inflammasome–mediated, IL-1β-dependent responses in severe, steroid-resistant asthma. *Am J Respir Crit Care Med.* (2017) 196:283–97. doi: 10.1164/rccm.201609-1830OC
33. Cero FT, Hillestad V, Sjaastad I, Yndestad A, Aukrust P, Ranheim T, et al. Absence of the inflammasome adaptor ASC reduces hypoxia-induced pulmonary hypertension in mice. *Am J Physiol-Lung Cell Mol Physiol.* (2015) 309:L378–87. doi: 10.1152/ajplung.00342.2014
34. Parpaleix A, Amsellem V, Houssaini A, Abid S, Breau M, Marcos E, et al. Role of interleukin-1 receptor 1/MyD88 signalling in the development and progression of pulmonary hypertension. *Eur Respir J.* (2016) 48:470–83. doi: 10.1183/13993003.01448-2015
35. Goldenberg NM, Hu Y, Hu X, Volchuk A, Zhao YD, Kucherenko MM, et al. Therapeutic targeting of high-mobility group box-1 in pulmonary arterial hypertension. *Am J Respir Crit Care Med.* (2019) 199:1566–9. doi: 10.1164/rccm.201808-1597LE
36. Bauer EM, Shapiro R, Billiar TR, Bauer PM. High mobility group box 1 inhibits human pulmonary artery endothelial cell migration via a toll-like receptor 4- and interferon response factor 3-dependent mechanism(s). *J Biol Chem.* (2013) 288:1365–73. doi: 10.1074/jbc.M112.434142
37. Steiner MK, Syrkina OL, Kolliputi N, Mark EJ, Hales CA, Waxman AB. Interleukin-6 overexpression induces pulmonary hypertension. *Circ Res.* (2009) 104:236–44. doi: 10.1161/CIRCRESAHA.108.182014
38. Ranchoux B, Bigorgne A, Hautefort A, Girerd B, Sitbon O, Montani D, et al. Gut–lung connection in pulmonary arterial hypertension. *Am J Respir Cell Mol Biol.* (2017) 56:402–5. doi: 10.1165/rcmb.2015-0404LE
39. Kang R, Tang D. PKR-dependent inflammatory signals. *Sci Signal.* (2012) 5:pe47. doi: 10.1126/scisignal.2003511
40. Lu B, Nakamura T, Inouye K, Li J, Tang Y, Lundbäck P, et al. Novel role of PKR in inflammasome activation and HMGB1 release. *Nature.* (2012) 488:670–4. doi: 10.1038/nature11290
41. Li Y, Li Y, Li L, Yin M, Wang J, Li X. PKR deficiency alleviates pulmonary hypertension via inducing inflammasome adaptor ASC inactivation. *Pulm Circ.* (2021) 11:204589402110461. doi: 10.1177/20458940211046156
42. Udjus C, Cero FT, Halvorsen B, Behmen D, Carlson CR, Bendiksen BA, et al. Caspase-1 induces smooth muscle cell growth in hypoxia-induced pulmonary hypertension. *Am J Physiol-Lung Cell Mol Physiol.* (2019) 316:L999–1012. doi: 10.1152/ajplung.00322.2018
43. Chen KW, Groß CJ, Sotomayor FV, Stacey KJ, Tschopp J, Sweet MJ, et al. The neutrophil NLRC4 inflammasome selectively promotes IL-1β maturation without pyroptosis during acute salmonella challenge. *Cell Rep.* (2014) 8:570–82. doi: 10.1016/j.celrep.2014.06.028
44. Lei-Leston AC, Murphy AG, Maloy KJ. Epithelial cell inflammasomes in intestinal immunity and inflammation. *Front Immunol.* (2017) 8:1168. doi: 10.3389/fimmu.2017.01168
45. Bai B, Yang Y, Wang Q, Li M, Tian C, Liu Y, et al. NLRP3 inflammasome in endothelial dysfunction. *Cell Death Dis.* (2020) 11:776. doi: 10.1038/s41419-020-02985-x
46. Cheng KT, Xiong S, Ye Z, Hong Z, Di A, Tsang KM, et al. Caspase-11–mediated endothelial pyroptosis underlies endotoxemia-induced lung injury. *J Clin Invest.* (2017) 127:4124–35. doi: 10.1172/JCI94495
47. Stacher E, Graham BB, Hunt JM, Gandjeva A, Groshong SD, McLaughlin VV, et al. Modern age pathology of pulmonary arterial hypertension. *Am J Respir Crit Care Med.* (2012) 186:261–72. doi: 10.1164/rccm.201201-0164OC
48. Yuan HY, Su W, Wei ZZ, Tang L, Qun HX, Hua ZS, et al. Elevated serum HMGB1 in pulmonary arterial hypertension secondary to congenital heart disease. *Vascul Pharmacol.* (2016) 85:66–72. doi: 10.1016/j.vph.2016.08.009
49. Soon E, Holmes AM, Treacy CM, Doughty NJ, Southgate L, Machado RD, et al. Elevated levels of inflammatory cytokines predict survival in idiopathic and familial pulmonary arterial hypertension. *Circulation.* (2010) 122:920–7. doi: 10.1161/CIRCULATIONAHA.109.933762
50. Ridker PM, Everett BM, Thuren T, MacFadyen JG, Chang WH, Ballantyne C, et al. Antiinflammatory therapy with canakinumab for atherosclerotic disease. *N Engl J Med.* (2017) 377:1119–31. doi: 10.1056/NEJMoa1707914
51. Trankle CR, Canada JM, Kadariya D, Markley R, De Chazal HM, Pinson J, et al. IL-1 blockade reduces inflammation in pulmonary arterial hypertension and right ventricular failure: a single-arm, open-label, phase IB/II pilot study. *Am J Respir Crit Care Med.* (2019) 199:381–4. doi: 10.1164/rccm.201809-1631LE
52. Swanson KV, Deng M, Ting JPY. The NLRP3 inflammasome: molecular activation and regulation to therapeutics. *Nat Rev Immunol.* (2019) 19:477–89. doi: 10.1038/s41577-019-0165-0
53. van Hout GPJ, Bosch L, Ellenbroek GHJM, de Haan JJ, van Solinge WW, Cooper MA, et al. The selective NLRP3-inflammasome inhibitor MCC950 reduces infarct size and preserves cardiac function in a pig model of myocardial infarction. *Eur Heart J.* (2017) 38:828–36. doi: 10.1093/eurheartj/ehw247
54. Ren P, Wu D, Appel R, Zhang L, Zhang C, Luo W, et al. Targeting the NLRP3 inflammasome with inhibitor MCC950 prevents aortic aneurysms and dissections in mice. *J Am Heart Assoc.* (2020) 9:e014044. doi: 10.1161/JAHA.119.014044
55. Coll RC, Robertson AAB, Chae JJ, Higgins SC, Muñoz-Planillo R, Inserra MC, et al. A small-molecule inhibitor of the NLRP3 inflammasome for the treatment of inflammatory diseases. *Nat Med.* (2015) 21:248–55. doi: 10.1038/nm.3806
56. Scott TE, Kemp-Harper BK, Hobbs AJ. Inflammasomes: a novel therapeutic target in pulmonary hypertension? *Br J Pharmacol.* (2019) 176:1880–96. doi: 10.1111/bph.14375
57. Hu JJ, Liu X, Xia S, Zhang Z, Zhang Y, Zhao J, et al. FDA-approved disulfiram inhibits pyroptosis by blocking gasdermin D pore formation. *Nat Immunol.* (2020) 21:736–5. doi: 10.1038/s41590-020-0669-6
58. Rathkey JK, Zhao J, Liu Z, Chen Y, Yang J, Kondolf HC, et al. Chemical disruption of the pyroptotic pore-forming protein gasdermin D inhibits inflammatory cell death and sepsis. *Sci Immunol.* (2018) 3:eaat2738. doi: 10.1126/sciimmunol.aat2738
59. Kariotis S, Jammeh E, Swietlik EM, Pickworth JA, Rhodes CJ, Otero P, et al. Biological heterogeneity in idiopathic pulmonary arterial hypertension identified through unsupervised transcriptomic profiling of whole blood. *Nat Commun.* (2021) 12:7104. doi: 10.1038/s41467-021-27326-0

60. Hemnes AR, Beck GJ, Newman JH, Abidov A, Aldred MA, Barnard J, et al. PVDOMICS: a multi-center study to improve understanding of pulmonary vascular disease through phenomics. *Circ Res.* (2017) 121:1136–9. doi: 10.1161/CIRCRESAHA.117.311737

Conflict of Interest: NG received funding from AstraZeneca Canada as part of the CIHR/Canadian Lung Association/AZ Canada Early Clinician Scientist Award. The funder was not involved in the study design, collection, analysis, interpretation of data, the writing of this article or the decision to submit it for publication.

The remaining authors declare that the research was conducted in the absence of any commercial or financial relationships that could be construed as a potential conflict of interest.

frontiers in Medicine

MINI REVIEW
published: 24 January 2022
doi: 10.3389/fmed.2021.814222

Therapeutic Approaches for Treating Pulmonary Arterial Hypertension by Correcting Imbalanced TGF-β Superfamily Signaling

Patrick Andre, Sachindra R. Joshi, Steven D. Briscoe, Mark J. Alexander, Gang Li and Ravindra Kumar*

Discovery Group, Acceleron Pharma (a wholly-owned subsidiary of Merck & Co., Inc.), Cambridge, MA, United States

Pulmonary arterial hypertension (PAH) is a rare disease characterized by high blood pressure in the pulmonary circulation driven by pathological remodeling of distal pulmonary arteries, leading typically to death by right ventricular failure. Available treatments improve physical activity and slow disease progression, but they act primarily as vasodilators and have limited effects on the biological cause of the disease—the uncontrolled proliferation of vascular endothelial and smooth muscle cells. Imbalanced signaling by the transforming growth factor-β (TGF-β) superfamily contributes extensively to dysregulated vascular cell proliferation in PAH, with overactive pro-proliferative SMAD2/3 signaling occurring alongside deficient anti-proliferative SMAD1/5/8 signaling. We review the TGF-β superfamily mechanisms underlying PAH pathogenesis, superfamily interactions with inflammation and mechanobiological forces, and therapeutic strategies under development that aim to restore SMAD signaling balance in the diseased pulmonary arterial vessels. These strategies could potentially reverse pulmonary arterial remodeling in PAH by targeting causative mechanisms and therefore hold significant promise for the PAH patient population.

Keywords: activin A, SMAD1/5/8, SMAD2/3, PAH, TGF-β, BMP, BMPRII, cell proliferation

OPEN ACCESS

Edited by:
Elena Goncharova, University of California, Davis, United States

Reviewed by:
Yen-Chun Lai, Indiana University, United States
Maryam Sharifi-Sanjani, University of Pittsburgh, United States

****Correspondence:***
Patrick Andre
pandre@acceleronpharma.com

Specialty section:
This article was submitted to Pulmonary Medicine, a section of the journal Frontiers in Medicine

Received: *12 November 2021*
Accepted: *15 December 2021*
Published: *24 January 2022*

Citation:
Andre P, Joshi SR, Briscoe SD, Alexander MJ, Li G and Kumar R (2022) Therapeutic Approaches for Treating Pulmonary Arterial Hypertension by Correcting Imbalanced TGF-β Superfamily Signaling. Front. Med. 8:814222. doi: 10.3389/fmed.2021.814222

TGF-β SUPERFAMILY DYSREGULATION IS A CRITICAL COMPONENT OF PAH

In pulmonary arterial hypertension (PAH), pathologic vascular remodeling distorts the gross- and micro-scale structure of the pulmonary arterial vasculature, severely disrupting blood flow patterns throughout the cardiopulmonary circulation. The primary pathology is thought to originate in the small distal arterioles, in which uncontrolled proliferation of vascular cells results in narrowing and occlusion of the vascular lumen. Loss of luminal space in turn increases pulmonary vascular resistance and pulmonary arterial pressure, leading to strain on the right cardiac ventricle and ultimately to heart failure (1).

Multiple cell types of the pulmonary arterial wall contribute to vascular remodeling in PAH (**Figure 1**) (2). Smooth muscle cells (SMCs) over-proliferate and thereby thicken vessel walls and cause vascular muscularization, including around the distal arterioles where SMCs are not normally found. Endothelial cells (ECs) also over-proliferate and in later stages of disease can form neointimal lesions that obstruct distal arterioles (3). Accordingly, targeting the proliferation

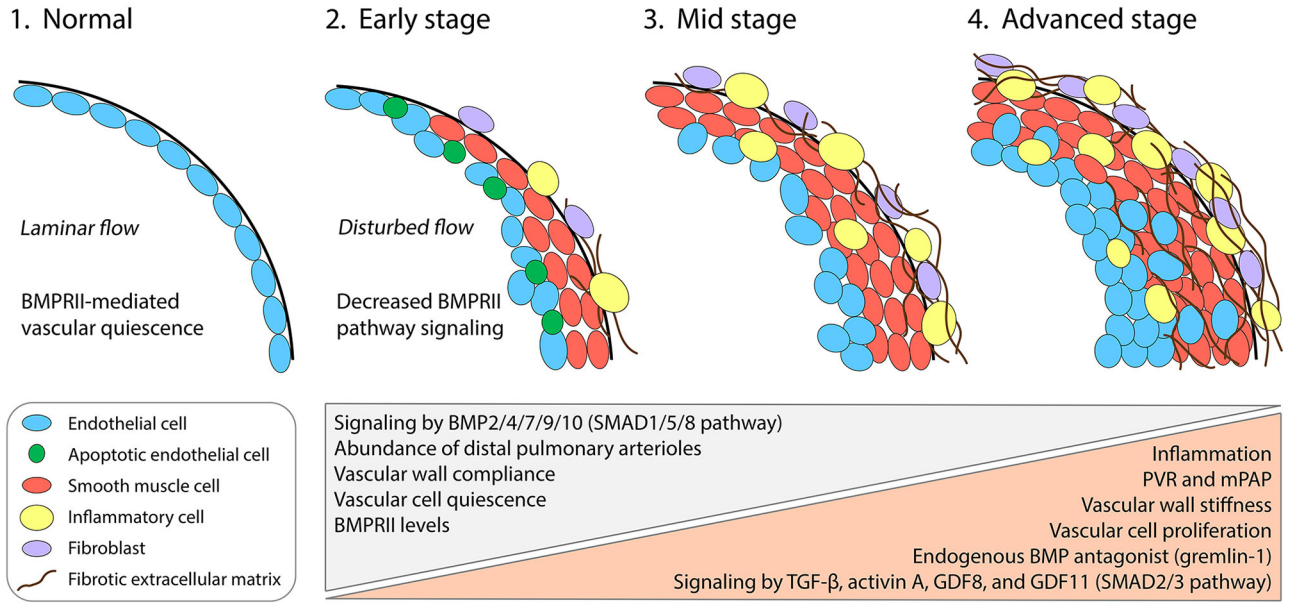

FIGURE 1 | Cellular, molecular, and biomechanical progression of PAH in the pulmonary arterial wall. Under normal conditions, the pulmonary distal arterioles comprise an intimal monolayer of ECs and are largely devoid of a medial layer with SMCs. Laminar blood flow patterns promote BMPRII-pathway signaling in ECs and maintain vascular quiescence (1). Genetic mutations or combined insults lead to insufficient BMPRII levels and SMAD1/5/8 signaling in multiple vascular cell types. Early events during PAH pathogenesis include the onset of vascular wall stiffening and inflammatory responses, including infiltration by diverse inflammatory cell types. Apoptotic ECs appear early but are progressively replaced by apoptosis-resistant and hyperproliferative ECs, which ultimately form disorganized neointimal lesions (2–4). SMAD2/3 pathway-activating ligands including TGF-β, activin A, GDF8, and GDF11 become upregulated and contribute to arterial remodeling. Gremlin-1, a key pathogenic protein in PAH, reduces BMPRII-pathway signaling by antagonizing specific BMPs. SMCs accumulate in the medial layer, causing distal muscularization. Fibroblasts in the adventitial layer become activated and synthesize fibrotic extracellular matrix. PVR, pulmonary vascular resistance; mPAP, mean pulmonary arterial pressure.

of SMCs and ECs to treat PAH has been the subject of extensive efforts over the last two decades. Studies on the platelet-derived growth factor receptor pathway, which is strongly upregulated in the distal pulmonary arteries of PAH patients and contributes to over-proliferation (4), have suggested that reversal of pathology is clinically achievable (5, 6)—although safer alternative strategies are desirable (7). Research into PAH disease mechanisms has also highlighted the critical roles of other signal transduction pathways, especially those of the transforming growth factor-β (TGF-β) superfamily, which interact with inflammatory processes and biomechanical forces to regulate EC and SMC proliferation.

The TGF-β superfamily features more than 30 ligands, which together regulate a great variety of developmental and homeostatic processes in all major organs including the vasculature (8). Indeed, dysregulation of TGF-β superfamily signaling has been implicated in numerous cardiomyopathies and vasculopathies, including atherosclerosis, vascular calcification, Marfan syndrome, Loeys-Dietz syndrome, and hereditary hemorrhagic telangiectasia, in addition to PAH (9–12). Typically, binding of a dimeric TGF-β superfamily ligand promotes assembly of a heterotetrameric signaling complex comprising two type I and two type II receptor serine/threonine kinases. Upon ligand binding, the constitutively active type II receptor phosphorylates the type I receptor, activating the type I receptor intracellular kinase domain. Signal is then propagated through various canonical (involving SMAD transcription factors) and non-canonical (or SMAD-independent) pathways. In PAH, recent evidence indicates a signaling imbalance between the two principal canonical pathways, with underactive SMAD1/5/8 signaling occurring alongside overactive SMAD2/3 signaling in pulmonary arterial ECs and SMCs (13). In the remaining sections, we describe how this SMAD signaling imbalance influences the exuberant cell proliferation underlying vascular remodeling and describe therapeutic approaches for either attenuating excessive SMAD2/3 signaling or restoring deficient SMAD1/5/8 signaling in diseased pulmonary vasculature (14–20). The potential involvement of non-canonical TGF-β superfamily pathways in PAH pathogenesis is poorly understood, but these signaling mechanisms have been implicated in related pathological conditions, such as fibrosis, and merit further study. We therefore refer the reader to previous reviews covering non-canonical signaling in disease (21–25).

DEFICIENT SIGNALING IN ANTI-PROLIFERATIVE SMAD1/5/8 PATHWAY

Studies exploring the human genetics of PAH have revealed important insights into PAH pathobiological mechanisms.

Mutations in *BMPR2*, which encodes bone morphogenetic protein receptor type II (BMPRII), were discovered in 2000 as the first known genetic cause of PAH (26, 27). Such mutations account for >70% of inherited PAH cases and 20% of spontaneous cases, by far the largest proportion for any single gene locus (28–30). Reduced levels of BMPRII protein have been found in other forms and etiologies of PAH, even in the absence of *BMPR2* mutation, suggesting that this signaling pathway could be a point of convergence among multiple distinct PAH disease etiologies (31–33).

BMPRII pathway activity is important in both pulmonary arterial ECs and SMCs, although the two vascular cell types appear to depend on different BMPRII ligands and on different BMPRII signaling outputs. Circulating bone morphogenetic protein 9 (BMP9) and BMP10 are thought to be critical quiescence factors in the pulmonary arteries and act primarily upon ECs (34). Mice with *Bmpr2* ablated selectively in ECs develop PAH-like disease, including proliferating ECs and SMCs, highlighting the importance of BMPRII signaling in the endothelium in particular (35). In addition, BMPRII-deficient human ECs in culture undergo enhanced transformation to a proliferative and synthetic mesenchymal phenotype, suggesting that BMPRII-mediated signaling in the endothelium preserves vascular structure by promoting EC quiescence (36, 37). In contrast, BMP2 and BMP7 promote SMC apoptosis through BMPRII (38), and BMP4 reduces SMC proliferation (39, 40). Thus, loss of BMPRII from SMCs could decrease BMP2/4/7 signaling and result in the accumulation of apoptosis-resistant and hyperproliferative SMCs—hallmarks of distal arterial muscularization in PAH. Gremlin-1, an endogenous antagonist of BMP2/4/7, is markedly upregulated in PAH (**Figure 1**) (41, 42), which could potentially account for reduced BMPRII pathway activity in patients with normal *BMPR2* expression. Notably, recent evidence indicates that BMPRII-deficient macrophages are also important contributors to vascular remodeling in PAH, underscoring the complexity of PAH pathogenesis and the interactions between vascular cell types of different lineages (43).

Interestingly, mutations associated with PAH have also been discovered for several TGF-β superfamily members that interact functionally with BMPRII in pulmonary ECs and SMCs (44, 45). Additional PAH risk genes include those encoding the BMPRII ligands BMP9 and BMP10 (46–48); the BMPRII signaling partners activin receptor-like kinase 1 (ALK1) and endoglin (49–51); the BMPRII transcriptional mediators SMAD1, SMAD4, and SMAD8 (52, 53); and the scaffolding protein caveolin-1 (54–56), which regulates BMPRII signaling through its localization and internalization. Although not all PAH risk factors are associated with BMPRII function, the striking enrichment for TGF-β superfamily members clearly identifies the BMPRII signaling axis as a pathway necessary for pulmonary vascular homeostasis (44). Together, evidence stemming from human genetics and preclinical experiments suggests that the BMP-BMPRII-SMAD1/5/8 pathway performs a protective function and is necessary to prevent vascular cell proliferation and consequent pathologic vascular remodeling (**Figure 1**). However, it is important to note that experiments *in vitro* reveal that BMPRII-deficient ECs could gain SMAD1/5 responsivity to TGF-β through lateral signaling (36), suggesting possible additional levels of signaling complexity in a tissue context. It will therefore be important to resolve the states of SMAD1/5/8 and SMAD2/3 phosphorylation in a cell type–specific manner in the lungs of PAH patients.

OVERACTIVE SIGNALING IN PRO-PROLIFERATIVE SMAD2/3 PATHWAY

Whereas the BMPs signal predominantly through the SMAD1/5/8 canonical pathway, other TGF-β superfamily members, notably TGF-β and the activin-class ligands, instead signal mainly through SMAD2/3. Recent evidence has revealed pathogenic roles for multiple SMAD2/3 pathway-activating ligands in PAH vascular remodeling and in the control of vascular cell proliferation (13, 57), providing important new targets for therapeutic development.

In PAH patients, elevated TGF-β levels have been detected in remodeled distal arterioles and in the circulation (**Figure 1**) (58–60). TGF-β can inhibit apoptosis of SMCs through activation of a non-canonical PI3K/AKT pathway and can promote SMC proliferation through a non-canonical PTEN-dependent pathway (61, 62). Blockade of signaling by one or more TGF-β isoforms using a soluble ligand trap (57), a pan–TGF-β antibody (63), or a TGF-β receptor antibody (64) demonstrates that TGF-β signaling plays a direct role in vascular remodeling and narrowing. Systemic administration of a TGF-β ligand trap decreases phosphorylated SMAD2 in the lungs of a PAH rat model, suggesting that TGF-β exerts at least some of its remodeling effects through canonical signaling in addition to non-canonical pathways (57). Beyond its direct effects in vascular remodeling, TGF-β also induces expression of endothelin-1 (ET-1) by ECs, an additional pathogenic factor in PAH (65). Increased levels of ET-1 reduce BMPRII expression (66), and BMPRII knockdown increases ET-1 (67), suggesting that a positive feedback loop could link diminished BMPRII output with enhanced signaling by TGF-β and ET-1 during PAH pathogenesis.

Activin-class ligands, which include activin A, growth differentiation factor 8 (GDF8), and GDF11, have more recently been implicated in PAH pathogenesis (13). These ligands, like TGF-β isoforms, activate SMAD2/3 signaling and might therefore act in concert with TGF-β, exerting pathogenic effects through overlapping or distinct mechanisms during pathologic vascular remodeling in PAH. Immunohistochemical evidence indicates that activin A, GDF8, and GDF11 are upregulated in small pulmonary arteries of PAH patients and PAH rodent models (**Figure 1**) (13). As we describe further below, concurrent inhibition of multiple activin-class ligands imparts robust protection in PAH rodent models and in phase 2 clinical trials. The individual contributions made by activin A (68) and GDF11 (69) have been explored in preclinical studies. Activin A in particular appears to play a substantial pathogenic role: it is upregulated by ECs in PAH lung tissues, can perturb EC function in culture, causes BMPRII downregulation, and

when overexpressed selectively in mouse ECs can cause PAH-like disease featuring muscularized pulmonary arteries and right heart hypertrophy (68). Selective ablation of *Gdf11* in mouse ECs protects against experimental PAH (69), suggesting that GDF11 might act similarly to activin A, a close phylogenic relative (70). Notably, GDF11 can signal through the type I receptor ALK5, better known as the principal SMAD2/3-activating receptor used by TGF-β (71, 72), providing a potential mechanism for convergence of GDF11- and TGF-β-mediated signals. Given emerging evidence of GDF8 involvement in vascular dysfunction and chronic inflammatory disease (11, 12, 73, 74), it will be important in future studies to dissect the pathogenic contributions made specifically by GDF8, if any, to vascular remodeling in PAH. Whether any of the activin-class ligands drive pathologic vascular remodeling processes through non-canonical signaling mechanisms has not yet been investigated to our knowledge.

In addition to their roles in pathologic vascular cell proliferation, TGF-β superfamily ligands also control the excessive deposition of extracellular matrix, or fibrosis, that leads to vascular wall stiffness in later stages of PAH progression (**Figure 1**) (75). TGF-β1 in particular has long been regarded as a master regulator of fibrosis, but accumulating evidence also implicates TGF-β2 and TGF-β3 isoforms in fibrotic processes potentially relevant to PAH vascular remodeling (58, 76, 77). Individually or in combination, the three TGF-β isoforms are thought to promote myofibroblast differentiation, drive the synthesis and deposition of extracellular matrix proteins, and might stimulate mesenchymal transformation of endothelial or other cell types in the pulmonary arteries (36, 78). Interestingly, lung BMPRII and phosphorylated SMAD1/5/8 levels were found to be decreased in a model of pulmonary hypertension associated with pulmonary fibrosis, suggesting that SMAD signaling balance might coordinately regulate fibrosis together with cell proliferation (79). Many important mechanisms of arterial fibrogenesis in PAH, including the potential involvement of activin-class ligands, require further study. It is clear, however, that PAH pathogenesis is characterized by multiple pathogenic ligands acting in parallel—in complex and potentially combinatorial modes—upon distinct classes of vascular cell types.

INTERPLAY BETWEEN INFLAMMATION AND TGF-β SUPERFAMILY SIGNALING IN PAH

Partial disruption of pulmonary vascular BMPRII signaling is not sufficient to initiate PAH pathogenesis because only a subset of mutation carriers is thought to develop overt disease. For *BMPR2* mutation carriers, penetrance is estimated to be ∼27% (14–42%) (28–30, 80, 81). As such, additional stimuli have been proposed as "second hits," which could potentially decrease BMPRII expression or activity below a certain threshold necessary for disease. Inflammation is considered one likely candidate for a second hit in PAH (82, 83). In animal models, inflammation precedes clear evidence of structural alterations and might be a key determinant of disease onset and progression (84). Multiple classes of immune cells, including macrophages, T cells, and neutrophils, have been identified in the vicinity of remodeled pulmonary arteries of PAH patients and PAH rodent models (**Figure 1**) (85, 86). Furthermore, inflammatory gene signatures have been found in cardiac and pulmonary tissues from patients and animal models of PAH (87).

Multiple lines of evidence indicate a close relationship between inflammation and BMPRII pathway signaling during PAH pathogenesis. For example, mice heterozygous for a *Bmpr2* null allele, but not wild-type controls, become more likely to develop PAH-like disease when overexpressing 5-lipoxygenase, which causes a sustained inflammatory response (88). Similarly, *Bmpr2* haploinsufficient rats are more prone to inflammation-induced PAH and exhibit evidence of apoptosis-resistant and proliferative ECs and enhanced mesenchymal transformation (89). Impaired BMPRII activity is also associated with pulmonary overexpression of inflammatory mediators including interleukin-6 (IL-6) and granulocyte-macrophage colony-stimulating factor, which are involved in leukocyte recruitment and PAH pathogenesis (90–92). Finally, mice with *Bmpr2* ablated from monocyte-lineage macrophages exhibited muscularized pulmonary arteries and increased right ventricular systolic pressure after Sugen-hypoxia treatment while depletion of macrophages with clodronate reversed these parameters (43). Together, these studies suggest that BMPRII-mediated signaling within the pulmonary vasculature normally protects against inflammation-induced vascular remodeling.

If levels of BMPRII activity become deficient, then otherwise innocuous inflammatory signals could initiate a feed-forward loop of pathological signaling by TGF-β (36), activin-class ligands (13), and other proinflammatory cytokines (43). IL-6 is a key inflammatory signal upregulated in the serum and lungs of patients with PAH (93). Transgenic mice overexpressing IL-6 in the lungs exhibit pulmonary arterial muscularization and proliferative arteriopathy, indicating that this molecule regulates multiple pathologic remodeling processes in PAH (90). At least some of these effects in IL-6 transgenic mice are probably mediated by enhanced TGF-β signaling, as IL-6 has been demonstrated to augment TGF-β1 responses by reducing turnover of TGF-β receptors from the plasma membrane (94). The observation that BMPRII pathway signaling normally inhibits IL-6 expression in pulmonary vasculature suggests a potential mechanism by which *BMPR2* haploinsufficiency provides a vulnerable setting for runaway inflammatory and fibrotic signaling (95).

INTERPLAY BETWEEN MECHANOBIOLOGY AND TGF-β SUPERFAMILY SIGNALING IN PAH

Biomechanical forces attributable to arterial physical properties and blood flow play prominent roles in vascular remodeling. Together with inflammatory signals, biomechanical forces and TGF-β superfamily signaling interact reciprocally during vascular homeostasis and disease initiation (96). Pathologic

vascular remodeling in PAH is characterized both by narrowing of the distal pulmonary arterioles and resultant dilation of the larger, more proximal arteries. Changes in the width of the vessel lumen are accompanied by increased thickness and stiffness of vessel walls, properties that together reinforce the development of turbulent blood flow patterns throughout the pulmonary arterial tree (**Figure 1**). Turbulent flow itself in turn contributes to dysfunction and excessive proliferation of ECs, leading to neointimal lesions, and vascular occlusion (75). These structural, biomechanical, and proliferative changes could establish a positive feedback loop of pathologic vascular remodeling, especially around vascular branch points where turbulent flow forces are most pronounced. Indeed, neointimal lesions of proliferative ECs are found primarily at branch points (75). Furthermore, detailed temporal analysis in rodent PAH models reveals that arterial stiffening occurs early in the disease process, prior to hemodynamic changes and right ventricular dysfunction, suggesting that vessel wall stiffening is one determinant of disease onset (97).

Changes in the mechanical properties of pulmonary blood flow are interpreted by TGF-β superfamily receptors located in endothelial cells and affect changes in canonical superfamily signaling pathways. For example, steady-state laminar flow, the pattern typical of healthy vasculature, promotes EC quiescence by facilitating activation of the BMPRII-SMAD1/5/8 axis (**Figure 1**) (98). This signaling pathway prevents cell cycle progression by ECs and contributes to the stabilization of EC cellular junctions, preventing vascular remodeling processes. Laminar blood flow also promotes expression of the key BMPRII partner ALK1 (98) and promotes its association with the coreceptor endoglin, mechanisms that sensitize ECs to BMP9 signaling and aid in BMPRII pathway activation (99, 100). ALK1 therefore acts as a critical molecular link between blood flow and vascular quiescence (101). Furthermore, caveolin-1, itself a PAH risk factor that is regulated by shear stress forces, is required for proper membrane localization of BMPRII (102, 103). In elegant contrast with the quiescence-promoting role for the BMPRII pathway, disturbed flow patterns stimulate arterial remodeling through a mechanism dependent upon endothelial SMAD2/3 and ALK5 signaling (104, 105). These studies suggest an interesting model for the onset of PAH pathogenesis in which loss of BMPRII or one of its signaling partners removes a flow-regulated brake upon SMAD2/3-driven remodeling processes by pulmonary vascular ECs. Inflammation could enhance this pathogenic process by further diminishing BMPRII levels, and remodeling could beget further remodeling by disrupting laminar flow patterns important for BMPRII pathway activity (**Figure 1**).

TGF-β isoforms are prominent among superfamily ligands that require mechanical activation from a latent state to engage cognate receptors (8). Briefly, TGF-β isoforms are synthesized as inactive precursors consisting of a prodomain—referred to as the latency-associated peptide (LAP)—together with the mature ligand and are attached to extracellular matrix proteins through association with latent TGF-β binding proteins (LTBPs). Release of an active signaling domain from the inert TGF-β/LTBP complex depends upon the physical stiffness of the extracellular environment. Thus, it has long been hypothesized that pathologic TGF-β signaling in PAH and related fibrotic conditions operates through a positive feedback loop of extracellular matrix deposition, increased stiffness, and further TGF-β activation (106, 107). Proper sequestration of latent TGF-β complexes by LTBP proteins is known to be critical for the spatial and temporal regulation of TGF-β activation during homeostasis and disease (108) and might facilitate rapid signaling responses to physical insults. As discussed further below, the many types of proteins that control TGF-β localization and activity, including RGD-integrins, metalloproteinases, and thrombospondin-1, provide potential therapeutic targets for PAH treatment (109).

TARGETING DEFICIENT SMAD1/5/8 PATHWAY SIGNALING

In the two decades since BMPRII deficiency was first implicated in the development of PAH, many approaches to promote SMAD1/5/8 pathway signaling in the pulmonary vasculature have been evaluated in PAH models and, in a few cases, clinically (**Table 1**).

Restoration of BMPRII Expression

Preclinical studies have investigated delivery of the wild-type *BMPR2* gene by various methods to remedy BMPRII deficiency (110, 111, 132–134). These studies indicate that delivery of exogenous *BMPR2* to the pulmonary vascular endothelium can improve cardiopulmonary parameters in two different rodent models of PAH, in some cases on a preventive basis and in other cases therapeutically. As noted previously (15), two limitations of using viral vectors to deliver *BMPR2* to the endothelium are the transient nature of adenoviral transgene expression and the potential for deleterious mutations following genomic integration. Alternative methods of *BMPR2* delivery are therefore under investigation (134, 135). *BMPR2* gene delivery has not yet been studied clinically.

Epigenetic mechanisms, notably including hypermethylation of the *BMPR2* promoter, are implicated in PAH pathogenesis (136). The transcriptional regulator switch-independent 3a (*SIN3a*), recently found to be dysregulated in PAH patients and rodent models, promotes *BMPR2* expression in PASMCs through demethylation of its promoter (112). Increased BMPRII levels in these cells were accompanied by higher levels of pSMAD1/5/8, confirming activation of this pathway. Intratracheal delivery of *SIN3a* by adenoviral vector restored BMPRII expression, increased levels of pSMAD1/5/8, and improved cardiopulmonary endpoints in two rat models of PAH (112). This virally mediated approach to indirectly elevating *BMPR2* expression is associated with the same limitations as those noted above for direct *BMPR2* delivery. In addition, as it relies on the endogenous *BMPR2* gene, this approach is expected to be more effective in patients with reduced expression of wild-type *BMPR2* than in patients harboring *BMPR2* inactivating mutations.

Other diverse approaches for elevating BMPRII levels have yielded positive results in preclinical models of PAH. A promising approach involves activation of the orphan nuclear receptor Nur77, which is a key regulator of proliferation

TABLE 1 | Agents targeting canonical TGF-β superfamily pathways for PAH.

Pathway branch	Target	Agent and mechanism	Preclinical activity	Clinical evaluation		
				Study type	NCT ID	Status
SMAD1/5/8	*BMPR2* gene	AdBMPR2 + Fab-9B9 or AdCMVBMPR2myc + Fab-9B9 (adenoviral delivery)	(110, 111)	–	–	–
	BMPR2 promoter hypermethylation	Adenoviral delivery of *SIN3a*	(112)	–	–	–
	BMPRII	miR-20a inhibitor (antagomiR disinhibits BMPRII expression)	(113)	–	–	–
		6-Mercaptopurine (activation of Nur77)	(114)	–	–	–
		4-Phenylbutyrate (rescue of misfolded BMPRII)	(115)	–	–	–
		Ataluren/PTC124 (translational read-through of premature termination mutations)	(116)	–	–	–
	BMP9	Recombinant BMP9 (activation of BMPRII)	(117)	–	–	–
		Anti-BMP9 antibody (immunoneutralization)	(118)	–	–	–
	BMP2, BMP4, BMP7	Anti-gremlin1 antibody (disinhibition of specific BMPs)	(119)	–	–	–
	BMPRII-ALK1 signaling	FK506/tacrolimus (disinhibition of ALK1)	(120, 121)	Phase 2a	01647945	(122)
				Other	–	(123)
	Downstream target genes	Stabilized apelin analogs (activation of APJ)	(124, 125)	Other	01457170	(126)
		Nutlin-3 (rescue of p53-PPARγ complex)	(127)	–	–	–
SMAD2/3	ALK5	SD-208, SB-525334 (TKI)	(128, 129)	–	–	–
	ALK5, TGFBRII	Anti-TGF-β receptor antibody (immunoneutralization)	(64)	–	–	–
	TGF-β1, TGF-β2, TGF-β3	Pan anti-TGF-β antibody (multi-ligand sequestration)	(63)	–	–	–
	TGF-β1, TGF-β3	TGFBRII-Fc (multi-ligand sequestration)	(57)	–	–	–
	Latent TGF-β stabilization	LSKL peptide (competitive antagonism of thrombospondin-1)	(130)	–	–	–
	Activin-class ligands (activin A, GDF8, GDF11, activin B)	ActRIIA-Fc (multi-ligand sequestration)	(13)	Phase 2	03496207	(131)
				Phase 2a	03738150	Ongoing
				Phase 3	04576988	Ongoing
					04811092	Ongoing
					04896008	Ongoing

APJ, apelin receptor; PPARγ, peroxisome proliferator-activated receptor gamma; TKI, tyrosine kinase inhibitor.

and inflammation in vascular cells. Treatment with 6-mercaptopurine increases expression of Nur77, BMPRII, pSMAD1/5/8, and target gene Id3 in pulmonary arterioles in a rat model of severe angioproliferative PAH (114). Moreover, therapeutic treatment with 6-mercaptopurine reversed abnormal vascular remodeling and RV hypertrophy in this model (114). In another approach, an antagonistic modified RNA oligonucleotide (antagomiR), which selectively targets the *BMPR2* negative regulator miR-20a, increased levels of BMPRII expression in lung tissue and improved cardiopulmonary parameters in a hypoxia-induced mouse model of PAH (113). A limitation of this study is that it did not evaluate therapeutic treatment in the context of established vascular pathology, which would better model the disease state in PAH patients with ongoing vascular remodeling. Other approaches have increased pulmonary expression of BMPRII in mice harboring certain *BMPR2* mutations either by rescuing misfolded BMPRII from the endoplasmic reticulum (115) or by facilitating translational read-through of premature *BMPR2* termination mutations (116). Such approaches provide support for future clinical evaluation in PAH patients with specific *BMPR2* mutations (116).

Of special note, the herbally-derived agent berberine was reported to improve cardiopulmonary endpoints in a hypoxia-induced mouse model by elevating expression of BMPRII and pSMAD1/5/8 while also reducing expression of TGF-β and pSMAD2/3 (137). Although investigation of target identity and further study are warranted, protective effects of berberine in this model underscore the potential benefit of rebalancing TGF-β superfamily signaling in PAH.

Stimulation With Exogenous BMPs

The finding that exogenous BMP9 can reverse established disease in rodent models of PAH (117) suggested that a similar approach could be beneficial in patients. However, this strategy is controversial because subsequent preclinical studies indicate that the role of BMP9 in pulmonary vascular homeostasis is complex and likely context dependent (118, 138–140). Importantly, loss of BMPRII reverses the endothelial response to BMP9, paradoxically causing enhanced proliferation (138), and BMP9 promotes pulmonary vascular remodeling in mice under conditions of chronic hypoxia (139). Even if these conflicting aspects of BMP9 function were to be resolved in favor of a beneficial role in PAH, the clinical value of this approach would depend on development of BMP9 agonists with extended circulating half-lives to avoid impractical dosing regimens in patients.

Disinhibition of Endogenous BMPs

BMP2, BMP4, and BMP7 exert anti-proliferative effects in pulmonary vessels through SMAD1/5/8 pathway activation. These ligands are selectively inhibited by the endogenous BMP antagonist gremlin-1, which is implicated as an important promoter of pathologic vascular remodeling in PAH (**Figure 1**) (141). Circulating levels of gremlin-1 stratify survival in PAH patients, hypoxia stimulates gremlin secretion by ECs, and *Grem1* haploinsufficiency reduces vascular remodeling in mice exposed to chronic hypoxia (41, 42). In addition, stretch-dependent secretion of gremlin-1 from pulmonary arterial cells is implicated in PAH induced by congenital systemic-to-pulmonary shunts and could potentially explain deficient BMPRII-pathway signaling in the many such patients whose *BMPR2* expression is normal (142). Importantly, therapeutic immunoneutralization of gremlin-1 reduces vascular remodeling in a mouse model of PAH (119). Despite its potential as a therapeutic candidate for PAH, anti–gremlin-1 antibody has not been evaluated clinically to our knowledge.

Disinhibition of BMPRII/ALK1 Signaling

The immunosuppressive agent tacrolimus (FK506) has been evaluated more extensively than other activators of SMAD1/5/8 pathway signaling as a potential treatment for PAH. A large-scale screen of FDA-approved drugs identified FK506 as an effective BMPRII signaling activator that disinhibits ALK1 kinase activity through inhibition of the immunophilin FK-binding protein-12 (120). FK506 reversed dysfunctional BMPRII signaling in pulmonary ECs from patients with idiopathic PAH and reversed cardiopulmonary functional deficits and vascular remodeling when administered therapeutically in a rat model of severe angio-obliterative PAH (120). Based on these promising preclinical results, FK506 was assessed in a phase 2a tolerability and safety study in PAH patients (NCT01647945, $N = 23$), but the results were inconclusive (122) and could warrant follow-up evaluation in a larger patient population. Intriguingly, FK506 treatment at this dose led to substantial improvement and stabilization of cardiovascular function in three patients with end-stage PAH who did not qualify for the foregoing trial (123). Recent findings suggest that targeting the BMPRII pathway with FK506 may exert direct protective effects on the right ventricle independent of its beneficial effects on the pulmonary vasculature (121).

Activation of Downstream Genes in Defective BMPRII Pathway

An alternative strategy to increase SMAD1/5/8 pathway activity is to promote expression of its downstream targets. One prominent target of BMPRII-mediated signaling in the endothelium is apelin (143), a peptide ligand of the apelin receptor whose activation opposes the renin-angiotensin-aldosterone system and regulates cardiovascular functions including hemodynamic homeostasis (144, 145). A genetic approach was used to identify apelin as a target gene of the BMP pathway in endothelial cells, and BMPRII-SMAD1/5/8 signaling was found to mediate downregulation of apelin expression by BMPs in such cells (146). However, the direction of this response is difficult to reconcile with later studies revealing apelin insufficiency in PAH lung and implicating apelin as beneficial in the context of PAH and cardiovascular disease more broadly. For example, circulating apelin levels are reduced in patients with PH, and apelin deficiency worsens hypoxia-induced PH in mice (147). Administration of a stabilized apelin analog, pyroglutamylated apelin-13, improves cardiopulmonary parameters in a monocrotaline rat model of PAH (124). In PAH patients undergoing right heart catheterization (NCT01457170, $N = 19$), this apelin analog reduced pulmonary vascular resistance and increased cardiac output without reducing mean pulmonary arterial pressure (126). Apelin receptor agonists with extended circulating half-lives are under development (125, 144), but substantial improvement will be needed for their use to become practical in a chronic clinical setting.

Additional agents have been evaluated preclinically as therapeutic activators of downstream targets in the SMAD1/5/8 pathway. One is nutlin-3, a small molecule which stabilizes a BMPRII-dependent transcription factor complex between p53 and PPARγ (peroxisome proliferator-activated receptor gamma) to activate a vasculoprotective gene regulation program downstream of BMPRII that includes the apelin gene (*APLN*) (127). This approach has been used to regenerate pulmonary microvessels and reverse persistent PH in mice with loss of BMPRII in pulmonary arterial ECs (127). Another therapeutic agent that can promote expression of BMPRII pathway effectors is tyrphostin-AG1296, a small-molecule tyrosine kinase inhibitor identified by screening compounds for improved survival of ECs from PAH patients (148). The tyrphostin-AG1296 mechanism of action remains to be defined but involves combined upregulation of BMPRII, SMAD1/5 coactivators, and cAMP response element-binding proteins, leading to an anti-PAH gene expression signature.

TARGETING OVERACTIVE SMAD2/3 PATHWAY SIGNALING

Inhibitors of the SMAD2/3 pathway have also been explored for treatment of PAH (**Table 1**) and could theoretically be used in combination with activators of the SMAD1/5/8 pathway as a strategy to rebalance superfamily signaling. As noted for

berberine in the preceding section, some individual agents could potentially exert superfamily rebalancing effects through complementary actions on both SMAD pathways, either directly or indirectly through known mechanistic links between them.

TGF-β

TGF-β inhibition was proposed more than a decade ago as a potential therapeutic approach to treat PAH (57, 63, 64, 128, 129, 149–151). Given the prominent roles of TGF-β in fibrotic diseases and cancer, diverse therapeutic approaches for inhibiting TGF-β-mediated signaling are being explored preclinically and clinically for those indications (152, 153) and could potentially be useful for treating PAH. Recent evidence indicates that there could be differential involvement of TGF-β-mediated signaling in patients with idiopathic PAH compared to those with hereditary PAH as well as differential involvement in rodent models of the disease (154).

Inhibition of TGF-β Receptors

Small-molecule inhibitors of ALK5 display efficacy in rodent models of PAH (128, 129) but have not been evaluated in PAH patients due in part to safety concerns and the potential for off-target effects (155). Such tyrosine kinase inhibitors are not selective for ALK5, as they also inhibit the closely related ALK4 and ALK7 receptors, which mediate activin signaling (156). Additionally, ALK5 inhibition is not selective for TGF-β signaling because this type I receptor also mediates signaling by GDF11 (71, 72). An antibody capable of inhibiting both type I and type II receptors for TGF-β was reported to be efficacious in a monocrotaline rat model of PAH (64), but such receptor immunoneutralization has not been evaluated in patients with PAH.

Inhibition of Active TGF-β Isoforms

More selective methods of TGF-β inhibition, including a pan anti–TGF-β antibody and a TGFBRII-Fc fusion protein that selectively sequesters TGF-β1 and TGF-β3, have displayed efficacy in rodent models of PAH (57, 63). Isoform selectivity in the latter case is thought to be advantageous partly due to major involvement of TGF-β2 in cardiac valve homeostasis and thus cardiotoxicity associated with ALK5 inhibition [see citations in ref. (57)]. These approaches for targeting TGF-β isoforms have not yet been evaluated clinically in PAH.

Stabilization of Latent TGF-β

An intensely explored approach to inhibit TGF-β signaling involves stabilization of latent ligand normally sequestered in the extracellular matrix, thereby preventing release of TGF-β and its binding to receptors. Such activation is regulated endogenously by interaction of TGF-β-containing latent complexes with several types of proteins, including integrins, proteases, thrombospondin-1, and glycoprotein-A repetitions predominant protein (GARP) (157–159). Thrombospondin-1 is implicated preclinically in PH caused by either hypoxia or the parasite *Schistosoma mansoni*, and thrombospondin-1 inhibition by the synthetic tetrapeptide Leu-Ser-Lys-Leu protects mice from PH caused by either factor (130). Further reinforcing the vascular connection, thrombospondin-1 contributes to arterial stiffening caused by disturbed blood flow (160). Although not investigated in experimental PAH, integrin inhibitors and antibody-mediated stabilization of latent TGF-β display efficacy in models of fibrosis or cancer (161–164), providing preclinical support for such approaches generally. Because endogenous mechanisms of TGF-β activation vary depending on cellular and tissue context (158), the therapeutic effects produced by the foregoing approaches would be predicted to differ according to their respective targets. Moreover, such approaches targeting TGF-β regulation would likely produce a subset of the effects seen by directly targeting active TGF-β isoforms and therefore provide precision which could be advantageous in certain contexts.

Inhibition of Activin-Class Ligands

Activin-class members of the SMAD2/3 signaling pathway have only recently been recognized widely as important contributors to PAH pathogenesis. Most prominent is the ligand trapping fusion protein ActRIIA-Fc, also known as sotatercept, which sequesters the activin-class ligands activin A, activin B, GDF8, and GDF11 with high affinity (165). As noted above, at least three of these ligands are upregulated in pulmonary vascular lesions of PAH patients and PAH rodent models (13). Protective administration of a murine ActRIIA-Fc fusion protein in rodent models markedly improves cardiopulmonary parameters and vascular remodeling, and therapeutic administration of this agent in a Sugen-hypoxia-normoxia model with established severe disease effectively alleviates PH and vascular remodeling (13). This activity is attributable in part to anti-proliferative effects on pulmonary arterial SMCs and ECs as well as to enhanced apoptosis in the vascular wall. Improvement in right ventricular structure and function may stem from indirect effects of reduced pulmonary vascular resistance and compliance. However, it could also arise from direct cardioprotective effects of ActRIIA-Fc consistent with those described previously with inhibition of activin receptor-mediated signaling in models of left ventricular failure associated with aging or systemic pressure overload (166, 167).

A phase 2 study of ActRIIA-Fc has been conducted in patients with PAH receiving background therapy (131). In this study (NCT03496207, $N = 106$), sotatercept produced significant improvement in the primary endpoint, pulmonary vascular resistance. It was also associated with clinically meaningful improvements in 6-min walk distance and circulating levels of N-terminal pro-B-type natriuretic peptide, a marker for cardiac dysfunction. Sotatercept has previously been evaluated in healthy volunteers and patients with conditions characterized by dysfunctional TGF-β superfamily signaling, including anemia associated with myelodysplastic syndromes, anemia associated with β-thalassemia, chemotherapy-induced anemia, end-stage kidney disease, bone loss, and multiple myeloma (168–174). As a result, substantial data are already available regarding sotatercept's safety profile. Ongoing clinical studies of sotatercept in PAH patients include a phase 2 study for detailed characterization of cardiopulmonary status by right heart catheterization with exercise (NCT03738150) and several phase 3 registration-enabling studies (NCT04576988,

NCT04811092, NCT04896008). Interestingly, several clinical studies have determined that sotatercept increases circulating hemoglobin concentrations under diverse conditions (169, 171–174). It has been observed that a large proportion of PAH patients exhibits anemia and could therefore receive sotatercept with acceptable erythropoietic effects (175). Further study is required to determine the potential benefits of increasing hemoglobin levels concurrently with targeting cardiopulmonary remodeling in PAH patients, particularly those with anemia.

CONCLUSIONS

Our growing understanding of mechanisms responsible for initiation and progression of PAH has not yet been matched by development of therapies effectively targeting those underlying disease processes. The TGF-β superfamily of ligands and receptors plays a critical role in the development and severity of PAH. More precisely, an imbalance in the intracellular SMAD2/3 vs. SMAD1/5/8 signaling pathways is now widely accepted to be an important contributor. Therapies targeting these two SMAD pathway branches have been evaluated preclinically and are in a few cases in clinical development. Importantly, there are indications that therapeutic interventions targeting the TGF-β superfamily have the potential to be disease modifying. Indeed, preclinical and clinical data generated with an ActRIIA-Fc ligand trap in particular support the view that targeting cellular proliferation through a rebalancing of SMAD activation could be a beneficial therapeutic approach for the underserved PAH patient population.

Further work is needed to establish whether other therapeutic modalities such as those targeting mechanisms of latent ligand activation could be developed to either reduce pro-proliferative or enhance anti-proliferative TGF-β superfamily pathways. Other interesting but underexplored possibilities are that either concomitant modulation of SMAD2/3 and SMAD1/5/8 pathways or combined inhibition of SMAD2/3 pathway-activating ligands (activin-class ligands together with one or more TGF-βs) could provide benefits beyond those observed to date with more restricted approaches. Such combinatorial strategies might also be useful in the context of Group 3 PH, a disease category characterized by pulmonary vasculopathy with fibrotic lung disease, most notably in subgroups associated with interstitial lung disease (PH-ILD) or chronic obstructive pulmonary disease (PH-COPD). In addition, it remains to be determined whether precisely targeting a single intracellular TGF-β superfamily pathway, including canonical and non-canonical effectors, could offer a different therapeutic window or greater ease of use than inhibition of ligand-receptor interactions. Hence, two decades after the seminal observations linking familial PAH with TGF-β superfamily signaling, there are signs that targeting this pathway—now thought to control multiple PAH disease processes—could offer hope for transformative PAH treatments.

AUTHOR CONTRIBUTIONS

PA, SB, and MA drafted the manuscript. PA, SJ, SB, MA, GL, and RK revised the manuscript critically for intellectual content. All authors contributed to the article and approved the submitted version.

FUNDING

The authors were supported by funding provided by Acceleron Pharma.

REFERENCES

1. Humbert M, Guignabert C, Bonnet S, Dorfmuller P, Klinger JR, Nicolls MR, et al. Pathology and pathobiology of pulmonary hypertension: state of the art and research perspectives. *Eur Respir J.* (2019) 53:2018. doi: 10.1183/13993003.01887-2018
2. Maron BA, Abman SH, Elliott CG, Frantz RP, Hopper RK, Horn EM, et al. Pulmonary arterial hypertension: diagnosis, treatment, and novel advances. *Am J Respir Crit Care Med.* (2021) 203:1472–87. doi: 10.1164/rccm.202012-4317SO
3. Sakao S, Tatsumi K, Voelkel NF. Endothelial cells and pulmonary arterial hypertension: apoptosis, proliferation, interaction and transdifferentiation. *Respir Res.* (2009) 10:95. doi: 10.1186/1465-9921-10-95
4. Humbert M, Monti G, Fartoukh M, Magnan A, Brenot F, Rain B, et al. Platelet-derived growth factor expression in primary pulmonary hypertension: comparison of HIV seropositive and HIV seronegative patients. *Eur Respir J.* (1998) 11:554–9.
5. Schermuly RT, Dony E, Ghofrani HA, Pullamsetti S, Savai R, Roth M, et al. Reversal of experimental pulmonary hypertension by PDGF inhibition. *J Clin Invest.* (2005) 115:2811–21. doi: 10.1172/JCI24838
6. Ghofrani HA, Morrell NW, Hoeper MM, Olschewski H, Peacock AJ, Barst RJ, et al. Imatinib in pulmonary arterial hypertension patients with inadequate response to established therapy. *Am J Respir Crit Care Med.* (2010) 182:1171–7. doi: 10.1164/rccm.201001-0123OC
7. Frost AE, Barst RJ, Hoeper MM, Chang HJ, Frantz RP, Fukumoto Y, et al. Long-term safety and efficacy of imatinib in pulmonary arterial hypertension. *J Heart Lung Transplant.* (2015) 34:1366–75. doi: 10.1016/j.healun.2015.05.025
8. Derynck R, Budi EH. Specificity, versatility, and control of TGF-β family signaling. *Sci Signal.* (2019) 12:aav5183. doi: 10.1126/scisignal.aav5183
9. Takeda N, Hara H, Fujiwara T, Kanaya T, Maemura S, Komuro I. TGF-β signaling-related genes and thoracic aortic aneurysms and dissections. *Int J Mol Sci.* (2018) 19:2125. doi: 10.3390/ijms19072125
10. Goumans MJ, Zwijsen A, ten Dijke P, Bailly S. Bone morphogenetic proteins in vascular homeostasis and disease. *Cold Spring Harb Perspect Biol.* (2018) 10:a031989. doi: 10.1101/cshperspect.a031989
11. Verzola D, Milanesi S, Bertolotto M, Garibaldi S, Villaggio B, Brunelli C, et al. Myostatin mediates abdominal aortic atherosclerosis progression by inducing vascular smooth muscle cell dysfunction and monocyte recruitment. *Sci Rep.* (2017) 7:46362. doi: 10.1038/srep46362
12. Esposito P, Verzola D, Picciotto D, Cipriani L, Viazzi F, Garibotto G. Myostatin/activin-A signaling in the vessel wall and vascular calcification. *Cells.* (2021) 10:2070. doi: 10.3390/cells10082070
13. Yung LM, Yang P, Joshi S, Augur ZM, Kim SSJ, Bocobo GA, et al. ACTRIIA-Fc rebalances activin/GDF versus BMP signaling in pulmonary hypertension. *Sci Transl Med.* (2020) 12:aaz5660. doi: 10.1126/scitranslmed.aaz5660
14. Guignabert C, Humbert M. Targeting transforming growth factor-β receptors in pulmonary hypertension. *Eur Respir J.* (2021) 57:2002341. doi: 10.1183/13993003.02341-2020
15. Dunmore BJ, Jones RJ, Toshner MR, Upton PD, Morrell NW. Approaches to treat pulmonary arterial hypertension by targeting BMPR2: from

cell membrane to nucleus. *Cardiovasc Res.* (2021) 117:2309–25. doi: 10.1093/cvr/cvaa350
16. Sharmin N, Nganwuchu CC, Nasim MT. Targeting the TGF-β signaling pathway for resolution of pulmonary arterial hypertension. *Trends Pharmacol Sci.* (2021) 42:510–3. doi: 10.1016/j.tips.2021.04.002
17. Lodberg A. Principles of the activin receptor signaling pathway and its inhibition. *Cytokine Growth Factor Rev.* (2021) 60:1–17. doi: 10.1016/j.cytogfr.2021.04.001
18. Tielemans B, Delcroix M, Belge C, Quarck R. TGFβ and BMPRII signalling pathways in the pathogenesis of pulmonary arterial hypertension. *Drug Discov Today.* (2019) 24:703–16. doi: 10.1016/j.drudis.2018.12.001
19. Orriols M, Gomez-Puerto MC, ten Dijke P. BMP type II receptor as a therapeutic target in pulmonary arterial hypertension. *Cell Mol Life Sci.* (2017) 74:2979–95. doi: 10.1007/s00018-017-2510-4
20. Dannewitz Prosseda S, Ali MK, Spiekerkoetter E. Novel advances in modifying BMPR2 signaling in PAH. *Genes.* (2021) 12:8. doi: 10.3390/genes12010008
21. Mu Y, Gudey SK, Landstrom M. Non-Smad signaling pathways. *Cell Tissue Res.* (2012) 347:11–20. doi: 10.1007/s00441-011-1201-y
22. Zhang YE. Non-smad signaling pathways of the TGF-β family. *Cold Spring Harb Perspect Biol.* (2017) 9:a022129. doi: 10.1101/cshperspect.a022129
23. Trojanowska M. Noncanonical transforming growth factor β signaling in scleroderma fibrosis. *Curr Opin Rheumatol.* (2009) 21:623–9. doi: 10.1097/BOR.0b013e32833038ce
24. Finnson KW, Almadani Y, Philip A. Non-canonical (non-SMAD2/3) TGF-β signaling in fibrosis: mechanisms and targets. *Semin Cell Dev Biol.* (2020) 101:115–22. doi: 10.1016/j.semcdb.2019.11.013
25. Meng XM, Nikolic-Paterson DJ, Lan HY. TGF-β: the master regulator of fibrosis. *Nat Rev Nephrol.* (2016) 12:325–38. doi: 10.1038/nrneph.2016.48
26. Lane KB, Machado RD, Pauciulo MW, Thomson JR, Phillips JA III, Loyd JE, et al. Heterozygous germline mutations in BMPR2, encoding a TGF-β receptor, cause familial primary pulmonary hypertension. *Nat Genet.* (2000) 26:81–4. doi: 10.1038/79226
27. Deng Z, Morse JH, Slager SL, Cuervo N, Moore KJ, Venetos G, et al. Familial primary pulmonary hypertension (gene PPH1) is caused by mutations in the bone morphogenetic protein receptor-II gene. *Am J Hum Genet.* (2000) 67:737–44. doi: 10.1086/303059
28. Newman JH, Trembath RC, Morse JA, Grunig E, Loyd JE, Adnot S, et al. Genetic basis of pulmonary arterial hypertension: current understanding and future directions. *J Am Coll Cardiol.* (2004) 43(12 Suppl S):S33–9. doi: 10.1016/j.jacc.2004.02.028
29. Cogan JD, Pauciulo MW, Batchman AP, Prince MA, Robbins IM, Hedges LK, et al. High frequency of BMPR2 exonic deletions/duplications in familial pulmonary arterial hypertension. *Am J Respir Crit Care Med.* (2006) 174:590–8. doi: 10.1164/rccm.200602-165OC
30. Aldred MA, Vijayakrishnan J, James V, Soubrier F, Gomez-Sanchez MA, Martensson G, et al. BMPR2 gene rearrangements account for a significant proportion of mutations in familial and idiopathic pulmonary arterial hypertension. *Hum Mutat.* (2006) 27:212–3. doi: 10.1002/humu.9398
31. Atkinson C, Stewart S, Upton PD, Machado R, Thomson JR, Trembath RC, et al. Primary pulmonary hypertension is associated with reduced pulmonary vascular expression of type II bone morphogenetic protein receptor. *Circulation.* (2002) 105:1672–8. doi: 10.1161/01.CIR.0000012754.72951.3D
32. Andruska A, Spiekerkoetter E. Consequences of BMPR2 deficiency in the pulmonary vasculature and beyond: contributions to pulmonary arterial hypertension. *Int J Mol Sci.* (2018) 19:2499. doi: 10.3390/ijms19092499
33. Sweatt A, Wells R, Purington N, Hedlin H, Sudheendra D, Hsi A, et al. Bone morphogenetic protein receptor 2 expression is reduced in blood across pulmonary arterial hypertension subtypes but does not reflect disease severity. *Am J Respir Crit Care Med.* (2018) 197:A2449.
34. Desroches-Castan A, Tillet E, Bouvard C, Bailly S. BMP9 and BMP10: two close vascular quiescence partners that stand out. *Dev Dyn.* (2021) 2021:1–20. doi: 10.1002/dvdy.395
35. Hong KH, Lee YJ, Lee E, Park SO, Han C, Beppu H, et al. Genetic ablation of the BMPR2 gene in pulmonary endothelium is sufficient to predispose to pulmonary arterial hypertension. *Circulation.* (2008) 118:722–30. doi: 10.1161/CIRCULATIONAHA.107.736801
36. Hiepen C, Jatzlau J, Hildebrandt S, Kampfrath B, Goktas M, Murgai A, et al. BMPR2 acts as a gatekeeper to protect endothelial cells from increased TGFβ responses and altered cell mechanics. *PLoS Biol.* (2019) 17:e3000557. doi: 10.1371/journal.pbio.3000557
37. Hiepen C, Jatzlau J, Knaus P. Biomechanical stress provides a second hit in the establishment of BMP/TGFβ-related vascular disorders. *Cell Stress.* (2020) 4:44–7. doi: 10.15698/cst2020.02.213
38. Zhang S, Fantozzi I, Tigno DD Yi ES, Platoshyn O, Thistlethwaite PA, Kriett JM, et al. Bone morphogenetic proteins induce apoptosis in human pulmonary vascular smooth muscle cells. *Am J Physiol Lung Cell Mol Physiol.* (2003) 285:L740–54. doi: 10.1152/ajplung.00284.2002
39. Yang X, Long L, Southwood M, Rudarakanchana N, Upton PD, Jeffery TK, et al. Dysfunctional smad signaling contributes to abnormal smooth muscle cell proliferation in familial pulmonary arterial hypertension. *Circ Res.* (2005) 96:1053–63. doi: 10.1161/01.RES.0000166926.54293.68
40. Yang J, Davies RJ, Southwood M, Long L, Yang X, Sobolewski A, et al. Mutations in bone morphogenetic protein type II receptor cause dysregulation of Id gene expression in pulmonary artery smooth muscle cells: implications for familial pulmonary arterial hypertension. *Circ Res.* (2008) 102:1212–21. doi: 10.1161/CIRCRESAHA.108.173567
41. Cahill E, Costello CM, Rowan SC, Harkin S, Howell K, Leonard MO, et al. Gremlin plays a key role in the pathogenesis of pulmonary hypertension. *Circulation.* (2012) 125:920–30. doi: 10.1161/CIRCULATIONAHA.111.038125
42. Wellbrock J, Harbaum L, Stamm H, Hennigs JK, Schulz B, Klose H, et al. Intrinsic BMP antagonist gremlin-1 as a novel circulating marker in pulmonary arterial hypertension. *Lung.* (2015) 193:567–70. doi: 10.1007/s00408-015-9735-5
43. West JD, Chen X, Ping L, Gladson S, Hamid R, Lloyd JE, et al. Adverse effects of BMPR2 suppression in macrophages in animal models of pulmonary hypertension. *Pulm Circ.* (2019) 10:2045894019856483. doi: 10.1177/2045894019856483
44. Morrell NW, Aldred MA, Chung WK, Elliott CG, Nichols WC, Soubrier F, et al. Genetics and genomics of pulmonary arterial hypertension. *Eur Respir J.* (2019) 53:1801899. doi: 10.1183/13993003.01899-2018
45. Southgate L, Machado RD, Graf S, Morrell NW. Molecular genetic framework underlying pulmonary arterial hypertension. *Nat Rev Cardiol.* (2020) 17:85–95. doi: 10.1038/s41569-019-0242-x
46. Wang G, Fan R, Ji R, Zou W, Penny DJ, Varghese NP, et al. Novel homozygous BMP9 nonsense mutation causes pulmonary arterial hypertension: a case report. *BMC Pulm Med.* (2016) 16:17. doi: 10.1186/s12890-016-0183-7
47. Graf S, Haimel M, Bleda M, Hadinnapola C, Southgate L, Li W, et al. Identification of rare sequence variation underlying heritable pulmonary arterial hypertension. *Nat Commun.* (2018) 9:1416. doi: 10.1038/s41467-018-03672-4
48. Wang XJ, Lian TY, Jiang X, Liu SF, Li SQ, Jiang R, et al. Germline BMP9 mutation causes idiopathic pulmonary arterial hypertension. *Eur Respir J.* (2019) 53:2018. doi: 10.1183/13993003.01609-2018
49. Harrison RE, Flanagan JA, Sankelo M, Abdalla SA, Rowell J, Machado RD, et al. Molecular and functional analysis identifies ALK-1 as the predominant cause of pulmonary hypertension related to hereditary haemorrhagic telangiectasia. *J Med Genet.* (2003) 40:865–71. doi: 10.1136/jmg.40.12.865
50. Fujiwara M, Yagi H, Matsuoka R, Akimoto K, Furutani M, Imamura S, et al. Implications of mutations of activin receptor-like kinase 1 gene (ALK1) in addition to bone morphogenetic protein receptor II gene (BMPR2) in children with pulmonary arterial hypertension. *Circ J.* (2008) 72:127–33. doi: 10.1253/circj.72.127
51. Harrison RE, Berger R, Haworth SG, Tulloh R, Mache CJ, Morrell NW, et al. Transforming growth factor-β receptor mutations and pulmonary arterial hypertension in childhood. *Circulation.* (2005) 111:435–41. doi: 10.1161/01.CIR.0000153798.78540.87
52. Shintani M, Yagi H, Nakayama T, Saji T, Matsuoka R, A. new nonsense mutation of SMAD8 associated with pulmonary arterial hypertension. *J Med Genet.* (2009) 46:331–7. doi: 10.1136/jmg.2008.062703
53. Nasim MT, Ogo T, Ahmed M, Randall R, Chowdhury HM, Snape KM, et al. Molecular genetic characterization of SMAD signaling molecules

in pulmonary arterial hypertension. *Hum Mutat.* (2011) 32:1385–9. doi: 10.1002/humu.21605
54. Austin ED, Ma L, LeDuc C, Berman Rosenzweig E, Borczuk A, Phillips JA 3rd, et al. Whole exome sequencing to identify a novel gene (caveolin-1) associated with human pulmonary arterial hypertension. *Circ Cardiovasc Genet.* (2012) 5:336–43. doi: 10.1161/CIRCGENETICS.111.961888
55. Copeland CA, Han B, Tiwari A, Austin ED, Loyd JE, West JD, et al. disease-associated frameshift mutation in caveolin-1 disrupts caveolae formation and function through introduction of a de novo ER retention signal. *Mol Biol Cell.* (2017) 28:3095–111. doi: 10.1091/mbc.e17-06-0421
56. Marsboom G, Chen Z, Yuan Y, Zhang Y, Tiruppathi C, Loyd JE, et al. Aberrant caveolin-1-mediated smad signaling and proliferation identified by analysis of adenine 474 deletion mutation (c.474delA) in patient fibroblasts: a new perspective in the mechanism of pulmonary hypertension. *Mol Biol Cell.* (2017) 28:1161–283. doi: 10.1091/mbc.E16-06-0380
57. Yung LM, Nikolic I, Paskin-Flerlage SD, Pearsall RS, Kumar R, Yu PB, et al. selective transforming growth factor-β ligand trap attenuates pulmonary hypertension. *Am J Respir Crit Care Med.* (2016) 194:1140–51. doi: 10.1164/rccm.201510-1955OC
58. Botney MD, Bahadori L, Gold LI. Vascular remodeling in primary pulmonary hypertension. Potential role for transforming growth factor-β. *Am J Pathol.* (1994) 144:286–95.
59. Selimovic N, Bergh CH, Andersson B, Sakiniene E, Carlsten H, Rundqvist B. Growth factors and interleukin-6 across the lung circulation in pulmonary hypertension. *Eur Respir J.* (2009) 34:662–8. doi: 10.1183/09031936.00174908
60. Yan Y, Wang XJ Li SQ, Yang SH, Lv ZC, Wang LT, He YY, et al. Elevated levels of plasma transforming growth factor-β1 in idiopathic and heritable pulmonary arterial hypertension. *Int J Cardiol.* (2016) 222:368–74. doi: 10.1016/j.ijcard.2016.07.192
61. Li L, Zhang X, Li X, Lv C, Yu H, Xu M, et al. TGF-β1 inhibits the apoptosis of pulmonary arterial smooth muscle cells and contributes to pulmonary vascular medial thickening via the PI3K/Akt pathway. *Mol Med Rep.* (2016) 13:2751–6. doi: 10.3892/mmr.2016.4874
62. Liu Y, Cao Y, Sun S, Zhu J, Gao S, Pang J, et al. Transforming growth factor-beta1 upregulation triggers pulmonary artery smooth muscle cell proliferation and apoptosis imbalance in rats with hypoxic pulmonary hypertension via the PTEN/AKT pathways. *Int J Biochem Cell Biol.* (2016) 77(Pt A):141–54. doi: 10.1016/j.biocel.2016.06.006
63. Megalou AJ, Glava C, Vilaeti AD, Oikonomidis DL, Baltogiannis GG, Papalois A, et al. Transforming growth factor-β inhibition and endothelin receptor blockade in rats with monocrotaline-induced pulmonary hypertension. *Pulm Circ.* (2012) 2:461–9. doi: 10.4103/2045-8932.105034
64. Megalou AJ, Glava C, Oikonomidis DL, Vilaeti A, Agelaki MG, Baltogiannis GG, et al. Transforming growth factor-β inhibition attenuates pulmonary arterial hypertension in rats. *Int J Clin Exp Med.* (2010) 3:332–40.
65. Castanares C, Redondo-Horcajo M, Magan-Marchal N, ten Dijke P, Lamas S, Rodriguez-Pascual F. Signaling by ALK5 mediates TGF-β-induced ET-1 expression in endothelial cells: a role for migration and proliferation. *J Cell Sci.* (2007) 120:1256–66. doi: 10.1242/jcs.03419
66. Maruyama H, Dewachter C, Sakai S, Belhaj A, Rondelet B, Remmelink M, et al. Bosentan reverses the hypoxia-induced downregulation of the bone morphogenetic protein signaling in pulmonary artery smooth muscle cells. *Life Sci.* (2016) 159:111–5. doi: 10.1016/j.lfs.2016.05.018
67. Star GP, Giovinazzo M, Langleben D. ALK2 and BMPR2 knockdown and endothelin-1 production by pulmonary microvascular endothelial cells. *Microvasc Res.* (2013) 85:46–53. doi: 10.1016/j.mvr.2012.10.012
68. Ryanto GRT, Ikeda K, Miyagawa K, Tu L, Guignabert C, Humbert M, et al. An endothelial activin A-bone morphogenetic protein receptor type 2 link is overdriven in pulmonary hypertension. *Nat Commun.* (2021) 12:1720. doi: 10.1038/s41467-021-21961-3
69. Yu X, Chen X, Zheng XD, Zhang J, Zhao X, Liu Y, et al. Growth differentiation factor 11 promotes abnormal proliferation and angiogenesis of pulmonary artery endothelial cells. *Hypertension.* (2018) 71:729–41. doi: 10.1161/HYPERTENSIONAHA.117.10350
70. Hinck AP, Mueller TD, Springer TA. Structural biology and evolution of the TGF-β family. *Cold Spring Harb Perspect Biol.* (2016) 8:a022103. doi: 10.1101/cshperspect.a022103
71. Andersson O, Reissmann E, Ibanez CF. Growth differentiation factor 11 signals through the transforming growth factor-β receptor ALK5 to regionalize the anterior–posterior axis. *EMBO Rep.* (2006) 7:831–7. doi: 10.1038/sj.embor.7400752
72. Goebel EJ, Corpina RA, Hinck CS, Czepnik M, Castonguay R, Grenha R, et al. Structural characterization of an activin class ternary receptor complex reveals a third paradigm for receptor specificity. *Proc Natl Acad Sci USA.* (2019) 116:15505–13. doi: 10.1073/pnas.1906253116
73. Fennen M, Weinhage T, Kracke V, Intemann J, Varga G, Wehmeyer C, et al. A myostatin-CCL20–CCR6 axis regulates Th17 cell recruitment to inflamed joints in experimental arthritis. *Sci Rep.* (2021) 11:14145. doi: 10.1038/s41598-021-93599-6
74. Pucci G, Ministrini S, Nulli Migliola E, Nunziangeli L, Battista F, D'Abbondanza M, et al. Relationship between serum myostatin levels and carotid-femoral pulse wave velocity in healthy young male adolescents. The Maciste Study. *J Appl Physiol.* (2021) 1:987–92. doi: 10.1152/japplphysiol.00782.2020
75. van der Feen DE, Bartelds B, de Boer RA, Berger RMF. Assessment of reversibility in pulmonary arterial hypertension and congenital heart disease. *Heart.* (2019) 105:276–82. doi: 10.1136/heartjnl-2018-314025
76. Sun T, Huang Z, Liang WC, Yin J, Lin WY, Wu J, et al. TGFβ2 and TGFβ3 isoforms drive fibrotic disease pathogenesis. *Sci Transl Med.* (2021) 13:abe0407. doi: 10.1126/scitranslmed.abe0407
77. Shin JY, Beckett JD, Bagirzadeh R, Creamer TJ, Shah AA, McMahan Z, et al. Epigenetic activation and memory at a TGFB2 enhancer in systemic sclerosis. *Sci Transl Med.* (2019) 11:aaw0790. doi: 10.1126/scitranslmed.aaw0790
78. Katsuno Y, Derynck R. Epithelial plasticity, epithelial-mesenchymal transition, and the TGF-β family. *Dev Cell.* (2021) 56:726–46. doi: 10.1016/j.devcel.2021.02.028
79. Jiang Q, Liu C, Liu S, Lu W, Li Y, Luo X, et al. Dysregulation of BMP9/BMPR2/SMAD signalling pathway contributes to pulmonary fibrosis and pulmonary hypertension induced by bleomycin in rats. *Br J Pharmacol.* (2021) 178:203–16. doi: 10.1111/bph.15285
80. Larkin EK, Newman JH, Austin ED, Hemnes AR, Wheeler L, Robbins IM, et al. Longitudinal analysis casts doubt on the presence of genetic anticipation in heritable pulmonary arterial hypertension. *Am J Respir Crit Care Med.* (2012) 186:892–6. doi: 10.1164/rccm.201205-0886OC
81. Soubrier F, Chung WK, Machado R, Grunig E, Aldred M, Geraci M, et al. Genetics and genomics of pulmonary arterial hypertension. *J Am Coll Cardiol.* (2013) 62(25 Suppl):D13–D21. doi: 10.1016/j.jacc.2013.10.035
82. Dorfmüller P, Perros F, Balabanian K, Humbert M. Inflammation in pulmonary arterial hypertension. *Eur Respir J.* (2003) 22:358–63. doi: 10.1183/09031936.03.00038903
83. Vonk-Noordegraaf A, Haddad F, Chin KM, Forfia PR, Kawut SM, Lumens J, et al. Right heart adaptation to pulmonary arterial hypertension: physiology and pathobiology. *J Am Coll Cardiol.* (2013) 62(25 Suppl):D22–33. doi: 10.1016/j.jacc.2013.10.027
84. Rabinovitch M, Guignabert C, Humbert M, Nicolls MR. Inflammation and immunity in the pathogenesis of pulmonary arterial hypertension. *Circ Res.* (2014) 115:165–75. doi: 10.1161/CIRCRESAHA.113.301141
85. Savai R, Pullamsetti SS, Kolbe J, Bieniek E, Voswinckel R, Fink L, et al. Immune and inflammatory cell involvement in the pathology of idiopathic pulmonary arterial hypertension. *Am J Respir Crit Care Med.* (2012) 186:897–908. doi: 10.1164/rccm.201202-0335OC
86. van Uden D, Koudstaal T, van Hulst JAC, Bergen IM, Gootjes C, Morrell NW, et al. Central role of dendritic cells in pulmonary arterial hypertension in human and mice. *Int J Mol Sci.* (2021) 22:1756. doi: 10.3390/ijms22041756
87. Rohm I, Grun K, Muller LM, Baz L, Forster M, Schrepper A, et al. Cellular inflammation in pulmonary hypertension: detailed analysis of lung and right ventricular tissue, circulating immune cells and effects of a dual endothelin receptor antagonist. *Clin Hemorheol Microcirc.* (2019) 73:497–522. doi: 10.3233/CH-180529
88. Song Y, Jones JE, Beppu H, Keaney JF Jr, Loscalzo J, Zhang YY. Increased susceptibility to pulmonary hypertension in heterozygous BMPR2-mutant mice *Circulation.* (2005) 112:553–62. doi: 10.1161/CIRCULATIONAHA.104.492488

89. Tian W, Jiang X, Sung YK, Shuffle E, Wu TH, Kao PN, et al. Phenotypically silent bone morphogenetic protein receptor 2 mutations predispose rats to inflammation-induced pulmonary arterial hypertension by enhancing the risk for neointimal transformation. *Circulation.* (2019) 140:1409–25. doi: 10.1161/CIRCULATIONAHA.119.040629
90. Steiner MK, Syrkina OL, Kolliputi N, Mark EJ, Hales CA, Waxman AB. Interleukin-6 overexpression induces pulmonary hypertension. *Circ Res.* (2009) 104:236–44. doi: 10.1161/CIRCRESAHA.108.182014
91. Sawada H, Saito T, Nickel NP, Alastalo TP, Glotzbach JP, Chan R, et al. Reduced BMPR2 expression induces GM-CSF translation and macrophage recruitment in humans and mice to exacerbate pulmonary hypertension. *J Exp Med.* (2014) 211:263–80. doi: 10.1084/jem.20111741
92. Golembeski SM, West J, Tada Y, Fagan KA. Interleukin-6 causes mild pulmonary hypertension and augments hypoxia-induced pulmonary hypertension in mice. *Chest.* (2005) 128(6 Suppl):572S−573S. doi: 10.1378/chest.128.6_suppl.572S-a
93. Humbert M, Monti G, Brenot F, Sitbon O, Portier A, Grangeot-Keros L, et al. Increased interleukin-1 and interleukin-6 serum concentrations in severe primary pulmonary hypertension. *Am J Respir Crit Care Med.* (1995) 151:1628–31. doi: 10.1164/ajrccm.151.5.7735624
94. Zhang XL, Topley N, Ito T, Phillips A. Interleukin-6 regulation of transforming growth factor (TGF)-β receptor compartmentalization and turnover enhances TGF-β1 signaling. *J Biol Chem.* (2005) 280:12239–45. doi: 10.1074/jbc.M413284200
95. Hagen M, Fagan K, Steudel W, Carr M, Lane K, Rodman DM, et al. Interaction of interleukin-6 and the BMP pathway in pulmonary smooth muscle. *Am J Physiol Lung Cell Mol Physiol.* (2007) 292:L1473–9. doi: 10.1152/ajplung.00197.2006
96. Hiepen C, Mendez PL, Knaus P. It takes two to tango: endothelial TGFβ/BMP signaling crosstalk with mechanobiology. *Cells.* (2020) 9:1965. doi: 10.3390/cells9091965
97. Liu F, Haeger CM, Dieffenbach PB, Sicard D, Chrobak I, Coronata AM, et al. Distal vessel stiffening is an early and pivotal mechanobiological regulator of vascular remodeling and pulmonary hypertension. *JCI Insight.* (2016) 1:e86987. doi: 10.1172/jci.insight.86987
98. Laux DW, Young S, Donovan JP, Mansfield CJ, Upton PD, Roman BL. Circulating Bmp10 acts through endothelial Alk1 to mediate flow-dependent arterial quiescence. *Development.* (2013) 140:3403–12. doi: 10.1242/dev.095307
99. Baeyens N, Larrivee B, Ola R, Hayward-Piatkowskyi B, Dubrac A, Huang B, et al. Defective fluid shear stress mechanotransduction mediates hereditary hemorrhagic telangiectasia. *J Cell Biol.* (2016) 214:807–16. doi: 10.1083/jcb.201603106
100. Franco CA, Gerhardt H. Blood flow boosts BMP signaling to keep vessels in shape. *J Cell Biol.* (2016) 214:793–5. doi: 10.1083/jcb.201609038
101. Corti P, Young S, Chen CY, Patrick MJ, Rochon ER, Pekkan K, et al. Interaction between alk1 and blood flow in the development of arteriovenous malformations. *Development.* (2011) 138:1573–82. doi: 10.1242/dev.060467
102. Mathew R. Pathogenesis of pulmonary hypertension: a case for caveolin-1 and cell membrane integrity. *Am J Physiol Heart Circ Physiol.* (2014) 306:H15–25. doi: 10.1152/ajpheart.00266.2013
103. Radel C, Rizzo V. Integrin mechanotransduction stimulates caveolin-1 phosphorylation and recruitment of Csk to mediate actin reorganization. *Am J Physiol Heart Circ Physiol.* (2005) 288:H936–45. doi: 10.1152/ajpheart.00519.2004
104. Deng H, Min E, Baeyens N, Coon BG, Hu R, Zhuang ZW, et al. Activation of Smad2/3 signaling by low fluid shear stress mediates artery inward remodeling. *Proc Natl Acad Sci USA.* (2021) 118:e2105339118. doi: 10.1073/pnas.2105339118
105. Mehta V, Pang KL, Givens CS, Chen Z, Huang J, Sweet DT, et al. Mechanical forces regulate endothelial-to-mesenchymal transition and atherosclerosis via an Alk5-Shc mechanotransduction pathway. *Sci Adv.* (2021) 7:eabg5060. doi: 10.1126/sciadv.abg5060
106. Aschner Y, Downey GP. Transforming growth factor-β: master regulator of the respiratory system in health and disease. *Am J Respir Cell Mol Biol.* (2016) 54:647–55. doi: 10.1165/rcmb.2015-0391TR
107. Sun W, Chan SY. Pulmonary arterial stiffness: an early and pervasive driver of pulmonary arterial hypertension. *Front Med.* (2018) 5:204. doi: 10.3389/fmed.2018.00204
108. Su CT, Urban Z. LTBP4 in health and disease. *Genes.* (2021) 12:795. doi: 10.3390/genes12060795
109. John AE, Graves RH, Pun KT, Vitulli G, Forty EJ, Mercer PF, et al. Translational pharmacology of an inhaled small molecule αvβ6 integrin inhibitor for idiopathic pulmonary fibrosis. *Nat Commun.* (2020) 11:4659. doi: 10.1038/s41467-020-18397-6
110. McMurtry MS, Moudgil R, Hashimoto K, Bonnet S, Michelakis ED, Archer SL. Overexpression of human bone morphogenetic protein receptor 2 does not ameliorate monocrotaline pulmonary arterial hypertension. *Am J Physiol Lung Cell Mol Physiol.* (2007) 292:L872–8. doi: 10.1152/ajplung.00309.2006
111. Reynolds AM, Xia W, Holmes MD, Hodge SJ, Danilov S, Curiel DT, et al. Bone morphogenetic protein type 2 receptor gene therapy attenuates hypoxic pulmonary hypertension. *Am J Physiol Lung Cell Mol Physiol.* (2007) 292:L1182–92. doi: 10.1152/ajplung.00020.2006
112. Bisserier M, Mathiyalagan P, Zhang S, Elmastour F, Dorfmuller P, Humbert M, et al. Regulation of the methylation and expression levels of the BMPR2 gene by SIN3a as a novel therapeutic mechanism in pulmonary arterial hypertension. *Circulation.* (2021) 144:52–73. doi: 10.1161/CIRCULATIONAHA.120.047978
113. Brock M, Samillan VJ, Trenkmann M, Schwarzwald C, Ulrich S, Gay RE, et al. AntagomiR directed against miR-20a restores functional BMPR2 signalling and prevents vascular remodelling in hypoxia-induced pulmonary hypertension. *Eur Heart J.* (2014) 35:3203–11. doi: 10.1093/eurheartj/ehs060
114. Kurakula K, Sun XQ, Happe C, da Silva Goncalves Bos D, Szulcek R, Schalij I, et al. Prevention of progression of pulmonary hypertension by the Nur77 agonist 6-mercaptopurine: role of BMP signalling. *Eur Respir J.* (2019) 54:2400. doi: 10.1183/13993003.02400-2018
115. Dunmore BJ, Yang X, Crosby A, Moore S, Long L, Huang C, et al. 4PBA restores signaling of a cysteine-substituted mutant BMPR2 receptor found in patients with pulmonary arterial hypertension. *Am J Respir Cell Mol Biol.* (2020) 63:160–71. doi: 10.1165/rcmb.2019-0321OC
116. Long L, Yang X, Southwood M, Moore S, Crosby A, Upton PD, et al. Targeting translational read-through of premature termination mutations in BMPR2 with PTC124 for pulmonary arterial hypertension. *Pulm Circ.* (2020) 10:1–14. doi: 10.1177/2045894020935783
117. Long L, Ormiston ML, Yang X, Southwood M, Graf S, Machado RD, et al. Selective enhancement of endothelial BMPR-II with BMP9 reverses pulmonary arterial hypertension. *Nat Med.* (2015) 21:777–85. doi: 10.1038/nm.3877
118. Tu L, Desroches-Castan A, Mallet C, Guyon L, Cumont A, Phan C, et al. Selective BMP-9 inhibition partially protects against experimental pulmonary hypertension. *Circ Res.* (2019) 124:846–55. doi: 10.1161/CIRCRESAHA.118.313356
119. Ciuclan L, Sheppard K, Dong L, Sutton D, Duggan N, Hussey M, et al. Treatment with anti–gremlin 1 antibody ameliorates chronic hypoxia/SU5416–induced pulmonary arterial hypertension in mice. *Am J Pathol.* (2013) 183:1461–73. doi: 10.1016/j.ajpath.2013.07.017
120. Spiekerkoetter E, Tian X, Cai J, Hopper RK, Sudheendra D, Li CG, et al. FK506 activates BMPR2, rescues endothelial dysfunction, and reverses pulmonary hypertension. *J Clin Invest.* (2013) 123:3600–13. doi: 10.1172/JCI65592
121. Boehm M, Tian X, Ali MK, Mao Y, Ichimura K, Zhao M, et al. Improving right ventricular function by increasing BMP signaling with FK506. *Am J Respir Cell Mol Biol.* (2021) 65:272–87. doi: 10.1165/rcmb.2020-0528OC
122. Spiekerkoetter E, Sung YK, Sudheendra D, Scott V, Del Rosario P, Bill M, et al. Randomised placebo-controlled safety and tolerability trial of FK506 (tacrolimus) for pulmonary arterial hypertension. *Eur Respir J.* (2017) 50:1602449. doi: 10.1183/13993003.02449-2016
123. Spiekerkoetter E, Sung YK, Sudheendra D, Bill M, Aldred MA, van de Veerdonk MC, et al. Low-dose FK506 (tacrolimus) in end-stage pulmonary arterial hypertension. *Am J Respir Crit Care Med.* (2015) 192:254–7. doi: 10.1164/rccm.201411-2061LE
124. Falcão-Pires I, Gonçalves N, Henriques-Coelho T, Moreira-Gonçalves D, Roncon-Albuquerque R Jr, Leite-Moreira AF. Apelin decreases myocardial

injury and improves right ventricular function in monocrotaline-induced pulmonary hypertension. *Am J Physiol Heart Circ Physiol.* (2009) 296:H2007–14. doi: 10.1152/ajpheart.00089.2009
125. Yang P, Read C, Kuc RE, Nyimanu D, Williams TL, Crosby A, et al. A novel cyclic biased agonist of the apelin receptor, MM07, is disease modifying in the rat monocrotaline model of pulmonary arterial hypertension. *Br J Pharmacol.* (2019) 176:1206–21. doi: 10.1111/bph.14603
126. Brash L, Barnes GD, Brewis MJ, Church AC, Gibbs SJ, Howard L, et al. Short-term hemodynamic effects of apelin in patients with pulmonary arterial hypertension. *JACC Basic Transl Sci.* (2018) 3:176–86. doi: 10.1016/j.jacbts.2018.01.013
127. Hennigs JK, Cao A, Li CG, Shi M, Mienert J, Miyagawa K, et al. PPARγ-p53-mediated vasculoregenerative program to reverse pulmonary hypertension. *Circ Res.* (2021) 128:401–18. doi: 10.1161/CIRCRESAHA.119.316339
128. Long L, Crosby A, Yang X, Southwood M, Upton PD, Kim DK, et al. Altered bone morphogenetic protein and transforming growth factor-β signaling in rat models of pulmonary hypertension: potential for activin receptor-like kinase-5 inhibition in prevention and progression of disease. *Circulation.* (2009) 119:566–76. doi: 10.1161/CIRCULATIONAHA.108.821504
129. Thomas M, Docx C, Holmes AM, Beach S, Duggan N, England K, et al. Activin-like kinase 5 (ALK5) mediates abnormal proliferation of vascular smooth muscle cells from patients with familial pulmonary arterial hypertension and is involved in the progression of experimental pulmonary arterial hypertension induced by monocrotaline. *Am J Pathol.* (2009) 174:380–9. doi: 10.2353/ajpath.2009.080565
130. Kumar R, Mickael C, Kassa B, Gebreab L, Robinson JC, Koyanagi DE, et al. TGF-β activation by bone marrow-derived thrombospondin-1 causes Schistosoma- and hypoxia-induced pulmonary hypertension. *Nat Commun.* (2017) 8:15494. doi: 10.1038/ncomms15494
131. Humbert M, McLaughlin V, Gibbs JSR, Gomberg-Maitland M, Hoeper MM, Preston IR, et al. Sotatercept for the treatment of pulmonary arterial hypertension. *N Engl J Med.* (2021) 384:1204–15. doi: 10.1056/NEJMoa2024277
132. Reynolds AM, Holmes MD, Danilov SM, Reynolds PN. Targeted gene delivery of BMPR2 attenuates pulmonary hypertension. *Eur Respir J.* (2012) 39:329–43. doi: 10.1183/09031936.00187310
133. Harper RL, Reynolds AM, Bonder CS, Reynolds PN. BMPR2 gene therapy for PAH acts via Smad and non-Smad signalling. *Respirology.* (2016) 21:727–33. doi: 10.1111/resp.12729
134. Harper RL, Maiolo S, Ward RJ, Seyfang J, Cockshell MP, Bonder CS, et al. BMPR2-expressing bone marrow-derived endothelial-like progenitor cells alleviate pulmonary arterial hypertension *in vivo*. *Respirology.* (2019) 24:1095–103. doi: 10.1111/resp.13552
135. Quarck R, Perros F. Rescuing BMPR2-driven endothelial dysfunction in PAH: a novel treatment strategy for the future? *Stem Cell Investig.* (2017) 4:56. doi: 10.21037/sci.2017.05.11
136. Liu D, Yan Y, Chen JW, Yuan P, Wang XJ, Jiang R, et al. Hypermethylation of BMPR2 promoter occurs in patients with heritable pulmonary arterial hypertension and inhibits BMPR2 expression. *Am J Respir Crit Care Med.* (2017) 196:925–8. doi: 10.1164/rccm.201611-2273LE
137. Chen M, Shen H, Zhu L, Yang H, Ye P, Liu P, et al. Berberine attenuates hypoxia-induced pulmonary arterial hypertension via bone morphogenetic protein and transforming growth factor-β signaling. *J Cell Physiol.* (2019) 234:17482–93. doi: 10.1002/jcp.28370
138. Theilmann AL, Hawke LG, Hilton LR, Whitford MKM, Cole DV, Mackeil JL, et al. Endothelial BMPR2 loss drives a proliferative response to BMP (bone morphogenetic protein) 9 via prolonged canonical signaling. *Arterioscler Thromb Vasc Biol.* (2020) 40:2605–18. doi: 10.1161/ATVBAHA.119.313357
139. Bouvard C, Tu L, Rossi M, Desroches-Castan A, Berrebeh N, Helfer E, et al. Different cardiovascular and pulmonary phenotypes for single- and double-knock-out mice deficient in BMP9 and BMP10. *Cardiovasc Res.* (2021) cvab187. doi: 10.1093/cvr/cvab187
140. Li W, Long L, Yang X, Tong Z, Southwood M, King R, et al. Circulating BMP9 protects the pulmonary endothelium during inflammation-induced lung injury in mice. *Am J Respir Crit Care Med.* (2020) 203:1419–30. doi: 10.1164/rccm.202005-1761OC
141. Costello CM, Cahill E, Martin F, Gaine S, McLoughlin P. Role of gremlin in the lung: development and disease. *Am J Respir Cell Mol Biol.* (2010) 42:517–23. doi: 10.1165/rcmb.2009-0101TR
142. Meng L, Teng X, Liu Y, Yang C, Wang S, Yuan W, et al. Vital roles of gremlin-1 in pulmonary arterial hypertension induced by systemic-to-pulmonary shunts. *J Am Heart Assoc.* (2020) 9:e016586. doi: 10.1161/JAHA.120.016586
143. Alastalo TP Li M, Perez Vde J, Pham D, Sawada H, Wang JK, et al. Disruption of PPARγ/β-catenin-mediated regulation of apelin impairs BMP-induced mouse and human pulmonary arterial EC survival. *J Clin Invest.* (2011) 121:3735–46. doi: 10.1172/JCI43382
144. Chapman FA, Nyimanu D, Maguire JJ, Davenport AP, Newby DE, Dhaun N. The therapeutic potential of apelin in kidney disease. *Nat Rev Nephrol.* (2021). doi: 10.1038/s41581-021-00461-z
145. Yang P, Maguire JJ, Davenport AP. Apelin, Elabela/Toddler, and biased agonists as novel therapeutic agents in the cardiovascular system. *Trends Pharmacol Sci.* (2015) 36:560–7. doi: 10.1016/j.tips.2015.06.002
146. Poirier O, Ciumas M, Eyries M, Montagne K, Nadaud S, Soubrier F. Inhibition of apelin expression by BMP signaling in endothelial cells. *Am J Physiol Cell Physiol.* (2012) 303:C1139–1145. doi: 10.1152/ajpcell.00168.2012
147. Chandra SM, Razavi H, Kim J, Agrawal R, Kundu RK, de Jesus Perez V, et al. Disruption of the apelin-APJ system worsens hypoxia-induced pulmonary hypertension. *Arterioscler Thromb Vasc Biol.* (2011) 31:814–20. doi: 10.1161/ATVBAHA.110.219980
148. Gu M, Donato M, Guo M, Wary N, Miao Y, Mao S, et al. iPSC–endothelial cell phenotypic drug screening and *in silico* analyses identify tyrphostin-AG1296 for pulmonary arterial hypertension. *Sci Transl Med.* (2021) 13:eaba6480. doi: 10.1126/scitranslmed.aba6480
149. Phillips JA III, Poling JS, Phillips CA, Stanton KC, Austin ED, Cogan JD, et al. Synergistic heterozygosity for TGFβ1 SNPs and BMPR2 mutations modulates the age at diagnosis and penetrance of familial pulmonary arterial hypertension. *Genet Med.* (2008) 10:359–65. doi: 10.1097/GIM.0b013e318172dcdf
150. Zaiman AL, Podowski M, Medicherla S, Gordy K, Xu F, Zhen L, et al. Role of the TGF-β/Alk5 signaling pathway in monocrotaline-induced pulmonary hypertension. *Am J Respir Crit Care Med.* (2008) 177:896–905. doi: 10.1164/rccm.200707-1083OC
151. Upton PD, Davies RJ, Tajsic T, Morrell NW. Transforming growth factor-β1 represses bone morphogenetic protein-mediated Smad signaling in pulmonary artery smooth muscle cells via Smad3. *Am J Respir Cell Mol Biol.* (2013) 49:1135–45. doi: 10.1165/rcmb.2012-0470OC
152. Budi EH, Schaub JR, Decaris M, Turner S, Derynck R. TGF-β as a driver of fibrosis: physiological roles and therapeutic opportunities. *J Pathol.* (2021). doi: 10.1002/path.5680
153. Teicher BA. TGFβ-directed therapeutics: 2020. *Pharmacol Ther.* (2021) 217:107666. doi: 10.1016/j.pharmthera.2020.107666
154. Sanada TJ, Sun XQ, Happe C, Guignabert C, Tu L, Schalij I, et al. Altered TGFβ/SMAD signaling in human and rat models of pulmonary hypertension: an old target needs attention. *Cells.* (2021) 10:84. doi: 10.3390/cells10010084
155. Anderton MJ, Mellor HR, Bell A, Sadler C, Pass M, Powell S, et al. Induction of heart valve lesions by small-molecule ALK5 inhibitors. *Toxicol Pathol.* (2011) 39:916–24. doi: 10.1177/0192623311416259
156. Vogt J, Traynor R, Sapkota GP. The specificities of small molecule inhibitors of the TGFβ and BMP pathways. *Cell Signal.* (2011) 23:1831–42. doi: 10.1016/j.cellsig.2011.06.019
157. Wang R, Zhu J, Dong X, Shi M, Lu C, Springer TA, et al. regulates the bioavailability and activation of TGFβ. *Mol Biol Cell.* (2012) 23:1129–39. doi: 10.1091/mbc.e11-12-1018
158. Robertson IB, Rifkin DB. Regulation of the bioavailability of TGF-β and TGF-β-related proteins. *Cold Spring Harb Perspect Biol.* (2016) 8:a021907. doi: 10.1101/cshperspect.a021907
159. Murphy-Ullrich JE, Suto MJ. Thrombospondin-1 regulation of latent TGF-β activation: a therapeutic target for fibrotic disease. *Matrix Biol.* (2018) 68–69:28–43. doi: 10.1016/j.matbio.2017.12.009
160. Kim CW, Pokutta-Paskaleva A, Kumar S, Timmins LH, Morris AD, Kang DW, et al. Disturbed flow promotes arterial stiffening through thrombospondin-1. *Circulation.* (2017) 136:1217–32. doi: 10.1161/CIRCULATIONAHA.116.026361

161. Slack RJ, Macdonald SJF, Roper JA, Jenkins RG, Hatley RJD. Emerging therapeutic opportunities for integrin inhibitors. *Nat Rev Drug Discov.* (2021). doi: 10.1038/s41573-021-00284-4
162. Demonbreun AR, Fallon KS, Oosterbaan CC, Vaught LA, Reiser NL, Bogdanovic E, et al. Anti-latent TGFβ binding protein 4 antibody improves muscle function and reduces muscle fibrosis in muscular dystrophy. *Sci Transl Med.* (2021) 13:eabf0376. doi: 10.1126/scitranslmed.abf0376
163. Welsh BT, Faucette R, Bilic S, Martin CJ, Schurpf T, Chen D, et al. Nonclinical development of SRK-181: an anti-latent TGFβ1 monoclonal antibody for the treatment of locally advanced or metastatic solid tumors. *Int J Toxicol.* (2021) 40:226–41. doi: 10.1177/1091581821998945
164. Zhang J, Wang T, Saigal A, Johnson J, Morrisson J, Tabrizifard S, et al. Discovery of a new class of integrin antibodies for fibrosis. *Sci Rep.* (2021) 11:2118. doi: 10.1038/s41598-021-81253-0
165. Aykul S, Martinez-Hackert E. Transforming growth factor-β family ligands can function as antagonists by competing for type II receptor binding. *J Biol Chem.* (2016) 291:10792–804. doi: 10.1074/jbc.M115.713487
166. Li CY, Chen YH, Wang Q, Hou JW, Wang H, Wang YP Li YG. Partial inhibition of activin receptor-like kinase 4 attenuates pressure overload-induced cardiac fibrosis and improves cardiac function. *J Hypertens.* (2016) 34:1766–77. doi: 10.1097/HJH.0000000000001020
167. Roh JD, Hobson R, Chaudhari V, Quintero P, Yeri A, Benson M, et al. Activin type II receptor signaling in cardiac aging and heart failure. *Sci Transl Med.* (2019) 11:aau8680. doi: 10.1126/scitranslmed.aau8680
168. Ruckle J, Jacobs M, Kramer W, Pearsall AE, Kumar R, Underwood KW, et al. Single-dose, randomized, double-blind, placebo-controlled study of ACE-011 (ActRIIA-IgG1) in postmenopausal women. *J Bone Miner Res.* (2009) 24:744–52. doi: 10.1359/jbmr.081208
169. Sherman ML, Borgstein NG, Mook L, Wilson D, Yang Y, Chen N, et al. Multiple-dose, safety, pharmacokinetic, and pharmacodynamic study of sotatercept (ActRIIA-IgG1), a novel erythropoietic agent, in healthy postmenopausal women. *J Clin Pharmacol.* (2013) 53:1121–30. doi: 10.1002/jcph.160
170. Abdulkadyrov KM, Salogub GN, Khuazheva NK, Sherman ML, Laadem A, Barger R, et al. Sotatercept in patients with osteolytic lesions of multiple myeloma. *Br J Haematol.* (2014) 165:814–23. doi: 10.1111/bjh.12835
171. Raftopoulos H, Laadem A, Hesketh PJ, Goldschmidt J, Gabrail N, Osborne C, et al. Sotatercept (ACE-011) for the treatment of chemotherapy-induced anemia in patients with metastatic breast cancer or advanced or metastatic solid tumors treated with platinum-based chemotherapeutic regimens: results from two phase 2 studies. *Support Care Cancer.* (2016) 24:1517–25. doi: 10.1007/s00520-015-2929-9
172. Komrokji R, Garcia-Manero G, Ades L, Prebet T, Steensma DP, Jurcic JG, et al. Sotatercept with long-term extension for the treatment of anaemia in patients with lower-risk myelodysplastic syndromes: a phase 2, dose-ranging trial. *Lancet Haematol.* (2018) 5:e63–72. doi: 10.1016/S2352-3026(18)30002-4
173. Cappellini MD, Porter J, Origa R, Forni GL, Voskaridou E, Galacteros F, et al. Sotatercept, a novel transforming growth factor β ligand trap, improves anemia in β-thalassemia: a phase II, open-label, dose-finding study. *Haematologica.* (2019) 104:477–84. doi: 10.3324/haematol.2018.198887
174. Coyne DW, Singh HN, Smith WT, Giuseppi AC, Connarn JN, Sherman ML, et al. Sotatercept safety and effects on hemoglobin, bone, and vascular calcification. *Kidney Int Rep.* (2019) 4:1585–97. doi: 10.1016/j.ekir.2019.08.001
175. Yang P, Bocobo GA Yu PB. Sotatercept for pulmonary arterial hypertension. *N Engl J Med.* (2021) 385:92–3. doi: 10.1056/NEJMc2107209

Conflict of Interest: All authors are past employees of Acceleron Pharma and are now employees of Merck Sharp and Dohme Corp., a subsidiary of Merck & Co., Inc., Kenilworth, NJ, USA and may own stock and hold stock options in the Company.

Publisher's Note: All claims expressed in this article are solely those of the authors and do not necessarily represent those of their affiliated organizations, or those of the publisher, the editors and the reviewers. Any product that may be evaluated in this article, or claim that may be made by its manufacturer, is not guaranteed or endorsed by the publisher.

frontiers in Medicine

ORIGINAL RESEARCH
published: 07 March 2022
doi: 10.3389/fmed.2022.851935

Lung Ventilation/Perfusion Scintigraphy for the Screening of Chronic Thromboembolic Pulmonary Hypertension (CTEPH): Which Criteria to Use?

Romain Le Pennec[1], Cécile Tromeur[2], Charles Orione[2], Philippe Robin[1], Raphaël Le Mao[2], Claire De Moreuil[2], Mitja Jevnikar[3], Clément Hoffman[2], Laurent Savale[3], Francis Couturaud[2], Olivier Sitbon[3], David Montani[3], Xavier Jaïs[3], Grégoire Le Gal[4,5], Pierre Yves Salaün[1], Marc Humbert[3] and Pierre Yves Le Roux[1]*

[1] Service de médecine nucléaire, EA3878 (GETBO) IFR 148, CHRU de Brest, Université de Bretagne Occidentale, Brest, France, [2] Département de Médecine Interne et Pneumologie, EA 3878 (GETBO), CHRU de Brest, Université de Bretagne Occidentale, Brest, France, [3] AP-HP, Service de Pneumologie, DHU Thorax Innovation, Hôpital Bicêtre, INSERM U999, LabEx LERMIT, Centre Chirurgical Marie Lannelongue, Université Paris-Sud, Paris, France, [4] Centre d'Investigation Clinique, Centre Hospitalier Régional et Universitaire de Brest, Brest, France, [5] Department of Medicine, Ottawa Hospital Research Institute, University of Ottawa, Ottawa, ON, Canada

OPEN ACCESS

Edited by:
Domenico Albano, University of Brescia, Italy

Reviewed by:
Francesco Dondi, Università degli Studi di Brescia, Italy
David John Macfarlane, The University of Queensland, Australia

***Correspondence:**
Romain Le Pennec
romain.lepennec@gmail.com

Specialty section:
This article was submitted to Nuclear Medicine, a section of the journal Frontiers in Medicine

Received: *10 January 2022*
Accepted: *31 January 2022*
Published: *07 March 2022*

Citation:
Le Pennec R, Tromeur C, Orione C, Robin P, Le Mao R, De Moreuil C, Jevnikar M, Hoffman C, Savale L, Couturaud F, Sitbon O, Montani D, Jaïs X, Le Gal G, Salaün PY, Humbert M and Le Roux PY (2022) Lung Ventilation/Perfusion Scintigraphy for the Screening of Chronic Thromboembolic Pulmonary Hypertension (CTEPH): Which Criteria to Use? Front. Med. 9:851935. doi: 10.3389/fmed.2022.851935

Objective: The diagnosis of chronic thromboembolic pulmonary hypertension (CTEPH) is a major challenge as it is a curable cause of pulmonary hypertension (PH). Ventilation/Perfusion (V/Q) lung scintigraphy is the imaging modality of choice for the screening of CTEPH. However, there is no consensus on the criteria to use for interpretation. The aim of this study was to assess the accuracy of various interpretation criteria of planar V/Q scintigraphy for the screening of CTEPH in patients with PH.

Methods: The eligible study population consisted of consecutive patients with newly diagnosed PH in the Brest University Hospital, France. Final diagnosis (CTEPH or non-CTEPH) was established in a referential center on the management of PH, based on the ESC/ERS guidelines and a minimum follow-up of 3 years. A retrospective central review of planar V/Q scintigraphy was performed by three nuclear physicians blinded to clinical findings and to final diagnosis. The number, extent (sub-segmental or segmental) and type (matched or mismatched) of perfusion defects were reported. Sensitivity and specificity were evaluated for various criteria based on the number of mismatched perfusion defects and the number of perfusion defects (regardless of ventilation). Receiver operating characteristic (ROC) curves were generated and areas under the curve (AUC) were calculated for both.

Results: A total of 226 patients with newly diagnosed PH were analyzed. Fifty six (24.8%) were diagnosed with CTEPH while 170 patients (75.2%) were diagnosed with non-CTEPH. The optimal threshold was 2.5 segmental mismatched perfusion defects, providing a sensitivity of 100 % (95% CI 93.6–100%) and a specificity of 94.7% (95%CI 90.3–97.2%). Lower diagnostic cut-offs of mismatched perfusion defects provided similar sensitivity but lower specificity. Ninety five percent of patients with CTEPH had

more than 4 segmental mismatched defects. An interpretation only based on perfusion provided similar sensitivity but a specificity of 81.8% (95%CI 75.3–86.9%).

Conclusion: Our study confirmed the high diagnostic performance of planar V/Q scintigraphy for the screening of CTEPH in patients with PH. The optimal diagnostic cut-off for interpretation was 2.5 segmental mismatched perfusion defects. An interpretation only based on perfusion defects provided similar sensitivity but lower specificity.

Keywords: chronic thromboembolic pulmonary hypertension, ventilation/perfusion scintigraphy, interpretation criteria, CTEPH, planar V/Q scintigraphy

INTRODUCTION

Chronic Thromboembolic Pulmonary Hypertension (CTEPH) is a rare complication of acute pulmonary embolism (PE) leading to severe right ventricular failure and death in the absence of treatment (1). CTEPH is characterized by the presence of macroscopic thromboembolic lesions in the proximal or distal pulmonary arteries and microscopic pulmonary vasculopathy, which obstruct blood flow and increases pressure in the pulmonary arteries (2). The incidence of CTEPH is probably underestimated because of non-specific symptoms and a high proportion of cases with no documented history of PE (3, 4). Diagnosing CTEPH is a major diagnostic challenge. Without treatment, the estimated 5-years survival of patients with CTEPH is poor, around 30% in patients with a mean Pulmonary Artery Pressure (mPAP) >40 mmHg (5, 6). However, in contrast with other groups of PH, CTEPH is potentially curable thanks to various treatment modalities including surgery, balloon pulmonary angioplasty and medical therapy (7–10).

According to the European Society of Cardiology (ESC) and the European Respiratory Society (ERS) guidelines for the diagnosis and treatment of pulmonary hypertension, Ventilation/Perfusion (V/Q) lung scintigraphy is the imaging modality of choice to exclude CTEPH at an early stage of the algorithm for diagnosing PH (10, 11). Indeed, V/Q lung scintigraphy is superior to Computed Tomography Pulmonary Angiography (CTPA), especially with a higher sensitivity (12).

While V/Q imaging has a key role in the screening of CTEPH (13), there is no consensus on the interpretation criteria to be used. According to ESC/ERS recommendations (10, 11), V/Q lung scintigraphy is considered positive for CTEPH if there are mismatched perfusion defects, but with no indication about the size and number of defects. Tunariu et al. demonstrated the superiority of planar V/Q lung scintigraphy over CTPA using the PIOPED criteria for V/Q scan interpretation (12). In this study, a high probability scan (i.e. at least two segmental mismatched perfusion defects) was suggestive of CTEPH while results were unclear for patients with an intermediate probability scintigraphy. In a recent study, Wang et al. used a lower threshold (14). V/Q lung scintigraphy was interpreted as positive for CTEPH if there was at least one segmental or two sub-segmental mismatched perfusion defects, as proposed by the European Association of Nuclear Medicine (EANM) guidelines for the diagnosis of acute PE (14–16). However, the pulmonary artery obstruction in patients with CTEPH is typically diffuse and multi-segmental and a low burden of pulmonary vascular obstruction, e.g., one segmental defect, is very unlikely to cause PH (14). On the other hand, given that V/Q lung scintigraphy is positioned as a screening tool in the diagnosis of CTEPH, a high sensitivity should remain the priority. Furthermore, an imaging technique using a perfusion-only scan along with a low-dose CT acquisitions (Q-LDCT), has been reported to exhibit adequate performance for CTEPH screening compared to V/Q lung scintigraphy, which may question the diagnostic value of V/Q mismatched defects as compared with perfusion defect regardless of the ventilation (17). So far, no study has evaluated and compared the diagnostic performances of V/Q scintigraphy according to interpretation criteria.

The aim of this study was to assess the accuracy of various interpretation criteria of planar V/Q lung scintigraphy for screening of CTEPH in patients with PH.

MATERIALS AND METHODS

Population

The eligible study population consisted of consecutive patients with newly diagnosed PH referred to Brest University Hospital, France for initial assessment, and included in a French National PH registry (authorization number 842063). All patients provided written informed consent.

The diagnosis of precapillary PH was established according to the 2015 guidelines [mPAP $\geq$ 25 mmHg and pulmonary artery wedge pressure (PAWP) $\leq$ 15 mmHg measured by right heart catheterization (RHC)] (18). Patients were managed according to ESC/ERS guidelines for the diagnosis and treatment of CTEPH (11), and classified into the different groups of PH based on clinical and imaging data. All patients with a possible CTEPH after initial assessment were referred to the National reference center in Paris Kremlin-Bicêtre, France, for diagnostic confirmation and to assess operability. The diagnosis of CTEPH was confirmed according to ESC/ERS guidelines (11). All patients diagnosed with CTEPH had pre-capillary PH diagnosed with RHC and typical morphological lesions of CTEPH on high resolution CT and/or conventional pulmonary angiography. All patients were followed up for minimum 3 years with multiple check-up review and RHC to assess evolution and avoid misdiagnosis.

Demographic data and history of acute PE were collected from the French PH registry. Hemodynamics results from RHC at initial screening (pulmonary vascular resistances (PVR)

expressed in dyn.sec.cm^{-5} and mPAP expressed in mmHg) were also collected in order to evaluate the correlation between the extent of perfusion defects and the alteration of hemodynamics parameters.

V/Q Scans Acquisition and Interpretation

Planar V/Q lung scans were performed according to the SFMN guidelines on lung scintigraphy protocols (15, 19). Perfusion images were obtained after administration of 140 MBq of ^{99m}Tc-macroaggregated albumin. Ventilation images were acquired either after inhalation of ^{99m}Tc-Technegas or ^{81m}Kr-Krypton gas. Imaging acquisition was performed in six views (anterior, posterior, left and right lateral, left and right posterior oblique).

A retrospective central review of all planar V/Q lung scintigraphy was performed by three nuclear physicians with different level of expertise, blinded to clinical results and to final diagnosis. Interpretation was determined via consensus reading. For each planar V/Q lung scintigraphy, the number, extent (sub-segmental or segmental) and type (matched or mismatched with ventilation images) of perfusion defects were reported. The extent of each defect was assessed visually. A defect was defined as segmental if it involved more than 75% of a segment and sub-segmental if it involved <75% (20).

Data Analysis

Continuous data were expressed as mean ± standard deviation (SD), and categorical data were expressed as frequency and percentage (%). Differences between the two groups were analyzed for significance with the unpaired Student *t* test for continuous variables and with the Chi2 test for categorical variables.

For each planar V/Q lung scintigraphy, the number of segmental perfusion defects or equivalent (2 sub-segments = 1 segment) was computed. This was performed for mismatched perfusion defects, and for perfusion defects regardless of the ventilation (i.e., mismatched or matched defects). Receiver operating characteristic (ROC) curves were generated and areas under the curve (AUC) were calculated. For determination of the optimal diagnostic cut-off for interpretation, the main criterion was to select a high sensitivity cutoff, as V/Q lung scintigraphy is positioned as a screening tool in the diagnostic algorithm for CTEPH. Then, if various thresholds provided similar sensitivity, the threshold with the highest specificity was chosen. Correlation between the extent of perfusion defects and PAPm/PVR alteration was analyzed using Pearson correlation test.

RESULTS

Population

A total of 288 patients referred to the Brest University Hospital were enrolled in the French National PH registry between January 2004 and January 2019. Among those 288 patients, 62 were excluded from the present study for the following reasons: 5 patients had a well-established diagnosis of a PH attributable to left heart disease with a post-capillary PH on RHC; 19 had V/Q SPECT imaging; three had a perfusion-only scan; images were not available in 28 patients; and seven patients died before undergoing assessment.

A total of 226 patients with newly diagnosed PH, who underwent V/Q planar scintigraphy for the screening of CTEPH, were therefore analyzed. Out of them, 56 (25%) were diagnosed with CTEPH at the reference center in Paris. Among 170 patients (75%) diagnosed with non-CTEPH, 92 were classified in group 1 of PH classification (41%), 24 in group 2 (10%), 40 in group 3 (18%), 4 in group 5 (2%), and 10 were classified as having mixed causes PH (mix from group 1, 2 and 3) (4%). Patients' characteristics in CTEPH and non-CTEPH groups are presented in **Table 1**.

TABLE 1 | Patient baseline characteristics.

	CTEPH patients (*N* = 56)	Non-CTEPH patients (*N* = 170)	*p*-value
Age (years)	68 (SD 57–81)	63 (SD 53–78)	$p = 0.043$
No PE history (%)	29 (39%)	160 (95%)	$p < 0.001$
mPAP (mmHg)	41.6 (SD 31.4–51.8)	43.2 (SD 32.4–54.1)	$p = 0.322$
PVR (dyn.sec.cm^{-5})	594.2 (SD 274.2–914.2)	595.6 (SD 253.2–937.9)	$p = 0.842$
Segmental mismatched perfusion defects	6.4 (SD 4.5–8.2)	0.3 (SD −0.95–1.6)	$p < 0.001$
Segmental perfusion defects	6.6 (SD 4.7–8.4)	1.1 (SD −0.6–1.2)	$p < 0.001$

Patients With CTEPH Diagnosis

Mean age of patients was 68 years old [SD (57–81)]. Mean time between first symptoms and diagnosis was 15 months. Among the 56 patients, 29 patients (39%) had no PE history. Planar V/Q lung scintigraphy was reported with a mean number of mismatched perfusion defects of 6.4 segments [SD (4.5–8.2)] and a mean number of perfusion defects of 6.6 segments [SD (4.7–8.4)]. **Figure 1** illustrates a typical planar V/Q lung scintigraphy in a patient with CTEPH. Mean PAPm and PVR were 41.6 mmHg [SD (31.4–51.8)] and 594.2 dyn.sec.cm-5 [SD (274.2–914.2)], respectively. No correlation was found between the extent of perfusion defects and the degree of PAPm or PVR alteration: based on mismatched perfusion defects, correlation coefficients were 0.03 and 0.20 for PAPm and PVR, respectively.

Patients With Non-CTEPH Diagnosis

Mean age of patients was 63 years old [SD (53–78)]. Mean time between first symptoms and diagnosis was 15 months. Among the 170 patients, 160 patients (95%) had no PE history. Planar V/Q lung scintigraphy was reported with a mean number of mismatched perfusion defects of 0.3 segments [SD (−0.95-1.6)] and a mean number of total perfusion defects of 1.1 segments [SD (−0.6–3.2)]. Mean PAPm and PVR were 43.2 mmHg [SD (32.4–54.1)] and 595.6 dyn.sec.cm^{-5} [SD (253.2–937.9)] respectively. Among the 170 non-CTEPH patients, 103 patients had a normal planar V/Q lung scintigraphy with no

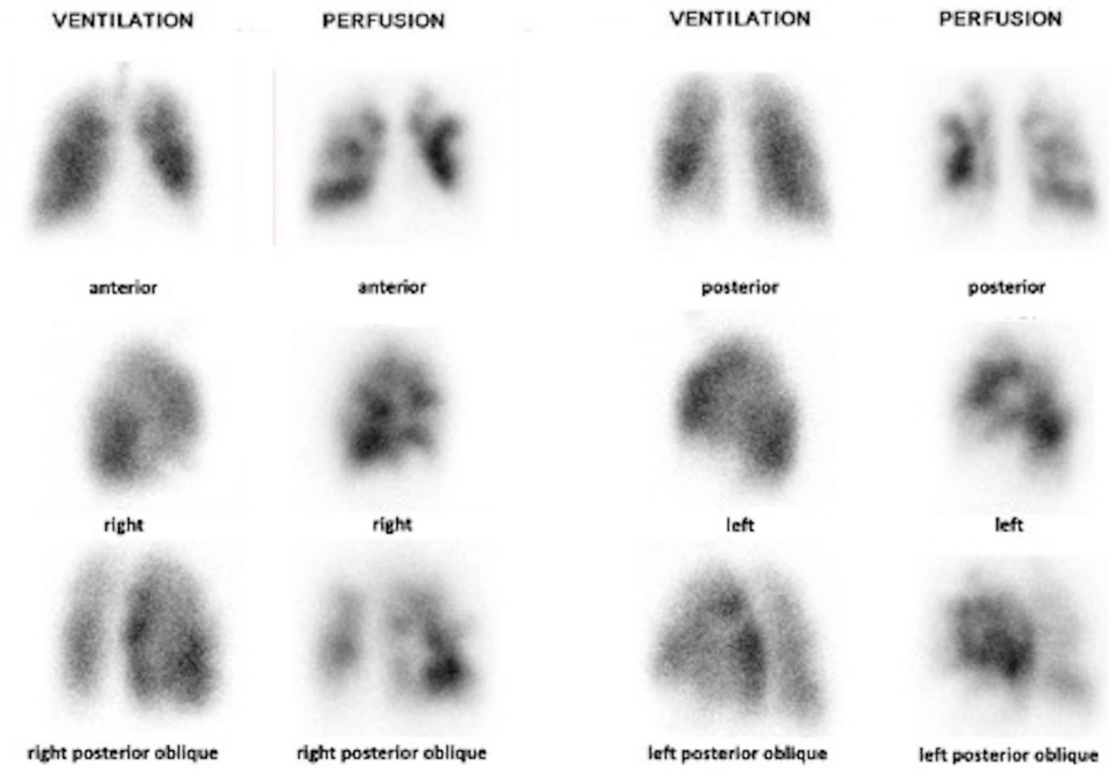

FIGURE 1 | Planar V/Q scintigraphy showing multiple segmental mismatched perfusion defects in a patient with confirmed CTEPH.

perfusion defect (mismatched or matched). Planar V/Q lung scintigraphy was normal in 64/92 patients (70%) from group 1, 12/24 patients (50%) from group 2, 21/40 patients (53%) from group 3, 3/4 patients (75%) from group 5, and 3/10 patients (30%) with a mixed cause of PH. Significant differences were found between CTEPH and non-CTEPH patients for PE history ($p < 0.0001$) and age ($p = 0.043$). But no significant difference was found between the two groups for PAPm ($p = 0.322$) and RVP ($p = 0.842$).

Diagnostic Performance of Planar V/Q According to Various Criteria of Interpretation

ROC curves generated according to the number of segmental mismatched perfusion defects and segmental perfusion defects are presented in **Figure 2**. **Figure 3** shows the histograms of distribution of mismatched segmental perfusion defects (**Figure 3A**) and segmental perfusion defects (**Figure 3B**) in the CTEPH and non-CTEPH groups. Sensitivity and specificity of lung scan according to various interpretation criteria are summarized in **Table 2**.

Based on perfusion mismatched defects, AUC was 0.98 (95%CI = 0.97–0.99). The optimal threshold was 2.5 segmental mismatched perfusion defects, providing a sensitivity of 100 % (95%CI 93.6–100%) and a specificity of 94.7% (95%CI 90.3–97.2%). Lower diagnostic cut-offs provided similar sensitivity but lower specificity: 91.8% (95%CI 87.7–95.0%) using 1 segmental mismatched defect (i.e., the EANM criteria) and 89.4% (95%CI 84.9–93.2%) using 0.5 segmental (=1 sub-segmental) mismatched defect, respectively. Out of the 56 patients with CTEPH, 53 patients (95%) had more than 4 segmental mismatched defects.

Based on perfusion defects regardless of ventilation, the AUC was 0.96 (95%CI 0.93–0.98). The optimal threshold was 2.5 segmental perfusion defects, providing a sensitivity of 100% (95%CI 93.6–100%) and a specificity of 81.8% (95%CI 75.3–86.9%). Lower diagnostic cut-offs provided similar sensitivity but lower specificity (See **Table 2**). **Figure 4** illustrates a planar V/Q lung scintigraphy with multiple bilateral perfusion defects matched to the ventilation in a non-CTEPH patient.

Using the optimal positivity threshold ($\geq$ 2.5 segmental mismatched perfusion defects), planar V/Q lung scintigraphy was falsely interpreted as positive for CTEPH in eight patients. Among them, four patients had a final diagnosis of PH due to advanced pulmonary disease with emphysema, chronic obstructive pulmonary disease or fibrosis with both mismatched and matched defects; one patient had pulmonary veno-occlusive disease; one patient was initially diagnosed with CTEPH but was finally classified as PH from undetermined cause during the

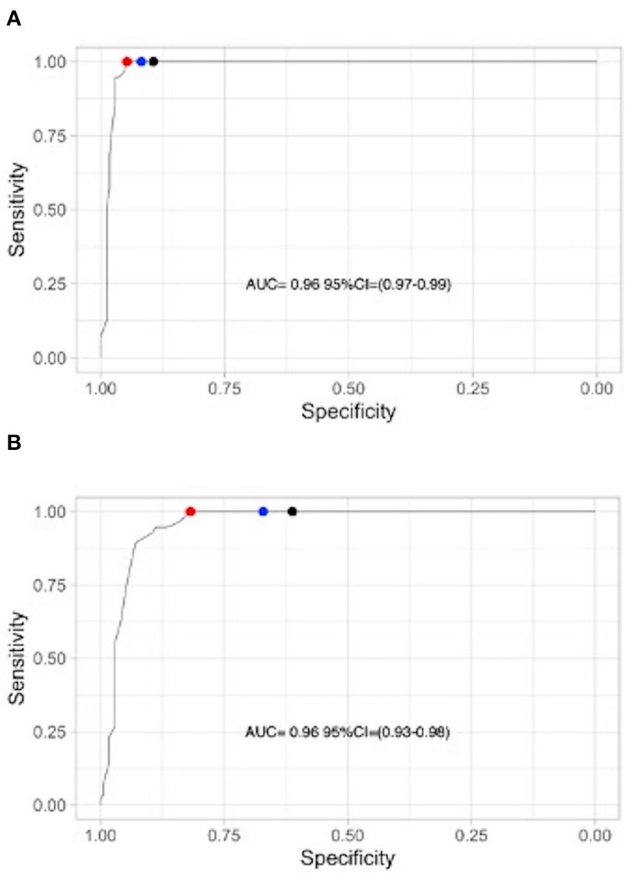

FIGURE 2 | (A) Segmental mismatched perfusion defects. **(B)** All segmental perfusion defects (regardless of ventilation). Red points: Cut-off at 2.5 segmental; Blue points: Cut-off at 1 segmental; Black points: Cut-off at 0.5 segmental.

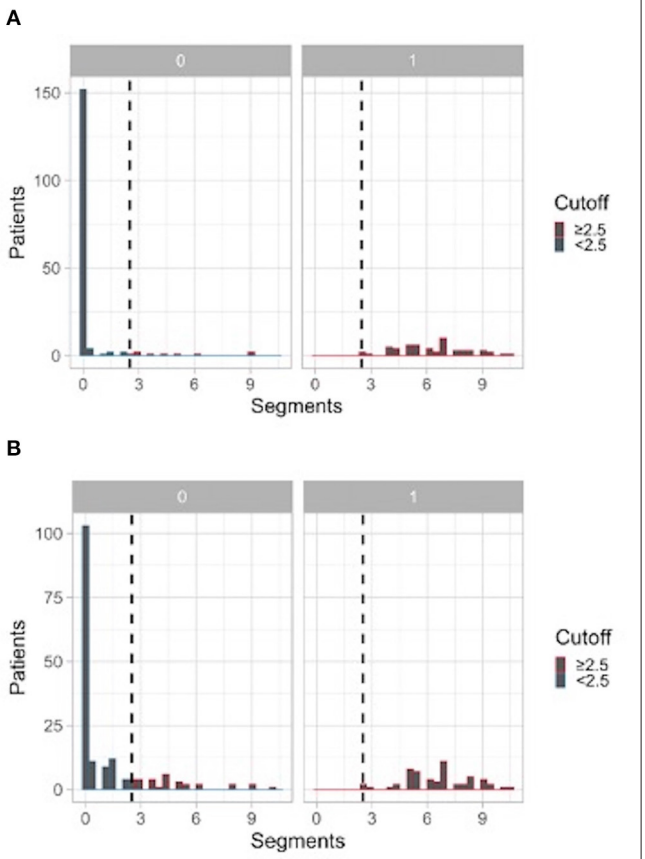

FIGURE 3 | (A) Histogram for V/Q scan interpreted on mismatched perfusion defects. **(B)** Histogram for V/Q scan interpreted on all segmental perfusion defects (regardless of ventilation). 0 = non-CTEPH patients; 1 = CTEPH patients; Red plots = positive V/Q scan; Blue plots = negative V/Q scan.

follow up; one patient had a porto-pulmonary hypertension; and one patient had pulmonary artery abnormality anatomy from congenital cause.

DISCUSSION

Our study confirms the high diagnostic performance of planar V/Q lung scintigraphy for screening CTEPH in patients with PH (12, 14). The optimal diagnostic cut-off for interpretation was 2.5 segmental mismatched perfusion defects, providing a sensitivity of 100% (CI 95% 93.6–100%) and a specificity of 94.7% (95%CI 90.3–97.2%), respectively. Our study also demonstrates the higher diagnostic value of mismatched perfusion defects over perfusion defects (regardless of ventilation) when screening CTEPH, as an interpretation only based on perfusion defects provided similar sensitivity but a lower specificity [81.8% (95%CI 75.3–86.9%)].

Diagnosing CTEPH is a major diagnostic challenge because it is the only curable form of PH (5, 17). Given that the V/Q lung scintigraphy is used as a screening tool for a potentially surgically curable condition, the test should be as sensitive as possible, ideally close to 100%. According to current recommendations (10, 11), all suspected cases of CTEPH on V/Q scan are then referred to an expert center to confirm the diagnosis, which implies additional testing and travels that may be invasive and costly. Therefore, V/Q lung scintigraphy should ideally also have a high specificity in order to limit unnecessary investigations.

In our study, the optimal cut-off was 2.5 segmental mismatched perfusion defects, providing a sensitivity of 100% (CI 95% 93.6–100%) and a specificity of 94.7% (95%CI 90.3–97.2%), respectively. This cut-off is roughly similar to that of a high probability planar V/Q scintigraphy according to PIOPED criteria (i.e., two segments). In the study from Tunariu et al. (12), a high probability V/Q lung scintigraphy had a sensitivity of 96.2% and a specificity of 94.6%, respectively. However, results were not straightforward for patients with an intermediate probability V/Q scintigraphy. Our study clarifies this situation, with no case of CTEPH diagnosed among patients with <2.5

segmental perfusion mismatched defects. In a recent study, Wang et al. (14) used as positivity threshold 1 segmental mismatched perfusion defect or equivalent (i.e., the EANM criteria) and reported 94.2% of sensitivity and 92.8% of specificity. Using the same criteria, we found a sensitivity of 100% (95%CI 93.6–100%) but a lower specificity of 91.8% (95%CI 87.7–95.0%). Finally, using the modified PISAPED criteria, which were also developed for the diagnosis of acute PE, the specificity was 89.4 (84.9–93.2) (21). The pulmonary artery obstruction in patients with CTEPH is typically diffuse and multi-segmental (2). In our study, the pulmonary vascular obstruction in patients diagnosed with CTEPH was 6.3 segmental mismatched perfusion defects on average (∼35% of the whole lung), consistent with data from other studies (14). Furthermore, among patients with CTEPH, 95% had at least 4 segmental mismatched perfusion defects (∼20% of the whole lung). Accordingly, although the V/Q lung scintigraphy is a screening tool in the management of patients with PH, not considering a single defect as a positive exam seems reasonable.

TABLE 2 | Sensitivity and specificity according to criteria tested.

Criteria		Sensitivity (%) CI 95%	Specificity (%) CI 95%
Mismatched perfusion defects	≥ 2.5 segmental	100 (93.6–100)	94.7 (90.3– 7.2)
	≥ 1 segmental (EANM)	100 (93.6–100)	91.8 (87.7–95.0)
	≥ 0.5 segmental	100 (93.6–100)	89.4 (84.9–93.2)
Perfusion defects (regardless of ventilation)	≥ 2.5 segmental	100 (93.6–100)	81.8 (75.3–86.9)
	≥ 1 segmental (EANM)	100 (93.6–100)	66.7 (60.7–74.7)
	≥ 0.5 segmental	100 (93.6–100)	60.6 (53.1–67.6)

More recently, new imaging modalities such as CTPA, Magnetic Resonance Imaging (MRI) or perfusion scan with a Low-Dose Computed Tomography (Q-LDCT) have emerged as alternatives to lung scintigraphy to diagnose CTEPH (13). All these techniques rely on the analysis of lung perfusion, without information on ventilation. The need for a ventilation scan is of particular interest with the COVID-19 pandemic as the ventilation procedure increases the potential risk of contamination by the aerosol secretion and the expired air (22). According to our results, an interpretation only based on perfusion images demonstrated similar high sensitivity but lower specificity: 100% (95%CI 93.6–100) and 81.8% (95%CI 75.3–86.9%) using the same 2.5 segments cut-off. Furthermore,

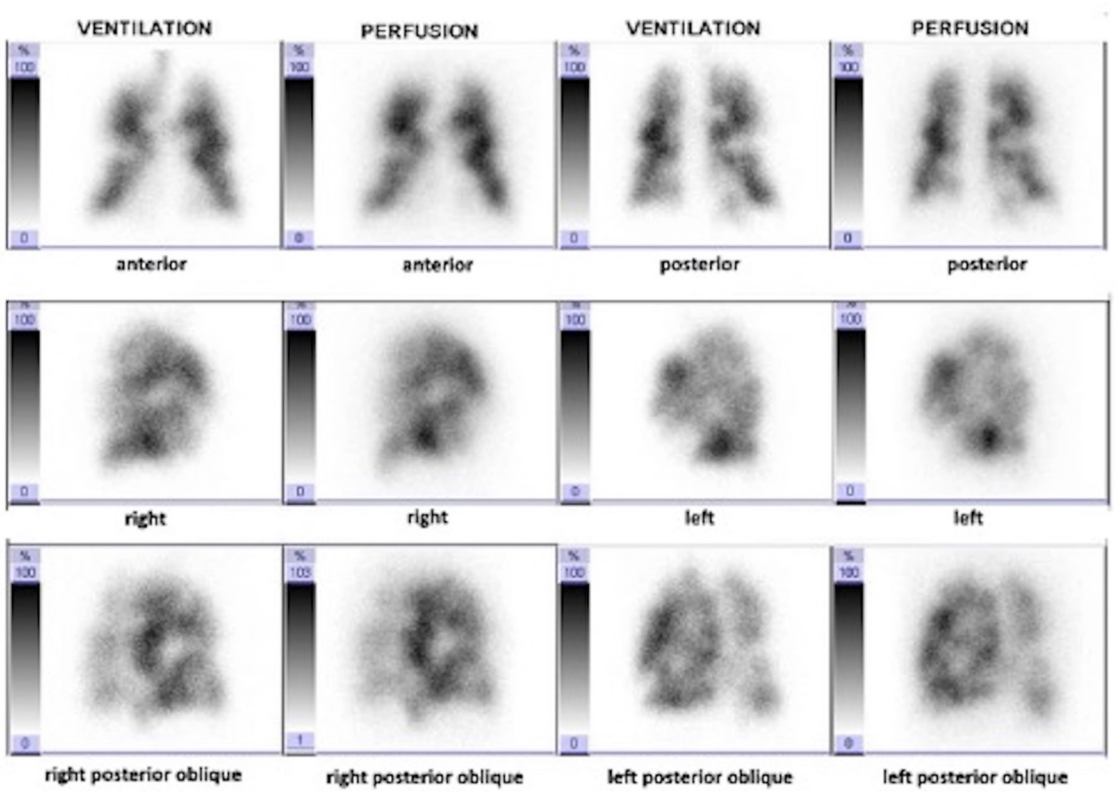

FIGURE 4 | Planar V/Q scan showing multiple perfusion defects matched with ventilation impairments: final diagnosis was a PH classified as mix from group 1, 2 and 3 of PH classification, which was confirmed during the follow-up.

an interpretation based on perfusion only would have led to unnecessary refer 20 patients (12%) to the reference center. The higher specificity of mismatched perfusion defects over perfusion defects is also illustrated by the lower number of mismatched perfusion defects (0.3 segments) than of perfusion defects (1.1 segments) in the non-CTEPH group. Finally, no patient with only matched perfusion defects was diagnosed with CTEPH.

In this study, we only focused the analysis on planar V/Q lung scintigraphy and not on SPECT imaging. Based on an expert consensus, the recent ERS statement on CTEPH proposed to perform SPECT imaging and to provide retro-projected planar images from SPECT data. Indeed, SPECT has largely replaced planar lung scintigraphy in nuclear medicine facilities for the diagnostic of PE (15, 23, 24). However, the diagnostic performance of planar images generated from V/Q SPECT is controversial (25) and data for V/Q SPECT in CTEPH are still sparse. Wang et al. recently reported that both techniques were highly effective for detecting or excluding CTEPH in individual patients, with no significant differences in sensitivity or specificity (14). Although both acute PE and CTEPH are caused by the obstruction of pulmonary arteries, their underlying pathologies differ substantially (2). For instance, pulmonary artery obstructions in patients with CTEPH are more diffuse and multi-segmental as demonstrated in our study with 95% of patient with CTEPH displaying more than 4 segmental mismatched perfusion defects. For the diagnosis of acute PE, SPECT has been reported to be more sensitive and to detect more perfusion defects than planar imaging. In that respect, and given that planar V/Q lung scintigraphy is already highly sensitive, the clinical relevance of using SPECT over planar scintigraphy for screening CTEPH may be questionable. The optimal diagnostic cut-off may also be higher with SPECT than with planar imaging. On the other hand, SPECT imaging may facilitate the co-registration with other imaging modality which may be of value for pre and post-operative assessment of patients with CTEPH. SPECT imaging may also better characterize micro-vascular disease by detecting peripherical perfusion amputation (13). Finally, it would be of interest to further assess the additional value of combining a low dose CT to SPECT imaging (SPECT/CT), which may allow to better characterize morphological abnormalities for alternative diagnosis of dyspnea and therefore increase specificity (26).

Surprisingly, no correlation was found between the extent of perfusion defects and PAPm or PVR impairment in patients with CTEPH. As reported by Azarian et al. (27), it could be explained by the presence of extensive microvascular disease associated with mechanical pulmonary vascular obstruction. Indeed, in our study, 3 out of the 11 patients with PVR $>$ 800 dyn.sec.cm^{-5} showed $<$6 perfusion defects. In these patients, high PVR may be explained not only by mechanical clots but also by a suspected small-vessel disease.

Our study has some limitations. Firstly, the index test and the reference standard were not completely independent as the result of the V/Q scan was used to classify patients according to the different group of PH, and especially to differentiate CTEPH and non-CTEPH cause of PH. The accuracy of V/Q lung scintigraphy could therefore have been artificially increased (28). However, our reference standard was based on the ERS/ESC guidelines for the diagnosis and treatment of PH (11). All patients with possible CTEPH were addressed to the National reference center in Paris and underwent an independent extensive work-up to assess morphology of the diseased pulmonary arteries with conventional catheter pulmonary angiography or high-resolution CT. In order to avoid misdiagnosis, all patients also had a mean follow-up of 3 years. Secondly, we performed a consensus reading and did not assess interobserver reproducibility. However, principles of interpretation, based on the recognition of mismatched perfusion defects, are similar for CTEPH screening and PE diagnosis and are therefore well-known by nuclear medicine physicians.

CONCLUSION

In this study, we confirm the high diagnostic performance of planar V/Q lung scintigraphy for screening CTEPH in patients with PH. The optimal diagnostic cut-off for interpretation was 2.5 segmental mismatched perfusion defects, providing 100% sensitivity and 94.7% specificity, respectively. We also confirmed the need for a ventilation scan as an interpretation only based on perfusion defects provided lower specificity (81.8%) and would have led to unnecessary additional explorations in 12% of patients.

DATA AVAILABILITY STATEMENT

The raw data supporting the conclusions of this article will be made available by the authors, without undue reservation.

ETHICS STATEMENT

Ethical review and approval was not required for the study on human participants in accordance with the local legislation and institutional requirements. The patients/participants provided their written informed consent to participate in this study.

AUTHOR CONTRIBUTIONS

Material preparation, data collection, and analysis were performed by RL, PL, PS, CO, and CT. The first draft of the manuscript was written by RL, PL, and CT. All authors contributed to the study conception, design, commented on previous versions of the manuscript, and read and approved the final manuscript.

ACKNOWLEDGMENTS

The authors would like to acknowledge Marie Guégan for her assistance.

REFERENCES

1. Held M, Hesse A, Gott F, Holl R, Hubner G, Kolb P, et al. A symptom-related monitoring program following pulmonary embolism for the early detection of CTEPH: a prospective observational registry study. *BMC Pulm Med.* (2014) 14:141. doi: 10.1186/1471-2466-14-141
2. Simonneau G, Torbicki A, Dorfmuller P, Kim N. The pathophysiology of chronic thromboembolic pulmonary hypertension. *Eur Respir Rev.* (2017) 26:160112. doi: 10.1183/16000617.0112-2016
3. Guerin L, Couturaud F, Parent F, Revel MP, Gillaizeau F, Planquette B, et al. Prevalence of chronic thromboembolic pulmonary hypertension after acute pulmonary embolism. Prevalence of CTEPH after pulmonary embolism. *Thromb Haemost.* (2014) 112:598–605. doi: 10.1160/TH13-07-0538
4. Bonderman D, Wilkens H, Wakounig S, Schafers HJ, Jansa P, Lindner J, et al. Risk factors for chronic thromboembolic pulmonary hypertension. *Eur Respir J.* (2009) 33:325–31. doi: 10.1183/09031936.00087608
5. Delcroix M, Lang I, Pepke-Zaba J, Jansa P, D'Armini AM, Snijder R, et al. Long-term outcome of patients with chronic thromboembolic pulmonary hypertension: results from an international prospective registry. *Circulation.* (2016) 133:859–71. doi: 10.1161/CIRCULATIONAHA.115.016522
6. Lang IM, Pesavento R, Bonderman D, Yuan JX. Risk factors and basic mechanisms of chronic thromboembolic pulmonary hypertension: a current understanding. *Eur Resp J.* (2013) 41:462–8. doi: 10.1183/09031936.00049312
7. Pepke-Zaba J, Delcroix M, Lang I, Mayer E, Jansa P, Ambroz D, et al. Chronic thromboembolic pulmonary hypertension (CTEPH): results from an international prospective registry. *Circulation.* (2011) 124:1973–81. doi: 10.1161/CIRCULATIONAHA.110.015008
8. Jenkins D, Madani M, Fadel E, D'Armini AM, Mayer E. Pulmonary endarterectomy in the management of chronic thromboembolic pulmonary hypertension. *Eur Respir Rev.* (2017) 26:160111. doi: 10.1183/16000617.0111-2016
9. Tromeur C, Jais X, Mercier O, Couturaud F, Montani D, Savale L, et al. Factors predicting outcome after pulmonary endarterectomy. *PloS one.* (2018) 13:e0198198. doi: 10.1371/journal.pone.0198198
10. Delcroix M, Torbicki A, Gopalan D, Sitbon O, Klok FA, Lang I, et al. ERS statement on chronic thromboembolic pulmonary hypertension. *Eur Respir J.* (2021) 57:2002828. doi: 10.1183/13993003.02828-2020
11. Galie N, Humbert M, Vachiery JL, Gibbs S, Lang I, Torbicki A, et al. 2015 ESC/ERS Guidelines for the diagnosis and treatment of pulmonary hypertension: the Joint Task Force for the Diagnosis and Treatment of Pulmonary Hypertension of the European Society of Cardiology (ESC) and the European Respiratory Society (ERS): Endorsed by: Association for European Paediatric and Congenital Cardiology (AEPC), International Society for Heart and Lung Transplantation (ISHLT). *Eur Respir J.* (2015) 46:903–75. doi: 10.1183/13993003.01032-2015
12. Tunariu N, Gibbs SJ, Win Z, Gin-Sing W, Graham A, Gishen P, et al. Ventilation-perfusion scintigraphy is more sensitive than multidetector CTPA in detecting chronic thromboembolic pulmonary disease as a treatable cause of pulmonary hypertension. *J Nucl Med.* (2007) 48:680–4. doi: 10.2967/jnumed.106.039438
13. Kim NH, Delcroix M, Jais X, Madani MM, Matsubara H, Mayer E, et al. Chronic thromboembolic pulmonary hypertension. *Eur Respir J.* (2019) 53:1801915. doi: 10.1183/13993003.01915-2018
14. Wang L, Wang M, Yang T, Wu D, Xiong C, Fang W, et al. Prospective, comparative study of ventilation-perfusion planar imaging and ventilation-perfusion SPECT for chronic thromboembolic pulmonary hypertension. *J Nucl Med.* (2020) 61:1832–8. doi: 10.2967/jnumed.120.243188
15. Bajc M, Schumichen C, Gruning T, Lindqvist A, Le Roux PY, Alatri A, et al. EANM guideline for ventilation/perfusion single-photon emission computed tomography (SPECT) for diagnosis of pulmonary embolism and beyond. *Eur J Nucl Med Mol imaging.* (2019) 46:2429–51. doi: 10.1007/s00259-019-04450-0
16. Le Roux PY, Robin P, Delluc A, Abgral R, Le Duc-Pennec A, Nowak E, et al. V/Q SPECT interpretation for pulmonary embolism diagnosis: which criteria to use? *J Nucl Med.* (2013) 54:1077–81. doi: 10.2967/jnumed.112.113639
17. Gopalan D, Delcroix M, Held M. Diagnosis of chronic thromboembolic pulmonary hypertension. *Eur Respir Rev.* (2017) 26:160108. doi: 10.1183/16000617.0108-2016
18. Simonneau G, Montani D, Celermajer DS, Denton CP, Gatzoulis MA, Krowka M, et al. Haemodynamic definitions and updated clinical classification of pulmonary hypertension. *Eur Respir J.* (2019) 53:1801913. doi: 10.1183/13993003.01913-2018
19. Le Roux PY, Blanc-Beguin F, Bonnefoy PB, Bourhis D, Camilleri S, Moreau-Triby C, et al. SFMN guideline for lung scintigraphy protocols. *Méd Nucl.* (2021) 45:85–92. doi: 10.1016/j.mednuc.2021.01.001
20. Investigators P. Value of the ventilation/perfusion scan in acute pulmonary embolism. Results of the prospective investigation of pulmonary embolism diagnosis (PIOPED). *JAMA.* (1990) 263:2753–9. doi: 10.1001/jama.263.20.2753
21. Watanabe N, Fettich J, Kucuk NO, Kraft O, Mut F, Choudhury P, et al. Modified PISAPED criteria in combination with ventilation scintigraphic finding for predicting acute pulmonary embolism. *World J Nucl Med.* (2015) 14:178–83. doi: 10.4103/1450-1147.163248
22. Le Roux PY, Bonnefoy PB, Bahloul A, Denizot B, Barres B, Moreau-Triby C, et al. Lung scintigraphy for pulmonary embolism diagnosis in COVID-19 patients: a multicenter study. *J Nucl Med.* (2021). doi: 10.2967/jnumed.121.262955. [Epub ahead of print].
23. Le Roux PY, Robin P, Tromeur C, Davis A, Robert-Ebadi H, Carrier M, et al. Ventilation/perfusion SPECT for the diagnosis of pulmonary embolism: A systematic review. *J Thromb Haemost.* (2020) 18:2910–20. doi: 10.1111/jth.15038
24. Le Roux PY, Pelletier-Galarneau M, De Laroche R, Hofman MS, Zuckier LS, Roach P, et al. Pulmonary scintigraphy for the diagnosis of acute pulmonary embolism: a survey of current practices in Australia, Canada, and France. *J Nucl Med.* (2015) 56:1212–7. doi: 10.2967/jnumed.115.157743
25. Le Roux PY, Abgral R, Jaffrelot M, Delluc A, Gut-Gobert C, Querellou S, et al. Diagnosis of pulmonary embolism: planar images generated from V/Q SPECT are not a reliable substitute for traditional planar V/Q scan. *Nucl Med Commun.* (2012) 33:695–700. doi: 10.1097/MNM.0b013e328352c7d2
26. Liu J, Larcos G. Radionuclide lung scans for suspected acute pulmonary embolism: Single photon emission computed tomography (SPECT) or hybrid SPECT/CT? *J Med Imaging Radiat Oncol.* (2019) 63:731–6. doi: 10.1111/1754-9485.12951
27. Azarian R, Wartski M, Collignon MA, Parent F, Herve P, Sors H, et al. Lung perfusion scans and hemodynamics in acute and chronic pulmonary embolism. *J Nucl Med.* (1997) 38:980–3.
28. Le Gal G, Le Roux PY. How to assess quality of primary research studies in the medical literature? *Semin Nucl Med.* (2019) 49:115–20. doi: 10.1053/j.semnuclmed.2018.11.007

Conflict of Interest: The authors declare that the research was conducted in the absence of any commercial or financial relationships that could be construed as a potential conflict of interest.

frontiers in Medicine

ORIGINAL RESEARCH
published: 14 March 2022
doi: 10.3389/fmed.2022.840196

CMR Measures of Left Atrial Volume Index and Right Ventricular Function Have Prognostic Value in Chronic Thromboembolic Pulmonary Hypertension

Yousef Shahin[1,2], Samer Alabed[1,2], Syed Rehan Quadery[3], Robert A. Lewis[3], Christopher Johns[2], Dheyaa Alkhanfar[1], Maria Sukhanenko[2], Faisal Alandejani[1], Pankaj Garg[1], Charlie A. Elliot[3], Abdul Hameed[1,3], Athaniosis Charalampopoulos[3], James M. Wild[1,4], Robin Condliffe[3], Andrew J. Swift[1,2,4] and David G. Kiely[1,3,4]*

[1] Department of Infection, Immunity and Cardiovascular Disease, University of Sheffield, Sheffield, United Kingdom, [2] Department of Clinical Radiology, Sheffield Teaching Hospitals NHS FT, Sheffield, United Kingdom, [3] Sheffield Pulmonary Vascular Disease Unit, Royal Hallamshire Hospital, Sheffield Teaching Hospitals NHS FT, Sheffield, United Kingdom, [4] INSIGNEO, Institute for in silico Medicine, University of Sheffield, Sheffield, United Kingdom

OPEN ACCESS

Edited by:
Elena Goncharova,
University of California, Davis,
United States

Reviewed by:
Roberto J. Bernardo,
University of Oklahoma Health Sciences Center, United States
Mark O. Wielpütz,
Heidelberg University, Germany

***Correspondence:**
Yousef Shahin
y.shahin@sheffield.ac.uk

Specialty section:
This article was submitted to Pulmonary Medicine, a section of the journal Frontiers in Medicine

Received: 20 December 2021
Accepted: 04 February 2022
Published: 14 March 2022

Citation:
Shahin Y, Alabed S, Rehan Quadery S, Lewis RA, Johns C, Alkhanfar D, Sukhanenko M, Alandejani F, Garg P, Elliot CA, Hameed A, Charalampopoulos A, Wild JM, Condliffe R, Swift AJ and Kiely DG (2022) CMR Measures of Left Atrial Volume Index and Right Ventricular Function Have Prognostic Value in Chronic Thromboembolic Pulmonary Hypertension. Front. Med. 9:840196. doi: 10.3389/fmed.2022.840196

Providing prognostic information is important when counseling patients and planning treatment strategies in chronic thromboembolic pulmonary hypertension (CTEPH). The aim of this study was to assess the prognostic value of gold standard imaging of cardiac structure and function using cardiac magnetic resonance imaging (CMR) in CTEPH. Consecutive treatment-naive patients with CTEPH who underwent right heart catheterization and CMR between 2011 and 2017 were identified from the ASPIRE (Assessing-the-Specturm-of-Pulmonary-hypertensIon-at-a-REferral-center) registry. CMR metrics were corrected for age and sex where appropriate. Univariate and multivariate regression models were generated to assess the prognostic ability of CMR metrics in CTEPH. Three hundred and seventy-five patients (mean+/-standard deviation: age 64+/-14 years, 49% female) were identified and 181 (48%) had pulmonary endarterectomy (PEA). For all patients with CTEPH, left-ventricular-stroke-volume-index-%predicted (LVSVI%predicted) ($p = 0.040$), left-atrial-volume-index (LAVI) ($p = 0.030$), the presence of comorbidities, incremental shuttle walking test distance (ISWD), mixed venous oxygen saturation and undergoing PEA were independent predictors of mortality at multivariate analysis. In patients undergoing PEA, LAVI ($p < 0.010$), ISWD and comorbidities and in patients not undergoing surgery, right-ventricular-ejection-fraction-%predicted (RVEF%pred) ($p = 0.040$), age and ISWD were independent predictors of mortality. CMR metrics reflecting cardiac function and left heart disease have prognostic value in CTEPH. In those undergoing PEA, LAVI predicts outcome whereas in patients not undergoing PEA RVEF%pred predicts outcome. This study highlights the prognostic value of imaging cardiac structure and function in CTEPH and the importance of considering left heart disease in patients considered for PEA.

Keywords: cardiac MRI, chronic thromboembolic pulmonary hypertension, left atrium, survival, left heart disease

INTRODUCTION

Pulmonary hypertension (PH) is heterogeneous and treatment depends on the underlying cause (1). Chronic thromboembolic pulmonary hypertension (CTEPH) is a potentially curable form of PH and a recent meta-analysis has identified a cumulative incidence of 2.9% in patients surviving an acute pulmonary embolism (2). It can also present as PH with no previous evidence of venous thromboembolism (3). It is characterized by non-resolution of thrombus and remodeling of the pulmonary arteries resulting in PH and right ventricular (RV) dysfunction (4) and without treatment a poor prognosis. Pulmonary endarterectomy (PEA), however, provides a potentially curative treatment for selected patients with CTEPH (5) with other options including pulmonary arterial hypertension (PAH) therapies and balloon pulmonary angioplasty (6). Increasingly patients with CTEPH are presenting with comorbidities and additional information that could aid decision making would be helpful.

Several clinical and haemodynamic measurements have been used to assess disease severity and risk stratify patients with PAH. These include an assessment of symptoms (WHO Functional class), exercise capacity (6-min walk test) and measures reflecting RV function including blood based biomarkers (N-terminal pro brain natriuretic peptide) and measures from cardiac catheterization (right atrial pressure, cardiac index and mixed venous oxygen saturation) (7–9). However, some of these measurements are limited by their subjectivity and invasive nature. Nonetheless, a multiparameter risk assessment incorporating a number of these measurements is now recommended in patients with PAH (9) and there is evidence that this approach can also be used in patients with CTEPH (10, 11).

Magnetic resonance imaging using CMR has been shown to have diagnostic value in suspected PH (12–14), prognostic value in PAH (15–17) and in screening for CTEPH using MR perfusion maps (18, 19) and aiding the surgical assessment of CTEPH using MR pulmonary angiography (12, 20). Septal angle, pulmonary artery area and ventricular mass index have additive value in a model to estimate pulmonary artery pressure (14, 21). Measures of RV function including stroke volume, right ventricular end systolic volume and right ventricular ejection fraction predict clinical worsening and mortality and left ventricular measures such as left ventricular end systolic volume predict mortality in PAH (15–17, 22). However, there is limited data on the utility of CMR measures of right ventricular function to aid mortality prediction in CTEPH and to our knowledge no data on the use of left ventricular or atrial measurements.

The aim of this study was, therefore, to assess the prognostic value of gold standard imaging of cardiac structure and function using CMR in a large cohort of patients with CTEPH.

MATERIALS AND METHODS

Patients

Consecutive treatment-naive patients diagnosed with CTEPH who had CMR and right heart catheterization (RHC) up to February 2017 were prospectively recorded in hospital databases as part of the ASPIRE (Assessing the Spectrum of Pulmonary Hypertension Identified at a Referral Center) registry as previously described (23, 24) (ClinicalTrials.gov identifier NCT02565030). Patients' demographics, imaging, and clinical metrics with follow-up data were prospectively collected using a census date of April 29th 2019. CMR and RHC metrics, exercise test, pulmonary function, and treatment were included.

The diagnosis of CTEPH required patients to have undergone RHC with a measured mean pulmonary artery pressure (mPAP) $\geq$ 25 mmHg at rest and at least one segmental perfusion defect on perfusion lung Q scan or pulmonary artery (PA) obstruction seen by multidetector computed tomography pulmonary angiography (CTPA) or conventional pulmonary angiography with other causes of PH excluded (9).

Following multi-modality imaging patients were discussed at a multi-professional meeting. Patients with CTEPH were subsequently discussed at the national pulmonary endarterectomy MDT at Papworth Hospital, Cambridge where surgical accessibility and suitability for surgery were assessed.

All patients were followed up until the date of death or census date. Ethical approval for this study was granted by our institutional review board (ref c06/Q2308/8). This study was funded by grants from the Wellcome Trust (A.J.S.). The funding body was not involved in the study design or data interpretation.

Cardiac MRI Acquisition

CMR was performed using an eight channel cardiac coil on a GE HDx (GE Healthcare, Milwaukee, WI) whole body scanner at 1.5 T, as previously described (15). Short-axis cine images were acquired using a cardiac gated multislice balanced SSFP sequence (20 frames per cardiac cycle; slice thickness, 8 mm; field of view, 48 cm; matrix, 2563256; BW, 125 kHz/pixel; TR/TE, 3.7/1.6 ms). A stack of images in the short-axis plane with slice thickness of 8 mm (2-mm inter-slice gap) were acquired fully covering both ventricles from base to apex. End-systole was considered to be the smallest cavity area. End-diastole was defined as the first cine phase of the R-wave triggered acquisition or largest volume. Through plane phase contrast imaging was performed orthogonal to the main pulmonary trunk. Phase contrast imaging parameters were as follows: repetition time, TR 5.6 ms; echo time, TE 2.7 ms; slice thickness, 10 mm; field of view, 48 cm, bandwidth, 62.5 kHz; matrix, 256 3128; 20 reconstructed cardiac phases; and velocity encoding of flow, 150 cm/s. Patients were in the supine position with a surface coil and with retrospective ECG gating.

Image Analysis

Image analysis was performed on a GE Advantage Workstation 4.1 with the observer blinded to the patient clinical information, and cardiac catheter parameters. Right and left endocardial and epicardial surfaces were manually traced from the stack of short-axis cine images, using proprietary MR workstation software to obtain RV end-diastolic volume (RVEDV) and RV end-systolic volume (RVESV), and left ventricular (LV) end-diastolic volume (LVEDV) and LV end-systolic volume (LVESV). From end-diastolic and end-systolic volumes, RVEF and LV ejection fraction (LVEF) and RV and LV stroke volumes (SV) were calculated. With the exception of RVEF and LVEF, these

measurements were all corrected for age and sex (%pred) based on previously published referenced data (25) and they were indexed for body surface area based on Mostellar formula (26). Based on previous work, SV was considered to be the most accurate from LV volumetry (27) and was used for MRI estimation of RV–PA coupling. For calculation of ventricular mass, the interventricular septum was considered as part of the LV. RV end-diastolic mass (RVEDM) and LV end-diastolic mass (LVEDM) were derived. Ventricular mass index (VMI) was defined as RV mass divided by LV mass, as previously described (28). Maximal and minimal PA areas were measured, and relative area change was defined by the following equation: relative area change = (maximum area – minimum area)/minimum area (29). Reproducibility for CMR measurements in our center has been described previously (15).

Right Heart Catheterization

RHC was performed using a balloon-tipped 7.5F thermodilution catheter (Becton-Dickinson, Franklin Lakes, NJ). RHC was usually performed via the internal jugular vein using a Swan-Ganz catheter. Measurements of right atrial pressure, pulmonary arterial wedge pressure (PAWP), cardiac output (CO) using thermodilution and mixed venous oxygen saturation were also made. Pulmonary vascular resistance (PVR) was calculated as [(mPAP-PAWP) / CO] / 80 and expressed as dyne.s.cm^{-5}.

Pulmonary Arterial Stiffness and Coupling Measurements

As previously described (15, 30–32), RV elastance (Ees) was estimated as mPAP divided by RVESV. PA elastance (Ea) was estimated using mPAP-PAWP divided by LVSV. Ees/Ea by a combined RHC and CMR approach was defined as follows: (mPAP/RVESV)/[(mPAP-PAWP)/LVSV]. CMR estimated Ees/Ea was defined by LVSV/RVESV. Distensibility, a measurement of PA stiffness, was defined as PA relative area change divided by pulse pressure.

Statistical Analysis

Continuous variables were expressed as mean (SD) for parametric variables and median (interquartile range) for non-parametric variables. Categorical data was presented as the number of subjects and percentage. Continuous variables were compared using independent sample *t*-test. Categorical variables were compared using Pearson's Chi-square test. Survival analysis was conducted using Kaplan-Meier plots and survival was compared using the log-rank test. Survival was calculated from date of diagnosis to date of death or census date to compare survival between the PEA and non-PEA groups. To assess the prognostic value of CMR metrics, survival was calculated from date of CMR to date of death or census date. Univariate Cox proportional hazard regression analysis was used to assess the prognostic value of CMR metrics in terms of biventricular volume, function, mass and PA stiffness metrics in the whole cohort, PEA and non-PEA groups. Hazard ratios (HR) generated from univariate analysis were scaled by dividing the actual individual value of the variable by SD. This is to allow direct comparison of HR. Multivariate Cox proportional hazard regression analysis was performed for predicted CMR variables / MRI coupling measurement, clinical variables and combined CMR and clinical variables. Selected variables were entered into multivariate models if they were reported in literature as predictors of mortality (33, 34), ≤ 10% missing values and a $p < 0.200$ at univariate analysis. Multivariate models for the whole cohort, PEA and non-PEA groups were generated. To overcome multicollinearity, highly correlated variables ($r > 0.80$) were entered separately in the models. Receiver operating characteristics (ROC) analysis was used to assess the prognostic significance of the CMR, clinical and combined CMR and clinical models generated on the whole, PEA and non-PEA cohorts and presented with area under the curve (AUC). In order to evaluate the stability (internal validation) of the CMR prognostic model of the whole cohort, PEA group and non-PEA groups, the bootstrap approach with 1,000 bootstrap samples (default settings) was performed (35). In the bootstrap, simple sampling method with bias-corrected and accelerated 95% confidence interval (95%

TABLE 1 | Patients demographics and results of baseline investigations for the whole CTEPH cohort, patients undergoing pulmonary endarterectomy, and not undergoing pulmonary endarterectomy.

Demographics	All patients (*n* = 375)	PEA (*n* = 181)	Non-PEA (*n* = 194)	*P*-value
Age, years	64 (14)	60 (14)	67 (13)	<0.001
Female, *n* (%)	185 (49)	88 (23)	97 (26)	0.836
BMI, kg/m^2	29 (6)	29 (6)	29 (6)	0.354
Comorbidities, *n* (%)				
Malignancy	52 (14)	14 (8)	38 (20)	0.035
CAD	45 (12)	18 (10)	27 (14)	0.237
Left Heart Failure	19 (5)	7 (4)	12 (6)	0.306
CKD	27 (7)	12 (7)	15 (8)	0.680
COPD	35 (9)	13 (7)	22 (11)	0.167
AF	46 (12)	28 (15)	18 (9)	0.068
CVA	26 (7)	17 (9)	9 (5)	0.070
Right heart catheter metrics				
mRAP, mmHg	10 (5)	11 (5)	10 (4)	0.618
mPAP, mmHg	44 (12)	44 (12)	44 (13)	0.840
PAWP, mmHg	12 (4)	12 (4)	12 (4)	0.815
PVR, dyne.s.cm^{-5}	587 (369)	597 (387)	578 (352)	0.680
CI, L/min/m^2	2.5 (0.7)	2.5 (0.7)	2.5 (0.7)	0.882
SvO_2, %	63 (8)	63 (8)	62 (7)	0.337
Lung function tests and exercise tests				
FEV1, L	2.17 (0.79)	2.33 (0.77)	2.02 (0.77)	<0.001
FVC, L	3.23 (1.10)	3.41 (1.09)	3.06 (1.07)	0.003
DLCO %pred	57 (20)	59 (21)	55 (18)	0.062
ISWD, m	248 (200)	283 (194)	215 (201)	0.001

Data is presented as mean (SD) unless otherwise stated.

BMI, body mass index; CAD, coronary artery disease; CI, cardiac index; CKD, chronic kidney disease; COPD, chronic obstructive pulmonary disease; CVA, cerebrovascular accident; DLCO, diffusing capacity of the lungs for carbon monoxide; FEV1, forced expiratory volume; FVC, forced vital capacity; ISWD, incremental shuttle walking distance; mPAP, mean pulmonary arterial pressure; mRAP, mean right atrial pressure; PAWP, pulmonary artery wedge pressure; PEA, pulmonary endarterectomy; PVR, pulmonary vascular resistance; SvO_2, mixed venous oxygen saturation; %pred, percentage predicted.

TABLE 2 | Cardiac MRI imaging parameters for the whole CTEPH cohort, patients undergoing pulmonary endarterectomy, and not undergoing pulmonary endarterectomy.

Cardiac MR metrics	All patients ($n = 375$)	PEA ($n = 181$)	Non-PEA ($n = 194$)	*P*-value
RVEDVI %pred	114 (43)	109 (42)	119 (44)	0.021
RVESVI %pred	227 (125)	207 (106)	245 (138)	0.003
RVEF %pred	58 (20)	59 (19)	57 (21)	0.283
RVSVI %pred	63 (25)	63 (27)	64 (24)	0.587
RVEDMI %pred	74 (36)	70 (30)	77 (41)	0.046
LVEDVI %pred	77 (21)	77 (22)	77 (20)	0.995
LVESVI %pred	83 (38)	85 (39)	82 (37)	0.440
LVEF %pred	97 (15)	95 (15)	98 (16)	0.178
LVSVI %pred	74 (23)	74 (23)	75 (23)	0.603
LVEDMI %pred	71 (15)	70 (14)	72 (15)	0.102
LAVI, ml/m^2	35 (16)	35 (16)	36 (17)	0.710
VMI, %	0.45 (0.21)	0.44 (0.19)	0.46 (0.22)	0.363
PA stiffness and RV-PA coupling metrics				
PA RAC, ratio	11 (10)	11 (10)	10 (9)	0.449
PA distensibility, (ΔV/V)/ΔP	0.2 (0.2)	0.2 (0.1)	0.2 (0.1)	0.628
Ees, mmHg/ml/m^2	1 (0.5)	1 (0.5)	1 (0.5)	0.323
Ea, mmHg/ml/m^2	1 (0.6)	1 (0.5)	1 (0.6)	0.448
Ees/Ea ratio	2 (1)	2 (1)	2 (1)	0.844
MRI Ees/Ea ratio	0.4 (0.1)	0.4 (0.1)	0.4 (0.1)	0.626

Data is presented as mean (SD) unless otherwise stated.
Ea, arterial load; Ees, right ventricle elastance; LAVI, left atrium volume index; LVEDMI, left ventricle end diastolic mass index; LVEDVI, left ventricle end diastolic volume index; LVEF, left ventricle ejection fraction; LVESVI, left ventricle end systolic volume index; LVSVI, left ventricle stroke volume index; MRI, magnetic resonance imaging; PA, pulmonary artery; PA RAC, pulmonary artery relative area change; RVEDMI, right ventricle end diastolic mass index; RVEDVI, right ventricle end diastolic volume index; RVEF, right ventricle ejection fraction; RVSP, right ventricle systolic pressure; RVESVI, right ventricle end systolic volume index; RVSVI, right ventricle stroke volume index; VMI, ventricular mass index. For other abbreviations see legend for ***Table 1****.*

C.I.) type were selected. Locally estimated scatterplot smoothing regression analysis (LOESS) was performed for 1 year mortality, where significance was demonstrated at multivariate analysis, for patients undergoing and not undergoing PEA. All statistical tests were two-sided and a *p*-value of < 0.050 was considered statistically significant. A Statistical Package for the Social Sciences Program (SPSS) version 26 for Windows (SPSS Inc. Chicago, IL) was used for statistical analysis and for presentation of data GraphPad Prism 8.3.0 (GraphPad Software, San Diego, CA) was used.

RESULTS

Baseline Demographics and Measurements

A total of 375 patients (mean+/-SD age 64+/- 14 years, 185 (49%) females) with CTEPH were included in the analysis. One hundred and eighty-one (48%) patients had PEA. **Table 1** shows demographic, RHC, and lung function results and **Table 2** CMR, RV-PA coupling metrics and pulmonary stiffness data, for the whole cohort and for the PEA and non-PEA groups. The mean+/- SD time delay between RHC and CMR was 45+/- 15 days.

TABLE 3 | Univariate Cox proportional hazards regression analysis in patients with CTEPH undergoing pulmonary endarterectomy (metrics shown where $p < 0.20$).

Covariate	Univariate hazard ratio	Scaled univariate hazard ratio	*P*-value
Age, years	1.028 (0.996–1.060)	1.035 (0.998–1.074)	0.087
ISWD, m	0.995 (0.992–0.998)	0.883 (0.871–0.990)	<0.001
Comorbidities, *n*			
Malignancy	3.611 (1.407–9.266)		0.008
CAD	4.577 (1.864–11.241)		0.001
Cardiac MR metrics			
LVESVI %pred	1.005 (0.999–1.011)	1.209 (0.953–1.534)	0.117
LVEF %pred	0.980 (0.958–1.001)	0.739 (0.535–1.019)	0.066
LVSVI %pred	0.987 (0.970–1.004)	0.650 (0.425–0.996)	0.135
LAVI, ml/m^2	1.029 (1.015–1.044)	1.513 (1.173–1.952)	<0.001
Right heart catheter metrics			
SvO_2, %	0.932 (0.883–0.984)	0.598 (0.403–0.887)	0.011
Lung function tests			
FEV1 %pred	0.463 (0.261–0.823)	0.641 (0.498–0.825)	0.009
DLCO %pred	0.660 (0.500–0.873)	0.479 (0.361–0.635)	0.004

Data in paracenteses is 95% confidence interval.
For abbreviations see legend for ***Tables 1****,* ***2****.*

Compared with the non-PEA group, patients in the PEA group were younger ($p < 0.001$), had a higher incremental shuttle walking distance (ISWD) ($p = 0.001$), lower RVESVI%pred (p=0.003), lower RVEDMI%pred ($p = 0.046$), higher forced expiratory volume at 1 min (FEV1) ($p < 0.001$) and higher forced vital capacity (FVC) ($p = 0.003$).

Survival Analysis

During the follow up period, 104 (28%) patients died. The median overall survival for the whole cohort was 143 months. Median survival of patients undergoing PEA was higher than patients not undergoing surgery (146 vs. 97 months, 95% C.I. (121–162); $p < 0.001$). Patients' demographics, CMR, RHC, lung function tests and pulmonary arterial stiffness data between survivors and non-survivors is summarized in **Supplementary Table 1**. Survivors were younger ($p < 0.001$) with a higher percentage of females ($p < 0.001$), had better lung function ($p < 0.001$), exercise capacity and less likely to have a history of malignancy, coronary artery disease, chronic kidney disease or COPD.

Univariate Analysis of Predictors of Mortality

Univariate Cox proportional hazard regression analysis for CMR metrics and clinical variables for the whole cohort is presented in **Supplementary Table 2**. Only variables with $p < 0.200$ are shown. CMR measures of RV size and function [RVEDVI%pred ($p = 0.002$), RVESVI%pred ($p < 0.001$), and RVEF%pred ($p < 0.001$)], LV function [LVSVI%pred ($p = 0.001$) and LVEF%pred ($p = 0.011$)], LA volume [LAVI ($p = 0.010$)] and invasive ($p = 0.027$) and non-invasive CMR-derived Ea/Ees ratio ($p = 0.001$), were significant predictors

TABLE 4 | Univariate Cox proportional hazards regression analysis in patients with CTEPH not undergoing pulmonary endarterectomy (metrics shown where $p < 0.20$).

Covariate	Univariate hazard ratio	Scaled univariate hazard ratio	*P*-value
Age, years	1.032 (1.011–1.054)	1.044 (1.020–1.062)	0.003
ISWD, m	0.997 (0.996–0.999)	0.799 (0.774–0.883)	0.001
Comorbidities, *n*			
Malignancy	1.747 (1.030–2.962)		0.038
CAD	2.455 (1.425–4.227)		0.001
COPD	1.692 (0.932–3.070)		0.087
Left Heart Failure	2.064 (0.944–4.514)		0.070
Cardiac MR metrics			
RVEDVI %pred	1.007 (1.002–1.011)	1.338 (1.095–1.634)	0.004
RVESVI %pred	1.002 (1.001–1.004)	1.322 (1.119–1.560)	0.001
RVEF %pred	0.983 (0.973–0.993)	0.706 (0.574–0.870)	0.001
RVEDMI %pred	1.005 (1.000–1.009)	1.192 (1.012–1.403)	0.035
LVEDVI %pred	0.988 (0.977–1.000)	0.792 (0.632–0.993)	0.043
LVEF %pred	0.984 (0.971–0.998)	0.789 (0.641–0.969)	0.010
LVSVI %pred	0.984 (0.974–0.994)	0.689 (0.547–0.867)	0.002
LVEDMI %pred	1.010 (0.995–1.024)	1.150 (0.930–1.423)	0.197
VMI, %	2.110 (0.869–5.110)	2.300 (0.996–5.220)	0.099
Right heart catheter metrics			
mPAP, mmHg	1.022 (1.003–1.041)	1.295 (1.035–1.609)	0.024
mRAP, mmHg	1.087 (1.041–1.136)	1.521 (1.221–1.893)	<0.001
CO, L/min	0.790 (0.663–0.942)	0.702 (0.540–0.914)	0.009
PVR, dyne.s.cm^{-5}	1.001 (1.000–1.002)	1.536 (1.190–1.981)	0.001
SvO_2, %	0.914 (0.888–0.941)	0.519 (0.421–0.639)	<0.001
Lung function tests			
FEV1 %pred	0.678 (0.472–0.973)	0.735 (0.552–0.979)	0.035
DLCO %pred	0.719 (0.609–0.850)	0.534 (0.389–0.734)	<0.001
PA stiffness and RV-PA coupling metrics			
Ees, mmHg/ml/m^2	0.552 (0.308–0.998)	0.756 (0.575–0.995)	0.046
Ea, mmHg/ml/m^2	1.341 (0.991–1.816)	1.196 (0.994–1.439)	0.057
Ees/Ea ratio	0.637 (0.475–0.855)	0.649 (0.472–0.893)	0.003
MRI Ees/Ea ratio	0.095 (0.021–0.443)	0.719 (0.582–0.889)	0.002

Data in paracenteses is 95% confidence interval.
*For abbreviations see legend for **Tables 1**, **2**.*

of mortality at univariate Cox regression analysis for the whole cohort. Separate univariate Cox regression analysis was performed for PEA and non-PEA groups and is shown in **Tables 3**, **4**, respectively.

Multivariate Analysis of Predictors of Mortality

Multivariate Cox proportional hazard regression analysis models of only CMR metrics, clinical variables and CMR metrics and clinical variables ($p < 0.200$) at univariate analysis are presented in **Table 5**. In the whole cohort, higher RVESVI%pred ($p = 0.007$), lower LVSVI%pred ($p = 0.001$) and higher LAVI ($p = 0.001$) were independent predictors of increased mortality in the CMR metrics model. The regression equation for

TABLE 5 | Multivariate cardiac MR metrics, clinical variables, and combined cardiac MR and clinical variables Cox regression model in the whole CTEPH cohort, endarterectomy and non-endarterectomy groups.

Covariate	Multivariate hazard ratio	*P*-value
Cardiac MR model		
Whole cohort		
RVESVI %pred	1.002 (1.001–1.003)	0.007
LVSVI %pred	0.984 (0.974–0.993)	0.001
LAVI, ml/m^2	1.013 (1.005–1.020)	0.001
PEA group		
LVSVI %pred	0.982 (0.966–0.999)	0.035
LAVI, ml/m^2	1.030 (1.017–1.044)	<0.001
Non-PEA group		
RVEF %pred	0.846 (0.739–0.968)	0.015
LVSVI %pred	0.986 (0.974–0.998)	0.024
Clinical model		
Whole cohort		
ISWD, m	0.997 (0.995–0.999)	0.001
PEA, *n*	0.384 (0.231–0.631)	<0.001
CAD, *n*	2.357 (1.398–3.973)	0.001
COPD, *n*	1.915 (1.056–3.472)	0.032
Malignancy, *n*	2.513 (1.454–4.433)	0.001
SvO_2, %	0.946 (0.917–0.977)	0.001
PEA group		
ISWD, m	0.995 (0.991–0.998)	0.004
CAD, *n*	3.543 (1.331–9.431)	0.011
Malignancy, *n*	2.897 (1.008–8.328)	0.042
Non-PEA group		
ISWD, m	0.998 (0.996–1.000)	0.015
CAD, *n*	1.956 (1.087–3.520)	0.025
Malignancy, *n*	1.948 (1.117–3.396)	0.019
mRAP, mmHg	1.094 (1.040–1.149)	<0.001
Combined cardiac MR and clinical model		
Whole cohort		
ISWD, m	0.997 (0.995–0.999)	0.002
PEA, *n*	0.467 (0.271–0.804)	0.006
CAD, *n*	2.605 (1.497–4.532)	0.001
Malignancy, *n*	1.952 (1.059–3.595)	0.032
CKD, *n*	2.092 (1.056–4.144)	0.034
SvO_2, %	0.953 (0.918–0.990)	0.013
LVSVI %pred	0.960 (0.924–0.998)	0.040
LAVI, ml/m^2	1.015 (1.001–1.028)	0.033
PEA group		
ISWD, m	0.993 (0.988–0.997)	<0.001
LAVI, ml/m^2	1.022 (1.020–1.032)	0.043
Malignancy, *n*	3.034 (1.043–8.823)	0.042
CAD, *n*	4.063 (1.681–9.817)	0.002
Non-PEA group		
Age, years	1.044 (1.013–1.075)	0.004
ISWD, m	0.998 (0.995–1.000)	0.024
RVEF %pred	0.961 (0.931–0.999)	0.017
RVEDVI %pred	1.025 (1.001–1.029)	0.039

Data in paracenteses is 95% confidence interval.
*For abbreviations see legend for **Tables 1**, **2**.*

the multivariate Cox regression model in the whole cohort is as follows: Expected hazard = (RVESV%pred*0.002)-(LVSVI%pred*0.019) + (LAVI*0.013). In the PEA group, lower LVSVI%pred ($p = 0.035$) and higher LAVI ($p < 0.001$) (Expected hazard = (LAVI*0.030) - (LVSVI%pred*0.018) and in the non-PEA group, lower RVEF%pred ($p = 0.015$) and lower LVSVI%pred ($p = 0.024$) were independent predictors of increased mortality [Expected hazard = (RVEF%pred*-0.167) - (LVSVI%pred*0.014)]. In the combined model, lower LVSVI%pred ($p = 0.040$) and higher LAVI ($p = 0.033$) in the whole cohort, higher LAVI ($p = 0.009$) in the PEA group and lower RVEF%pred ($p = 0.040$) in the non-PEA group were predictors of increased mortality.

Figure 1 shows Kaplan-Meier survival analysis of the PEA group (LVSVI%pred and LAVI) and non-PEA group (LVSVI%pred and RVEF%pred). LAVI is plotted above and below a value of 41 ml/m^2 based on previous work and for other values based on median (36). **Figure 2** shows LOESS regression analysis for risk of 1 year mortality for LVSVI%pred and LAVI for patients undergoing PEA and for LVSVI%pred and RVEF%pred for the Non-PEA group.

Accuracy, Sensitivity, and Specificity of Prognostic Models

The accuracy of the multivariate Cox models for the whole, PEA and non-PEA cohorts was tested using ROC analysis and presented as AUC. The prognostic accuracy of the CMR model in the whole cohort (AUC, 0.69, $p = 0.001$), clinical model (AUC, 0.62, $p < 0.001$) and in the combined CMR and clinical model (AUC, 0.65, $p < 0.001$). Sensitivity and specificity of the CMR whole cohort model was 71% (95% CI, 65–76) and 62% (95% CI, 52–72) respectively, clinical model 78% (95% CI, 69–86) and 43% (95% CI, 37–50) and for the combined clinical and CMR model 70% (95% CI, 63–76) and 55% (95% CI, 45–65), respectively (**Figure 3A**). In the PEA cohort, the prognostic accuracy of the CMR model (AUC, 0.73, $p < 0.001$), clinical model (AUC, 0.69, $p = 0.002$) and in the combined clinical and CMR model (AUC, 0.76, $p < 0.001$). Sensitivity and specificity of the CMR PEA model 80% (95% CI, 61–91) and 53% (95% CI, 46–62), respectively, clinical model 72% (95% CI, 65–79) and 65% (95% CI, 46–79) and for the combined model 80% (95% CI, 61–91) and 53% (95% CI, 46–62), respectively (**Figure 3B**). The prognostic accuracy of the CMR model in the non-PEA group (AUC, 0.63, $p = 0.003$), clinical model (AUC, 0.63, $p = 0.003$) and for the combined model (AUC, 0.56, $p = 0.030$). The sensitivity and specificity were 65% (95% CI, 56–73) and 60% (95% CI, 50–71), respectively for the CMR model, 60% (95% CI, 48–70) and 58% (95% CI, 50–67), respectively for the clinical model and 60% (95% CI, 48–70) and 58% (95% CI, 50–67), respectively for the combined model (**Figure 3C**).

Internal Validation and Bootstrapping

Internal validation was performed using the bootstrap method as previously described. **Supplementary Table 3** summarizes the results of the multivariate Cox regression model using the bootstrap method for the whole cohort CMR model. Variables remained significant with no bias after performing 1,000 bootstraps using bias corrected and accelerated confidence intervals. Similarly, variables for CMR prognostic model for the PEA and non-PEA groups remained significant after the bootstrap method (All $p < 0.050$).

DISCUSSION

To our knowledge this is the first study to demonstrate that CMR has prognostic value in patients with CTEPH. We have also highlighted the importance of considering left heart disease in patients considered for PEA, by showing the prognostic value of LAVI in patients undergoing PEA, whilst confirming the value of established prognostic markers of RV function in patients with CTEPH who do not undergo PEA.

Despite extensive study of the potential value of CMR in patients with PAH, where measures of RV function are strongly prognostic (15, 17, 25, 37–43), there is only limited data on the use of CMR in patients with CTEPH with large cohort studies in CTEPH primarily reporting on the utility of clinical, exercise and haemodynamic measures to predict mortality (24, 34, 44). Studies using CMR in CTEPH (45, 46) have focussed on changes in CMR metrics following PEA. Schoenfeld et al. (45) showed an improvement in RV mass and function 12 days post PEA and Mauritz et al. (46) showed an improvement in RV systolic wall stress 6 months post PEA. Non cardiac focused MRI based techniques such as MR pulmonary perfusion maps and MR pulmonary angiography for the screening of CTEPH and surgical planning have also shown to have diagnostic value (12, 18–20, 47). Combining CMR with MR pulmonary perfusion maps and MR pulmonary angiography provides a potential one-stop shop for comprehensive cardiopulmonary of evaluation of suspected PH with MR imaging, providing information on the likelihood of PH, its severity and potential causes.

In this study we have shown that a number of measures reflecting RV function, including RVESVI%pred which is strongly prognostic in PAH (15, 25) and RVEF (%pred), were predictors of mortality in the whole cohort (**Supplementary Table 1**) and in those not undergoing PEA (**Table 5**), at univariate analysis. At multivariate analysis LVSVI %predicted, a measure of global cardiac function was an independent predictor of outcome in the whole cohort whilst RVEF%pred a measure of RV function was an independent predictor of outcome in patients not undergoing PEA. Increases in RV afterload in idiopathic PAH impair RV function resulting in reductions in LVSVI which has been shown to have prognostic value (39) and aid monitoring of treatment (40). In contrast, neither RV size nor RV functional metrics prior to PEA were predictors of mortality in patients undergoing surgery at univariate analysis. In carefully selected patients with surgical disease, PEA can dramatically reduce afterload, normalize pulmonary hemodynamics and improve RV function (45, 48–50) and may explain in significant part why pre-operative measures of RV function are not prognostic in these patients.

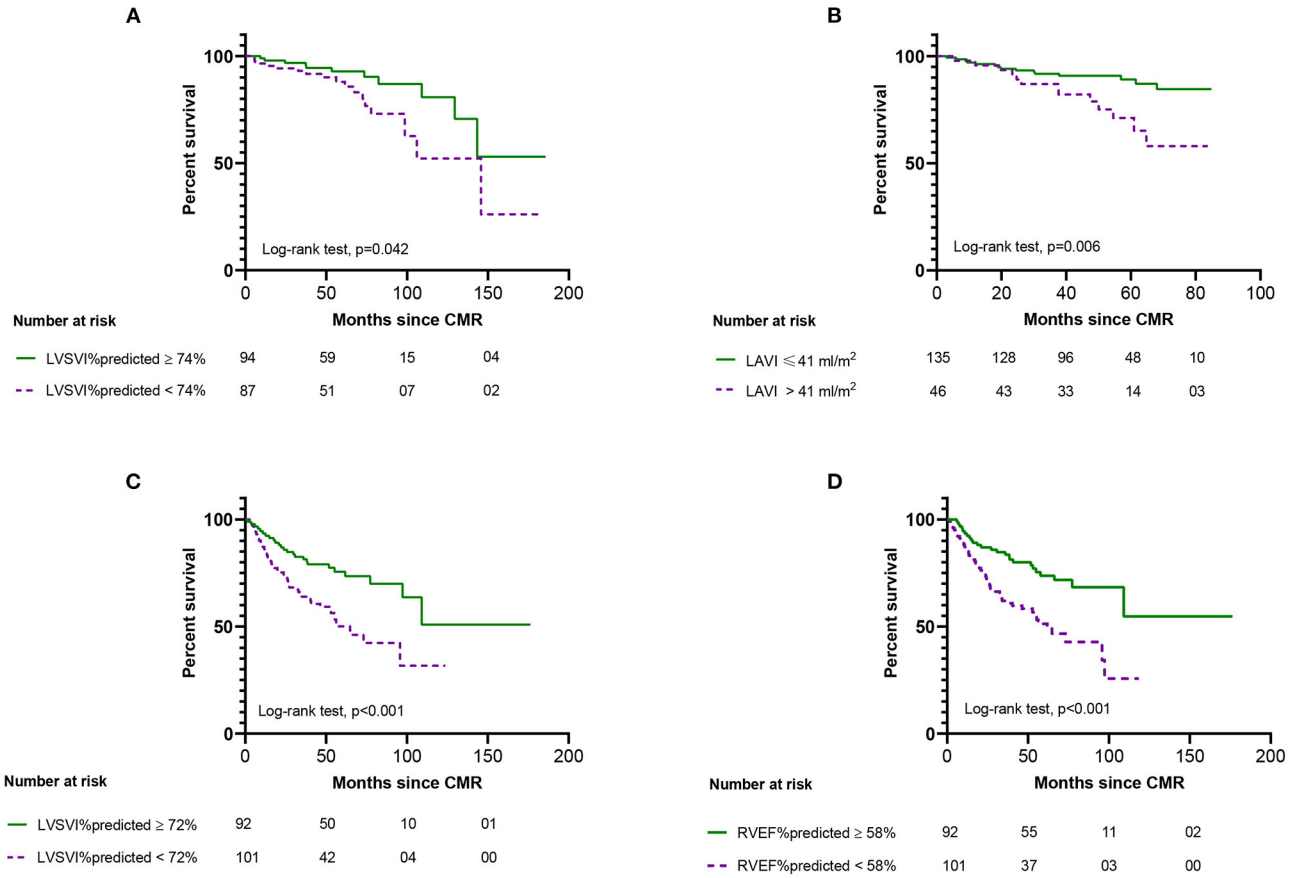

FIGURE 1 | Kaplan-Meier survival analysis from date of cardiac MR showing the outcome of patients undergoing pulmonary endarterectomy (top) based on left ventricular stroke volume index %predicted **(A)** and left atrial volume index **(B)** and for patients not undergoing pulmonary endarterectomy (bottom) based on left ventricular stroke volume index %predicted **(C)** and right ventricular ejection fraction %predicted **(D)**. Numbers at risk for each group are presented below the plot.

A novel finding of this study relates to prognostic value of LA size in patients with CTEPH. LAVI was a significant independent predictor of mortality in the whole cohort and in patients undergoing PEA, highlighting the importance of considering left heart disease when considering the risk and benefits of PEA in CTEPH. Although a LAVI of >41 ml/m^2 is used as a threshold to identify an enlarged left atrium on transthoracic echocardiography a normal LA size in patients undergoing PEA cannot be used to exclude left heart disease, and this may be unmasked following surgery. PEA results in increased LA and LV filling post-surgery (46) and increases in LAVI of ∼20% post PEA have previously been noted and correlated with changes in PVR (51).

Markers of PA stiffness based on using a CMR only measurement method or a combination of CMR and RHC measurement methods were also predictors of mortality at univariate analysis but were not shown to be independent predictors of mortality in the whole, PEA or non-PEA cohorts. Vanderpool et al. (30) reported superior prognostic significance of CMR-derived estimate of RV-arterial coupling Ees/Ea over other invasive and non-invasive measures of RV function in patients referred with pulmonary hypertension. However, no additional prognostic value of a CMR-only measurement of RV–PA coupling over volumetric indices was demonstrated in the present study in patients with CTEPH.

This study also confirms findings from the International CTEPH Registry (52) and our previous work from the ASPIRE Registry regarding the prognostic impact of demographics such as age, comorbidities including malignancy, coronary artery disease and chronic kidney disease, pulmonary hemodynamics and measures of exercise capacity and lung function on outcomes in patients with CTEPH. However, despite inclusion of these prognostic factors MRI metrics still had independent predictive value (**Table 5**). The prognostic accuracy of the CMR only model was higher compared to the accuracy of the clinical only model and combining both models did not increase the prognostic ability of the model only for the PEA group (**Figure 3**).

Study Limitations

This was a single center study with retrospective analysis of prospectively collected data which might have introduced selection or misclassification bias. CMR metrics were corrected

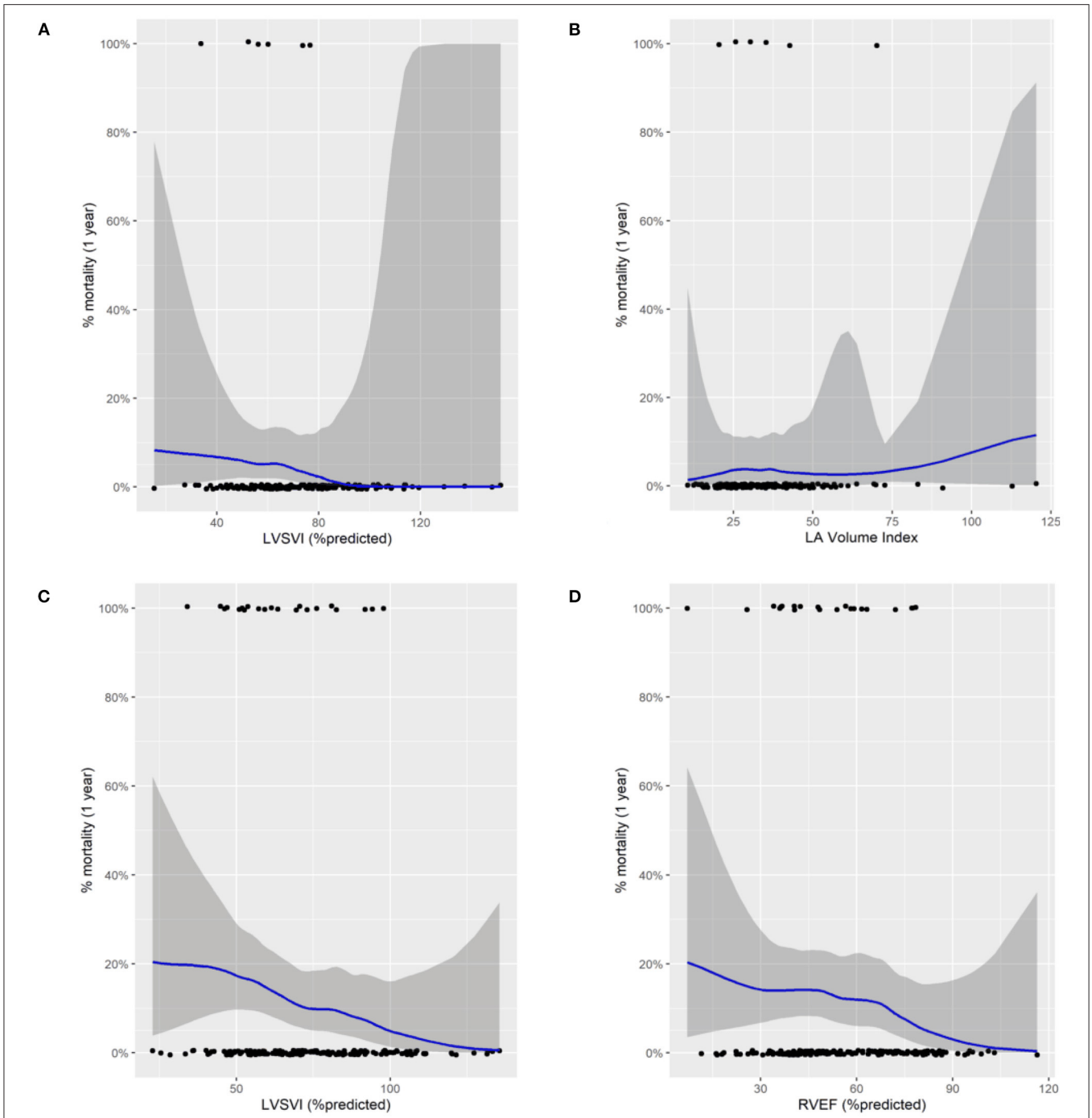

FIGURE 2 | Locally estimated scatterplot smoothing regression analysis (LOESS) for risk of 1 year mortality for patients undergoing pulmonary endarterectomy (top) for left ventricular stroke volume index %predicted **(A)** and left atrial volume index **(B)** and patients not undergoing pulmonary endarterectomy for left ventricular stroke volume index %predicted **(C)** and for right ventricular ejection fraction %predicted **(D)**. Black dots represent status (alive at the bottom and dead at the top). The blue line correspond to a smoothing function fitted by loess regression.

for age and sex but not for race, which impacts on CMR metrics (53). Despite identifying LAVI as an independent predictor of outcome in the whole cohort and patients undergoing PEA further work is required to identify thresholds to aid clinical decision making. This study also used CMR as a gold standard technique to assess cardiac volumetric and functional data rather than echocardiography and echocardiography may be able to provide comparative data although this is not answered by this study. Balloon pulmonary angioplasty has only recently been available in the UK and we were unable therefore to provide any

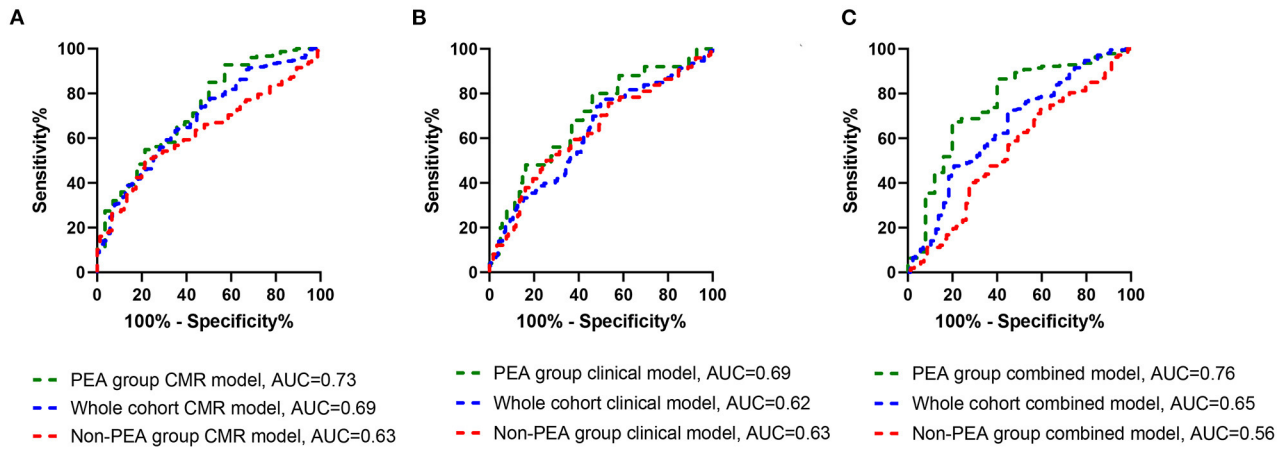

FIGURE 3 | Receiver operating curves for CMR model (green dashes), clinical model (blue dashes) and combined clinical and CMR models (red dashes) in the whole cohort **(A)**, PEA group **(B)**, and in the non-PEA **(C)** showing area under the curve (AUC) for overall mortality.

data regarding the potential for CMR to assess for outcomes in patients undergoing this intervention.

CONCLUSION

CMR metrics reflecting RV function and the presence of left heart disease are of prognostic value in patients with CTEPH. In those undergoing PEA an elevated left atrial volume index predicts a worse outcome highlighting the importance of considering left heart disease in patients considered for PEA. This study also demonstrates the prognostic value of CMR imaging metrics in determining outcome in patients with CTEPH not-undergoing surgery. Whether CMR has a role in serial monitoring of such patients requires further evaluation.

DATA AVAILABILITY STATEMENT

The raw data supporting the conclusions of this article will be made available by the authors, without undue reservation.

ETHICS STATEMENT

The studies involving human participants were reviewed and approved by University of Sheffield, ref c06/Q2308/8. Written informed consent for participation was not required for this study in accordance with the national legislation and the institutional requirements.

AUTHOR CONTRIBUTIONS

YS, AS, and DK conceived the idea for the study and prepared tables and figures. YS, SA, MS, DA, and RL collected and analyzed data for study. YS and AS did statistical analysis. SA, PG, CJ, and SR assisted with the demographic and MRI data. JW, RC, CE, AC, AH, AS, and DK supported this study management and assisted in the writing of the manuscript. AS and DK edited the final manuscript. All authors read and approved the manuscript.

FUNDING

This study was funded in part by the Wellcome Trust to AS, grant number: AJS 205188/Z/16/Z.

SUPPLEMENTARY MATERIAL

The Supplementary Material for this article can be found online at: https://www.frontiersin.org/articles/10.3389/fmed.2022.840196/full#supplementary-material

REFERENCES

1. Kiely DG, Elliot CA, Sabroe I, Condliffe R. Pulmonary hypertension: diagnosis and management. *BMJ.* (2013) 346:f2028. doi: 10.1136/bmj.f2028
2. Ende-Verhaar YM, Cannegieter SC, Vonk Noordegraaf A, Delcroix M, Pruszczyk P, Mairuhu AT, et al. Incidence of chronic thromboembolic pulmonary hypertension after acute pulmonary embolism: a contemporary view of the published literature. *Eur Respir J.* (2017) 49:1601792. doi: 10.1183/13993003.01792-2016
3. Hoeper MM, Mayer E, Simonneau G, Rubin LJ. Chronic thromboembolic pulmonary hypertension. *Circulation.* (2006) 113:2011–20. doi: 10.1161/CIRCULATIONAHA.105.602565
4. Moser KM, Braunwald NS. Successful surgical intervention in severe chronic thromboembolic pulmonary hypertension. *Chest.* (1973) 64:29–35. doi: 10.1378/chest.64.1.29
5. Bonderman D, Skoro-Sajer N, Jakowitsch J, Adlbrecht C, Dunkler D, Taghavi S, et al. Predictors of outcome in chronic thromboembolic pulmonary hypertension. *Circulation.* (2007) 115:2153–8. doi: 10.1161/CIRCULATIONAHA.106.661041

6. Delcroix M, Torbicki A, Gopalan D, Sitbon O, Klok FA, Lang I, et al. ERS statement on chronic thromboembolic pulmonary hypertension. *Eur Respir J.* (2021) 57:2002828. doi: 10.1183/13993003.02828-2020
7. Benza RL, Miller DP, Gomberg-Maitland M, Frantz RP, Foreman AJ, Coffey CS, et al. Predicting survival in pulmonary arterial hypertension: insights from the Registry to Evaluate Early and Long-Term Pulmonary Arterial Hypertension Disease Management (REVEAL). *Circulation.* (2010) 122:164–72. doi: 10.1161/CIRCULATIONAHA.109.898122
8. D'Alonzo GE, Barst RJ, Ayres SM, Bergofsky EH, Brundage BH, Detre KM, et al. Survival in patients with primary pulmonary hypertension. Results from a national prospective registry. *Ann Intern Med.* (1991) 115:343–9. doi: 10.7326/0003-4819-115-5-343
9. Galie N, Humbert M, Vachiery JL, Gibbs S, Lang I, Torbicki A, et al. 2015 ESC/ERS Guidelines for the diagnosis and treatment of pulmonary hypertension: the Joint Task Force for the Diagnosis and Treatment of Pulmonary Hypertension of the European Society of Cardiology (ESC) and the European Respiratory Society (ERS): endorsed by: association for European Paediatric and Congenital Cardiology (AEPC), International Society for Heart and Lung Transplantation (ISHLT). *Eur Respir J.* (2015) 46:903–75. doi: 10.1183/13993003.01032-2015
10. Benza RL, Farber HW, Frost A, Grünig E, Hoeper MM, Busse D, et al. REVEAL risk score in patients with chronic thromboembolic pulmonary hypertension receiving riociguat. *J Heart Lung Transplant.* (2018) 37:836–43. doi: 10.1016/j.healun.2018.02.015
11. Sandqvist A, Kylhammar D, Bartfay SE, Hesselstrand R, Hjalmarsson C, Kavianipour M, et al. Risk stratification in chronic thromboembolic pulmonary hypertension predicts survival. *Scand Cardiovasc J.* (2021) 55:43–9. doi: 10.1080/14017431.2020.1783456
12. Swift AJ, Wild JM, Nagle SK, Roldán-Alzate A, François CJ, Fain S, et al. Quantitative magnetic resonance imaging of pulmonary hypertension: a practical approach to the current state of the art. *J Thorac Imaging.* (2014) 29:68–79. doi: 10.1097/RTI.0000000000000079
13. Johns CS, Kiely DG, Rajaram S, Hill C, Thomas S, Karunasaagarar K, et al. Diagnosis of pulmonary hypertension with cardiac MRI: derivation and validation of regression models. *Radiology.* (2019) 290:61–8. doi: 10.1148/radiol.2018180603
14. Whitfield AJ, Solanki R, Johns CS, Kiely D, Wild J, Swift AJ, et al. Prediction of precapillary pulmonary hypertension according to the sixth world symposium on pulmonary hypertension. *Radiology.* (2020) 294:482. doi: 10.1148/radiol.2019192078
15. Swift AJ, Capener D, Johns C, Hamilton N, Rothman A, Elliot C, et al. Magnetic resonance imaging in the prognostic evaluation of patients with pulmonary arterial hypertension. *Am J Respir Crit Care Med.* (2017) 196:228–39. doi: 10.1164/rccm.201611-2365OC
16. Kiely DG, Levin D, Hassoun P, Ivy DD, Jone PN, Bwika J, et al. EXPRESS: statement on imaging and pulmonary hypertension from the Pulmonary Vascular Research Institute (PVRI). *Pulm Circ.* (2019) 2019:2045894019841990. doi: 10.1177/2045894019841990
17. Alabed S, Shahin Y, Garg P, Alandejani F, Johns CS, Lewis RA, et al. Cardiac-MRI predicts clinical worsening and mortality in pulmonary arterial hypertension: a systematic review and meta-analysis. *JACC Cardiovasc Imaging.* (2021) 14:931–42. doi: 10.1016/j.jcmg.2020.08.013
18. Johns CS, Swift AJ, Rajaram S, Hughes PJC, Capener DJ, Kiely DG, et al. Lung perfusion: MRI vs. SPECT for screening in suspected chronic thromboembolic pulmonary hypertension. *J Magn Reson Imaging.* (2017) 46:1693–7. doi: 10.1002/jmri.25714
19. Rajaram S, Swift AJ, Telfer A, Hurdman J, Marshall H, Lorenz E, et al. 3D contrast-enhanced lung perfusion MRI is an effective screening tool for chronic thromboembolic pulmonary hypertension: results from the ASPIRE Registry. *Thorax.* (2013) 68:677–8. doi: 10.1136/thoraxjnl-2012-203020
20. Rajaram S, Swift AJ, Capener D, Telfer A, Davies C, Hill C, et al. Diagnostic accuracy of contrast-enhanced MR angiography and unenhanced proton MR imaging compared with CT pulmonary angiography in chronic thromboembolic pulmonary hypertension. *Eur Radiol.* (2012) 22:310–7. doi: 10.1007/s00330-011-2252-x
21. Johns CS, Wild JM, Rajaram S, Tubman E, Capener D, Elliot C, et al. Identifying at-risk patients with combined pre- and postcapillary pulmonary hypertension using interventricular septal angle at cardiac MRI. *Radiology.* (2018) 289:61–8. doi: 10.1148/radiol.2018180120
22. Lewis RA, Johns CS, Cogliano M, Capener D, Tubman E, Elliot CA, et al. Identification of cardiac magnetic resonance imaging thresholds for risk stratification in pulmonary arterial hypertension. *Am J Respir Crit Care Med.* (2020) 201:458–68. doi: 10.1164/rccm.201909-1771OC
23. Hurdman J, Condliffe R, Elliot CA, Davies C, Hill C, Wild JM, et al. ASPIRE registry: assessing the Spectrum of Pulmonary hypertension Identified at a REferral centre. *Eur Respir J.* (2012) 39:945–55. doi: 10.1183/09031936.00078411
24. Quadery SR, Swift AJ, Billings CG, Thompson AAR, Elliot CA, Hurdman J, et al. The impact of patient choice on survival in chronic thromboembolic pulmonary hypertension. *Eur Respir J.* (2018) 52:589. doi: 10.1183/13993003.00589-2018
25. Swift AJ, Rajaram S, Campbell MJ, Hurdman J, Thomas S, Capener D, et al. Prognostic value of cardiovascular magnetic resonance imaging measurements corrected for age and sex in idiopathic pulmonary arterial hypertension. *Circ Cardiovasc Imaging.* (2014) 7:100–6. doi: 10.1161/CIRCIMAGING.113.000338
26. Mosteller RD. Simplified calculation of body-surface area. *N Engl J Med.* (1987) 317:1098. doi: 10.1056/NEJM198710223171717
27. Mauritz GJ, Marcus JT, Boonstra A, Postmus PE, Westerhof N, Vonk-Noordegraaf A. Non-invasive stroke volume assessment in patients with pulmonary arterial hypertension: left-sided data mandatory. *J Cardiovasc Magn Reson.* (2008) 10:51. doi: 10.1186/1532-429X-10-51
28. Saba TS, Foster J, Cockburn M, Cowan M, Peacock AJ. Ventricular mass index using magnetic resonance imaging accurately estimates pulmonary artery pressure. *Eur Respir J.* (2002) 20:1519–24. doi: 10.1183/09031936.02.00014602
29. Sanz J, Kariisa M, Dellegrottaglie S, Prat-González S, Garcia MJ, Fuster V, et al. Evaluation of pulmonary artery stiffness in pulmonary hypertension with cardiac magnetic resonance. *JACC Cardiovasc Imaging.* (2009) 2:286–95. doi: 10.1016/j.jcmg.2008.08.007
30. Vanderpool RR, Pinsky MR, Naeije R, Deible C, Kosaraju V, Bunner C, et al. RV-pulmonary arterial coupling predicts outcome in patients referred for pulmonary hypertension. *Heart.* (2015) 101:37–43. doi: 10.1136/heartjnl-2014-306142
31. Sanz J, Garcia-Alvarez A, Fernandez-Friera L, Nair A, Mirelis JG, Sawit ST, et al. Right ventriculo-arterial coupling in pulmonary hypertension: a magnetic resonance study. *Heart.* (2012) 98:238–43. doi: 10.1136/heartjnl-2011-300462
32. Najjar SS, Schulman SP, Gerstenblith G, Fleg JL, Kass DA, O'Connor F, et al. Age and gender affect ventricular-vascular coupling during aerobic exercise. *J Am Coll Cardiol.* (2004) 44:611–7. doi: 10.1016/j.jacc.2004.04.041
33. Escribano-Subías P, Del Pozo R, Román-Broto A, Domingo Morera JA, Lara-Padrón A, Elías Hernández T, et al. Management and outcomes in chronic thromboembolic pulmonary hypertension: From expert centers to a nationwide perspective. *Int J Cardiol.* (2016) 203:938–44. doi: 10.1016/j.ijcard.2015.11.039
34. Delcroix M, Lang I, Pepke-Zaba J, Jansa P, D'Armini AM, Snijder R, et al. Long-term outcome of patients with chronic thromboembolic pulmonary hypertension: results from an International Prospective Registry. *Circulation.* (2016) 133:859–71. doi: 10.1161/CIRCULATIONAHA.115.016522
35. Altman DG, Andersen PK. Bootstrap investigation of the stability of a cox regression model. *Stat Med.* (1989) 8:771–83. doi: 10.1002/sim.4780080702
36. Aune E, Baekkevar M, Roislien J, Rodevand O, Otterstad JE. Normal reference ranges for left and right atrial volume indexes and ejection fractions obtained with real-time three-dimensional echocardiography. *Eur J Echocardiogr.* (2009) 10:738–44. doi: 10.1093/ejechocard/jep054
37. Swift AJ, Telfer A, Rajaram S, Condliffe R, Marshall H, Capener D, et al. Dynamic contrast enhanced magnetic resonance imaging in patients with pulmonary arterial hypertension. *Pulm Circ.* (2014) 4:61–70. doi: 10.1086/674882
38. Gan CTJ, Lankhaar JW, Westerhof N, Marcus JT, Becker A, Twisk JW, et al. Noninvasively assessed pulmonary artery stiffness predicts mortality in pulmonary arterial hypertension. *Chest.* (2007) 132:1906–12. doi: 10.1378/chest.07-1246
39. van Wolferen SA, Marcus JT, Boonstra A, Marques KM, Bronzwaer JG, Spreeuwenberg MD, et al. Prognostic value of right ventricular mass, volume,

and function in idiopathic pulmonary arterial hypertension. *Eur Heart J.* (2007) 28:1250–7. doi: 10.1093/eurheartj/ehl477
40. Van de Veerdonk MC, Kind T, Marcus JT, Mauritz GJ, Heymans MW, Bogaard HJ, et al. Progressive right ventricular dysfunction in patients with pulmonary arterial hypertension responding to therapy. *J Am Coll Cardiol.* (2011) 58:2511–9. doi: 10.1016/j.jacc.2011.06.068
41. Freed BH, Gomberg-Maitland M, Chandra S, Mor-Avi V, Rich S, Archer SL, et al. Late gadolinium enhancement cardiovascular magnetic resonance predicts clinical worsening in patients with pulmonary hypertension. *J Cardiovasc Magn Reson.* (2012) 14:11. doi: 10.1186/1532-429X-14-11
42. Yamada Y, Okuda S, Kataoka M, Tanimoto A, Tamura Y, Abe T, et al. Prognostic value of cardiac magnetic resonance imaging for idiopathic pulmonary arterial hypertension before initiating intravenous prostacyclin therapy. *Circ J.* (2012) 76:1737–43. doi: 10.1253/circj.CJ-11-1237
43. Cho IJ, Oh J, Chang HJ, Park J, Kang KW, Kim YJ, et al. Tricuspid regurgitation duration correlates with cardiovascular magnetic resonance-derived right ventricular ejection fraction and predict prognosis in patients with pulmonary arterial hypertension. *Eur Heart J Cardiovasc Imaging.* (2014) 15:18–23. doi: 10.1093/ehjci/jet094
44. Riedel M, Stanek V, Widimsky J, Prerovsky I. Longterm follow-up of patients with pulmonary thromboembolism. Late prognosis and evolution of hemodynamic and respiratory data. *Chest.* (1982) 81:151–8. doi: 10.1378/chest.81.2.151
45. Schoenfeld C, Cebotari S, Hinrichs J, Renne J, Kaireit T, Olsson KM, et al. MR imaging-derived regional pulmonary parenchymal perfusion and cardiac function for monitoring patients with chronic thromboembolic pulmonary hypertension before and after pulmonary endarterectomy. *Radiology.* (2016) 279:925–34. doi: 10.1148/radiol.2015150765
46. Mauritz GJ, Vonk-Noordegraaf A, Kind T, Surie S, Kloek JJ, Bresser P, et al. Pulmonary endarterectomy normalizes interventricular dyssynchrony and right ventricular systolic wall stress. *J Cardiovasc Magn Reson.* (2012) 14:5. doi: 10.1186/1532-429X-14-5
47. Tsuchiya N, van Beek EJ, Ohno Y, Hatabu H, Kauczor HU, Swift A, et al. Magnetic resonance angiography for the primary diagnosis of pulmonary embolism: a review from the international workshop for pulmonary functional imaging. *World J Radiol.* (2018) 10:52–64. doi: 10.4329/wjr.v10.i6.52
48. Berman M, Gopalan D, Sharples L, Screaton N, Maccan C, Sheares K, et al. Right ventricular reverse remodeling after pulmonary endarterectomy: magnetic resonance imaging and clinical and right heart catheterization assessment. *Pulm Circ.* (2014) 4:36–44. doi: 10.1086/674884
49. Kreitner KF, Ley S, Kauczor HU, Mayer E, Kramm T, Pitton MB, et al. Chronic thromboembolic pulmonary hypertension: pre- and postoperative assessment with breath-hold MR imaging techniques. *Radiology.* (2004) 232:535–43. doi: 10.1148/radiol.2322030945
50. Rolf A, Rixe J, Kim WK, Börgel J, Möllmann H, Nef HM, et al. Right ventricular adaptation to pulmonary pressure load in patients with chronic thromboembolic pulmonary hypertension before and after successful pulmonary endarterectomy—a cardiovascular magnetic resonance study. *J Cardiovasc Magn Reson.* (2014) 16:96. doi: 10.1186/s12968-014-0096-7
51. Marston NA, Auger WR, Madani MM, Kimura BJ, Strachan GM, Raisinghani AB, et al. Assessment of left atrial volume before and after pulmonary thromboendarterectomy in chronic thromboembolic pulmonary hypertension. *Cardiovasc Ultrasound.* (2014) 12:32. doi: 10.1186/1476-7120-12-32
52. Pepke-Zaba J, Delcroix M, Lang I, Mayer E, Jansa P, Ambroz D, et al. Chronic thromboembolic pulmonary hypertension (CTEPH): results from an international prospective registry. *Circulation.* (2011) 124:1973–81. doi: 10.1161/CIRCULATIONAHA.110.015008
53. Kawut SM, Lima JA, Barr RG, Chahal H, Jain A, Tandri H, et al. Sex and race differences in right ventricular structure and function: the multi-ethnic study of atherosclerosis-right ventricle study. *Circulation.* (2011) 123:2542–51. doi: 10.1161/CIRCULATIONAHA.110.985515

Conflict of Interest: The authors declare that the research was conducted in the absence of any commercial or financial relationships that could be construed as a potential conflict of interest.

Publisher's Note: All claims expressed in this article are solely those of the authors and do not necessarily represent those of their affiliated organizations, or those of the publisher, the editors and the reviewers. Any product that may be evaluated in this article, or claim that may be made by its manufacturer, is not guaranteed or endorsed by the publisher.

GLOSSARY

CTEPH, chronic thromboembolic pulmonary hypertension; PAH, pulmonary arterial hypertension; mPAP, mean pulmonary artery pressure; RHC, right heart catheter; DLCO, diffusing capacity of the lungs for carbon monoxide; FEV1, forced expiratory volume; FVC, forced vital capacity; ISWD, incremental shuttle walking distance; mPAP, mean pulmonary arterial pressure; mRAP, mean right atrial pressure; PAWP, pulmonary artery wedge pressure; PEA, pulmonary endarterectomy; PVR, pulmonary vascular resistance; SvO2, mixed venous oxygen saturation; %pred, percentage predicted; Ea, arterial load; Ees, right ventricle elastance; LAVI, left atrium volume index; LVEDMI, left ventricle end diastolic mass index; LVEDVI, left ventricle end diastolic volume index; LVEF, left ventricle ejection fraction; LVESVI, left ventricle end systolic volume index; LVSVI, left ventricle stroke volume index; MRI, magnetic resonance imaging; PA, pulmonary artery; PA RAC, pulmonary artery relative area change; RVEDMI, right ventricle end diastolic mass index; RVEDVI, right ventricle end diastolic volume index; RVEF, right ventricle ejection fraction; RVSP, right ventricle systolic pressure; RVESVI, right ventricle end systolic volume index; RVSVI, right ventricle stroke volume index; VMI, ventricular mass index.

frontiers | Frontiers in Medicine

ORIGINAL RESEARCH
published: 12 May 2022
doi: 10.3389/fmed.2022.894584

Integrated Bioinformatic Analysis Reveals TXNRD1 as a Novel Biomarker and Potential Therapeutic Target in Idiopathic Pulmonary Arterial Hypertension

Wenchao Lin, Yiyang Tang, Mengqiu Zhang, Benhui Liang, Meijuan Wang, Lihuang Zha and Zaixin Yu**

Department of Cardiology, Xiangya Hospital, Central South University, Changsha, China

OPEN ACCESS

Edited by:
Soban Umar,
University of California, Los Angeles, United States

Reviewed by:
Jason Hong,
UCLA Health System, United States
Zhiyu Dai,
University of Arizona, United States

***Correspondence:**
Zaixin Yu
yuzaixin@126.com
Lihuang Zha
zhalihuang@csu.edu.cn

Specialty section:
This article was submitted to Pulmonary Medicine, a section of the journal Frontiers in Medicine

Received: *11 March 2022*
Accepted: *27 April 2022*
Published: *12 May 2022*

Citation:
Lin W, Tang Y, Zhang M, Liang B, Wang M, Zha L and Yu Z (2022) Integrated Bioinformatic Analysis Reveals TXNRD1 as a Novel Biomarker and Potential Therapeutic Target in Idiopathic Pulmonary Arterial Hypertension. Front. Med. 9:894584. doi: 10.3389/fmed.2022.894584

Idiopathic pulmonary arterial hypertension (IPAH) is a life-threatening cardiopulmonary disease lacking specific diagnostic markers and targeted therapy, and its mechanism of development remains to be elucidated. The present study aimed to explore novel diagnostic biomarkers and therapeutic targets in IPAH by integrated bioinformatics analysis. Four eligible datasets (GSE117261, GSE15197, GSE53408, GSE48149) was firstly downloaded from GEO database and subsequently integrated by Robust rank aggregation (RRA) method to screen robust differentially expressed genes (DEGs). Then functional annotation of robust DEGs was performed by GO and KEGG enrichment analysis. The protein-protein interaction (PPI) network was constructed followed by using MCODE and CytoHubba plug-in to identify hub genes. Finally, 10 hub genes were screened including ENO1, TALDO1, TXNRD1, SHMT2, IDH1, TKT, PGD, CXCL10, CXCL9, and CCL5. The GSE113439 dataset was used as a validation cohort to appraise these hub genes and TXNRD1 was selected for verification at the protein level. The experiment results confirmed that serum TXNRD1 concentration was lower in IPAH patients and the level of TXNRD1 had great predictive efficiency (AUC:0.795) as well as presents negative correlation with mean pulmonary arterial pressure (mPAP) and pulmonary vascular resistance (PVR). Consistently, the expression of TXNRD1 was proved to be inhibited in animal and cellular model of PAH. In addition, GSEA analysis was performed to explore the functions of TXNRD1 and the results revealed that TXNRD1 was closely correlated with mTOR signaling pathway, MYC targets, and unfolded protein response. Finally, knockdown of TXNRD1 was shown to exacerbate proliferative disorder, migration and apoptosis resistance in PASMCs. In conclusion, our study demonstrates that TXNRD1 is a promising candidate biomarker for diagnosis of IPAH and plays an important role in PAH pathogenesis, although further research is necessary.

Keywords: bioinformatic analysis, TXNRD1, pulmonary hypertension, biomarker, RRA, GEO

INTRODUCTION

Pulmonary arterial hypertension (PAH) is a progressive cardiovascular disease characterized by vasodilation dysfunction and irreversible vascular remodeling, eventually leading to pulmonary pressure elevation and right heart failure (1). According to WHO classification, PAH is divided into five groups and idiopathic pulmonary arterial hypertension (IPAH) is the most common subtype of PAH occurred in the absence of etiology (2). Although considerable target therapy for PAH have been developed to well relieve symptoms, this devastating disease still carries a poor prognosis with a 5-year survival of 61.2% in newly diagnosed patients (3). In the early stage of PAH, pulmonary vasculature presents sustained constriction which can be reversed by anti-vasoconstrictor drugs. As the disease progresses, vascular remodeling including distal artery hypertrophy, inflammation, fibrosis, and neovascularization, predominately accelerate the deterioration of the disease (4). Current therapies mainly focus on improving pulmonary vasodilation rather than targeting proliferative vascular remodeling and that is the reason why target therapy gradually lose efficacy in the advanced stage of the disease (5). Therefore, there is urgent need to explore novel therapeutic target to directly address the pathological remodeling that underpins the disease.

In the past decades, microarray and RNA sequencing technology have been widely used for gene expression analysis in lung tissue or cell from PAH patients or experimental animal, which has already identified multiple therapeutic genes target and yielded some achievements in pathogenesis knowledge (6–8). However, currently most PAH lung tissue gene expression profiles have not yet been uploaded, and analysis among the uploaded datasets are very inconsistent due to the limited sample size. Therefore, it is very necessary to integrate the existing PAH datasets. Robust rank aggregation (RRA) method is a dataset integration method based on gene ranking list comparison. It hypothesizes that each gene is randomly ordered, if a gene is upregulated or downregulated in all gene lists, then the gene is considered robust (9). Up to now, there have been several studies that integrated PAH datasets adopting batch normalization method for consolidation while there are rare studies using RRA method for data integration (10, 11), which facilitated this study.

In this study, we performed an integrated bioinformatics analysis to identify robust differentially expressed genes (DEGs) in IPAH. The gene expression profiles of GSE117261, GSE53408, GSE48149, and GSE15197 were downloaded from GEO database. After screening DEGs in each dataset, the RRA method was applied to identify 169 robust DEGs and enrichment analysis was conducted. Then, we uploaded robust DEGs to the STRING database to construct global protein-protein interaction network. The module analysis was performed by the MCODE plug-in of Cytoscape based on the entire network and hub genes identification was carried out by the plug-in Cytohubba. Through verification of independent dataset and experimental validation, TXNRD1 was finally identified as a candidate molecular biomarker and potential therapeutic target in IPAH.

MATERIALS AND METHODS

Gene Expression Omnibus Datasets Selection

We screened the Gene Expression Omnibus (GEO) database[1] according to the following inclusion criteria: (1) Samples from human lung tissue; (2) Containing at least five IPAH cases and at least five controls; (3) Raw data or gene expression profiling were available for downloading in GEO. Finally, a total of 5 datasets were obtained: GSE117261, GSE53408, GSE48149, and GSE15197 were used for RRA analysis, and GSE113439 was used as the validation dataset. The detailed information of datasets was listed in **Table 1**.

Identification of Robust Differentially Expressed Genes Among Each Gene Expression Omnibus Dataset

For each dataset, we firstly downloaded the gene expression matrix and annotation document from GEO database, then the microarray probes were mapped to corresponding gene symbol and the not available gene symbols were removed from the expression matrix. If multiple probes annotated with the same symbol, the mean value was adopted. To determine DEGs between IPAH and control group, we utilized limma R package to analyze with the cut-off criteria of $|\log2 \text{ fold-change (FC)}| > 0.5$ and P-value < 0.05. Identified DEGs from each dataset were integrated using the Robust Rank Aggregation (RRA) method to minimize the inconsistency. RRA analysis was performed with an R package "Robust Rank Aggreg." Genes with P-value < 0.05 were regarded as robust DEGs.

Gene Ontology and Kyoto Encyclopedia of Genes and Genomes Pathway Enrichment Analysis

In order to excavate the function of robust DEGs, we performed Gene Ontology (GO) enrichment analysis and Kyoto Encyclopedia of Genes and Genomes (KEGG) pathway analysis *via* R package "clusterprofiler" (12). Terms with $P < 0.05$ was considered to be significant enrichment.

Protein-Protein Interaction Network Analysis

The organization of protein-protein interaction (PPI) network was managed by the Search Tool for the Retrieval of Interacting Genes (STRING[2]). Interaction with combined score ≥ 0.4 was set as cut-off point. To visualize the global PPI network, Cytoscape (3.8.0) software was applied. The MCODE plug-in of Cytoscape software was used to identify significant modules with default parameters (degree of cut off = 2, node score cutoff = 0.2, k-core = 2, and max depth = 100). To seek for important hub genes among robust DEGs, the Cytohubba plug-in of Cytoscape software was applied, which provided top 10 hub genes by combing different algorithm.

[1]https://www.ncbi.nlm.nih.gov/geo/

[2]http://string-db.org

TABLE 1 | Datasets detailed information.

References	Sample	GEO	Platform	IPAH	Control
Stearman et al.	Lung tissue	GSE117261	GPL6244	32	25
Hsu et al.	Lung tissue	GSE48149	GPL16221	8	9
Rajkumar et al.	Lung tissue	GSE15197	GPL6480	13	18
Zhao et al.	Lung tissue	GSE53408	GPL6244	12	11
Mura M. et al.	Lung tissue	GSE113439	GPL6244	6	11

Clinical Blood Sampling and Enzyme-Linked Immunosorbent Assay

To test whether TXNRD1 was reduced in the blood of IPAH patients, 9 diagnosed IPAH patients were recruited from the Department of Cardiology of the Xiangya Hospital, and 13 healthy controls with matched age and gender were recruited during physical check-up. The patient data and samples collection were approved by the Medical Ethics Committee of the Xiangya Hospital of Central South University and informed consent was obtained from all subjects or their legal guardians. All methods were carried out in accordance with the approved guidelines. Clinical features include age, sex, BMI, 6-min walk distance (6MWD), NT-proBNP, mPAP, and PVR. Blood samples were collected through vein puncture and subsequently processed to serum as soon as possible. TXNRD1 levels were determined using the human TrxR enzyme immunoassay kit (CSB-E09731h, CUSABIO, Wuhan, China) according to the manufacturer's instructions. Receiver operating characteristic (ROC) curve analysis was completed by the Hipplot online tool[3] to determine the sensitivity and specificity of TXNRD1.

Animal Experiment

This study was approved by the Institutional Animal Care and Use Committee of Central South University. Fourteen 180–200 g male SD rats were raised under standard laboratory conditions and followed the National Institutes of Health guide for the care and use of rat. One week later, rats were randomly divided into control group and MCT group (n = 7) which received intraperitoneal injection with saline and MCT (60 mg/kg, Sigma-Aldrich, St Louis, MO, United States) respectively. After 21 days, the rats were anesthetized and the right ventricle systolic pressure (RVSP) was measured through right heart catheterization. Then, the rats were sacrificed, and lung and heart tissues were collected for histological analysis and western blotting. The RV hypertrophy index was calculated as the weight ratio of RV to (LV + ventricular septum).

Cell Culture Experiments

Primary rat PASMCs were isolated and cultured following previously described protocol (13). Briefly, rats were sacrificed under anesthetized condition and lung tissue were quickly separated. Then the distal pulmonary arteries were peeled off and connective tissue was removed in PBS. Pulmonary artery was then cut into small pieces and incubated in HBSS containing 1 mg/ml collagenase I (Sigma-Aldrich, St Louis, MO, United States) at 37°C for 20 min under shaking until the tissue block is digested. Tissue lysate was then filtered through 0.45 μm cell strainer and centrifuged to collect cells which were cultivated in DMEM/F12 containing 20% fetal bovine serum (FBS) till reaching confluence. Cell purity was confirmed by immunofluorescence with smooth muscle cell actin (1:400, 67735-1-Ig, ProteinTech). PASMCs of passages 3–5 at 70–80% confluence were used for experiments. As for stimulation of PASMC proliferation, cells were starved in 0.5% FBS supplemented medium for 24 h and then treated with 20 ng/ml PDGF-BB (Peprotech, Rocky Hill, NJ, United States) for 24 h. For gene knockdown in PASMCs, cells were transfected with control siRNA or si-TXNRD1 in antibiotic-free medium for 48 h following the manufacturer's instructions. The siRNA was synthesized by Ribobio (China) and the sequence was as follows: si-TXNRD1, 5′-GGAAGAGATTCTTG TACAA-3′.

Western Blot

For the analysis of total proteins, lung tissue or PASMC were lysed in RIPA containing protease inhibitor. Following this, the lysates were centrifuged at 12,000g for 10 min, and the supernatant was collected. The BCA Protein Assay Kit (Beyotime) was used to determine protein concentrations. Total lysates were loaded on 10% SDS-PAGE to separate the proteins electrophoretically and the proteins were then transferred to a PVDF membrane. Blocked membranes in 5% bovine serum albumin were probed using the following antibodies: TXNRD1 (1:1,000, sc-28321, Santa Cruz Biotech), PCNA (1:2000, 10205-2-AP, Proteintech), Bcl-2 (1:1000, 60178-1-Ig, Proteintech), BAX (1:5000, 60267-1-Ig, Proteintech), cleaced-PARP (1:1000,

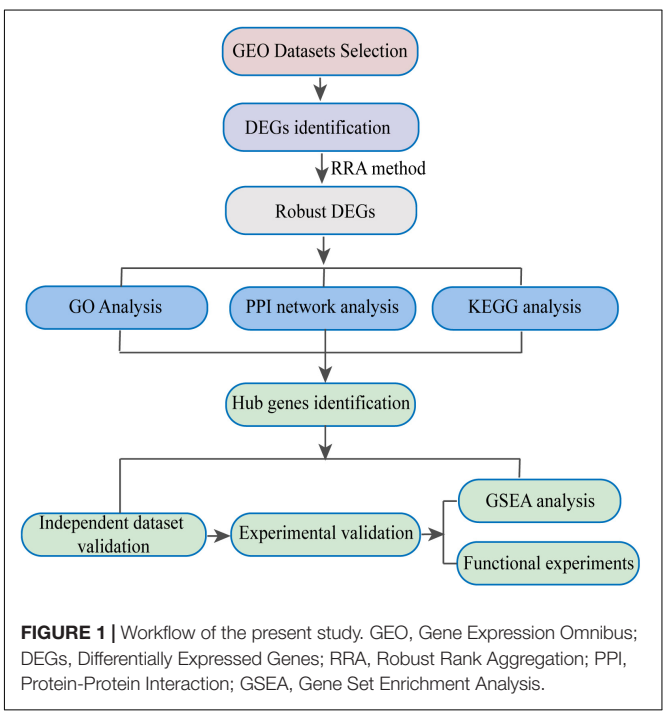

FIGURE 1 | Workflow of the present study. GEO, Gene Expression Omnibus; DEGs, Differentially Expressed Genes; RRA, Robust Rank Aggregation; PPI, Protein-Protein Interaction; GSEA, Gene Set Enrichment Analysis.

[3]https://hiplot.com.cn/basic

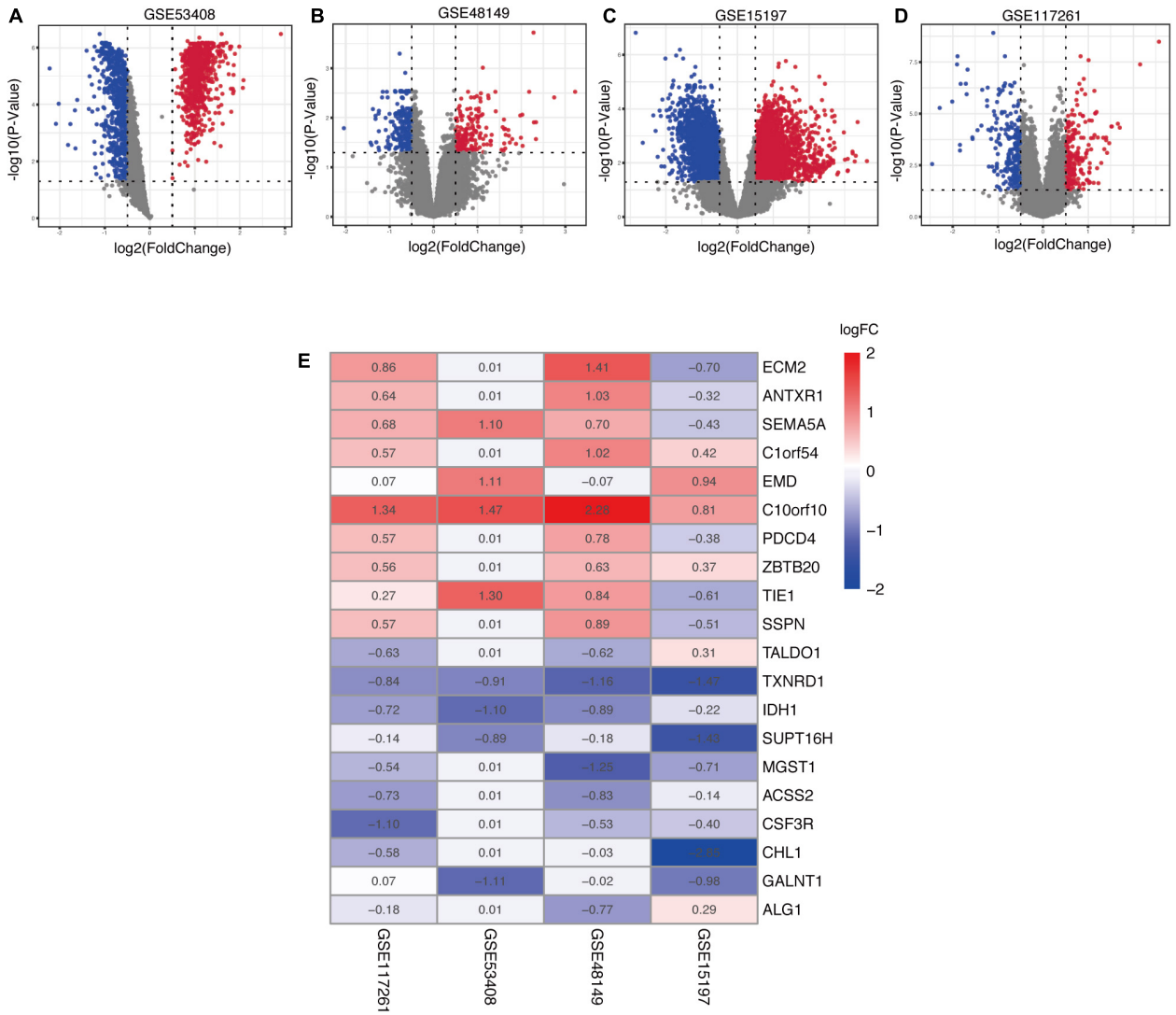

FIGURE 2 | Identification of robust DEGs among each GEO dataset. **(A–D)** The volcano plots of the distribution of DEGs in each dataset. **(E)** The heatmap of robust DEGs in the RRA analysis. The values in a cell represent |log2 fold-change (FC)| of each gene in a dataset. DEG, differentially expressed gene; GEO, Gene Expression Omnibus; RRA, robust rank aggregation.

94885, CST), β-actin (1:2000, 20536-1-AP, Proteintech). Reactive bands were visualized with the chemiluminescent protocol, recorded with the ChemiDoc MP Imaging System (Bio-Rad).

RNA Extraction and Real-Time qPCR

In order to assess the knockdown efficiency of TXNRD1, total RNA was extracted from PASMCs using RNA Extraction Kit (#6834, OMEGA biotek) according to the manufacturer's instructions. First-strand cDNA was reverse transcribed from total RNA using the First-Strand cDNA Synthesis Kit (GeneCopeia). mRNA level of TXNRD1 was quantified by Real-time PCR using SYBR Green qPCR Mix Kit (GeneCopeia) on QuantStudio 5 (Thermo) with following primer: 5′-GGTGAAAGGCCGCGCTA-3′ (forward), 5′ATAGGACGCGCCAACCACTA-3′ (reverse). Data were analyzed using the 2-ΔΔCT method with GAPDH as an internal control.

Gene Set Enrichment Analysis

Gene set enrichment analysis was conducted using "clusterprofiler" to explore the potential signaling pathways related to TXNRD1 in IPAH. The MSigDB gene set, "h.all.v7.4.entrez.gmt," was defined as reference. Terms with $P < 0.05$ and FDR < 0.25 were defined as significant.

Cell Proliferation and Migration Assays

EdU assay kit (Ribobio) was used to measure the PASMC proliferation according to manufacturer's instruction (Ribobio, China). Briefly, PASMCs were cultured in 24-well culture plates

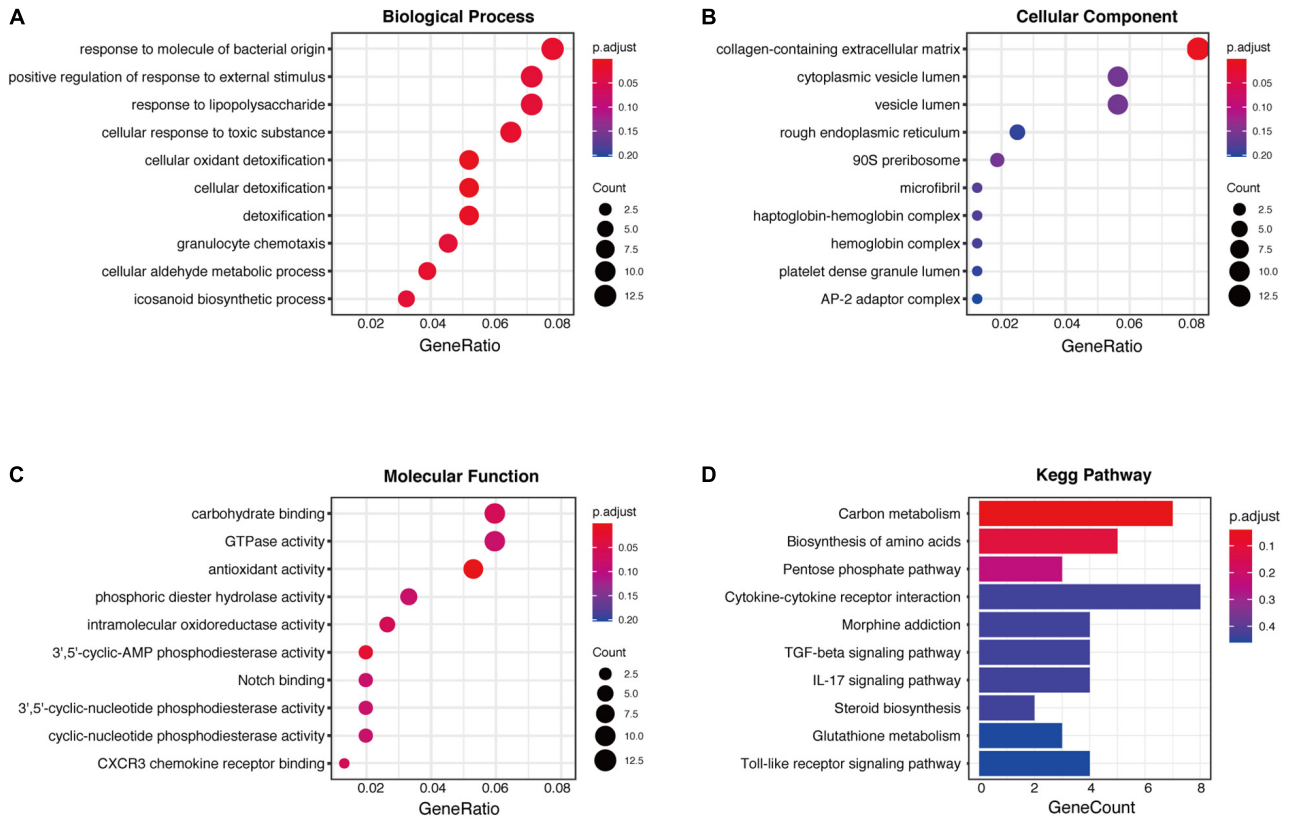

FIGURE 3 | GO and KEGG enrichment analysis of robust DEGs. **(A)** Biological process GO terms for robust DEGs. **(B)** Cellular component GO terms for robust DEGs. **(C)** Molecular function GO terms for robust DEGs. **(D)** KEGG analysis for robust DEGs. DEG, differentially expressed gene; GO, Gene Ontology; KEGG, Kyoto Encyclopedia of Genes and Genomes.

and were subcultured with EdU labeling solution for 2 h after 48 h transfection with or without PDGF-BB stimulation. Then the cells were fixed by paraformaldehyde and incubated with EdU detection solution for 1 h. The stained cells were examined using a fluorescent-inverted microscope. Cell proliferation rate was calculated as the number of EdU-stained cells/the number of Hoechst–stained cells. Cell migration was determined by the wound-healing assay. In brief, cell medium was switched to starvation medium with or without PDGF-BB treatment after transfection, then a line scratch was drawn in the cell layer and photographed immediately as initial image (0 h). The second image (24 h) of the same line scratch was taken after 24 h of culturing, and cell migration was determined by measuring the decreased width of corresponding scratch from 0 to 24 h.

Statistical Analysis

Statistical analysis was conducted using R software (Version 3.5.3) and GraphPad Prism 8. Student *t*-test and one-way ANOVA were used to compare two and multiple groups. Pearson's correlation test and linear regression analysis were applied to specify the relationships between TXNRD1 levels and clinical parameters. Data was presented as mean ± SEM and $P < 0.05$ was considered statistically significant.

Data Availability

The authors declare that all data supporting the findings of this study are available in Zenodo (DOI: 10.5281/zenodo.5840973). If any other requirements were requested, please contact the author at convenience.

RESULTS

Identification of Differentially Expressed Genes Among Each Selected Dataset

In the present study, robust DEGs and hub genes were determined based on various GEO datasets by integrated bioinformatics analysis (**Figure 1**). After filtering the GEO datasets based on the given eligibility criteria, four PAH-associated datasets were included, and their detailed information was listed in **Table 1**. There was a total of 128 profiles including 65 IPAH patients and 63 controls selected for data processing. After the normalization and annotation of expression matrix, we used the "limma" package to screen DEGs among each dataset. Overall, 501 DEGs including 235 upregulated and 266 downregulated genes were selected in GSE117261 dataset (**Supplementary Table 1**). There were 963 DEGs in the GSE48149 dataset, including 552 upregulated

TABLE 2 | GO and KEGG enrichment terms.

Term	Description	Gene Count	Adjusted *P*-value
GO:0098869	Cellular oxidant detoxification	8	0.006
GO:1990748	Cellular detoxification	8	0.0062
GO:0098754	Detoxification	8	0.0133
GO:0002237	Response to molecule of bacterial origin	12	0.0202
GO:0006081	Cellular aldehyde metabolic process	6	0.0178
GO:0097237	Cellular response to toxic substance	10	0.0178
GO:0071621	Granulocyte chemotaxis	7	0.0254
GO:0032103	Positive regulation of response to external stimulus	11	0.0254
GO:0046456	Icosanoid biosynthetic process	5	0.0254
GO:0032496	Response to lipopolysaccharide	11	0.0254
GO:0001569	Branching involved in blood vessel morphogenesis	4	0.0299
GO:0006739	NADP metabolic process	4	0.0299
GO:0071216	Cellular response to biotic stimulus	9	0.0316
GO:0097530	Granulocyte migration	7	0.0327
GO:0030593	Neutrophil chemotaxis	6	0.0348
GO:0006098	Pentose-phosphate shunt	3	0.0348
GO:0019321	Pentose metabolic process	3	0.0348
GO:0046184	Aldehyde biosynthetic process	3	0.0348
GO:0062023	Collagen-containing extracellular matrix	13	0.0080
GO:0016209	Antioxidant activity	8	0.0002
GO:0004115	3′,5′-cyclic-AMP phosphodiesterase activity	3	0.0236
hsa01200	Carbon metabolism	7	0.0403

and 411 downregulated genes (**Supplementary Table 2**). Additionally, 1562 DEGs were screened from the GSE53408 dataset including 858 upregulated and 704 downregulated genes (**Supplementary Table 3**). A total of 5971 DEGs were found in GSE15197 dataset including 3214 upregulated and 2847 downregulated genes (**Supplementary Table 4**). The volcano plots of DEGs among each dataset were shown in **Figures 2A–D**.

Selection of Robust Differentially Expressed Genes by Robust Rank Aggregation Method

In order to explore DEGs with similar expression pattern in these datasets, we applied RRA method to decrease inconsistency of DEGs screened from each dataset. Finally, a total of 169 significantly robust DEGs were determined including 98 upregulated and 71 downregulated genes (**Supplementary Table 5**). The top 10 upregulated and downregulated genes were illustrated by a heatmap (**Figure 2E**), and the heatmap of 169 robust DEGs was shown in **Supplementary Figure 1**. Among the robust upregulated genes, ECM2 was ranked as the first one (p = 5.91E-05), followed by ANTXR1 (p = 4.33E-04) and SEMA5A (p = 1.05E-03). Meanwhile, TALDO1 (p = 5.99E-05), TXNRD1 (p = 1.66E-04), and IDH1 (p = 5.46E-04) were ranked as the top three robust downregulated genes.

Enrichment Analysis of Robust Differentially Expressed Genes

To explore the biological role of selected robust DEGs in IPAH, we performed GO annotation and KEGG pathway enrichment analysis. Several biological processes in GO terms were enriched, such as response to molecule of bacterial origin, response to lipopolysaccharide and cellular oxidant detoxification (**Figure 3A**). Collagen-containing extracellular matrix was the most enriched cellular component in GO terms (**Figure 3B**). In terms of molecular function, antioxidant activity and 3′,5′-cyclic-AMP phosphodiesterase activity were identified as the significant enriched GO terms (**Figure 3C**). In the KEGG analysis, the robust DEGs were mostly associated with carbon metabolism (**Figure 3D**). The detailed results of enrichment analysis were shown in **Table 2**. The above results indicated that the robust DEGs were significantly enriched in PAH-related biological processes.

Protein-Protein Interaction Network Establishment and Hub Genes Identification

To explore potential connection and identify hub genes among 169 robust DEGs, the STRING database was used to create global PPI network which was visualized by Cytoscape software (**Figure 4A**). Then MCODE plug-in was applied to find key modules (**Figures 4B,C** and **Table 3**). The genes in module 1 contains PGD, ENO1, TALDO1, IDH1, TXNRD1, TKT, SHMT2, which are associated with metabolic reprogramming and NADP metabolic process. The genes in module 2 correlates with cytokine-cytokine receptor interaction, including GBP5, CCL5, CD69, CXCL9, IL7R, GZMB, CXCL10. In addition, we utilized cytohubba plug-in to further determine the top 10 hub genes of DEGs including ENO1, TALDO1, TXNRD1, SHMT2, IDH1, TKT, PGD, CXCL10, CXCL9, and CCL5 (**Figure 4D**).

Validation of TXNRD1 in Clinical Samples

Based on verification analysis in GSE113439, we found that TXNRD1 showed consistently downregulated in IPAH group while other hub genes showed no difference (**Figure 5A**). Therefore, we selected TXNRD1 for further experimental validation. Firstly, we collected the blood samples from 9 IPAH patients and 13 healthy controls to detect the serum TXNRD1 concentration. The clinical baseline characteristics of study subjects were shown in **Table 4**. As a result, we found that serum TXNRD1 concentration was lower in IPAH patients compared with healthy controls (**Figure 5B**). The ability of TXNRD1 levels to diagnose IPAH was assessed using

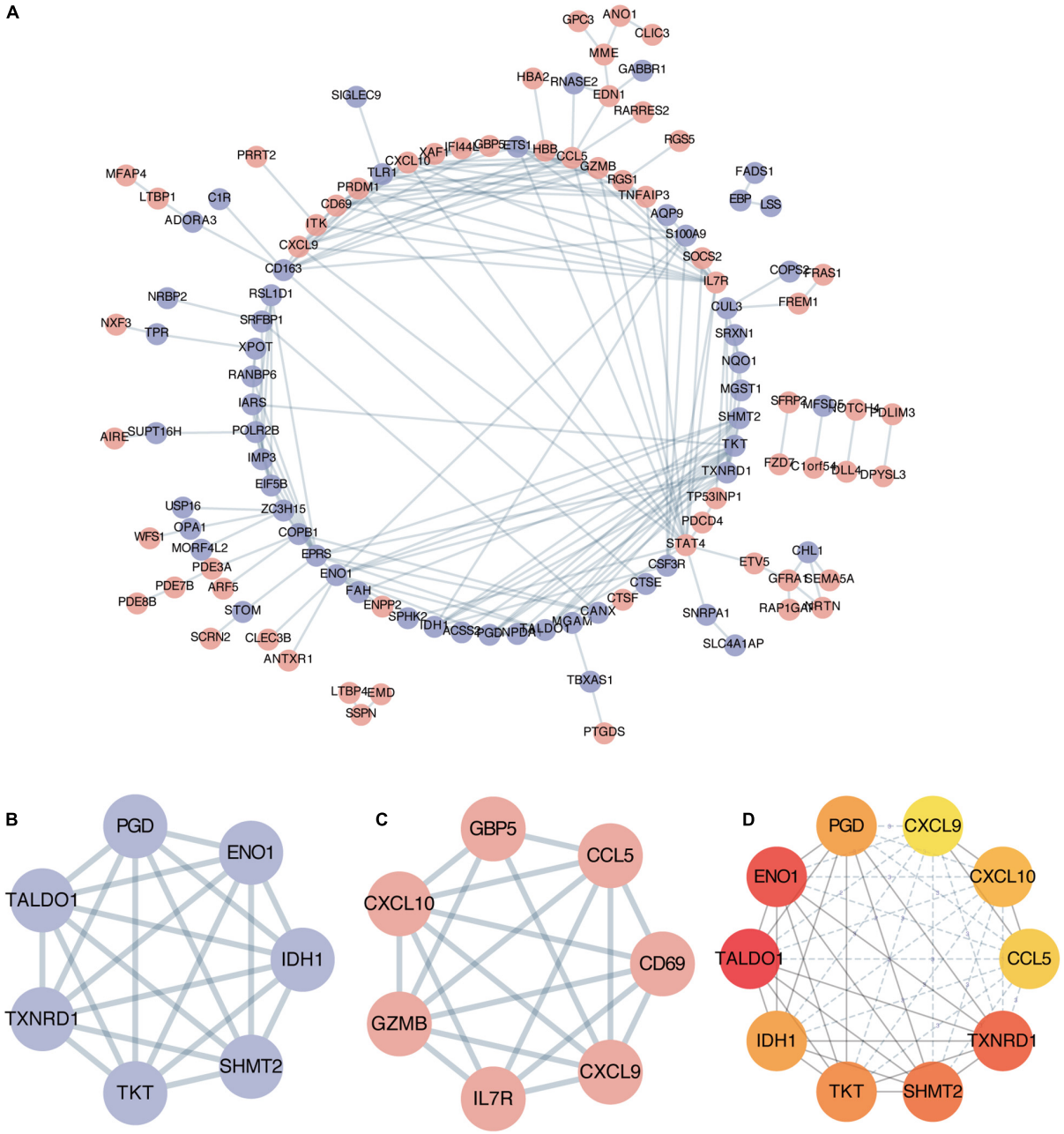

FIGURE 4 | Establishment of protein-protein interaction (PPI) network and hub genes identification. **(A)** Entire PPI network of robust DEGs. The red nodes represent upregulated DEGs and the purple nodes represent downregulated DEGs. **(B)** The significant module 1 identified from PPI network *via* MCODE (score = 7). **(C)** The significant module 2 identified from PPI network *via* MCODE (score = 6.3). **(D)** The top 10 hub genes with highest degrees identified by cytoHubba analysis, the shade of red color represents the degree of importance.

ROC curve analysis which showed that the sensitivity and specificity were 92.3 and 66.7%, respectively, at the optimal expression cutoff value of 0.60, and AUC value of 0.795 exhibited great predictive efficiency of TXNRD1 as diagnosis biomarker (**Figure 5C**). We subsequently analyzed the relationship between serum TXNRD1 levels and clinical characteristics of IPAH patients, and the results revealed that TXNRD1 levels were negatively correlated with mPAP and PVR (**Figures 5D,E**) but had no significant correlation with 6MWD and NT-proBNP (**Supplementary Figure 2**).

In vitro and *in vivo* Experimental Validation and Gene Set Enrichment Analysis Analysis of TXNRD1

Besides blood samples, TXNRD1 expression was also verified by Western blotting using lung homogenate of monocrotaline

TABLE 3 | MCODE module.

	Genes	Description	log10 (*P*-value)
Module 1	PGD, ENO1, TALDO1, IDH1, TXNRD1, TKT, SHMT2	Carbon metabolism	−13.57
		Metabolic reprogramming	−12.81
		Biosynthesis of amino acids	−11.61
		NADP metabolic process	−10.16
Module 2	GBP5, CCL5, CD69, CXCL9, IL7R, GZMB, CXCL10	Cytokine-cytokine receptor interaction	−6.55

(MCT) treated rat which was a well-recognized animal model of PAH. As shown in **Figure 6A**, MCT-treated rats exhibited markedly increased RVSP and RV/(LV + S) as well as pulmonary vascular remodeling. Lung homogenates from MCT rats were measured by Western blot analysis and the results indicated TXNRD1 was significantly downregulated compared with controls (**Figure 6B**). The result was also confirmed by immunofluorescence staining in which TXNRD1 was predominantly expressed in the medial layer of vasculature (**Figure 6C**). Since excessive proliferation of pulmonary artery smooth muscle cell (PASMC) is a pivotal pathophysiological process of PAH, we isolated the rat PASMCs which were confirmed by immunofluorescence with alpha-sma (see **Supplementary Figure 3**) and stimulated it with PDGF-BB (platelet-derived growth factor-BB), a cytokine which has been proposed to be a key mediator of PASMC proliferation in the progression of PAH. Following PDGF-BB stimulation, we observed that TXNRD1 expression was suppressed, which was consistent with our previous results (**Figure 6D**). To decipher the molecular mechanisms leading to deregulation of TXNRD1 in PAH, we analyzed the correlation between TXNRD1 and other genes in multiple datasets and performed GSEA enrichment analysis. As shown in **Figures 6E,F**, there were three GSEA terms that were collectively enriched among different datasets, namely HALLMARK_MTORC1_SIGNALING, HALLMARK_MYC_TARGETS_V1, and HALLMARK_UNFOLDED_PROTEIN_RESPONSE. The entire list of GSEA terms of each datasets could be found as **Supplementary Tables 6–10**.

Knockdown of TXNRD1 Promotes Proliferation, Migration, and Apoptosis Resistance in Pulmonary Artery Smooth Muscle Cell

In order to further explore the functions of TXNRD1 in PASMC, we knocked down the TXNRD1 in transcriptional level to evaluate if silencing TXNRD1 exacerbated PASMC malignant phenotype, including uncontrolled proliferation, migration and apoptosis resistance. We firstly silenced TXNRD1 in PASMC with siRNA that targets TXNRD1 (**Figure 7A**) and exposed them to normal condition or PDGF stimulation for 24 h. As shown in **Figures 7B–E**, knockdown of TXNRD1 aggravated PDGF-induced PCNA expression (a proliferation marker) and EdU incorporation while concomitantly inhibited the expression of cleaved-PARP and BAX/Bcl-2 (apoptosis markers), suggesting TXNRD1 plays a pivotal part in PDGF-BB-induced proliferation and apoptosis resistance in PASMC. Consistently, we then estimated whether TXNRD1 is essential for PDGF-BB-induced PASMC migration and the wound healing assay showed that TXNRD1 interference significantly accelerated the migratory quantity of PASMC (**Figures 7F,G**). In conclusion, these results suggest that TXNRD1 may protect PASMC from switching to a malignant phenotype following the PDGF-BB induction.

DISCUSSION

In this study, we performed an integrated bioinformatics analysis on four datasets containing 65 IPAH samples based on the RRA method. A total of 169 robust differential genes were screened, including 98 up-regulated genes and 71 down-regulated genes. GO and KEGG enrichment analysis showed that these DEGs were significantly enriched in some PAH-related functions and pathways. By constructing a PPI network and screening hub genes, we selected TXNRD1 for further research based on validation in independent datasets. We verified that the expression of TXNRD1 was decreased not only in the serum of IPAH patients but *in vivo* and *in vitro* experiments, which is in line with the predicted results. Furthermore, the GSEA analysis indicated that TXNRD1 may correlate with mTORC1 signaling pathway and MYC targets. Finally, *in vitro* experiments revealed that TXNRD1-knockdown PASMC exhibited exacerbated phenotype including hyperproliferation, migration and apoptosis resistance. This study is the first report to prove that TXNRD1 may be used as a clinical predictive molecule and potential therapeutic target for IPAH.

In recent years, more and more researchers have tried to explore the potential targets of pulmonary hypertension and explore the underlying pathogenesis through bioinformatics analysis. However, since some studies only adopted a single GEO dataset for analysis, or only take the intersection of the results, it may lead to bias and a large number of DEGs that have no biological effect. Regarding this issue, the RRA method has become a reliable method for obtaining important DEG (14). Based on the above integrated bioinformatics analysis, 10 significant hub genes have been identified. Among them, ENO1 and IDH1 were demonstrated to be aberrantly expressed in pulmonary hypertension, which provided strong support for our results. ENO1 encodes alpha-enolase, a glycolytic enzyme that catalyzes the conversion of 2-phosphoglycerate to phosphoenolpyruvate, which had been reported to mediate the malignant phenotypes of PASMCs in pulmonary hypertension, including hyperproliferation, apoptosis resistance, and metabolic conversion (15). Another document also confirmed that

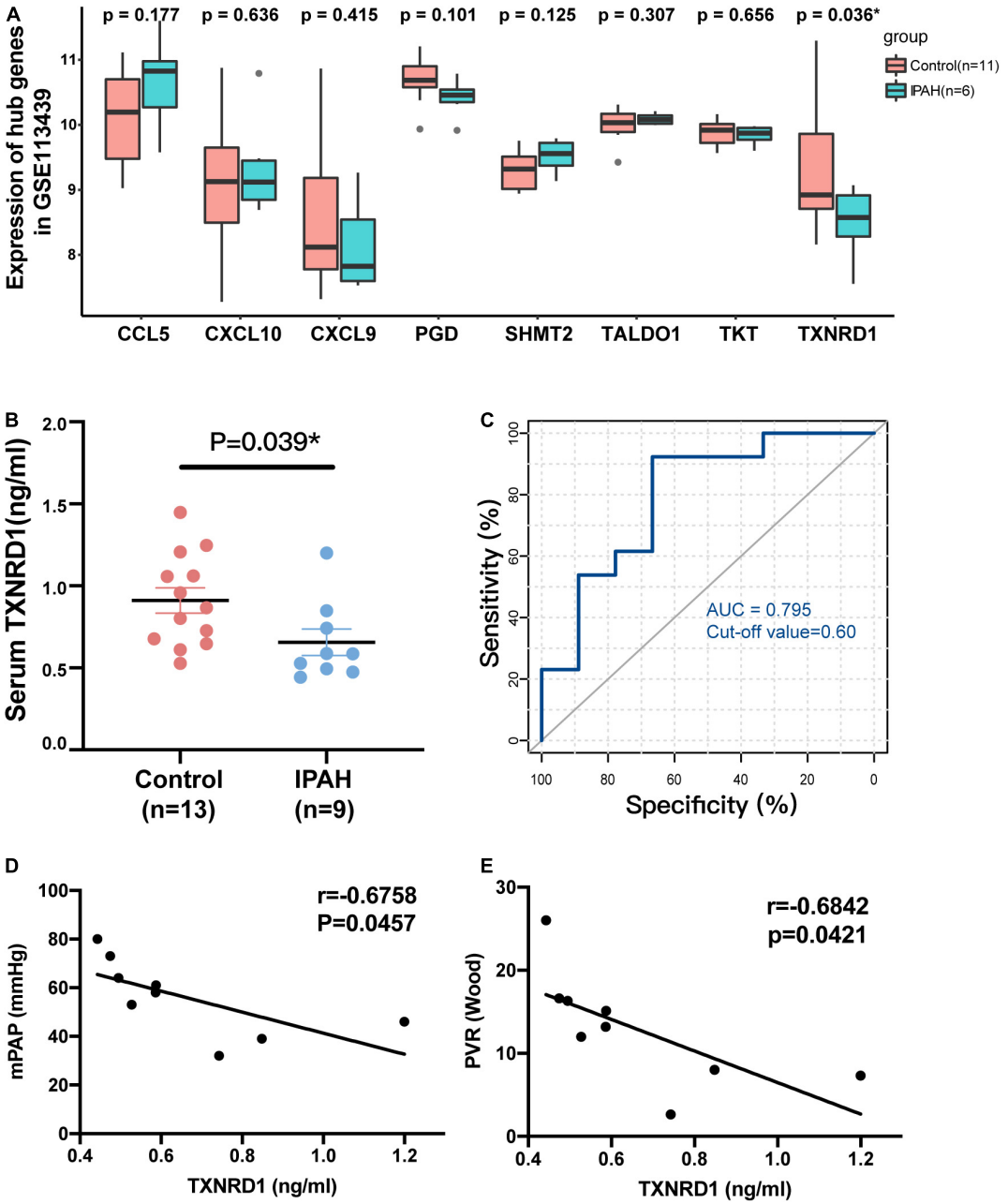

FIGURE 5 | Validation of TXNRD1 in clinical samples. **(A)** Gene expression of hub genes in GSE113439. **(B)** Serum TXNRD1 was decreased in IPAH patients. **(C)** The ability of serum TXNRD1 levels to diagnose IPAH was assessed using ROC curve analysis. **(D,E)** The relationship between serum TXNRD1 and mPAP as well as PVR analyzed by Spearman's correlation analysis.

autoantibody against alpha enolase-1 in the blood of PAH patients with systemic lupus erythematosus could promote the proliferation and migration of PASMCs *in vitro* (16). IDH1 catalyzes the conversion of the citrate isomer isocitrate to alpha-ketoglutarate, which was reportedly elevated in PAH-PASMC (7). However, our results showed that ENO1 and IDH1 were reduced in IPAH patients, which was inconsistent with the above-mentioned literature. The possible reason is that the chip data measures the expression level at the transcription level rather than the protein level, and ENO1 and IDH1 may have post-transcriptional modification. Another possible reason is that the selected research objects are different: our research object is the lung tissue of IPAH patients, and the above-mentioned literature selected the isolated PASMCs from PAH patients for research.

In addition, it is worth noting that other hub genes including TALDO1, SHMT2, TKT, and PGD, are key enzymes involved in the pentose phosphate pathway (PPP), and their expression was inhibited in IPAH group. As we all know, aerobic glycolysis is

TABLE 4 | Clinical characteristics of the study population.

Characteristics	IPAH (*n* = 9)	Control (*n* = 13)	*P*-value
Age (years)	38.5 ± 3.6	34.4 ± 0.7	0.201
BMI (kg/m^2)	20.6 ± 0.8	19.6 ± 0.3	0.236
NT-proBNP (pg/ml)	2414 ± 857		
6MMW (m)	409.5 ± 16.8		
mPAP (mmHg)	56.22 ± 5.18		
PVR (wood)	13.01 ± 2.25		

one of the characteristics of PAH pathogenesis (17). Increased glycolysis can synthesize nucleotides *via* the pentose phosphate pathway to promote cell proliferation, thereby targeting the pentose phosphate pathway is one of the potential strategies to correct metabolic reprogramming. Similar to our results, Varghese et al. reported that the deficiency of the glucose-6-phosphate dehydrogenase (G6PD), the rate-limiting enzyme in PPP, could promote PAH development (18). Counterintuitively, G6PD deficiency did not reduce PPP flux but activated collateral pathways at the cost of increased oxidative stress. Combining the literature and our results, the inhibition of metabolic enzymes in PPP may be one of the unique molecular patterns of IPAH. However, apart from G6PD, genes related to PPP have not yet been elucidated in PAH. Therefore, the above-mentioned PPP-related genes that we have screened deserves to be further studied. These genes have been confirmed to regulate metabolic reprogramming in tumors (19, 20). Besides PPP-related genes, we also screened out several chemokines: CXCL10, CXCL9, CCL5. The dysregulation of chemokine and chemokine receptors had been shown to be implicated in PAH progression (21). Similar to our results, both CXCL10 and CXCL9 have been reported to have relatively elevated serum concentrations in IPAH patients (22, 23). While CCL5 is claimed to promote the PAH progression *via* the BMPR2 signaling pathway, and CCL5 receptor CCR5 has been reported to be involved in the interaction between macrophages and smooth muscle cells (24, 25).

Through the validation analysis of GSE113439, we identified TXNRD1 as the research object for further experimental verification. TXNRD1 is a critical antioxidant enzyme that catalyzes thioredoxin reduction to maintain the cell redox homeostasis (26). Most literatures reported that TXNRD1 was overexpressed in a variety of solid cancers (27, 28). The use of TXNRD1 inhibitors auranofin can overload tumor cells with ROS and promote tumor cell death (29). However, there were also literatures supporting that TXNRD1 could prevent tumorigenesis (30). At present, TXNRD1 has not yet been reported in pulmonary hypertension, while the substrate of TXNRD1, thioredoxin1 (Trx1), was claimed to be increased in hypoxia-induced PASMC proliferation (31), whereas Zimmer et al. observed that MCT-induced PAH animal model promoted a reduction in Trx1 (32). Potential reasons for this contradiction may arise from different stimuli or different stages of disease development. In addition, it is worth noted that numerous studies have reported the reduced expression or activity inhibition of antioxidant enzymes in PAH or PH animal model, such as SOD and GPXs (33). Our experimental results revealed for the first time that serum TXNRD1 of IPAH patients was lower than healthy controls and negatively correlated with mPAP and PVR, which suggested TXNRD1 could be a potential diagnostic marker for IPAH. Not only that, in the PAH animal model induced by MCT, the expression of TXNRD1 was also significantly decreased, which was in agreement with Zimmer's observation. TXNRD1 inhibition had also been confirmed in PDGF-induced PASMC proliferation. Preliminary exploration of TXNRD1 function revealed that silencing of TXNRD1 exacerbated PDGF-induced uncontrolled proliferation, migration, and apoptosis resistance in PASMC. Since TXNRD is closely related to ROS production, we speculate based on our findings that the decreased expression of TXNRD1 increases the production of ROS to a certain extent, which can promote the proliferation of PASMC, but this hypothesis requires further research to prove.

In addition, through GSEA analysis of TXNRD1 related genes, we also found that TXNRD1 was closely correlated with mTORC1 signaling pathway, MYC targets and unfolded protein response, which provided some clues for future exploration of the mechanism involving TXNRD1 dysregulation in IPAH. mTORC1 is a serine/threonine protein kinase complex that regulates protein synthesis and acts as a cellular nutrient, energy, and redox sensor (34). It is reported that mTORC1 signaling is activated in PAH and required for PASMC proliferation induced by chronic hypoxia *in vivo* and *in vitro* (35, 36). mTORC1 activation can modulates cellular redox state through regulating SOD1 activity to ensure adequate proliferation while minimize oxidative damages (37). Myc is a well-known oncogenic transcription factor that serves as a downstream effector of many signaling pathways in PAH (38). Myc has been reported to potentially regulate the transcription of at least 15% of the entire genome (39), and the ChIP-seq data from the ENCODE consortium also demonstrated that Myc binds directly to the Nrf2 locus (an important antioxidant transcription factor) and increases its transcription (40). In view of this, we believe that the role of TXNRD1 in the pathogenesis of PAH be partly achieved by affecting the redox regulation mediated by mTORC1 or Myc. However, there is currently a lack of direct evidence to support this notion. At the same time, the correlation between TXNRD1 and mTOR as well as Myc has not yet been clarified in PAH, which deserves further research to validate.

There were some limitations in our study. First, the serum samples of IPAH patients we have collected are insufficient, so future studies consist of larger sample size are required to corroborate our results. Second, due to the limitations of laboratory conditions, the PAH animal model we used is relatively simple, so future researches are needed to verify the expression of TXNRD1 using other animal models such as hypoxia + Sugen5416 treated mice. Third, we did not conduct experiments to verify the activity of TXNRD1. Future studies are worth exploring the detailed mechanism of TXNRD1.

In conclusion, after integrating combined analysis by RRA method, we identified TXNRD1 as a potential biomarker for diagnosis of IPAH and potentially even a therapeutic target. Further research is needed to validate the function of TXNRD1 in IPAH pathogenesis.

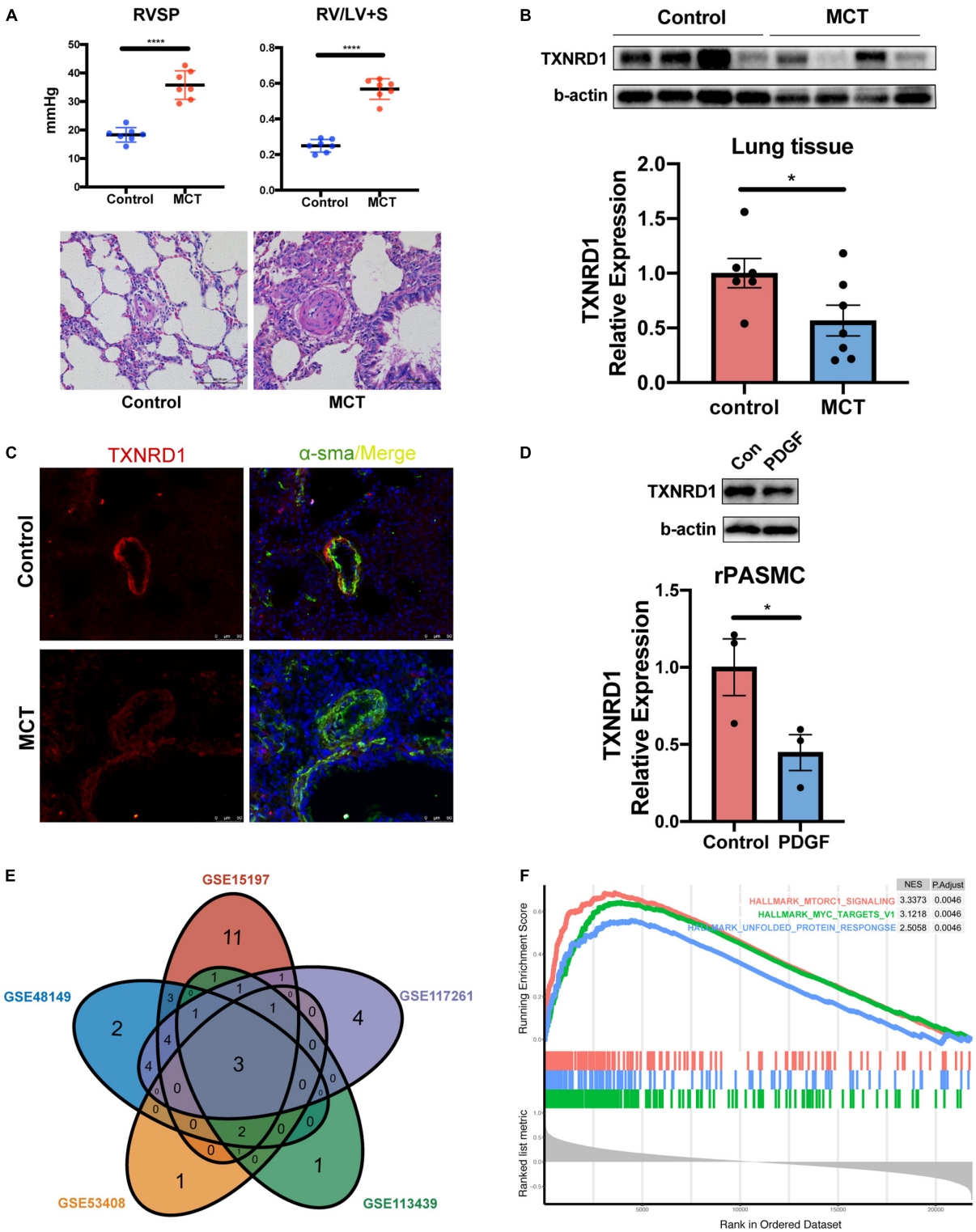

FIGURE 6 | *In vitro* and *in vivo* experimental validation and GSEA analysis of TXNRD1. **(A)** The hemodynamic data and HE staining of lung tissue in animal experiments. **(B)** Representative Western blots and quantification of TXNRD1 and β-actin in the lungs of monocrotaline treated rats and controls ($n = 7$ each, $^*P < 0.05$), data represent the mean ± SEM and Student *t*-test was used to compare two groups. **(C)** Immunofluorescence images of lung distal PA from MCT rats and controls. **(D)** Representative Western blots and quantification of TXNRD1 levels in rat PASMCs under PDGF-BB stimulation (30 ng/ml) normalized to a β-actin internal control ($n = 3$ each,$^*P < 0.05$). **(E)** Venn diagram of GSEA terms among five datasets based on correlation analysis of TXNRD1. **(F)** The overlapping three GSEA terms correlated with TXNRD1. $^{****}P < 0.0001$.

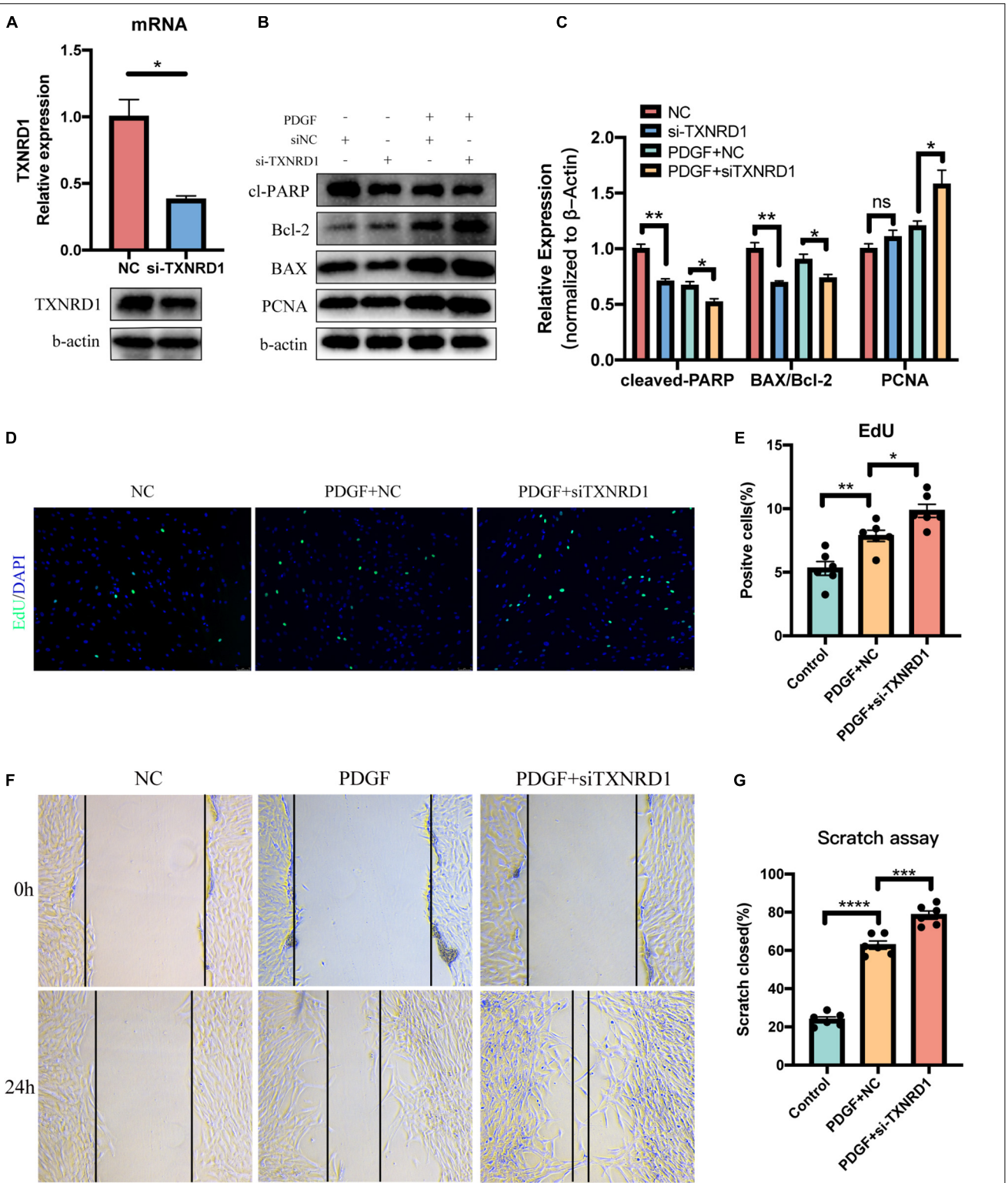

FIGURE 7 | Silencing of TXNRD1 exacerbated PDGF-induced PASMC malignant phenotype. **(A)** Knockdown efficiency of TXNRD1 was verified by qPCR and Western Blot. **(B)** PASMCs were transfected with siRNA for 48 h before treatment with PDGF-BB (20 ng/ml) for another 24 h, and western blotting was used to detect proliferative and apoptotic markers in cell lysates. **(C)** Normalized quantification of cleaved-PARP, BAX/Bcl-2 and PCNA expression ($n = 3$ each, $^*P < 0.05$). **(D)** Cell proliferative ability was determined by EdU assay in siTXNRD1-PASMC under PDGF stimulation. **(E)** Calculation of EdU-stained cells rate ($n = 6$ each, $^*P < 0.05$). **(F)** Cell migration was measured by scratch assay in siTXNRD1-PASMC under PDGF stimulation. **(G)** Calculation of scratch closed percentage ($n = 6$ each, $^*P < 0.05$). Data represent the mean ± SEM. Student *t*-test and one-way ANOVA were used to compare two and multiple groups. $^{**}P < 0.01$, $^{***}P < 0.001$, $^{****}P < 0.0001$.

DATA AVAILABILITY STATEMENT

The datasets presented in this study can be found in online repositories. The names of the repository/repositories and accession number(s) can be found in the article/ **Supplementary Material**.

ETHICS STATEMENT

The studies involving human participants were reviewed and approved by the Medical Ethics Committee of the Xiangya Hospital of Central South University. The patients/participants provided their written informed consent to participate in this study. The animal study was reviewed and approved by the Institutional Animal Care and Use Committee of Central South University.

AUTHOR CONTRIBUTIONS

ZY and LZ conceived and designed the study. WL performed this study and drafted the manuscript. YT and MZ reviewed the manuscript. BL and MW assisted in collecting clinical samples. All authors read and approved the manuscript.

FUNDING

This study was supported by the National Natural Science Foundation of China (Nos. 82070055, 81873416, and 82100071) and the Key Research and Development Program of Hunan Province (2020SK2065).

ACKNOWLEDGMENTS

We are grateful to thank Professor Li Ming for her technical assistance.

SUPPLEMENTARY MATERIAL

The Supplementary Material for this article can be found online at: https://www.frontiersin.org/articles/10.3389/fmed.2022.894584/full#supplementary-material

REFERENCES

1. Zolty R. Pulmonary arterial hypertension specific therapy: the old and the new. *Pharmacol Ther.* (2020) 214:107576. doi: 10.1016/j.pharmthera.2020.107576
2. Ghataorhe P, Rhodes CJ, Harbaum L, Attard M, Wharton J, Wilkins MR. Pulmonary arterial hypertension - progress in understanding the disease and prioritizing strategies for drug development. *J Intern Med.* (2017) 282:129–41. doi: 10.1111/joim.12623
3. Farber HW, Miller DP, Poms AD, Badesch DB, Frost AE, Muros-Le Rouzic E, et al. Five-year outcomes of patients enrolled in the REVEAL registry. *Chest.* (2015) 148:1043–54. doi: 10.1378/chest.15-0300
4. Thenappan T, Ormiston ML, Ryan JJ, Archer SL. Pulmonary arterial hypertension: pathogenesis and clinical management. *BMJ.* (2018) 360:j5492. doi: 10.1136/bmj.j5492
5. Thompson AAR, Lawrie A. Targeting vascular remodeling to treat pulmonary arterial hypertension. *Trends Mol Med.* (2017) 23:31–45. doi: 10.1016/j.molmed.2016.11.005
6. Stearman RS, Bui QM, Speyer G, Handen A, Cornelius AR, Graham BB, et al. Systems analysis of the human pulmonary arterial hypertension lung transcriptome. *Am J Respir Cell Mol Biol.* (2019) 60:637–49. doi: 10.1165/rcmb.2018-0368OC
7. Li D, Shao NY, Moonen JR, Zhao Z, Shi M, Otsuki S, et al. ALDH1A3 coordinates metabolism with gene regulation in pulmonary arterial hypertension. *Circulation.* (2021) 143:2074–90. doi: 10.1161/CIRCULATIONAHA.120.048845
8. Kikuchi N, Satoh K, Kurosawa R, Yaoita N, Elias-Al-Mamun M, Siddique MAH, et al. Selenoprotein P promotes the development of pulmonary arterial hypertension: possible novel therapeutic target. *Circulation.* (2018) 138:600–23. doi: 10.1161/circulationaha.117.033113
9. Kolde R, Laur S, Adler P, Vilo J. Robust rank aggregation for gene list integration and meta-analysis. *Bioinformatics.* (2012) 28:573–80. doi: 10.1093/bioinformatics/btr709
10. Ma Y, Chen SS, Feng YY, Wang HL. Identification of novel biomarkers involved in pulmonary arterial hypertension based on multiple-microarray analysis. *Biosci Rep.* (2020) 40:BSR20202346. doi: 10.1042/BSR20202346
11. Dong H, Li X, Cai M, Zhang C, Mao W, Wang Y, et al. Integrated bioinformatic analysis reveals the underlying molecular mechanism of and potential drugs for pulmonary arterial hypertension. *Aging (Albany NY).* (2021) 13:14234–57. doi: 10.18632/aging.203040
12. Yu GC, Wang LG, Han YY, He QY. clusterProfiler: an R package for comparing biological themes among gene clusters. *Omics.* (2012) 16:284–7. doi: 10.1089/omi.2011.0118
13. Siques P, Pena E, Brito J, El Alam S. Oxidative stress, kinase activation, and inflammatory pathways involved in effects on smooth muscle cells during pulmonary artery hypertension under hypobaric hypoxia exposure. *Front Physiol.* (2021) 12:690341. doi: 10.3389/fphys.2021.690341
14. Sun G, Li Y, Peng Y, Lu D, Zhang F, Cui X, et al. Identification of differentially expressed genes and biological characteristics of colorectal cancer by integrated bioinformatics analysis. *J Cell Physiol.* (2019) 234:15215–24. doi: 10.1002/jcp.28163
15. Dai J, Zhou Q, Chen J, Rexius-Hall ML, Rehman J, Zhou G. Alpha-enolase regulates the malignant phenotype of pulmonary artery smooth muscle cells via the AMPK-Akt pathway. *Nat Commun.* (2018) 9:3850. doi: 10.1038/s41467-018-06376-x
16. Kato Y, Kasama T, Soejima M, Kubota T. Anti-enolaseantibodies from a patient with systemic lupus erythematosus accompanied by pulmonary arterial hypertension promote migration of pulmonary artery smooth muscle cells. *Immunol Lett.* (2020) 218:22–9. doi: 10.1016/j.imlet.2019.12.005
17. Humbert M, Guignabert C, Bonnet S, Dorfmuller P, Klinger JR, Nicolls MR, et al. Pathology and pathobiology of pulmonary hypertension: state of the art and research perspectives. *Eur Respir J.* (2019) 53:1801887. doi: 10.1183/13993003.01887-2018
18. Varghese MV, James J, Rafikova O, Rafikov R. Glucose-6-phosphate dehydrogenase deficiency contributes to metabolic abnormality and pulmonary hypertension. *Am J Physiol Lung Cell Mol Physiol.* (2021) 320:L508–21. doi: 10.1152/ajplung.00165.2020
19. Kim D, Fiske BP, Birsoy K, Freinkman E, Kami K, Possemato RL, et al. SHMT2 drives glioma cell survival in ischaemia but imposes a dependence on glycine clearance. *Nature.* (2015) 520:363–7. doi: 10.1038/nature14363
20. Tseng CW, Kuo WH, Chan SH, Chan HL, Chang KJ, Wang LH. Transketolase regulates the metabolic switch to control breast cancer cell metastasis via the alpha-ketoglutarate signaling pathway. *Cancer Res.* (2018) 78:2799–812. doi: 10.1158/0008-5472.CAN-17-2906
21. Mamazhakypov A, Viswanathan G, Lawrie A, Schermuly RT, Rajagopal S. The role of chemokines and chemokine receptors in pulmonary arterial hypertension. *Br J Pharmacol.* (2021) 178:72–89. doi: 10.1111/bph.14826
22. Koudstaal T, van Uden D, van Hulst JAC, Heukels P, Bergen IM, Geenen LW, et al. Plasma markers in pulmonary hypertension subgroups correlate

with patient survival. *Respir Res.* (2021) 22:137. doi: 10.1186/s12931-021-01716-w
23. Li Z, Jiang J, Gao S. Potential of C-X-C motif chemokine ligand 1/8/10/12 as diagnostic and prognostic biomarkers in idiopathic pulmonary arterial hypertension. *Clin Respir J.* (2021) 15:1302–9. doi: 10.1111/crj.13421
24. Abid S, Marcos E, Parpaleix A, Amsellem V, Breau M, Houssaini A, et al. CCR2/CCR5-mediated macrophage-smooth muscle cell crosstalk in pulmonary hypertension. *Eur Respir J.* (2019) 54:1802308. doi: 10.1183/13993003.02308-2018
25. Nie X, Tan J, Dai Y, Liu Y, Zou J, Sun J, et al. CCL5 deficiency rescues pulmonary vascular dysfunction, and reverses pulmonary hypertension via caveolin-1-dependent BMPR2 activation. *J Mol Cell Cardiol.* (2018) 116:41–56. doi: 10.1016/j.yjmcc.2018.01.016
26. Dagnell M, Schmidt EE, Arner ESJ. The A to Z of modulated cell patterning by mammalian thioredoxin reductases. *Free Radic Biol Med.* (2018) 115:484–96. doi: 10.1016/j.freeradbiomed.2017.12.029
27. Rodriguez-Garcia A, Hevia D, Mayo JC, Gonzalez-Menendez P, Coppo L, Lu J, et al. Thioredoxin 1 modulates apoptosis induced by bioactive compounds in prostate cancer cells. *Redox Biol.* (2017) 12:634–47. doi: 10.1016/j.redox.2017.03.025
28. Bhatia M, McGrath KL, Di Trapani G, Charoentong P, Shah F, King MM, et al. The thioredoxin system in breast cancer cell invasion and migration. *Redox Biol.* (2016) 8:68–78. doi: 10.1016/j.redox.2015.12.004
29. Lee D, Xu IM, Chiu DK, Leibold J, Tse AP, Bao MH, et al. Induction of oxidative stress through inhibition of thioredoxin reductase 1 is an effective therapeutic approach for hepatocellular carcinoma. *Hepatology.* (2019) 69:1768–86. doi: 10.1002/hep.30467
30. Carlson BA, Yoo MH, Tobe R, Mueller C, Naranjo-Suarez S, Hoffmann VJ, et al. Thioredoxin reductase 1 protects against chemically induced hepatocarcinogenesis via control of cellular redox homeostasis. *Carcinogenesis.* (2012) 33:1806–13. doi: 10.1093/carcin/bgs230
31. Chen B, Nelin VE, Locy ML, Jin Y, Tipple TE. Thioredoxin-1 mediates hypoxia-induced pulmonary artery smooth muscle cell proliferation. *Am J Physiol Lung Cell Mol Physiol.* (2013) 305:L389–95. doi: 10.1152/ajplung.00432.2012
32. Zimmer A, Teixeira RB, Constantin RL, Fernandes-Piedras TRG, Campos-Carraro C, Türck P, et al. Thioredoxin system activation is associated with the progression of experimental pulmonary arterial hypertension. *Life Sci.* (2021) 284:119917. doi: 10.1016/j.lfs.2021.119917
33. Masri FA, Comhair SA, Dostanic-Larson I, Kaneko FT, Dweik RA, Arroliga AC, et al. Deficiency of lung antioxidants in idiopathic pulmonary arterial hypertension. *Clin Transl Sci.* (2008) 1:99–106. doi: 10.1111/j.1752-8062.2008.00035.x
34. Babicheva A, Makino A, Yuan JX. mTOR signaling in pulmonary vascular disease: pathogenic role and therapeutic target. *Int J Mol Sci.* (2021) 22:2144. doi: 10.3390/ijms22042144
35. Goncharov DA, Kudryashova TV, Ziai H, Ihida-Stansbury K, DeLisser H, Krymskaya VP, et al. Mammalian target of rapamycin complex 2 (mTORC2) coordinates pulmonary artery smooth muscle cell metabolism, proliferation, and survival in pulmonary arterial hypertension. *Circulation.* (2014) 129:864–74. doi: 10.1161/CIRCULATIONAHA.113.004581
36. Li Y, Yang L, Dong L, Yang ZW, Zhang J, Zhang SL, et al. Crosstalk between the Akt/mTORC1 and NF-kappaB signaling pathways promotes hypoxia-induced pulmonary hypertension by increasing DPP4 expression in PASMCs. *Acta Pharmacol Sin.* (2019) 40:1322–33. doi: 10.1038/s41401-019-0272-2
37. Tsang CK, Chen M, Cheng X, Qi Y, Chen Y, Das I, et al. . SOD1 phosphorylation by mTORC1 couples nutrient sensing and redox regulation. *Mol Cell.* (2018) 70: 502–515.e8. doi: 10.1016/j.molcel.2018.03.029
38. Dong L, Liu X, Wu B, Li C, Wei X, Wumaier G, et al. Mxi1-0 promotes hypoxic pulmonary hypertension via ERK/c-Myc-dependent proliferation of arterial smooth muscle cells. *Front Genet.* (2022) 13:810157. doi: 10.3389/fgene.2022.810157
39. Dang CV, O'Donnell KA, Zeller KI, Nguyen T, Osthus RC, Li F. The c-Myc target gene network. *Semin Cancer Biol.* (2006) 16:253–64. doi: 10.1016/j.semcancer.2006.07.014
40. DeNicola GM, Karreth FA, Humpton TJ, Gopinathan A, Wei C, Frese K, et al. Oncogene-induced Nrf2 transcription promotes ROS detoxification and tumorigenesis. *Nature.* (2011) 475:106–9. doi: 10.1038/nature10189

Conflict of Interest: The authors declare that the research was conducted in the absence of any commercial or financial relationships that could be construed as a potential conflict of interest.

Publisher's Note: All claims expressed in this article are solely those of the authors and do not necessarily represent those of their affiliated organizations, or those of the publisher, the editors and the reviewers. Any product that may be evaluated in this article, or claim that may be made by its manufacturer, is not guaranteed or endorsed by the publisher.

frontiers | Frontiers in Medicine

ORIGINAL RESEARCH
published: 28 June 2022
doi: 10.3389/fmed.2022.886868

Akt-Dependent Glycolysis-Driven Lipogenesis Supports Proliferation and Survival of Human Pulmonary Arterial Smooth Muscle Cells in Pulmonary Hypertension

Lifeng Jiang[1], Dmitry A. Goncharov[1], Yuanjun Shen[1], Derek Lin[1], Baojun Chang[2], Andressa Pena[2], Horace DeLisser[3], Elena A. Goncharova[1†] and Tatiana V. Kudryashova[1†]*

[1] Lung Center, Division of Pulmonary, Critical Care and Sleep Medicine, Department of Internal Medicine, School of Medicine, University of California, Davis, Davis, CA, United States, [2] Pittsburgh Heart, Lung, and Blood Vascular Medicine Institute, University of Pittsburgh, Pittsburgh, PA, United States, [3] Department of Medicine, Perelman School of Medicine, University of Pennsylvania, Philadelphia, PA, United States

OPEN ACCESS

Edited by:
Soban Umar,
University of California, Los Angeles,
United States

Reviewed by:
Olivier Boucherat,
Laval University, Canada
Werner Seeger,
University of Giessen, Germany

***Correspondence:**
Tatiana V. Kudryashova
tkud@ucdavis.edu

[†]These authors share senior authorship

Specialty section:
This article was submitted to Pulmonary Medicine, a section of the journal Frontiers in Medicine

Received: 01 March 2022
Accepted: 31 May 2022
Published: 28 June 2022

Citation:
Jiang L, Goncharov DA, Shen Y, Lin D, Chang B, Pena A, DeLisser H, Goncharova EA and Kudryashova TV (2022) Akt-Dependent Glycolysis-Driven Lipogenesis Supports Proliferation and Survival of Human Pulmonary Arterial Smooth Muscle Cells in Pulmonary Hypertension. Front. Med. 9:886868. doi: 10.3389/fmed.2022.886868

Hyper-proliferation of pulmonary arterial vascular smooth muscle cells (PAVSMC) is an important pathological component of pulmonary vascular remodeling in pulmonary arterial hypertension (PAH). Lipogenesis is linked to numerous proliferative diseases, but its role in PAVSMC proliferation in PAH remains to be elucidated. We found that early-passage human PAH PAVSMC had significant up-regulation of key fatty acids synthesis enzymes ATP-citrate lyase (ACLY), acetyl-CoA carboxylase (ACC), and fatty acid synthase (FASN), and increased unstimulated proliferation compared to control human PAVSMC. Treatment with an allosteric ACC inhibitor 5-tetradecyloxy-2-furoic acid (TOFA) significantly decreased proliferation and induced apoptosis of human PAH PAVSMC. Intracellular lipid content and proliferation of PAH PAVSMC were not reduced by incubation in lipid-depleted media but suppressed by a non-metabolizable analog of glucose 2-Deoxy-D-glucose (2-DG) and partially restored by addition of pyruvate. Protein kinase Akt was upregulated in human PAH PAVSMC in a sirtuin 7 (SIRT7)- and c-Jun N-terminal kinase (JNK)-dependent manner. Pharmacological inhibition of Akt down-regulated ACLY and ACC, significantly reduced intracellular lipid content, inhibited proliferation and induced apoptosis of human PAH PAVSMC. Taken together, these data demonstrate that human PAH PAVSMC have up-regulated lipogenesis, which is supported in an Akt- and glycolysis-dependent manner and is required for increased proliferation and survival. Our data suggest that there is a mechanistic link between glycolysis, lipogenesis, and the proliferation of human PAH PAVSMC and call for further studies to determine the potential attractiveness of a SIRT7/JNK-Akt-lipogenesis axis as a target pathway to inhibit PAVSMC hyper-proliferation in PAH.

Keywords: pulmonary arterial hypertension, lipogenesis, vascular smooth muscle, proliferation, apoptosis, JNK, SIRT7, Akt

INTRODUCTION

Pulmonary arterial hypertension (PAH) is a devastating progressive disease leading to a deteriorating quality of life and high morbidity and mortality rates (1–3). Continuous vasoconstriction and excessive remodeling of pulmonary arteries (PA) cause an increase in pulmonary arterial pressure and pulmonary vascular resistance, leading to elevated right ventricular (RV) afterload and ultimately right heart failure and death (4, 5). At present, available vasodilatory therapies do not stop disease progression, and currently there are no vascular remodeling-focused therapies available for PAH patients (4, 6). All three layers of small pulmonary arteries—intima, media and adventitia—contribute to pulmonary vascular remodeling (7, 8). One of the important features of pulmonary vascular remodeling is the increased proliferation and survival of pulmonary arterial vascular smooth muscle cells (PAVSMC) (9, 10) in the medial layer of small muscular PAs (11). Over the last decades significant progress was achieved in dissecting the signaling molecules and pathways supporting the pathological pro-proliferative/pro-survival nature of PAVSMC in PAH. However, the underlying mechanisms are still not completely understood.

We and others previously demonstrated that PAH PAVSMC undergo a complex metabolic reprogramming required to maintain energy consuming pro-proliferative phenotype (9, 10, 12, 13). In contrast to non-diseased cells, PAH PAVSMC demonstrate increased ATP generation, proliferation and survival which depend predominantly on glycolytic metabolism (10) and undergo a metabolic shift from mitochondrial oxidative phosphorylation to glycolysis, similar to the "Warburg effect" in cancer cells (9, 10, 14). Multiple crucial metabolic regulators and enzymes, including AMP-activated protein kinase (AMPK), mechanistic target of rapamycin (mTOR) complex 2 (mTORC2) (10), hypoxia-induced factor (HIF) 1α (9), nuclear factor of activated T-cells (NFAT) (15), peroxisome proliferator-activated receptor (PPAR)γ (16), pyruvate dehydrogenase (PDH) (17), PDH kinase (PDK) (18), 6-phosphofructo-2-kinase/fructose-2,6-bisphosphatase 3 (PFKFB3) (19), pyruvate carboxylase (PC) (20), and enolase (21), support this glycolytic shift in PAH PAVSMC (9, 10, 22). A stable isotope metabolomics-based study confirmed that PAH PAVSMC have increased glucose uptake and utilization by glycolysis and the pentose shunt, but intriguingly no changes in fatty acid or glutamine uptake or utilization were detected (23).

Besides increased ATP levels, hyper-proliferative cells require increased amounts of intracellular essential "building blocks" such as lipids, proteins, and nucleic acids (24). The fact that highly proliferative PAH PAVSMC do not demonstrate increased fatty acid uptake (23) indicates that lipid metabolism in these cells might be re-organized to produce and accumulate the required amount of lipids internally. Indeed, several lines of evidence indicate that lipid metabolism is deregulated in PAH PAVSMC (25). RNAseq-based analysis identified up-regulation of fatty acid biosynthesis and metabolism pathways in isolated human PAH PASMC (26). Up-regulation of a key enzyme in fatty acid synthesis, fatty acid synthase (FASN) (27), and a key rate-limiting enzyme of mitochondrial fatty acid β-oxidation, carnitine palmitoyltransferase (CPT) (28), was reported in PAVSMC in rats with monocrotaline (MCT)-induced PH. Interestingly, a similar metabolic adaptation to satisfy high lipids demand is observed in most cancer cells, which have elevated endogenous fatty acid synthesis supported by the increased glycolysis and an increased ability to synthesize lipids (29, 30). *De novo* fatty acid synthesis makes a major contribution to the intracellular fatty acid pool in tumor cells (31) suggesting that PAVSMC in PAH might use similar strategies to support their highly proliferative phenotype. However, in contrast to the role of lipid metabolism in right ventricle (RV) function in PAH (25), the potential role of the lipogenic process and underlying mechanisms in PAH PAVSMC require further investigation.

In this study, we aimed to evaluate the status and role of lipogenesis in PAH PAVSMC proliferation and survival. Our data demonstrate that the pro-proliferative/pro-survival phenotype of PAVSMC in PAH is supported by glycolysis-dependent *de novo* lipid synthesis and suggest the potential role of Sirtuin 7 (SIRT7)- c-Jun N-terminal kinase (JNK)-Akt axis as a regulator of lipogenesis and a potential molecular target for anti-remodeling therapy.

MATERIALS AND METHODS

Cell Culture

Early-passage (3–8 passage) human PAVSMC isolated from small (≤1 mm outer diameter) PAs of patients with PAH and non-diseased subjects were provided by UC Davis Lung Center Pulmonary Vascular Disease Program human specimens biobank, University of Pittsburgh Vascular Medicine Institute Cell Processing Core, and the Pulmonary Hypertension Breakthrough Initiative (PHBI) under approved protocols in accordance with Institutional Review Board (IRB) and Committee for Oversight of Research and Clinical Training Involving Decedents (*CORID*) policies. Cells isolation, characterization and maintenance were performed under PHBI-approved protocols as described previously (10, 32). Cells were maintained in complete PromoCell Smooth Muscle Cell Growth Medium 2 with SupplementPack and Antibiotic-Antimycotic. Before experiments, cells were incubated for 24–48 h in basal media supplemented with 0.1% bovine serum albumin (BSA) if not stated otherwise. For functional experiments (Ki-67, cell counts, TUNEL) a minimum of three technical replicas was performed within one experiment, minimum of 100 cells/subject was analyzed.

Exogenous Lipids Removal

To achieve the lipid-deprived cell culture condition, cell culture grade fetal bovine serum (FBS) and BSA were delipidated using Cleanascite^{TM} Lipid Removal Reagent (Biotech Support Group; Monmouth Junction, NJ, United States) according to the manufacturer's protocol with modification. Briefly, Cleanascite^{TM} was added to the FBS or BSA (1:4 volume ratio). The mixture was incubated for four hours at 4°C with gentle shaking and centrifuged at 16,000 *g* for 10 min. Supernatant was collected, then a second dose of Cleanascite^{TM} Lipid Removal Reagent was added (1:4 volume ratio), and incubation and centrifugation steps were repeated as described above.

The supernatants, consisting of lipid depleted FBS or BSA, were then used as cell culture media supplements to prepare lipid-depleted media.

Intracellular Lipid Detection

Intracellular lipid detection was performed using a fluorescent probe for lipid droplets BODIPY 493/503 as previously described in Qiu et al. (33) with modifications. Briefly, cells were washed twice with PBS and then incubated with 2 μM BODIPY 493/503 staining solution (#D3922 Thermo Fisher Scientific, Chicago, IL, United States) for 15 min at 37°C. Then cells were fixed in 4% paraformaldehyde/phosphate-buffered saline (PBS), followed by DAPI staining to detect nuclei. Immunostaining was visualized and images were taken using a Keyence BZ-X800 (Keyence Corporation of America, Itasca, IL, United States) and Zeiss LSM700 confocal microscope (White Plains, NY, United States). A minimum of 100 cells per condition was analyzed.

Cell Proliferation Assay

Cell proliferation was assessed using Ki-67 immunostaining as described previously (10, 32, 34). Briefly, cells were washed with PBS, fixed in 4% paraformaldehyde/PBS, and permeabilized using Triton X-100/PBS solution. Then cells were incubated in blocking solution (2% BSA/PBS), followed by overnight incubation with primary anti-Ki-67 antibody (#9129, Cell Signaling, Danvers, MA, United States) in blocking solution. Next day, the slides were washed with PBS, followed by incubation with secondary chicken anti-rabbit IgG (H + L) Alexa Fluor 594 antibody (#A-21442, Invitrogen, Waltham, MA, United States) and 4′,6-diamidino-2-phenylindole (DAPI) to detect nuclei. Images were taken using a Keyence BZ-X800 microscope.

Cell Growth Assay

Cell growth analysis was performed as described previously (10, 32, 34). Briefly, 300,000 cells per well were plated in a six well plate in cell culture media supplemented with 5% FBS. Forty-eight hours later, when cells attached and spread (day 0), the media was changed to 0.1% BSA with or without lipids and incubated for six more days (media was renewed every 48 h). Then, cell counting was performed using the Countess II FL Automated Cell Counter (Thermo Fisher Scientific, Waltham, MA, United States) according to manufacturer's protocol.

Apoptosis Analysis

Apoptosis analysis was performed using the *In situ* Cell Death Detection Kit (Roche, Nutley, NJ, United States) based on terminal deoxynucleotidyltransferase-mediated dUTP-biotin nick end labeling (TUNEL) technology following the manufacturer's protocol.

Immunoblot Analysis

Immunoblot analysis was performed as described previously (10, 32, 34). Antibodies for ACLY (#4332), P-S79-ACC (#11818), ACC (#3676), FASN (#3180), P-S473-Akt (#4060), P-T450-Akt (#12178), Akt (#9272), PThr183/Tyr185-JNK (#4668), JNK (#9252), α/β-Tubulin (#2148), CPT1A (#97361), hexokinase II (HKII) (#2867), phosphofructokinase (PFKP) (#8164) were purchased from Cell Signaling (Danvers, MA, United States). The antibody for P-S455-ACLY (#PA5-97395) was purchased from Thermo Fisher Scientific (Chicago, IL, United States). The antibody for malonyl CoA decarboxylase (MLYCD) (#15265-1-AP) were purchased from Proteintech (Rosemont, IL, United States). Secondary HRP conjugated anti-mouse antibody (ab205719) was purchased from Abcam (Boston, MA, United States), secondary HRP-conjugated anti-rabbit antibody (#7074) was purchased from Cell Signaling (Danvers, MA, United States).

Inhibitors and Activators

2-Deoxy-D-glucose (2-DG, D6134), IL-6 (I1395), PDGF-BB (GF149), and Akt inhibitor VIII (SIAL-124018) were purchased from Millipore Sigma (St. Louis, MO, United States), 5-tetradecyloxy-2-furoic acid (TOFA, sc-200653) was purchased from Santa Cruz Biotechnology (Dallas, TX, United States), JNK inhibitor (bentamapimod, HY-14761) was purchased from MedChemExpress (Monmouth Junction, NJ, United States).

Lactate Assay

To measure intracellular lactate amount, the lactate assay kit (#MAK064, Millipore Sigma) was used according to the manufacturer protocol with modifications. Briefly, 2×10^6 cell were homogenized in 200 μL of lactate assay buffer and centrifuged at 21,000 *g* for 5 min to remove cell debris. The supernatant was deproteinized with a 10 kDa MWCO spin filter (#UFC5003, Millipore Sigma) to remove lactate dehydrogenase, and the lactate assay was performed. Protein concentrations were determined in the supernatants before deproteinization using the BCA protein assay kit (#23227, Thermo Fisher Scientific) and lactate content was normalized to the amount of total protein used for the assay.

Data Analysis

Immunoblots, BODIPY 493/503, Ki-67 and apoptosis assays were analyzed using ImageJ (NIH, Bethesda, MD, United States), StatView (SAS Institute, Cary, NC, United States) and GraphPad Prizm 9.02 (GraphPad Software, San Diego, CA, United States). Immunocytochemical analyses were detected and captured using the Keyence BZ-X800 system and software (Keyence Corporation of America, Itasca, IL, United States) and Zeiss LSM700 confocal microscope and software (ZEN, 2009; White Plains, NY, United States). Statistical comparisons between the two groups were performed by Mann–Whitney *U* test. Statistical comparisons among three or more groups were performed by the Kruskal–Wallis rank test with Dunn pairwise comparison *post hoc* test. Statistical significance was defined as $p \leq 0.05$.

RESULTS

Increased Lipid Synthesis Is Required for Hyper-Proliferation and Survival of Human PAH PAVSMC

In order to evaluate the status of lipogenesis in PAH PAVSMC, we first tested the expression of key lipogenic enzymes

driving the biosynthesis of fatty acids. Immunoblot analysis demonstrated significant increase in phosphorylated ACLY, and elevated protein levels of ACC and FASN in early-passage distal human PAH PAVSMC compared to cells from non-diseased subjects (CTRL) (**Figures 1A–D** and **Supplementary Figure 1A**). Interestingly, we detected no significant differences between non-diseased and PAH PAVSMC in protein levels of CPT1A (**Figures 1A,E**) and MLYCD (**Supplementary Figure 1B**), the regulatory enzymes in fatty acid β-oxidation and synthesis, in spite of previously reported up-regulation of CPT1A in

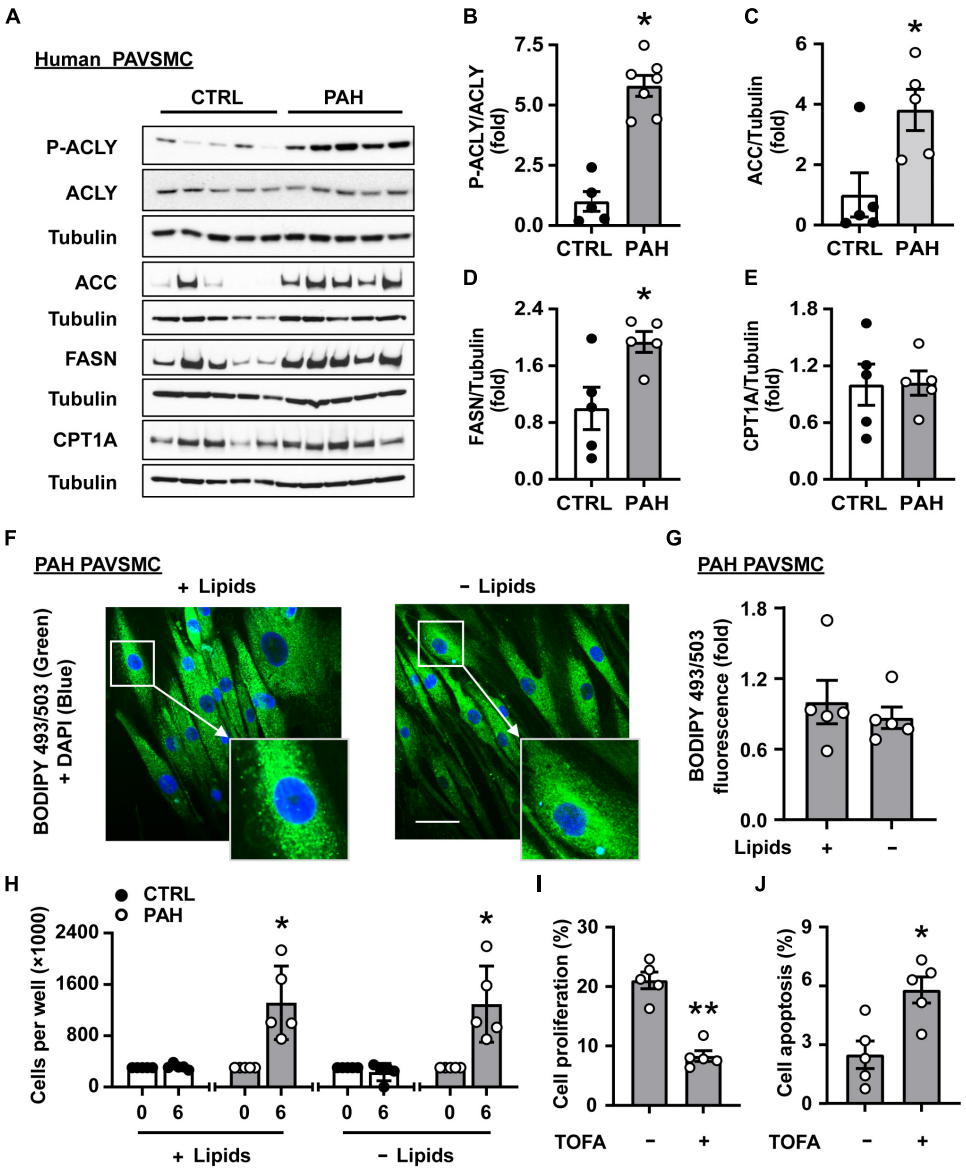

FIGURE 1 | Increased lipid synthesis is required for hyper-proliferation and survival of human PAH PAVSMC. **(A–E)** Early passage distal primary human PAVSMC from non-diseased (CTRL) and PAH subjects were serum-deprived for 48 hours and subjected to immunoblot analysis to detect indicated proteins. $n = 5$ (CTRL), $n = 7$ (PAH for P-ACLY, ACLY, see **Supplementary Figure 1A** for additional immunoblots used for statistical analysis) or $n = 5$ (PAH for ACC, FASN, CPT1A). Data are means ± SE, fold to control. **(F,G)** Human PAH PAVSMC were incubated for 48 h in serum deprived media supplemented with regular (+ Lipids) or lipid-deprived (-Lipids) 0.1% BSA and subjected to fluorescent BODIPY 493/503 staining (green) to detect intracellular neutral lipids followed by DAPI (blue) staining to detect nuclei. Representative images with enlarged area **(F)** and statistical analysis **(G)** are shown. Bar equals 50 μm. Data are means ± SE from $n = 5$ subjects/group, fold to cells incubated in regular 0.1% BSA (+ Lipids) group. **(H)** Equal amount of human PAVSMC from five PAH and five control subjects were seeded to 6 well plates. 48 h later (day 0), media was changed to the serum-free media supplemented with regular (+ Lipids) or lipid-deprived (-Lipids) 0.1% BSA; six days later, cell count assay was performed. Data are means ± SE, $n = 5$ subjects/group. **(I)** PAH PAVSMC were treated with ACC inhibitor TOFA (20 μM) for 48 h followed by proliferation analysis (Ki-67). Data are means ± SE, percentage of Ki-67 positive cells/total number of cells, $n = 5$ subjects/group. **(J)** PAH PAVSMC were treated with ACC inhibitor TOFA (20 μM) for 48 h followed by apoptosis analysis. Data are means ± SE, percentage of TUNEL-positive cells/total number of cells, $n = 5$ subjects/group. $^{*}p < 0.05$, $^{**}p < 0.01$ by Mann–Whitney *U* test.

smooth muscle cells in rats with monocrotaline-induced PH and protective effect of MLYCD deletion against development of hypoxia-induced PH in mice (28, 35). Observed up-regulation of key fatty acid synthesis enzymes suggested that *de novo* lipid synthesis is altered in PAH PAVSMC. To confirm our observations, we performed immunocytochemical detection of lipid droplets (a major storage depot for neutral lipids, primarily triglycerides) using a fluorescent probe (BODIPY 493/503) to visualize neutral lipid accumulation in PAH PAVSMC. We found that lipid accumulation detected in PAH PAVSMC was preserved in media deprived from exogenous lipids (**Figures 1F,G**), indicating that PAH PAVSMC have an ability to generate lipids *de novo*. Importantly, PAH PAVSMC, in contrast to control cells, demonstrated increased growth not only in serum-deprived media, but in lipid-deprived serum-deprived media (**Figure 1H**). Moreover, 5-tetradecyloxy-2-furoic acid (TOFA), an allosteric inhibitor of ACC, a key enzyme regulating fatty acid synthesis, significantly decreased proliferation and induced apoptosis in PAH PAVSMC (**Figures 1I,J**), demonstrating that lipogenesis is required for PAH PAVSMC hyper-proliferation and survival. Taken together, these data show that *de novo* lipid synthesis is up-regulated and required for maintaining the pro-proliferative/pro-survival phenotype of human PAH PAVSMC.

Increased Lipid Synthesis in Human PAH PAVSMC Is Glucose-Dependent

Since fatty acid uptake is not altered in PAH PAVSMC (23) and we found that PAH PAVSMC growth was maintained

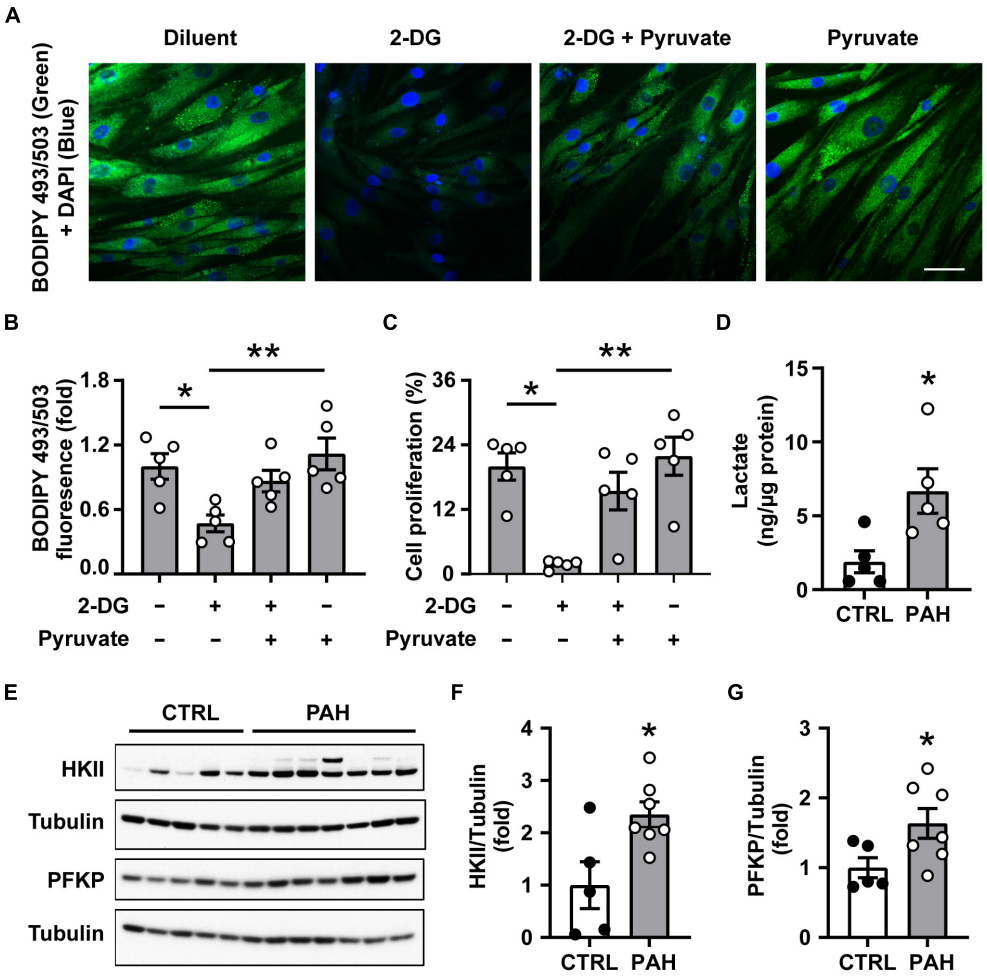

FIGURE 2 | Increased lipid synthesis in human PAH PAVSMC is glucose dependent. **(A–C)** Human PAH PAVSMC were incubated in serum deprived media supplemented with 0.1% lipid-deprived BSA in presence of 2-Deoxy-D-glucose (2-DG, 100 mM) and/or pyruvate (10 mM) or vehicle (–). Forty-eight hours later neutral lipid accumulation **(A,B)** was evaluated by fluorescent BODIPY 493/503 staining (green) followed by DAPI co-staining (blue) to detect nuclei and cell proliferation (Ki-67) **(C)** was analyzed. Representative images **(A)** and statistical analysis **(B,C)** are shown. Bar equals 50 μm. Data are means ± SE, $n = 5$ subjects/group, fold to vehicle-treated group **(B)**, percentage of Ki-67 positive cells/total **(C)**, $^{*}p < 0.05$, $^{**}p < 0.01$ by Kruskal–Wallis rank test with Dunn pairwise comparison *post hoc* test. **(D)** Intracellular lactate levels were measured in PAVSMC from five non-diseased and five PAH subjects. **(E–G)** Early passage distal primary human PAVSMC from five non-diseased (CTRL) and seven PAH subjects were serum deprived for 48 h and subjected to immunoblot analysis to detect indicated proteins. **(D,F,G)** Data are means ± SE, fold to control **(F,G)**, $^{*}p < 0.05$ by Mann–Whitney *U* test.

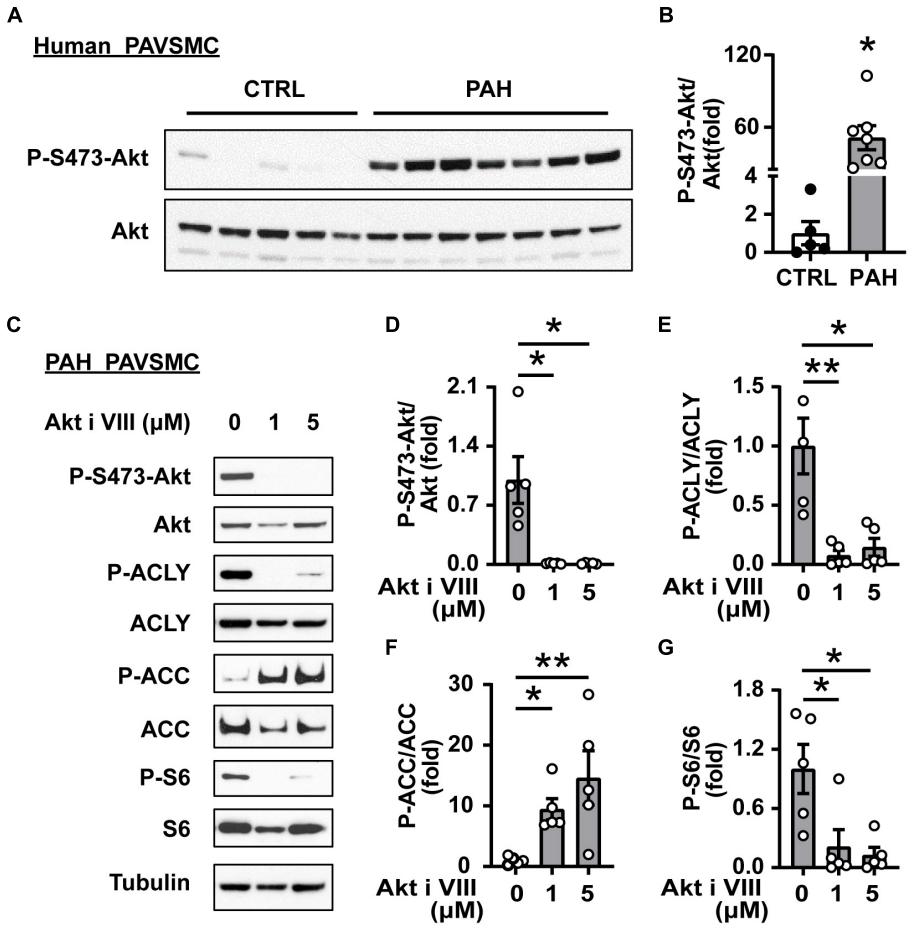

FIGURE 3 | Akt supports ACLY and ACC up-regulation in human PAH PAVSMC. **(A,B)** Early passage distal human PAVSMC from five non-diseased (CTRL) and seven PAH subjects were serum deprived for 48 h and subjected to immunoblot analysis to detect indicated proteins. Immunoblots **(A)** and statistical analysis **(B)** are shown. Data are means ± SE, fold to control, $^{*}p < 0.05$ by Mann–Whitney *U* test. **(C–G)** Early passage human PAH PAVSMC were treated with Akt inhibitor VIII (1, 5 μM) or vehicle (0) for 24 h followed by immunoblot analysis. Data are fold to vehicle-treated group, $n = 5$ subjects/group, $^{*}p < 0.05$, $^{**}p < 0.01$ by Kruskal–Wallis rank test with Dunn pairwise comparison *post hoc* test.

in lipid-deprived media, we hypothesized that glucose could be a potential source for *de novo* lipid synthesis in PAH. We found that intracellular lipid content in PAH PAVSMC in lipid-deprived conditions was significantly depleted by the treatment with the non-metabolizable analog of glucose 2-DG. Importantly, co-treatment with glucose metabolite pyruvate significantly attenuated 2-DG-dependent inhibition of intracellular lipid accumulation in human PAH PAVSMC (**Figures 2A,B**). Furthermore, 2-DG-induced inhibition of PAH PAVSMC proliferation in lipid-deprived conditions was also partially reversed by pyruvate (**Figure 2C**). These data demonstrate that glucose, metabolized through the glycolysis, serves as the main source for *de novo* lipid synthesis and supports lipid accumulation and increased proliferation of PAH PAVSMC. Confirming up-regulation of glycolysis, intracellular lactate levels were significantly higher in PAH PAVSMC compared to non-diseased cells (**Figure 2D**). Moreover, protein levels of key glycolytic enzymes PFKP and HKII were significantly higher in human PAH PAVSMC compared to controls (**Figures 2E–G**), and HIF1α over accumulation was detected in six out of seven PAVSMC from PAH patients compared to one out of five non-diseased (control) subjects (**Supplementary Figure 2**). This is in good agreement with previously published data demonstrating the importance of glycolysis for PH (19, 36, 37). Together, our data demonstrate that glycolysis-metabolized glucose serves as a main source for increased *de novo* lipid synthesis in PAH PAVSMC, supporting a pro-proliferative cell phenotype.

Akt Supports ACLY and ACC Up-Regulation in Human PAH PAVSMC

One of the key regulators of glucose and lipid metabolism is a serine/threonine kinase Akt (38–42), which stimulates glucose uptake and glycolysis (43) and promotes *de novo* lipid synthesis through sterol regulatory binding protein (SREBP)-dependent expression of lipogenic enzymes (43, 44). Accumulating evidence from multiple groups, including ours, demonstrate pathological role of Akt as a regulator of pulmonary vascular cell

metabolism, proliferation, pulmonary vascular remodeling, and overall PH (10, 45, 46). This allowed us to hypothesize that Akt might coordinate glucose metabolism and *de novo* lipid synthesis supporting PAVSMC hyper-proliferation in PAH. In agreement with published studies reporting Akt activation in PAH (10, 32), we found that S473-Akt phosphorylation was significantly increased in human PAH PAVSMC (**Figures 3A,B**). Importantly, Akt inhibitor VIII suppressed activation of both key lipogenesis enzymes, ACLY and ACC; ACLY deactivation was detected by decrease in S455-ACLY phosphorylation (47), and ACC deactivation was detected by an increase in inhibitory S79-ACC (48) phosphorylation (**Figures 3C–F** and **Supplementary Figures 3A,B**), suggesting that Akt supports increased lipogenesis in human PAH PAVSMC. Moreover, Akt inhibitor suppressed phosphorylation of ribosomal protein S6 (**Figures 3C,G**), the main downstream effector of mTOR complex 1 (mTORC1), a known activator of cell growth, proliferation, and lipid biogenesis (49). In summary, these data demonstrate that *de novo* lipid synthesis in PAH PAVSMC is regulated by Akt.

SIRT7 Up-Regulates Akt and Lipogenic Enzymes in Human PAH PAVSMC

Next, we aimed to identify the factor(s) regulating *de novo* Akt-dependent lipid synthesis in PAH. Several studies demonstrate that lysine deacetylase SIRT7 coordinates cellular metabolic balance by regulating glucose sensing/homeostasis, glycolysis, mitochondria and ribosomal biogenesis, DNA damage response, fatty acid synthesis and overall lipid metabolism (50–56). Moreover, it was recently shown that SIRT7 modulates aortic vascular smooth muscle cell proliferation in wire injury model of the femoral artery (57) and promotes cancer progression by activating Akt (56, 58) and mTORC1 effector S6K1 (59). We found that SIRT7 protein levels were significantly higher in human PAH PAVSMC compared to non-diseased PAVSMC (**Figures 4A,B**). Importantly, shRNA-induced depletion of SIRT7 in PAH PAVSMC significantly reduced S473 Akt phosphorylation (**Figures 4C,D**) and activatory phosphorylation of ACLY, and significantly increased inhibitory phosphorylation of ACC in human PAH PAVSMC (**Figures 4C,E,F**), suggesting that Akt-mediated lipogenesis in human PAH PAVSMC is regulated by SIRT7.

SIRT7-Dependent JNK Activation Is Required for Akt and Lipogenic Enzymes Up-Regulation in Human PAH PAVSMC

Since SIRT7 does not possess kinase activity, its regulation of Akt phosphorylation status most likely is mediated by intermediate player(s) and one of the potential SIRT7 pro-survival targets is JNK (54). Indeed, we found that shSIRT7 significantly decreased phosphorylation of JNK in PAH PAVSMC (**Figures 4C,G**), also suggesting that SIRT7 regulates Akt and lipogenesis through JNK. Previous studies have shown that Akt activation *via* phosphorylation at S473 is achieved through a series of phosphorylation steps, and the initial priming phosphorylation of T450 can be regulated by JNK (60). We found a significant increase in T183/185 JNK phosphorylation in human PAH PAVSMC compared to control PAVSMC (**Figures 5A,B**), indicating that JNK is activated in PAH PAVSMC. JNK inhibitor HY-14761 significantly reduced both S473 and priming Thr450 Akt phosphorylation in PAH PAVSMC (**Figures 5C–E**). JNK inhibitor-mediated deactivation of Akt was associated with de-activation of lipogenic enzymes ACLY and ACC in human PAH PAVSMC (**Figures 5C,F,G** and **Supplementary Figures 3C,D**). These data indicate that Akt-mediated lipogenesis in human PAH PAVSMC is at least in part regulated by JNK.

In PAH, Akt activation in resident pulmonary vascular cells could be induced by excessive amounts of growth factors and pro-inflammatory mediators. To start determining pro-PH agents modulating SIRT7/JNK axis in PAVSMC, we treated non-diseased human PAVSMC with PDGF and IL-6. Interestingly, while both PGDF and IL-6 significantly increased JNK phosphorylation, only PDGF induced significant increase of SIRT7 protein levels (**Supplementary Figures 4A,B**), similar to those seen in human PAH PAVSMC. Together, these data suggest that SIRT7/JNK-dependent Akt activation in PAVSMC could be induced by PDGF.

Akt Supports Lipid Accumulation, Proliferation and Survival of Human PAH PAVSMC

To further clarify the role of Akt in lipid accumulation, hyper-proliferation, and survival of human PAH PAVSMC, we treated cells with Akt inhibitor VIII. Immunocytochemical analysis demonstrated that intracellular lipid accumulation in PAH PAVSMC, maintained in lipid-deprived media, was significantly downregulated by Akt inhibitor VIII (**Figures 6A,B**). Moreover, treatment with Akt inhibitor VIII significantly reduced proliferation and promoted apoptosis of PAH PAVSMC (**Figures 6C,D**), demonstrating that Akt supports increased cell proliferation, survival, and lipogenesis in PAH PAVSMC (**Figure 6E**). Furthermore, inhibition of Akt did not augment 2-DG-dependent inhibition of PAH PAVSMC proliferation (**Supplementary Figures 5A,B**), suggesting that Akt regulates PAH PAVSMC proliferation at the level of or downstream of glycolytic enzymes. Taken together, our data demonstrate that human PAH PAVSMC have up-regulated lipogenesis supported in an Akt- and glycolysis-dependent manner to sustain increased proliferation and survival, and that Akt signaling is regulated, at least in part, by SIRT7-JNK axis (**Figure 6E**).

DISCUSSION

Increased proliferation and survival of PAVSMC in small PAs are critical components of pulmonary vascular remodeling in PAH, the mechanisms of which are not completely understood. Here we report that human PAH PAVSMC have up-regulated lipogenesis, which is required to support increased cell proliferation and survival. We also show that observed *de novo* lipid synthesis is glucose-dependent and is regulated by Akt. We further demonstrate that SIRT7 and JNK are up-regulated in PAH PAVSMC, and support Akt activation and lipogenesis. Lastly, we show that Akt activation is required for increased lipid

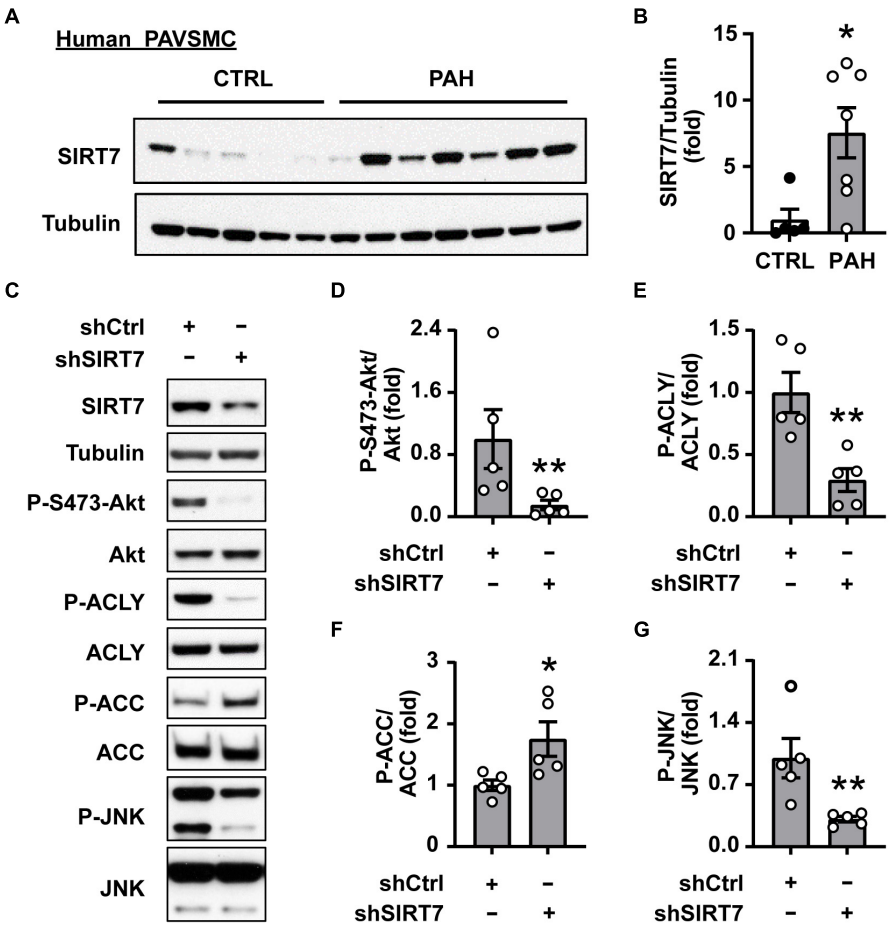

FIGURE 4 | SIRT7 regulates Akt status and lipogenic enzymes activation in human PAH PAVSMC. **(A,B)** Early passage distal human PAVSMC from five non-diseased (CTRL) and seven PAH subjects were serum deprived for 48 h and subjected to immunoblot analysis to detect indicated proteins. Immunoblots **(A)** and statistical analysis **(B)** are shown. Data are means ± SE, fold to control. **(C–G)** Human PAH PAVSMC were transfected with shRNA SIRT7 (shSIRT7), or control scramble shRNA (shCtrl) for 72 h followed by immunoblot analysis. Data represent fold to shCtrl. Data are means ± SE, $n = 5$ subjects/group. $^{*}p < 0.05$, $^{**}p < 0.01$ by Mann–Whitney *U* test.

accumulation, cell proliferation and survival of PAH PAVSMC. Overall, although further studies are needed, our data suggest that the SIRT7/JNK-Akt-lipogenesis axis could be considered as a potential target pathway for developing novel anti-remodeling therapy for PAH.

Metabolic alterations in glucose homeostasis and glycolysis, similar to the "Warburg effect" in cancer cells, support increased PAVSMC proliferation and pulmonary vascular remodeling in PAH (9, 10, 12). Increased glucose uptake coupled with unaltered fatty acid uptake by PAH PAVSMC (23) indicates that intracellular demand in lipids in these highly proliferative cells is fulfilled by alternative internal pathways. This phenomenon is well known in cancer, since tumor cells demonstrate elevated endogenous fatty acid synthesis, supported by the increased glycolysis, to maintain hyper-proliferation (29). Glucose serves as major source supporting lipid synthesis. Glucose is converted to pyruvate through glycolysis. Pyruvate, in turn, enters mitochondria for citrate generation. Through mitochondrial carrier Slc25a1, citrate can be exported into the cytosol, wherein it is cleaved by ACLY to produce acetyl-CoA, which is processed for *de novo* lipogenesis by ACC and FASN (61). We demonstrate that all the key enzymes of fatty acid synthesis, ACLY, ACC, and FASN are up-regulated in human PAH PAVSMC. Moreover, we found that PAH PAVSMC maintain hyper-proliferation and glucose-dependent accumulation of intracellular lipids even in the absence of an extracellular lipid source but require activation of intracellular *de novo* lipid synthesis machinery. This is an important observation, confirming that lipid synthesis plays a crucial role not only in RV disfunction in PAH (62, 63) but also in smooth muscle proliferation and pulmonary vascular remodeling. It also supports previous studies suggesting that targeting lipid metabolism in PAH VSM needs to be considered for developing on anti-remodeling therapeutic options for PAH treatment (27, 28).

Besides glucose, glutamine can also contribute carbon to lipogenic acetyl-coenzyme A (acetyl-CoA) through glutamine-derived α-ketoglutarate (α-KG). Generated α-KG could be, in turn, converted into citrate *via* an isocitrate dehydrogenase-1

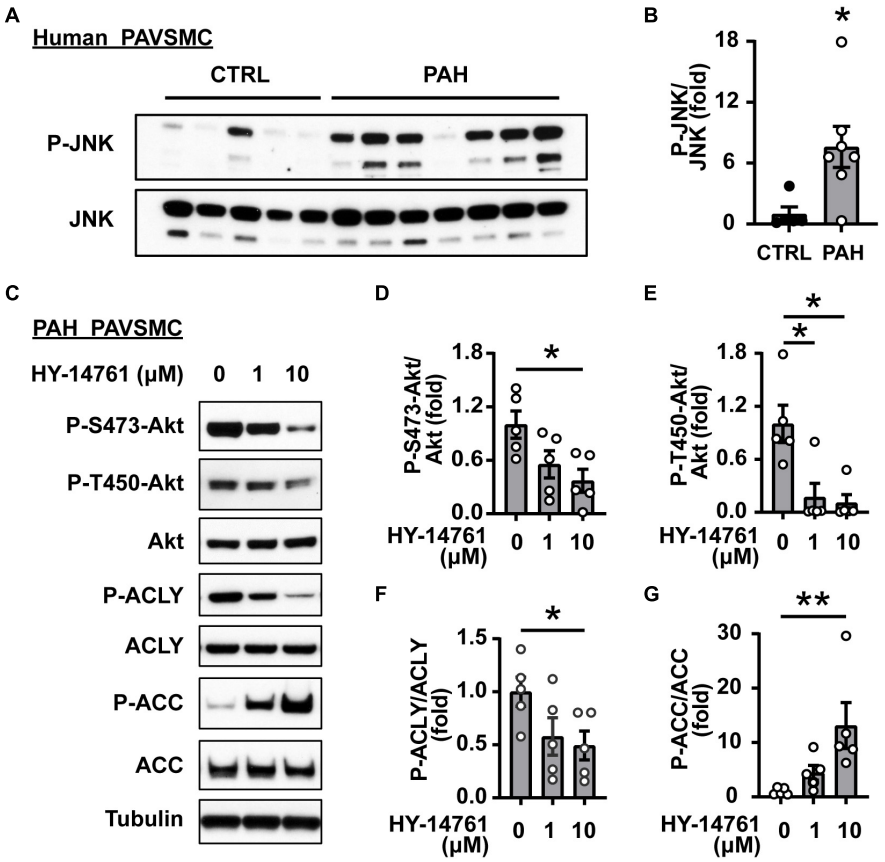

FIGURE 5 | JNK regulates Akt and lipogenic enzymes in human PAH PAVSMC. **(A,B)** Early passage distal human PAVSMC from five non-diseased (CTRL) and seven PAH subjects were serum deprived for 48 h and subjected to immunoblot analysis to detect indicated proteins. Immunoblots **(A)** and statistical analysis **(B)** are shown. Data are means ± SE, fold to control, $^{*}p < 0.05$ by Mann–Whitney *U* test. **(C–G)** Early passage human PAH PAVSMC were treated with JNK inhibitor HY-14761 (1, 10 μM) or vehicle (0) for 48 h followed by immunoblot analysis. Data represent fold to vehicle-treated group, $n = 5$ subjects/group, $^{*}p < 0.05$, $^{**}p < 0.01$ by Kruskal–Wallis rank test with Dunn pairwise comparison *post hoc* test.

(IDH1)-dependent mitochondrial or cytosolic pathway (64, 65). In our present study, we have shown that PAH PAVSMC *de novo* lipogenesis depends on glucose, but whether α-KG contributes to this process remains unstudied.

Akt signaling is tightly related to the regulation of glycolysis and lipogenesis (66–68). Akt stimulates aerobic glycolysis in cancer cells, supporting continued growth and survival, mediates bioenergetic stability in epithelial cells (68), and stimulates hepatic SREBP1c and lipogenesis through mTORC1-dependent and independent pathways (69), suggesting that Akt might be involved in regulation of lipid synthesis and accumulation in PAH PAVSMC. Our data demonstrate that Akt not only supports glycolysis-driven lipogenesis in PAH PAVSMC, but also regulates proliferation and survival of PAH PAVSMC. Since Akt is a major player, coordinating multiple processes directly involved in cell survival, growth, metabolism, proliferation, migration and differentiation (70), pharmacological targeting of Akt is a highly attractive therapeutic approach for proliferative diseases such as cancer. Multiple Akt inhibitors are now in various stages of clinical development (71, 72). However, since Akt activation occurs through various mechanisms, clinical efficacies of Akt inhibitors are limited (73), and Akt targeting still remains a challenge. Thus, inhibiting Akt *via* modulating its upstream regulators might represent an alternative, potentially attractive strategy for therapeutic intervention.

The members of the sirtuin family of lysine deacylases are important regulators of metabolic pathways and energy homeostasis (50, 74) which are also known regulators of Akt (75). Sirtuins have been implicated in multiple metabolic diseases, including aging, cancers, cardiovascular diseases, obesity, and diabetes mellitus (50) and are considered potential targets for the therapeutic interventions (76). Unlike other sirtuins, SIRT7 demonstrates a relatively weak deacetylase activity, but is involved in regulating cellular energy metabolism homeostasis, lipid metabolism, cell migration, and was recently shown to control VSMC proliferation (50, 57, 77, 78). SIRT7 is also considered an attractive target for anti-cancer therapy (79). Despite being the least well-characterized member of the sirtuin family, accumulating evidence shows that SIRT7 acts as an Akt upstream regulator in other cell types (58, 59, 80). Here we demonstrate that SIRT7 acts as an upstream positive regulator of Akt in PAH PAVSMC

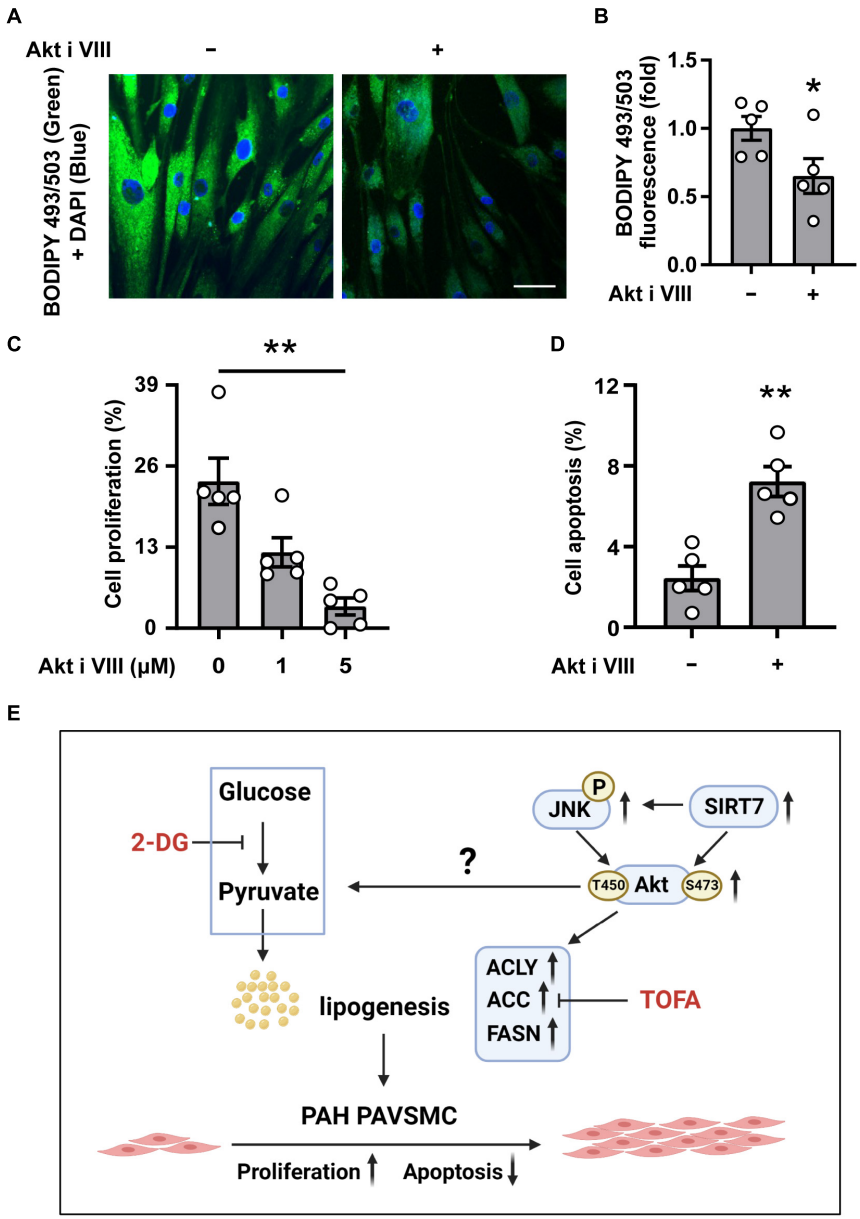

FIGURE 6 | Akt supports intracellular lipid levels, proliferation and survival of human PAH PAVSMC. **(A,B)** Human PAH PAVSMC were incubated in serum deprived media supplemented with 0.1% lipid deprived BSA in presence of Akt inhibitor VIII (10 μM) or diluent. Forty-eight hours later neutral lipid accumulation was evaluated by fluorescent BODIPY 493/503 staining (green) followed by DAPI co-staining (blue) to detect nuclei. Representative images **(A)** and statistical analysis **(B)** are shown. Bar equals 50 μm. Data are means ± SE, fold to the diluent-treated cells, $n = 5$ subjects/group, $^*p < 0.05$ by Mann–Whitney *U* test. **(C)** Human PAH PAVSMC were serum deprived in media, supplemented with regular 0.1% BSA, and were treated with 1, 5 μM **(C)** or 10 μM **(D)** Akt inhibitor VIII or vehicle (0/-) for 48 h followed by proliferation (Ki-67) **(C)** or apoptosis **(D)** analyses. Data are percentage of Ki-67- or TUNEL- positive cells/total number of cells, means ± SE, $n = 5$ subjects/group. $^*p < 0.05$ Kruskal–Wallis rank test with Dunn pairwise comparison *post hoc* test **(C)** or by Mann–Whitney *U* test **(D)**. **(E)** Schematic representation of the proposed regulation of the *de novo* lipid synthesis, required for increased proliferation and survival of PAVSMC in PAH.

and supports Akt phosphorylation in a JNK-dependent manner. We found that pharmacological inhibition of JNK significantly reduced both S473 and T450 Akt phosphorylation in PAH PAVSMC. This finding is in agreement with previous studies, demonstrating that JNK regulates Akt reactivation through T450 phosphorylation in cardiomyocyte survival after hypoxia (60).

Our study, however, has limitations. Although use of cells from PAH and non-diseased human subjects strongly suggests the translational significance of our findings, we only verified the role of SIRT7-JNK-Akt-*de novo* lipid synthesis *in vitro*, and further studies are needed to determine the role of this axis *in vivo*. Also, further pre-clinical studies are needed to evaluate whether the link between SIRT7-JNK and Akt-dependent

de novo lipid synthesis, required for increased proliferation and survival of PAH PAVSMC, could be a potential target pathway for therapeutic intervention.

In summary, we found that human PAH PAVSMC have up-regulated lipogenesis supported in an Akt- and glycolysis-dependent manner to sustain increased cell proliferation. We also show that inhibition of the Akt-lipogenesis axis reduces proliferation and induces apoptosis of human PAH PAVSMC. In aggregate, our data provide a link between glycolysis, lipogenesis and proliferation of human PAH PAVSMC and call for further studies to determine the potential attractiveness of the SIRT7/JNK-Akt-lipogenesis axis as a target pathway for therapeutic intervention.

DATA AVAILABILITY STATEMENT

The data that support the findings of this study are available from the corresponding author upon reasonable request.

AUTHOR CONTRIBUTIONS

EG and TK: conception and design. LJ, TK, HD, EG, DG, AP, BC, YS, and DL: experimental work, analysis, and interpretation. LJ, EG, and TK: drafting the manuscript and intellectual content. All authors contributed to the article and approved the submitted version.

FUNDING

This work was supported by NIH/NHLBI R01HL113178 (EG), R01HL130261 (EG), and R01HL150638 (EG). The Pulmonary Hypertension Breakthrough Initiative is supported by NIH/NHLBI R24HL123767.

SUPPLEMENTARY MATERIAL

The Supplementary Material for this article can be found online at: https://www.frontiersin.org/articles/10.3389/fmed.2022.886868/full#supplementary-material

Supplementary Figure 1 | (A,B) Early passage distal primary human PAVSMC from non-diseased (CTRL) and PAH subjects were serum-deprived for 48 h and subjected to immunoblot analysis to detect indicated proteins. **(A)** $n = 5$ (CTRL), $n = 7$ (PAH) (see **Figure 1B** for statistical analysis). **(B)** Data are means ± SE, fold to control, $n = 5$ subjects/group.

Supplementary Figure 2 | Early passage PAVSMC from five non-diseased (CTRL) and seven PAH subjects were serum deprived for 48 h and subjected to immunoblot analysis to detect indicated proteins. Immunoblots **(A)** and statistical analysis **(B)** are shown. **(B)** Data are means ± SE, fold to control.

Supplementary Figure 3 | Early passage human PAH PAVSMC were treated with Akt inhibitor VIII, JNK inhibitor HY-14761, or diluent (0) and subjected to immunoblot analysis to detect indicated proteins. Data are fold to diluent-treated group. $^{*}p < 0.05$ by Kruskal–Wallis rank test with Dunn pairwise comparison *post hoc* test.

Supplementary Figure 4 | Early passage human control (non-diseased) PAVSMC were treated with **(A)** PDGF-BB (60 ng/ml) or **(B)** IL-6 (20 ng/ml) and appropriate vehicles for 48 h followed by immunoblot analyses of indicated proteins. Representative immunoblots and statistical analyses are shown. Data are means ± SE, $n = 3$ subjects/group, $^{*}p < 0.05$, by Mann–Whitney *U* test.

Supplementary Figure 5 | Early passage human PAH PAVSMC were incubated in serum deprived media in presence of 2-Deoxy-D-glucose (2-DG) 10 mM **(A)** or 1 mM **(B)** and/or Akt inhibitor VIII (1 μM) or vehicle (–). Forty-eight hours later cell proliferation (Ki-67) was analyzed. Data are means ± SE, percentage of Ki-67-positive cells/total. $^{*}p < 0.05$, $^{**}p < 0.01$ by Kruskal–Wallis rank test with Dunn pairwise comparison *post hoc* test.

REFERENCES

1. Lai YC, Potoka KC, Champion HC, Mora AL, Gladwin MT. Pulmonary arterial hypertension: the clinical syndrome. *Circ Res.* (2014) 115:115–30. doi: 10.1161/circresaha.115.301146
2. Besinque GM, Lickert CA, Pruett JA. The myth of the stable pulmonary arterial hypertension patient. *Am J Manag Care.* (2019) 25:S47–52.
3. Sarzynska K, Swiatoniowska-Lonc N, Dudek K, Jonas K, Kopec G, Gajek J, et al. Quality of life of patients with pulmonary arterial hypertension: a meta-analysis. *Eur Rev Med Pharmacol Sci.* (2021) 25:4983–98. doi: 10.26355/eurrev_202108_26455
4. Humbert M, Guignabert C, Bonnet S, Dorfmuller P, Klinger JR, Nicolls MR, et al. Pathology and pathobiology of pulmonary hypertension: state of the art and research perspectives. *Eur Respir J.* (2019) 53:1801887. doi: 10.1183/13993003.01887-2018
5. Thenappan T, Ormiston ML, Ryan JJ, Archer SL. Pulmonary arterial hypertension: pathogenesis and clinical management. *BMJ.* (2018) 360:j5492. doi: 10.1136/bmj.j5492
6. Sommer N, Ghofrani HA, Pak O, Bonnet S, Provencher S, Sitbon O, et al. Current and future treatments of pulmonary arterial hypertension. *Br J Pharmacol.* (2021) 178:6–30. doi: 10.1111/bph.15016
7. Hassoun PM. Pulmonary arterial hypertension. *N Engl J Med.* (2021) 385:2361–76. doi: 10.1056/NEJMra2000348
8. Tuder RM. Pulmonary vascular remodeling in pulmonary hypertension. *Cell Tissue Res.* (2017) 367:643–9. doi: 10.1007/s00441-016-2539-y
9. Archer SL, Gomberg-Maitland M, Maitland ML, Rich S, Garcia JG, Weir EK. Mitochondrial metabolism, redox signaling, and fusion: a mitochondria-ROS-HIF-1alpha-Kv1.5 O2-sensing pathway at the intersection of pulmonary hypertension and cancer. *Am J Physiol Heart Circ Physiol.* (2008) 294:H570–8. doi: 10.1152/ajpheart.01324.2007
10. Goncharov DA, Kudryashova TV, Ziai H, Ihida-Stansbury K, DeLisser H, Krymskaya VP, et al. Mammalian target of rapamycin complex 2 (mTORC2) coordinates pulmonary artery smooth muscle cell metabolism, proliferation, and survival in pulmonary arterial hypertension. *Circulation.* (2014) 129:864–74. doi: 10.1161/circulationaha.113.004581
11. Crosswhite P, Sun Z. Molecular mechanisms of pulmonary arterial remodeling. *Mol Med.* (2014) 20:191–201. doi: 10.2119/molmed.2013.00165
12. Tuder RM, Davis LA, Graham BB. Targeting energetic metabolism: a new frontier in the pathogenesis and treatment of pulmonary hypertension. *Am J Respir Crit Care Med.* (2012) 185:260–6. doi: 10.1164/rccm.201108-1536PP
13. Kudryashova TV, Goncharov DA, Pena A, Ihida-Stansbury K, DeLisser H, Kawut SM, et al. Profiling the role of mammalian target of rapamycin in the vascular smooth muscle metabolome in pulmonary arterial hypertension. *Pulm Circ.* (2015) 5:667–80. doi: 10.1086/683810
14. Xu W, Janocha AJ, Erzurum SC. Metabolism in pulmonary hypertension. *Annu Rev Physiol.* (2021) 83:551–76. doi: 10.1146/annurev-physiol-031620-123956
15. Bonnet S, Rochefort G, Sutendra G, Archer SL, Haromy A, Webster L, et al. The nuclear factor of activated T cells in pulmonary arterial hypertension can

be therapeutically targeted. *Proc Natl Acad Sci U S A.* (2007) 104:11418–23. doi: 10.1073/pnas.0610467104
16. Hansmann G, Calvier L, Risbano MG, Chan SY. Activation of the metabolic master regulator PPARgamma: a potential PIOneering therapy for pulmonary arterial hypertension. *Am J Respir Cell Mol Biol.* (2020) 62:143–56. doi: 10.1165/rcmb.2019-0226PS
17. Sutendra G, Dromparis P, Bonnet S, Haromy A, McMurtry MS, Bleackley RC, et al. Pyruvate dehydrogenase inhibition by the inflammatory cytokine TNFalpha contributes to the pathogenesis of pulmonary arterial hypertension. *J Mol Med (Berl).* (2011) 89:771–83. doi: 10.1007/s00109-011-0762-2
18. Michelakis ED, Gurtu V, Webster L, Barnes G, Watson G, Howard L, et al. Inhibition of pyruvate dehydrogenase kinase improves pulmonary arterial hypertension in genetically susceptible patients. *Sci Transl Med.* (2017) 9:eaao4583. doi: 10.1126/scitranslmed.aao4583
19. Kovacs L, Cao Y, Han W, Meadows L, Kovacs-Kasa A, Kondrikov D, et al. PFKFB3 in smooth muscle promotes vascular remodeling in pulmonary arterial hypertension. *Am J Respir Crit Care Med.* (2019) 200:617–27. doi: 10.1164/rccm.201812-2290OC
20. Valuparampil Varghese M, James J, Eccles CA, Niihori M, Rafikova O, Rafikov R. Inhibition of anaplerosis attenuated vascular proliferation in pulmonary arterial hypertension. *J Clin Med.* (2020) 9:443. doi: 10.3390/jcm9020443
21. Dai J, Zhou Q, Chen J, Rexius-Hall ML, Rehman J, Zhou G. Alpha-enolase regulates the malignant phenotype of pulmonary artery smooth muscle cells via the AMPK-Akt pathway. *Nat Commun.* (2018) 9:3850. doi: 10.1038/s41467-018-06376-x
22. Pullamsetti SS, Savai R, Seeger W, Goncharova EA. Translational advances in the field of pulmonary hypertension. From cancer biology to new pulmonary arterial hypertension therapeutics. targeting cell growth and proliferation signaling hubs. *Am J Respir Crit Care Med.* (2017) 195:425–37. doi: 10.1164/rccm.201606-1226PP
23. Hernandez-Saavedra D, Sanders L, Freeman S, Reisz JA, Lee MH, Mickael C, et al. Stable isotope metabolomics of pulmonary artery smooth muscle and endothelial cells in pulmonary hypertension and with TGF-beta treatment. *Sci Rep.* (2020) 10:413. doi: 10.1038/s41598-019-57200-5
24. Zhu J, Thompson CB. Metabolic regulation of cell growth and proliferation. *Nat Rev Mol Cell Biol.* (2019) 20:436–50. doi: 10.1038/s41580-019-0123-5
25. Culley MK, Chan SY. Mitochondrial metabolism in pulmonary hypertension: beyond mountains there are mountains. *J Clin Invest.* (2018) 128:3704–15. doi: 10.1172/JCI120847
26. Mumby S, Perros F, Hui C, Xu BL, Xu W, Elyasigomari V, et al. Extracellular matrix degradation pathways and fatty acid metabolism regulate distinct pulmonary vascular cell types in pulmonary arterial hypertension. *Pulm Circ.* (2021) 11:2045894021996190. doi: 10.1177/2045894021996190
27. Singh N, Manhas A, Kaur G, Jagavelu K, Hanif K. Inhibition of fatty acid synthase is protective in pulmonary hypertension. *Br J Pharmacol.* (2016) 173:2030–45. doi: 10.1111/bph.13495
28. Zhuang W, Lian G, Huang B, Du A, Gong J, Xiao G, et al. CPT1 regulates the proliferation of pulmonary artery smooth muscle cells through the AMPK-p53-p21 pathway in pulmonary arterial hypertension. *Mol Cell Biochem.* (2019) 455:169–83. doi: 10.1007/s11010-018-3480-z
29. Menendez JA, Lupu R. Fatty acid synthase and the lipogenic phenotype in cancer pathogenesis. *Nat Rev Cancer.* (2007) 7:763–77. doi: 10.1038/nrc2222
30. Baron A, Migita T, Tang D, Loda M. Fatty acid synthase: a metabolic oncogene in prostate cancer? *J Cell Biochem.* (2004) 91:47–53. doi: 10.1002/jcb.10708
31. Zaidi N, Lupien L, Kuemmerle NB, Kinlaw WB, Swinnen JV, Smans K. Lipogenesis and lipolysis: the pathways exploited by the cancer cells to acquire fatty acids. *Progr Lipid Res.* (2013) 52:585–9. doi: 10.1016/j.plipres.2013.08.005
32. Kudryashova TV, Goncharov DA, Pena A, Kelly N, Vanderpool R, Baust J, et al. HIPPO-Integrin-linked Kinase cross-talk controls self-sustaining proliferation and survival in pulmonary hypertension. *Am J Respir Crit Care Med.* (2016) 194:866–77. doi: 10.1164/rccm.201510-2003OC
33. Qiu B, Simon MC. BODIPY 493/503 staining of neutral lipid droplets for microscopy and quantification by flow cytometry. *Bio Protoc.* (2016) 6:e1912. doi: 10.21769/BioProtoc.1912
34. Kudryashova TV, Dabral S, Nayakanti S, Ray A, Goncharov DA, Avolio T, et al. Noncanonical HIPPO/MST signaling via BUB3 and FOXO drives pulmonary vascular cell growth and survival. *Circ Res.* (2022) 130:760–78. doi: 10.1161/CIRCRESAHA.121.319100
35. Sutendra G, Bonnet S, Rochefort G, Haromy A, Folmes KD, Lopaschuk GD, et al. Fatty acid oxidation and malonyl-CoA decarboxylase in the vascular remodeling of pulmonary hypertension. *Sci Transl Med.* (2010) 2:44ra58. doi: 10.1126/scitranslmed.3001327
36. Zhang YL, Zhang R, Shen YF, Huang KY, He YY, Zhao JH, et al. 3-Bromopyruvate attenuates experimental pulmonary hypertension via inhibition of glycolysis. *Am J Hypertens.* (2019) 32:426–32. doi: 10.1093/ajh/hpy191
37. He S, Zhu T, Fang Z. The role and regulation of pulmonary artery smooth muscle cells in pulmonary hypertension. *Int J Hypertens.* (2020) 2020:1478291. doi: 10.1155/2020/1478291
38. Lee J, Kim MS. The role of GSK3 in glucose homeostasis and the development of insulin resistance. *Diabetes Res Clin Pract.* (2007) 77(Suppl. 1):S49–57. doi: 10.1016/j.diabres.2007.01.033
39. Tappy L, Dussoix P, Iynedjian P, Henry S, Schneiter P, Zahnd G, et al. Abnormal regulation of hepatic glucose output in maturity-onset diabetes of the young caused by a specific mutation of the glucokinase gene. *Diabetes.* (1997) 46:204–8. doi: 10.2337/diab.46.2.204
40. Lin HV, Accili D. Hormonal regulation of hepatic glucose production in health and disease. *Cell Metab.* (2011) 14:9–19. doi: 10.1016/j.cmet.2011.06.003
41. Krycer JR, Sharpe LJ, Luu W, Brown AJ. The Akt-SREBP nexus: cell signaling meets lipid metabolism. *Trends Endocrinol Metab.* (2010) 21:268–76. doi: 10.1016/j.tem.2010.01.001
42. Porstmann T, Santos CR, Griffiths B, Cully M, Wu M, Leevers S, et al. SREBP activity is regulated by mTORC1 and contributes to Akt-dependent cell growth. *Cell Metab.* (2008) 8:224–36. doi: 10.1016/j.cmet.2008.07.007
43. Hoxhaj G, Manning BD. The PI3K-AKT network at the interface of oncogenic signalling and cancer metabolism. *Nat Rev Cancer.* (2020) 20:74–88. doi: 10.1038/s41568-019-0216-7
44. Shimano H, Sato R. SREBP-regulated lipid metabolism: convergent physiology - divergent pathophysiology. *Nat Rev Endocrinol.* (2017) 13:710–30. doi: 10.1038/nrendo.2017.91
45. Garat CV, Crossno JT Jr., Sullivan TM, Reusch JE, Klemm DJ. Inhibition of phosphatidylinositol 3-kinase/Akt signaling attenuates hypoxia-induced pulmonary artery remodeling and suppresses CREB depletion in arterial smooth muscle cells. *J Cardiovasc Pharmacol.* (2013) 62:539–48. doi: 10.1097/FJC.0000000000000014
46. Houssaini A, Abid S, Mouraret N, Wan F, Rideau D, Saker M, et al. Rapamycin reverses pulmonary artery smooth muscle cell proliferation in pulmonary hypertension. *Am J Respir Cell Mol Biol.* (2013) 48:568–77. doi: 10.1165/rcmb.2012-0429OC
47. Baardman J, Verberk SGS, van der Velden S, Gijbels MJJ, van Roomen C, Sluimer JC, et al. Macrophage ATP citrate lyase deficiency stabilizes atherosclerotic plaques. *Nat Commun.* (2020) 11:6296. doi: 10.1038/s41467-020-20141-z
48. Minokoshi Y, Kim YB, Peroni OD, Fryer LG, Muller C, Carling D, et al. Leptin stimulates fatty-acid oxidation by activating AMP-activated protein kinase. *Nature.* (2002) 415:339–43. doi: 10.1038/415339a
49. Goncharova EA. mTOR and vascular remodeling in lung diseases: current challenges and therapeutic prospects. *FASEB J.* (2013) 27:1796–807. doi: 10.1096/fj.12-222224
50. Yan WW, Liang YL, Zhang QX, Wang D, Lei MZ, Qu J, et al. Arginine methylation of SIRT7 couples glucose sensing with mitochondria biogenesis. *EMBO Rep.* (2018) 19:e46377. doi: 10.15252/embr.201846377
51. Shin J, He M, Liu Y, Paredes S, Villanova L, Brown K, et al. SIRT7 represses Myc activity to suppress ER stress and prevent fatty liver disease. *Cell Rep.* (2013) 5:654–65. doi: 10.1016/j.celrep.2013.10.007
52. Yoshizawa T, Karim MF, Sato Y, Senokuchi T, Miyata K, Fukuda T, et al. SIRT7 controls hepatic lipid metabolism by regulating the ubiquitin-proteasome pathway. *Cell Metab.* (2014) 19:712–21. doi: 10.1016/j.cmet.2014.03.006
53. Tang M, Tang H, Tu B, Zhu WG. SIRT7: a sentinel of genome stability. *Open Biol.* (2021) 11:210047. doi: 10.1098/rsob.210047
54. Kiran S, Oddi V, Ramakrishna G. Sirtuin 7 promotes cellular survival following genomic stress by attenuation of DNA damage, SAPK activation and p53 response. *Exp Cell Res.* (2015) 331:123–41. doi: 10.1016/j.yexcr.2014.11.001
55. Wu D, Li Y, Zhu KS, Wang H, Zhu WG. Advances in cellular characterization of the sirtuin isoform, SIRT7. *Front Endocrinol (Lausanne).* (2018) 9:652. doi: 10.3389/fendo.2018.00652

56. Tang X, Li G, Shi L, Su F, Qian M, Liu Z, et al. Combined intermittent fasting and ERK inhibition enhance the anti-tumor effects of chemotherapy via the GSK3beta-SIRT7 axis. *Nat Commun.* (2021) 12:5058. doi: 10.1038/s41467-021-25274-3
57. Kimura Y, Izumiya Y, Araki S, Yamamura S, Hanatani S, Onoue Y, et al. Sirt7 deficiency attenuates neointimal formation following vascular injury by modulating vascular smooth muscle cell proliferation. *Circ J.* (2021) 85:2232–40. doi: 10.1253/circj.CJ-20-0936
58. Zhao Y, Ye X, Chen R, Gao Q, Zhao D, Ling C, et al. Sirtuin 7 promotes non-small cell lung cancer progression by facilitating G1/S phase and epithelial-mesenchymal transition and activating AKT and ERK1/2 signaling. *Oncol Rep.* (2020) 44:959–72. doi: 10.3892/or.2020.7672
59. Li H, Tian Z, Qu Y, Yang Q, Guan H, Shi B, et al. SIRT7 promotes thyroid tumorigenesis through phosphorylation and activation of Akt and p70S6K1 via DBC1/SIRT1 axis. *Oncogene.* (2019) 38:345–59. doi: 10.1038/s41388-018-0434-6
60. Shao Z, Bhattacharya K, Hsich E, Park L, Walters B, Germann U, et al. c-Jun N-terminal kinases mediate reactivation of Akt and cardiomyocyte survival after hypoxic injury in vitro and in vivo. *Circ Res.* (2006) 98:111–8. doi: 10.1161/01.RES.0000197781.20524.b9
61. Mashima T, Seimiya H, Tsuruo T. De novo fatty-acid synthesis and related pathways as molecular targets for cancer therapy. *Br J Cancer.* (2009) 100:1369–72. doi: 10.1038/sj.bjc.6605007
62. Agrawal V, Lahm T, Hansmann G, Hemnes AR. Molecular mechanisms of right ventricular dysfunction in pulmonary arterial hypertension: focus on the coronary vasculature, sex hormones, and glucose/lipid metabolism. *Cardiovasc Diagn Ther.* (2020) 10:1522–40. doi: 10.21037/cdt-20-404
63. Koop AC, Bossers GPL, Ploegstra MJ, Hagdorn QAJ, Berger RMF, Sillje HHW, et al. Metabolic remodeling in the pressure-loaded right ventricle: shifts in glucose and fatty acid Metabolism-A systematic review and meta-analysis. *J Am Heart Assoc.* (2019) 8:e012086. doi: 10.1161/JAHA.119.012086
64. Metallo CM, Gameiro PA, Bell EL, Mattaini KR, Yang J, Hiller K, et al. Reductive glutamine metabolism by IDH1 mediates lipogenesis under hypoxia. *Nature.* (2011) 481:380–4. doi: 10.1038/nature10602
65. Baenke F, Peck B, Miess H, Schulze A. Hooked on fat: the role of lipid synthesis in cancer metabolism and tumour development. *Dis Model Mech.* (2013) 6:1353–63. doi: 10.1242/dmm.011338
66. Lamming DW, Sabatini DM. A central role for mTOR in lipid homeostasis. *Cell Metab.* (2013) 18:465–9. doi: 10.1016/j.cmet.2013.08.002
67. Martinez Calejman C, Trefely S, Entwisle SW, Luciano A, Jung SM, Hsiao W, et al. mTORC2-AKT signaling to ATP-citrate lyase drives brown adipogenesis and de novo lipogenesis. *Nat Commun.* (2020) 11:575. doi: 10.1038/s41467-020-14430-w
68. Elstrom RL, Bauer DE, Buzzai M, Karnauskas R, Harris MH, Plas DR, et al. Akt stimulates aerobic glycolysis in cancer cells. *Cancer Res.* (2004) 64:3892–9. doi: 10.1158/0008-5472.Can-03-2904
69. Yecies JL, Zhang HH, Menon S, Liu S, Yecies D, Lipovsky AI, et al. Akt stimulates hepatic SREBP1c and lipogenesis through parallel mTORC1-dependent and independent pathways. *Cell Metab.* (2011) 14:21–32. doi: 10.1016/j.cmet.2011.06.002
70. Manning BD, Toker A. AKT/PKB signaling: navigating the network. *Cell.* (2017) 169:381–405. doi: 10.1016/j.cell.2017.04.001
71. Martorana F, Motta G, Pavone G, Motta L, Stella S, Vitale SR, et al. AKT inhibitors: new weapons in the fight against breast cancer? *Front Pharmacol.* (2021) 12:662232. doi: 10.3389/fphar.2021.662232
72. Brown JS, Banerji U. Maximising the potential of AKT inhibitors as anti-cancer treatments. *Pharmacol Ther.* (2017) 172:101–15. doi: 10.1016/j.pharmthera.2016.12.001
73. He Y, Sun MM, Zhang GG, Yang J, Chen KS, Xu WW, et al. Targeting PI3K/Akt signal transduction for cancer therapy. *Signal Transduct Target Ther.* (2021) 6:425. doi: 10.1038/s41392-021-00828-5
74. Mei Z, Zhang X, Yi J, Huang J, He J, Tao Y. Sirtuins in metabolism, DNA repair and cancer. *J Exp Clin Cancer Res.* (2016) 35:182. doi: 10.1186/s13046-016-0461-5
75. Pillai VB, Sundaresan NR, Gupta MP. Regulation of Akt signaling by sirtuins: its implication in cardiac hypertrophy and aging. *Circ Res.* (2014) 114:368–78. doi: 10.1161/CIRCRESAHA.113.300536
76. Carafa V, Rotili D, Forgione M, Cuomo F, Serretiello E, Hailu GS, et al. Sirtuin functions and modulation: from chemistry to the clinic. *Clin Epigenetics.* (2016) 8:61. doi: 10.1186/s13148-016-0224-3
77. Blank MF, Grummt I. The seven faces of SIRT7. *Transcription.* (2017) 8:67–74. doi: 10.1080/21541264.2016.1276658
78. Chen KL, Li L, Yang FX, Li CM, Wang YR, Wang GL. SIRT7 depletion inhibits cell proliferation, migration, and increases drug sensitivity by activating p38MAPK in breast cancer cells. *J Cell Physiol.* (2018) 233:6767–78. doi: 10.1002/jcp.26398
79. Kim JH, Kim D, Cho SJ, Jung KY, Kim JH, Lee JM, et al. Identification of a novel SIRT7 inhibitor as anticancer drug candidate. *Biochem Biophys Res Commun.* (2019) 508:451–7. doi: 10.1016/j.bbrc.2018.11.120
80. Yu J, Qin B, Wu F, Qin S, Nowsheen S, Shan S, et al. Regulation of serine-threonine kinase Akt activation by NAD(+)-Dependent deacetylase SIRT7. *Cell Rep.* (2017) 18:1229–40. doi: 10.1016/j.celrep.2017.01.009

Conflict of Interest: The authors declare that the research was conducted in the absence of any commercial or financial relationships that could be construed as a potential conflict of interest.

frontiers | Frontiers in Medicine

ORIGINAL RESEARCH
published: 28 July 2022
doi: 10.3389/fmed.2022.940784

Altered Lung Microbiome and Metabolome Profile in Children With Pulmonary Arterial Hypertension Associated With Congenital Heart Disease

Runwei Ma[1†], Liming Cheng[2†], Yi Song[3], Yi Sun[1], Wenting Gui[1], Yao Deng[1], Chao Xie[2] and Min Liu[1]*

[1] Department of Cardiovascular Surgery, Fuwai Yunnan Cardiovascular Hospital, Kunming, China, [2] Department of Anesthesiology, Kunming Children's Hospital, Kunming, China, [3] Department of Extracorporeal Circulation, Fuwai Yunnan Cardiovascular Hospital, Kunming, China

OPEN ACCESS

Edited by:
Ivette Buendia-Roldan,
Instituto Nacional de Enfermedades Respiratorias-México (INER), Mexico

Reviewed by:
Kongkiat Kespechara,
Oregon Health and Science University, United States
Brittany Needham,
California Institute of Technology, United States

***Correspondence:**
Runwei Ma
marw0102@163.com

[†] These authors have contributed equally to this work

Specialty section:
This article was submitted to Pulmonary Medicine, a section of the journal Frontiers in Medicine

Received: 10 May 2022
Accepted: 13 June 2022
Published: 28 July 2022

Citation:
Ma R, Cheng L, Song Y, Sun Y, Gui W, Deng Y, Xie C and Liu M (2022) Altered Lung Microbiome and Metabolome Profile in Children With Pulmonary Arterial Hypertension Associated With Congenital Heart Disease. Front. Med. 9:940784. doi: 10.3389/fmed.2022.940784

Backgrounds: Pulmonary arterial hypertension (PAH) is characterized by progressive pulmonary vascular functional and structural changes, resulting in increased pulmonary vascular resistance and eventually right heart failure and death. Congenital Left-to-Right shunts (LTRS) is one type of congenital heart disease (CHD) and PAH associated with the congenital Left-to-Right shunt (PAH-LTRS) is a severe disease in children. However, changes in the lung microbiome and their potential impact on PAH-LTRS have not been not fully studied. We hypothesized that lung microbiota and their derived metabolites have been disturbed in children with PAH-LTRS, which might contribute to the progression and outcomes of PAH-LTRS.

Methods: In this study, 68 age- and sex-matched children of three different groups (patients with PAH-LTRS cohort, patients with LTRS but have no pathologic features of PAH cohort, and healthy reference cohort) were enrolled in the current study. Bronchoalveolar lavage fluid samples from these participants were conducted for multi-omics analysis, including 16S rRNA sequencing and metabolomic profiling. Data progressing and integration analysis were performed to identify pulmonary microbial and metabolic characteristics of PAH-LTRS in children.

Results: We found that microbial community density was not significantly altered in PAH-LTRS based on α-diversity analysis. Microbial composition analysis indicated phylum of Bacteroidetes was that less abundant while Lactobacillus, Alicycliphilus, and Parapusillimonas were significantly altered and might contribute to PAH in children with LTRS. Moreover, metabolome profiling data showed that metabolites involved in Purine metabolism, Glycerophospholipid metabolism, Galactose metabolism, and Pyrimidine metabolism were also significantly disturbed in the PAH-LTRS cohort. Correlation analysis between microbes and metabolites indicated that alterations in the microbial composition from the lung microbiota could eventually result in the disturbance in certain metabolites, and might finally contribute to the pathology of PAH-LTRS.

Conclusion: Lung microbial density was not significantly altered in patients with PAH-LTRS. Composition analysis results showed that the relative microbiome abundance was different between groups. Metabolome profiling and correlation analysis with microbiota showed that metabolome also altered in children with PAH-LTRS. This study indicated that pulmonary microbes and metabolites disturbed in PAH-LTRS could be potentially effective biomarkers and provides valuable perspectives on clinical diagnosis, treatment, and prognosis of pediatric PAH-LTRS.

Keywords: pulmonary arterial hypertension, congenital heart disease, left to right shunt, lung, microbiome, metabolome

INTRODUCTION

PAH is a multifactorial disease characterized by progressive loss and obstructive remodeling of the pulmonary arteries (1). The disease leads to elevated pulmonary vascular resistance (PVR) together with pulmonary arterial pressure (mPAP), ultimately resulting in irreversible right ventricular failure and death (2–5), and median survival in patients with PAH is only 5–7 yr (6). Although significant efforts have been made in the last decades, PAH is still incurable and needs life-long treatments (7), significantly influencing morbidity and mortality. The 6th World Symposium on pulmonary hypertension modified the definition for pulmonary hypertension as mPAP $>$ 20 mmHg and PVR $\geq$ 3 Wood Units (WU) instead of only mPAP $>$ 25-mmHg (3).

PAH is a complication widely found in patients with various congenital heart diseases (CHD) (8), including LTRS (9, 10). LTRS contributes to pulmonary vasculature remodeling and increased PVR, ultimately leading to PAH. Pediatric PAH has similar characteristics to adults but not the same in treatment and outcomes (11). Pediatric cardiovascular medicine and surgery still were the main therapeutic strategies for these patients (12). Correction is critical to preventing pulmonary vascular remodeling and progression of PAH-LTRS. If not, it might ultimately develop into Eisenmenger's syndrome, the most severe phenotype of PAH associated with CHD (13–15). For patients with end-stage PAH, lung function is severely disrupted, and difficulty in breathing. In that case, although lung transplantation was the only established treatment option (16–18), organ rejection and infection will be the most significant challenge after surgery. Early diagnosis or early treatment of LTRS or PAH-LTRS will effectively reduce the progression and mortality rate of PAH (19). Closure of cardiac defects in early childhood could effectively prevent the occurrence and progression of PAH and has a favorable outcome (20). However, not all children can be repaired timely and successfully, especially in developing countries (20). For them, they may continue to suffer from PAH their whole life. Although children with PAH-LTRS performed atrial septal defect closure at an appropriate time, most might persist immediately or initiate PAH months or years later despite the lack of any residual shunt named post-operation PAH. Postoperative PAH has the poorest prognosis, even worse than uncorrected subjects or Eisenmenger syndrome (21), significantly influencing the survival.

Although there have been notable advances in therapies for PAH, there are still considerable challenges in the cure and prognosis of the disease, specifically associated with CHD. Physical activity, pathology, and biomarkers are used for prognostic evaluation of PAH treatment in children but are far from sufficient to treat (22–25). Therefore, new treatment strategies or diagnostic biomarkers for PAH associated with CHD are urgently required in therapies or prognoses in the future. Microbiota facilitates many physiological functions by affecting host systemic immune regulation, energy homeostasis and metabolism, vitamin synthesis and degradation, and is widely considered involved in various diseases (26–30). Gut microbiota dysbiosis in patients with PAH was observed by extensive studies (31–34). Gut microbiota-derived metabolites were also involved in PAH through effects on the gut-lung axis (35, 36).

The lung is similar to the gut in immunity, epithelial barrier functions, and microbiomes. The microbiome in pulmonary is also the source of clinical variation in critical illness (37–39), despite the biomass of lung microbiota being smaller than the gut. The lung microbiome and metabolome could contribute to respiratory infections and inflammation, relating to human health and resulting in various pulmonary diseases, and could be the novel therapeutic target for the prevention and treatment or predicting clinical outcomes of human diseases (40–42). Knowledge of pulmonary microbiota and their derived metabolites have not been fully characterized in patients with PAH, especially in patients with PAH-LTRS. Lung is the local tissue where PAH occurs and severe PAH in patients with LTRS eventually results in lung transplantation without treatment (18). Therefore, it seems reasonable to assume that lung microbiome and metabolome have changed in patients with PAH-LTRS. Identification and characterization of lung-specific bacteria and metabolites in PAH-LTRS could lead to the development of targeted therapies in the future.

With the emerging role of the microbiome in disease, lung microbiota composition and function were potentially crucial for diagnosis, treatment, and improving clinical outcomes for patients with PAH-LTRS. Thus, our objective in this study was to evaluate the hypothesis that children with PAH-LTRS have a unique microbiome and metabolome profile in the lung that potentially, in turn, contribute to the pathogenesis and outcomes of PAH. Our results demonstrate that the lung microbiome

was not changed globally but significantly altered in some taxa, in terms of composition at phylum and genus levels. These disturbances might contribute to the alteration of metabolites and might contribute to the pathology of PAH-LTRS.

MATERIALS AND METHODS

Patients and Bronchoalveolar Lavage Fluid Collection

Patients who underwent clinical bronchoscopy at the Fuwai Yunnan Cardiovascular Hospital (Kunming, China) were recruited in our study. The pulmonary microbial community was easily affected by multi-factors and subjects were excluded from our study if they (1) have other cardiopulmonary diseases, lung comorbidities, pulmonary infection, metabolic diseases, and other systemic diseases; (2) take any special drugs, such as antibiotics, in the 3 months before enrollment; (3) have special diets such as feeding with breast or formula; and (4) participate in other clinical studies or were unable to provide consent for care or BALF collection. Finally, a total of 68 patients were enrolled in the current research. Bronchoalveolar lavage fluid (BALF) was collected into the sterile tube according to a standardized protocol with minimum oral contamination (43). Two milliliter BALF was collected from each participant and flash-frozen in liquid nitrogen and transferred to −80°C later until further processing.

16S rRNA High-Throughput Sequencing and Data Processing

Bacterial genomic DNA was extracted from BALF samples with CTAB/SDS method according to the previously reported (44). 16S rRNA high-throughput sequencing was performed with the 16S MetaVx^{TM} system (GENEWIZ). Total genomic DNA with ∼3 ng was conducted to first step PCR to amplify 16S rRNA genes (V3–V4) as per manufacturer's instructions. Purified PCR products were processed for second step PCR to construct sequencing libraries. 16S rRNA was sequenced on the Illumina MiSeq platform, and paired-end reads were obtained. Data processing according to previously described (34). In summary, raw data was firstly performed to eliminate adaptors by Cutadapt (1.9.1), and then input into Vsearch (1.9.6) and Qiime (1.9.1) for further filtration and operational taxonomic units (OUTs) analysis. Alpha diversity indexes, including observed species, Chao1, Shannon, and PD whole tree, evaluated by Qiime, were employed to analyze the complexity of bacterial diversity, and the *P*-values were adjusted by the Benjamini-Hochberg correction. Unsupervised analysis methods, such as principal coordinate analyses (PCoA), could significantly detect the difference between groups. However, when the differences between the groups are not significantly different and the obvious differences existed within groups, unsupervised analysis is difficult to find and distinguish the differences between the groups. Partial least squares-discriminant analysis (PLS-DA), as the supervised method, could achieve dimensionality reduction for clustering but with full awareness of the group labels and was also performed to analyze the potential differences among different groups in our study. Online data processing tool LEfSe (http://huttenhower.sph.harvard.edu/galaxy/root?tool_id=lefse_upload) was used to find dominant taxa in each group. Wilcoxon rank sum test was performed to evaluate taxonomic abundance in different groups. If not specified, figures were drawn by R packages.

Metabolomic Profiling by Liquid Chromatography and Mass Spectrometry and Data Processing

BALF samples used for metabolomic assay were taken from liquid nitrogen and thawed on ice, and metabolite extraction was performed using methanol and L-2-chlorobenzalanine. Metabolomic analysis of all samples was performed using the UHPLC -Q Exactive HF-X system (Thermo). The instrument was equipped with an ACQUITY UPLC HSS T3 (100 mm × 2.1 mm i.d., 1.8 μm; Waters, Milford, USA), and the column temperature was maintained at 40°C. Gradient elution of analytes was performed as previously described (45). Quality control samples are prepared by mixing equal volumes of all assay samples and are used to evaluate assay system stability. Obtained metabolism data were progressed according to previously reported (46). Briefly, Principal Component Analysis (PCA) was conducted to analyze global similarities containing quality control samples (QC). Student's *t*-test combined with multivariate analysis Orthogonal partial least-squares discriminate analysis (OPLS-DA) method was utilized to screen out the differential metabolites between groups (VIP $>$ 1, p-value $<$ 0.05). Differential metabolites (DMs) were performed based on fisher's exact test and clustering of DMs according to the Pearson coefficient. Differentially enriched KEGG (Kyoto Encyclopedia of Genes and Genomes) was performed to investigate the metabolomic pathways potentially involved in the pathogenesis of PAH-LTRS pathways by integrating databases of HMDB, KEGG compound and LIPID MAPS.

Correlation Between the Lung Microbiota and the Metabolome

Pearson correlation analysis was performed to reveal the correlation between lung microbiota and the metabolites with the Cytoscape software as previously described (47). $P < 0.05$ was regarded as statistically significant, $P < 0.01$ was considered as very significant, and $P < 0.001$ was regarded as extremely significant. A heatmap was used to show the correlation between lung bacteria and metabolites.

Statistical Analysis

All data were shown as the mean ± standard error of mean (s.e.m.). Patient's baseline characters and F/B ratio were graphically plotted using GraphPad Prism 7 (GraphPad Software Inc. San Diego, CA, USA). One-way ANOVA was used for assessing differences among multiple groups. Differences were considered statistically significant at $p < 0.05$.

TABLE 1 | Characteristics of participants.

Characteristic	All patients (*N* = 68)
Mean age (s.e.m.), yr	3.377 (0.411)
Sex	
Male, *n* (%)	41 (60.3)
Female, *n* (%)	27 (39.7)
Groups	
LTRS, *n* (%)	26 (38.2)
PAH-LTRS, *n* (%)	21 (30.9)
REF, *n* (%)	21 (30.9)
Diagnosis	
VSD, *n*	19
ASD, *n*	9
VSD + PFO, *n*	12
VSD + ASD, *n*	5
VSD + PDA, *n*	1
VSD + PDA + PFO, *n*	1

Values are mean ± s.e.m., proportiinton.
LTRS, congenital left to right shunts heart disease; PAH-LTRS, Pulmonary arterial hypertension associated with the congenital left to right shunts heart disease; REF, healthy reference; VSD, Ventricular Septal defect; ASD, Atrial Septal Defect; PFO, Patent Foramen Ovale; PDA, patent ductus arteriosus.

RESULTS

Study Populations

Six-eight anticipants, in three cohorts [21 children with PAH-LTRS cohort, 26 children with only LTRS cohort, and 21 healthy reference (REF) cohort] were recruited in our current study. The average age of these participants was 3.377 years, and the proportion of males and females was 60.3 and 39.7%, respectively. There were no significant differences in age and sex among the three groups. Baseline characteristics of anticipants are shown in **Table 1**.

BALF specimens were obtained from three cohorts as our study objects ($n = 68$) and were conducted for microbiome and metabolome profiling. Since some BLAF specimens were not sufficient for both analyses at the same time, of these 68 samples, 47 dispersed in different groups were used for 16S rRNA sequencing, while 59 were conducted for metabolomics profiling. All PAH-LTRS participants met the clinical definition of PAH, with exceeding mean PAP 20 mmHg and PVR > 3 Wood units measured by right heart catheterization.

Bacterial Diversity and Community Structure Were Not Significantly Disturbed in Children With PAH-LTRS

We firstly analyzed bacterial diversity in each cohort. A mass of operational taxonomic units (OTUs) was identified in our study (**Supplementary Table 1**), with common and distinct OTUs among different cohorts (**Figure 1A**). The number of species detected in PAH-LTRS and LTRS patients was slightly lower than that in REF but with no significant differences (PAH-LTRS vs. REF with padj = 0.43, LTRS vs. REF with padj = 0.16, and LTRS vs. PAH-LTRS with padj = 0.83) (**Figure 1B**). α-diversity analysis was then conducted to evaluate the richness and evenness of species diversity within each cohort. The result showed that PD whole tree index decreased in LTRS compared with REF and PAH-LTRS (padj = 0.005, 0.043, respectively). However, community diversity was not significantly altered globally among these cohorts indicated by the indexes of Chao1 (PAH-LTRS vs. REF with padj = 0.39, LTRS vs. REF with padj = 0.16 and LTRS vs. PAH-LTRS with padj = 0.86) and Shannon (PAH-LTRS vs. REF with padj = 0.39, LTRS vs. REF with padj = 0.99 and LTRS vs. PAH-LTRS with padj = 0.45) (**Figure 1C**). These results showed that microbiota community diversity was not significantly altered among different cohorts.

To further assess the similarities of bacterial communities among groups, PCoA plot based on the bray-curtis distance (**Supplementary Figure 1A**) were performed at the OTUs levels based on β-diversity analysis. The PCoA results showed no separation of the PAH-LTRS patients from other groups, indicating that the main composition of the lung microbiome of the PAH-LTRS cohort was not significantly altered. Supervised PLS-DA was then considered to find and distinguish the possible differences in OTUs between the groups and there was discernable boundaries among different cohorts (**Figure 1D**). Taken together, the results demonstrated that the microbial community in patients with PAH-LTRS was not globally different from other groups.

PAH-LTRS Patients Have Distinct Lung Microbiome Composition

To determine the differences among the three cohorts, we next focused on the bacteria composition, which contributes to the microbiota ecosystem. The predominant phyla in three cohorts were Proteobacteria, Firmicutes, Bacteroidetes, Actinobacteria, and Fusobacteria (**Figure 2A**; **Supplementary Table 2**). Although many taxa were common among the three subjects, the relative abundance was not the same. In PAH-LTRS, Bacteroidetes (5.77 vs. 8.3% and 13.55%) and Fusobacteria (0.65 vs. 1.43% and 4.8%) were decreased, Compared with REF and LTRS groups while the Bacteroidetes was one of the most important composition contributed to gut microbial homeostasis. Furthermore, we conducted a differential analysis of the relative abundance components between different groups based on the Wilcoxon rank sum test. The proportion of Deinococcus–Thermus and Euryarchaeota were significantly increased ($p = 0.002$, 0.047, respectively) in PAH-LTRS compared with REF (**Figure 2B**, middle; **Supplementary Table S2**). Bacteroidetes and Fusobacteria were significantly decreased ($p = 0.014$, 9.12E-05, respectively) in PAH-LTRS compared with LTRS (**Figure 2B**, right; **Supplementary Table 2**).

At genus level, the most common bacteria in three groups included Streptococcus, Pseudomonas, Haemophilus, Neisseria and Moraxella (**Figure 2C**; **Supplementary Table 2**). We found that the proportion of Haemophilus (4.56 vs. 9.69% and 6.33%) decreased, while Lactobacillus increased in PAH-LTRS compared with REF (2.71 vs. 1.22%) and LTRS (2.71 vs.

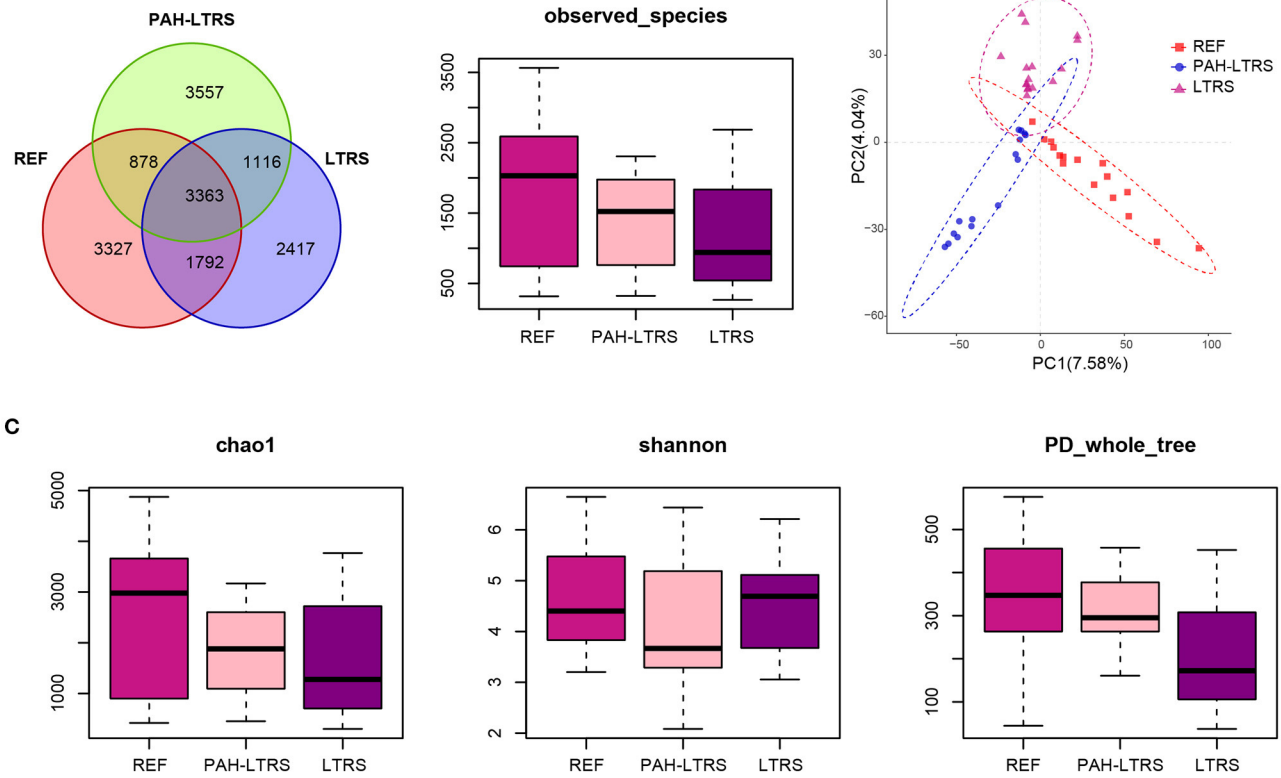

FIGURE 1 | Pulmonary bacterial community diversity in different cohorts and Principal Coordinate Analysis (PCoA) clustering. **(A)** Venn diagram of OUTs detected in three cohorts. **(B)** The number of species identified in three groups. **(C)** α-diversity among three cohorts measured by the Chao, Shannon and PD whole tree. Results were present as means ± s.e.m. **(D)** PLS-DA was conducted to compare the overall similarities in the bacterial taxonomy based on β-diversity. Each principal component represents most of the variation between samples. PAH-LTRS, patients with pulmonary arterial hypertension associated with Left-to-Right shunt ($n = 15$); REF, healthy reference ($n = 16$); LTRS, patients with Left-to-Right shunts but without PAH ($n = 16$).

0.48%) groups. Compared with REF, among the top 20 most variable genera, Alicycliphilus ($p = 0.01$), Rothia ($p = 0.03$), Providencia ($p = 0.001$) and Diaphorobacter ($p = 0.006$) were significantly increased, while Ruminococcus_gnavus_group ($p = 6.68E\text{-}05$), Fusicatenibacter ($p = 0.001$) and Enterococcus ($p = 0.02$) tend to be decreased in PAH-LTRS group (**Figure 2D**, middle; **Supplementary Table 2**). Compared with LTRS group, Moraxella ($p = 0.02$), Porphyromonas ($p = 0.003$), Campylobacter ($p = 0.003$) and Fusicatenibacter ($p = 0.002$) were significantly decreased while Alicycliphilus ($p = 0.004$) and Lactobacillus ($p = 0.039$) were increased in PAH-LTRS group (**Figure 2D**, right; **Supplementary Table 2**). Taxa composition at phylum and genus levels in each sample were showed in **Supplementary Figures 1B,D**.

LEfSe tool was considered to analyze bacterial communities in BALF samples and to find potentially essential differential taxa. The cladogram shows that Lactobacillaceae, acteroidales_S24-7_group, and Lactobacillaceae families were the predominant taxa and potentially involved in the pathology of PAH-LTRS (**Figure 3A**). Furthermore, the enriched genera in the PAH-LTRS group included Lactobacillus, Alicycliphilus, Castellaniella, Propionibacterium, Providencia, Parapusillimonas and Diaphorobacter (with LDA threshold 3) (**Figure 3B**). Collectively, these observations suggested composition of lung microbiota had been altered in PAH-LTRS, leading to dysbiosis in the pulmonary microenvironment and the Lactobacillus genus might have an essential influence on PAH-LTRS.

The Lung Metabolome Is Altered in PAH-LTRS

Accumulating evidence shows that PAH is a systemic metabolic disease. To explore the metabolites that contribute to the pulmonary microenvironment, we then conducted a non-targeted metabolism profiling on a total of 59 BALF samples. PCA analysis containing QC samples was shown in **Supplementary Figure 2A**. OPLS-DA analysis between any two of three groups showed clear boundaries, despite LTRS and PAH-LTRS were not completely separated in the clustering (**Figure 4A**). Differential analysis was then performed between groups, and the significantly altered metabolites were selected based on the variable importance in the projection (VIP) values and p-values (VIP > 1 and $p < 0.05$). Under this criterion, 88, 3, and 79 metabolites were found to be disturbed in REF vs. PAH-LTRS, REF vs. LTRS, and LTRS vs. PAH-LTRS, respectively

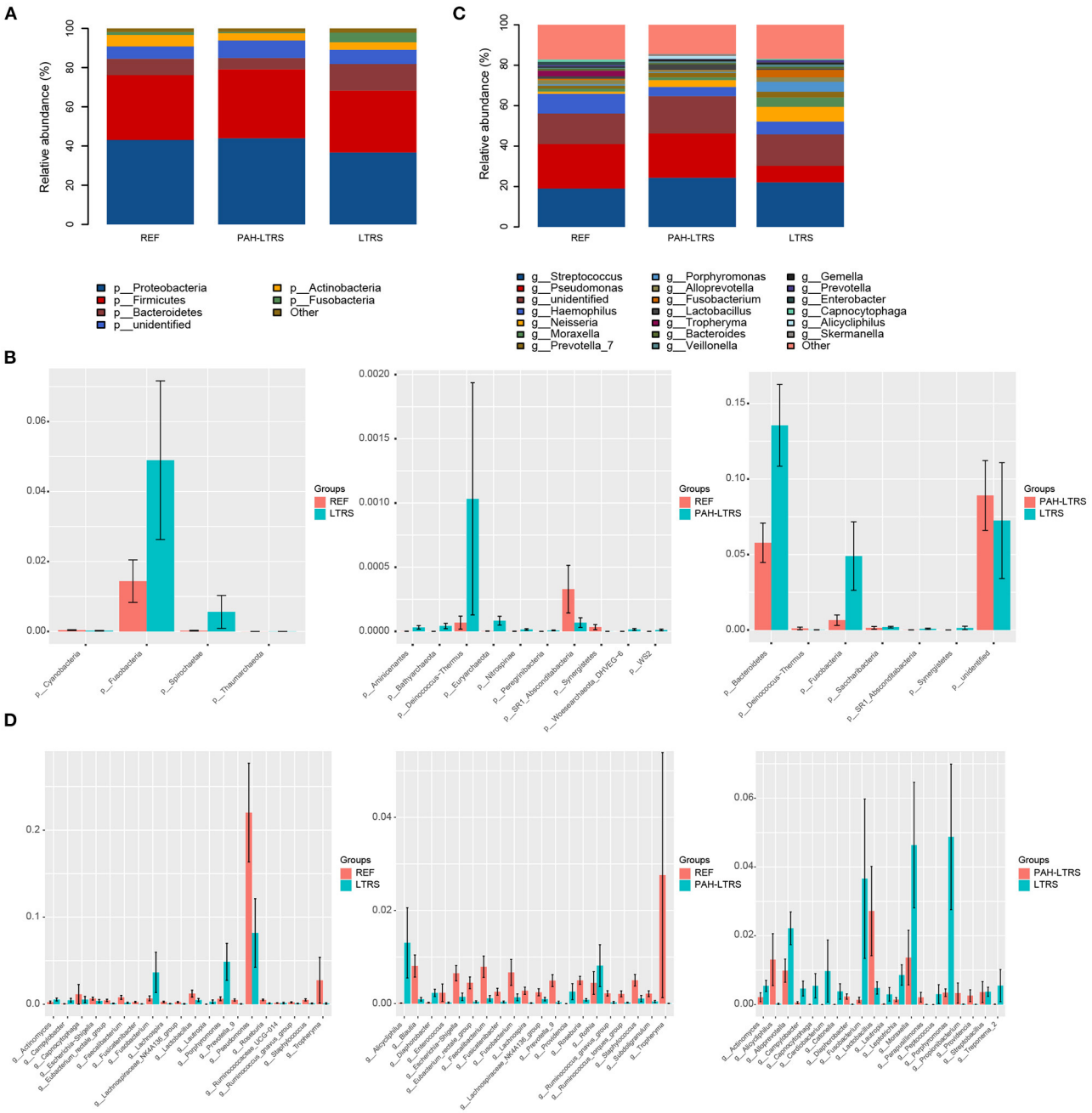

FIGURE 2 | Taxonomic composition of the lung microbiota among three cohorts. **(A)** The relative frequency of top abundant taxa in each cohort at the phylum level. **(B)** The relative abundance analysis of top altered phylum in three pair of comparisons (means ± s.e.m.). **(C)** The relative frequency of top abundant taxa in each cohort at the genus level. **(D)** Analysis of the relative abundance of top fluctuated genera between any two different cohorts (means ± s.e.m.). Wilcoxon rank sum test, $p < 0.05$. PAH-LTRS, patients with pulmonary arterial hypertension associated with Left-to-Right shunt ($n = 15$); REF, healthy reference ($n = 16$); LTRS, patients with Left-to-Right shunts but without PAH ($n = 16$).

(**Figures 4B,C**). Detailed information on these differential metabolites is available in **Supplementary Table 3**.

In the comparison of PAH-LTRS and REF, the most differential metabolites were identified and clustered into 5 clusters (**Supplementary Figure 2**B) with different expressed tendencies (**Figure 5A**). The significantly altered metabolites included Pos-22909 (2-piperidone), neg_1486 (UDP-glucose), neg_15140 (Glycerophosphocholine), neg_532 (ADP-ribose), neg_3243 (Adenosine monophosphate), pos_25479 (Dimethylethanolamine), neg_3243 (Adenosine

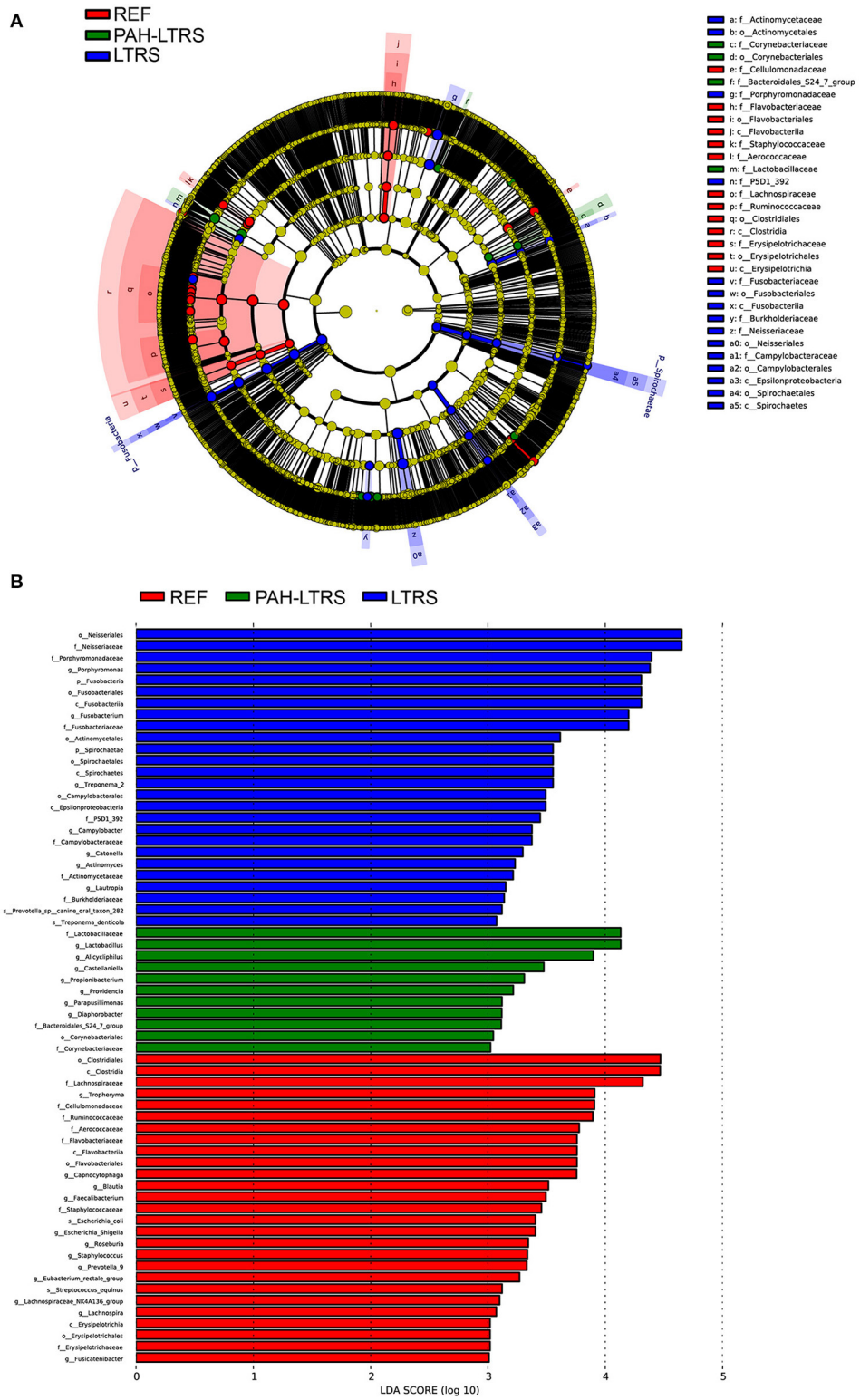

FIGURE 3 | LEfSe analysis to visualize differences in bacterial taxa among different groups. **(A)** The phylogenetic distribution of significantly enriched bacteria in different groups were showed by the cladogram. Nodes with different color represent different microbial taxa that are significantly abundant in the groups and significantly contribute to the differences between cohorts. **(B)** LDA bar graphs were utilized to identify the microbiota taxa with potentially significant effects in the three groups. Linear discriminant analysis (LDA, score > 2.0) scores are shown on the x-axis and taxa with the larger LDA score, the greater effect they might have in this group. PAH-LTRS, patients with pulmonary arterial hypertension associated with Left-to-Right shunt ($n = 15$); REF, healthy reference ($n = 16$); LTRS, patients with Left-to-Right shunts but without PAH ($n = 16$).

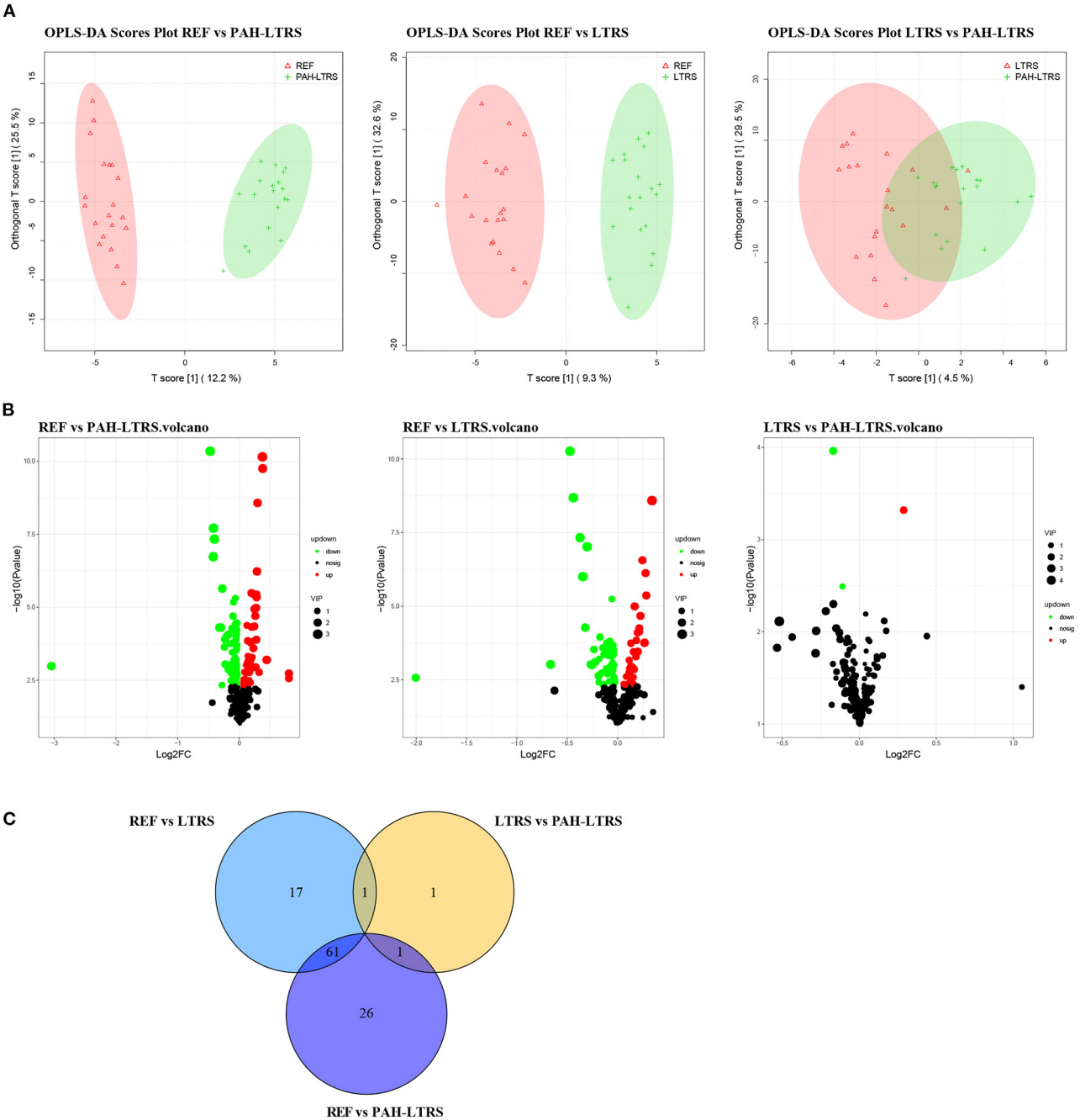

FIGURE 4 | Differential lung metabolites between different groups. **(A)** OPLS-DA was used to discriminate between different groups. **(B)** volcano plot of the differential metabolisms for any two groups (VIP > 1, $P < 0.05$). **(C)** Venn diagram showed the altered metabolites overlap among three pair of comparisions. PAH-LTRS, patients with pulmonary arterial hypertension associated with Left-to-Right shunt ($n = 19$); REF, healthy reference ($n = 20$); LTRS, patients with Left-to-Right shunts but without PAH ($n = 20$).

monophosphate), and pos_147 (Uridine). To further identify the biological significance associated with PAH-LTRS, we applied the Kyoto Encyclopedia of Genes and Genomes (KEGG) database to focus on the discrepant KEGG annotation with differential metabolites was firstly performed (**Supplementary Figure 2C**), and the significantly enriched terms (with the metabolic pathways most affected) included FoXO signaling pathway, mTOR signaling pathway, PI3K-Akt

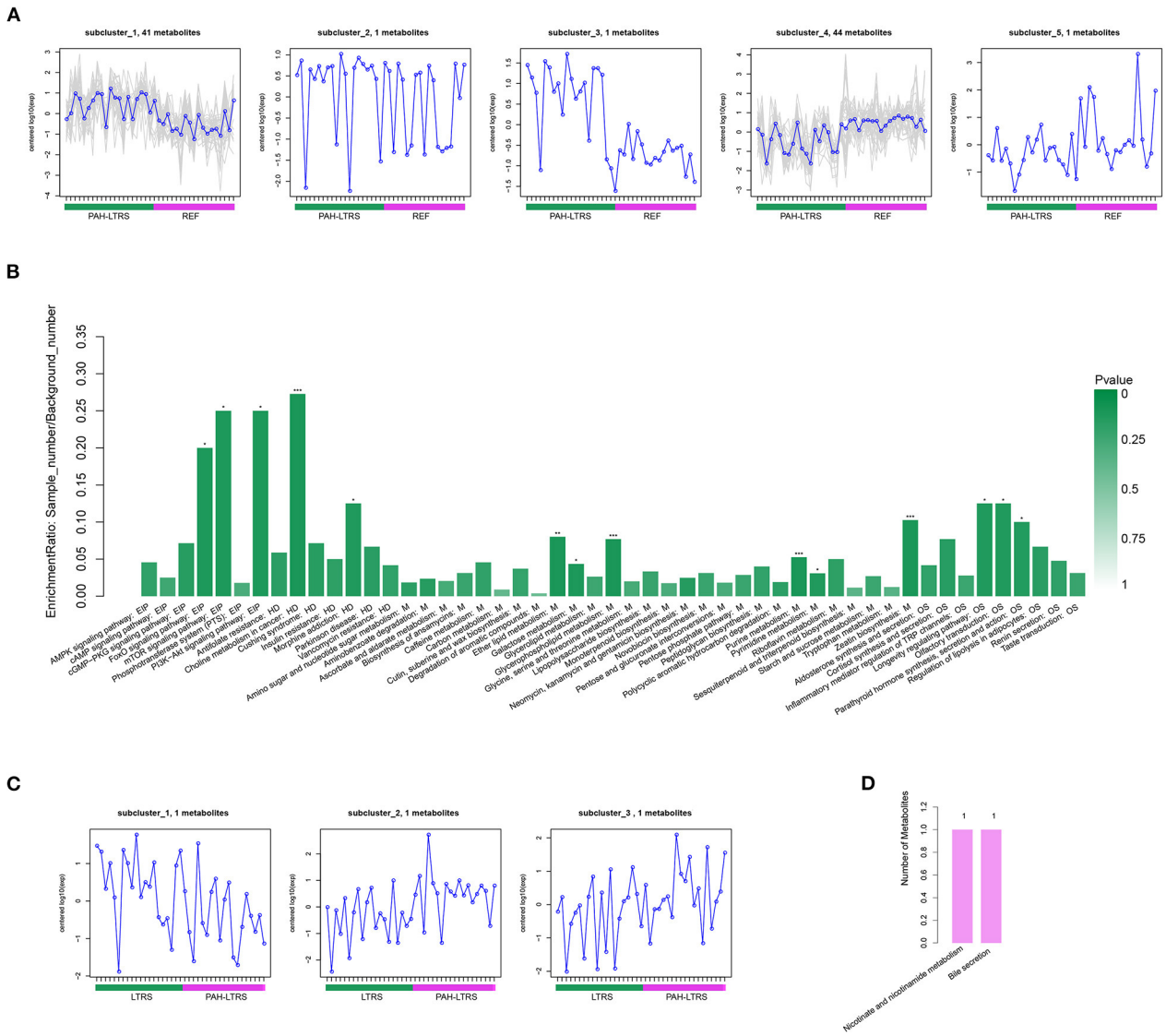

FIGURE 5 | Differential metabolites clustering and KEGG enrichment. **(A)** Differential metabolites in REF vs. PAH-LTRS were clustered into 5 clusters. These sub-clusters had different expression trend in two groups. **(B)** KEGG enrichment of these differential metabolites in REF vs. PAH. **(C)** Three differential metabolites in LTRS vs. PAH-LTRS also shown with different abundance in two groups. **(D)** Three differential metabolites in LTRS vs. PAH-LTRS were annotated into two pathways without significantly enrichment. EIP, Environmental Information Processing; HD, Human Diseases; M, Metabolism; OS, Organismal Systems. PAH-LTRS, patients with pulmonary arterial hypertension associated with Left-to-Right shunt ($n = 19$); REF, healthy reference ($n = 20$); LTRS, patients with Left-to-Right shunts but without PAH ($n = 20$).

signaling pathway, Eher lipid metabolism, Choline metabolism in cancer, Galactose metabolism, Glycerophospholipid metabolism, Purine metabolism, Pyrimidine metabolism and Zeatin biosynthesis (**Figure 5B**). Other classical signal pathways involved in PAH, such as the cGMP-PKG signaling pathway and Insulin resistance, were also dysregulated in PAH-LTRS, although not significantly ($P = 0.06$, 0.08, respectively).

Furthermore, there were only three differential metabolites were found in LTRS vs. PAH-LTRS, 2-piperidone, Pos-25441 (Trigonellinamide) and Pos-18930 (DL-2-Aminooctanoic acid). 2-piperidone was significantly decreased in PAH-LTRS (**Figure 5C**; **Supplementary Figure 2D**). These differential metabolites were annotated to Nicotinate and nicotinamide metabolism and bile secretion (**Figure 5D**). Overall, patients with PAH-LRTS exhibited a distinct metabolic signature compared with that in REF or the LRTS group. These changes in metabolites and related KEGG pathways might both contribute to the alteration of the lung microenvironment in patients with PAH-LTRS.

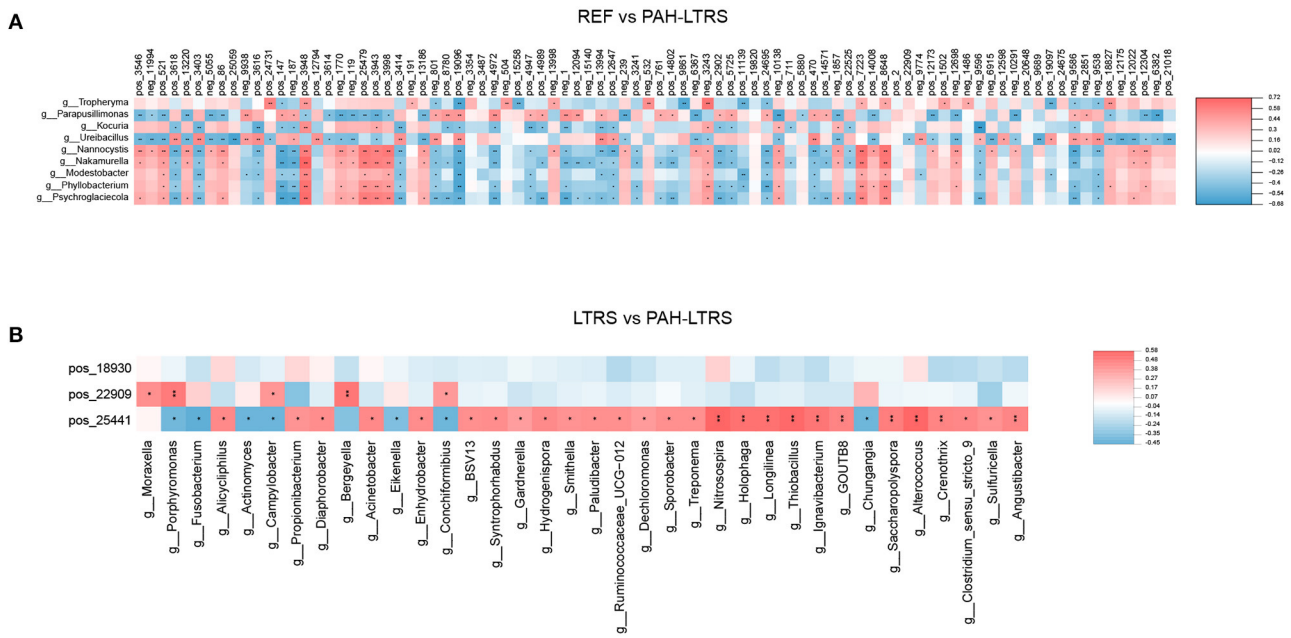

FIGURE 6 | Significant correlation between lung bacteria and differential metabolites. Heatmap indicated positive (red) and negative (blue) correlations between metabolites and the microbiota at the genus level detected in REF compared with PAH-LTRS cohort **(A)** and LTRS compared with PAH-LTRS cohort **(B)**. The legend shows correlation values from −1 to 1. *Represents significantly negative or positive correlations (*$P < 0.05$, **$P < 0.01$). PAH-LTRS, patients with pulmonary arterial hypertension associated with Left-to-Right shunt ($n = 19$); REF, healthy reference ($n = 20$); LTRS, patients with Left-to-Right shunts but without PAH ($n = 20$).

Microbes and Their Derived Metabolites Can Be Biomarkers for Targeted Therapy of PAH-LTRS

We next analyzed the correlation between differential metabolites and microorganisms at the genus level. We found those differential metabolites were correlated with microbes at varying degrees (**Supplementary Table 4**). We focused on the significant positive or negative correlations between metabolites and microbial taxa ($p < 0.05$). Parapusillimonas was significantly enriched in **PAH-LTRS** (**Figure 3A**) and was positively correlated with differential metabolites, such as Uridine, neg_9938 (Glycoursodeoxycholic acid) and pos_19096 (Laudanosine), while negatively with Dimethylethanolamine. Compared with **REF**, UDP-glucose, pos_24731 (Guanidylic acid), Adenosine monophosphate, pos_18827 (2,4-DPD), and pos_12304 (Cinnamic acid) were significantly decreased in PAH-LTRS. These decreased metabolites were positively correlated with the genera, such as Tropheryma, and negatively correlated with the genera, such as Nannocystis (**Figure 6A**).

In the comparison of LTRS vs. PAH, DL-2-Aminooctanoic acid had no significant correlation with any differential bacteria, while Trigonellinamide and 2-piperidone were significantly correlated with related microbes. 2-piperidone was decreased considerably in PAH-LTRS compared with LTRS or REF ($p = 0.005$, 0.009, respectively), Integration analysis showed that 2-piperidone was significantly positively correlated with Moraxella, Porphyromonas, and Campylobacter, which with reduced abundance in PAH-LTRS (**Figure 6B**). Trigonellinamide was enriched in PAH-LTRS compared to LTRS ($P = 0.001$), and there was also a significant positive correlation with the genera enriched in PAH-LTRS, such as Alicycliphilus, Diaphorobacter, and Propionibacterium. Taken together, differential metabolites and their significantly correlated microbial taxa are expected to serve as diagnostic biomarkers and therapeutic targets for PAH-LTRS in children.

DISCUSSION

PAH is considered a severe disease associated with congenital Left-to-Right shunts heart disease (48, 49). Lung transplantation would be the only intervention for end-stage patients with PAH (18). Numerous studies on gut microbes in PAH, either in animal models or humans, elucidate the essential role of gut microbiota in this disease (32, 34, 35). However, there is a lack of information on the lung microbiota impact on the pathology and prognosis of PAH-LTRS. In the present work, we used multiple omics approaches to study the character of the lung microbiome, metabolome, and the correlation of them in children with PAH-LTRS.

In the current study, we found that there was no significant difference in alpha diversity among the three groups, indicating no significant differences globally in microbial communities, consistent with an earlier study of PAH in gut microbiota (34). In contrast, reduced lung microbial richness and diversity were found in other diseases (50, 51). PCoA, as the unsupervised analysis, could significantly detect the difference between groups.

However, our PCoA results indicated that there was no significant clustering in Bray–Curtis distance matrices between groups. We assumed that there were individual differences among recruited participants and further studies with large cohorts size are needed to provide more evidence of global differences of lung microbes with PCoA clustering. PLS-DA, as the supervised method, could achieve clustering for different groups but with full awareness of the group labels (52–54). Composition analysis showed that there were bacterial disturbances in some taxa, despite the most common phyla and genera reported previously (39, 50) being the same among the three groups. Previous studies have shown that the Firmicutes (F) to Bacteroidetes (B) ratio (F/B), as the hallmark of gut dysbiosis (34, 35, 55), increased in the gut. F/B also tended to increase in PAH-LTRS (**Supplementary Figure 1**C). This ratio was mainly driven by less abundant Bacteroidetes phylum, propionate-producing bacteria and highly relevant in dysbiosis and disease (56–58). In contrast, there was no apparent change in the relative presence of Firmicutes phylum, which was consistent with previous findings in the gut (34). F/B was correlated with inflammation in gut microbiome studies, but the association of F/B with clinical significance in PAH-LTRS needs to be further addressed.

Lactobacillus, Alicycliphilus, Castellaniella, Propionibacterium, Providencia, Parapusillimonas, and Diaphorobacter genera were enriched in PAH-LTRS based on LEfSe analysis. In particular, Lactobacillus was thought to be reduced in PAH-LTRS in the gut (59). Lactobacillus in the lung was found to be significantly higher than in other groups and were the dominant taxa in PAH-LTRS. This discrepancy might result from different sub-type of PAH, tissue the microbes from, patient location, and the sampling time. The role of Lactobacillus in the lung of PAH-LTRS may be different from the gut. It might act as a beneficial bacterium as the short-term self-healing mechanism to resist PAH-LTRS development in the early stage. Further research needs to be done to explain the Lactobacillus variation in different studies and its role in PAH. Alicycliphilus phylum was considered involved in hypoxic energy metabolism involved in PAH, similar to the result of other studies concerning the lung bacteria (60), potentially as a marker of PAH-LTRS.

In the comparison of PAH-LTRS and REF, there were 88 differential metabolites disturbed. These metabolites were significantly enriched in a variety of metabolism pathways, including Galactose metabolism, Glycerophospholipid metabolism, Purine metabolism, Pyrimidine metabolism and Zeatin biosynthesis. Consistent with our result, Glycerophospholipid metabolism, Pyrimidine metabolism, and Purine metabolism were reported dysregulated in PAH (31, 61, 62). Glycerophospholipid metabolism was reported to be dysregulated in PAH by affecting lipid metabolism (63) and was close with inflammation (64), while inflammation is a prominent pathologic feature in PAH (65). However, there were only three different expressed metabolites in the PAH-LTRS cohort compared with LTRS, which exceeded our expectations. Such few differences may be due to the individual variability of the subjects and the insufficient sample size. 2-piperidone, which was significantly decreased in PAH-LTRS, was significantly positively correlated with Moraxella and Porphyromonas, which were decreased in abundance in PAH-LTRS. Porphyromonas was one of the most important genera of the phylum of Bacteroidetes and was reported involved in inflammatory diseases (66–68) and other human diseases (69, 70). Bacteroidetes might play a role in prohibiting PAH progression in patients with LTRS by Porphyromonas through related metabolites, such as 2-piperidone. 2-piperidone was reported to be disturbed in some human diseases, such as ovarian cancer (60), which indicated that it might be a biomarker for PAH-LTRS patients. Further evidence was warranted to clarify the mechanism of the significant correlation between the lung microbiota and metabolites.

However, our current study has some limitations. First, further study is required to clarify whether lung dysbiosis plays a pathophysiological role in the development of PAH-LTRS or is just secondary to pulmonary pathology resulting from the disease. If the former is true, these alterations might be helpful in investigating the underlying mechanisms of PAH-LTRS and open new avenues for therapeutic intervention. Second, further investigations consisting of larger sample sizes or samples from different centers or other geographical locations are needed in our future work. Third, BLAF samples were only collected from patients before surgery in this study, while samples from patients after surgery and collected at different time points after surgery will be more beneficial to predict or improve the clinical prognosis of PAH-LTRS. Fourth, BLAF collection was a method of invasive sampling. Instead, the upper airway method including oropharyngeal swabs and nasopharyngeal were much more convenient compared with BLAF collection (71, 72), and to what extent they can reflect the pathology of PAH-LTRS was worthy to study in the future.

In summary, our results demonstrate that bacterial composition and metabolic activity in lung were disturbed significantly in patients with PAH-LTRS. At the phylum level, Bacteroidetes was less abundant in PAH-LTRS. Lactobacillus, Alicycliphilus, Castellaniella, Propionibacterium, Providencia, Parapusillimonas, and Diaphorobacter were the predominant genus in PAH-LTRS. 2-piperidone and correlated microbes of Moraxella and Porphyromonas were significantly decreased in PAH-LTRS. Glycerophospholipid metabolism, Pyrimidine metabolism, and Purine metabolism were dysregulated in PAH-LTRS. Our study highlighted potentially unknown roles of pulmonary bacteria and metabolites in children with PAH-LTRS and might be the biomarkers providing a clue to improving the therapeutic, diagnostic, and clinical outcomes of PAH-LTRS.

DATA AVAILABILITY STATEMENT

The data presented in the study are deposited in the National Genomics Data Center (https://ngdc.cncb.ac.cn/omix/) repository, accession number OMIX001230.

ETHICS STATEMENT

The studies involving human participants were reviewed and approved by Ethics Committee of Fuwai Yunnan Cardiovascular Hospital. Written informed consent to participate in this study was provided by the participants' legal guardian/next of kin.

AUTHOR CONTRIBUTIONS

RM and LC conceived and designed the experiments, wrote, revised, and finalized the manuscript. LC, YSo, YSu, WG, YD, CX, and ML performed the experiments and analyzed the data. All authors reviewed the content and approved the final version for publication.

FUNDING

This work was supported by Foundation of Medical Specialist (YNWR-MY-2020-044) and Foundation Program of Yunnan Provincial Cardiovascular Clinical Medical Center (FZX2019-06-01-05).

ACKNOWLEDGMENTS

The authors thank all the subjects participated in this study.

SUPPLEMENTARY MATERIAL

The Supplementary Material for this article can be found online at: https://www.frontiersin.org/articles/10.3389/fmed.2022.940784/full#supplementary-material

REFERENCES

1. Heath D, Edwards JE. The pathology of hypertensive pulmonary vascular disease; a description of six grades of structural changes in the pulmonary arteries with special reference to congenital cardiac septal defects. *Circulation.* (1958) 18:533–47. doi: 10.1161/01.CIR.18.4.533
2. Thenappan T, Ormiston ML, Ryan JJ, Archer SL. Pulmonary arterial hypertension: pathogenesis and clinical management. *BMJ.* (2018) 360:j5492. doi: 10.1136/bmj.j5492
3. Simonneau G, Montani D, Celermajer DS, Denton CP, Gatzoulis MA, Krowka M, et al. Haemodynamic definitions and updated clinical classification of pulmonary hypertension. *Eur Respir J.* (2019) 53:1801913. doi: 10.1183/13993003.01913-2018
4. Kovacs G, Dumitrescu D, Barner A, Greiner S, Grunig E, Hager A, et al. Definition, clinical classification and initial diagnosis of pulmonary hypertension: updated recommendations from the Cologne Consensus Conference 2018. *Int J Cardiol.* (2018) 272S:11–9. doi: 10.1016/j.ijcard.2018.08.083
5. Humbert M, Guignabert C, Bonnet S, Dorfmuller P, Klinger JR, Nicolls MR, et al. Pathology and pathobiology of pulmonary hypertension: state of the art and research perspectives. *Eur Respir J.* (2019) 53:1801887. doi: 10.1183/13993003.01887-2018
6. Benza RL, Miller DP, Barst RJ, Badesch DB, Frost AE, McGoon MD. An evaluation of long-term survival from time of diagnosis in pulmonary arterial hypertension from the REVEAL registry. *Chest.* (2012) 142:448–56. doi: 10.1378/chest.11-1460
7. Galie N, Channick RN, Frantz RP, Grunig E, Jing ZC, Moiseeva O, et al. Risk stratification and medical therapy of pulmonary arterial hypertension. *Eur Respir J.* (2019) 53:1801889. doi: 10.1183/13993003.01889-2018
8. Dimopoulos K, Wort SJ, Gatzoulis MA. Pulmonary hypertension related to congenital heart disease: a call for action. *Eur Heart J.* (2014) 35:691–700. doi: 10.1093/eurheartj/eht437
9. D'Alto M, Diller GP. Pulmonary hypertension in adults with congenital heart disease and Eisenmenger syndrome: current advanced management strategies. *Heart.* (2014) 100:1322–8. doi: 10.1136/heartjnl-2014-305574
10. Muneuchi J, Nagatomo Y, Watanabe M, Joo K, Onzuka T, Ochiai Y, et al. Relationship between pulmonary arterial resistance and compliance among patients with pulmonary arterial hypertension and congenital heart disease. *J Thorac Cardiovasc Surg.* (2016) 152:507–13. doi: 10.1016/j.jtcvs.2016.03.080
11. Rosenzweig EB, Abman SH, Adatia I, Beghetti M, Bonnet D, Haworth S, et al. Paediatric pulmonary arterial hypertension: updates on definition, classification, diagnostics and management. *Eur Respir J.* (2019) 53:1801916. doi: 10.1183/13993003.01916-2018
12. Moons P, Bovijn L, Budts W, Belmans A, Gewillig M. Temporal trends in survival to adulthood among patients born with congenital heart disease from 1970 to 1992 in Belgium. *Circulation.* (2010) 122:2264–72. doi: 10.1161/CIRCULATIONAHA.110.946343
13. Wood P. The Eisenmenger syndrome or pulmonary hypertension with reversed central shunt. I. *Br Med J.* (1958) 2:701–9. doi: 10.1136/bmj.2.5098.701
14. Arvanitaki A, Giannakoulas G, Baumgartner H, Lammers AE. Eisenmenger syndrome: diagnosis, prognosis and clinical management. *Heart.* (2020) 106:1638–45. doi: 10.1136/heartjnl-2020-316665
15. Arvanitaki A, Gatzoulis MA, Opotowsky AR, Khairy P, Dimopoulos K, Diller GP, et al. Eisenmenger syndrome: JACC state-of-the-art review. *J Am Coll Cardiol.* (2022) 79:1183–98. doi: 10.1016/j.jacc.2022.01.022
16. Hansmann G. Pulmonary hypertension in infants, children, and young adults. *J Am Coll Cardiol.* (2017) 69:2551–69. doi: 10.1016/j.jacc.2017.03.575
17. Galie N, Humbert M, Vachiery JL, Gibbs S, Lang I, Torbicki A, et al. 2015 ESC/ERS guidelines for the diagnosis and treatment of pulmonary hypertension: the joint task force for the diagnosis and treatment of pulmonary hypertension of the European Society of Cardiology (ESC) and the European Respiratory Society (ERS): Endorsed by: Association for European Paediatric and Congenital Cardiology (AEPC), International Society for Heart and Lung Transplantation (ISHLT). *Eur Heart J.* (2016) 37:67–119. doi: 10.1093/eurheartj/ehv317
18. Hansmann G, Diekmann F, Chouvarine P, Ius F, Carlens J, Schwerk N, et al. Full recovery of right ventricular systolic function in children undergoing bilateral lung transplantation for severe PAH. *J Heart Lung Transplant.* (2022) 41:187–98. doi: 10.1016/j.healun.2021.10.014
19. Report of the British Cardiac Society Working P. Grown-up congenital heart (GUCH) disease: current needs and provision of service for adolescents and adults with congenital heart disease in the UK. *Heart.* (2002) 88 (Suppl. 1):i1–14. doi: 10.1136/heart.88.suppl_1.i1
20. Arafuri N, Murni IK, Idris NS, Uiterwaal C, Savitri AI, Nugroho S, et al. Survival of left-to-right shunt repair in children with pulmonary arterial hypertension at a tertiary hospital in a low-to-middle-income country. *Glob Heart.* (2021) 16:25. doi: 10.5334/gh.831
21. Alonso-Gonzalez R, Lopez-Guarch CJ, Subirana-Domenech MT, Ruiz JMO, Gonzalez IO, Cubero JS, et al. Pulmonary hypertension and congenital heart disease: an insight from the REHAP national registry. *Int J Cardiol.* (2015) 184:717–23. doi: 10.1016/j.ijcard.2015.02.031
22. Bernus A, Wagner BD, Accurso F, Doran A, Kaess H, Ivy DD. Brain natriuretic peptide levels in managing pediatric patients with pulmonary arterial hypertension. *Chest.* (2009) 135:745–51. doi: 10.1378/chest.08-0187
23. van Loon RL, Roofthooft MT, Delhaas T, van Osch-Gevers M, ten Harkel AD, Strengers JL, et al. Outcome of pediatric patients with pulmonary arterial hypertension in the era of new medical therapies. *Am J Cardiol.* (2010) 106:117–24. doi: 10.1016/j.amjcard.2010.02.023
24. Zijlstra WMH, Ploegstra MJ, Vissia-Kazemier T, Roofthooft MTR, Sarvaas GDM, Bartelds B, et al. Physical activity in pediatric pulmonary arterial

hypertension measured by accelerometry. A candidate clinical endpoint. *Am J Respir Crit Care Med.* (2017) 196:220–7. doi: 10.1164/rccm.201608-1576OC
25. Bittner V, Weiner DH, Yusuf S, Rogers WJ, McIntyre KM, Bangdiwala SI, et al. Prediction of mortality and morbidity with a 6-minute walk test in patients with left ventricular dysfunction. SOLVD Investigators. *JAMA.* (1993) 270:1702–7. doi: 10.1001/jama.1993.03510140062030
26. Nagpal R, Yadav H. Bacterial translocation from the gut to the distant organs: an overview. *Ann Nutr Metab.* (2017) 71 (Suppl. 1):11–6. doi: 10.1159/000479918
27. Li X, Watanabe K, Kimura I. Gut microbiota dysbiosis drives and implies novel therapeutic strategies for diabetes mellitus and related metabolic diseases. *Front Immunol.* (2017) 8:1882. doi: 10.3389/fimmu.2017.01882
28. Emoto T, Yamashita T, Sasaki N, Hirota Y, Hayashi T, So A, et al. Analysis of gut microbiota in coronary artery disease patients: a possible link between gut microbiota and coronary artery disease. *J Atheroscler Thromb.* (2016) 23:908–21. doi: 10.5551/jat.32672
29. Cho I, Blaser MJ. The human microbiome: at the interface of health and disease. *Nat Rev Genet.* (2012) 13:260–70. doi: 10.1038/nrg3182
30. Wang Z, Zhao Y. Gut microbiota derived metabolites in cardiovascular health and disease. *Protein Cell.* (2018) 9:416–31. doi: 10.1007/s13238-018-0549-0
31. Kim S, Rigatto K, Gazzana MB, Knorst MM, Richards EM, Pepine CJ, et al. Altered gut microbiome profile in patients with pulmonary arterial hypertension. *Hypertension.* (2020) 75:1063–71. doi: 10.1161/HYPERTENSIONAHA.119.14294
32. Yang T, Santisteban MM, Rodriguez V, Li E, Ahmari N, Carvajal JM, et al. Gut dysbiosis is linked to hypertension. *Hypertension.* (2015) 65:1331–40. doi: 10.1161/HYPERTENSIONAHA.115.05315
33. Aldred MA. Food for thought: the emerging role of intestinal microbiota in pulmonary arterial hypertension. *Am J Respir Cell Mol Biol.* (2022) 66:361–2. doi: 10.1165/rcmb.2022-0005ED
34. Callejo M, Mondejar-Parreno G, Barreira B, Izquierdo-Garcia JL, Morales-Cano D, Esquivel-Ruiz S, et al. Pulmonary arterial hypertension affects the rat gut microbiome. *Sci Rep.* (2018) 8:9681. doi: 10.1038/s41598-018-27682-w
35. Sanada TJ, Hosomi K, Shoji H, Park J, Naito A, Ikubo Y, et al. Gut microbiota modification suppresses the development of pulmonary arterial hypertension in an SU5416/hypoxia rat model. *Pulm Circ.* (2020) 10:2045894020929147. doi: 10.1177/2045894020929147
36. Sobko T, Reinders CI, Jansson E, Norin E, Midtvedt T, Lundberg JO. Gastrointestinal bacteria generate nitric oxide from nitrate and nitrite. *Nitric Oxide.* (2005) 13:272–8. doi: 10.1016/j.niox.2005.08.002
37. Barcik W, Boutin RCT, Sokolowska M, Finlay BB. The role of lung and gut microbiota in the pathology of asthma. *Immunity.* (2020) 52:241–55. doi: 10.1016/j.immuni.2020.01.007
38. Liu NN, Ma Q, Ge Y, Yi CX, Wei LQ, Tan JC, et al. Microbiome dysbiosis in lung cancer: from composition to therapy. *NPJ Precis Oncol.* (2020) 4:33. doi: 10.1038/s41698-020-00138-z
39. Khan FH, Bhat BA, Sheikh BA, Tariq L, Padmanabhan R, Verma JP, et al. Microbiome dysbiosis and epigenetic modulations in lung cancer: from pathogenesis to therapy. *Semin Cancer Biol.* (2021). doi: 10.1016/j.semcancer.2021.07.005
40. Dickson RP, Schultz MJ, van der Poll T, Schouten LR, Falkowski NR, Luth JE, et al. Lung microbiota predict clinical outcomes in critically ill patients. *Am J Respir Crit Care Med.* (2020) 201:555–63. doi: 10.1164/rccm.201907-1487OC
41. Moffatt MF, Cookson WO. The lung microbiome in health and disease. *Clin Med.* (2017) 17:525–9. doi: 10.7861/clinmedicine.17-6-525
42. Li J, Hu Y, Liu L, Wang Q, Zeng J, Chen C. PM2.5 exposure perturbs lung microbiome and its metabolic profile in mice. *Sci Total Environ.* (2020) 721:137432. doi: 10.1016/j.scitotenv.2020.137432
43. Segal LN, Alekseyenko AV, Clemente JC, Kulkarni R, Wu B, Gao Z, et al. Enrichment of lung microbiome with supraglottic taxa is associated with increased pulmonary inflammation. *Microbiome.* (2013) 1:19. doi: 10.1186/2049-2618-1-19
44. Cheng C, Wang Z, Wang J, Ding C, Sun C, Liu P, et al. Characterization of the lung microbiome and exploration of potential bacterial biomarkers for lung cancer. *Transl Lung Cancer Res.* (2020) 9:693–704. doi: 10.21037/tlcr-19-590
45. Niu JL, Zhang J, Wei LQ, Zhang WJ, Nie CX. Effect of fermented cottonseed meal on the lipid-related indices and serum metabolic profiles in broiler chickens. *Animals.* (2019) 9:930. doi: 10.3390/ani9110930
46. Lord T, Nixon B. Metabolic changes accompanying spermatogonial stem cell differentiation. *Dev Cell.* (2020) 52:399–411. doi: 10.1016/j.devcel.2020.01.014
47. Duan Y, Xiong D, Wang Y, Li H, Dong H, Zhang J. Toxic effects of ammonia and thermal stress on the intestinal microbiota and transcriptomic and metabolomic responses of *Litopenaeus vannamei*. *Sci Total Environ.* (2021) 754:141867. doi: 10.1016/j.scitotenv.2020.141867
48. Clavel T, Desmarchelier C, Haller D, Gerard P, Rohn S, Lepage P, et al. Intestinal microbiota in metabolic diseases: from bacterial community structure and functions to species of pathophysiological relevance. *Gut Microbes.* (2014) 5:544–51. doi: 10.4161/gmic.29331
49. Friedrich MJ. Microbiome project seeks to understand human body's microscopic residents. *JAMA.* (2008) 300:777–8. doi: 10.1001/jama.300.7.777
50. Lee SH, Sung JY, Yong D, Chun J, Kim SY, Song JH, et al. Characterization of microbiome in bronchoalveolar lavage fluid of patients with lung cancer comparing with benign mass like lesions. *Lung Cancer.* (2016) 102:89–95. doi: 10.1016/j.lungcan.2016.10.016
51. Hufnagl K, Pali-Scholl I, Roth-Walter F, Jensen-Jarolim E. Dysbiosis of the gut and lung microbiome has a role in asthma. *Semin Immunopathol.* (2020) 42:75–93. doi: 10.1007/s00281-019-00775-y
52. Li R, Chen X, Liu Z, Chen Y, Liu C, Ye L, et al. Characterization of gut microbiota associated with clinical parameters in intrahepatic cholestasis of pregnancy. *BMC Gastroenterol.* (2020) 20:395. doi: 10.1186/s12876-020-01510-w
53. Jia W, Zhen J, Liu A, Yuan J, Wu X, Zhao P, et al. Long-term vegan meditation improved human gut microbiota. *Evid Based Complement Alternat Med.* (2020) 2020:9517897. doi: 10.1155/2020/9517897
54. Song H, Xiao K, Chen Z, Long Q. Analysis of conjunctival sac microbiome in dry eye patients with and without Sjogren's syndrome. *Front Med.* (2022) 9:841112. doi: 10.3389/fmed.2022.841112
55. Marques FZ, Mackay CR, Kaye DM. Beyond gut feelings: how the gut microbiota regulates blood pressure. *Nat Rev Cardiol.* (2018) 15:20–32. doi: 10.1038/nrcardio.2017.120
56. Parker BJ, Wearsch PA, Veloo ACM, Rodriguez-Palacios A. The genus alistipes: gut bacteria with emerging implications to inflammation, cancer, and mental health. *Front Immunol.* (2020) 11:906. doi: 10.3389/fimmu.2020.00906
57. Qin J, Li Y, Cai Z, Li S, Zhu J, Zhang F, et al. A metagenome-wide association study of gut microbiota in type 2 diabetes. *Nature.* (2012) 490:55–60. doi: 10.1038/nature11450
58. Karlsson FH, Tremaroli V, Nookaew I, Bergstrom G, Behre CJ, Fagerberg B, et al. Gut metagenome in European women with normal, impaired and diabetic glucose control. *Nature.* (2013) 498:99–103. doi: 10.1038/nature12198
59. Hong W, Mo Q, Wang L, Peng F, Zhou Y, Zou W, et al. Changes in the gut microbiome and metabolome in a rat model of pulmonary arterial hypertension. *Bioengineered.* (2021) 12:5173–83. doi: 10.1080/21655979.2021.1952365
60. Chan SY, Rubin LJ. Metabolic dysfunction in pulmonary hypertension: from basic science to clinical practice. *Eur Respir Rev.* (2017) 26:170094. doi: 10.1183/16000617.0094-2017
61. Liu D, Qin S, Su D, Wang K, Huang Y, Huang Y, et al. Metabolic reprogramming of the right ventricle and pulmonary arteries in a flow-associated pulmonary arterial hypertension rat model. *ACS Omega.* (2022) 7:1273–87. doi: 10.1021/acsomega.1c05895
62. Savale L, Akagi S, Tu L, Cumont A, Thuillet R, Phan C, et al. Serum and pulmonary uric acid in pulmonary arterial hypertension. *Eur Respir J.* (2021) 58:2000332. doi: 10.1183/13993003.00332-2020
63. Chen C, Luo F, Wu P, Huang Y, Das A, Chen S, et al. Metabolomics reveals metabolite changes of patients with pulmonary arterial hypertension in China. *J Cell Mol Med.* (2020) 24:2484–96. doi: 10.1111/jcmm.14937
64. Wang S, Tan KS, Beng H, Liu F, Huang J, Kuai Y, et al. Protective effect of isosteviol sodium against LPS-induced multiple organ injury by regulating of glycerophospholipid metabolism and reducing macrophage-driven inflammation. *Pharmacol Res.* (2021) 172:105781. doi: 10.1016/j.phrs.2021.105781
65. Hu Y, Chi L, Kuebler WM, Goldenberg NM. Perivascular inflammation in pulmonary arterial hypertension. *Cells.* (2020) 9:2338. doi: 10.3390/cells9112338
66. Yoshida K, Yoshida K, Fujiwara N, Seyama M, Ono K, Kawai H, et al. Extracellular vesicles of *P. gingivalis*-infected macrophages

induce lung injury. *Biochim Biophys Acta Mol Basis Dis.* (2021) 1867:166236. doi: 10.1016/j.bbadis.2021.166236
67. Liang S, Desai AA, Black SM, Tang H. Cytokines, chemokines, and inflammation in pulmonary arterial hypertension. *Adv Exp Med Biol.* (2021) 1303:275–303. doi: 10.1007/978-3-030-63046-1_15
68. Huertas A, Tu L, Humbert M, Guignabert C. Chronic inflammation within the vascular wall in pulmonary arterial hypertension: more than a spectator. *Cardiovasc Res.* (2020) 116:885–93. doi: 10.1093/cvr/cvz308
69. Okumura S, Konishi Y, Narukawa M, Sugiura Y, Yoshimoto S, Arai Y, et al. Gut bacteria identified in colorectal cancer patients promote tumourigenesis via butyrate secretion. *Nat Commun.* (2021) 12:5674. doi: 10.1038/s41467-021-25965-x
70. Olsen I, Kell DB, Pretorius E. Is *Porphyromonas gingivalis* involved in Parkinson's disease? *Eur J Clin Microbiol Infect Dis.* (2020) 39:2013–8. doi: 10.1007/s10096-020-03944-2
71. Ubags NDJ, Marsland BJ. Mechanistic insight into the function of the microbiome in lung diseases. *Eur Respir J.* (2017) 50:1602467. doi: 10.1183/13993003.02467-2016
72. Marsh RL, Kaestli M, Chang AB, Binks MJ, Pope CE, Hoffman LR, et al. The microbiota in bronchoalveolarlavage from young children with chronic lung disease includes taxa present in both the oropharynx and nasopharynx. *Microbiome.* (2016) 4:37. doi: 10.1186/s40168-016-0182-1

Conflict of Interest: The authors declare that the research was conducted in the absence of any commercial or financial relationships that could be construed as a potential conflict of interest.

frontiers | Frontiers in Medicine

TYPE Original Research
PUBLISHED 20 September 2022
DOI 10.3389/fmed.2022.908639

OPEN ACCESS

EDITED BY
Elena Goncharova,
University of California, Davis,
United States

REVIEWED BY
Laszlo Farkas,
The Ohio State University,
United States
Wen Tian,
Stanford University, United States

*CORRESPONDENCE
Akiko Mammoto
amammoto@mcw.edu
Tadanori Mammoto
tmammoto@mcw.edu

†These authors have contributed equally to this work

SPECIALTY SECTION
This article was submitted to Pulmonary Medicine, a section of the journal Frontiers in Medicine

RECEIVED 30 March 2022
ACCEPTED 29 August 2022
PUBLISHED 20 September 2022

CITATION
Kyi P, Hendee K, Hunyenyiwa T, Matus K, Mammoto T and Mammoto A (2022) Endothelial senescence mediates hypoxia-induced vascular remodeling by modulating PDGFB expression. *Front. Med.* 9:908639. doi: 10.3389/fmed.2022.908639

Endothelial senescence mediates hypoxia-induced vascular remodeling by modulating PDGFB expression

Priscilla Kyi[1,2], Kathryn Hendee[1], Tendai Hunyenyiwa[1,2], Kienna Matus[1], Tadanori Mammoto[1,3*†] and Akiko Mammoto[1,2*†]

[1]Department of Pediatrics, Medical College of Wisconsin, Milwaukee, WI, United States, [2]Department of Cell Biology, Neurobiology and Anatomy, Medical College of Wisconsin, Milwaukee, WI, United States, [3]Department of Pharmacology and Toxicology, Medical College of Wisconsin, Milwaukee, WI, United States

Uncontrolled accumulation of pulmonary artery smooth muscle cells (PASMCs) to the distal pulmonary arterioles (PAs) is one of the major characteristics of pulmonary hypertension (PH). Cellular senescence contributes to aging and lung diseases associated with PH and links to PH progression. However, the mechanism by which cellular senescence controls vascular remodeling in PH is not fully understood. The levels of senescence marker, $p16^{INK4A}$ and senescence-associated β-galactosidase (SA-β-gal) activity are higher in PA endothelial cells (ECs) isolated from idiopathic pulmonary arterial hypertension (IPAH) patients compared to those from healthy individuals. Hypoxia-induced accumulation of α-smooth muscle actin (αSMA)-positive cells to the PAs is attenuated in *p16*$^{fl/fl}$*-Cdh5(PAC)-Cre*^{ERT2} (*p16*$^{i\Delta EC}$) mice after tamoxifen induction. We have reported that endothelial TWIST1 mediates hypoxia-induced vascular remodeling by increasing platelet-derived growth factor (PDGFB) expression. Transcriptomic analyses of IPAH patient lungs or hypoxia-induced mouse lung ECs reveal the alteration of senescence-related gene expression and their interaction with TWIST1. Knockdown of $p16^{INK4A}$ attenuates the expression of PDGFB and TWIST1 in IPAH patient PAECs or hypoxia-treated mouse lungs and suppresses accumulation of αSMA–positive cells to the supplemented ECs in the gel implanted on the mouse lungs. Hypoxia-treated mouse lung EC-derived exosomes stimulate DNA synthesis and migration of PASMCs *in vitro* and in the gel implanted on the mouse lungs, while *p16*$^{i\Delta EC}$ mouse lung EC-derived exosomes inhibit the effects. These results suggest that endothelial senescence modulates TWIST1-PDGFB signaling and controls vascular remodeling in PH.

KEYWORDS

pulmonary hypertension, hypoxia, endothelial cell, senescence, TWIST1, PDGFB

Introduction

PH is a cardiopulmonary disorder characterized by a sustained elevation of PA pressure, resulting in right-side heart failure and eventual death (1–4). Remodeling of distal PAs is a key feature of PH and involves marked accumulation of PASMCs to normally non-muscularized distal PAs, which narrows and blocks the PAs, increasing PA pressure (5, 6). ECs secrete angiocrine factors and regulate various physiological functions (7, 8). Disrupted PAEC signaling and dysfunctional secretion of angiocrine factors stimulate PASMC proliferation and accumulation to distal PAs (3, 9–11), highlighting EC dysfunction as a critical contributor to PH pathology.

Accumulation of senescent cells, the cells that irreversibly lose the ability to proliferate (12), promotes aging and exacerbates age-related pathologies (12–18), including chronic lung disease (19–21) and cancer (22–24). Although senescent cells are unable to replicate, they secrete senescence-associated secretory phenotype (SASP) factors such as inflammatory cytokines, chemokines, growth factors, and proteases (13, 18, 25–28), which allow the cells to be metabolically active. Senescent ECs play a key role in vascular aging and age-related cardiovascular and degenerative diseases (12, 13, 15), and senolytic reagents are extensively studied in the aging research (28, 29). Cellular senescence also contributes to idiopathic pulmonary fibrosis (IPF) and chronic obstructive pulmonary disease (COPD) (19–21) associated with PH (30, 31). Recently, it is reported that EC senescence is involved in PH (32, 33), however the underlying mechanism is not fully understood.

TWIST1 is a bHLH family transcription factor and contributes to chronic lung diseases associated with PH such as IPF (31, 34, 35). We have reported that TWIST1 is upregulated in IPAH patients-derived PAECs and mediates hypoxia-induced increases in right ventricular systolic pressure (RVSP) and accumulation of PASMCs to PAs (11, 36). TWIST1 contributes to age-dependent inhibition of angiogenesis and lung regeneration (37) and is involved in cellular senescence to promote tumor cell proliferation (38), suggesting that endothelial TWIST1 and senescence may contribute to vascular remodeling in PH.

Exosomes are one of the types of extracellular vesicles with size typically from 30 to 150 nm in diameter and contain various proteins, lipids, and nucleic acids (DNA, mRNA, miRNA, non-coding RNA) (39–41). Exosomes are produced by ECs and other cell types, and serve as a messenger of signals for cell-cell communications (39–43). Exosomes also remove unused or harmful molecules and proteins (39, 40, 42, 44, 45) to maintain tissue homeostasis in normal physiology and contribute to disease pathology [e.g., aging (46), cancer (45), atherosclerosis (47)]. SASP factors such as inflammatory cytokines, membrane organization and signaling proteins (48, 49) are enriched in exosomes from senescence cells (50), which constitutes part of the SASP and mediates paracrine effects on the microenvironment (45, 51, 52). It has been reported that human mesenchymal stem cell (MSC)-derived exosomes suppress PH and other lung diseases such as bronchopulmonary dysplasia (BPD), airway inflammation, and pulmonary fibrosis in animal models (53–61). We have demonstrated that exosomes collected from ECs promote angiogenesis (41). However, the role of EC-derived exosomes in PH pathology has not been well characterized.

Here we have demonstrated that EC senescence modulates TWIST1-PDGFB signaling and mediates hypoxia-induced αSMA-positive cell accumulation to PAs in the mouse lungs. Inhibition of EC senescence suppresses accumulation of αSMA-positive cells to IPAH patient lung ECs and exosomes collected from $p16^{INK4A}$ knocked down ECs inhibit hypoxia-induced αSMA-positive cell recruitment in the gel implanted on the mouse lungs. Understanding the mechanism by which EC senescence mediates vascular remodeling in PH will lead to the development of novel therapeutics to manage PH and exosomes derived from ECs, in which cellular senescence is modulated, could be one of the sound strategies to prevent PH.

Materials and methods

Materials

Anti-$p16^{INK4A}$, -TWIST1, -PDGFB, -VE-cadherin, -SLUG, -ERG, and -αSMA antibodies were purchased from Abcam (Cambridge, MA). Anti-p21 and -Flotillin-1 antibodies were from Cell Signaling (Danvers, MA). Anti-GM130 antibody was from BD Biosciences (Franklin Lakes, NJ). Anti-CD63 antibody was from Santa Cruze Biotechnology (Dallas, TX). Phospho-gamma-H2AX (Ser139) antibody was from Thermo Fisher Scientific (Waltham, MA). β-actin antibody was from Sigma (Burlington, MA). ABT-263 was purchased from Selleckchem (Houston, TX). Human pulmonary artery smooth muscle cells (HPASMCs) were purchased from Lonza and cultured in DMEM containing 5% FBS.

De-identified human IPAH patient ECs were obtained from unused donor control lungs at time of transplantation *via* the Pulmonary Hypertension Breakthrough Initiative (PHBI) Network, which is funded by the Cardiovascular Medical and Education Fund (CMREF) and NIH-NHLBI. The study using these de-identified human cells has been determined and approved as Non-Human Subjects Research by the Medical College of Wisconsin Institutional Review Board (IRB PRO00029154). We obtained ECs isolated from PA (>5 mm in diameter) from females and males (5 control samples; 45.6 ± 2.6 years old, 5 IPAH samples; 34.4 ± 2.5 years old). The patient demographic information is in Table 1. These ECs were cultured in ECM medium containing 5% FBS and growth factors (VEGF, bFGF and PDGF, Science Cell, Carlsbad, CA).

TABLE 1 Sample demographics.

ID	Age	Sex	Race
Con-1	36	Female	White
Con-2	45	Female	White
Con-3	47	Male	White
Con-4	49	Female	White
Con-5	51	Male	White
PAH-1	27	Female	White
PAH-2	32	Male	White
PAH-3	33	Female	White
PAH-4	40	Male	White
PAH-5	40	Female	White

Plasmid construction and gene knockdown

ON-TARGET plus human $p16^{INK4A}$ siRNA SMARTPool was purchased from Horizon Discovery (Lafayette, CO). As a control, siRNA with irrelevant sequences was used (36, 41). Lentiviral construct targeting human $p16^{INK4A}$ ($p16^{INK4A}$ shRNA, CCGGAGTAACCATGCCCGCATAGATCTCGA-GATCTATGCGGGCATGGTTACTTTTTTG) was obtained from Sigma. As a control, plasmid with vector only was used. Generation of lentiviral vectors was accomplished by a five-plasmid transfection procedure as reported (36, 41, 62). Viral supernatants were collected starting 48 h after transfection, for four consecutive times every 12 h, pooled, and filtered through a 0.45 μm filter. Viral supernatants were then concentrated 100-fold by ultracentrifugation in a Beckman centrifuge for 1.5 h at 16,500 rpm. PAECs were incubated with viral stocks in the presence of 5 μg/ml polybrene (Sigma) and 90–100% infection was achieved 3 days later (41, 62).

Molecular biological and biochemical methods

Quantitative reverse transcription (qRT)-PCR was performed with the iScript reverse transcription and iTaq SYBR Green qPCR kit (BioRad, Hercules, CA) using the BioRad real time PCR system (BioRad). β2 microglobulin and cyclophilin controlled for overall cDNA content as a reference gene. The primers used for human β2 microglobulin, human TWIST1, mouse Twist1, and mouse cyclophilin were previously described (35, 36, 62, 63). Human $p16^{INK4A}$ primers, forward; GATCCAGGTGGGTAGAAGGTC, reverse; CCCCTGCAAACTTCGTCCT, human p21 primers, forward; TGTCCGTCAGAACCCATGC, reverse; AAAGTCGAAGTTCCATCGCTC, mouse $p16^{INK4A}$ primers, forward; CGCAGGTTCTTGGTCACTGT, reverse; TGTTCACGAAAGCCAGAGCG, mouse αSMA primers, forward; CCCAGACATCAGGGAGTAATGG, reverse; TCTATCGGATACTTCAGCGTCA, and mouse Pdgfb primers forward; CATCCGCTCCTTTGATCTT, reverse; GTGCTCGGGTCATGTTCAAGT. The protein levels of human PDGFB were measured using ELISA (R&D systems, Minneapolis, MN) and normalized by the protein levels of total cell lysate. Senescence β-galactosidase activity was measured using SA β-gal staining kit (Cell Signaling).

Mouse hypoxic exposure model *in vivo*

The *in vivo* animal study was carried out in strict accordance with the recommendations in the Guide for the Care and Use of Laboratory Animals of the National Institutes of Health. The protocols were reviewed and approved by the Animal Care and Use Committee of Medical College of Wisconsin. $p16^{fl/fl}$ mice (B6;129S4-*Cdkn2a*$^{tm2.1Nesh}$/Mmnc, 043540-UNC, MMRRC) (64) were crossed with *Cdh5(PAC)-Cre*^{ERT2} mice [obtained from Dr. Ralf Adams (65)] to develop $p16^{i\Delta EC}$ mice. Eight to Ten-week old male $p16^{i\Delta EC}$, $p16^{fl/fl}$, and *Cdh5(PAC)-Cre*^{ERT2} mice as a control were treated with tamoxifen (125 μg/mouse, 5 days), housed in plexiglass chambers, and exposed to 8.5 ± 0.5% O_2 for 3 weeks. After 3 weeks of exposure, right ventricular systolic pressure (RVSP) was measured (36); after IP injection of ketamine/xylazine, right jugular vein was exposed and a pressure transducer catheter (Millar Instruments, Houston, TX) was inserted into the jugular vein *via* a minimal incision. The catheter was advanced into the right ventricle and the position of the catheter was confirmed by the ventricular wave form. RVSP measurements were recorded and analyzed using a Quad Bridge Amplifier connected to a Power Lab device (AD Instruments, Colorado Springs, CO). We also measured Fulton's index; hearts and pulmonary vasculature were perfused *in situ* with cold 1X PBS injection into the right ventricle (RV); hearts were excised and used for Fulton's Index measurements (ratio of RV weight over left ventricle (LV) plus septal (S) weight, RV/[LV + S]) (36). Both ventricles were weighed first, then the right ventricular free wall was dissected and the remaining LV and ventricular septum was weighed. For pulmonary histological analysis, lungs were inflated by tracheotomy and perfused with 4% paraformaldehyde (PFA), excised, and fixed in 4% PFA overnight at 4°C followed by OCT embedding and cryosectioning.

Mouse EC isolation

Mouse lung ECs were isolated from tamoxifen-induced $p16^{i\Delta EC}$ or $p16^{fl/fl}$ mouse lungs using anti-CD31 conjugated magnetic beads (41, 66). We cut lung tissue from $p16^{i\Delta EC}$ or

$p16^{fl/fl}$ mouse into small pieces using small scissors and treated the tissue with collagenase A (5 ml, 1 mg/ml) for 30 min at 37°C. The tissue suspension was filtered through a 40 μm cell strainer (Falcon) to remove the undigested cell clumps and separate single cells. Cells were centrifuged (1,000 rpm, 5 min) at room temperature (RT) and the pellet was resuspended into 0.5 ml RBC Lysis Buffer (sigma, 1 min, RT). The lysis reaction was stopped by adding 10 ml 10% FBS/DMEM, centrifuged (1,000 rpm, 5 min, RT), and the pellet was resuspended into 0.5 ml 4% FBS/PBS with APC anti-mouse CD31 (Biolegend, 1/100), incubated (20 min, on ice) and washed three times with 4% FBS/PBS. Cells were centrifuged (1,000 rpm, 5 min, RT) and resuspended into 0.1 ml 4% FBS/PBS with anti-APC conjugated microbeads (Miltenyl Biotec, Somerville, MA), incubated (10 min, on ice) and washed three times with 4% FBS/PBS. The cells were then resuspended in 0.5 ml 4% FBS/PBS and CD31-positive ECs were magnetically separated using MACS column (Miltenyi Biotec) according to manufacturer's instruction. To increase the purity of the magnetically separated fraction, the eluted fraction was enriched over a second new MACS column. Using this method, we obtained 5×10^5 cells/mouse and FACS analysis confirmed that more than 80% of the cells are $CD31^+$ and VE-$cadherin^+$ cells [not shown (41, 66)].

Fibrin gel implantation on the mouse lung

Fibrin gel was fabricated as described (35, 36, 41, 66, 67). Briefly, we added thrombin (2.5 U/ml) to the fibrinogen solution (12.5 mg/ml), mixed well, supplemented the gel with human ECs labeled with GFP using lentiviral transduction (1×10^6 cells), incubated the mixture at 37°C for 30 min until they solidified, and implanted on non-obese diabetic/severe combined immunodeficiency gamma (NSG, Jackson Laboratories, stock # 005557) mouse lungs. We also supplemented the gel with exosomes (5 μg/gel) isolated from tamoxifen-induced and hypoxia-treated $p16^{i\Delta EC}$ or $p16^{fl/fl}$ mouse lung ECs, incubated the mixture at 37°C for 30 min until they solidified, and implanted on $p16^{fl/fl}$ mouse lungs. We used NSG mice for implantation of gel supplemented with human ECs to enhance engraftment of cells in the gel. In case of implantation of gel containing exosomes isolated from $p16^{fl/fl}$ or $p16^{i\Delta EC}$ mouse lung ECs, we used a syngeneic mouse implantation model, in which gel was implanted on the mouse of the same genetic background ($p16^{fl/fl}$). Since the syngeneic mice retain intact immune systems, we selected this model rather than the immunocompromised NSG mouse model when we don't implant human cells. It is known that the NOD genetic background eliminates hemolytic complement and reduces dendritic cell and macrophage functions to inhibit immune system. NOD mice also express a unique variant of the Sirp-alpha protein to superior human cell engraftment. To date, NSG mouse line is one of the most standard mouse lines for human cell engraftment and therefore, we have been using NSG mice for our human cell implantation (11, 36, 37, 68–70). It is important to note that diabetes in NOD mice results from an autoimmune response, in which endogenous T cells attack and destroy beta cells in the pancreas, and therefore immune-deficient NOD-*scid* mice that lack these T cells do not become diabetic. For gel implantation on the mouse lungs, NSG or $p16^{fl/fl}$ mice were mechanically ventilated and thoracotomy was performed in the fifth left intercostal space (35, 36, 41, 66, 67). After thoracotomy, a small area of the left visceral pleura (0.5 mm^2) was scraped using forceps and the fabricated fibrin gel was implanted on the mouse lung surface using fibrin glue. For histological analysis, gels were fixed in 4% PFA overnight at 4°C followed by OCT embedding and cryosectioning. Fluorescent images were taken on a Nikon A1 confocal imaging system. Fluorescently labeled supplemented EC-derived vascular structures and accumulation of αSMA-positive cells in the gel were evaluated in five different areas of the gel using ImageJ software (35, 36, 41, 62, 66, 67).

Microarray data analysis

Publicly available microarray datasets from 6 IPAH patient lungs and 11 healthy adult human frozen lung tissues (NCBI GEO, GSE113439) were utilized, and differential gene expression analysis was performed by GEO2R. The total number of genes identified by the array was 33,297, with 19,919 being downregulated and 13,378 upregulated. Of these, 790 downregulated and 1,285 upregulated genes possessed adjusted p-values < 0.001 following Benjamini and Hochberg false discovery rate multiple-testing correction of p-values, resulting in a total of 2,075 significantly differentially expressed genes. The 2,075 significantly differentially expressed genes underwent Biological Processes Gene Ontology (BP GO) Term analysis through the Functional Annotation Chart tool of the Database for Annotation, Visualization, and Integrated Discovery (DAVID) software, v6.8, and total 235 BP GO term categories were identified (Supplementary Table 1). Among these total 235 GO Term categories, 113 BP GO Term categories contain genes related to SASP/senescence and classified into transcription/gene expression, protein/RNA processing, cell cycle, inflammatory/immune response, cell signaling/signal transduction, or miscellaneous groups (Supplementary Table 2). To select GO Terms linked to Senescence/SASP, we used the master list curated from the literature [SASP Atlas (71), CellAge: the Database of cell senescence Genes https://genomics.senescence.info/cells/query.php]. Although the senescence/SASP genes were originally identified using biased analysis including the antibody arrays which selectively measure the secretion of pro-inflammatory cytokines, proteases and protease inhibitors, and growth factors, a recent comprehensive proteomic analysis demonstrated

that SASP is more dynamic and heterogeneous dependent on cell types and senescence inducers. Therefore, we utilized unbiased genomic and proteomic database [SASP Atlas (71), CellAge] to create the master list that includes diverse senescence/SASP and aging genes, which covers broad range of genes related to senescence/SASP, while containing genes of normal pathways such as cell division, cell adhesion indirectly related to senescence/SASP. All genes from 113 BP GO Term categories containing senescence/SASP genes were made into a network and color-coded using Ingenuity Pathway Analysis (IPA) software. These genes were linked to TWIST1 and PDGFB agnostically by adding TWIST1 and PDGFB to the network. Basically, we identified (1) the shortest interaction between TWIST1 and all genes from 113 BP GoTerms, (2) the shortest interaction between PDGFB and all genes from 113 BP GoTerms, and (3) the shortest interaction between the genes from TWIST1 network and PDGFB networks. In the resulting network, all genes that are connected to <4 nodes are removed to reduce the number of genes in the interactome. In a separate analysis, we confirmed the involvement of narrower categories of major senescence/SASP genes (e.g., pro-inflammatory cytokines, proteases and protease inhibitors, and growth factors) using a master list curated from the literature (32); The 128 major senescence/SASP genes were identified in the total number of genes identified by the array (33,297). These senescence/SASP genes were further narrowed down following Benjamini and Hochberg false adjustment and filtered to adjusted p-values of <0.05, resulting in a total of 31 significantly differentially expressed senescence/SASP genes, with 16 being significantly downregulated and 15 being significantly upregulated (Supplementary Figure 1C). Heatmaps of these senescence/SASP-related genes were generated in Excel using data from the profile graph generated by GEO2R.

RNA sequencing and analysis

ECs were isolated from male C57BL6 mouse lungs treated with normoxia or hypoxia for 3 weeks (8 week old, $n = 3$ per group) using anti-CD31 conjugated magnetic beads (41, 66) and isolated ECs were validated by FACS for EC markers ($CD31^+$, VE-$Cadherin^+$, $CD45^-$). RNA was extracted using RNeasy mini kit (QIAGEN). Total RNA samples were submitted to the Institute for Systems Biology Molecular and Cell Core (Seattle, WA) for RNA sequencing. Library preparation was employed using the Illumina TruSeq Stranded mRNA kit. Sequencing was performed using the Illumina NextSeq500. Paired end sequencing was performed on a high output 150 cycle kit v2.5. The RNA sequencing reads were aligned to the mouse genome (mm10 reference genome). Differential gene expression analysis and Fragments Per Kilobase Million (FPKM) calculation were performed with Basepair Tech (www.basepairtech.com) using the DEseq2 pipeline. Significantly differentially expressed genes (335 upregulated and 403 downregulated) were defined as having a log2 fold change >1, and a p-adjusted value calculated by the Benjamini-Hochberg adjustment and filtered to <0.05 (Supplementary Table 3). BP GO Term analysis of significant targets was done *via* DAVID v 6.8 using the Functional Annotation Chart tool. Charts were filtered by BP GO Terms and sorted by p-value. The 317 BP GO term categories were identified (Supplementary Table 4). Genes related to cellular senescence or the SASP gathered from the GeneCards and CellAge database were agnostically identified in the 178 BP GO Term categories (Supplementary Table 5). The top 50 BP GO Terms were color-coded into groups relating to: transcription/gene expression, protein/RNA processing, cell cycle, inflammatory/immune response, and cell signaling/signal transduction (Supplementary Figure 3A). All genes from top 50 BP GO Term categories containing senescence and SASP genes were made into a network and color-coded using IPA software. The network mapped the shortest interactions among Twist1, Pdgfb, and the genes from top 50 BP GO Term categories related to cellular senescence and SASP. The 133 major senescence and SASP genes curated from literature (32) were identified in the total number of genes identified by the Basepair (19,068). These 133 senescence/SASP genes were further narrowed down to adjusted p-values of <0.05 following Benjamini and Hochberg false discovery rate multiple-testing correction of p-values, resulting in a total of 14 significantly differentially expressed senescence/SASP genes, with 7 being downregulated and 7 being upregulated. Heatmaps of the 7 upregulated and 7 downregulated senescence/SASP-related genes were generated by Basepair. RNAseq results are available in NCBI Geo (GSE193272).

Exosome isolation

ECs isolated from tamoxifen-induced $p16^{i\Delta EC}$ or $p16^{fl/fl}$ mouse lungs were plated (1×10^6 cells per 6 cm dish), cultured with media containing exosome free FBS, and conditioned media was collected after 24 h. Exosomes were isolated using Total Exosome Isolation Reagent from Cell Culture Media (Thermo Fisher Scientific, Waltham, MA) according to the manufacturer's protocol (41, 72). The exosome pellet was resuspended in 25 μl of 0.2 μm filtered PBS. Isolated exosomes were confirmed with exosome marker proteins (CD63, flotillin-1) using immunoblotting (IB). For transmission electron microscopy (TEM) to analyze the ultrastructure of the exosome, resuspended exosomes were adsorbed onto freshly ionized, 400 mesh formvar/carbon grids, washed once with distilled water, and negatively stained with 2% aqueous Uranyl acetate. Exosome preparations were viewed in a Hitachi H600 transmission electron microscope and images were recorded with a Hamamatsu ccd camera using AMT image capture software. Size and concentration distributions of exosomes

were determined using nanoparticle tracking analysis (NTA; NanoSight LM10 system, Malvern instruments, Malvern, UK) (41, 72).

In vitro cell biological assay

HPASMCs (DMEM with 2% serum) were treated with exosomes isolated from tamoxifen-induced $p16^{i\Delta EC}$ or $p16^{fl/fl}$ mouse lung ECs with or without hypoxia treatment, and DNA synthesis of HPASMCs was analyzed by an EdU assay (36, 41, 70). HPASMC migration was analyzed using a modified transwell migration assay (41, 70). The cells that migrated toward the 0.5% serum DMEM or supplemented with exosomes (10 μg/ml) through the membrane were stained with Giemsa and counted.

Proteomics analysis

Proteomics analysis was performed by the Northwestern University Proteomics Core Facility (41) and the Mass Spectrometry Technology Access Center at McDonnell Genome Institute (MTAC@MGI) at Washington University School of Medicine. Isolated exosomes (100 μg) were briefly tip sonicated (∼10 s) to break the exosome membrane and purified proteins by acetone/TCA precipitation. Then, the proteins were reduced, alkylated, and digested with trypsin according to the optimized protocol. Digested peptides were desalted on C18 columns then subjected to mass spec analysis. Data was searched against a *Mus musculus* database. Proteomics data analysis on three control (normoxia) and three hypoxia (3 weeks) treated C57BL6 mouse lung EC exosome replicates was performed using Scaffold 5.1.0 software. Total 438 proteins were identified in the control and hypoxia sample replicates (Supplementary Table 6). A cutoff threshold of <8 Total Spectrum Counts in at least one overall replicate was used to further narrow the list of protein of interest, resulting in 37 proteins. Among them, 10 proteins were significantly differentially expressed in the hypoxia- vs. normoxia-treated exosomes. Out of 37 proteins, 30 SASP related proteins were identified using the "SASP Atlas" (50). These 30 SASP related proteins underwent BP GO analysis *via* the Functional Annotation Chart feature of the DAVID v6.8 software and the 51 BP GO term categories were identified (Supplementary Table 7, red bold: significantly differentially expressed proteins). The proteomics data are available *via* ProteomeXchange with identifier PXD033549.

Statistical analysis

All phenotypic analysis was performed by masked observers unaware of the identity of experimental groups. Error bars (SEM) and *p*-values were determined from the results of three or more independent experiments. Student's *t*-test was used for statistical significance for two groups. For more than two groups, one-way ANOVA with a *post-hoc* analysis using the Bonferroni test was conducted.

Results

Senescence increases in IPAH patient PAECs *in vitro*

It has been reported that cellular senescence contributes to PH pathology (32, 33), however, the mechanism by which EC senescence controls PH phenotype is not fully understood. Differential expression analysis of publicly available microarray data (GSE113439) comparing 11 control and 6 IPAH patient lungs resulted in 2,075 genes with known gene names at a significance threshold of adjusted p-value < 0.001. These genes were sorted into BP GO term categories and 113 BP GO Term categories were found to contain 48 senescence/SASP related genes compiled from the GeneCards database (Supplementary Table 2; Figure 1A; Supplementary Figure 1B). In the separate analysis, 128 major senescence/SASP genes selectively related to pro-inflammatory cytokines, proteases and protease inhibitors, and growth factors curated from literature (32) were identified in the total number of genes (33,297). These senescence/SASP genes were further narrowed down following Benjamini and Hochberg false adjustment and filtered to adjusted p-values of <0.05, resulting in 16 downregulated and 15 upregulated genes identified (Supplementary Figure 1C). Gene network analysis of microarray dataset using IPA software reveals that genes from 113 BP GO Term categories containing cellular senescence/SASP genes of normal vs. IPAH patient lungs, which is classified into transcription/gene expression, protein/RNA processing, cell cycle, inflammatory/immune response, cell signaling/signal transduction, or miscellaneous groups, directly or indirectly interacted with TWIST1 (Supplementary Figure 1A). Endothelial TWIST1 mediates hypoxia-induced vascular remodeling by increasing PDGFB expression (11). Although the direct link between TWIST1 and PDGFB was not identified, significantly differentially expressed genes of healthy vs. IPAH patient lungs that interacted with TWIST1 also interacted with PDGFB (Supplementary Figure 1A).

Consistent with microarray data, the mRNA levels of major senescence markers $p16^{INK4A}$ and p21 were 1.8- and 1.5-times higher, respectively, in IPAH patient-derived PAECs compared to those in control healthy PAECs (Figure 1B). Immunocytochemical (ICC) and immunoblotting (IB) data confirmed that the expression of $p16^{INK4A}$ and p21 is upregulated in the PAECs of IPAH patients (Figure 1C; Supplementary Figure 2A). SA β-Gal activity and an early

A

Biological Processes	PValue	Fold Enrichment
DNA repair	3.20154E-09	2.325100449
transcription, DNA-templated	9.11255E-08	1.347530357
cell division	1.48872E-07	1.923546111
regulation of transcription, DNA-templated	1.96299E-07	1.394800771
cell-cell adhesion	1.23134E-06	1.980226891
cellular response to DNA damage stimulus	2.27992E-06	2.110914942
mRNA splicing, via spliceosome	2.46414E-06	2.065696144
protein sumoylation	4.88597E-06	2.501825117
ubiquitin-dependent protein catabolic process	1.49348E-05	2.09081099
DNA duplex unwinding	1.73993E-05	3.548042893
double-strand break repair	7.88521E-05	2.80886729
sister chromatid cohesion	9.06157E-05	2.368232513
covalent chromatin modification	0.000158532	2.245000591
DNA replication	0.000201123	2.014372739
mitotic sister chromatid cohesion	0.000209305	5.575495974
chromatin remodeling	0.000348403	2.382552059
mitotic nuclear division	0.000397589	1.731101573
DNA synthesis involved in DNA repair	0.000513139	3.345297584
RNA processing	0.000697536	2.212954588
positive regulation of intracellular protein transport	0.00102101	3.991548254
G2/M transition of mitotic cell cycle	0.001420001	1.922935655
rRNA processing	0.001953008	1.686978338
I-kappaB kinase/NF-kappaB signaling	0.002490947	2.439279489
strand displacement	0.003439212	3.377463907
telomere maintenance via recombination	0.003839584	3.049099361
DNA recombination	0.004000656	2.116001484
cell cycle	0.004518348	1.61869238
viral process	0.005463545	1.50109507
mRNA export from nucleus	0.005778439	1.951423591
viral entry into host cell	0.006538601	2.073387565
protein K63-linked deubiquitination	0.006546603	3.393780158
ER-associated ubiquitin-dependent protein catabolic proc	0.006834964	2.276660856
nucleic acid phosphodiester bond hydrolysis	0.008303827	2.081518497
telomere maintenance	0.008871759	2.710310543
proteasome-mediated ubiquitin-dependent protein catabol	0.008978345	1.586132475

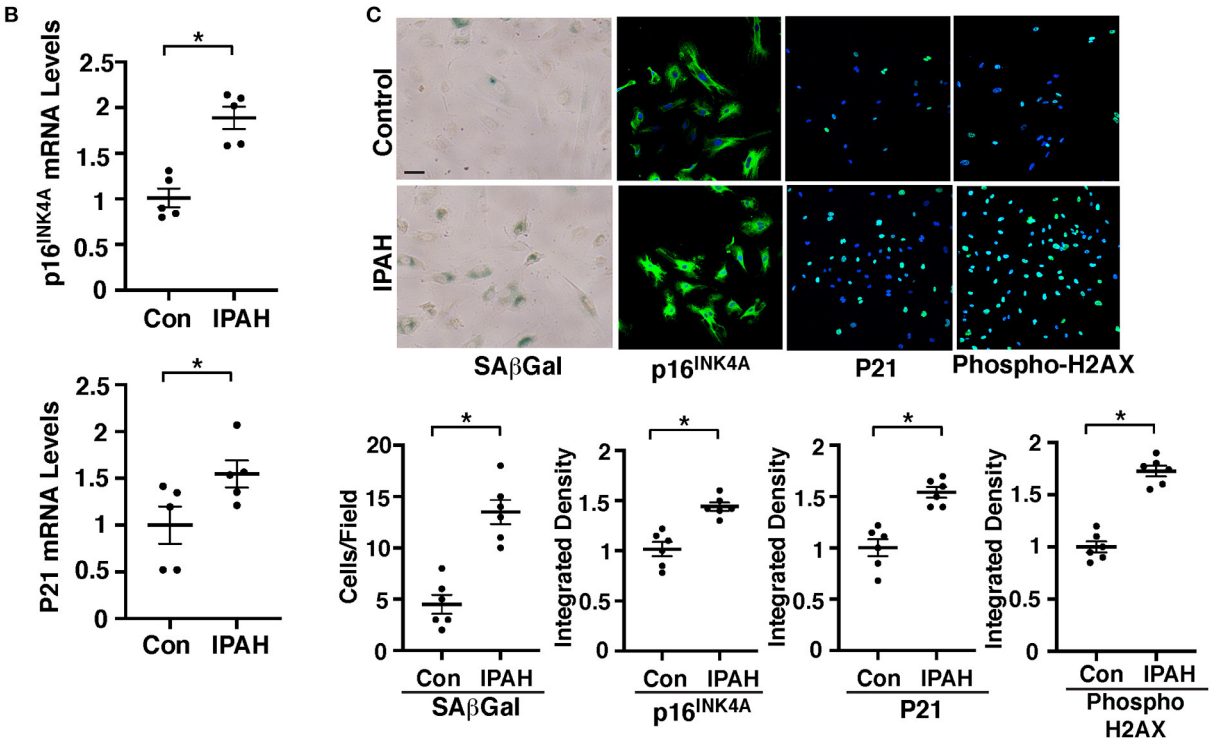

FIGURE 1
EC senescence increases in IPAH patient lung ECs. **(A)** List of top 35 BP GO term categories derived from significantly differentially expressed genes related to cellular senescence and SASP in control vs. IPAH patient lungs. **(B)** Graphs showing the mRNA levels of $p16^{INK4A}$ (*top*) and p21 (*bottom*) in PAECs from IPAH patients or healthy individuals ($n = 5$, $*p < 0.05$). Error bars represent SEM. **(C)** Micrographs of PAECs from IPAH patients or healthy individuals showing SAβGal activity (*left*). Immunofluorescence (IF) micrographs of $p16^{INK4A}$ expression and DAPI (*2nd*), p21 expression and DAPI (*3rd*), and the levels of phospho-gamma H2AX and DAPI (*right*). Scale bar, 20 μm. Graphs showing the number of SAβGal-positive cells and integrated fluorescent density of $p16^{INK4A}$, p21, and phospho-gamma H2AX ($n = 6$, $*p < 0.05$). Error bars represent SEM.

induction of cellular senescence with accumulated DNA damage detected by phospho gamma H2AX staining and IB were also upregulated in IPAH patient-derived PAECs (Figure 1C; Supplementary Figure 2A), suggesting that EC senescence increases in PH.

Knockdown of endothelial p16^{INK4A} attenuates hypoxia-induced vascular remodeling in the mouse lung

Cellular senescence is upregulated in the IPAH patient PAECs (Figure 1). We next examined whether p16^{INK4A} knockdown in ECs attenuates SMC accumulation to the distal PAs (10–100 μm in diameter) in a hypoxia-induced mouse PH model. Consistent with IPAH patient PAECs, when we exposed control *p16$^{fl/fl}$* mice (8–10 week old) to hypoxia (8.5% O_2) for 3 weeks, p16^{INK4A} mRNA levels increased by 2.1-times in mouse lung ECs compared to that treated with normoxia (Figure 2E). Hypoxia-treated *p16$^{fl/fl}$* mice exhibited accumulation of αSMA-positive cells to distal PAs (Figures 2A,B), upregulated αSMA mRNA expression (Figure 2F), increased right ventricular hypertrophy evaluated by a Fulton's index (36) (Figure 2C), and raised RVSP (Figure 2D) compared with those treated with normoxia. These effects were attenuated in tamoxifen-induced *p16$^{i\Delta EC}$* mice (Figures 2A–D,F), in which p16^{INK4A} expression was 52% lower in lung ECs (Figure 2E). To examine the effects of Cre gene, we also treated tamoxifen-induced *Cdh5(PAC)-Cre^{ERT2}* control mice with hypoxia and examined the effects on accumulation of αSMA-positive cells to distal PAs, right ventricular hypertrophy, and RVSP. Hypoxia stimulated accumulation of αSMA-positive cells to distal PAs and increased Fulton's index and RVSP in *Cdh5(PAC)-Cre^{ERT2}* mice, suggesting that inhibition of αSMA-positive cell accumulation, right ventricular hypertrophy, and RVSP in *p16$^{i\Delta EC}$* mice is not because of the effects of Cre gene (Supplementary Figures 2B–E). We and others have reported that hypoxia induces vascular remodeling by increasing PDGFB expression (11, 73). Hypoxia-induced increases in PDGFB expression were suppressed in *p16$^{i\Delta EC}$* mouse lungs when analyzed using IHC (Figures 2A,B) and qRT-PCR (Figure 2F), indicating that EC senescence increases PDGFB expression and mediates the hypoxia-induced pathological accumulation of αSMA–positive cells to distal PAs.

Endothelial p16^{INK4A} mediates hypoxia-induced TWIST1 expression in the mouse lung

We have reported that endothelial TWIST1 mediates hypoxia-induced vascular remodeling through PDGFB signaling (11). Network analysis of publicly available microarray data (GSE113439) of control and IPAH patient lungs revealed that the cellular senescence/SASP genes network with one another as well as with TWIST1 or PDGFB (Supplementary Figure 1A). RNAseq analysis of ECs from hypoxia (8.5% O_2, 3 weeks)—or normoxia-treated mouse lungs also revealed that a total of 19,068 genes were altered. This list was filtered for genes with a >2-fold change and an adjusted p-value < 0.01, which narrowed the list to 738 genes (335 upregulated and 403 downregulated) that were significantly differentially expressed (Supplementary Table 3, GSE193272) and 317 BP GO Terms categories were generated (Supplementary Table 4). Of these GO Term categories, 178 categories were identified as categories with senescence/SASP-related genes appeared on a master list comprised of GeneCards and relating to transcription/gene expression, protein/RNA processing, cell cycle, inflammatory/immune response, and cell signaling/signal transduction (Supplementary Table 5; Supplementary Figure 3A). IPA network analysis demonstrated that genes from top 50 BP GO Term categories relating to cellular senescence/SASP interact closely with Twist1 and Pdgfb (Figure 3A). We have reported that (1) TWIST1 overexpression increases the expression of PDGFB in human pulmonary arterial endothelial (HPAE) cells, (2) Twist1 knockdown suppresses hypoxia-induced upregulation of PDGFB expression and accumulation of αSMA–positive cells in the mouse lungs, and (3) IPAH patient-derived PAE cells stimulate accumulation of αSMA–positive cells through endothelial TWIST1-PDGFB signaling (11). Therefore, we next examined whether EC senescence controls TWIST1 expression in the hypoxia-treated mouse lungs. The levels of TWIST1 were 1.8-times higher in the hypoxia-treated *p16$^{fl/fl}$* mouse lungs, while the levels were not significantly altered in the tamoxifen-induced *p16$^{i\Delta EC}$* mouse lungs (Figure 3B). Consistently, the mRNA levels of Twist1 increased in hypoxia-treated *p16$^{fl/fl}$* mouse lungs compared to those under normoxia, while the effects were suppressed in *p16$^{i\Delta EC}$* mouse lungs (Figure 3C). We also confirmed the results using IPAH patient PAECs; p16^{INK4A} knockdown using siRNA transfection decreased the levels of TWIST1 in IPAH PAECs (Figure 3D). These results suggest that EC senescence increases TWIST1 signaling and mediates hypoxia-induced vascular remodeling.

Inhibition of EC senescence suppresses accumulation of αSMA-positive cells to IPAH ECs in the gel implanted on the mouse lungs

To further examine the effects of EC senescence on vascular structures and PASMC accumulation in the mouse lungs, we implanted fibrin gel mixed with IPAH patient ECs or

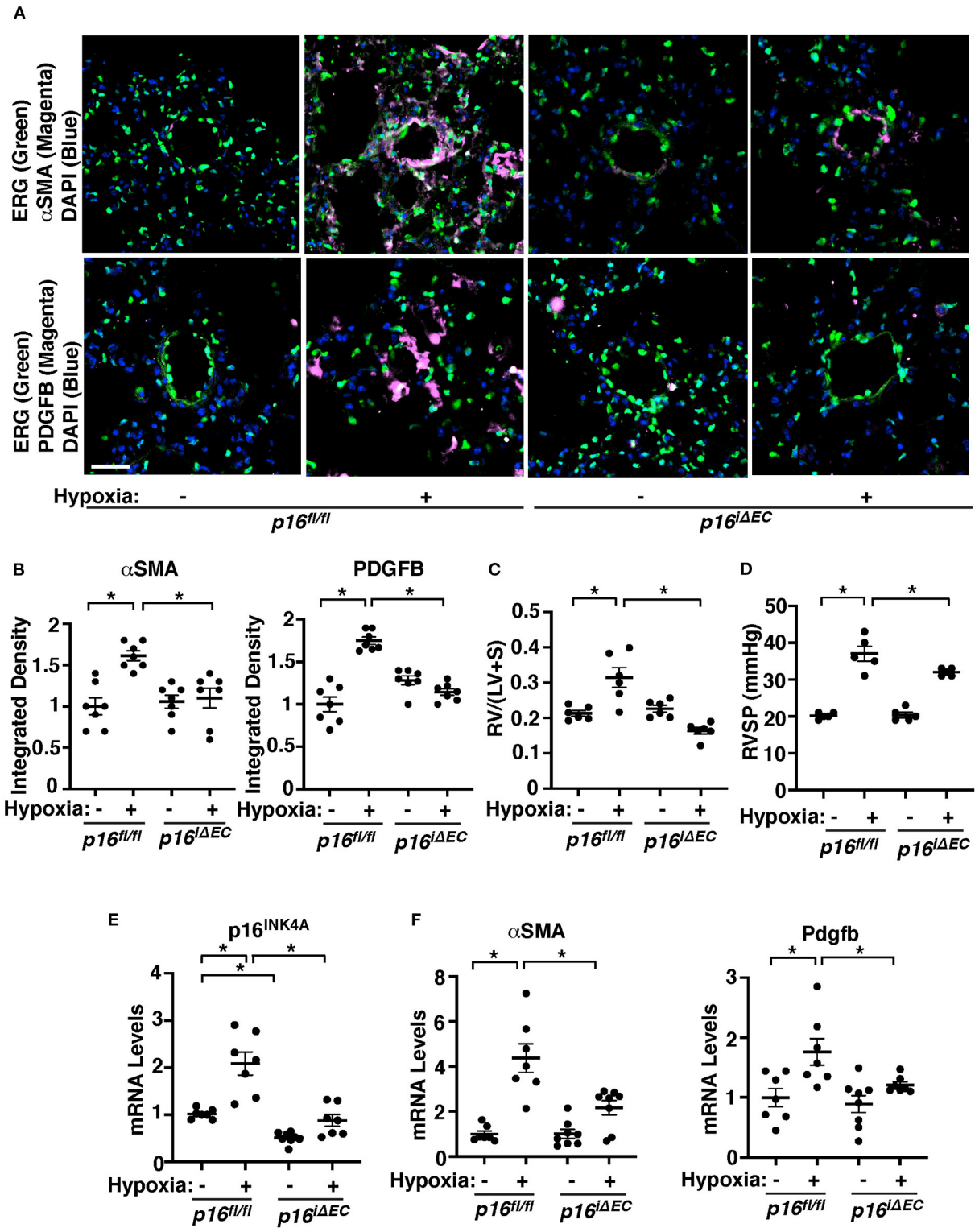

FIGURE 2
Endothelial p16^{INK4A} mediates hypoxia-induced vascular remodeling in pulmonary arterioles in the mouse lung. **(A)** IF images of representative pulmonary arterioles in the lungs of tamoxifen-induced *p16*$^{fl/fl}$ or *p16*$^{i\Delta EC}$ mice treated with normoxia or hypoxia for 3 weeks stained for αSMA, ERG, and DAPI (*top*) or PDGFB, ERG, and DAPI (*bottom*). Scale bar: 25 μm. **(B)** Graphs showing integrated fluorescent density of αSMA and PDGFB in tamoxifen-induced *p16*$^{fl/fl}$ or *p16*$^{i\Delta EC}$ mice treated with normoxia or hypoxia for 3 weeks ($n = 7$, mean ± SEM, $^*p < 0.05$). **(C)** Graph
(Continued)

FIGURE 2 (Continued)
showing Fulton's index (right ventricle/[left ventricle + septum], [RV/(LV + S)]) of tamoxifen-induced $p16^{fl/fl}$ or $p16^{i\Delta EC}$ mice treated with normoxia or hypoxia for 3 weeks ($n = 6$, mean ± SEM, $^*p < 0.05$). **(D)** Graph showing right ventricular systolic pressure (RVSP) of tamoxifen-induced $p16^{fl/fl}$ or $p16^{i\Delta EC}$ mice treated with normoxia or hypoxia for 3 weeks ($n = 5$, mean ± SEM, $^*p < 0.05$). **(E)** Graph showing the mRNA levels of $p16^{INK4A}$ in the ECs isolated from tamoxifen-induced $p16^{fl/fl}$ or $p16^{i\Delta EC}$ mouse lungs treated with normoxia or hypoxia for 3 weeks ($n = 7–8$, mean ± SEM, $^*p < 0.05$). **(F)** Graphs showing the mRNA levels of αSMA and Pdgfb in the tamoxifen-induced $p16^{fl/fl}$ or $p16^{i\Delta EC}$ mouse lungs treated with normoxia or hypoxia for 3 weeks ($n = 7–8$, mean ± SEM, $^*p < 0.05$).

in combination with modulation EC senescence on the lung surface of living mice (35, 36, 41, 66, 67). When we implanted fibrin gel supplemented with PAECs from IPAH patients or healthy individuals on the immunocompromised NOD scid gamma (NSG) mouse lung (8–10 week old) for 7 days (35, 36, 41, 66, 67), GFP-labeled healthy ECs supplemented in the gel formed a well-developed vascular structure in the gel (Figure 4A). Supplementation of IPAH patient-derived PAECs reduced blood vessel formation, increased PDGFB expression, and induced recruitment of αSMA-positive cells from host mouse lungs to accumulate in the gel compared to that in the gel supplemented with healthy ECs (Figure 4A); the levels of αSMA and PDGFB were 1.8- and 1.5-times higher in the gel mixed with IPAH PAECs, while $p16^{INK4A}$ knockdown using lentivirus expressing $p16^{INK4A}$ shRNA or treatment the gel with a senolytic reagent, ABT-263 (1 μg/gel) inhibited accumulation of αSMA-positive cells and PDGFB expression in the gel (Figure 4A).

We also examined the effects of inhibition of EC senescence on PDGFB expression in IPAH patient PAECs. Consistent with the results of hypoxia-treated $p16^{i\Delta EC}$ mouse lungs (Figures 2A,B,F), the PDGFB protein levels were significantly higher in IPAH PAECs compared to those in healthy human PAECs when analyzed using ELISA (Figures 4B,C), while the effects were suppressed when $p16^{INK4A}$ was knocked down in IPAH PAECs using siRNA transfection compared to those treated with scrambled control siRNA (Figure 4B) or IPAH PAECs were treated with ABT-263 (250 nM, Figure 4C). These results suggest that EC senescence increases PDGFB expression and mediates αSMA-positive cell accumulation to IPAH PAECs.

Exosomes from hypoxia-treated mouse lung ECs stimulate SMC recruitment in the fibrin gel implanted on the mouse lungs

It has been reported that human MSC-derived exosomes suppress various lung diseases including PH in animal models (53–61). However, the role of EC exosomes in PH pathology and the involvement of EC senescence have not been studied before. When exosomes were isolated from pre-filtered (0.2 μm) conditioned media of ECs (1×10^6 cells) isolated from tamoxifen-induced $p16^{fl/fl}$ or $p16^{i\Delta EC}$ mouse lungs treated with hypoxia (41, 72, 74, 75), the isolated exosome population was positive for exosome markers (CD63, Flotillin-1) and negative for the cellular marker GM130 when analyzed using IB (Figure 5A). NTA revealed that isolated EC exosomes were heterogeneous in diameter with 90–130 nm (Figure 5B). TEM images exhibited the typical round vesicular like morphology with ∼50–100 nm in size (Figure 5C).

Proteomics analysis of exosomes isolated from conditioned media of three normoxia- vs. three hypoxia-treated mouse lung EC replicates identified 438 proteins present in the control and hypoxia sample replicates (Supplementary Table 6). Proteins with total spectrum count of ≥8 identified 37 proteins, 10 of which were significantly differentially expressed in hypoxia- vs. normoxia-treated exosomes. Out of these 37 proteins, 30 proteins were identified as SASP related proteins based on the "SASP Atlas" (50). These 30 proteins underwent BP GO analysis *via* the Functional Annotation Chart feature of the DAVID v6.8 software and 51 total BP GO term categories were identified (Supplementary Table 7). The top 20 BP GO Term categories derived from the 30 SASP-related proteins were classified as cell differentiation, tissue development, cell signaling/signal transduction, and extracellular matrix (ECM)/cellular junction assembly, which contribute to vascular remodeling and cell-cell communications (Figure 5D). When we treated PASMCs with exosomes collected from hypoxia-treated $p16^{fl/fl}$ mouse lung ECs, PASMC DNA synthesis and migration were induced by 1.7- and 1.6-times, respectively, compared to those treated with normoxia-treated $p16^{fl/fl}$ mouse lung EC-derived exosomes when analyzed using an EdU assay and a transwell migration assay, respectively (Figures 5E,F). However, these effects were suppressed when PASMCs were treated with exosomes derived from hypoxia-treated $p16^{i\Delta EC}$ mouse lung ECs (Figures 5E,F).

To confirm the effects of hypoxia-treated mouse lung EC-derived exosomes on PASMC behaviors in the lungs, we implanted fibrin gel supplemented with exosomes (5 μg/gel) isolated from conditioned media of normoxia- or hypoxia-treated $p16^{fl/fl}$ or $p16^{i\Delta EC}$ mouse lung ECs. Recruitment of αSMA-positive cells from the host mouse lungs was significantly stimulated in the gel containing hypoxia-treated $p16^{fl/fl}$ mouse lung EC-derived exosomes compared to that supplemented with exosomes from normoxia-treated $p16^{fl/fl}$ mouse lung ECs (Figure 5G). Exosomes isolated from conditioned media of hypoxia-treated $p16^{i\Delta EC}$ mouse lung ECs suppressed recruitment of host mouse lung αSMA-positive cells in the gel (Figure 5G), suggesting that senescence-related factors in the

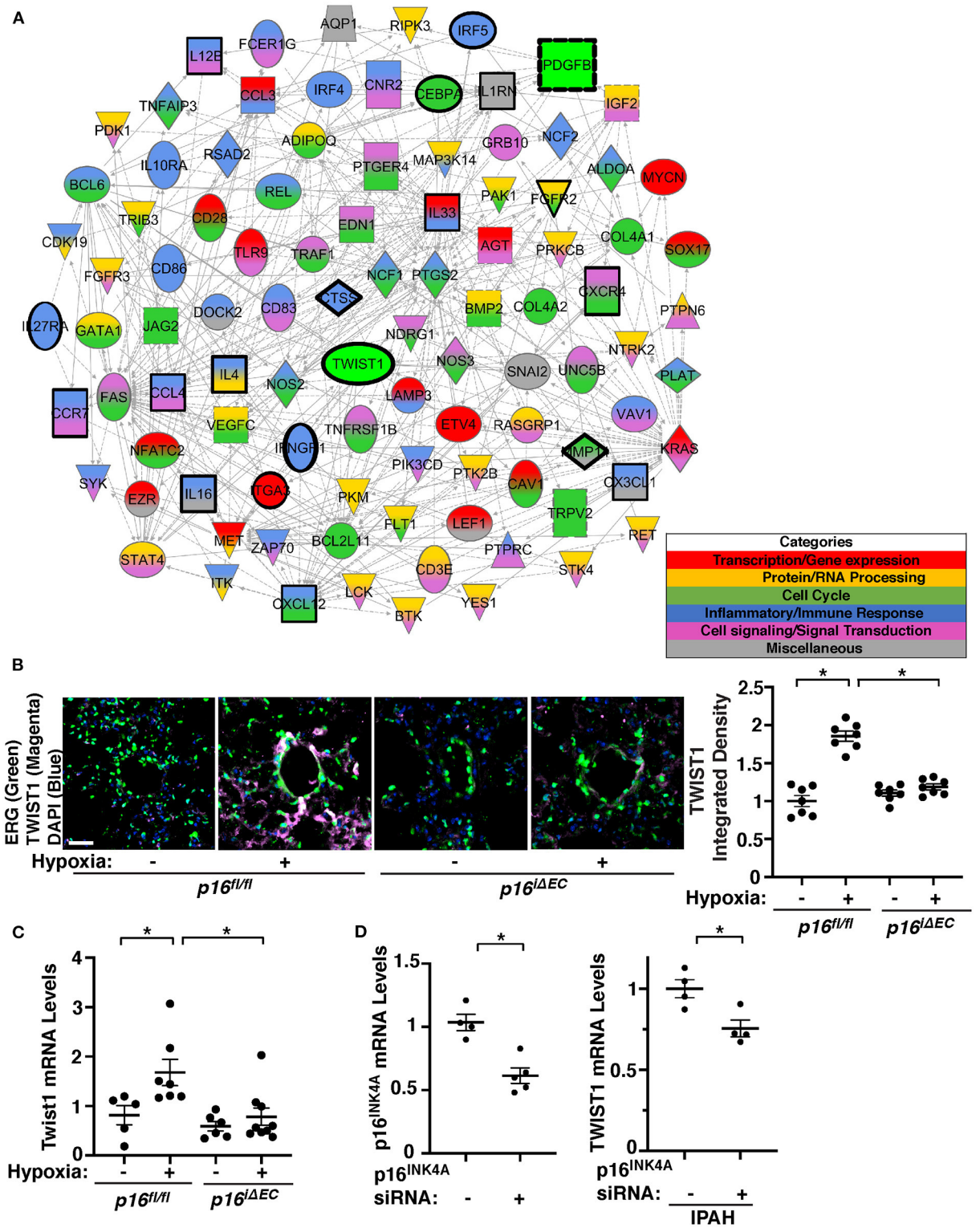

FIGURE 3
Endothelial p16^{INK4A} mediates hypoxia-induced TWIST1 expression in the mouse lung. **(A)** Gene network demonstrating interactions between Twist1, Pdgfb, and differentially expressed genes listed in the top 50 BP GO Term categories relating to senescence/SASP in ECs isolated from mouse lungs treated with hypoxia for 3 weeks compared to those from normoxia-treated mouse lung ECs. Red: Transcription/gene expression, Gold: Protein/RNA processing, Green: Cell cycle. Blue: Inflammatory/immune response. Pink: Cell signaling/signal transduction, Gray:
(Continued)

FIGURE 3 (Continued)
Miscellaneous. **(B)** IF images of representative pulmonary arterioles in the lungs of tamoxifen-induced $p16^{fl/fl}$ or $p16^{i\Delta EC}$ mice treated with normoxia or hypoxia for 3 weeks stained for TWIST1, ERG, and DAPI. Scale bar: 25 μm. Graph showing integrated fluorescent density of TWIST1 in tamoxifen-induced $p16^{fl/fl}$ or $p16^{i\Delta EC}$ mouse lungs treated with normoxia or hypoxia for 3 weeks ($n = 7$, mean ± SEM, $^*p < 0.05$). **(C)** Graph showing the mRNA levels of Twist1 in tamoxifen-induced $p16^{fl/fl}$ or $p16^{i\Delta EC}$ mouse lungs treated with normoxia or hypoxia for 3 weeks ($n =$ 5–9, mean ± SEM, $^*p < 0.05$). **(D)** Graph showing the mRNA levels of $p16^{INK4A}$ in PAECs treated with $p16^{INK4A}$ siRNA or scrambled control siRNA (*left*, $n = 4$–5, mean ± SEM, $^*p < 0.05$). Graph showing the mRNA levels of TWIST1 in IPAH PAECs treated with $p16^{INK4A}$ siRNA or scrambled control siRNA (*right*, $n = 4$, mean ± SEM, $^*p < 0.05$).

hypoxia-treated mouse lung EC-derived exosomes are required for SMC recruitment in the implanted gel.

Discussion

Here, we have demonstrated that endothelial senescence mediates PH pathology. The levels of senescence markers are higher in IPAH patient PAECs compared to those from healthy individuals. Hypoxia-induced accumulation of αSMA-positive cells to the PAs is attenuated in tamoxifen-induced $p16^{i\Delta EC}$ mice. The levels of PDGFB and TWIST1 increase in hypoxia-treated mouse lungs or IPAH patient PAECs, while the effects are attenuated by knocking down $p16^{INK4A}$ in ECs or treating ECs with senolytic reagent. Exosomes collected from hypoxia-treated mouse lung ECs stimulate SMC DNA synthesis and migration *in vitro* and recruitment of αSMA-positive cells in the gel implanted on the mouse lungs, while exosomes from $p16^{INK4A}$ knocked down ECs inhibit the effects. These results suggest that EC senescence stimulates TWIST1-PDGFB signaling and mediates PH pathology. Modulation of EC senescence could be an effective strategy to manage PH.

Our microarray analysis of control vs. IPAH lungs suggests that among significantly differentially expressed 2075 genes (p adj value < 0.001) applied for the BP GO analysis regardless the ranking order, 48 genes were categorized as SASP/senescence-related genes curated from unbiased genomic and proteomic database [SASP Atlas (71), CellAge] (Supplementary Figure 1B). In a separate analysis, we confirmed the involvement of narrower categories of major senescence/SASP genes (e.g., pro-inflammatory cytokines, proteases and protease inhibitors, and growth factors) using a master list curated from the literature (32); 16 downregulated and 15 upregulated significantly differentially expressed senescence/SASP genes were identified (Supplementary Figure 1C). These transcriptome data suggest that senescence/SASP are directly or indirectly involved in the PH pathology.

In the microarray data, while PDGFB was significantly differentially expressed between control vs. IPAH lungs (adjusted p-value, 0.0019), TWIST1 was not (adjusted p-value, 0.485). We were not able to identify the direct link between TWIST1 and PDGFB in our microarray and RNAseq analyses, however the IPA network indicates that TWIST1 and PDGFB link indirectly through interaction between senescence/SASP genes (Figure 3A; Supplementary Figure 1A). Since TWIST1 phosphorylation is necessary for its nuclear translocation, transcriptional activity, and gene interaction (35, 36), even TWIST1 expression levels were not significantly changed, TWIST1-PDGFB may contribute the PH phenotype. In fact, (1) TWIST1 overexpression increases the expression of PDGFB in HPAE cells, (2) Twist1 knockdown suppresses hypoxia-induced upregulation of PDGFB expression and accumulation of αSMA–positive cells, and (3) IPAH patient-derived PAECs stimulate accumulation of αSMA–positive cells through endothelial TWIST1-PDGFB signaling (11). In addition, (4) PDGFB promoter region has putative TWIST1 binding site, (5) $p16^{INK4A}$ knockdown decreased TWIST1 and PDGFB expression in a hypoxia-induced pulmonary hypertension model and IPAH patient cells (Figures 2–4), (6) significantly differentially expressed genes of healthy vs. IPAH patient lungs that interacted with TWIST1 also interacted with PDGFB (Supplementary Figure 1A). Therefore, although there is no direct link between TWIST1 and PDGFB in the IPA interactome of senescence/SASP related genes, endothelial senescence may control vascular remodeling in PH through TWIST1-PDGFB signaling, and we focused on this signaling in this study. Post-translational modification of TWIST1 or cell type-specific expression of TWIST1 may contribute to the direct interaction between TWIST1 and PDGFB, which is undetectable in the IPA network. Although $p16^{INK4A}$ is a major senescence marker and our results reveal that (1) the levels of $p16^{INK4A}$ are higher in IPAH patient PAECs (Figure 1), (2) knockdown of $p16^{INK4A}$ in ECs prevents hypoxia-induced accumulation of αSMA-positive cells and increases in RVSP (Figure 2), and (3) knockdown of $p16^{INK4A}$ in ECs also decreases TWIST1 and PDGFB expression under hypoxia (Figures 2, 3), $p16^{INK4A}$ was not significantly differentially expressed in ECs isolated from hypoxia-treated mouse lungs in our bulk RNAseq analysis. This may be because of the spatiotemporal changes in the expression of $p16^{INK4A}$ during PH pathology or differential expression of $p16^{INK4A}$ in specific EC subpopulations. Given that there is a spatial and temporal heterogeneity in pulmonary ECs (76), the susceptibility and the level of senescence in response to hypoxia as well as SASP gene profiles (77) may be different among subpopulations of ECs, which directs spatiotemporal differences in vascular remodeling in PH. While the SASP reinforces the senescence through autocrine positive-feedback loop and induces neighbor cells to undergo senescence through paracrine

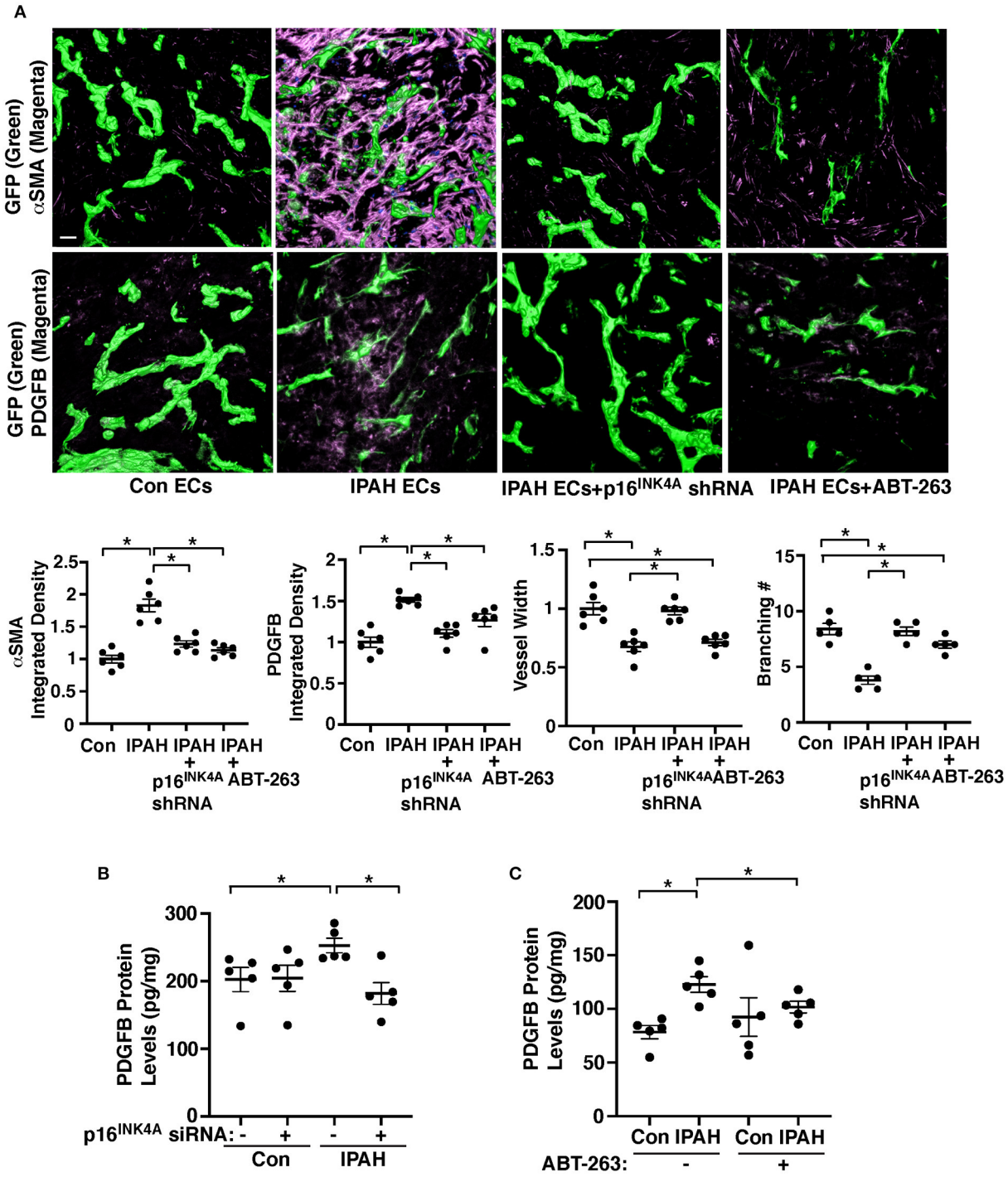

FIGURE 4
Inhibition of EC senescence suppresses accumulation of αSMA-positive cells and PDGFB expression in the gel implanted on the mouse lung. **(A)** IF micrographs of fibrin gel supplemented with GFP-labeled healthy or IPAH patient ECs or in combination with treatment with $p16^{INK4}$ shRNA or ABT-263 and implanted on the NSG mouse lungs for 7 days; GFP-labeled blood vessels and αSMA expression (*top*) and GFP-labeled blood vessels and PDGFB expression (*bottom*) in the fibrin gel. Scale bar, 50 μm. Graphs showing integrated fluorescent density of αSMA (*left*) and PDGFB (*2nd*, $n = 6$, mean ± SEM, $*p < 0.05$), vessel width (*3rd*, $n = 6$, mean ± SEM, $*p < 0.05$), and branching number (*right*, $n = 5$, mean ± SEM, $*p < 0.05$). **(B)** Graph showing the protein levels of PDGFB measured by ELISA in healthy or IPAH patient PAECs or in combination with treatment with $p16^{INK4}$ siRNA or scrambled control siRNA ($n = 5$, mean ± SEM, $*p < 0.05$). **(C)** Graph showing the protein levels of PDGFB measured by ELISA in healthy or IPAH patient PAECs or in combination with treatment with ABT-263 (250 nM, $n = 5$, mean ± SEM, $*p < 0.05$).

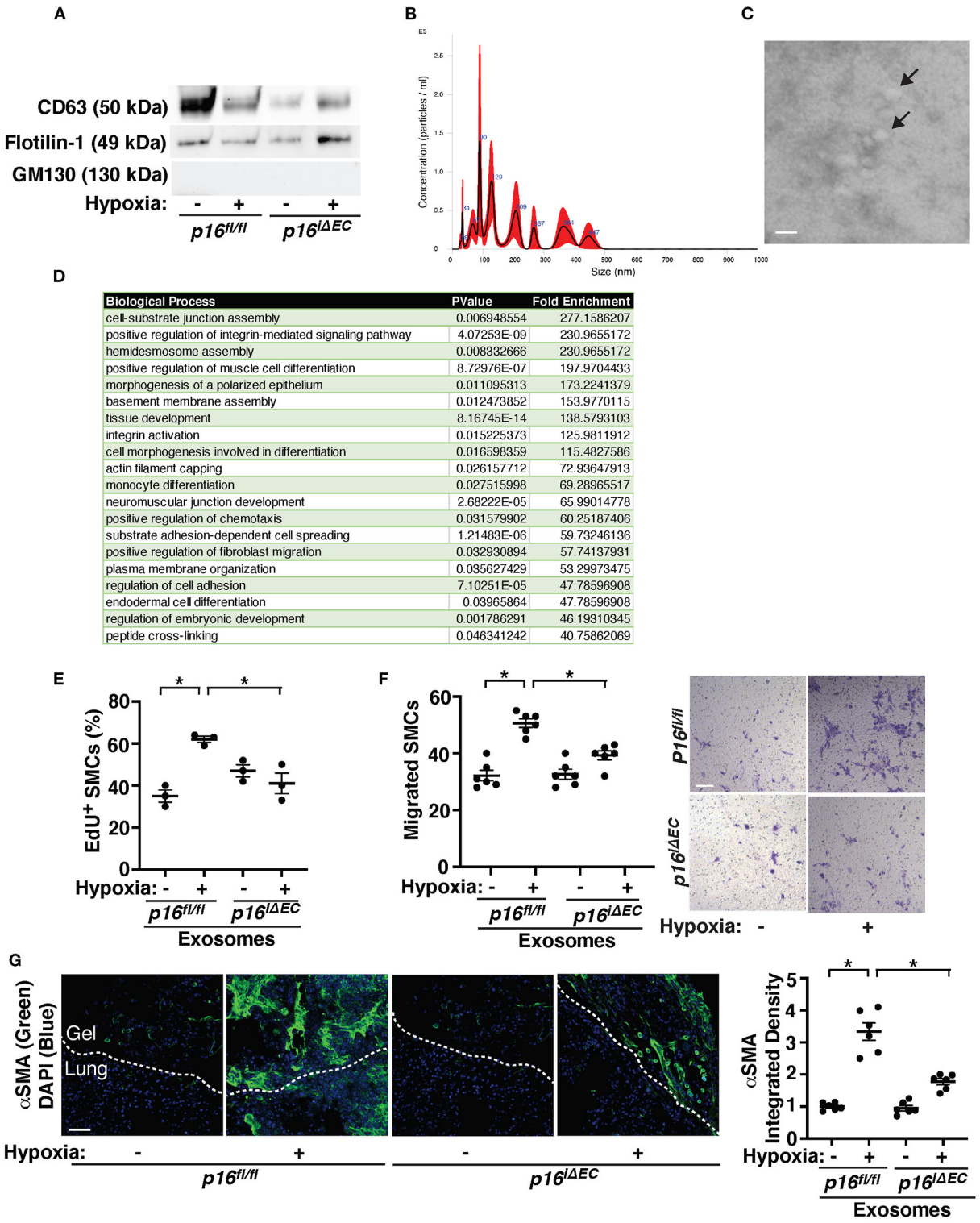

Biological Process	PValue	Fold Enrichment
cell-substrate junction assembly	0.006948554	277.1586207
positive regulation of integrin-mediated signaling pathway	4.07253E-09	230.9655172
hemidesmosome assembly	0.008332666	230.9655172
positive regulation of muscle cell differentiation	8.72976E-07	197.9704433
morphogenesis of a polarized epithelium	0.011095313	173.2241379
basement membrane assembly	0.012473852	153.9770115
tissue development	8.16745E-14	138.5793103
integrin activation	0.015225373	125.9811912
cell morphogenesis involved in differentiation	0.016598359	115.4827586
actin filament capping	0.026157712	72.93647913
monocyte differentiation	0.027515998	69.28965517
neuromuscular junction development	2.68222E-05	65.99014778
positive regulation of chemotaxis	0.031579902	60.25187406
substrate adhesion-dependent cell spreading	1.21483E-06	59.73246136
positive regulation of fibroblast migration	0.032930894	57.74137931
plasma membrane organization	0.035627429	53.29973475
regulation of cell adhesion	7.10251E-05	47.78596908
endodermal cell differentiation	0.03965864	47.78596908
regulation of embryonic development	0.001786291	46.19310345
peptide cross-linking	0.046341242	40.75862069

FIGURE 5
Exosomes from hypoxia-treated mouse lung ECs stimulate recruitment of αSMA-positive cells in the fibrin gel implanted on the mouse lungs. **(A)** IB analysis of CD63, Flotillin-1, and GM130 in exosomes collected from conditioned media of ECs isolated from tamoxifen-induced *p16*$^{fl/fl}$ or *p16*$^{i\Delta EC}$ mouse lungs treated with normoxia or hypoxia for 3 weeks. **(B)** Size distribution and particle concentration of isolated exosomes analyzed using NTA. **(C)** TEM image of exosome morphology. Scale bar: 150 nm. Arrows indicate exosomes. **(D)** List of top 20 BP GO terms of proteins differentially enriched in exosomes isolated from conditioned media of mouse lung ECs isolated from C57BL6 mouse lungs treated

(Continued)

FIGURE 5 (Continued)
with normoxia or hypoxia for 3 weeks. **(E)** Graph showing EdU-positive PASMCs treated with exosomes (10 μg/ml) collected from conditioned media of ECs isolated from tamoxifen-induced $p16^{fl/fl}$ or $p16^{i\Delta EC}$ mouse lungs treated with normoxia or hypoxia for 3 weeks ($n = 3$, mean ± SEM, $^*p < 0.05$). **(F)** Graph showing PASMCs migrating toward medium containing exosomes (10 μg/ml) collected from conditioned media of ECs isolated from tamoxifen-induced $p16^{fl/fl}$ or $p16^{i\Delta EC}$ mouse lungs treated with normoxia or hypoxia for 3 weeks (*left*, $n = 6$, mean ± SEM, $^*p < 0.05$). Representative micrographs showing PASMCs migrating toward medium containing exosomes (10 μg/ml) collected from conditioned media of ECs isolated from tamoxifen-induced $p16^{fl/fl}$ or $p16^{i\Delta EC}$ mouse lungs treated with normoxia or hypoxia for 3 weeks (*right*, Wright Giemsa staining). Scale bar, 50 μm. **(G)** IF micrographs of αSMA expression and DAPI in the fibrin gel supplemented with exosomes collected from conditioned media of ECs isolated from tamoxifen-induced $p16^{fl/fl}$ or $p16^{i\Delta EC}$ mouse lungs treated with normoxia or hypoxia for 3 weeks and implanted on the $p16^{fl/fl}$ mouse lung for 7 days. Scale bar, 50 μm. Graph showing integrated fluorescent density of αSMA ($n = 6$, mean ± SEM, $^*p < 0.05$).

signaling, paracrine signaling of the SASP also promotes proliferation and migration of neighbor cells (27, 77, 78). These functional complexities of senescent ECs drive an endothelial heterogeneity in PH pathology. Further investigation using scRNAseq analysis may elucidate the mechanism.

Our results suggest that EC senescence stimulates TWIST1-PDGFB signaling and mediates PH pathology; knockdown of endothelial $p16^{INK4A}$ inhibits hypoxia-induced accumulation of PASMCs, RV hypertrophy, and expression of TWIST1 and PDGFB in the mouse lungs (Figures 2, 3). Although hypoxia-induced accumulation of PASMCs to PAs was inhibited in $p16^{i\Delta EC}$ mouse lungs, the hypoxia-induced PH phenotype was further accelerated in p16-3MR mice (not shown), in which other types of $p16^{INK4A+}$ senescent cells are also eliminated upon treatment with ganciclovir (GCV) (79); while inhibition of EC senescence in $p16^{i\Delta EC}$ mice suppresses PASMC accumulation to PAs, PASMC senescence may also be inhibited in p16-3MR mice, which stimulates proliferation and migration of PASMCs to accumulate to PAs. It is important to note that treatment the gel with the senolytics ABT-263 suppressed both vascular network formation and PASMC accumulation to PAs in the gel (Figure 4A). This inconsistency may be because of the differences in the experimental condition (e.g., senolytics vs. gene knockdown, treatment timeline, and sensitivity of the senolytics to different cell types). The senolytic effects of ABT-263 on other recruited cells, which inhibits SASP factor secretion to inhibit not only SMC accumulation but also EC angiogenic activity to suppress vascular network formation in the gel. In addition to SMCs, EC senescence and subsequent stimulation of secretion of PDGFB and SASP factors may also alter behaviors of other αSMA-positive cells (e.g., pericytes and myofibroblasts) and other lung cells (e.g., epithelial cells and immune cells) (80) to indirectly change vascular structures and αSMA-positive cell accumulation in the hypoxia-treated mouse lungs. Furthermore, in $p16^{i\Delta EC}$ mice $p16^{INK4A}$ expression is knocked down in ECs not only in the lungs but also in other organs. Suppression of EC senescence in other organs (e.g., cardiac ECs) and associated changes in the systemic metabolism may affect hypoxia-induced PH phenotype in $p16^{i\Delta EC}$ mice. Knockdown of $p16^{INK4A}$ in these other cell types or other organs, or PA-specific knockdown of $p16^{INK4A}$ will further elucidate the mechanism.

We have demonstrated that hypoxia-induced PH phenotype was attenuated in $p16^{i\Delta EC}$ mice (Figures 2, 3) and knock down of $p16^{INK4A}$ inhibits increases in the levels of TWIST1 in hypoxia-treated mouse lungs and IPAH patient PAECs (Figure 3). Senescence-related signaling molecules being up- or down-regulated in IPAH patient lungs and hypoxia-treated mouse lung ECs interact with TWIST1 (Figure 3; Supplementary Figure 1), which may directly or indirectly control TWIST1 expression and activity during PH progression. For example, HIF1α expression is significantly increased in IPAH patient lungs and interacts with TWIST1 (Supplementary Figure 1). Since the promoter region of TWIST1 has a HIF1α binding site [−651, −82, CACGT (81)], HIF1α may control TWIST1 transcription in PH ECs. Our IPA network analysis also reveals that HIF1α and other senescence-related genes differentially expressing in IPAH patient lungs interact with PDGFB (Supplementary Figure 1A). Since the promoter region of PDGFB also has HIF1α binding sites [−62, −486, −489, CACGT (81)] and HIF1α is known to control PDGFB expression in breast cancer cells (82), HIF1α may also directly control PDGFB expression in PAECs in PH. Recently it is reported that HIF1 mediates hypoxia-induced endothelial deficiency of iron-sulfur (Fe-S) biogenesis to induce endothelial senescence and PH phenotype (33). Thus, differential and reciprocal regulation of HIF1-3α genes is necessary for PH pathology (83). Although HIF1α controls multiple hypoxia-induced signaling pathways (81) to mediate PH pathology, HIF1α expression was not significantly differentially expressed in our RNAseq data from hypoxia-treated mouse lung ECs (3 weeks). Also while HIF3α was significantly increased in hypoxia-treated mouse lung ECs (Supplementary Figure 3B), HIF3α expression was significantly lower in IPAH patient lungs (Supplementary Figure 1C). In fact, the BP GO term categories in the microarray data of IPAH patient lungs and RNAseq data of hypoxia-treated mouse lung ECs are not identical; BP GO terms of transcription and cell cycle genes are altered more in the IPAH patient lungs, while inflammatory gene categories are changed more in the hypoxia-treated mouse lung ECs. This may be because of the differences in the sample conditions (whole lung samples vs. ECs, human vs. mouse, sample demographics, time course, contribution of factors other than hypoxia). Further

investigation of the gene expression patterns and sample profiles will elucidate the mechanism.

In addition to PDGFB (11), TWIST1 is a bHLH transcription factor and controls expression of other angiogenic genes that contain an E-box in their promoter region [e.g., TGFβ2 (84), VEGFR2 (85), Tie2 (63), TGFβR2 (36)] (86), which mediates PH phenotype in a cooperative way. It is known that TWIST1 is also involved in endothelial to mesenchymal transition (EndMT) (36, 87–89). We have reported that hypoxia-treated HPAECs exhibit EndMT, which is inhibited by TWIST1 knockdown that attenuates the accumulation of PASMCs to distal PA in a mouse hypoxia-induced PH model (36). It has been demonstrated that senescent ECs show EndMT phenotype (90). Consistently, IPAH patient-derived PAECs exhibited EndMT phenotype; SLUG expression increased, while VE-cadherin-positive cell–cell junctional structures were disrupted in IPAH patient-derived PAECs compared with control healthy human PAECs when analyzed by ICC (Supplementary Figure 2F). These effects were attenuated when $p16^{INK4A}$ expression was knocked down using siRNA transfection (Supplementary Figure 2F). Thus, cellular senescence may contribute to PH pathology through EndMT signaling as well. Other pathways known to mediate the PH pathology [e.g., eNOS (91), High Mobility Group AT-hook 1 (HMGA1) (92), SMAD (36, 93), PGC1α/TFAM (94)] may also be involved in the mechanism. For example, mitochondrial dysfunction that stimulates cellular senescence during aging (95, 96) contributes to PH pathology (94). TWIST1 controls expression of PGC1α that stimulates mitochondrial biogenesis (97–99) and angiogenesis (98, 100, 101) to mediate age-dependent inhibition of angiogenesis and lung regeneration (37). Inhibition of TWIST1 activity also increases the expression of PGC1α in fat cells (102). PGC1α controls age-dependent mitochondrial metabolism (97) and mediates aging-related cardiovascular diseases (98, 103–105). Thus, although our results suggest that cellular senescence induces TWIST1 expression, there may be a feedback mechanism; TWIST1 may control cellular senescence as reported in mesenchymal stem cells (106) and tumor cells (107) and contribute to PH phenotype through mitochondrial signaling.

We have demonstrated that exosomes isolated from hypoxia-treated $p16^{fl/fl}$ mouse lung ECs induce SMC accumulation to ECs in the gel implanted on the mouse lungs, while these effects are inhibited when treated with exosomes from $p16^{i\Delta EC}$ mouse lung ECs (Figure 5). This is consistent with the data demonstrating that senolytics prevent vascular remodeling of IPAH patient ECs (Figure 4). Although senolytics are known to attenuate tissue injury, extend lifespan and delay age-related conditions (28), given the beneficial effects of senescent cells on tissue regeneration/repair (18, 28), senolytics may have harmful side effects. In fact, although senolytic ABT-263 inhibits SMC accumulation, vascular network formation was also suppressed in the gel (Figure 4A). It is known that senescent cells can mediate paracrine effects on adjacent cells (45, 51, 52) through release of exosomes that contain SASP factors and other proteins/nucleic acids regulating cellular senescence (45, 50–52, 77, 108–110). Since exosomes contain multiple proteins and nucleic acids (e.g., ECM molecules, cytoskeleton remodeling molecules), they may reduce the adverse effects of senolytics alone. Furthermore, exosomes are small in size and protected from degradation due to their lipid bilayer structure, which facilitates delivery to their target with a low immune response (39, 40, 42, 44, 45, 111, 112). In fact, MSC-derived exosomes suppress PH and various lung diseases associated with PH (e.g., BPD, airway inflammation, and pulmonary fibrosis) (53–61). Understanding the effects of EC exosomes on PH pathology, combination of senolytic reagents with EC exosomes, and appropriate therapeutic timing will lead to the development of promising strategies for the management of PH. In our results, CD63 levels were lower in exosomes isolated from hypoxia-treated mouse lung ECs or $p16^{i\Delta EC}$ mouse lung ECs (Figure 5A). This is consistent with others' reports demonstrating that the expression of CD63 is suppressed in exosomes isolated from hypoxia treated cells (113), while upregulated in the plasma exosomes collected from aged mice, in which senescence is upregulated (114). Given that $CD63^{+}$ exosomes are key effectors in old exosomes (114), investigation of the role of exosome subfraction in PH pathology would further elucidate the mechanism.

We have been using a unique method to implant fibrin gel supplemented with fluorescently labeled control vs. IPAH ECs, in which gene expression is manipulated, or to implant the gel containing senolytic agent on the lung surface of a living mouse (Figure 4A) (35, 36, 41, 66, 67, 115). This method is important and significant to study vascular structures and function in the lung microenvironment, which is significantly different from the systemic vascular system (e.g., negative pleural pressure and low PA pressure) (116, 117). This method also enables us to clearly visualize the lung specific vascular structures and precisely analyze the process and mechanisms of blood vessel formation and interactions between ECs and other resident lung cells recruited from the host lung (e.g., SMCs, alveolar epithelial cells, immune cells, and fibroblasts) in the gel (35, 36, 41, 66, 67, 115), which cannot be done using the subcutaneous gel implantation. In fact, (1) recruited blood vessels are derived from PA (35); when PA is ligated, the blood vessel recruitment into the gel is significantly attenuated, and (2) the morphology of blood vessels is significantly different in the gel implanted on the lung compared to those in the gel implanted under the skin (66). The recruited host lung cells [e.g., alveolar capillaries, epithelial cells, and macrophages (35)] secrete angiogenic/growth factors, and may create lung-specific microenvironment in the gel. Further investigation using this system will enable elucidating the paracrine signaling mechanism by which senescent ECs control behaviors of

SMCs in the gel in the lung-specific microenvironment by manipulating gene expression in ECs.

We have investigated the role of EC senescence in αSMA-positive cell accumulation using ECs isolated from IPAH patient PAs, the region >5 mm in diameter. We excluded the samples from >55 years old patients, which are more susceptible to cellular senescence and senescence-related lung diseases such as COPD or IPF that affect PH phenotype in different ways. However, the heterogeneity of the samples due to cardiopulmonary condition (e.g., chronic lung diseases, inflammation), obesity, sex, race, and type-2 bone morphogenetic protein receptor (BMPR2) mutations, which contribute to severity of PH phenotype (3, 118), may impact EC senescence and vascular remodeling. DNA damage inhibits BMPR2 expression and reduced BMPR2 signaling impairs DNA damage repair processes (32, 119), suggesting the involvement of reciprocal interaction of cellular senescence and BMPR2 mutant in severity of PH. While we investigated the effects of EC senescence on SMC accumulation in this study, it is also reported that EC senescence drives the transition from a reversible to irreversible pulmonary vascular phenotype at end-stage of PH progression (32). Obesity is also associated with PH (120) and cellular senescence is induced in an obese condition (121), in which angiogenesis is impaired through TWIST1 signaling (70). Further investigation in another cohort with a larger sample size including the patients with BMPR2 mutation and/or different stages will elucidate the mechanism of EC senescence in the PH pathology.

In summary, we have demonstrated that endothelial senescence increases TWIST1 and PDGFB expression and mediates PH pathology. Knockdown of $p16^{INK4A}$ in ECs attenuates the levels of PDGFB and TWIST1 in IPAH patient PAECs or hypoxia-treated mouse lungs and suppresses accumulation of αSMA–positive cells to PAs in the mouse lungs. These findings suggest that modulation of endothelial senescence will lead to the development of better strategy for the management of PH.

Data availability statement

The datasets presented in this study can be found in online repositories. The names of the repository/repositories and accession number(s) can be found in the article/Supplementary material.

Ethics statement

The animal study was reviewed and approved by Animal Care and Use Committee of Medical College of Wisconsin.

Author contributions

Conceived and designed the experiments: TM and AM. Performed the experiments: PK, KH, TH, KM, TM, and AM. Analyzed the data and contributed reagents/materials/analysis tools: PK, KH, TH, TM, and AM. Wrote the paper: PK, TM, and AM. All authors contributed to the article and approved the submitted version.

Funding

This work was supported by funds fromNIHR21AG054830, R01HL139638, R21AG062893, and NIH R01HL142578 (to AM and TM), and American Heart Association (AHA) 18TPA34170129 (to AM) as well as 967800 (to AM). Proteomics analysis was performed by the Northwestern Proteomics Core Facility supported by NCI CCSG P30 CA060553 awarded to the Robert H. Lurie Comprehensive Cancer Center, instrumentation award (S10OD025194) from NIH Office of Director, and the National Resource for Translational and Developmental Proteomics supported by P41 GM108569 as well as the Mass Spectrometry Technology Access Center at McDonnell Genome Institute (MTAC@MGI) at Washington University School of Medicine.

Conflict of interest

The authors declare that the research was conducted in the absence of any commercial or financial relationships that could be construed as a potential conflict of interest.

Publisher's note

Supplementary material

The Supplementary Material for this article can be found online at: https://www.frontiersin.org/articles/10.3389/fmed.2022.908639/full#supplementary-material

SUPPLEMENTARY FIGURE 1
Gene networks of TWIST1, PDGFB and senescence-related genes differentially expressed in IPAH patient lungs. **(A)** Network of genes from 113 GO Term categories containing cellular senescence/SASP genes and their relationship to TWIST1 and PDGFB. Red: Transcription/Gene Expression, Gold: Protein/RNA processing, Green: Cell cycle, Blue:

Inflammatory/Immune Response, Pink: Cell Signaling/Signal Transduction, Gray: Miscellaneous. **(B)** Heatmap of the 37 upregulated and 11 downregulated cellular senescence/SASP related genes in the 113 BP GO Term categories in control vs. IPAH patient lungs. **(C)** Heatmap of the 15 upregulated and 16 downregulated major cellular senescence/SASP genes in control vs. IPAH patient lungs.

SUPPLEMENTARY FIGURE 2
Cellular senescence mediates EndMT in IPAH patient derived ECs. **(A)** Representative IB showing the expression of $p16^{INK4}$, p21, phospho gamma H2AX, and β-actin in PAECs from IPAH patients or healthy individuals. Graph showing the protein levels of $p16^{INK4}$, p21, and phospho gamma H2AX in PAECs from IPAH patients or healthy individuals ($n = 3$, mean ± SEM, $^*p < 0.05$). **(B)** IF images of representative pulmonary arterioles in the lungs of tamoxifen-induced *Cdh5(PAC)-Cre^{ERT2}* mice treated with normoxia or hypoxia for 3 weeks stained for αSMA, ERG, and DAPI (*top*) or PDGFB, ERG, and DAPI (*bottom*). Scale bar: 25 μm. **(C)** Graphs showing integrated fluorescent density of αSMA and PDGFB in tamoxifen-induced *Cdh5(PAC)-Cre^{ERT2}* mouse lungs treated with normoxia or hypoxia for 3 weeks ($n = 6$, mean ± SEM, $^*p < 0.05$). **(D)** Graph showing Fulton's index (right ventricle/[left ventricle + septum], [RV/(LV + S)]) of tamoxifen-induced *Cdh5(PAC)-Cre^{ERT2}* mice treated with normoxia or hypoxia for 3 weeks ($n = 5$–6, mean ± SEM, $^*p < 0.05$). **(E)** Graph showing right ventricular systolic pressure (RVSP) of tamoxifen-induced *Cdh5(PAC)-Cre^{ERT2}* mice treated with normoxia or hypoxia for 3 weeks ($n = 5$, mean ± SEM, $^*p < 0.05$). **(F)** IF micrographs of VE-cadherin and SLUG expression and DAPI in healthy or IPAH patient PAECs or in combination with treatment with $p16^{INK4}$ siRNA or scrambled control siRNA. Scale bar, 20 μm.

SUPPLEMENTARY FIGURE 3
BP GO term categories of senescence-related genes differentially expressed in hypoxia-treated mouse lung ECs. **(A)** Top 50 BP GO Term categories of senescence-related genes derived from significantly differentially expressing genes in control vs. hypoxia-treated mouse lung ECs. The color-coding corresponds to the network color key. Red: Transcription/Gene Expression, Gold: Protein/RNA processing, Green: Cell cycle, Blue: Inflammatory/Immune Response, Pink: Cell Signaling/Signal Transduction, Gray: Miscellaneous. **(B)** Heatmap of the 7 upregulated and 7 downregulated cellular senescence/SASP genes in normoxia- vs. hypoxia-treated mouse lung ECs.

References

1. Farber HW, Loscalzo J. Pulmonary arterial hypertension. *N Engl J Med.* (2004) 351:1655–65. doi: 10.1056/NEJMra035488

2. Mahapatra S, Nishimura RA, Sorajja P, Cha S, McGoon MD. Relationship of pulmonary arterial capacitance and mortality in idiopathic pulmonary arterial hypertension. *J Am Coll Cardiol.* (2006) 47:799–803. doi: 10.1016/j.jacc.2005.09.054

3. Rabinovitch M. Molecular pathogenesis of pulmonary arterial hypertension. *J Clin Invest.* (2012) 122:4306–13. doi: 10.1172/JCI60658

4. Guignabert C, Tu L, Girerd B, Ricard N, Huertas A, Montani D, et al. New molecular targets of pulmonary vascular remodeling in pulmonary arterial hypertension: importance of endothelial communication. *Chest.* (2015) 147:529–37. doi: 10.1378/chest.14-0862

5. Humbert M, Morrell NW, Archer SL, Stenmark KR, MacLean MR, Lang IM, et al. Cellular and molecular pathobiology of pulmonary arterial hypertension. *J Am Coll Cardiol.* (2004) 43(Suppl. S):13S—24S. doi: 10.1016/j.jacc.2004.02.029

6. Pietra GG, Capron F, Stewart S, Leone O, Humbert M, Robbins IM, et al. Pathologic assessment of vasculopathies in pulmonary hypertension. *J Am Coll Cardiol.* (2004) 43(Suppl. S):25S—32S. doi: 10.1016/j.jacc.2004.02.033

7. Mammoto A, Mammoto T. Vascular Niche in Lung Alveolar Development, Homeostasis, and Regeneration. *Front Bioeng Biotechnol.* (2019) 7:318. doi: 10.3389/fbioe.2019.00318

8. Gomez-Salinero JM, Itkin T, Rafii S. Developmental angiocrine diversification of endothelial cells for organotypic regeneration. *Dev Cell.* (2021) 56:3042–51. doi: 10.1016/j.devcel.2021.10.020

9. Rabinovitch M, Bothwell T, Hayakawa BN, Williams WG, Trusler GA, Rowe RD, et al. Pulmonary artery endothelial abnormalities in patients with congenital heart defects and pulmonary hypertension. A correlation of light with scanning electron microscopy and transmission electron microscopy. *Lab Invest.* (1986) 55:632–53.

10. Rosenberg HC, Rabinovitch M. Endothelial injury and vascular reactivity in monocrotaline pulmonary hypertension. *Am J Physiol.* (1988) 255(6 Pt 2):H1484–1491. doi: 10.1152/ajpheart.1988.255.6.H1484

11. Mammoto A, Hendee K, Muyleart M, Mammoto T. Endothelial Twist1-PDGFB signaling mediates hypoxia-induced proliferation and migration of αSMA-positive cells. *Sci Rep.* (2020) 10:7563. doi: 10.1038/s41598-020-64298-5

12. Campisi J. Aging, cellular senescence, and cancer. *Annu Rev Physiol.* (2013) 75:685–705. doi: 10.1146/annurev-physiol-030212-183653

13. van Deursen JM. The role of senescent cells in ageing. *Nature.* (2014) 509:439–46. doi: 10.1038/nature13193

14. Sharpless NE, Sherr CJ. Forging a signature of *in vivo* senescence. *Nat Rev Cancer.* (2015) 15:397–408. doi: 10.1038/nrc3960

15. Baker DJ, Childs BG, Durik M, Wijers ME, Sieben CJ, Zhong J, et al. Naturally occurring p16(Ink4a)-positive cells shorten healthy lifespan. *Nature.* (2016) 530:184–9. doi: 10.1038/nature16932

16. Jeon OH, Kim C, Laberge RM, Demaria M, Rathod S, Vasserot AP, et al. Local clearance of senescent cells attenuates the development of post-traumatic osteoarthritis and creates a pro-regenerative environment. *Nat Med.* (2017) 23:775–81. doi: 10.1038/nm.4324

17. Konstantinov IE, Ye XT, Fricke TA. From cellular senescence to regeneration: a quest for the holy grail for the next generation of surgeons? *J Thorac Cardiovasc Surg.* (2017) 154:953–4. doi: 10.1016/j.jtcvs.2017.05.036

18. Hamsanathan S, Alder JK, Sellares J, Rojas M, Gurkar AU, Mora AL. Cellular senescence: the trojan horse in chronic lung diseases. *Am J Respir Cell Mol Biol.* (2019) 61:21–30. doi: 10.1165/rcmb.2018-0410TR

19. Tsuji T, Aoshiba K, Nagai A. Alveolar cell senescence in patients with pulmonary emphysema. *Am J Respir Crit Care Med.* (2006) 174:886–93. doi: 10.1164/rccm.200509-1374OC

20. Noureddine H, Gary-Bobo G, Alifano M, Marcos E, Saker M, Vienney N, et al. Pulmonary artery smooth muscle cell senescence is a pathogenic mechanism for pulmonary hypertension in chronic lung disease. *Circ Res.* (2011) 109:543–53. doi: 10.1161/CIRCRESAHA.111.241299

21. Parikh P, Wicher S, Khandalavala K, Pabelick CM, Britt RD Jr, Prakash YS. Cellular senescence in the lung across the age spectrum. *Am J Physiol Lung Cell Mol Physiol.* (2019) 316:L826–42. doi: 10.1152/ajplung.00424.2018

22. Krtolica A, Parrinello S, Lockett S, Desprez PY, Campisi J. Senescent fibroblasts promote epithelial cell growth and tumorigenesis: a link between cancer and aging. *Proc Natl Acad Sci U S A.* (2001) 98:12072–7. doi: 10.1073/pnas.211053698

23. Collado M, Blasco MA, Serrano M. Cellular senescence in cancer and aging. *Cell.* (2007) 130:223–33. doi: 10.1016/j.cell.2007.07.003

24. Kang TW, Yevsa T, Woller N, Hoenicke L, Wuestefeld T, Dauch D, et al. Senescence surveillance of pre-malignant hepatocytes limits liver cancer development. *Nature.* (2011) 479:547–51. doi: 10.1038/nature10599

25. Rodier F, Coppe JP, Patil CK, Hoeijmakers WA, Munoz DP, Raza SR, et al. Persistent DNA damage signalling triggers senescence-associated inflammatory cytokine secretion. *Nat Cell Biol.* (2009) 11:973–9. doi: 10.1038/ncb1909

26. Baker DJ, Wijshake T, Tchkonia T, LeBrasseur NK, Childs BG, van de Sluis B, et al. Clearance of p16Ink4a-positive senescent cells delays ageing-associated disorders. *Nature.* (2011) 479:232–6. doi: 10.1038/nature10600

27. Acosta JC, Banito A, Wuestefeld T, Georgilis A, Janich P, Morton JP, et al. A complex secretory program orchestrated by the inflammasome controls paracrine senescence. *Nat Cell Biol.* (2013) 15:978–90. doi: 10.1038/ncb2784

28. Watanabe S, Kawamoto S, Ohtani N, Hara E. Impact of senescence-associated secretory phenotype and its potential as a therapeutic target for senescence-associated diseases. *Cancer Sci.* (2017) 108:563–9. doi: 10.1111/cas.13184

29. Gasek NS, Kuchel GA, Kirkland JL, Xu M. Strategies for targeting senescent cells in human disease. *Nat Aging.* (2021) 1:870–9. doi: 10.1038/s43587-021-00121-8

30. Chaouat A, Naeije R, Weitzenblum E. Pulmonary hypertension in COPD. *Eur Respir J.* (2008) 32:1371–85. doi: 10.1183/09031936.00015608

31. Farkas L, Gauldie J, Voelkel NF, Kolb M. Pulmonary hypertension and idiopathic pulmonary fibrosis: a tale of angiogenesis, apoptosis, and growth factors. *Am J Respir Cell Mol Biol.* (2011) 45:1–15. doi: 10.1165/rcmb.2010-0365TR

32. van der Feen DE, Bossers GPL, Hagdorn QAJ, Moonen JR, Kurakula K, Szulcek R, et al. Cellular senescence impairs the reversibility of pulmonary arterial hypertension. *Sci Transl Med.* (2020) 12:aaw4974. doi: 10.1126/scitranslmed.aaw4974

33. Culley MK, Zhao J, Tai YY, Tang Y, Perk D, Negi V, et al. Frataxin deficiency promotes endothelial senescence in pulmonary hypertension. *J Clin Invest.* (2021) 131:459. doi: 10.1172/JCI136459

34. Pozharskaya V, Torres-Gonzalez E, Rojas M, Gal A, Amin M, Dollard S, et al. Twist: a regulator of epithelial-mesenchymal transition in lung fibrosis. *PLoS ONE.* (2009) 4:e7559. doi: 10.1371/journal.pone.0007559

35. Mammoto T, Jiang A, Jiang E, Mammoto A. The role of twist1 phosphorylation in angiogenesis and pulmonary fibrosis. *Am J Respir Cell Mol Biol.* (2016) 55:633–44. doi: 10.1165/rcmb.2016-0012OC

36. Mammoto T, Muyleart M, Konduri GG, Mammoto A. Twist1 in hypoxia-induced pulmonary hypertension through TGFβ-Smad signaling. *Am J Respir Cell Mol Biol.* (2018) 58:194–207. doi: 10.1165/rcmb.2016-0323OC

37. Hendee K, Hunyenyiwa T, Matus K, Toledo M, Mammoto A, Mammoto T. Twist1 signaling in age-dependent decline in angiogenesis and lung regeneration. *Aging (Albany NY).* (2021) 13:202875. doi: 10.18632/aging.202875

38. Tran PT, Shroff EH, Burns TF, Thiyagarajan S, Das ST, Zabuawala T, et al. Twist1 suppresses senescence programs and thereby accelerates and maintains mutant Kras-induced lung tumorigenesis. *PLoS Genet.* (2012) 8:e1002650. doi: 10.1371/journal.pgen.1002650

39. Thery C, Zitvogel L, Amigorena S. Exosomes: composition, biogenesis and function. *Nat Rev Immunol.* (2002) 2:569–79. doi: 10.1038/nri855

40. Kourembanas S. Exosomes: vehicles of intercellular signaling, biomarkers, and vectors of cell therapy. *Annu Rev Physiol.* (2015) 77:13–27. doi: 10.1146/annurev-physiol-021014-071641

41. Mammoto T, Hunyenyiwa T, Kyi P, Hendee K, Matus K, Rao S, et al. Hydrostatic pressure controls angiogenesis through endothelial YAP1 during lung regeneration. *Front Bioeng Biotechnol.* (2022) 10:823642. doi: 10.3389/fbioe.2022.823642

42. Pant S, Hilton H, Burczynski ME. The multifaceted exosome: biogenesis, role in normal and aberrant cellular function, and frontiers for pharmacological and biomarker opportunities. *Biochem Pharmacol.* (2012) 83:1484–94. doi: 10.1016/j.bcp.2011.12.037

43. Davidson SM, Riquelme JA, Zheng Y, Vicencio JM, Lavandero S, Yellon DM. Endothelial cells release cardioprotective exosomes that may contribute to ischaemic preconditioning. *Sci Rep.* (2018) 8:15885. doi: 10.1038/s41598-018-34357-z

44. Thery C, Ostrowski M, Segura E. Membrane vesicles as conveyors of immune responses. *Nat Rev Immunol.* (2009) 9:581–93. doi: 10.1038/nri2567

45. Jakhar R, Crasta K. Exosomes as emerging pro-tumorigenic mediators of the senescence-associated secretory phenotype. *Int J Mol Sci.* (2019) 20:574. doi: 10.3390/ijms20102547

46. Xie Y, Gao Y, Zhang L, Chen Y, Ge W, Tang P. Involvement of serum-derived exosomes of elderly patients with bone loss in failure of bone remodeling *via* alteration of exosomal bone-related proteins. *Aging Cell.* (2018) 17:e12758. doi: 10.1111/acel.12758

47. Chang YJ, Li YS, Wu CC, Wang KC, Huang TC, Chen Z, et al. Extracellular microRNA-92a mediates endothelial cell-macrophage communication. *Arterioscler Thromb Vasc Biol.* (2019) 39:2492–504. doi: 10.1161/ATVBAHA.119.312707

48. Effenberger T, von der Heyde J, Bartsch K, Garbers C, Schulze-Osthoff K, Chalaris A, et al. Senescence-associated release of transmembrane proteins involves proteolytic processing by ADAM17 and microvesicle shedding. *FASEB J.* (2014) 28:4847–56. doi: 10.1096/fj.14-254565

49. Schumacher N, Meyer D, Mauermann A, von der Heyde J, Wolf J, Schwarz J, et al. Shedding of endogenous interleukin-6 receptor (IL-6R) is governed by A disintegrin and metalloproteinase (ADAM) proteases while a full-length IL-6R isoform localizes to circulating microvesicles. *J Biol Chem.* (2015) 290:26059–71. doi: 10.1074/jbc.M115.649509

50. Basisty N, Kale A, Jeon OH, Kuehnemann C, Payne T, Rao C, et al. A proteomic atlas of senescence-associated secretomes for aging biomarker development. *PLoS Biol.* (2020) 18:e3000599. doi: 10.1371/journal.pbio.3000599

51. Kadota T, Fujita Y, Yoshioka Y, Araya J, Kuwano K, Ochiya T. Emerging role of extracellular vesicles as a senescence-associated secretory phenotype: insights into the pathophysiology of lung diseases. *Mol Aspects Med.* (2018) 60:92–103. doi: 10.1016/j.mam.2017.11.005

52. Terlecki-Zaniewicz L, Lammermann I, Latreille J, Bobbili MR, Pils V, Schosserer M, et al. Small extracellular vesicles and their miRNA cargo are anti-apoptotic members of the senescence-associated secretory phenotype. *Aging (Albany NY).* (2018) 10:1103–32. doi: 10.18632/aging.101452

53. Lee C, Mitsialis SA, Aslam M, Vitali SH, Vergadi E, Konstantinou G, et al. Exosomes mediate the cytoprotective action of mesenchymal stromal cells on hypoxia-induced pulmonary hypertension. *Circulation.* (2012) 126:2601–11. doi: 10.1161/CIRCULATIONAHA.112.114173

54. Cruz FF, Borg ZD, Goodwin M, Sokocevic D, Wagner DE, Coffey A, et al. Systemic administration of human bone marrow-derived mesenchymal stromal cell extracellular vesicles ameliorates aspergillus hyphal extract-induced allergic airway inflammation in immunocompetent mice. *Stem Cells Transl Med.* (2015) 4:1302–16. doi: 10.5966/sctm.2014-0280

55. Willis GR, Fernandez-Gonzalez A, Anastas J, Vitali SH, Liu X, Ericsson M, et al. Mesenchymal stromal cell exosomes ameliorate experimental bronchopulmonary dysplasia and restore lung function through macrophage immunomodulation. *Am J Respir Crit Care Med.* (2018) 197:104–16. doi: 10.1164/rccm.201705-0925OC

56. Genschmer KR, Russell DW, Lal C, Szul T, Bratcher PE, Noerager BD, et al. Activated PMN exosomes: pathogenic entities causing matrix destruction and disease in the lung. *Cell.* (2019) 176:113–26.e115. doi: 10.1016/j.cell.2018.12.002

57. Mansouri N, Willis GR, Fernandez-Gonzalez A, Reis M, Nassiri S, Mitsialis SA, et al. Mesenchymal stromal cell exosomes prevent and revert experimental pulmonary fibrosis through modulation of monocyte phenotypes. *JCI Insight.* (2019) 4:128060. doi: 10.1172/jci.insight.128060

58. Dinh PC, Paudel D, Brochu H, Popowski KD, Gracieux MC, Cores J, et al. Inhalation of lung spheroid cell secretome and exosomes promotes lung repair in pulmonary fibrosis. *Nat Commun.* (2020) 11:1064. doi: 10.1038/s41467-020-14344-7

59. Klinger JR, Pereira M, Del Tatto M, Brodsky AS, Wu KQ, Dooner MS, et al. Mesenchymal stem cell extracellular vesicles reverse sugen/hypoxia pulmonary hypertension in rats. *Am J Respir Cell Mol Biol.* (2020) 62:577–87. doi: 10.1165/rcmb.2019-0154OC

60. Mohan A, Agarwal S, Clauss M, Britt NS, Dhillon NK. Extracellular vesicles: novel communicators in lung diseases. *Respir Res.* (2020) 21:175. doi: 10.1186/s12931-020-01423-y

61. Sindi HA, Russomanno G, Satta S, Abdul-Salam VB, Jo KB, Qazi-Chaudhry B, et al. Therapeutic potential of KLF2-induced exosomal microRNAs in pulmonary hypertension. *Nat Commun.* (2020) 11:1185. doi: 10.1038/s41467-020-14966-x

62. Mammoto A, Connor KM, Mammoto T, Yung CW, Huh D, Aderman CM, et al. A mechanosensitive transcriptional mechanism that controls angiogenesis. *Nature.* (2009) 457:1103–8. doi: 10.1038/nature07765

63. Mammoto T, Jiang E, Jiang A, Lu Y, Juan AM, Chen J, et al. Twist1 controls lung vascular permeability and endotoxin-induced pulmonary edema by altering Tie2 expression. *PLoS ONE.* (2013) 8:73407. doi: 10.1371/journal.pone.0073407

64. Monahan KB, Rozenberg GI, Krishnamurthy J, Johnson SM, Liu W, Bradford MK, et al. Somatic p16(INK4a) loss accelerates melanomagenesis. *Oncogene.* (2010) 29:5809–17. doi: 10.1038/onc.2010.314

65. Wang Y, Nakayama M, Pitulescu ME, Schmidt TS, Bochenek ML, Sakakibara A, et al. Ephrin-B2 controls VEGF-induced angiogenesis and lymphangiogenesis. *Nature.* (2010) 465:483–6. doi: 10.1038/nature09002

66. Mammoto T, Muyleart M, Mammoto A. Endothelial YAP1 in regenerative lung growth through the angiopoietin-Tie2 pathway *Am J Respir Cell Mol Biol.* (2019) 60:117–27. doi: 10.1165/rcmb.2018-0105OC

67. Mammoto T, Mammoto A. Implantation of fibrin gel on mouse lung to study lung-specific angiogenesis. *J Vis Exp.* (2014) 94:52012. doi: 10.3791/52012

68. Mammoto A, Muyleart M, Kadlec A, Gutterman D, Mammoto T. YAP1-TEAD1 signaling controls angiogenesis and mitochondrial biogenesis through PGC1α. *Microvasc Res.* (2018) 119:73–83. doi: 10.1016/j.mvr.2018.04.003

69. Mammoto T, Torisawa YS, Muyleart M, Hendee K, Anugwom C, Gutterman D, et al. Effects of age-dependent changes in cell size on endothelial cell proliferation and senescence through YAP1. *Aging.* (2019) 11:102236. doi: 10.18632/aging.102236

70. Hunyenyiwa T, Hendee K, Matus K, Kyi P, Mammoto T, Mammoto A. Obesity inhibits angiogenesis through TWIST1-SLIT2 signaling. *Front Cell Dev Biol.* (2021) 9:693410. doi: 10.3389/fcell.2021.693410

71. Coppe JP, Desprez PY, Krtolica A, Campisi J. The senescence-associated secretory phenotype: the dark side of tumor suppression.

Annu Rev Pathol. (2010) 5:99–118. doi: 10.1146/annurev-pathol-121808-102144

72. Gartz M, Darlington A, Afzal MZ, Strande JL. Exosomes exert cardioprotection in dystrophin-deficient cardiomyocytes *via* ERK1/2-p38/MAPK signaling. *Sci Rep.* (2018) 8:16519. doi: 10.1038/s41598-018-34879-6

73. Sheikh AQ, Saddouk FZ, Ntokou A, Mazurek R, Greif DM. Cell Autonomous and non-cell autonomous regulation of SMC progenitors in pulmonary hypertension. *Cell Rep.* (2018) 23:1152–65. doi: 10.1016/j.celrep.2018.03.043

74. Doyle LM, Wang MZ. Overview of extracellular vesicles, their origin, composition, purpose, and methods for exosome isolation and analysis. *Cells.* (2019) 8:727. doi: 10.3390/cells8070727

75. Gartz M, Lin CW, Sussman MA, Lawlor MW, Strande JL. Duchenne muscular dystrophy (DMD) cardiomyocyte-secreted exosomes promote the pathogenesis of DMD-associated cardiomyopathy. *Dis Model Mech.* (2020) 13:045559. doi: 10.1242/dmm.045559

76. Gillich A, Zhang F, Farmer CG, Travaglini KJ, Tan SY, Gu M, et al. Capillary cell-type specialization in the alveolus. *Nature.* (2020) 586:785–9. doi: 10.1038/s41586-020-2822-7

77. Herranz N, Gil J. Mechanisms and functions of cellular senescence. *J Clin Invest.* (2018) 128:1238–46. doi: 10.1172/JCI95148

78. Nelson G, Wordsworth J, Wang C, Jurk D, Lawless C, Martin-Ruiz C, et al. A senescent cell bystander effect: senescence-induced senescence. *Aging Cell.* (2012) 11:345–9. doi: 10.1111/j.1474-9726.2012.00795.x

79. Demaria M, Ohtani N, Youssef SA, Rodier F, Toussaint W, Mitchell JR, et al. An essential role for senescent cells in optimal wound healing through secretion of PDGF-AA. *Dev Cell.* (2014) 31:722–33. doi: 10.1016/j.devcel.2014.11.012

80. Stevens T, Phan S, Frid MG, Alvarez D, Herzog E, Stenmark KR. Lung vascular cell heterogeneity: endothelium, smooth muscle, and fibroblasts. *Proc Am Thorac Soc.* (2008) 5:783–91. doi: 10.1513/pats.200803-027HR

81. Schodel J, Oikonomopoulos S, Ragoussis J, Pugh CW, Ratcliffe PJ, Mole DR. High-resolution genome-wide mapping of HIF-binding sites by ChIP-seq. *Blood.* (2011) 117:e207–217. doi: 10.1182/blood-2010-10-314427

82. Bos R, van Diest PJ, de Jong JS, van der Groep P, van der Valk P, van der Wall E. Hypoxia-inducible factor-1alpha is associated with angiogenesis, and expression of bFGF, PDGF-BB, and EGFR in invasive breast cancer. *Histopathology.* (2005) 46:31–6. doi: 10.1111/j.1365-2559.2005.02045.x

83. Chen YR, Dai AG, Hu RC, Jiang YL. Differential and reciprocal regulation between hypoxia-inducible factor-alpha subunits and their prolyl hydroxylases in pulmonary arteries of rat with hypoxia-induced hypertension. *Acta Biochim Biophys Sin.* (2006) 38:423–34. doi: 10.1111/j.1745-7270.2006.00174.x

84. Xue G, Restuccia DF, Lan Q, Hynx D, Dirnhofer S, Hess D, et al. Akt/PKB-mediated phosphorylation of Twist1 promotes tumor metastasis *via* mediating cross-talk between PI3K/Akt and TGF-beta signaling axes. *Cancer Discov.* (2012) 2:248–59. doi: 10.1158/2159-8290.CD-11-0270

85. Li J, Liu CH, Sun Y, Gong Y, Fu Z, Evans LP, et al. Endothelial TWIST1 promotes pathological ocular angiogenesis. *Invest Ophthalmol Vis Sci.* (2014) 55:8267–77. doi: 10.1167/iovs.14-15623

86. Lee KW, Lee NK, Ham S, Roh TY, Kim SH. Twist1 is essential in maintaining mesenchymal state and tumor-initiating properties in synovial sarcoma. *Cancer Lett.* (2014) 343:62–73. doi: 10.1016/j.canlet.2013.09.013

87. Wirrig EE, Yutzey KE. Conserved transcriptional regulatory mechanisms in aortic valve development and disease. *Arterioscler Thromb Vasc Biol.* (2014) 34:737–41. doi: 10.1161/ATVBAHA.113.302071

88. Mendoza FA, Piera-Velazquez S, Farber JL, Feghali-Bostwick C, Jimenez SA. Endothelial cells expressing endothelial and mesenchymal cell gene products in Systemic Sclerosis-associated interstitial lung disease lung tissues. *Arthritis Rheumatol.* (2015) 68:210–17. doi: 10.1002/art.39421

89. Ranchoux B, Antigny F, Rucker-Martin C, Hautefort A, Pechoux C, Bogaard HJ, et al. Endothelial-to-mesenchymal transition in pulmonary hypertension. *Circulation.* (2015) 131:1006–18. doi: 10.1161/CIRCULATIONAHA.114.008750

90. Fleenor BS, Marshall KD, Rippe C, Seals DR. Replicative aging induces endothelial to mesenchymal transition in human aortic endothelial cells: potential role of inflammation. *J Vasc Res.* (2012) 49:59–64. doi: 10.1159/000329681

91. Frump AL, Datta A, Ghose S, West J, de Caestecker MP. Genotype-phenotype effects of Bmpr2 mutations on disease severity in mouse models of pulmonary hypertension. *Pulm Circ.* (2016) 6:597–607. doi: 10.1086/688930

92. Hopper RK, Moonen JR, Diebold I, Cao A, Rhodes CJ, Tojais NF, et al. In pulmonary arterial hypertension, reduced BMPR2 promotes endothelial-to-mesenchymal transition *via* HMGA1 and its target slug. *Circulation.* (2016) 133:1783–94. doi: 10.1161/CIRCULATIONAHA.115.020617

93. Orriols M, Gomez-Puerto MC, Ten Dijke P. BMP type II receptor as a therapeutic target in pulmonary arterial hypertension. *Cell Mol Life Sci.* (2017) 74:2979–95. doi: 10.1007/s00018-017-2510-4

94. Diebold I, Hennigs JK, Miyagawa K, Li CG, Nickel NP, Kaschwich M, et al. BMPR2 preserves mitochondrial function and DNA during reoxygenation to promote endothelial cell survival and reverse pulmonary hypertension. *Cell Metab.* (2015) 21:596–608. doi: 10.1016/j.cmet.2015.03.010

95. Wiley CD, Velarde MC, Lecot P, Liu S, Sarnoski EA, Freund A, et al. Mitochondrial dysfunction induces senescence with a distinct secretory phenotype. *Cell Metab.* (2016) 23:303–14. doi: 10.1016/j.cmet.2015.11.011

96. Wiley CD, Campisi J. The metabolic roots of senescence: mechanisms and opportunities for intervention. *Nat Metab.* (2021) 3:1290–301. doi: 10.1038/s42255-021-00483-8

97. Austin S, St-Pierre J. PGC1alpha and mitochondrial metabolism–emerging concepts and relevance in ageing and neurodegenerative disorders. *J Cell Sci.* (2012) 125:4963–71. doi: 10.1242/jcs.113662

98. Patten IS, Arany Z. PGC-1 coactivators in the cardiovascular system. *Trends Endocrinol Metab.* (2012) 23:90–7. doi: 10.1016/j.tem.2011.09.007

99. Fan W, Evans R. PPARs and ERRs: molecular mediators of mitochondrial metabolism. *Curr Opin Cell Biol.* (2015) 33:49–54. doi: 10.1016/j.ceb.2014.11.002

100. Arany Z, Foo SY, Ma Y, Ruas JL, Bommi-Reddy A, Girnun G, et al. HIF-independent regulation of VEGF and angiogenesis by the transcriptional coactivator PGC-1alpha. *Nature.* (2008) 451:1008–12. doi: 10.1038/nature06613

101. Kluge MA, Fetterman JL, Vita JA. Mitochondria and endothelial function. *Circ Res.* (2013) 112:1171–88. doi: 10.1161/CIRCRESAHA.111.300233

102. Pan D, Fujimoto M, Lopes A, Wang YX. Twist-1 is a PPARdelta-inducible, negative-feedback regulator of PGC-1alpha in brown fat metabolism. *Cell.* (2009) 137:73–86. doi: 10.1016/j.cell.2009.01.051

103. Kadlec AO, Chabowski DS, Ait-Aissa K, Gutterman DD. Role of PGC-1alpha in vascular regulation: implications for atherosclerosis. *Arterioscler Thromb Vasc Biol.* (2016) 36:1467–74. doi: 10.1161/ATVBAHA.116.307123

104. Mora AL, Bueno M, Rojas M. Mitochondria in the spotlight of aging and idiopathic pulmonary fibrosis. *J Clin Invest.* (2017) 127:405–14. doi: 10.1172/JCI87440

105. Prakash YS, Pabelick CM, Sieck GC. Mitochondrial dysfunction in airway disease. *Chest.* (2017) 125:618–26. doi: 10.1016/j.chest.2017.03.020

106. Voskamp C, Anderson LA, Koevoet WJ, Barnhoorn S, Mastroberardino PG, van Osch GJ, et al. TWIST1 controls cellular senescence and energy metabolism in mesenchymal stem cells. *Eur Cell Mater.* (2021) 41:401–14. doi: 10.22203/eCM.v042a25

107. Nayak D, Kumar A, Chakraborty S, Rasool RU, Amin H, Katoch A, et al. Inhibition of Twist1-mediated invasion by Chk2 promotes premature senescence in p53-defective cancer cells. *Cell Death Differ.* (2017) 24:1275–87. doi: 10.1038/cdd.2017.70

108. Lehmann BD, Paine MS, Brooks AM, McCubrey JA, Renegar RH, Wang R, et al. Senescence-associated exosome release from human prostate cancer cells. *Cancer Res.* (2008) 68:7864–71. doi: 10.1158/0008-5472.CAN-07-6538

109. van Balkom BW, de Jong OG, Smits M, Brummelman J, den Ouden K, de Bree PM, et al. Endothelial cells require miR-214 to secrete exosomes that suppress senescence and induce angiogenesis in human and mouse endothelial cells. *Blood.* (2013) 121:S3991–S3915. doi: 10.1182/blood-2013-02-478925

110. Weiner-Gorzel K, Dempsey E, Milewska M, McGoldrick A, Toh V, Walsh A, et al. Overexpression of the microRNA miR-433 promotes resistance to paclitaxel through the induction of cellular senescence in ovarian cancer cells. *Cancer Med.* (2015) 4:745–58. doi: 10.1002/cam4.409

111. Vickers KC, Remaley AT. Lipid-based carriers of microRNAs and intercellular communication. *Curr Opin Lipidol.* (2012) 23:91–7. doi: 10.1097/MOL.0b013e328350a425

112. Lai RC, Yeo RW, Tan KH, Lim SK. Exosomes for drug delivery - a novel application for the mesenchymal stem cell. *Biotechnol Adv.* (2013) 31:543–51. doi: 10.1016/j.biotechadv.2012.08.008

113. Patton MC, Zubair H, Khan MA, Singh S, Singh AP. Hypoxia alters the release and size distribution of extracellular vesicles in pancreatic cancer cells to support their adaptive survival. *J Cell Biochem.* (2020) 121:828–39. doi: 10.1002/jcb.29328

114. Alibhai FJ, Lim F, Yeganeh A, DiStefano PV, Binesh-Marvasti T, Belfiore A, et al. Cellular senescence contributes to age-dependent changes in circulating extracellular vesicle cargo and function. *Aging Cell.* (2020) 19:e13103. doi: 10.1111/acel.13103

115. Mammoto T, Chen J, Jiang E, Jiang A, Smith LE, Ingber DE, et al. LRP5 Regulates development of lung microvessels and

alveoli through the angiopoietin-Tie2 pathway. *PLoS ONE.* (2012) 7:e41596. doi: 10.1371/journal.pone.0041596

116. Stenmark KR, Mecham RP. Cellular and molecular mechanisms of pulmonary vascular remodeling. *Annu Rev Physiol.* (1997) 59:89–144. doi: 10.1146/annurev.physiol.59.1.89

117. McLoughlin P, Keane MP. Physiological and pathological angiogenesis in the adult pulmonary circulation. *Compr Physiol.* (2011) 1:1473–508. doi: 10.1002/cphy.c100034

118. Soubrier F, Chung WK, Machado R, Grunig E, Aldred M, Geraci M, et al. Genetics and genomics of pulmonary arterial hypertension. *J Am Coll Cardiol.* (2013) 62:D13–21. doi: 10.1016/j.jacc.2013.10.035

119. Li M, Vattulainen S, Aho J, Orcholski M, Rojas V, Yuan K, et al. Loss of bone morphogenetic protein receptor 2 is associated with abnormal DNA repair in pulmonary arterial hypertension. *Am J Respir Cell Mol Biol.* (2014) 50:1118–28. doi: 10.1165/rcmb.2013-0349OC

120. Min J, Feng R, Badesch D, Berman-Rosenzweig E, Burger C, Chakinala M, et al. Obesity in pulmonary arterial hypertension (PAH): the pulmonary hypertension association registry (PHAR). *Ann Am Thorac Soc.* (2020) 18:229–37. doi: 10.1164/ajrccm-conference.2019.199.1_MeetingAbstracts.A2510

121. Conley SM, Hickson LJ, Kellogg TA, McKenzie T, Heimbach JK, Taner T, et al. Human obesity induces dysfunction and early senescence in adipose tissue-derived mesenchymal stromal/stem cells. *Front Cell Dev Biol.* (2020) 8:197. doi: 10.3389/fcell.2020.00197

frontiers | Frontiers in Medicine

TYPE Review
PUBLISHED 30 November 2022
DOI 10.3389/fmed.2022.1041236

OPEN ACCESS

EDITED BY
Judit Pongracz,
University of Pécs, Hungary

REVIEWED BY
Marco Massari,
Independent Researcher,
Reggio Emilia, Italy
Ashraf Roshdy,
Alexandria University, Egypt

*CORRESPONDENCE
Rudolf K. F. Oliveira
rudolf.oliveira@unifesp.br

†These authors have contributed equally to this work and share first authorship

SPECIALTY SECTION
This article was submitted to Pulmonary Medicine, a section of the journal Frontiers in Medicine

RECEIVED 10 September 2022
ACCEPTED 14 November 2022
PUBLISHED 30 November 2022

CITATION
Oliveira RKF, Nyasulu PS, Iqbal AA, Hamdan Gul M, Ferreira EVM, Leclair JW, Htun ZM, Howard LS, Mocumbi AO, Bryant AJ, Tamuzi JL, Avdeev S, Petrosillo N, Hassan A, Butrous G and de Jesus Perez V (2022) Cardiopulmonary disease as sequelae of long-term COVID-19: Current perspectives and challenges. *Front. Med.* 9:1041236. doi: 10.3389/fmed.2022.1041236

Cardiopulmonary disease as sequelae of long-term COVID-19: Current perspectives and challenges

Rudolf K. F. Oliveira[1*†], Peter S. Nyasulu[2†], Adeel Ahmed Iqbal[3†], Muhammad Hamdan Gul[4†], Eloara V. M. Ferreira[1], John William Leclair[5], Zin Mar Htun[6], Luke S. Howard[7], Ana O. Mocumbi[8,9], Andrew J. Bryant[10], Jacques L. Tamuzi[2], Sergey Avdeev[11], Nicola Petrosillo[12], Ahmed Hassan[13], Ghazwan Butrous[14] and Vinicio de Jesus Perez[15]

[1]Division of Respiratory Diseases, Department of Medicine, Federal University of São Paulo (UNIFESP), São Paulo, Brazil, [2]Division of Epidemiology and Biostatistics, Department of Global Health, Faculty of Medicine and Health Sciences, Stellenbosch University, Stellenbosch, South Africa, [3]National Health System (NHS), Global Clinical Network, London, United Kingdom, [4]Department of Internal Medicine, University of Kentucky, Lexington, KY, United States, [5]Department of Medicine, Stanford University, Stanford, CA, United States, [6]Division of Pulmonary and Critical Care, National Institute of Health, University of Maryland, College Park, College Park, MD, United States, [7]National Heart and Lung Institute, Imperial College London, London, United Kingdom, [8]Faculty of Medicine, Universidade Eduardo Mondlane, Maputo, Mozambique, [9]Non-communicable Diseases Division, Instituto Nacional de Saúde, Marracuene, Mozambique, [10]College of Medicine, University of Florida, Gainesville, FL, United States, [11]Department of Pulmonology, I.M. Sechenov First Moscow State Medical University (Sechenov University), Moscow, Russia, [12]Infection Prevention and Control-Infectious Disease Service, Foundation University Hospital Campus Bio-Medico, Rome, Italy, [13]Department of Cardiology, Cairo University, Cairo, Egypt, [14]Medway School of Pharmacy, University of Kent at Canterbury, Canterbury, United Kingdom, [15]Division of Pulmonary, Allergy and Critical Care Medicine, Stanford University Medical Center, Stanford, CA, United States

COVID-19 infection primarily targets the lungs, which in severe cases progresses to cytokine storm, acute respiratory distress syndrome, multiorgan dysfunction, and shock. Survivors are now presenting evidence of cardiopulmonary sequelae such as persistent right ventricular dysfunction, chronic thrombosis, lung fibrosis, and pulmonary hypertension. This review will summarize the current knowledge on long-term cardiopulmonary sequelae of COVID-19 and provide a framework for approaching the diagnosis and management of these entities. We will also identify research priorities to address areas of uncertainty and improve the quality of care provided to these patients.

KEYWORDS

COVID-19, pulmonary hypertension, interstitial lung disease, thrombosis, right ventricular dysfunction

Introduction

The post-COVID-19 syndrome (or long COVID) is defined by the persistence of symptoms with a history of probable or confirmed SARS-CoV-2 infection, usually 3 months from the onset and lasts at least 2 months in the absence of an alternative diagnosis (1). CDC defines long COVID in the context of lingering symptoms that can last greater than 4 weeks and even months in a patient who had the onset of COVID-19 infection 4 weeks prior (2). The main symptoms are fatigue, muscle weakness, dyspnea, sleep, and cognitive disturbances. The proposed hypotheses to explain these findings relate to the viral toxicity itself, systemic inflammatory response, persistent impairment of gas exchange, restrictive lung disease, perfusion abnormality due to micro and macro vascular thrombosis, chronic myocardial dysfunction, corticosteroids use, prolonged hospitalization with immobility, and post-traumatic stress syndrome (3, 4).

Even though the burden of long COVID symptoms correlates with the severity of COVID-19 acute infection (5, 6), patients with milder COVID-19 also have a substantial burden of long COVID symptoms on follow-up. In a study that compared COVID-19 patients who were hospitalized vs. home-isolated patients at 6 months, the persistence of symptoms was noted in 81 vs. 55% of patients respectively (7). In a clinical follow-up of 150 non-critically ill COVID-19 patients after 3 months, 66% of the patients reported symptoms—40% reported asthenia, 30% reported dyspnea, and 23% reported anosmia or dysgeusia (8). In a multistate telephonic survey of 274 patients who had been tested positive for COVID-19 as outpatient, 35% of the patients had not returned to their usual state of health when interviewed 2–3 weeks after being tested positive (9).

A significant economic burden on the healthcare system is expected with the increasing long COVID cases, and further studies exploring this aspect are encouraged. The full spectrum and burden of long COVID in terms of symptoms and cardiopulmonary sequelae such as pulmonary hypertension will be more apparent in the coming years. This narrative review will focus on the most prevalent cardiopulmonary sequelae reported in COVID-19 survivors. We will address the current understanding of the pathobiological mechanisms potentially involved in developing these conditions and focus on areas of uncertainties that should be prioritized in research efforts. We will also review the management strategies for these commonly encountered post-COVID-19 conditions. As the pool of patients recovering from COVID-19 continues to increase, healthcare providers will need to learn to recognize these cardiopulmonary sequelae early and develop a management plan, including focusing on rehabilitation techniques that will prevent further deterioration and improve the quality of life for these patients.

Long-term cardiovascular complications in COVID-19

Cardiovascular complications in COVID-19 infection, including myocardial injury, myocarditis, heart failure, and arrhythmias, have been well-reported during the acute phase since the pandemic's start (10). The incidence of long-term cardiovascular complications after 30 days of COVID-19 was studied in the US database on a cohort of 153,760 veterans, and an increased risk of strokes, dysrhythmias, myocarditis, ischemic heart diseases, heart failure, cardiac arrest, pulmonary embolism, and deep vein thrombosis was observed (11). The higher risk of cardiovascular complications also extended to COVID-19 survivors who were not hospitalized in this large study (11). These findings were comparable to the results from another large retrospective cohort study (12). In another study of 587 COVID-19 patients, who were followed 1 year after discharge, 11 patients were thought to have died from complications due to COVID-19, including cardiovascular complications such as acute myocardial infarction, acute heart failure and sudden death related to malignant arrhythmia and pulmonary thromboembolism (13). Additionally, new-onset diabetes and major cardiovascular adverse events have also been reported in COVID-19 patients after hospital discharge (14). Regarding the dynamic changes in the ECG or arrhythmias observed during the acute phase of COVID-19, they tend to resolve by 6 months post-COVID-19 (15, 16). However, sinus tachycardia is prevalent in post-COVID-19 survivors (15, 17) and postural orthostatic tachycardia may be the etiology in the setting of persistent complaints of dizziness (18). The cardiovascular impact of COVID-19 infection has also been studied in autopsy studies.

Risk of myocarditis in post-COVID-19 survivors

In an extensive multicenter study screening for myocarditis in 1,597 athletes who underwent cardiac magnetic resonance (CMR) imaging, 2.3% were diagnosed with COVID-19 myocarditis—9 had clinical and 27 had subclinical myocarditis. Follow-up CMR in the 4–14 weeks demonstrated resolution of T2 elevation in all 27 athletes and late gadolinium enhancement in 11 athletes (3). In another observational cohort study following athletes, clinically indicated CMR had a higher yield of myocarditis [15 of 119 (12.6%)] vs. primary screening CMR [6 of 198 (3.0%)]. In post-COVID-19 patients with cardiac symptoms, cardiac edema (54%) and late gadolinium enhancement (31%) on CMR imaging has been reported (15). However, in a study involving 32 patients post-COVID-19 with persistent cardiovascular symptoms, only 3 (9%) met the criteria of acute myocarditis on CMR imaging, and none of those patients met criteria for myocarditis on endomyocardial

biopsy (19). In a meta-analysis, the overall prevalence of myocarditis in athletes who had recovered from COVID-19 ranged from 1 to 4% (20). In a study of post-COVID-19 patients (average time since COVID-19 was 4 months) where myocarditis was diagnosed with biopsy in six patients, SARS-CoV-2 was found in four biopsies, lymphocytic myocarditis was found in five, and one patient had giant cell myocarditis (21). The presence of COVID-19 in myocardial tissue months after infection with COVID-19 explains the persistence of chronic inflammation in patients with myocarditis. In a meta-analysis of 277 post-mortem examinations, COVID-19 related histopathological changes such as macro or microvascular thrombi, inflammation, or intraluminal megakaryocytes were common; however, the true prevalence of myocarditis was likely less than 2% based on the pathological analysis. Global uniformity with the use of an autopsy checklist was suggested in reporting cardiovascular pathology findings in COVID-19 (22).

These data indicate that post-COVID-19 survivors can have lingering cardiovascular morbidities in the long-term. Increased burden of cardiovascular complications is also found in COVID-19 patients who may not be hospitalized for COVID-19. During the clinic's follow-up visits of COVID-19 patients, the possibility of long-term cardiovascular complications should be entertained, especially in the presence of symptoms, and referred to the appropriate specialty clinic when needed. Long-term cardiovascular complications with increased risk in COVID-19 are presented in **Table 1**.

Right ventricular dysfunction

Prevalence and pathogenesis of right ventricular dysfunction

Right ventricular dysfunction is a known cardiovascular complication of COVID-19 infection observed in 20–31% of cases and associated with increased mortality (23–27). Additionally, worse right ventricular function is associated with elevated troponin and worse clinical presentation (23) and impaired longitudinal strain on echocardiography (27, 28). In a meta-analysis of 1,450 patients, those with right ventricular dysfunction had twofold mortality compared to those without (48.5 vs. 24.7%) (29).

It is known that the thin-walled right ventricle is susceptible to ischemia and dysfunction in response to sudden increases in afterload or coronary occlusion, which in turn may compromise left ventricular function (30). Increased right ventricular afterload in SARS-CoV-2 infection can be secondary to pulmonary parenchymal abnormalities combined with macro- or micro pulmonary vascular disease. In this context, the extent of local tissue damage and the cytokine storm triggered by the host immune response may contribute to the severity of the disease and right ventricular dysfunction (31). Furthermore, activation of the inflammatory cells present in atherosclerotic plaques may lead to coronary plaque rupture and subsequent myocardial ischemia (32). Finally, cardiac CMR imaging findings of patients recovered from COVID-19 infection point to myocardial tissue abnormalities and impaired right ventricular function in otherwise healthy subjects, ultimately suggesting chronic cardiac disease as a consequence of SARS-CoV-2 infection (33). Potential mechanisms of right ventricular dysfunction in COVID-19 are summarized in **Figure 1**.

TABLE 1 Long-term cardiovascular complications with increased risk in COVID-19.

Arrhythmias; atrial fibrillation, sinus tachycardia, sinus bradycardia, atrial flutter, ventricular arrhythmias
Inflammatory heart diseases; myocarditis, pericarditis
Ischemic heart disease: acute coronary syndrome, myocardial infarction, ischemic cardiomyopathy, angina
Other cardiac disorders: heart failure, non-ischemic cardiomyopathy, cardiac arrest
Thrombotic complications; DVT, pulmonary embolism, superficial venous thrombosis
Cerebrovascular disorders; stroke, TIA

Management of right ventricular dysfunction

Management of acute right ventricular dysfunction depends on treating the underlying etiology in addition to the optimization of the intravascular volume, reducing the right ventricular afterload, and enhancing ventricular contractility. Milrinone, a phosphodiesterase-3 inhibitor, enhances right ventricular contractility and reduces pulmonary vascular resistance (34) and may be used instead of dobutamine; however, it might induce hypotension and arrhythmias (35). Inhaled nitric oxide, a selective pulmonary vasodilator, may be beneficial in reducing and stabilizing the pulmonary artery systolic pressure and might reduce the risk of right ventricular failure in COVID-19 (36). Levosimendan, a calcium sensitizer with the advantages of improving the right ventricular contractility and reducing right ventricular afterload with no increase in myocardial oxygen consumption (37), may increase cardiac output and decrease mean pulmonary artery pressure, right atrial pressure, and peripheral systemic resistance in the setting of acute heart failure. Nevertheless, no randomized controlled trials support improved mortality (38–41). Finally, in the presence of severe right ventricular dysfunction, venoarterial, venovenous, venovenous-arterial, or venopulmonary-arterial extracorporeal membrane oxygenation may be required to augment the right ventricle function (42, 43).

In the setting of chronic right heart failure, long-term supplemental oxygen use is recommended for patients with

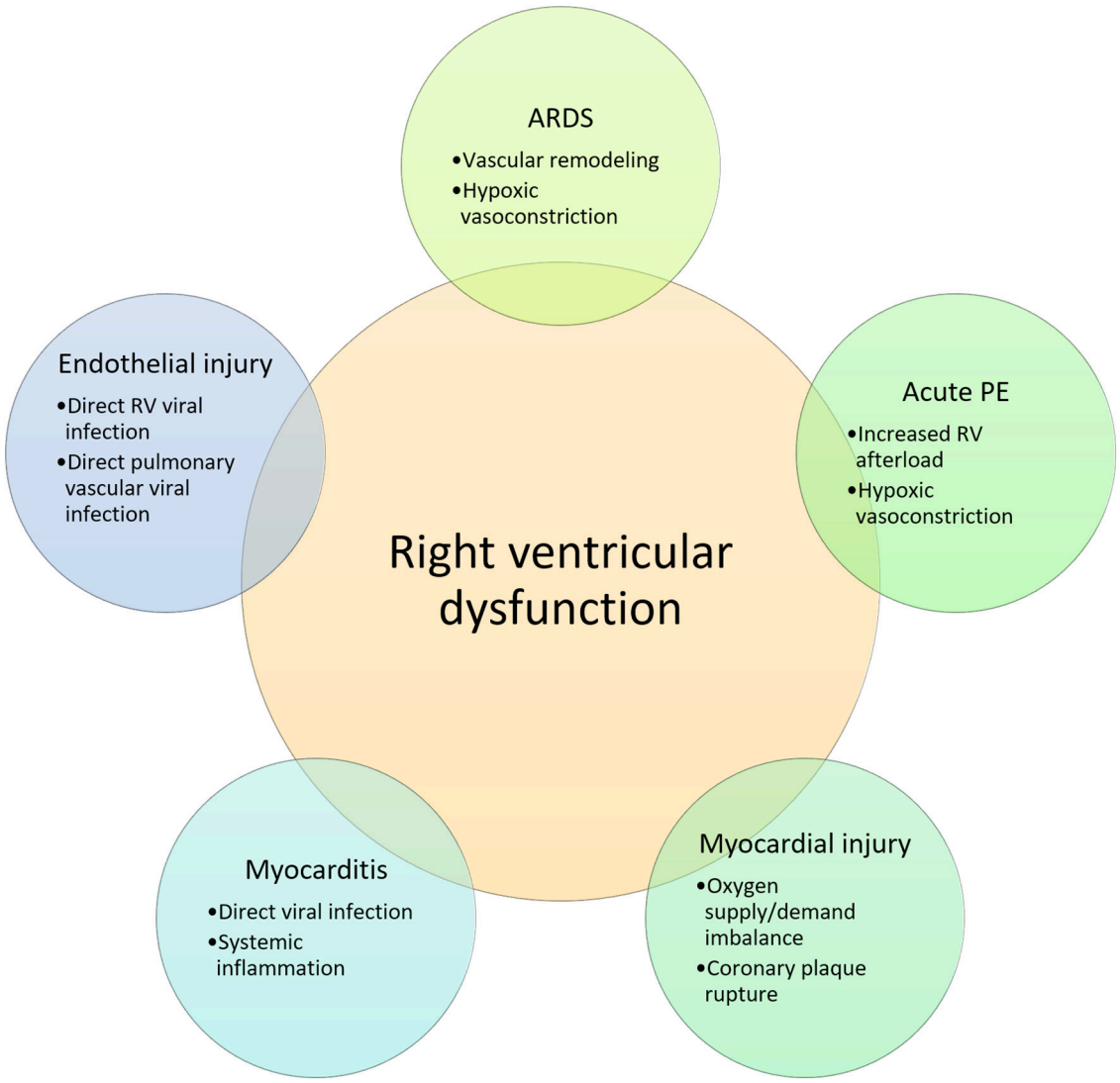

FIGURE 1
Potential mechanisms of right ventricular dysfunction in COVID-19. RV, right ventricular; ARDS, acute respiratory distress syndrome; PE, pulmonary embolism; IL, interleukin.

resting or exercise-induced hypoxemia, aiming to reduce hypoxic vasoconstriction and avoid an increase in pulmonary vascular resistance (44). Volume overload should be treated with diuretics. In the setting of isolated right heart failure due to pulmonary embolism, while being cautious of avoiding volume depletion, low-dose diuretics may be used (45). In the setting of decreased left ventricular ejection fraction, goal-directed medical therapy should be employed (46). Whether pulmonary vasodilators can be used or not depends on the primary etiology of pulmonary hypertension, which is further discussed in the section of post-COVID-19 pulmonary hypertension.

Right ventricular dysfunction may not be fully reversible in some COVID-19 survivors, depending on the chronicity of the ischemic insult. In a canine study that involved banding of the pulmonary artery inducing right heart failure, reversibility of the right ventricle was shown to be more profound in those in which pulmonary afterload was reduced early (47). In another canine study, depressed right ventricular function due to severe pulmonary artery obstruction was restored after right coronary artery hyper perfusion (48). However, chronic hypoxia in rats has been shown to induce non-reversible right ventricular dysfunction (49). Additionally, direct or indirect injury of right ventricular myocytes and endothelial cells by SARS-CoV-2 or systemic inflammation might chronically impact right ventricular myocardial and endothelial viability resulting in right ventricular dysfunction. Also, we should point out that the development of chronic thromboembolic pulmonary hypertension (CTEPH) can be accompanied by right ventricular

dysfunction (50), which is further discussed in the section of post-COVID-19 pulmonary hypertension. Further studies on the reversibility of right ventricular dysfunction in COVID-19 patients should be pursued and patients with right ventricular dysfunction will require close follow-up for signs of heart failure.

Post-COVID-19 lung fibrosis

Overview of lung function recovery post-COVID-19

A subgroup of post-COVID-19 patients will evolve with persistent chest imaging abnormalities (51) and/or reduced lung diffusion capacity (52, 53). Additionally, post-COVID-19 patients reporting persistent dyspnea, are more likely to have a restrictive pattern, lower carbon monoxide diffusion capacity, reduced functional capacity, and increased exertional desaturation (54). There findings were confirmed by a systematic review of studies assessing pulmonary function post-COVID-19, where altered carbon monoxide diffusion capacity, restrictive pattern, and obstructive pattern were observed in 39, 15, and 7% of patients, respectively, between 1 and 3 months after COVID-19 (55).

In a large study undertaken during the first wave of the COVID-19 epidemic in Wuhan, China, 1,733 of 2,469 discharged patients with COVID-19 were followed up 6 months after hospital discharge. Patients with higher severity scores were found to have lower 6-min walking distance, decreased carbon monoxide diffusion capacity on the pulmonary function test, and worse imaging findings corroborated by high computed tomography (CT) scores (56). Although the pathological characterization of postmortem lung samples from patients who died early after COVID-19 has been extensively reported (57, 58), little is known about the residual pathological changes in the lungs of patients within 2 years of survival of acute COVID-19 (11).

Taken together, these studies suggest that patients with greater severity of acute COVID-19 may have a higher risk for long-term pulmonary complications. These persisting abnormalities are attributed to diffusion impairment and structural pulmonary abnormalities such as pulmonary fibrosis (59).

Evolving pulmonary fibrotic changes in COVID-19

Pulmonary fibrosis is the consequence of aberrant wound healing, which results in a cascade of pathological changes that replaces the lung parenchyma with an extracellular matrix (60). On imaging, pulmonary fibrosis is suggested by the parenchymal bands, reticular opacities, traction bronchiectasis, and honeycombing (61). Pulmonary fibrosis is among the most feared chronic pulmonary complications of COVID-19. It can be challenging to separate the fibrotic changes from the reversible lingering opacities from COVID-19 pneumonia based on the imaging in the post-COVID-19 setting. Often encountered are the imaging findings denoting "grey areas," which represent evolving immature fibroblastic changes in the background of the diffuse alveolar damage (DAD) remodeling over time (62). It is thus preferred to use the term post-COVID interstitial lung disease (PCILD), which covers a broader spectrum of evolving pulmonary changes seen in patients who have recovered from COVID-19 pneumonia and leaves the prospect of reversibility an open question (62, 63).

Reticular changes suggestive of fibrotic changes were found in half of COVID-19 survivors (23 out of 46) screened at 2 weeks intervals after the onset of severe COVID-19, and these changes persisted at the 4-week follow-up (64). Han et al. showed fibrotic changes in 35% of survivors of severe COVID-19 pneumonia at a 6-month follow-up chest CT (61). According to Vasarmidi et al., the rate of COVID-induced fibrosis may exceed 30% (65, 66). Wu et al. demonstrated that 24% of patients had abnormal CT images at 12 months (67). Similarly, Huang et al. found that at 2 months post-discharge, extensive fibrosis was evident on the CT imaging of 42 out of 81 (52%) patients (68).

The prevalence of PCILD disease varied across all these studies. While interpreting the results of these studies, it is essential to realize that in post-SARS-CoV-2 respiratory syndrome, CT findings suggestive of fibrosis at initial imaging may eventually improve or even resolve with further follow-up (69, 70), but several cases of progressive pulmonary fibrosis have been described in patients with COVID-19 (71–73). Based on the observational studies on SARS-CoV-1, the residual lung damage decreased by the end of the first year (74, 75); however, it persisted after that in the 15 years of follow-up (76). Given that post-COVID-19 pulmonary fibrosis can result in severe chronic hypoxic respiratory failure with significantly debilitating dyspnea, patients with irreversible PCILD after approximately a year may be potential candidates for a lung transplant. Flaifel et al. described the lung pathology of such a population of patients before the lung transplant (77). At 8–11 months after COVID-19 diagnosis, the significant changes noted were described as proliferative and fibrotic phases of DAD, diffuse type 2 pneumocyte hyperplasia, prominent interstitial capillary neo-angiogenesis, and mononuclear cells, specifically macrophages (77).

Risk factors of pulmonary fibrosis in COVID-19

Numerous risk factors have been attributed to the development of PCILD, such as the length of stay in the hospital and the ICU, the use of high-flow nasal oxygen,

mechanical ventilation, and the occurrence of acute respiratory distress (66, 78). Acute respiratory distress syndrome (ARDS) is a condition well known for high rates of development of pulmonary fibrosis (79–81). Ventilator-associated lung injury, in the setting of non-adherence to protective lung strategies, can further worsen lung injury (82). Among survivors of severe COVID-19, 20% of non-mechanically ventilated and 72% of mechanically ventilated individuals had fibrotic-like radiographic abnormalities 4 months after hospitalization (83). Greater initial severity of the disease and a longer duration of mechanical ventilation were independent risk factors for the development of fibrosis-like abnormalities. Similar findings were also reported in another study that found most COVID-19 patients with pulmonary fibrosis (81%) during acute COVID-19 infection were admitted to an ICU, and 63% required mechanical ventilation (84).

Patient-related risk factors included male gender, older age, active smoking, persistent breathlessness, and alcohol abuse (68, 85–88). Men are three times more likely to develop PCILD (85). Han et al. identified age >50 years and heart rate >100 beats per minute at admission as independent predictors of fibrotic-like changes in survivors of severe COVID-19 pneumonia at a 6-month follow-up (61). Finally, cytokines such as interleukin-6 and upregulation of other growth factors such as TGF-β1, FGF, and EGF also contribute to the development of pulmonary fibrosis (89, 90). Neutrophil extracellular traps play a key role in the interplay between inflammation and thrombotic changes in the lung. They may have a role in the development of lung fibrosis (91) and therefore can be a potential therapeutic target (92).

Link between idiopathic pulmonary fibrosis and COVID-19

Gene-environment interactions and genetic susceptibility factors may play a role in the development of PCILD. Fadista et al. found a genetic correlation between idiopathic pulmonary fibrosis and COVID-19 severity, pointing several variants associated with both increased idiopathic pulmonary fibrosis risk and increased risk of severe COVID-19 (93). Additionally, genome-wide association studies have identified multiple genetic signals associated with severe COVID-19, including a variant within the DPP9 gene related to increased idiopathic pulmonary fibrosis risk (94). Four genetic association signals showed evidence of a shared causal variant between idiopathic pulmonary fibrosis and at least one COVID-19 phenotype, namely loci at 7q22.1, near MUC5B, near ATP11A, and near DPP9 (94). Finally, shorter blood leukocyte telomere lengths are independent risk factors for developing fibrotic-like abnormalities in COVID-19 (83). Thus, this genomic biomarker may predict increased susceptibility to the development of post-COVID-19 pulmonary fibrosis.

Diagnosis of post-COVID interstitial lung disease

A diagnosis of PCILD should be based on clinical, radiologic, and pathologic findings. While the appropriate timing for the diagnosis of irreversible fibrosis has not yet been established, serial evaluation with lung function test, including assessment for carbon monoxide diffusion capacity and 6-min walk test, can be tailored to the patient's clinical course, symptoms, and oxygen requirement. Further evaluation may involve the need for a chest CT (90, 95). Earlier in the pandemic, more frequent serial evaluations at 3, 6, 9, and 12 months were recommended, as there was a need for further research studies in this area (95, 96). Although there is no specific finding from laboratory testing, immunohistochemical analysis of TGF-b, IL-1α, and IFN-β may play a role in predicting PCILD. In this context, a recent study found that high IL-1α and TGF-β and low plasma levels of IFN-β could predict an increased relative risk of lung fibrosis-like changes in PCILD (97). More research is needed to confirm the prognostic role of genetic tests such as telomere shortening in PCILD.

Management of post-COVID interstitial lung disease

The role of treatment with antifibrotic and anti-inflammatory drugs (65, 98–100) in improving PCILD symptoms remains unclear and inconclusive. There is still little data on the safety and effectiveness of those treatments in COVID-19 patients with PCILD, and most clinical trials have yet to be completed. Recent evidence has shown that the use of high-dose vs. low-dose prednisolone in a randomized control trial of 130 patients with PCILD did not show significant improvement in symptoms after 6 weeks of follow-up (101). In contrast, three observational studies have reported improvement with glucocorticoids in symptomatic patients with PCILD (102–104). However, these findings should be interpreted cautiously because the two studies had small sample sizes (103, 104). A recent trial found that Pycnogenol® and Centellicum® may improve the residual clinical picture in PCILD patients and reduce the number of subjects progressing to lung fibrosis (100). However, this result should be viewed in the context of small sample size and a poorly designed study. Randomized clinical trials with Pycnogenol® and Centellicum® in PCILD patients are highly recommended. Other suggested therapies include mesenchymal stem cells, cytokine Inhibitors, spironolactone, TGF-β1 Inhibitors, CD147 Inhibitors, poly-(ADP-Ribose) polymerase Inhibitor, galectin-3 (e.g., BIO 300), and Chinese medicine drugs for pulmonary fibrosis in convalescent sequelae of COVID-19 (99, 105).

Presently, the treatment for PCILD remains supportive. Referral to pulmonary rehabilitation programs and evaluation

for supplemental oxygen therapy should be considered for patients meeting the criteria. The role of treatment with antifibrotic drugs remains unclear whose lung function continues to deteriorate.

Persisting coagulation abnormalities in COVID-19 survivors

Various coagulation abnormalities such as increased D-dimer, fibrinogen, factor VIII levels, mild thrombocytopenia, and slightly prolonged prothrombin time have been noted in the setting of the inflammatory milieu featured in COVID-19 (106–110). These coagulation abnormalities predispose COVID-19 patients to acute macro and micro thromboembolic events (111). The predisposition to coagulopathy is manifested in the form of microangiopathy with widespread thrombosis observed in COVID-19 autopsied lungs (112). The 90-day incidence rate of venous thromboembolism may range from 0.2 to 0.8% in COVID-19 cases and up to 4.5% in hospitalized patients (113).

Persistent hypercoagulability has been observed in COVID-19 survivors. A study on 208 COVID-19 survivors 2 months after onset, identified significant activation of endothelial cells and *in vivo* thrombin generation in at least one out of four COVID-19 survivors (114). At 3 months, 203 COVID-19 survivors were found to have increased endothelin-1, thrombin-antithrombin complex, von-Willebrand factor, and inflammatory cytokines (115). Others have identified increased thrombin generation capacity and hypofibrinolytic activity in the setting of increased Factor VIII levels and decreased plasminogen-activator inhibitor 1 (116). In 39 COVID-19 survivors followed for coagulation abnormalities after a year, elevated D-dimer, factor VIII, von-Willebrand factor antigen and interleukin-6 was reported. In a prospective registry study of 4,906 hospitalized patients followed at the mean of 92 days, venous thromboembolic event rates of 1.55% were noted, more than half of which included pulmonary embolism (117). Other smaller studies had thromboembolic events ranging from 0.2 to 2.5% (118–121). Thus, persisting hypercoagulopathy and higher rates of pulmonary thromboembolism have been noted in the post-discharge period in COVID-19 survivors.

Pulmonary hypertension

The vascular remodeling and luminal microthrombi noted in acute SARS-CoV-2 infection raise the suspicion that SARS-CoV-2 infection could be a risk factor for the future development of pulmonary arterial hypertension (122). Thickened pulmonary vascular walls, one of the hallmarks of pulmonary arterial hypertension, were reported in SARS-CoV-2 infection. In an autopsy study, the pulmonary vascular wall thickness was more than twice thicker than those of patients who died from H1N1 influenza (123).

The role of ACE2 in the pathogenesis of pulmonary vascular disease in COVID-19

The vascular endothelium is one of the primary targets of SARS-CoV-2 and the molecular pathways and cellular abnormalities observed in SARS-CoV-2 pulmonary vascular injury are similar to the pathogenesis pathway of pulmonary arterial hypertension (124). Direct viral infection and inflammatory cytokines outbursts are plausible mechanisms for endothelial damage caused by SARS-CoV-2. The host receptor for the virus (ACE2) is widely expressed in endothelial cells. Monteil et al. showed that SARS-CoV-2 can directly infect engineered human blood vessels, which can be inhibited by human recombinant soluble ACE2 (125). Varga et al. demonstrated in an autopsy study that viral particles were present in the endothelial cells of the glomerular capillary loops by electron microscopy of kidney tissue (126).

The presence of ACE2 within normal levels in the lung seems to be essential to combat inflammatory lung disease (127). In PAH, angiotensin II is upregulated and its level correlates with disease severity. Downregulation of ACE2 during SARS-CoV-2 infection can potentially increase angiotensin II circulating levels. Perivascular lymphocytic infiltration has been found in lung biopsies from patients with SARS-CoV-2 infection (125, 126). An autopsy study by Ackermann et al. demonstrated severe endothelial injury in SARS-CoV-2 infection, mediated by the entry of the virus into the endothelial cells, resulting in micro and macrovascular thrombosis. These features are distinct compared to patients who died from ARDS secondary to H1N1 influenza (112). The mechanisms described earlier may also contribute to developing pulmonary arterial hypertension in COVID-19 survivors.

Pulmonary fibrosis and development of pulmonary hypertension in COVID-19

Pulmonary fibrosis can be further complicated by pulmonary hypertension (25), which in turn has been noted to be a major determinant of higher mortality (26). The severity of pulmonary fibrosis is not correlated with the development of pulmonary hypertension, and numerous mechanisms involving dysregulation of molecular pathways resulting in vascular remodeling have been suggested (25). Vascular remodeling is now considered an essential contributor to pulmonary hypertension besides the traditionally known factors of hypoxic vasoconstriction and capillary bed destruction in pulmonary

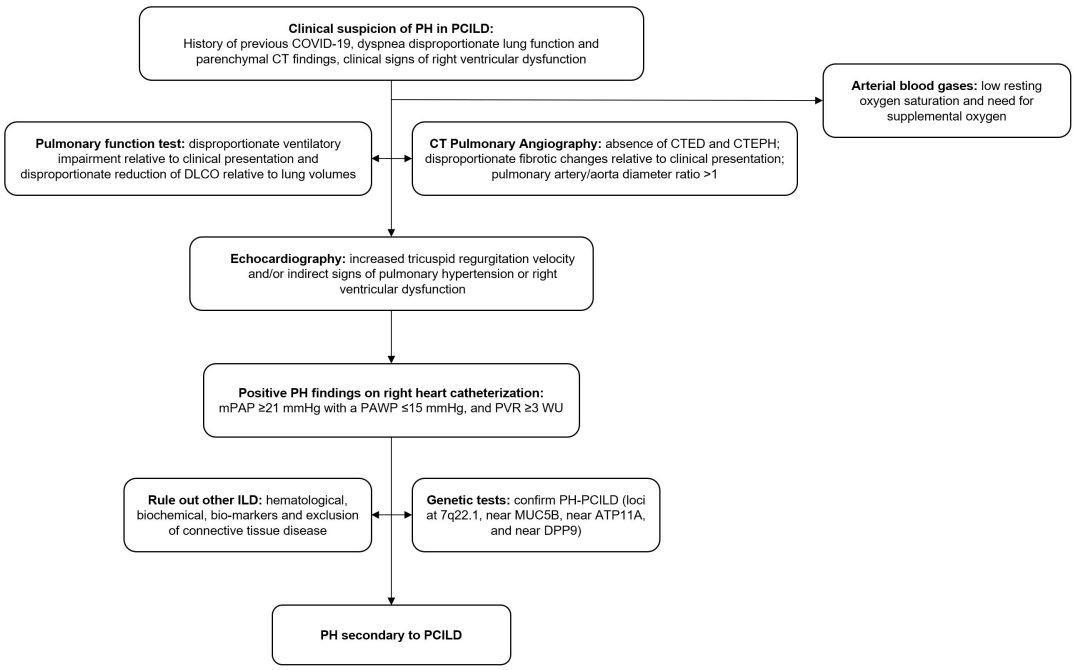

FIGURE 2
Proposed algorithm for the diagnosis of pulmonary hypertension in PCILD. PH, pulmonary hypertension; PCILD, post-COVID-19 interstitial lung disease; CT, computed tomography; DLCO, diffusion capacity for carbon monoxide; CTED, chronic thromboembolic disease; CTEPH, chronic thromboembolic pulmonary hypertension; mPAP, mean pulmonary arterial pressure; PAWP, pulmonary arterial wedge pressure; PVR, pulmonary vascular resistance; ILD, interstitial lung disease.

fibrosis. Loss of BMPR2 signaling, upregulation of A2BAR, and endothelial-to-mesenchymal transition have been speculated to be involved in the vascular remodeling process in pulmonary fibrosis (23, 27). The entry of the virus into the endothelial cells of pulmonary capillaries has been implicated in the vascular remodeling in COVID-19. The incidence of pulmonary hypertension in PCILD needs to be studied further. In general, transthoracic echocardiography in chronic lung diseases is insufficient to confirm or rule out pulmonary hypertension (29). Right heart catheterization is considered the gold standard for diagnosing pulmonary hypertension in this population (29). A proposed algorithm for the diagnosis of pulmonary hypertension in PCILD is shown in **Figure 2**.

Chronic thromboembolic disease and chronic thromboembolic pulmonary hypertension in COVID-19

While most acute pulmonary embolisms and clots resolve with anticoagulation, clot persistence can lead to continued post-embolic symptoms of shortness of breath and the development of chronic thromboembolic disease (CTED). About 30–50% of the patients have persistent defects up to 1 year after diagnosis (128). CTEPH refers to the development of pulmonary hypertension in the setting of CTED. CTEPH is estimated to have a 0.5–5% prevalence after PE (129–132). In the European CTEPH registry, pulmonary endarterectomy mortality rate was 4.7% (133). Additionally, untreated or undiagnosed CTEPH patients have a poor prognosis and a mean pulmonary arterial pressure >30 mmHg is associated with mortality rates >50% in 10 years (134).

In COVID-19 patients, persistent coagulation abnormalities have been noted 4 months after discharge (116, 135), making COVID-19 patients further prone to CTED. Endothelial dysfunction, which can lead to inflammation and thrombosis, is the common pathology in COVID-19 and CTEPH (136). This supports the concept of *in situ* thrombosis in COVID-19, which is a different phenotype than traditional venous thromboembolism (137). The histological evaluation of lungs in COVID-19 patients showed pulmonary vascular endotheliitis with widespread micro thrombosis (112). Whether severe COVID-19 patients without acute pulmonary embolism and ongoing long-term respiratory symptoms may have developed pulmonary hypertension in the setting of micro-thrombosis needs further evaluation. Dyspnea and prolonged hypoxia being common post-COVID-19 symptoms due to other etiologies such as PCILD, make an early diagnosis of COVID-19-related CTED and CTEPH challenging.

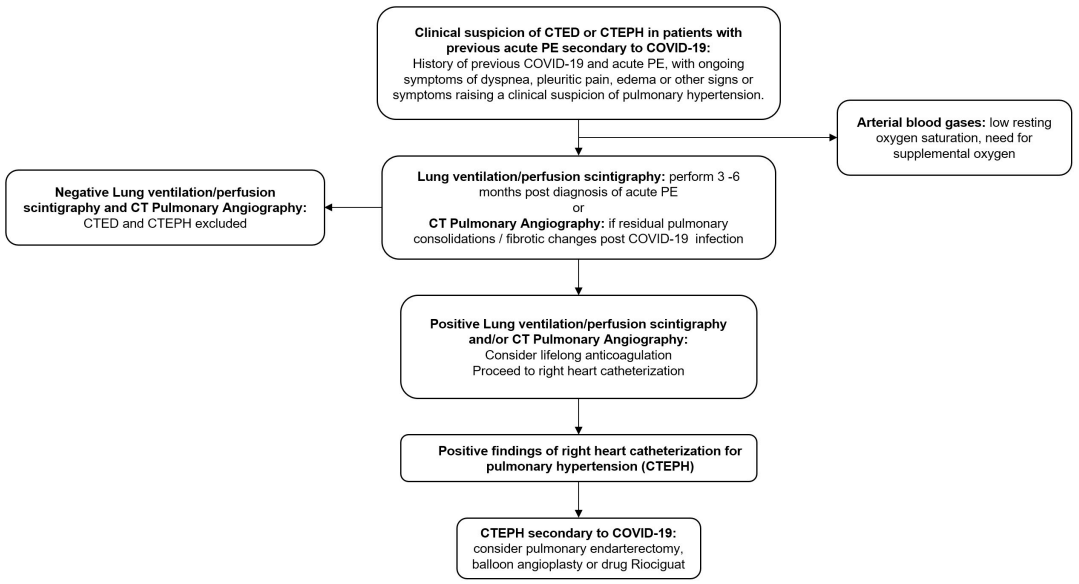

FIGURE 3
Proposed algorithm for investigation and management of chronic thromboembolic disease and chronic thromboembolic pulmonary hypertension secondary to COVID-19. CTED, chronic thromboembolic disease; CTEPH, chronic thromboembolic pulmonary hypertension; PE, pulmonary embolism; CT, computed tomography.

In the absence of scientific evidence specific to COVID-19 for CTED and CTEPH, we recommend standard follow-ups for all patients diagnosed with acute pulmonary embolism during the first 2 years. These patients should be monitored for recurrent thromboembolism and right heart failure symptoms and the optimal timing for initiating diagnostic testing is 3–6 months after acute pulmonary embolism diagnosis (138). Lung ventilation/perfusion scintigraphy (V/Q scan) is the screening test of choice (139). However, residual pulmonary consolidations and fibrosis from post-ARDS changes from COVID-19 might cause abnormalities in ventilation and make interpretation challenging. In such patients, CT pulmonary angiography is a reasonable alternative imaging modality (139, 140). Right heart catheterization is the gold standard confirmation test for CTEPH. Where available, referral to CTEPH centers should be initiated simultaneously with workup once the diagnosis is suspected.

Presently, there are no evidence-based guidelines on the optimal management of CTED and CTEPH in COVID-19 survivors. Most societies recommend a minimum of 3 months of anticoagulation for acute pulmonary embolism and lifelong anticoagulation for CTED or CTEPH (139, 141, 142). If CTEPH is the clinical diagnosis, then pulmonary endarterectomy is the definitive therapy for CTEPH (139). Percutaneous balloon angioplasty shows benefit for inoperable patients and patients with residual CTEPH after endarterectomy (143, 144). For those patients not eligible for endarterectomy or angioplasty, Riociguat is the drug of choice (145). A proposed algorithm for CTED and CTEPH in post-COVID-19 patients is shown in Figure 3.

Post-COVID-19 pulmonary hypertension

Although theoretically, it is expected that post-COVID-19 patients can develop new onset pulmonary hypertension in the setting of interstitial lung disease and pulmonary vasculopathy; however, literature on post-COVID-19 pulmonary hypertension remains scant. We speculate that the complete picture of the burden of post-COVID-19 pulmonary hypertension will be more apparent in the upcoming years, as was the case with HIV and the use of anti-obesity drugs. Additionally, the interaction between parasites such as schistosomiasis in endemic areas and COVID-19 in the development of pulmonary hypertension would be worth exploring further.

Post-COVID-19 pulmonary hypertension has only been mentioned in the setting of case-reports so far. Cueto-Robledo et al. described a case of the development of severe pulmonary hypertension in a patient 3 months post-COVID-19. The finding of pulmonary trunk dilatation on imaging and the echocardiographic results prompted right heart catheterization, which confirmed severe pulmonary hypertension (146). In another case, new pulmonary hypertension was diagnosed on right heart catheterization 6 weeks after discharge from COVID-19 (147). In cases of severe pulmonary hypertension, right heart catheterization will be essential to confirm the pressure

readings in the pulmonary vasculature and also to determine further if there is a component of WHO group 1 pulmonary arterial hypertension in addition to WHO group 3 pulmonary hypertension due to PCILD. Pulmonary arterial hypertension-specific therapy or pulmonary arterial vasodilators are rarely indicated in group 3 pulmonary hypertension unless the right heart catheterization findings and pulmonary function testing, demonstrate pulmonary hypertension out of proportion to the chronic lung disease (146, 148). Such patients should be referred to pulmonary hypertension centers for expert-opinion.

The role of pulmonary rehabilitation in post-COVID-19

Pathogenesis of exercise intolerance in post-COVID-19

Most of the evidence regarding the etiology of exercise intolerance in post-COVID syndrome comes from the cardiopulmonary exercise tests, which have been summarized in **Table 2**. Based on these studies, it has been suggested that exercise intolerance could result from deconditioning, defined as loss of physical fitness due to the inability to maintain an optimal level of physical activity or training (16, 149–158). In cardiopulmonary exercise findings, deconditioning is the reduction of peak oxygen uptake in the absence of known central and peripheral cardiocirculatory diseases. However, post-COVID-19 exercise intolerance may be attributed to impaired peripheral oxygen utilization or extraction due to mitochondrial injury. Evaluating patients with persistent symptoms after COVID-19 infection, Singh et al. elegantly demonstrated through an invasive cardiopulmonary exercise test that oxygen delivery was normal; however, reduced peripheral oxygen extraction and uptake were noted, indicating lower diffusive oxygen delivery to the mitochondria (159). Corroborating peripheral muscle impairment in the setting of myopathy due to inflammatory changes and mitochondrial cellular respiration dysfunction, a case series of 16 patients post-COVID-19 who were evaluated for fatigue and myalgia and who performed muscle biopsy, had muscle fiber atrophy (38%) with signs of regeneration (56%) and mitochondrial and inflammatory changes(62%) (160). This may be the result of myopathy because of viral injury, which may be responsible for the persistence of fatigue in long COVID. Nonetheless, a more recent report demonstrated that in post-COVID-19 patients with fatigue vs. non-fatigue, the only difference in cardiopulmonary exercise test was lower peak oxygen uptake (ml/kg/min), without other noticeable differences in exercise responses (161).

Ventilatory inefficiencies such as an increase in the minute ventilation to carbon dioxide output ratio during exercise or an increase in the dead space to tidal volume observed in the studies may explain the persistent dyspneic symptoms in the long COVID patients (151, 152, 159, 162). These findings can result from increased central chemosensitivity, dysfunctional breathing, and persistent pulmonary or microvascular injury.

Pulmonary rehabilitation in post-COVID syndrome

After hospital discharge, patients need to follow-up with a multidisciplinary approach to control and improve their symptoms and sequelae. For this reason, referring the patient with persistent symptoms after COVID-19 infection to a pulmonary rehabilitation program is crucial to accelerate the improvement in symptoms and health status and allow the patient to return to a productive life. The main goal of the pulmonary rehabilitation program is to restore physical, psychological, and social functions, improve the quality of life in COVID-19 survivors and decrease the incidence of long-term disabilities (163–165). In a large longitudinal cohort in China, within 1 year after acute infection, most hospital survivors with COVID-19 had an excellent physical and functional recovery over the months and had returned to their original work and life (166). Therefore, follow-up evaluations are needed, and rehabilitation might be helpful in post-COVID-19 patients.

Each patient will need a specific program based on education, self-management, and exercise training. However, data on the efficacy of particular rehabilitation approaches in the acute and post-acute phases are still scarce (167–174). An open randomized clinical trial comprising 72 elderly patients more than 6 months after contracting COVID-19 showed an improvement in pulmonary function, exercise capacity, and quality of life with 6-week pulmonary rehabilitation therapy (174). Other cohort studies yielded similar results (175, 176).

In terms of rehabilitation modality, a randomized controlled trial showed that low-intensity aerobic training combined with resistance training has better effects on handgrip strength, kinesiophobia status, and quality of life than high-intensity aerobic training combined with resistance training in post-COVID-19 older adults with sarcopenia. However, the intragroup analysis showed that both groups had significant improvement in the muscle bulk irrespective of exercise intensity (172). With the relocation of health professionals from outpatient activities to hospitals (176, 177), telerehabilitation was used to provide a much-needed resource to address the needs of COVID-19 survivors. In a prospectively randomized program, patients allocated to virtual and home physical therapy had improved outcomes (168). A more robust study was performed to compare supervised home telerehabilitation program with no rehabilitation for post-COVID-19. In this trial, the tele-rehabilitation program was superior to no rehabilitation in terms of functional exercise capacity by six-minute walk test, dyspnea-free symptoms, and physical quality of life. (170).

TABLE 2 Mechanisms of exercise intolerance in post-COVID syndrome.

Time of the evaluation after hospitalization-sample (*n*)	Comparison subgroups	Findings
Gao et al. (182) 1-month post-discharge follow-up (*n* = 10)	Pre-rehabilitation patients with post-COVID-19	• Reduction in $_{PEAK}V'O_2$ 66.2 ± 10.5% pred (*n* = 10) • Decreasing oxygen pulse relative to predicted values (*n* = 7) • DLCO <80% (*n* = 3) and high $V'E/V'CO_2$ at AT (*n* = 2)
Raman et al. (16) >2–3 months of disease-onset (*n* = 58)	Moderate to severe COVID-19 vs. controls	• 54.9% of patients ($_{PEAK}V'O_2$ <80% pred) • Lower $_{PEAK}V'O_2$ • Lower OUES • Higher $V'E/V'CO_2$ (worse in MRI lung parenchymal abnormalities, and it correlated with markers of inflammation)
Liu et al. (183) 7 months (*n* = 41)	Persistence or absence of pulmonary fibrosis on chest CT	• $_{PEAK}V'O_2$: 16.4 ± 3.6 ml/kg/min (with fibrosis) vs. 20.2 ± 3.7 ml/kg/min (no fibrosis) • Older and more severe hospitalization • Lower $_{PEAK}V'O_2$ • Lower METS • Higher $V'E/V'CO_2$
Debeaumont et al. (153) 6 months (*n* = 23)	ICU vs. ward	• 52% of patients ($_{PEAK}V'O_2$ <85% prev) • Higher $\Delta V'E/\Delta V'CO_2$
Dorelli et al. (184) 5 months (*n* = 28)	$\Delta V'E/\Delta V'CO_2$ >31 or ≤31	• Mean $_{PEAK}V'O_2$: 29.2 ± 8.3 ml/kg/min • No difference in pulmonary function variables at rest and in CPET responses
Baratto et al. (162) At time of hospital discharge (*n* = 18)	COVID-19 vs. control participants	• $_{PEAK}V'O_2$ 59% pred (IQR 32) • Lower slope $V'O_2$/WR 8.1 (1.2) ml/min/W • Lower O_2 pulse 9.1 (2.0) beat/L • Higher $V'E/V'CO_2$ 40 (9.0) related to hypocapnia • Lower Ca-vO_2/CaO_2: 0.66 (0.19) • Higher VD/VT at rest with elevated VD/VT during exercise
Rinaldo et al. (150) 3 months (*n* = 75)	Reduced or normal $_{PEAK}V'O_2$	• 55% of patients ($_{PEAK}V'O_2$ <85% prev) • Lower lactate threshold • Lower $\Delta V'O_2/\Delta WR$ • Lower pulse O_2
Skjørten et al. (151) 3 months (*n* = 156)	Post-COVID and normal population without COVID-19 by *z*-score (20% in ICU)	• 31% of patients ($_{PEAK}V'O_2$ <80% prev) • 15% reduced lactate threshold • 16% ventilatory limitation • 23% desaturation >4% • 15% increased $\Delta V'E/\Delta V'CO_2$
Motiejunaite et. (152) 3 months (*n* = 114)	DLCO ≤ or >75% prev	• 75% of patients (PEAKV′O2 <85% prev) • Lower PEAKV′O2 • Lower lactate threshold • Tendency to greater limitation to exercise
Clavario et al. (154) 3 months (*n* = 200)	$_{PEAK}V'O_2$ < or >85% pred	• 49.5% of patients ($_{PEAK}V'O_2$ <85% pred) • 61% normal lactate threshold, among those: ◇ 14.8% respiratory limitation ◇ 34.4% cardiac limitation ◇ 50.8% non-cardiopulmonary limitation • Predictors of low $V'O_2$: FEV1, DLCO% pred, and maximal muscle strength • 80% had one disabling symptoms and was not related to lower $_{PEAK}V'O_2$
Barbagelata et al. (185) 80 ± 21 days after COVID-19 (*n* = 200)	Post-COVID-19 syndrome (PASC 56%) and asymptomatic post COVID	• $_{PEAK}V'O_2$ 27.2 ± 8.9 ml/min/kg • Lower $_{PEAK}V'O_2$ • More symptoms during the CPET • Lower probability of reaching AT • 89.5% normal O_2 pulse and 44.5% normal OUES • Patients with PASC compared to asymptomatic patients had 3.2 ml/min/kg less $_{PEAK}V'O2$ (95% CI −0.9 to −5.5)
Singh et al. (159) 11 months (*n* = 10)	Unexplained exercise intolerance vs. control participants	• Reduced $_{PEAK}V'O_2$ (70 ± 11% pred) • Normal oxygen delivery (DO_2) • Reduced systemic oxygen extraction (EO_2) • Ventilatory inefficiency (high $V'E/V'CO_2$ 35 ± 5) with a normal decrease in dead space ventilation

(Continued)

TABLE 2 (Continued)

Time of the evaluation after hospitalization-sample (*n*)	Comparison subgroups	Findings
Rinaldo et al. (149) 3 months (n = 75)	The severity of hospitalization: mild-moderate, severe, and critical	• 54% of patients ($_{PEAK}V'O_2$ <85% prev) • Older and had greater residual pulmonary sequelae • No difference in lung function • There was no difference in peak$V'O_2$ related to cardiocirculatory and gas exchange responses • Mild increase of $V'E/V'CO_2$ in the critical vs. mild-moderate group
Acar et al. (155) >3 months (n = 51)		• $_{PEAK}V'O_2$ 85 ± 10% pred (or 24 ± 4.6 ml/kg/min) • No difference in acute disease severity • Lower slope $V'O_2$/WR (5.6 ± 1.4 ml/min/W)
Mancini et al. (186) >3 months after the onset of symptoms (n = 71)	Post-COVID-19 vs. control	• Lower $_{PEAK}V'O_2$ • Lower anaerobic threshold • Lower HR and oxygen pulse • Lower cardiac output during exercise • Higher peak O_2 extraction • No difference in $V'E/V'CO_2$, f, and VT
Cassar et al. (156) 2–3 and 6 months (n = 58)	Post-COVID and controls	• Reduced $_{PEAK}V'O_2$ at 2–3 months By 6 months, $V'O_2$ improved (31% persisted with lower $V'O_2$) but was still reduced relative to controls • $V'E/V'CO_2$ abnormal at 2–3 months and improved at 6 months • Lower O_2 pulse at 2–3 months with improvement at 6 months and comparable to controls • Slower HRR at 2–3 months and comparable to controls at 6 months • Severity was not associated with lower $V'O_2$ • Improvement of CPET and MRI were not correlated with cardiopulmonary symptoms
Szekely et al. (187) 3–15 months (n = 41)	Normal breathing pattern vs. dysfunctional breathing	• 59% of patients ($_{PEAK}V'O_2$ <80% pred) • Only 2 CPET (5%) were considered normal • Dysfunctional breathing (n = 26) • 5 patients with preload failure and symptoms of ME/CFS
de Boer et al. (188) 6 ± 4 months (n = 50)	PASC	• 32% of patients ($_{PEAK}V'O_2$ ≤84% pred) • None ventilatory limitation • 56% cardiovascular limitation • Higher arterial lactate levels and low FATox
Vonbank et al. (157) 3–6 months (n = 100)	Moderate/critical vs. asymptomatic/mild vs. normal control	• Lower $_{PEAK}V'O_2$ and $_{atAT}$ • Lower work peak • Lower lactate level • Lower HR • Higher $V'E/V'CO_2$
Ladlow et al. (189) >6 months (n = 205)	25% dysautonomia vs. non-dysautonomia	• HR $_{atrest}$ and HR $_{atAT}$ were higher • Slowly HRR • Lower work rate $_{atAT}$ and $_{PEAK}$ with same lactate level • Lower $V'O_2$ $_{atAT}$ and $_{atpeak}$ exercise • Mild elevated $V'E/V'CO_2$
Ambrosino et al. (190) >2 months (n = 36)	Normal vs. reduced exercise capacity	• 77.8% of patients ($_{PEAK}V'O_2$ <20 ml/kg/min) • Lower lactate threshold • Lower peak ventilation • Higher $V'E/V'CO_2$ and no VD/VT reduction in 87.5% of patients • Lower vascular reactivity (FMD) with slope $V'E/V'CO_2$ ≥36
Freìsard et al. (191) >6 weeks of persistent dyspnea (median 119 ± 89 days) (n = 51)		• Preserved $_{PEAK}V'O_2$ 22.9 (20.0–25.5) ml/kg/min in DB patients • DB (chaotic ventilatory pattern) mostly without hyperventilation in 29.4% (n = 15) • Respiratory limitation with gas exchange abnormalities in 54.9% (n = 28) • Normal CPET or O_2 delivery/utilization impairment 15.7% (n = 8) • $_{PEAK}V'O_2$ >84% pred and workload at the peak were within the normal range for DB patients. No relation to hyperventilation was found (normal $V'E/V'CO_2$ and $PaCO_2$ at rest).

(Continued)

TABLE 2 (Continued)

Time of the evaluation after hospitalization-sample (*n*)	Comparison subgroups	Findings
Ribeiro Baptista et al. (158) 3 months (n = 105)	$_{PEAK}V'O_2$ < (reduced) or > (normal exercise capacity) 80% pred	• 35% of patients ($_{PEAK}V'O_2$ <80% pred) • No difference in acute disease severity • 38.9% sarcopenia • Lower lactate threshold and O_2 pulse (no ventilatory or gas exchange analysis) • Obs: relation with low $V'O_2$ were: reduced pulmonary function (DLCO) and a decrease in muscular mass index
Schaeffer et al. (161) >3 months (n = 49)	Fatigue (n = 34) or non-fatigue (n = 15)	• Lower $_{PEAK}V'O_2$ in ml/kg/min (not in % pred). Obs: greater proportion of obese patients. • METs were lower • Dyspnea intensity ratings, dyspnea intensity-ventilation, and -$V'O_2$ slopes were higher • No difference in mechanical constraint

mMRC, Medical Research Council modified dyspnea scale; peak$V'O_2$, peak exercise oxygen consumption; CPET, cardiopulmonary exercise testing; WR, work rate; $V'E/V'CO_2$, minute ventilation by carbon dioxide output; DLCO, carbon monoxide diffusion; FEV1, forced expiratory volume in one second; CT chest, chest computed tomography; ICU, intensive care unit; ME/CFS, myalgic encephalomyelitis/chronic fatigue syndrome; FMD, endothelial-dependent flow mediate dilation; MRI, magnetic resonance imaging; PASC, post-acute sequelae of SARS-CoV-2 infection; FATox, beta-oxidation of mitochondrial substrates fatty acids; iCPET, invasive cardiopulmonary exercise testing; AT, anaerobic threshold; DO_2, oxygen delivery; EO_2, systemic oxygen extraction; OUES, oxygen uptake efficiency; f, respiratory rate; VT, tidal volume; METS, peak metabolic equivalents of task.

Before starting rehabilitation therapy, it is essential to evaluate the exercise capacity, which could be done by field tests, such as the 6-min walking test, shuttle walking test, step test, etc., or a more complex test, such as cardiopulmonary exercise testing. Patients should be reevaluated in 6–12 weeks. Although the exercise program is essential, which includes aerobic and strengthening exercises for peripheral and respiratory muscles, it is vital to include breathing retraining, airway clearance, energy conservation techniques, and psychological counseling (163, 165, 178–181). Referring the patient with persistent symptoms after COVID-19 infection to a rehabilitation program is crucial to accelerate the improvement in symptoms and health status and allow the patient to return to a productive life.

Conclusion

COVID-19 survivors may present signs of cardiopulmonary sequelae such as persistent lung fibrosis, chronic thrombosis, right ventricular dysfunction, pulmonary hypertension, and exercise intolerance. Pulmonary fibrosis is among the most feared chronic pulmonary complications of COVID-19. A diagnosis of PCILD should be based on clinical, radiological, and pathological findings. The role of treatment with antifibrotic and anti-inflammatory drugs in improving PCILD symptoms remains inconclusive. A substantial proportion of patients with COVID-19 have coagulation abnormalities. Acute pulmonary embolism in COVID-19 can lead to the development of CTED and CTEPH or even other forms of pulmonary hypertension, which could increase in prevalence over time during the COVID-19 pandemic. Right ventricular dysfunction is prevalent in patients hospitalized with SARS-CoV-2 and is more likely related to systemic consequences rather than direct viral myocardial infection. In terms of mechanisms of exercise intolerance after COVID-19 infection, exercise limitation can be due to a central or peripheral cardiocirculatory origin, decreased oxygen uptake, and with or without ventilatory or gas exchange limitation. Referring the patient with persistent symptoms after COVID-19 infection to a pulmonary rehabilitation program is crucial to accelerate the improvement in symptoms and health status and allow the patient to return to a productive life. We anticipate that as the pool of patients recovering from COVID-19 continues to increase, healthcare providers will need to learn to recognize these long-term cardiopulmonary sequelae early and create a management plan to prevent further deterioration and improve the quality of life of these patients. Furthermore, carefully designed research programs and long-term monitoring of these patients will help clinicians to manage these patients in the long run.

Author contributions

All authors made substantial contributions to the conception or design of the work; or the acquisition, analysis, or interpretation of data for the work, drafted the work or revising it critically for important intellectual content, provided approval for publication of the content, and agreed to be accountable for all aspects of the work in ensuring that questions related to the accuracy or integrity of any part of the work were appropriately investigated and resolved.

Conflict of interest

The authors declare that the research was conducted in the absence of any commercial or financial relationships that could be construed as a potential conflict of interest.

Publisher's note

References

1. Soriano JB, Murthy S, Marshall JC, Relan P, Diaz JV, WHO Clinical Case Definition Working Group. A clinical case definition of post-COVID-19 condition by a Delphi consensus. *Lancet Infect Dis.* (2022) 22:e102–7. doi: 10.1016/S1473-3099(21)00703-9

2. CDC. *Long COVID or Post-COVID Conditions*. Atlanta, GA: CDC (2022).

3. Daniels CJ, Rajpal S, Greenshields JT, Rosenthal GL, Chung EH, Terrin M, et al. Prevalence of clinical and subclinical myocarditis in competitive athletes with recent SARS-CoV-2 infection: results from the big ten COVID-19 cardiac registry. *JAMA Cardiol.* (2021) 6:1078–87.

4. Choutka J, Jansari V, Hornig M, Iwasaki A. Unexplained post-acute infection syndromes. *Nat Med.* (2022) 28:911–23. doi: 10.1038/s41591-022-01810-6

5. González J, Zuil M, Benítez ID, de Gonzalo-Calvo D, Aguilar M, Santisteve S, et al. One year overview and follow-up in a post-COVID consultation of critically ill patients. *Front Med.* (2022) 9:897990. doi: 10.3389/fmed.2022.897990

6. Carfì A, Bernabei R, Landi F, Gemelli Against Covid-19 Post-Acute Care Study Group. Persistent symptoms in patients after acute COVID-19. *JAMA.* (2020) 324:603–5. doi: 10.1001/jama.2020.12603

7. Blomberg B, Mohn KG-I, Brokstad KA, Zhou F, Linchausen DW, Hansen B-A, et al. Long COVID in a prospective cohort of home-isolated patients. *Nat Med.* (2021) 27:1607–13. doi: 10.1038/s41591-021-01433-3

8. Carvalho-Schneider C, Laurent E, Lemaignen A, Beaufils E, Bourbao-Tournois C, Laribi S, et al. Follow-up of adults with noncritical COVID-19 two months after symptom onset. *Clin Microbiol Infect.* (2021) 27:258–63. doi: 10.1016/j.cmi.2020.09.052

9. Tenforde MW, Kim SS, Lindsell CJ, Billig Rose E, Shapiro NI, Files DC, et al. Symptom duration and risk factors for delayed return to usual health among outpatients with COVID-19 in a multistate health care systems network—United States, March–June 2020. *Morb Mortal Wkly Rep Cent Dis Control Prev.* (2020) 69:993–8. doi: 10.15585/mmwr.mm6930e1

10. Azevedo RB, Botelho BG, de Hollanda JVG, Ferreira LVL, Junqueira de Andrade LZ, Oei SSML, et al. Covid-19 and the cardiovascular system: a comprehensive review. *J Hum Hypertens.* (2021) 35:4–11. doi: 10.1038/s41371-020-0387-4

11. Xie Y, Xu E, Bowe B, Al-Aly Z. Long-term cardiovascular outcomes of COVID-19. *Nat Med.* (2022) 28:583–90. doi: 10.1038/s41591-022-01689-3

12. Wang W, Wang C-Y, Wang S-I, Wei JC-C. Long-term cardiovascular outcomes in COVID-19 survivors among non-vaccinated population: a retrospective cohort study from the TriNetX US collaborative networks. *EClinicalMedicine* (2022) 53:101619. doi: 10.1016/j.eclinm.2022.101619

13. Maestre-Muñiz MM, Arias Á, Mata-Vázquez E, Martín-Toledano M, López-Larramona G, Ruiz-Chicote AM, et al. Long-term outcomes of patients with coronavirus disease 2019 at one year after hospital discharge. *J Clin Med MDPI.* (2021) 10:2945. doi: 10.3390/jcm10132945

14. Ayoubkhani D, Khunti K, Nafilyan V, Maddox T, Humberstone B, Diamond I, et al. Post-covid syndrome in individuals admitted to hospital with covid-19: retrospective cohort study. *BMJ.* (2021) 372:n693. doi: 10.1136/bmj.n693

15. Raman B, Bluemke DA, Lüscher TF, Neubauer S. Long COVID: post-acute sequelae of COVID-19 with a cardiovascular focus. *Eur Heart J.* (2022) 43:1157–72. doi: 10.1093/eurheartj/ehac031

16. Raman B, Cassar MP, Tunnicliffe EM, Filippini N, Griffanti L, Alfaro-Almagro F, et al. Medium-term effects of SARS-CoV-2 infection on multiple vital organs, exercise capacity, cognition, quality of life and mental health, post-hospital discharge. *EClinicalMedicine.* (2021) 31:100683. doi: 10.1016/j.eclinm.2020.100683

17. Radin JM, Quer G, Ramos E, Baca-Motes K, Gadaleta M, Topol EJ, et al. Assessment of prolonged physiological and behavioral changes associated with COVID-19 infection. *JAMA Netw Open.* (2021) 4:e2115959. doi: 10.1001/jamanetworkopen.2021.15959

18. Blitshteyn S, Whitelaw S. Postural orthostatic tachycardia syndrome (POTS) and other autonomic disorders after COVID-19 infection: a case series of 20 patients. *Immunol Res.* (2021) 69:205–11. doi: 10.1007/s12026-021-09185-5

19. Tanacli R, Doeblin P, Götze C, Zieschang V, Faragli A, Stehning C, et al. COVID-19 vs. classical myocarditis associated myocardial injury evaluated by cardiac magnetic resonance and endomyocardial biopsy. *Front Cardiovasc Med.* (2021) 8:737257. doi: 10.3389/fcvm.2021.737257

20. Modica G, Bianco M, Sollazzo F, Di Murro E, Monti R, Cammarano M, et al. Myocarditis in athletes recovering from covid-19: a systematic review and meta-analysis. *Int J Environ Res Public Health MDPI.* (2022) 19:4279. doi: 10.3390/ijerph19074279

21. Blagova O, Ainetdinova DH, Lutokhina YUA, Novosadov VM, Rud' RS, Zaitsev AYU, et al. Post-COVID myocarditis diagnosed by endomyocardial biopsy and/or magnetic resonance imaging 2–9 months after acute COVID-19. *Eur Heart J.* (2021) 42:1751. doi: 10.1093/eurheartj/ehab724.1751

22. Halushka MK, Vander Heide RS. Myocarditis is rare in COVID-19 autopsies: cardiovascular findings across 277 postmortem examinations. *Cardiovasc Pathol.* (2021) 50:107300. doi: 10.1016/j.carpath.2020.107300

23. Szekely Y, Lichter Y, Taieb P, Banai A, Hochstadt A, Merdler I, et al. Spectrum of cardiac manifestations in COVID-19: a systematic echocardiographic study. *Circulation.* (2020) 142:342–53. doi: 10.1161/CIRCULATIONAHA.120.047971

24. Zhou F, Yu T, Du R, Fan G, Liu Y, Liu Z, et al. Clinical course and risk factors for mortality of adult inpatients with COVID-19 in Wuhan, China: a retrospective cohort study. *Lancet.* (2020) 395:1054–62. doi: 10.1016/S0140-6736(20)30566-3

25. Bhatraju PK, Ghassemieh BJ, Nichols M, Kim R, Jerome KR, Nalla AK, et al. Covid-19 in critically ill patients in the seattle region–case series. *N Engl J Med* (2020) 382:2012–22. doi: 10.1056/NEJMoa2004500

26. Cao Y, Zhang M, Guo Y, Zhang Y. The overlooked chamber in coronavirus disease 2019. *ESC Heart Fail.* (2020) 7:3483–6. doi: 10.1002/ehf2.12976

27. Argulian E, Sud K, Vogel B, Bohra C, Garg VP, Talebi S, et al. Right ventricular dilation in hospitalized patients with covid-19 infection. *JACC Cardiovasc Imaging.* (2020) 13:2459–61. doi: 10.1016/j.jcmg.2020.05.010

28. Li Y, Li H, Zhu S, Xie Y, Wang B, He L, et al. Prognostic value of right ventricular longitudinal strain in patients with COVID-19. *JACC Cardiovasc Imaging.* (2020) 13:2287–99. doi: 10.1016/j.jcmg.2020.04.014

29. Paternoster G, Bertini P, Innelli P, Trambaiolo P, Landoni G, Franchi F, et al. Right ventricular dysfunction in patients with COVID-19: a systematic review and meta-analysis. *J Cardiothorac Vasc Anesth.* (2021) 35:3319–24. doi: 10.1053/j.jvca.2021.04.008

30. Park JF, Banerjee S, Umar S. In the eye of the storm: the right ventricle in COVID-19. *Pulm Circ.* (2020) 10:2045894020936660. doi: 10.1177/2045894020936660

31. Hendren NS, Drazner MH, Bozkurt B, Cooper LT. Description and proposed management of the acute COVID-19 cardiovascular syndrome. *Circulation.* (2020) 141:1903–14. doi: 10.1161/CIRCULATIONAHA.120.047349

32. Fox SE, Li G, Akmatbekov A, Harbert JL, Lameira FS, Brown JQ, et al. Unexpected features of cardiac pathology in covid-19 infection. *Circulation.* (2020) 142:1123–5. doi: 10.1161/CIRCULATIONAHA.120.049465

33. Huang L, Zhao P, Tang D, Zhu T, Han R, Zhan C, et al. Cardiac involvement in patients recovered from covid-2019 identified using magnetic resonance imaging. *JACC Cardiovasc Imaging.* (2020) 13:2330–9. doi: 10.1016/j.jcmg.2020.05.004

34. Rieg AD, Suleiman S, Perez-Bouza A, Braunschweig T, Spillner JW, Schröder T, et al. Milrinone relaxes pulmonary veins in guinea pigs and humans. *PLoS One.* (2014) 9:e87685. doi: 10.1371/journal.pone.0087685

35. Mathew R, Di Santo P, Jung RG, Marbach JA, Hutson J, Simard T, et al. Milrinone as compared with dobutamine in the treatment of cardiogenic shock. *N Engl J Med.* (2021) 385:516–25. doi: 10.1056/NEJMoa2026845

36. Feng W-X, Yang Y, Wen J, Liu Y-X, Liu L, Feng C. Implication of inhaled nitric oxide for the treatment of critically ill COVID-19 patients with pulmonary hypertension. *ESC Heart Fail.* (2021) 8:714–8. doi: 10.1002/ehf2.13023

37. Kerbaul F, Rondelet B, Demester J-P, Fesler P, Huez S, Naeije R, et al. Effects of levosimendan versus dobutamine on pressure load-induced right ventricular failure*. *Crit Care Med.* (2006) 34:2814–9. doi: 10.1097/01.CCM.0000242157.19347.50

38. Slawsky MT, Colucci WS, Gottlieb SS, Greenberg BH, Haeusslein E, Hare J, et al. Acute hemodynamic and clinical effects of levosimendan in patients with severe heart failure, study investigators. *Circulation.* (2000) 102:2222–7. doi: 10.1161/01.CIR.102.18.2222

39. Russ MA, Prondzinsky R, Carter JM, Schlitt A, Ebelt H, Schmidt H, et al. Right ventricular function in myocardial infarction complicated by cardiogenic shock: improvement with levosimendan. *Crit Care Med.* (2009) 37:3017–23. doi: 10.1097/CCM.0b013e3181b0314a

40. Alibaz-Oner F, Gurbuz OZ, Oner E, Yurdakul S, Erguney M. Impact of levosimendan on right ventricular functions by using novel tissue Doppler derived indices in patients with ischaemic left ventricular failure. *Kardiol Pol.* (2013) 71:1036–41. doi: 10.5603/KP.2013.0258

41. Hansen MS, Andersen A, Nielsen-Kudsk JE. Levosimendan in pulmonary hypertension and right heart failure. *Pulm Circ.* (2018) 8:204589401879090. doi: 10.1177/2045894018790905

42. Lorusso R, Raffa GM, Heuts S, Lo Coco V, Meani P, Natour E, et al. Pulmonary artery cannulation to enhance extracorporeal membrane oxygenation management in acute cardiac failure. *Interact Cardiovasc Thorac Surg.* (2020) 30:215–22. doi: 10.1093/icvts/ivz245

43. Mustafa AK, Alexander PJ, Joshi DJ, Tabachnick DR, Cross CA, Pappas PS, et al. Extracorporeal membrane oxygenation for patients with covid-19 in severe respiratory failure. *JAMA Surg.* (2020) 155:990–2. doi: 10.1001/jamasurg.2020.3950

44. Haddad F, Doyle R, Murphy DJ, Hunt SA. Right ventricular function in cardiovascular disease, part II: pathophysiology, clinical importance, and management of right ventricular failure. *Circ Am Heart Assoc.* (2008) 117:1717–31. doi: 10.1161/CIRCULATIONAHA.107.653584

45. Arrigo M, Huber LC, Winnik S, Mikulicic F, Guidetti F, Frank M, et al. Right ventricular failure: pathophysiology, diagnosis and treatment. *Cardiac Fail Rev.* (2019) 5:140. doi: 10.15420/cfr.2019.15.2

46. Ameri P, Inciardi RM, Di Pasquale M, Agostoni P, Bellasi A, Camporotondo R, et al. Pulmonary embolism in patients with COVID-19: characteristics and outcomes in the Cardio-COVID Italy multicenter study. *Clin Res Cardiol.* (2021) 110:1020–8. doi: 10.1007/s00392-020-01766-y

47. Hsieh C-M, Mishkel GJ, Cardoso PFG, Rakowski H, Dunn SC, Butany J, et al. Production and reversibility of right ventricular hypertrophy and right heart failure in dogs. *Ann Thorac Surg.* (1992) 54:104–10. doi: 10.1016/0003-4975(92)91152-Y

48. Brooks H, Kirk ES, Vokonas PS, Urschel CW, Sonnenblick EH. Performance of the right ventricle under stress: relation to right coronary flow. *Am Soc Clin Investig.* (1971) 50:2176–83. doi: 10.1172/JCI106712

49. Bonnet P, Bonnet S, Boissière J, Net J-LL, Gautier M, Dumas de la Roque E, et al. Chronic hypoxia induces nonreversible right ventricle dysfunction and dysplasia in rats. *Am J Physiol Heart Circ Physiol.* (2004) 287:H1023–8. doi: 10.1152/ajpheart.00802.2003

50. Vonk Noordegraaf A, Westerhof BE, Westerhof N. The relationship between the right ventricle and its load in pulmonary hypertension. *J Am Coll Cardiol.* (2017) 69:236–43. doi: 10.1016/j.jacc.2016.10.047

51. Solomon JJ, Heyman B, Ko JP, Condos R, Lynch DA. CT of post-acute lung complications of COVID-19. *Radiology.* (2021) 301:E383–95. doi: 10.1148/radiol.2021211396

52. Froidure A, Mahsouli A, Liistro G, De Greef J, Belkhir L, Gérard L, et al. Integrative respiratory follow-up of severe COVID-19 reveals common functional and lung imaging sequelae. *Respir Med.* (2021) 181:106383. doi: 10.1016/j.rmed.2021.106383

53. Bellan M, Soddu D, Balbo PE, Baricich A, Zeppegno P, Avanzi GC, et al. Respiratory and psychophysical sequelae among patients with covid-19 four months after hospital discharge. *JAMA Netw Open.* (2021) 4:e2036142. doi: 10.1001/jamanetworkopen.2020.36142

54. Cortés-Telles A, López-Romero S, Figueroa-Hurtado E, Pou-Aguilar YN, Wong AW, Milne KM, et al. Pulmonary function and functional capacity in COVID-19 survivors with persistent dyspnoea. *Respir Physiol Neurobiol.* (2021) 288:103644. doi: 10.1016/j.resp.2021.103644

55. Torres-Castro R, Vasconcello-Castillo L, Alsina-Restoy X, Solis-Navarro L, Burgos F, Puppo H, et al. Respiratory function in patients post-infection by COVID-19: a systematic review and meta-analysis. *Pulmonology.* (2021) 27:328–37. doi: 10.1016/j.pulmoe.2020.10.013

56. Huang C, Huang L, Wang Y, Li X, Ren L, Gu X, et al. 6-month consequences of COVID-19 in patients discharged from hospital: a cohort study. *Lancet.* (2021) 397:220–32. doi: 10.1016/S0140-6736(20)32656-8

57. De Michele S, Sun Y, Yilmaz MM, Katsyv I, Salvatore M, Dzierba AL, et al. Forty postmortem examinations in covid-19 patients. *Am J Clin Pathol.* (2020) 154:748–60. doi: 10.1093/ajcp/aqaa156

58. Borczuk AC, Salvatore SP, Seshan SV, Patel SS, Bussel JB, Mostyka M, et al. COVID-19 pulmonary pathology: a multi-institutional autopsy cohort from Italy and New York City. *Mod Pathol.* (2020) 33:2156–68. doi: 10.1038/s41379-020-00661-1

59. Nalbandian A, Sehgal K, Gupta A, Madhavan MV, McGroder C, Stevens JS, et al. Post-acute COVID-19 syndrome. *Nat Med.* (2021) 27:601–15. doi: 10.1038/s41591-021-01283-z

60. Yu QY, Tang XX. Irreversibility of pulmonary fibrosis. *Aging Dis JKL Int LLC.* (2022) 13:73. doi: 10.14336/AD.2021.0730

61. Han X, Fan Y, Alwalid O, Li N, Jia X, Yuan M, et al. Six-month follow-up chest CT findings after severe COVID-19 pneumonia. *Radiology.* (2021) 299:E177–86. doi: 10.1148/radiol.2021203153

62. Wells AU, Devaraj A, Desai SR. Interstitial lung disease after COVID-19 infection: a catalog of uncertainties. *Radiology.* (2021) 299:E216–8. doi: 10.1148/radiol.2021204482

63. Garg M, Maralakunte M, Dhooria S. Sequelae of COVID-19 pneumonia: is it correct to label everything as post-COVID lung fibrosis? *J Postgrad Med.* (2021) 67:224–7. doi: 10.4103/jpgm.jpgm_550_21

64. Hu Q, Guan H, Sun Z, Huang L, Chen C, Ai T, et al. Early CT features and temporal lung changes in COVID-19 pneumonia in Wuhan, China. *Eur J Radiol.* (2020) 128:109017. doi: 10.1016/j.ejrad.2020.109017

65. Bazdyrev E, Rusina P, Panova M, Novikov F, Grishagin I, Nebolsin V. Lung fibrosis after COVID-19: treatment prospects. *Pharmaceuticals (Basel).* (2021) 14:807. doi: 10.3390/ph14080807

66. Vasarmidi E, Tsitoura E, Spandidos DA, Tzanakis N, Antoniou KM. Pulmonary fibrosis in the aftermath of the COVID-19 era (Review). *Exp Ther Med.* (2020) 20:2557–60. doi: 10.3892/etm.2020.8980

67. Wu Q, Zhong L, Li H, Guo J, Li Y, Hou X, et al. Follow-up study of lung function and chest computed tomography at 6 months after discharge in patients with coronavirus disease 2019. *Can Respir J.* (2021) 2021:6692409. doi: 10.1155/2021/6692409

68. Huang W, Wu Q, Chen Z, Xiong Z, Wang K, Tian J, et al. The potential indicators for pulmonary fibrosis in survivors of severe COVID-19. *J Infect.* (2021) 82:e5–7. doi: 10.1016/j.jinf.2020.09.027

69. Zou J-N, Sun L, Wang B-R, Zou Y, Xu S, Ding Y-J, et al. The characteristics and evolution of pulmonary fibrosis in COVID-19 patients as assessed by AI-assisted chest HRCT. *PLoS One.* (2021) 16:e0248957. doi: 10.1371/journal.pone.0248957

70. Li X, Shen C, Wang L, Majumder S, Zhang D, Deen MJ, et al. Pulmonary fibrosis and its related factors in discharged patients with new corona virus pneumonia: a cohort study. *Respir Res.* (2021) 22:203. doi: 10.1186/s12931-021-01798-6

71. Doane JJ, Hirsch KS, Baldwin JO, Wurfel MM, Pipavath SN, West TE. Progressive pulmonary fibrosis after non-critical covid-19: a case report. *Am J Case Rep.* (2021) 22:e933458. doi: 10.12659/AJCR.933458

72. Udwadia ZF, Koul PA, Richeldi L. Post-COVID lung fibrosis: the tsunami that will follow the earthquake. *Lung India.* (2021) 38:S41–7. doi: 10.4103/lungindia.lungindia_818_20

73. Hall DJ, Schulte JJ, Lewis EE, Bommareddi SR, Rohrer CT, Sultan S, et al. Successful lung transplantation for severe post covid-19 pulmonary fibrosis. *Ann Thorac Surg.* (2021) 114:e17–9. doi: 10.1016/j.athoracsur.2021.10.004

74. Hui DS, Joynt GM, Wong KT, Gomersall CD, Li TS, Antonio G, et al. Impact of severe acute respiratory syndrome (SARS) on pulmonary function, functional capacity and quality of life in a cohort of survivors. *Thorax.* (2005) 60:401–9. doi: 10.1136/thx.2004.030205

75. Wong K, Antonio GE, Hui DS, Ho C, Chan P, Ng W, et al. Severe acute respiratory syndrome: thin-section computed tomography features, temporal changes, and clinicoradiologic correlation during the convalescent period. *J Comput Assist Tomogr.* (2004) 28:790–5. doi: 10.1097/00004728-200411000-00010

76. Zhang P, Li J, Liu H, Han N, Ju J, Kou Y, et al. Correction: long-term bone and lung consequences associated with hospital-acquired severe acute respiratory

syndrome: a 15-year follow-up from a prospective cohort study. *Bone Res.* (2020) 8:1–1. doi: 10.1038/s41413-020-00113-1

77. Flaifel A, Kwok B, Ko J, Chang S, Smith D, Zhou F, et al. pulmonary pathology of end-stage covid-19 disease in explanted lungs and outcomes after lung transplantation. *Am J Clin Pathol.* (2022) 157:908–26. doi: 10.1093/ajcp/aqab208

78. Guler SA, Ebner L, Aubry-Beigelman C, Bridevaux P-O, Brutsche M, Clarenbach C, et al. Pulmonary function and radiological features 4 months after COVID-19: first results from the national prospective observational Swiss COVID-19 lung study. *Eur Respir J.* (2021) 57:2003690. doi: 10.1183/13993003.03690-2020

79. Zapol WM, Trelstad RL, Coffey JW, Tsai I, Salvador RA. Pulmonary fibrosis in severe acute respiratory failure. *Am Rev Respir Dis.* (1979) 119:547–54.

80. Marshall R, Bellingan G, Laurent G. The acute respiratory distress syndrome: fibrosis in the fast lane. *Thorax.* (1998) 53:815–7. doi: 10.1136/thx.53.10.815

81. Thille AW, Esteban A, Fernández-Segoviano P, Rodriguez J-M, Aramburu J-A, Vargas-Errázuriz P, et al. Chronology of histological lesions in acute respiratory distress syndrome with diffuse alveolar damage: a prospective cohort study of clinical autopsies. *Lancet Respir Med.* (2013) 1:395–401. doi: 10.1016/S2213-2600(13)70053-5

82. Senzi A, Bindi M, Cappellini I, Zamidei L, Consales G. COVID-19 and VILI: developing a mobile app for measurement of mechanical power at a glance. *Intensive Care Med Exp.* (2021) 9:6. doi: 10.1186/s40635-021-00372-0

83. McGroder CF, Zhang D, Choudhury MA, Salvatore MM, D'Souza BM, Hoffman EA, et al. Pulmonary fibrosis 4 months after COVID-19 is associated with severity of illness and blood leucocyte telomere length. *Thorax.* (2021) 76:1242–5. doi: 10.1136/thoraxjnl-2021-217031

84. Farghaly S, Badedi M, Ibrahim R, Sadhan MH, Alamoudi A, Alnami A, et al. Clinical characteristics and outcomes of post-COVID-19 pulmonary fibrosis: a case-control study. *Medicine (Baltimore).* (2022) 101:e28639. doi: 10.1097/MD.0000000000028639

85. Aul DR, Gates DJ, Draper DA, Dunleavy DA, Ruickbie DS, Meredith DH, et al. Complications after discharge with COVID-19 infection and risk factors associated with development of post-COVID pulmonary fibrosis. *Respir Med.* (2021) 188:106602. doi: 10.1016/j.rmed.2021.106602

86. Jutant E-M, Meyrignac O, Beurnier A, Jaïs X, Pham T, Morin L, et al. Respiratory symptoms and radiologic findings in post-acute COVID-19 syndrome. *ERJ Open Res.* (2021) 8:00479–2021. doi: 10.1183/23120541.00479-2021

87. Yu M, Liu Y, Xu D, Zhang R, Lan L, Xu H. Prediction of the development of pulmonary fibrosis using serial thin-section CT and clinical features in patients discharged after treatment for covid-19 pneumonia. *Korean J Radiol.* (2020) 21:746–55. doi: 10.3348/kjr.2020.0215

88. Wallis TJM, Heiden E, Horno J, Welham B, Burke H, Freeman A, et al. Risk factors for persistent abnormality on chest radiographs at 12-weeks post hospitalisation with PCR confirmed COVID-19. *Respir Res.* (2021) 22:157. doi: 10.1186/s12931-021-01750-8

89. Moodley YP, Scaffidi AK, Misso NL, Keerthisingam C, McAnulty RJ, Laurent GJ, et al. Fibroblasts isolated from normal lungs and those with idiopathic pulmonary fibrosis differ in interleukin-6/gp130-mediated cell signaling and proliferation. *Am J Pathol.* (2003) 163:345–54. doi: 10.1016/S0002-9440(10)63658-9

90. Vianello A, Guarnieri G, Braccioni F, Lococo S, Molena B, Cecchetto A, et al. The pathogenesis, epidemiology and biomarkers of susceptibility of pulmonary fibrosis in COVID-19 survivors. *Clin Chem Lab Med.* (2022) 60:307–16. doi: 10.1515/cclm-2021-1021

91. Pandolfi L, Bozzini S, Frangipane V, Percivalle E, De Luigi A, Violatto MB, et al. Neutrophil extracellular traps induce the epithelial-mesenchymal transition: implications in post-COVID-19 fibrosis. *Front Immunol.* (2021) 12:663303. doi: 10.3389/fimmu.2021.663303

92. Gavillet M, Martinod K, Renella R, Wagner DD, Williams DA. A key role for Rac and Pak signaling in neutrophil extracellular traps (NETs) formation defines a new potential therapeutic target. *Am J Hematol.* (2018) 93:269–76. doi: 10.1002/ajh.24970

93. Fadista J, Kraven LM, Karjalainen J, Andrews SJ, Geller F, Covid-19 Host Genetics Initiative, et al. Shared genetic etiology between idiopathic pulmonary fibrosis and COVID-19 severity. *EBioMedicine.* (2021) 65:103277. doi: 10.1016/j.ebiom.2021.103277

94. Allen RJ, Guillen-Guio B, Croot E, Kraven LM, Moss S, Stewart I, et al. Genetic overlap between idiopathic pulmonary fibrosis and COVID-19. *medRxiv.* (2021) [Preprint]. doi: 10.1101/2021.12.08.21267459

95. Raghu G, Wilson KC. COVID-19 interstitial pneumonia: monitoring the clinical course in survivors. *Lancet Respir Med.* (2020) 8:839–42. doi: 10.1016/S2213-2600(20)30349-0

96. Lee JH, Yim J-J, Park J. Pulmonary function and chest computed tomography abnormalities 6–12 months after recovery from COVID-19: a systematic review and meta-analysis. *Respir Res.* (2022) 23:1–16. doi: 10.1186/s12931-022-02163-x

97. Colarusso C, Maglio A, Terlizzi M, Vitale C, Molino A, Pinto A, et al. Post-COVID-19 patients who develop lung fibrotic-like changes have lower circulating levels of ifn-β but higher levels of il-1α and TGF-β. *Biomedicines.* (2021) 9:1931. doi: 10.3390/biomedicines9121931

98. George PM, Wells AU, Jenkins RG. Pulmonary fibrosis and COVID-19: the potential role for antifibrotic therapy. *Lancet Respir Med.* (2020) 8:807–15. doi: 10.1016/S2213-2600(20)30225-3

99. Rumende CM, Susanto EC, Sitorus TP. The management of pulmonary fibrosis in COVID-19. *Acta Med Indones.* (2021) 53:233–41.

100. Cesarone MR, Hu S, Belcaro G, Cornelli U, Feragalli B, Corsi M, et al. Pycnogenol®-Centellicum® supplementation improves lung fibrosis and post-COVID-19 lung healing. *Minerva Med.* (2022) 113:135–40. doi: 10.23736/S0026-4806.20.07225-0

101. Dhooria S, Chaudhary S, Sehgal IS, Agarwal R, Arora S, Garg M, et al. High-dose versus low-dose prednisolone in symptomatic patients with post-COVID-19 diffuse parenchymal lung abnormalities: an open-label, randomised trial (the COLDSTER trial). *Eur Respir J.* (2022) 59:2102930. doi: 10.1183/13993003.02930-2021

102. Myall KJ, Mukherjee B, Castanheira AM, Lam JL, Benedetti G, Mak SM, et al. Persistent post-COVID-19 interstitial lung disease. An observational study of corticosteroid treatment. *Ann Am Thorac Soc.* (2021) 18:799–806. doi: 10.1513/AnnalsATS.202008-1002OC

103. Kostorz-Nosal S, Jastrzębski D, Chyra M, Kubicki P, Zieliński M, Ziora D. A prolonged steroid therapy may be beneficial in some patients after the COVID-19 pneumonia. *Eur Clin Respir J.* (2021) 8:1945186. doi: 10.1080/20018525.2021.1945186

104. Segala FV, Sgalla G, Salvati F, Berardini L, Negri M, Nardella E, et al. Adjunctive corticosteroid treatment for organizing pneumonia in COVID-19 patients with persistent respiratory failure. *Respir Med.* (2021) 187:106571. doi: 10.1016/j.rmed.2021.106571

105. Shen H, Zhang N, Liu Y, Yang X, He Y, Li Q, et al. The interaction between pulmonary fibrosis and COVID-19 and the application of related anti-fibrotic drugs. *Front Pharmacol.* (2021) 12:805535. doi: 10.3389/fphar.2021.805535

106. Tang N, Li D, Wang X, Sun Z. Abnormal coagulation parameters are associated with poor prognosis in patients with novel coronavirus pneumonia. *J Thromb Haemost.* (2020) 18:844–7. doi: 10.1111/jth.14768

107. Guan W-J, Ni Z-Y, Hu Y, Liang W-H, Ou C-Q, He J-X, et al. Clinical characteristics of coronavirus disease 2019 in China. *N Engl J Med.* (2020) 382:1708–20. doi: 10.1056/NEJMoa2002032

108. Naymagon L, Zubizarreta N, Feld J, van Gerwen M, Alsen M, Thibaud S, et al. Admission D-dimer levels, D-dimer trends, and outcomes in COVID-19. *Thromb Res.* (2020) 196:99–105. doi: 10.1016/j.thromres.2020.08.032

109. Huang C, Wang Y, Li X, Ren L, Zhao J, Hu Y, et al. Clinical features of patients infected with 2019 novel coronavirus in Wuhan, China. *Lancet.* (2020) 395:497–506. doi: 10.1016/S0140-6736(20)30183-5

110. Panigada M, Bottino N, Tagliabue P, Grasselli G, Novembrino C, Chantarangkul V, et al. Hypercoagulability of COVID-19 patients in intensive care unit: a report of thromboelastography findings and other parameters of hemostasis. *J Thromb Haemost.* (2020) 18:1738–42. doi: 10.1111/jth.14850

111. Levi M, Thachil J, Iba T, Levy JH. Coagulation abnormalities and thrombosis in patients with COVID-19. *Lancet Haematol.* (2020) 7:e438–40. doi: 10.1016/S2352-3026(20)30145-9

112. Ackermann M, Verleden SE, Kuehnel M, Haverich A, Welte T, Laenger F, et al. Pulmonary vascular endothelialitis, thrombosis, and angiogenesis in Covid-19. *N Engl J Med.* (2020) 383:120–8. doi: 10.1056/NEJMoa2015432

113. Burn E, Duarte-Salles T, Fernandez-Bertolin S, Reyes C, Kostka K, Delmestri A, et al. Venous or arterial thrombosis and deaths among COVID-19 cases: a European network cohort study. *Lancet Infect Dis.* (2022) 8:1142–52. doi: 10.1016/S1473-3099(22)00223-7

114. Gerotziafas GT, Van Dreden P, Sergentanis TN, Politou M, Rousseau A, Grusse M, et al. Persisting Endothelial cell activation and hypercoagulability after COVID-19 recovery–the prospective observational ROADMAP-post COVID-19 study. *Hemato.* (2022) 3:111–21. doi: 10.3390/hemato3010010

115. Willems LH, Nagy M, Ten Cate H, Spronk HMH, Groh LA, Leentjens J, et al. Sustained inflammation, coagulation activation and elevated endothelin-1 levels

without macrovascular dysfunction at 3 months after COVID-19. *Thrombos Res.* (2022) 209:106–14. doi: 10.1016/j.thromres.2021.11.027

116. von Meijenfeldt FA, Havervall S, Adelmeijer J, Lundström A, Magnusson M, Mackman N, et al. Sustained prothrombotic changes in COVID-19 patients 4 months after hospital discharge. *Blood Adv.* (2021) 5:756–9. doi: 10.1182/bloodadvances.2020003968

117. Giannis D, Allen SL, Tsang J, Flint S, Pinhasov T, Williams S, et al. Postdischarge thromboembolic outcomes and mortality of hospitalized patients with COVID-19: the CORE-19 registry. *Blood.* (2021) 137:2838–47. doi: 10.1182/blood.2020010529

118. Roberts LN, Whyte MB, Georgiou L, Giron G, Czuprynska J, Rea C, et al. Postdischarge venous thromboembolism following hospital admission with COVID-19. *Blood Am Soc Hematol.* (2020) 136:1347–50. doi: 10.1182/blood.2020008086

119. Patell R, Bogue T, Koshy A, Bindal P, Merrill M, Aird WC, et al. Postdischarge thrombosis and hemorrhage in patients with COVID-19. *Blood Am Soc Hematol.* (2020) 136:1342–6. doi: 10.1182/blood.2020007938

120. Rashidi F, Barco S, Kamangar F, Heresi GA, Emadi A, Kaymaz C, et al. Incidence of symptomatic venous thromboembolism following hospitalization for coronavirus disease 2019: prospective results from a multi-center study. *Thromb Res.* (2021) 198:135–8. doi: 10.1016/j.thromres.2020.12.001

121. Engelen MM, Vandenbriele C, Balthazar T, Claeys E, Gunst J, Guler I, et al. Venous thromboembolism in patients discharged after COVID-19 hospitalization. *Semin Thromb Hemost.* (2021) 47:362–71. doi: 10.1055/s-0041-1727284

122. Suzuki YJ, Nikolaienko SI, Shults NV, Gychka SG. COVID-19 patients may become predisposed to pulmonary arterial hypertension. *Med Hypotheses.* (2021) 147:110483. doi: 10.1016/j.mehy.2021.110483

123. Suzuki YJ, Nikolaienko SI, Dibrova VA, Dibrova YV, Vasylyk VM, Novikov MY, et al. CoV-2 spike protein-mediated cell signaling in lung vascular cells. *Vascul Pharmacol.* (2021) 137:106823. doi: 10.1016/j.vph.2020.106823

124. Potus XF, Mai V, Lebret M, Malenfant XS, Breton-gagnon E, Lajoie XAC, et al. Novel insights on the pulmonary vascular consequences of COVID-19. *Am J Physiol Lung Cell Mol Physiol.* (2020) 319:L277–88. doi: 10.1152/ajplung.00195.2020

125. Monteil V, Kwon H, Prado P, Hagelkrüys A, Wimmer RA, Stahl M, et al. Inhibition of SARS-CoV-2 infections in engineered human tissues using clinical-grade soluble human ACE2. *Cell.* (2020) 181:905.e–13.e. doi: 10.1016/j.cell.2020.04.004

126. Varga Z, Flammer AJ, Steiger P, Haberecker M, Andermatt R, Zinkernagel AS, et al. Endothelial cell infection and endotheliitis in COVID-19. *Lancet.* (2020) 395:1417–8. doi: 10.1016/S0140-6736(20)30937-5

127. Jia H. Pulmonary angiotensin-converting enzyme 2 (ACE2) and inflammatory lung disease. *Shock.* (2016) 46:239–48. doi: 10.1097/SHK.0000000000000633

128. Nijkeuter M, Hovens MMC, Davidson BL, Huisman MV. Resolution of thromboemboli in patients with acute pulmonary embolism: a systematic review. *Chest.* (2006) 129:192–7. doi: 10.1378/chest.129.1.192

129. Klok FA, van Kralingen KW, van Dijk APJ, Heyning FH, Vliegen HW, Huisman MV. Prospective cardiopulmonary screening program to detect chronic thromboembolic pulmonary hypertension in patients after acute pulmonary embolism. *Haematologica.* (2010) 95:970–5. doi: 10.3324/haematol.2009.018960

130. Pengo V, Lensing AWA, Prins MH, Marchiori A, Davidson BL, Tiozzo F, et al. Incidence of chronic thromboembolic pulmonary hypertension after pulmonary embolism. *N Engl J Med.* (2004) 350:2257–64. doi: 10.1056/NEJMoa032274

131. Ende-Verhaar YM, Cannegieter SC, Vonk Noordegraaf A, Delcroix M, Pruszczyk P, Mairuhu ATA, et al. Incidence of chronic thromboembolic pulmonary hypertension after acute pulmonary embolism: a contemporary view of the published literature. *Eur Respir J.* (2017) 49:1601792. doi: 10.1183/13993003.01792-2016

132. Guérin L, Couturaud F, Parent F, Revel M-P, Gillaizeau F, Planquette B, et al. Prevalence of chronic thromboembolic pulmonary hypertension after acute pulmonary embolism. Prevalence of CTEPH after pulmonary embolism. *Thromb Haemost.* (2014) 112:598–605. doi: 10.1160/TH13-07-0538

133. Pepke-Zaba J, Delcroix M, Lang I, Mayer E, Jansa P, Ambroz D, et al. Chronic thromboembolic pulmonary hypertension (CTEPH): results from an international prospective registry. *Circulation.* (2011) 124:1973–81. doi: 10.1161/CIRCULATIONAHA.110.015008

134. Riedel M, Stanek V, Widimsky J, Prerovsky I. Longterm follow-up of patients with pulmonary thromboembolism. Late prognosis and evolution of hemodynamic and respiratory data. *Chest.* (1982) 81:151–8. doi: 10.1378/chest.81.2.151

135. Townsend L, Fogarty H, Dyer A, Martin-Loeches I, Bannan C, Nadarajan P, et al. Prolonged elevation of D-dimer levels in convalescent COVID-19 patients is independent of the acute phase response. *J Thromb Haemost.* (2021) 19:1064–70. doi: 10.1111/jth.15267

136. Nuche J, Segura de la Cal T, Jiménez López Guarch C, López-Medrano F, Delgado CP, Ynsaurriaga FA, et al. Effect of coronavirus disease 2019 in pulmonary circulation. the particular scenario of precapillary pulmonary hypertension. *Diagnostics (Basel).* (2020) 10:E548. doi: 10.3390/diagnostics10080548

137. van Dam LF, Kroft LJM, van der Wal LI, Cannegieter SC, Eikenboom J, de Jonge E, et al. Clinical and computed tomography characteristics of COVID-19 associated acute pulmonary embolism: a different phenotype of thrombotic disease? *Thromb Res.* (2020) 193:86–9. doi: 10.1016/j.thromres.2020.06.010

138. Delcroix M, Torbicki A, Gopalan D, Sitbon O, Klok FA, Lang I, et al. ERS statement on chronic thromboembolic pulmonary hypertension. *Eur Respir J.* (2021) 57:2002828. doi: 10.1183/13993003.02828-2020

139. Kim NH, Delcroix M, Jais X, Madani MM, Matsubara H, Mayer E, et al. Chronic thromboembolic pulmonary hypertension. *Eur Respir J.* (2019) 53:1801915. doi: 10.1183/13993003.01915-2018

140. He J, Fang W, Lv B, He J-G, Xiong C-M, Liu Z-H, et al. Diagnosis of chronic thromboembolic pulmonary hypertension: comparison of ventilation/perfusion scanning and multidetector computed tomography pulmonary angiography with pulmonary angiography. *Nucl Med Commun.* (2012) 33:459–63. doi: 10.1097/MNM.0b013e32835085d9

141. Moores LK, Tritschler T, Brosnahan S, Carrier M, Collen JF, Doerschug K, et al. Prevention, diagnosis, and treatment of VTE in patients with coronavirus disease 2019: CHEST guideline and expert panel report. *Chest.* (2020) 158:1143–63. doi: 10.1016/j.chest.2020.05.559

142. NIH. *Antithrombotic Therapy. COVID-19 Treatment Guidelines*. Bethesda, MD: NIH (2022).

143. Brenot P, Jaïs X, Taniguchi Y, Garcia Alonso C, Gerardin B, Mussot S, et al. French experience of balloon pulmonary angioplasty for chronic thromboembolic pulmonary hypertension. *Eur Respir J.* (2019) 53:1802095. doi: 10.1183/13993003.02095-2018

144. Li W, Yang T, Quan R-L, Chen X-X, An J, Zhao Z-H, et al. Balloon pulmonary angioplasty reverse right ventricular remodelling and dysfunction in patients with inoperable chronic thromboembolic pulmonary hypertension: a systematic review and meta-analysis. *Eur Radiol.* (2021) 31:3898–908. doi: 10.1007/s00330-020-07481-6

145. Ghofrani H-A, D'Armini AM, Grimminger F, Hoeper MM, Jansa P, Kim NH, et al. Riociguat for the Treatment of Chronic Thromboembolic Pulmonary Hypertension. *N Engl J Med.* (2013) 369:319–29. doi: 10.1056/NEJMoa1209657

146. Cueto-Robledo G, Porres-Aguilar M, Puebla-Aldama D, del Pilar Barragán-Martínez M, Jurado-Hernández MY, García-César M, et al. Severe pulmonary hypertension: an important sequel after severe post-acute COVID-19 pneumonia. *Curr Probl Cardiol.* (2022) 47:101004. doi: 10.1016/j.cpcardiol.2021.101004

147. Salcin S, Fontem F. Recurrent SARS-CoV-2 infection resulting in acute respiratory distress syndrome and development of pulmonary hypertension: a case report. *Respir Med Case Rep.* (2021) 33:101314. doi: 10.1016/j.rmcr.2020.101314

148. Kolb TM, Hassoun PM. Right ventricular dysfunction in chronic lung disease. *Cardiol Clin.* (2012) 30:243–56. doi: 10.1016/j.ccl.2012.03.005

149. Rinaldo RF, Mondoni M, Parazzini EM, Baccelli A, Pitari F, Brambilla E, et al. Severity does not impact on exercise capacity in COVID-19 survivors. *Respir Med.* (2021) 187:106577. doi: 10.1016/j.rmed.2021.106577

150. Rinaldo RF, Mondoni M, Parazzini EM, Pitari F, Brambilla E, Luraschi S, et al. Deconditioning as main mechanism of impaired exercise response in COVID-19 survivors. *Eur Respir J.* (2021) 58:2100870. doi: 10.1183/13993003.00870-2021

151. Skjørten I, Ankerstjerne OAW, Trebinjac D, Brønstad E, Rasch-Halvorsen Ø, Einvik G, et al. Cardiopulmonary exercise capacity and limitations 3 months after COVID-19 hospitalisation. *Eur Respir J.* (2021) 58:2100996. doi: 10.1183/13993003.00996-2021

152. Motiejunaite J, Balagny P, Arnoult F, Mangin L, Bancal C, Vidal-Petiot E, et al. Hyperventilation as one of the mechanisms of persistent dyspnoea in SARS-CoV-2 survivors. *Eur Respir J.* (2021) 58:2101578. doi: 10.1183/13993003.01578-2021

153. Debeaumont D, Boujibar F, Ferrand-Devouge E, Artaud-Macari E, Tamion F, Gravier F-E, et al. Cardiopulmonary exercise testing to assess persistent symptoms at 6 months in people with covid-19 who survived hospitalization: a pilot study. *Phys Ther.* (2021) 101:zab099. doi: 10.1093/ptj/pzab099

154. Clavario P, De Marzo V, Lotti R, Barbara C, Porcile A, Russo C, et al. Cardiopulmonary exercise testing in COVID-19 patients at 3 months follow-up. *Int J Cardiol.* (2021) 340:113–8. doi: 10.1016/j.ijcard.2021.07.033

155. Acar RD, Sarıbaş E, Güney PA, Kafkas Ç, Aydınlı D, Taşçı E, et al. COVID-19: the new cause of dyspnoea as a result of reduced lung and peripheral muscle performance. *J Breath Res.* (2021) 15:047103. doi: 10.1088/1752-7163/ac22bb

156. Cassar MP, Tunnicliffe EM, Petousi N, Lewandowski AJ, Xie C, Mahmod M, et al. Symptom Persistence Despite Improvement in Cardiopulmonary Health - Insights from longitudinal CMR, CPET and lung function testing post-COVID-19. *EClinicalMedicine.* (2021) 41:101159. doi: 10.1016/j.eclinm.2021.101159

157. Vonbank K, Lehmann A, Bernitzky D, Gysan MR, Simon S, Schrott A, et al. Predictors of prolonged cardiopulmonary exercise impairment after COVID-19 Infection: a prospective observational study. *Front Med (Lausanne).* (2021) 8:773788. doi: 10.3389/fmed.2021.773788

158. Ribeiro Baptista B, d'Humières T, Schlemmer F, Bendib I, Justeau G, Al-Assaad L, et al. Identification of factors impairing exercise capacity after severe COVID-19 pulmonary infection: a 3-month follow-up of prospective COVulnerability cohort. *Respir Res.* (2022) 23:68. doi: 10.1186/s12931-022-01977-z

159. Singh I, Joseph P, Heerdt PM, Cullinan M, Lutchmansingh DD, Gulati M, et al. Persistent exertional intolerance after COVID-19. *Chest.* (2021) 161:54–63. doi: 10.1016/j.chest.2021.08.010

160. Hejbøl EK, Harbo T, Agergaard J, Madsen LB, Pedersen TH, Østergaard LJ, et al. Myopathy as a cause of fatigue in long-term post-COVID-19 symptoms: evidence of skeletal muscle histopathology. *Eur J Neurol.* (2022) 29:2832–41. doi: 10.1111/ene.15435

161. Schaeffer MR, Cowan J, Milne KM, Puyat JH, Voduc N, Corrales-Medina V, et al. Cardiorespiratory physiology, exertional symptoms, and psychological burden in post-COVID-19 fatigue. *Respir Physiol Neurobiol.* (2022) 302:103898. doi: 10.1016/j.resp.2022.103898

162. Baratto C, Caravita S, Faini A, Perego GB, Senni M, Badano LP, et al. Impact of COVID-19 on exercise pathophysiology: a combined cardiopulmonary and echocardiographic exercise study. *J Appl Physiol.* (2021) 130:1470–8. doi: 10.1152/japplphysiol.00710.2020

163. Spruit MA, Holland AE, Singh SJ, Tonia T, Wilson KC, Troosters T. COVID-19: interim guidance on rehabilitation in the hospital and post-hospital phase from a European respiratory society and American thoracic society-coordinated international task force. *Eur Respir J.* (2020) 56:2002197. doi: 10.1183/13993003.02197-2020

164. Li J. Rehabilitation management of patients with COVID-19: lessons learned from the first experience in China. *Eur J Phys Rehabil Med.* (2020) 56:335–8. doi: 10.23736/S1973-9087.20.06292-9

165. Dixit S, Borghi-Silva A, Bairapareddy KC. Revisiting pulmonary rehabilitation during COVID-19 pandemic: a narrative review. *Rev Cardiovasc Med.* (2021) 22:315–27. doi: 10.31083/j.rcm2202039

166. Huang L, Yao Q, Gu X, Wang Q, Ren L, Wang Y, et al. 1-year outcomes in hospital survivors with COVID-19: a longitudinal cohort study. *Lancet.* (2021) 398:747–58. doi: 10.1016/S0140-6736(21)01755-4

167. de Sire A, Andrenelli E, Negrini F, Patrini M, Lazzarini SG, Ceravolo MG, et al. Rehabilitation and COVID-19: a rapid living systematic review by cochrane rehabilitation field updated as of December 31st, 2020 and synthesis of the scientific literature of 2020. *Eur J Phys Rehabil Med.* (2021) 57:181–8. doi: 10.23736/S1973-9087.21.06870-2

168. Hameed F, Palatulan E, Jaywant A, Said R, Lau C, Sood V, et al. Outcomes of a COVID-19 recovery program for patients hospitalized with SARS-CoV-2 infection in New York City: a prospective cohort study. *PM R.* (2021) 13:609–17. doi: 10.1002/pmrj.12578

169. Gonzalez-Gerez JJ, Saavedra-Hernandez M, Anarte-Lazo E, Bernal-Utrera C, Perez-Ale M, Rodriguez-Blanco C. Short-term effects of a respiratory telerehabilitation program in confined covid-19 patients in the acute phase: a pilot study. *Int J Environ Res Public Health.* (2021) 18:7511. doi: 10.3390/ijerph18147511

170. Li J, Xia W, Zhan C, Liu S, Yin Z, Wang J, et al. A telerehabilitation programme in post-discharge COVID-19 patients (TERECO): a randomised controlled trial. *Thorax.* (2021) 77:697–706. doi: 10.1136/thoraxjnl-2021-217382

171. De Marchi T, Frâncio F, Ferlito JV, Weigert R, de Oliveira C, Merlo AP, et al. Effects of photobiomodulation therapy combined with static magnetic field in severe COVID-19 patients requiring intubation: a pragmatic randomized placebo-controlled trial. *J Inflamm Res.* (2021) 14:3569–85. doi: 10.2147/JIR.S318758

172. Nambi G, Abdelbasset WK, Alrawaili SM, Elsayed SH, Verma A, Vellaiyan A, et al. Comparative effectiveness study of low versus high-intensity aerobic training with resistance training in community-dwelling older men with post-COVID 19 sarcopenia: a randomized controlled trial. *Clin Rehabil.* (2022) 36:59–68. doi: 10.1177/02692155211036956

173. Mohamed AA, Alawna M. The effect of aerobic exercise on immune biomarkers and symptoms severity and progression in patients with COVID-19: a randomized control trial. *J Bodyw Mov Ther.* (2021) 28:425–32. doi: 10.1016/j.jbmt.2021.07.012

174. Liu K, Zhang W, Yang Y, Zhang J, Li Y, Chen Y. Respiratory rehabilitation in elderly patients with COVID-19: a randomized controlled study. *Complement Ther Clin Pract.* (2020) 39:101166. doi: 10.1016/j.ctcp.2020.101166

175. Güler T, Yurdakul FG, Acar Sivas F, Kiliç Z, Adigüzel E, Yaşar E, et al. Rehabilitative management of post-acute COVID-19: clinical pictures and outcomes. *Rheumatol Int.* (2021) 41:2167–75. doi: 10.1007/s00296-021-05003-1

176. Bouteleux B, Henrot P, Ernst R, Grassion L, Raherison-Semjen C, Beaufils F, et al. Respiratory rehabilitation for Covid-19 related persistent dyspnoea: a one-year experience. *Respir Med.* (2021) 189:106648. doi: 10.1016/j.rmed.2021.106648

177. Holland AE, Cox NS, Houchen-Wolloff L, Rochester CL, Garvey C, ZuWallack R, et al. Defining modern pulmonary rehabilitation. An official American thoracic society workshop report. *Ann Am Thorac Soc* (2021) 18:e12–29. doi: 10.1513/AnnalsATS.202102-146ST

178. Spruit MA, Singh SJ, Garvey C, ZuWallack R, Nici L, Rochester C, et al. An official American thoracic society/European respiratory society statement: key concepts and advances in pulmonary rehabilitation. *Am J Respir Crit Care Med* (2013) 188:e13–64.

179. Bolton CE, Bevan-Smith EF, Blakey JD, Crowe P, Elkin SL, Garrod R, et al. British thoracic society guideline on pulmonary rehabilitation in adults. *Thorax* (2013) 68(Suppl. 2):ii1–30. doi: 10.1136/thoraxjnl-2013-203808

180. Radtke T, Crook S, Kaltsakas G, Louvaris Z, Berton D, Urquhart DS, et al. ERS statement on standardisation of cardiopulmonary exercise testing in chronic lung diseases. *Eur Respir Rev.* (2019) 28:180101. doi: 10.1183/16000617.0101-2018

181. Holland AE, Spruit MA, Troosters T, Puhan MA, Pepin V, Saey D, et al. An official European respiratory society/American thoracic society technical standard: field walking tests in chronic respiratory disease. *Eur Respir J.* (2014) 44:1428–46. doi: 10.1183/09031936.00150314

182. Gao Y, Chen R, Geng Q, Mo X, Zhan C, Jian W, et al. Cardiopulmonary exercise testing might be helpful for interpretation of impaired pulmonary function in recovered COVID-19 patients. *Eur Respir J.* (2021) 57:2004265. doi: 10.1183/13993003.04265-2020

183. Liu M, Lv F, Huang Y, Xiao K. Follow-up study of the chest CT characteristics of COVID-19 survivors seven months after recovery. *Front Med.* (2021) 8:636298. doi: 10.3389/fmed.2021.636298

184. Dorelli G, Braggio M, Gabbiani D, Busti F, Caminati M, Senna G, et al. Importance of cardiopulmonary exercise testing amongst subjects recovering from COVID-19. *Diagnostics.* (2021) 11:507. doi: 10.3390/diagnostics11030507

185. Barbagelata L, Masson W, Iglesias D, Lillo E, Migone JF, Orazi ML, et al. Cardiopulmonary exercise testing in patients with post-COVID-19 syndrome. *Med Clin (Barc).* (2021) 159:6–11. doi: 10.1016/j.medcli.2021.07.007

186. Mancini DM, Brunjes DL, Lala A, Trivieri MG, Contreras JP, Natelson BH. Use of cardiopulmonary stress testing for patients with unexplained dyspnea post–coronavirus disease. *JACC Heart Fail.* (2021) 9:927–37. doi: 10.1016/j.jchf.2021.10.002

187. Szekely Y, Lichter Y, Sadon S, Lupu L, Taieb P, Banai A, et al. Cardiorespiratory abnormalities in patients recovering from coronavirus disease 2019. *J Am Soc Echocardiogr* (2021) 34:1273–1284.e9. doi: 10.1016/j.echo.2021.08.022

188. de Boer E, Petrache I, Goldstein NM, Olin JT, Keith RC, Modena B, et al. Decreased fatty oxidation and altered lactate production during exercise in post-acute COVID-19 patients. *Am J Respir Crit Care Med.* (2021) 205:126–9. doi: 10.1164/rccm.202108-1903LE

189. Ladlow P, O'Sullivan O, Houston A, Barker-Davies R, May S, Mills D, et al. Dysautonomia following COVID-19 is not associated with subjective limitations or symptoms but is associated with objective functional limitations. *Heart Rhythm.* (2022) 19:613–20. doi: 10.1016/j.hrthm.2021.12.005

190. Ambrosino P, Parrella P, Formisano R, Perrotta G, D'Anna SE, Mosella M, et al. Cardiopulmonary exercise performance and endothelial function in convalescent covid-19 patients. *J Clin Med.* (2022) 11:1452. doi: 10.3390/jcm11051452

191. Frésard I, Genecand L, Altarelli M, Gex G, Vremaroiu P, Vremaroiu-Coman A, et al. Dysfunctional breathing diagnosed by cardiopulmonary exercise testing in "long COVID" patients with persistent dyspnoea. *BMJ Open Respir Res.* (2022) 9:e001126. doi: 10.1136/bmjresp-2021-001126

Frontiers in Medicine

Translating medical research and innovation into improved patient care

A multidisciplinary journal which advances our medical knowledge. It supports the translation of scientific advances into new therapies and diagnostic tools that will improve patient care.

Discover the latest Research Topics

See more →

Frontiers

Avenue du Tribunal-Fédéral 34
1005 Lausanne, Switzerland
frontiersin.org

Contact us

+41 (0)21 510 17 00
frontiersin.org/about/contact